Sedimentology and tectonic history of late Archaean sedimentary successions in Zimbabwe: a study in greenstone belt geology

Dissertation zur Erlangung des Grades
"Doktor der Naturwissenschaften" am Fachbereich Geowissenschaften
der Johannes Gutenberg-Universität in Mainz

Axel Hofmann
geb. in Bad Kreuznach

Mainz, im Dezember 2001

Tag der mündlichen Prüfung: 30. Januar 2002

Versicherung
für das Gesuch um Zulassung zur Promotion in den Fachbereichen 17-22

Hiermit versichere ich gemäß §11(3)d der Promotionsordnung vom 30. April 1990:

a) Ich habe die jetzt als Dissertation vorgelegte Arbeit selbst angefertigt und alle benutzten Hilfsmittel (Literatur, Apparaturen, Material) in der Arbeit angegeben.
b) Ich habe oder hatte die jetzt als Dissertation vorgelegte Arbeit nicht als Prüfungsarbeit für eine staatliche oder andere wissenschaftliche Prüfung eingereicht.
c) Ich hatte weder die jetzt als Dissertation vorgelegte Arbeit noch Teile davon bei einer anderen Fakultät bzw. einem anderen Fachbereich als Dissertation eingereicht.

Sämtliche Beobachtungen und Interpretationen in dieser kumulativen Dissertation stammen vom Autor. Die Arbeit wurde finanziell von Projekt 1998-2001/13 des niederländischen Stichting Dr. Schürmannfonds unterstützt, so daß die Projektantragssteller Paul H.G.M. Dirks and Hielke A. Jelsma als Co-Autoren in Kapitel 2-8 genannt werden. In Kapitel 5 wird Robert Bolhar als Co-Autor genannt, da ich als Endglieder für die Provenanzmodellierung (Abbildung 5.11, Tabelle 5.3) bis jetzt unveröffentlichte Gesteinsanalysen aus seiner Dissertation (als Quelle angegeben) benutzt habe. In Kapitel 8 wird Nikadzino Matura als Co-Autor genannt, da ich die geologische Karte seiner bis jetzt unveröffentlichten M.Sc. Arbeit (als Quelle angegeben) in modifizierter Form als Abbildung 8.13 benutzt habe.

Mainz, den 16. Dezember 2001

TABLE OF CONTENTS

Abstract

The study of ~2.65 Ga old sedimentary rocks in three greenstone belts of the Zimbabwe craton has provided important constraints on Archaean geology and the evolution of Archaean greenstone belts in Zimbabwe. In the Belingwe greenstone belt, a mid-Archaean granitoid basement is overlain by an allochthonous unit which consists of a submarine mafic-ultramafic lava sequence and a sedimentary foreland basin succession. The sedimentary unit comprises a drowned carbonate ramp sequence overlain by a thick turbidite sequence. Sedimentological and stratigraphic constraints, geochemical provenance analyses and structural evidence for thin-skinned thrusting and tectonic stacking suggest horizontal tectonic processes as an important factor in the evolution of this greenstone belt. The carbonate ramp comprises one of the best preserved successions of Archaean carbonates so far observed. Importantly, carbonate facies are arranged into shallowing-upward cycles, similar to those of the Proterozoic and Phanerozoic rock record. High-frequency eustatic sea-level changes, possibly tuned by Milankovitch-type orbital cyclic forcing, are suggested as the controlling mechanism for the cyclicity.

Late Archaean sediments in the Midlands greenstone belt occur as a shear zone-bounded lithotectonic unit wedged in between complexly deformed mafic volcanic rocks and mid-Archaean gneisses. The facies sequence of lower, deep-marine turbidites and upper, shallow-marine shelf sandstones and coarse clastic alluvial deposits, combined with geological and geochemical data from the adjacent rock units, is consistent with deposition in a foreland or forearc basin that formed during collision of a continental fragment and an oceanic plateau-island arc sequence.

In the Bindura-Shamva greenstone belt, late Archaean sediments occur as distinct, shear zone-bounded tectonstratigraphic units, an alluvial fan—fluvial braid-plain—marine shoreface sequence with detritus derived from a mid-Archaean granitoid-gneiss terrain, and a deep-marine—shallow-marine—fluvial sequence with an intermediate to felsic volcanic source. Sediment supply and subsidence rate must have been high. Basin initiation may have been related to extensional tectonics, possibly on stretched continental crust. Later stages of basin history may have been similar to compressional foreland or forearc settings, because sedimentation was followed by layer-parallel shearing during thrust belt-style tectonic deformation.

Thin, bedding-parallel horizons of ironstone, lithologically similar to banded iron-formation, but interpreted as silicified and sulphide-impregnated shear zones, commonly occupy the contacts between the sedimentary sequences and the volcanic rocks of the greenstone belts studied. The formation of these “tectonic ironstones” is attributed to in-situ hydrothermal alteration of rocks adjacent to and within fault zones during deformation. Shearing is indicated by the truncation of bedding/foliation and duplication of statigraphic units along the ironstone horizons and gave rise to the imbrication of volcanic and sedimentary rock units.

Zusammenfassung

Die Erforschung von ca. 2,65 Milliarden Jahre alten Sedimentgesteinen in Grünsteingürteln des Simbabwe Kratons haben wichtige Erkenntnisse für die Geologie des Archaikums und für die Entstehung von archaischen Grünsteingürteln in Simbabwe erbracht. In dem Belingwe Grünsteingürtel ist mittelarchaisches Grundgebirge von einer allochthonen Einheit aus submarinen, mafisch-ultramafischen Laven und Vorlandbeckensedimenten überlagert. Die sedimentäre Abfolge besteht aus Flachwasserkalken und darüberliegenden, tiefer marinen Turbiditen. Sedimentologische und stratigraphische Daten, geochemische Provenanzanalysen und deutliche Hinweise für Deckenüberschiebungen zeigen die Bedeutung horizontaler tektonischer Prozesse für die Entwicklung dieses Grünsteingürtels an. Die untersuchten Kalksteine sind im Vergleich zu anderen archaischen Karbonatvorkommen ungewöhnlich gut erhalten. Interessanterweise sind unterschiedliche Faziestypen in sedimentäre Verflachungszyklen angeordnet, ganz ähnlich zu proterozoischen und phanerozoischen Karbonaten. Hochfrequenzielle, eustatische Meeresspiegelschwankungen, möglicherweise von orbitalen Milankovitch-Zyklen gesteuert, werden als Ursache der zyklischen Sedimentation angenommen.

Spätarchaische Sedimente des Midlands Grünsteingürtels bilden eine lithotektonische Einheit, welche, von Scherzonen begrenzt, zwischen komplex deformierten, mafischen Vulkaniten und mittelarchaischen Gneisen lagert. Die Art der Abfolge sedimentärer Fazies, beginnend mit tiefmarinen Turbiditen und überlagert von flachmarinen Schelfsedimenten und grob-klastischen, alluvialen Ablagerungen, läßt auf Ablagerung in einem Becken vor einem Orogen oder vulkanischen Bogen schließen. Unterstützt von geologischen und geochemischen Hinweisen aus den benachbarten Gesteinsabfolgen wird die Kollision eines kontinentalen Krustenfragmentes mit einem ozeanischen Plateau und Inselbogen als Ursache für die Bildung des Sedimentbeckens angenommen.

In dem Bindura-Shamva Grünsteingürtel können zwei tektonostratigraphische Sedimenteinheiten unterschieden werden, eine alluvial—fluviatil—flachmarine Abfolge, deren Sedimente sich von einem mittelarchaischen Granit-Gneis Gebiet ableiten, und eine tiefmarin—flachmarin—fluviatile Abfolge mit einem aus intermediär-felsischen Vulkaniten zusammengesetzten Liefergebiet. Sedimentations- und Subsidenzraten waren erheblich. Extensionstektonik verursachte wahrscheinlich die Bildung des Sedimentbeckens, möglicherweise auf gestreckter kontinentaler Kruste. Die spätere Phase der Bekkenbildung war jedoch ähnlich jener in modernen Vorlandbecken, da Deckenüberschiebungen schichtparallele Deformation in den Sedimenten kurz nach der Ablagerung verursachte.

Geringmächtige, schichtparallele Eisensteinhorizonte, den gebänderten Eisensteinformationen lithologisch sehr ähnlich, sind in den untersuchten Grünsteingürteln häufig entlang von Sediment-Vulkanit-Kontakten zu finden. Diese Gesteine werden als silifizierte und von Sulfiden imprägnierte Scherzonen interpretiert. Syntektonische hydrothermale Alteration von Gesteinen entlang von Störungszonen führte zur Bildung dieser “tektonischen Eisensteine”. Das Abschneiden von Schichtung oder Schieferung sowie die tektonische Verdopplung von Gesteinseinheiten zeigt Scherungsdeformation an, welche zu komplizierten Überschiebungen von vulkanischen und sedimentären Gesteinen führte.

Zusammenfassung für Fachfremde

Gesteine des Erdaltertums (Archaikums), eine sich von 4,0 bis 2,5 Milliarden Jahren vor heute erstreckende geologische Epoche, sind auf bestimmte Erdkrustenteile (Kratone) beschränkt. Ein solcher Kraton nimmt im südlichen Afrika den überwiegenden Teil von Simbabwe ein. Archaische Sedimentgesteine, in Wechsellagerung mit durch metamorphe Veränderungen grün gefärbten vulkanischen Gesteinen (Grünsteine), sind in 50-200 km langen, und 10-50 km breiten Gesteinsgürteln zu finden. Diese Grünsteingürtel sind von granitischen Gesteinen umgeben; ihre Entstehung ist nicht geklärt. Genauso sind Art und Umfang oberflächennaher und erdinnerer Prozesse im Archaikum controvers. Sedimentgesteine sind Zeugen solcher Prozesse. Ihre Zusammensetzung und ihr Aufbau sind das Resultat von Wechselwirkungen zwischen der Atmosphäre, Hydrosphäre und Biosphäre. Die Bildung von Sedimentationsraum, Ablagerung und Sedimenterhalt hingegen sind von den Kräften im Erdinneren abhängig.

Eine durch ein spätarchaisches Alter (ca. 2,65 Milliarden Jahre), Entstehungsart und relative Position zu angrenzenden vulkanischen Gesteinen charakterisierte Sedimentgesteinsgruppe wurde in verschiedenen Grünsteingürteln Simbabwes untersucht. Die sedimentologischen, strukturellen und teilweise geochemischen Merkmale der Gesteine wurden erfaßt, um Gemeinsamkeiten und Unterschiede zu viel jüngeren Gesteinen oder Sedimenten aufzuzeigen, Ablagerungsmodelle zu erstellen und die Bildung von sedimentären Becken im Archaikum zu charakterisieren. Im Vergleich mit heutigen oberflächennahen Prozessen zeigten sich keine bedeutenden Unterschiede in den angenommenen Prozessverläufen, die zur Sedimentbildung im Archaikum führten, mit Ausnahme von Kennzeichen, die auf eine unterschiedliche Zusammensetzung der archaischen Atmosphäre (z.B. hoher CO_2 Gehalt) und fehlende Vegetation hinweisen. Die Sedimente wurden in Ablagerungsräumen ähnlich derer heutiger, kontinentnaher Ozeane, Schelfgebiete, Küsten und Flußmündungen gebildet. Die horizontale und vertikale Abfolge von Sedimenteinheiten ist bestimmten modernen Sedimentationsräumen (z.B. das Vorland junger Gebirge oder vulkanischer Inselbögen) sehr ähnlich. Interessanterweise wurden in einer flachmeerischen Kalksteinabfolge sedimentäre Zyklen beobachtet, welche mit frühen Meerespiegelschwankungen in Verbindung gebracht werden konnten. Ähnliche Schwankungen des Meeresspiegels waren in der geologisch jungen Vergangenheit an den Wechsel von Warm- und Eiszeiten geknüpft.

Kurz nach der Bildung von Sedimentationsraum und Ablagerung unterlagen die untersuchten Gesteinsserien komplizierten Deformationsprozessen, welche in Verfaltung, schichtparalleler Scherung und Überschiebung resultierte. Solche Verformungen sind heute in den Vorlandgebieten von vielen Gebirgen (z.B. den Alpen) zu finden. Als Ursache werden horizontale Bewegungen von kontinentalen und ozeanischen Erdkrustenplatten angenommen welche, bei gegensinniger Bewegungsrichtung, kompressive Deformation ihrer Ränder erfahren. Ähnliche Prozesse von horizontalen Krustenbewegungen und Deformation an Plattengrenzen können für die Strukturen der spätarchaischen Gesteine angenommen werden.

Acknowledgements

I acknowledge financial support by the Deutscher Akademischer Austauschdienst (Hochschulsonderprogramm III) and a grant from the University of Mainz (Landesgraduiertenförderung). Field work was financially supported by grants from Stichting Dr. Schürmannfonds (1998-2001/13). Data from the area around Shamva Mine are presented with permission of Independence Gold Mining Zimbabwe (Pvt) Ltd.

CHAPTER 1

Preface

INTRODUCTION

Granite-greenstone terrains around the world are characterized by granite-gneiss domes bordered by synforms of volcano-sedimentary sequences (greenstone belts). They are a characteristic feature of the Archaean (4.0-2.5 Ga) and contain much of the Earth´s mineral wealth. It has been suggested that greenstone belts may reflect a tectonic setting somewhat different from that of today which is dominated by plate tectonic processes. The current debate whether or not modern plate tectonic models can be applied to Archaean rock successions is mainly based on uncertainties in the way in which heat transfer mechanisms evolved over time. There is general consensus that the Earth's mantle in the Archaean was hotter than at present, partly due to higher abundances of radio-nuclides. Greater heat loss may have occurred through a greater global length of ocean spreading ridges, faster spreading rates and plate motions, or enhanced activity of mantle plumes. Different modes of heat loss and mantle convection may strongly influence the mode of crust formation and tectonic processes (e.g., Stein and Hofmann, 1994).

Two main tectonic models to explain the formation of Archaean crust are currently favoured. The horizontal accretion model suggests that greenstone terrains represent remnant oceanic crust or island arc material that was amalgamated with continental fragments via a modernistic, subduction-accretion related process (e.g., de Wit, 1998). In a contrasting model, greenstone belts are interpreted as rift-related sequences deposited on continental crust, possibly in fixed position above mantle plumes. Much of the subsequent compressional deformation is attributed to vertical processes including solid state granite diapirism and post-tectonic strike-slip faulting (non-uniformitarian model; Campbell and Hill, 1988; Bouhallier et al., 1993; Bickle et al., 1994; Hamilton, 1998).

The Zimbabwe craton (Fig. 1.1) is a segment of continental crust that attained stability c. 2.6 Ga ago. The oldest nucleus and earliest depositional stage of the craton is represented by the Tokwe Gneiss Complex and greenstones belonging to the Sebakwean Group (~3.5 Ga). The majority of the rocks were formed between 2.9-2.6 Ga ago and include volcanic and sedimentary rocks of the Belingwean, Lower Bulawayan, Upper Bulawayan and Shamvaian Group, and voluminous granitoid plutons that have been assigned to the Chingezi, Sesombi, Wedza and Chilimanzi suite (Table 1.1; Wilson et al., 1995). The Zimbabwe craton is generally quoted as a typical example of vertically accreted crust (Bickle et al., 1975; Blenkinsop et al., 1993; Bickle et al., 1994; Shackleton, 1995; Wilson et al., 1995; Jelsma et al., 1996; Hunter et al., 1998; Horstwood et al., 1999). This view is based on a range of arguments including: (a) the tri-cuspate outcrop pattern of greenstone belts enveloping subelliptical batholiths (Macgregor, 1951); (b) the recognition of unconformities at the

base of major greenstone sequences apparently overlying older continental crust (Bickle et al., 1975); (c) the recognition of a large-scale stratigraphy in the Belingwe belt that appears to be non-repetitive and has been correlated across much of the Zimbabwe craton (Wilson et al., 1995), suggesting that prior to the diapiric rise of granite-gneiss domes, the continental crust of Zimbabwe was covered by one extensive greenstone basin or a series of smaller, linked greenstone basins.

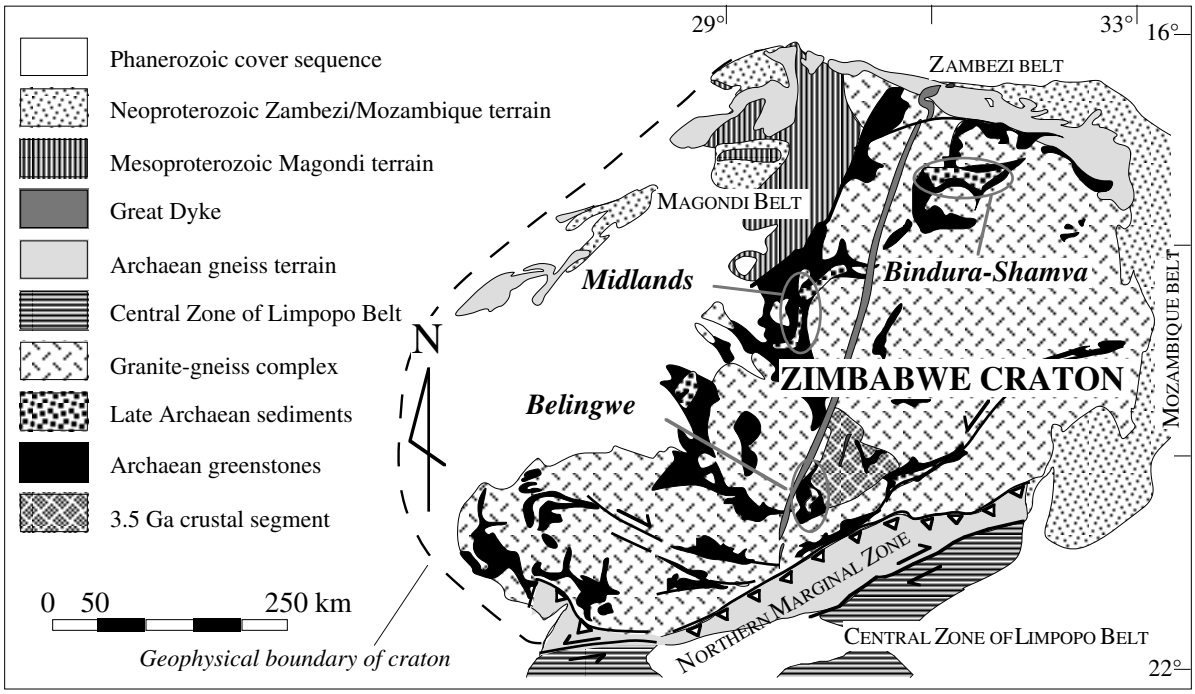

Fig. 1.1. Simplified geological map of the Zimbabwe craton and adjacent mobile belts. Study areas are indicated.

Particularly the last argument has resulted in an evolutionary concept for the Zimbabwe craton, herein referred to as the "Belingwe Model", which states that the craton developed during a series of growth stages that can be recognized throughout the craton (Wilson et al., 1995; Jelsma et al., 1996; Horstwood et al., 1999). Each stage involved an early episode of continental rifting associated with the deposition (above an unconformity) of a characteristic stratigraphic sequence (dominated by volcanics), followed by closure of the rift basin during a stage of magmatic underplating and diapirism. The "Belingwe Model" relies on a tectonically undisturbed stratigraphic sequence and the presence of basal unconformities underlying each major stratigraphic unit. The model predicts that: (a) the current stratigraphy reflects the stratigraphy as it was originally laid down; (b) all units were deposited on continental crust, and oceanic basins were not involved in the evolution of the craton; (c) the stratigraphy described in the Belingwe belt may be correlated craton-wide.

In contrast, it has been suggested that tectonic stacking of the stratigraphy may have played an important role in the evolution of the greenstone sequences (Kusky and Kidd, 1992; Kusky and Winsky, 1995; Dirks and Jelsma, 1998; Kusky, 1998; Jelsma and Dirks, 2000). The occurrence of detachment surfaces in the Archaean stratigraphy implies that the concept of a craton-wide

stratigraphy based on the "Belingwe Model" is incorrect, that oceanic crust may well exist in the greenstone sequences, that stratigraphic thicknesses are incorrect, and that the Zimbabwe craton developed in a similar way as other Archaean cratons where horizontal accretion tectonics played a significant role (e.g., Yilgarn craton, Myers, 1995; Superior Province, Card, 1990).

Table 1.1. Simplified stratigraphic nomenclature for greenstones and granitoids of the Zimbabwe craton (modified after Wilson, 1995).

Age (in Ga)	Greenstones	Granitoids
c. 2.6		Chilimanzi suite
c. 2.65	Shamvaian Group	Wedza suite
c. 2.7	Upper Bulawayan Group	Sesombi suite
c. 2.85	Lower Bulawayan Group	
c. 2.9	Belingwean Group	Chingezi suite
c. 3.5	Sebakwean Group	Tokwe suite

The main rock formation episode in the Zimbabwe craton occurred in the late Archaean with the formation of Upper Bulawayan greenstones, dominated by thick units of tholeiitic basalt with komatiite intercalations, followed by deposition of Shamvaian clastic sediments, including conglomerate, sandstone, shale and minor felsic volcaniclastics. This was followed by final stabilization of the craton after emplacement of the voluminous, crustally derived Chilimanzi suite of granites. To understand the tectonics that led to the formation of the Zimbabwe craton requires a coherent explanation for the structural and igneous events that accompanied the late Archaean tectonism. So far the "Belingwe Model" has been the main guide to explain the evolution of the Zimbabwe craton. Yet, new evidence for thrusting cannot be ignored and must be considered.

In this study the problem of the role of lateral accretion and thrusting in the Zimbabwe craton has been tackled in an integrated manner, involving mainly sedimentological and structural techniques in a number of well documented greenstone belts. The Belingwe belt is critical, because it represents the type locality where the stratigraphy was first defined and claimed to be tectonically undisturbed. It has the added advantage of good exposure, relatively low metamorphic grade and a well preserved sedimentary sequence (the Cheshire Formation) that contains an, as yet undocumented, wealth of information regarding the structural and sedimentary history of the belt. Other belts targeted include the Bindura-Shamva and Midlands greenstone belts, both of which have been extensively studied in the past and contain well-preserved sedimentary sequences that are intercalated with the greenstone volcanics. The objectives of this study are threefold: First, detailed mapping in critical areas (Belingwe, Shamva and Midlands belts) was needed to define (a) the exact nature of the stratigraphic sequence in the greenstone belts; (b) the nature of the contacts between stratigraphic units (depositional or sheared contacts); (c) the structural histories of the areas in the context of the entire craton; (d) sedimentological models that can be linked to the tectonic evolution of the areas.

Second, detailed structural-sedimentological mapping was needed to fully classify the deformation history of the areas and to see whether there is a causal relationship between deformation and sedimentation. Third, the sedimentological and structural data had to be integrated to define the depositional and tectonic setting in which the volcano-sedimentary sequences were formed.

Structural analysis of the volcanic rocks in the greenstone belts is complicated by a number of factors that include: (a) the general absence of clear stratification and younging directions, (b) the lateral discontinuity of many volcanic units and the absence of good marker horizons, and (c) the common occurrence of layer-parallel shear zones bounding lensoidal stratigraphic units. However, sedimentary sequences in the greenstone piles preserve layering and younging directions and show a reasonable degree of lateral continuity. These sequences tend to preserve the complex geometries that characterize the greenstone belts in a relatively clear manner. They consist of a variety of lithofacies, ranging from coarse clastic, molasse-type sediments to turbiditic, flysch-type deposits, and commonly preserve evidence for syn-sedimentary tectonism.

This dissertation is a collection of seven papers which concentrate on the geological history of late Archaean sedimentary sequences of the Zimbabwe craton. The data presented are important for the understanding of the formation of Archaean crust in Zimbabwe and provide new insights into: (a) the regional geology of Zimbabwe, because the late Archaean sedimentary sequences have never been studied in detail before; (b) the evolution and stabilization of the Zimbabwe craton as an Archaean continent; (c) the evolution of Archaean granite-greenstone terrains in general; and (d) the nature of plate tectonics in the Archaean.

STUDY AREAS

Belingwe greenstone belt

The Belingwe greenstone belt is situated in the southern part of Zimbabwe (Fig. 1.1) and contains rocks assigned to the Upper Bulawayan, termed the Ngezi Group. At the base of the Ngezi Group is a unit of clastic sediments (Manjeri Formation) that has been deposited unconformably on granitoid basement (Bickle et al., 1975). The Manjeri Formation is overlain by komatiitic and tholeiitic lavas (Reliance and Zeederbergs Formations) and a second sedimentary unit (Cheshire Formation). The Ngezi Group has been interpreted by many workers (e.g., papers in Bickle and Nisbet, 1993; Blenkinsop et al., 1993; Bickle et al., 1994; Brake, 1996; Hunter et al., 1998; Silva, 1997) as an autochtonous sequence deposited in an intracontinental rift basin. In contrast, Kusky and Kidd (1992) and Kusky and Winsky (1995) reported a major detachment zone between the Manjeri Formation and the overlying Reliance and Zeederbergs Formations, which they interpreted as the obducted part of an oceanic plateau that was emplaced as a large allochtonous sheet on a felsic basement. This diverging interpretation resulted in a heated dispute in the literature (e.g., Blenkinsop et al., 1994; Kusky et al., 1994; Dirks et al., 1999), but no consensus was reached. A detailed study of the Cheshire Formation, the youngest unit of the greenstone sequence, is presented here to place additional constraints on the evolution of the Belingwe belt.

Midlands greenstone belt

The Midlands greenstone belt in central Zimbabwe (Fig. 1.1) consists of marginal units of Bulawayan mafic to felsic volcanic and volcaniclastic rocks and a central unit of Shamvaian siliciclastic sediments striking north-south. A c. 3.5 Ga old granitoid-gneiss terrain flanks the belt to the east. Several large-scale shear zones run sub-parallel to the contacts between the greenstones, sediments and gneisses.

A layer-cake stratigraphic model for the Midlands greenstone belt is generally assumed with a gneissic basement overlain by Bulawayan volcanics and, in turn, overlain by Shamvaian sediments. Contacts between stratigraphic units have been regarded as unconformities (Macgregor, 1951; Harrison, 1970; Robertson, 1976; Wilson et al., 1995), even though many such contacts are strongly sheared (e.g., Campbell and Pitfield, 1994). The structure of the Midlands greenstone belt has been explained by a two-stage tectonic model, namely an early event of upright folding linked to vertical tectonic processes (granite diapirism) and a later event of multistage strike-slip faulting forming a complex network of shear zones (e.g., Campbell and Pitfield, 1994; Herrington, 1995). Campbell and Pitfield (1994) suggested that deposition of the Shamvaian sediments took place in narrow, fault-bounded transtensional or transpressional basins during strike-slip faulting.

Dirks et al. (2001) presented a different view in suggesting an early episode of west-directed thrusting of lithotectonic domains that underwent different structural-metamorphic histories prior to their juxtaposition. Strike-slip faulting reactivating the earlier thrust faults is assumed to have occurred late in the tectonic history, postdating deposition of the Shamvaian sediments. A study of the Shamvaian clastic sediments has therefore been undertaken to shed some light on the conflicting evolutionary models for the Midlands belt so far proposed.

Bindura-Shamva greenstone belt

The Bindura-Shamva greenstone belt occurs in the northern part of the Zimbabwe craton (Fig. 1.1). Upper Bulawayan lithologies occupy the flanks of the greenstone belt, whereas the clastic sediments of the Shamvaian occur as a folded sequence within the core, a configuration similar to the Midlands greenstone belt. The greenstones consist of tholeiitic basalts to felsic volcanics and volcaniclastics with intercalated sedimentary rocks. The contacts between the greenstones and the overlying Shamvaian sediments are in places unconformable but mostly tectonized (Jelsma et al., 1993). The Shamvaian has been subdivided into two stratigraphic units (Stidolph, 1977), the Lower Shamvaian, predominantly represented by felsic volcanics and volcaniclastic sediments, and the Upper Shamvaian, a sedimentary association composed of conglomerate, sandstone and shale. The stratigraphic succession of the Bindura-Shamva greenstone belt has previously been interpreted as intact and tectonically undisturbed (e.g., Wilson et al., 1995) with deformation resulting in a simple configuration of an upright synclinorium due to the diapiric rise of surrounding granitoid batholiths (Ramsay, 1989; Jelsma et al., 1993). In contrast, Dirks and Jelsma (1998) described a network of layer-parallel shear zones in the greenstone belt and argued that these shear zones accommodated

horizontal stacking of (possibly oceanic) greenstone fragments and continental (island arc) crust, resulting in crustal thickening, melting and the emplacement of diapirs. Deposition of the Shamvaian sediments was inferred to have taken place syntectonically with thrusting. A detailed investigation of the Shamvaian was therefore undertaken in order to constrain the tectonic setting of the sedimentary sequence.

STRUCTURE OF THE THESIS

The sedimentology and stratigraphy of the Cheshire Formation of the Belingwe greenstone belt is described in Chapter 2. The succession is c. 1.3 km thick and consists of shallow-water carbonates at the base that are overlain by, and grade laterally to the east into, deeper water (sub-wave base) conglomerate, shale and minor sandstone representing high- to low-density turbidity current deposits. The contact between the carbonate ramp sequence and deep-water (submarine ramp) siliciclastics is formed by a karstic limestone breccia. Sediment was mainly derived from the erosion of Zeederbergs Formation volcanic rocks from the east. A foreland-type sedimentary basin model for the Cheshire Formation is presented which is constrained by the stratigraphy, facies distribution and palaeogeographic parameters.

Shortly after deposition, the Cheshire Formation and underlying volcanics were affected by a northwest-directed, thin-skinned thrusting event. Structural features related to this event such as the deformation of semi-consolidated sediments, local duplication of the stratigraphy, and the juxtaposition of a thrust slice of Zeederbergs basalts onto Cheshire sediments are described in Chapter 3. Bedding-parallel ductile shear zones separate the volcanic sequence and the overlying sediments and occur between the carbonate and siliciclastic units. The structural geology provides additional evidence that the deposition of the Cheshire Formation clastic rocks took place syntectonically with thrusting in a foreland-type basin. Evidence for early thrusting suggests that horizontal tectonic processes played an important role in the evolution of the Belingwe greenstone belt and that the volcanic rocks of the Ngezi Group most probably represent a tectonic thrust slice obducted onto granitoid basement.

The Cheshire Formation comprises one of the best preserved successions of Archaean carbonates so far observed (Martin et al., 1980; Grotzinger, 1989). During sedimentological-structural mapping of the Cheshire Formation, a previously unrecognized outcrop of the Cheshire carbonates was discovered which is described in detail in Chapter 4. The section comprises subtidal shale, shallow subtidal grainstone, intertidal microbial laminite, and supratidal breccia and tufa-like microbial boundstone facies. These facies are arranged into asymmetric, metre-scale shallowing-upward cycles. High-frequency eustatic sea-level changes are suggested as the controlling mechanism for the cyclicity. Hierarchies of stratigraphic cyclicity occur on different scales and may be the result of the combined effects of several orders of sea level oscillations. The data presented agree well with a Milankovitch-type model of orbital cyclic forcing. The deposition of metre-scale cycles is attributed to small-scale eustatic changes in tune with orbital precession with a frequency

of c. 12 ka. The bundling into groups of 9-10 cycles suggests modulation by the ~100 ka eccentricity cycle. The shallowing-upward cycles of the Cheshire Formation are similar to those of the Proterozoic and Phanerozoic rock record. This observation suggests that the mechanisms controlling shallow marine carbonate deposition have not significantly changed in the last 2650 million years. This paper is the first detailed description of possibly orbitally controlled shallowing-upward carbonate cycles of Archaean age.

The geochemistry of shales of the Zeederbergs and Cheshire Formations is presented in Chapter 5. Major, trace and rare earth element systematics and weathering indices indicate local derivation of Zeederbergs shale from submarine reworking of the surrounding basaltic rocks. Cheshire shale has geochemical characteristics indicative of a mixed mafic and felsic provenance. A systematic change in rare earth element patterns and concentrations of transition metals and high field strength elements upwards in the sedimentary succession indicates erosion of progressively more ultramafic volcanic rocks and unroofing of granitoid crust. Weathering indices suggest intense chemical weathering of the source terrain in late Archaean times.

Sedimentological data of the Shamvaian sediments in the Midlands greenstone belt are presented in Chapter 6. The sedimentary sequence occurs as a shear zone-bounded lithotectonic unit and consists of deep-water sandstone and shale that were deposited by turbidity currents and derived from a granitoid-gneiss source. The deep-water sediments are overlain by shallow-water shelf sandstones which grade upsection into coarse clastic alluvial deposits. Deposition took place in a northward deepening basin with local felsic volcanic input and with fluvial systems draining a sedimentary source. Basin formation is related to a west-directed thrusting event, and the sediments were incorporated into the thrust stack soon after deposition. A plate tectonic scenario for the evolution of the Midlands greenstone belt is presented in which the Shamvaian sedimentary basin formed along a suture zone during collision of a continental fragment with an oceanic plateau that developed into an island arc.

The Shamvaian sediments of the Bindura-Shamva greenstone belt are described in Chapter 7. The lower part of the sedimentary succession represents a transgressive, fining-upward sequence of alluvial fan, fluvial braid-plain, and marine shoreface siliciclastics derived from a granitoid-gneiss terrain. Shallow shelf sedimentation was followed by sub-wave base deposition of fine to coarse clastic turbidites and subsequent sedimentation of shallow-marine and fluvial clastics, predominantly derived from an intermediate and felsic volcanic terrain, possibly a volcanic arc. Deposition was followed by horizontal tectonic deformation disrupting and juxtaposing original stratigraphic units. Basin initiation may have been related to extensional tectonics, whereas later stages of basin history may have been similar to compressional foreland or forearc settings. Sedimentary facies, stratigraphy, and facies distribution are remarkably similar to some late Archaean sedimentary sequences of the Superior Province in Canada.

Field work in the greenstone belts discussed above has shown that thin, bedding-parallel horizons of ironstone lithologically similar to banded iron-formation, but interpreted as silicified and

sulphide-impregnated shear zones, are a common component of the late Archaean greenstone stratigraphy of the Zimbabwe craton. These "tectonic ironstones" occur along contacts between distinct lithotectonic units and are described in Chapter 8. Ironstone formation is attributed to in situ silicification and iron (sulphide)-impregnation of rocks adjacent to and within fault zones during deformation. Shearing is indicated by local truncation of bedding and foliation and duplication of statigraphic units along the ironstone horizons and gave rise to the imbrication of volcanic and sedimentary rock units. As a result, the "layer-cake" model for the Archaean stratigraphy of Zimbabwe is invalid.

REFERENCES

Bickle, M.J., and Nisbet, E.G., Eds., (1993). The geology of the Belingwe Greenstone Belt, Zimbabwe. Spec. Publ. Geol. Soc. Zim., 2, 239 pp.

Bickle, M.J., Martin, A., and Nisbet, E.G. (1975). Basaltic and peridotitic komatiites, stromatolites and a basal unconformity in the Belingwe greenstone belt, Rhodesia. Earth Planet. Sci. Lett., 27, 155-162.

Bickle, M.J., Nisbet, E.G., and Martin, A. (1994). Archaean greenstone belts are not oceanic crust. J. Geol., 102, 121-138.

Blenkinsop, T.G., Fedo, C.M., Bickle, M.J., Eriksson, K.A., Martin, A., Nisbet, E.G., and Wilson, J.F. (1993). Ensialic origin for the Ngezi group, Belingwe greenstone belt, Zimbabwe. Geology, 21, 1135-1138.

Blenkinsop, T.G., Fedo, C.M., Bickle, M.J., Eriksson, K.A., Martin, A., Nisbet, E.G., Wilson, J.F., and Orpen, J.L. (1994). Ensialic origin for the Ngezi group, Belingwe greenstone belt, Zimbabwe. Reply, Geology, 22, 767-768.

Bouhallier, H., Choukroune, P., and Ballèvre, M. (1993). Diapirism, bulk homogeneous shortening and transcurrent shearing in the Archaean Dharwar craton, the Holenarsipur area, southern India. Precambrian Res., 63, 43-58.

Brake, C. (1996). Tholeiitic magmatism in the Belingwe greenstone belt, Zimbabwe. Ph.D. thesis, University of Edinburgh, 184 pp.

Campbell, I.H., and Hill, R.I. (1988). A two-stage model for the formation of the granite-greenstone terrain of the Kalgoorlie-Norseman area, Western Australia. Earth Planet. Sci. Lett., 90, 11-25.

Campbell, S.D.G., and Pitfield, P.E.J. (1994). Structural controls of gold mineralization in the Zimbabwe Craton: Exploration guidelines. Geol. Surv. Zim. Bull., 101, 278 pp.

Card, K.D. (1990). A review of the Superior Province of the Canadian Schield, a product of Archaean accretion. Precambrian Res., 48, 99-156.

de Wit, M.J. (1998). On Archaean granites, greenstones, cratons and tectonics: does the evidence demand a verdict? Precambrian Res., 91, 181-226.

Dirks, P.H.G.M., and Jelsma, H.A. (1998). Horizontal accretion and stabilization of the Archean Zimbabwe Craton. Geology, 26, 11-14.

Dirks, P.H.G.M., Jelsma, H.A., and Hofmann, A. (1999). Continental extensional setting for the Archean Belingwe greenstone belt, Zimbabwe. Comment, Geology, 27, 667.

Dirks, P.H.G.M., Jelsma, H.A., and Hofmann, A. (2001). Accretion of an Archaean greenstone belt in the Midlands of Zimbabwe. J. Struct. Geol., in press.

Grotzinger, J.P. (1989). Facies and evolution of Precambrian carbonate depositional systems: emergence of the modern platform archetype. In: Crevello, P.D., Wilson, J.L., Sarg, J.F., and Read, J.F. (Eds.), Controls on carbonate platform and basin evolution. Spec. Publ. Soc. Econ. Paleontol. Mineral., 44, pp. 79-106.

Hamilton, W.B. (1998). Archean magmatism and deformation were not products of plate tectonics. Precambrian Res., 91, 143-179.

Harrison, N.M. (1970). The geology of the country around Que Que. Rhod. Geol. Surv. Bull., 67, 125p.

Herrington, R.J. (1995). Late Archean structure and gold mineralization in the Kadoma region of the Midlands greenstone belt, Zimbabwe. In: Coward, M.P., and Ries, A.C. (Eds.), Early Precambrian Processes. Geol. Soc. Spec. Publ., 95, pp. 173-191.

Horstwood, M.S.A., Nesbitt, R.W., Noble, S.R., and Wilson, J.F. (1999). U-Pb zircon evidence for an extensive early Archaean craton in Zimbabwe: A reassessment of the timing of craton formation, stabilization, and growth. Geology, 27, 707-710.

Hunter, M.A., Bickle, M.J., Nisbet, E.G., Martin, A., and Chapman, H.J. (1998). Continental extensional setting for the Archean Belingwe Greenstone Belt, Zimbabwe. Geology, 26, 883-886.

Jelsma, H.A., and Dirks, P.H.G.M. (2000). Tectonic evolution of a greenstone sequence in northern Zimbabwe: sequential early stacking and pluton diapirism. Tectonics, 19, 135-152.

Jelsma, H.A., van der Beek, P.A., and Vinyu, M.L. (1993). Tectonic evolution of the Bindura-Shamva greenstone belt (northern Zimbabwe): Progressive deformation around diapiric batholiths. J. Struct. Geol., 15, 163-176.

Jelsma, H.A., Vinyu, M.L., Valbracht, P.J., Davies, G.R., Wijbrans, J.R., and Verdurmen, E.A.T. (1996). Constraints on Archaean crustal evolution of the Zimbabwe craton: a U-Pb zircon, Sm-Nd and Pb-Pb whole-rock isotope study. Contrib. Mineral. Petrol., 124, 55-70.

Kusky, T.M. (1998). Tectonic setting and terrane accretion of the Archean Zimbabwe craton. Geology, 26, 163-166.

Kusky, T.M., and Kidd, W.S.F. (1992). Remnants of an Archaean oceanic plateau, Belingwe Greenstone Belt, Zimbabwe. Geology, 20, 43-46.

Kusky, T.M., and Winsky, P.A. (1995). Structural relationships along a greenstone/shallow water shelf contact, Belingwe greenstone belt, Zimbabwe. Tectonics, 14, 448-471.

Kusky, T.M., Winsky, P.A., and Kidd, W.S.F. (1994). Ensialic origin for the Ngezi group, Belingwe greenstone belt, Zimbabwe. Comment, Geology, 22, 766-767.

Macgregor, A.M. (1951). Some milestones in the Precambrian of Southern Rhodesia. Proc. Geol. Soc. S. Afr., 54, 27-71.

Martin, A., Nisbet, E.G., and Bickle, M.J. (1980). Archaean stromatolites of the Belingwe Greenstone Belt. Precambrian Res., 13, 337-362.

Myers, J.S. (1995). The generation and assembly of an Archaean super continent: evidence from the Yilgarn craton, western Australia. In: Coward, M.P. and Ries, A.C. (Eds.), Early Precambrian Processes. Geol. Soc. Spec. Publ., 95, pp. 143-154.

Ramsay, J.G. (1989). Emplacement kinematics of a granite diapir: The Chinamora Batholith, Zimbabwe. J. Struct. Geol., 11, 191-209.

Robertson, I.D.M. (1976). The geology of the country around Battlefields, Gatooma District. Geol. Surv. Rhod. Bull., 76, 258pp.

Shackleton, R.M. (1995). Tectonic evolution of greenstone belts. In: Coward, M.P. and Ries, A.C. (Eds.), Early Precambrian Processes. Geol. Soc. Spec. Publ., 95, pp. 53-65.

Silva, K.E. (1997). Komatiites from the Belingwe greenstone belt, Zimbabwe: constraints on the development of Archaean greenstone belts. Ph.D. thesis, University of London, UK.

Stein, M., and Hofmann, A.W. (1984). Mantle plumes and episodic crustal growth. Nature, 372, 63-68.

Stidolph, P.A. (1977). The geology of the country around Shamva. Geol. Surv. Rhod. Bull., 78, 249pp.

Wilson, J.F., Nesbitt, R.W., and Fanning, C.M. (1995). Zircon geochronology of Archaean felsic sequences in the Zimbabwe craton: a revision of greenstone stratigraphy and a model for crustal growth. In: Coward, M.P. and Ries, A.C. (Eds.), Early Precambrian Processes. Geol. Soc. Spec. Publ., 95, pp. 109-126.

CHAPTER 2

Late Archaean foreland basin deposits, Belingwe greenstone belt, Zimbabwe

Axel Hofmann, Paul H.G.M. Dirks, and Hielke A. Jelsma
Sedimentary Geology, 141-142, 131-168

Abstract—The c. 2.65 Ga old sedimentary Cheshire Formation of the Belingwe greenstone belt, central Zimbabwe, has been studied in detail to shed some light on the much debated evolution of this classical belt. The Cheshire Formation rests sharply on a mafic volcanic unit (Zeederbergs Formation) and comprises a basal, eastward-sloping carbonate ramp sequence built of shallowing-upward, metre-scale sedimentary cycles. The cycles strongly resemble Proterozoic and Phanerozoic carbonate cycles and may have formed as a result of small-scale eustatic sea level changes. The top of the carbonate ramp is represented by a karst surface. The carbonates are overlain by, and grade laterally to the east into deeper water (sub-wave base) siliciclastic facies. Conglomerate, shale and minor sandstone were deposited by high- to low-density turbidity currents and were derived from the erosion of Zeederbergs-like volcanic rocks from the east. Shortly after deposition, the Cheshire Formation and underlying volcanics were affected by a northwest-directed thrusting event. Thrusting gave rise to the deformation of semi-consolidated sediments and resulted in the juxtaposition of a thrust slice of Zeederbergs basalts onto Cheshire sediments. The stratigraphy, asymmetric facies and sediment thickness distribution, palaeogeographic constraints and evidence for an early horizontal tectonic event all suggest that the Cheshire Formation formed in a foreland-type sedimentary basin.

INTRODUCTION

The evolution of greenstone belts has been a topic of considerable debate, and two models are currently favoured. In the first model, greenstone belts are envisaged to have formed in intracratonic extensional basins with magma under- and overplating above mantle plumes, with later deformation mainly due to non-uniformitarian vertical tectonic processes (e.g., solid state granite diaprism). Vertical accretion processes have been put forward for the Dharwar Craton, India (Bouhallier et al., 1993) and the Zimbabwe Craton (see references in Blenkinsop et al., 1997). The second model claims that greenstone belts have been formed (and deformed) as a result of actualistic plate tectonic processes including sea-floor spreading followed by subduction-accretion-collision of crustal fragments. Examples of Archaean crust whose formation is attributed to horizontal accretion include the Yilgarn Block, Australia (Myers, 1995), the Kaapvaal Craton, South Africa (de Wit et al., 1992) and the Superior Province, Canada (Card, 1990). Along this line, the Zimbabwe Craton has been recently reinterpreted by Kusky (1998), Dirks and Jelsma (1998) and Jelsma and Dirks (2000) to represent an amalgamation of crustal fragments that accreted due to plate tectonic processes. Late Archaean sedimentary sequences in Zimbabwe (c. 2.65 Ga) feature strongly in this debate. Various tectonic regimes responsible for sedimentary basin formation have been proposed ranging from intracontinental plume-related rift basins (Blenkinsop et al., 1993; Bickle et al., 1994; Wilson et al., 1995; Hunter et al., 1998), transtensional pull-apart basins (Campbell and Pitfield, 1993; Kusky, 1998), foreland basins (Kusky and Winsky, 1995; Dirks and Jelsma, 1998; Jelsma and Dirks, 2000) and piggy-back basins that formed on actively moving thrust sheets (Kusky and Kidd, 1992). These models have never been tested by rigorous sedimentological work, partly because studies of the sedimentary rocks are hampered by poor exposure as well as varying degrees of chemical and physical alteration during metamorphism, deformation and emplacement of granitoids.

In the Belingwe greenstone belt most supracrustal rocks have undergone low grade metamorphism and limited deformation (see papers in Bickle and Nisbet, 1993). As a result, original sedimentary features are preserved well enough to conduct a sedimentary facies analysis which can be used to interpret the structural setting of sediment deposition. Additionally, most of the lithological contacts in the Belingwe belt show primary features of their origin and are not severely overprinted by later tectonic movements. A correct interpretation of the contacts, whether tectonic or depositional in origin, is fundamental to an understanding of the tectonic setting during deposition of the supracrustal sequences. In this paper sedimentological data from the c. 2.65 Ga old Cheshire Formation, the youngest unit of the Belingwe greenstone belt, is presented in order to clarify the tectonic environment in which this sedimentary sequence formed.

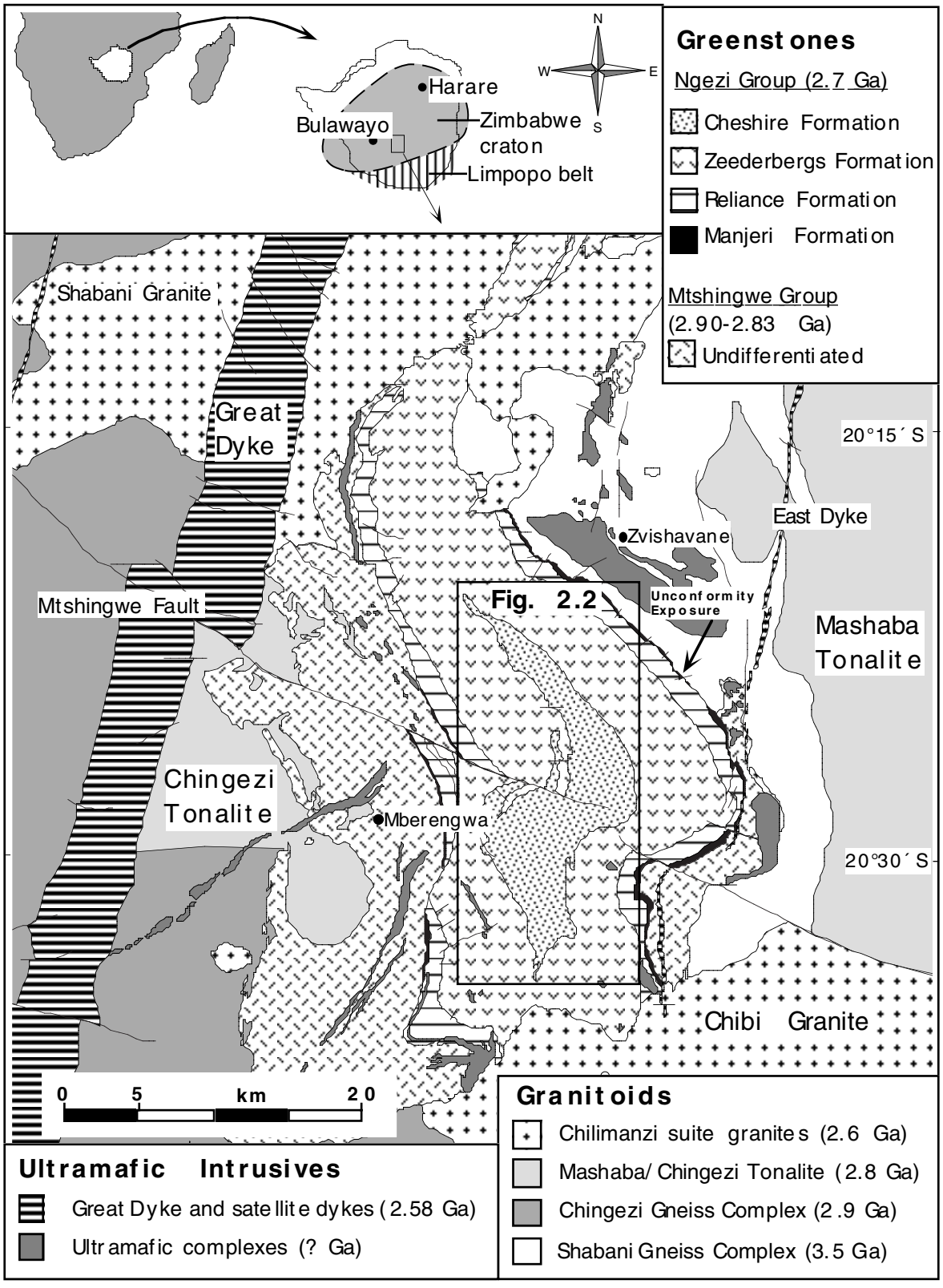

Fig. 2.1. Geological map of the Belingwe greenstone belt (after Martin et al., 1993, Fig. 2.1).

GEOLOGICAL SETTING

The Belingwe greenstone belt (BGB) is situated in the southern part of the Zimbabwe craton, north of the Limpopo belt and east of the Great Dyke (Fig. 2.1). It contains a well preserved, ~2.9-2.65 Ga old volcano-sedimentary sequence which overlies, and is surrounded by, a granitoid-gneiss terrain dominated by the c. 3.5 Ga Shabani gneiss complex to the east and the c. 2.9 Ga Chingezi gneiss complex to the west. The greenstone sequence is divided into two distinct units, the lower Mtshingwe and upper Ngezi Groups. The Mtshingwe Group is confined to the southern and western parts of the belt. It comprises ultramafic to mafic lavas and volcaniclastics, minor felsic volcaniclastics and sedimentary rocks including conglomerate, sandstone, shale and ironstone (Martin et al., 1993). U/Pb zircon dates of Mtshingwe Group rocks range from 2.90 to 2.83 Ga (Wilson et al., 1995).

The Ngezi Group forms the central part of the BGB, stretching the entire length of the belt with a maximum exposure width of 20 km. It overlies the Shabani Gneiss Complex to the east and north-east and the Mtshingwe Group to the south-east and west. Chilimanzi Suite monzogranites intrude the Ngezi Group in the northern and southern parts of the BGB (Fig. 2.1).

The Ngezi Group comprises a basal sedimentary succession (Manjeri Formation), overlain by ultramafic and mafic volcanics (Reliance and Zeederbergs Formations), and capped by a sedimentary succession (Cheshire Formation). The Reliance and Zeederbergs Formations are collectively termed Ngezi volcanics. The Manjeri Formation is a thin (0-120 m) clastic sedimentary unit which lies unconformably on rocks of the Mtshingwe Group and oversteps onto granitoid basement (Fig. 2.1; Bickle et al., 1975; Hunter et al., 1998). Its lower part consists of fluvial to shallow-water sediments including conglomerate, sandstone, shale, ironstone and localized stromatolitic limestone. The upper part comprises immature, alluvial fan to fan delta clastics, mainly conglomerate and sandstone capped by ironstone (Hunter et al., 1998).

The Reliance Formation is c. 1 km thick and can be divided into three stratigraphic units. The basal unit (500-600 m) consists of tholeiitic and komatiitic basalt forming partly pillowed lava flows and pyroclastic tuffs. The central unit (300 m) comprises a komatiite suite of pillows and flows with a few cross-cutting dykes. The upper unit (200 m) includes poorly exposed komatiitic basalt, tholeiitic basalt and tuff and passes without a distinctive geological break into the lavas of the Zeederbergs Formation (Scholey, 1992). Ion microprobe trace element data of glass inclusions of Reliance Formation komatiites are similar to modern plume-related oceanic plateau and oceanic island basalts (McDonough and Ireland, 1993).

The Zeederbergs Formation (c. 2.8 km thick, Brake, 1996) consists mainly of pillowed and massive basalts which form randomly intercalated units from several metres up to 200 metres in thickness. Massive basalt is locally gradational to pillow basalt, indicating that the massive variety represents at least in part extrusive lava flows. Pillows are typically 0.5-1 m in diameter and always young towards the synclinal axis the belt. Dark grey chilled margins as well as calcite- and quartz-filled vesicles (up to 1 cm across) are common. Pillow basalt and, less

frequently, massive basalt commonly contain light grey spherical ocelli, typically 0.5-1 cm across. Intrusive rocks are rare in the Zeederbergs Formation and include narrow (< 2 m), cross-cutting basaltic dykes and up to several metres thick ultramafic sills (Brake, 1996).

Hyaloclastites form a minor proportion of the sequence. Spherical, ellipsoidal or irregular shard-like basalt clasts, ranging from sand size to 2 cm in diameter, form crudely parallel-stratified, continuous horizons, several decimetres up to 10 metres thick, intercalated with basalt flows. Pillow breccias commonly fill the space between pillows or forms rare discrete horizons.

Rare epiclastic sedimentary rocks include continuous, several decimetres thick beds of shale. Graded beds, 0.1-1 m thick, also occur. The base generally consists of normally graded, fine basalt pebble conglomerate with varying amounts of angular, medium to coarse basalt pebbles. Conglomerate grades into parallel- and ripple-laminated sand- to siltstone. Load and water escape structures are common. The graded beds show partial and complete Bouma sequences indicative of turbidity current deposits.

The c. 1.3 km thick sedimentary Cheshire Formation forms the uppermost stratigraphic unit of the Belingwe greenstone belt and is distributed along the synclinal axis of the belt. The sedimentology and basin analysis of the Cheshire Formation forms the subject of this paper.

Precise age data are scarce for the Ngezi Group. Komatiitic basalts of the Reliance Formation have been dated by the whole-rock Pb/Pb isochron method at 2692±9 Ma (Chauvel et al., 1993). Bolhar et al. (2000) determined whole-rock Pb/Pb isochron dates of 2698±48 Ma and 2600±48 Ma for stromatolitic limestones of the Manjeri and Cheshire Formations, respectively. A minimum age for deposition of the Cheshire Formation is provided by the intrusion of the Chibi granite (Fig. 2.1) which is part of the Chilimanzi Suite granites. Granites of this suite have yielded U-Pb zircon dates of 2634±17 in the central part of the craton (Horstwood, 1998). Taken all this data into account, the Cheshire Formation was probably deposited around 2650 Ma ago.

Controversy surrounds the tectonic setting in which the supracrustal rocks formed. The Ngezi Group has been interpreted by many authors (e.g., papers in Bickle and Nisbet, 1993; Blenkinsop et al., 1993; Bickle et al., 1994; Hunter et al., 1998) as an autochthonous sequence deposited in a rift basin on pre-existing continental crust. Intracontinental extension is attributed to the ascent of a mantle plume beneath the Zimbabwe Craton, which caused uplift of the crust and rifting. The Ngezi Group is interpreted as a synrift sequence (Manjeri Formation), overlain by plume-related lavas (Ngezi volcanics) that erupted from crustal magma chambers, and capped by late syn- to post-volcanic fluvial to shallow-water sediments (Cheshire Formation). Grotzinger et al. (1993) interpreted the Cheshire Formation to have been deposited in an extensional basin with carbonate breccias, interpreted as mass flow deposits and conglomerates shed from active scarps.

In contrast, Kusky and Kidd (1992), Kusky and Winsky (1995) and Kusky (1998) suggested the presence of a major detachment zone at the top of the Manjeri Formation. They argued that the Ngezi volcanics originated from an oceanic plateau and were emplaced as a large allochthonous sheet, the Mberengwa allochthon, onto the Manjeri Formation. Kusky and

Winsky (1995) interpreted the Cheshire Formation as either a foreland basin or as an extensional basin that formed after collapse of the thickened crust after obduction.

In order to test these two contrasting models, a detailed sedimentological-structural study of the Cheshire Formation was undertaken. Emphasis was placed on the investigation of the nature of the contacts between stratigraphic units (depositional or sheared contacts), the distribution of lithofacies, the depositional environment, and the sedimentological and structural history of the sedimentary basin fill in order to (a) determine whether there was a causal relationship between deformation and sedimentation and (b) to define a sedimentological model that can be linked to the tectonic evolution of the area.

GEOLOGY OF THE CHESHIRE FORMATION

Stratigraphy

The Cheshire Formation can be subdivided into two informal members, the carbonate member which consists of limestone-shale cycles and their brecciated equivalents, and the siliciclastic member which is dominated by shale and conglomerate.

The carbonate member is restricted to two occurrences in the western part of the Cheshire outcrop (Figs. 2.2 and 2.3). The westernmost occurrence varies between 100-350 m in thickness. It consists of cyclically stacked shallow marine limestone and shale and is capped by a laterally continuous limestone breccia (see also Fig. 2.4). This unit is overlain by siliciclastic facies with discontinuous intercalations of limestone breccia. The rocks are locally folded and sheared and show features similar to a tectonic mélange (see below). The deformed zone is in contact with the siliciclastic member in the south of the Cheshire Formation and overlain by an inlier of mafic volcanics in the centre (Fig. 2.2). The volcanics include pillowed basalts with minor massive basalts and hyaloclastites, and are lithologically identical to those of the Zeederbergs Formation. Towards the north the carbonates are probably sheared out but reappear c. 1.5 km further to the north where they are in contact with the siliciclastic member along an ironstone horizon (Fig. 2.2). The second outcrop of cyclic carbonates (250-350 m thick) is situated at the western margin of the central Cheshire outcrop where it is bounded by ironstone (Fig. 2.3). The ironstone horizon separating the carbonates from the siliciclastic member to the east extends to the north without a break to form the contact between the volcanics and the siliciclastics. Carbonate brecciation is restricted to several zones that are perpendicular to strike (Fig. 2.3).

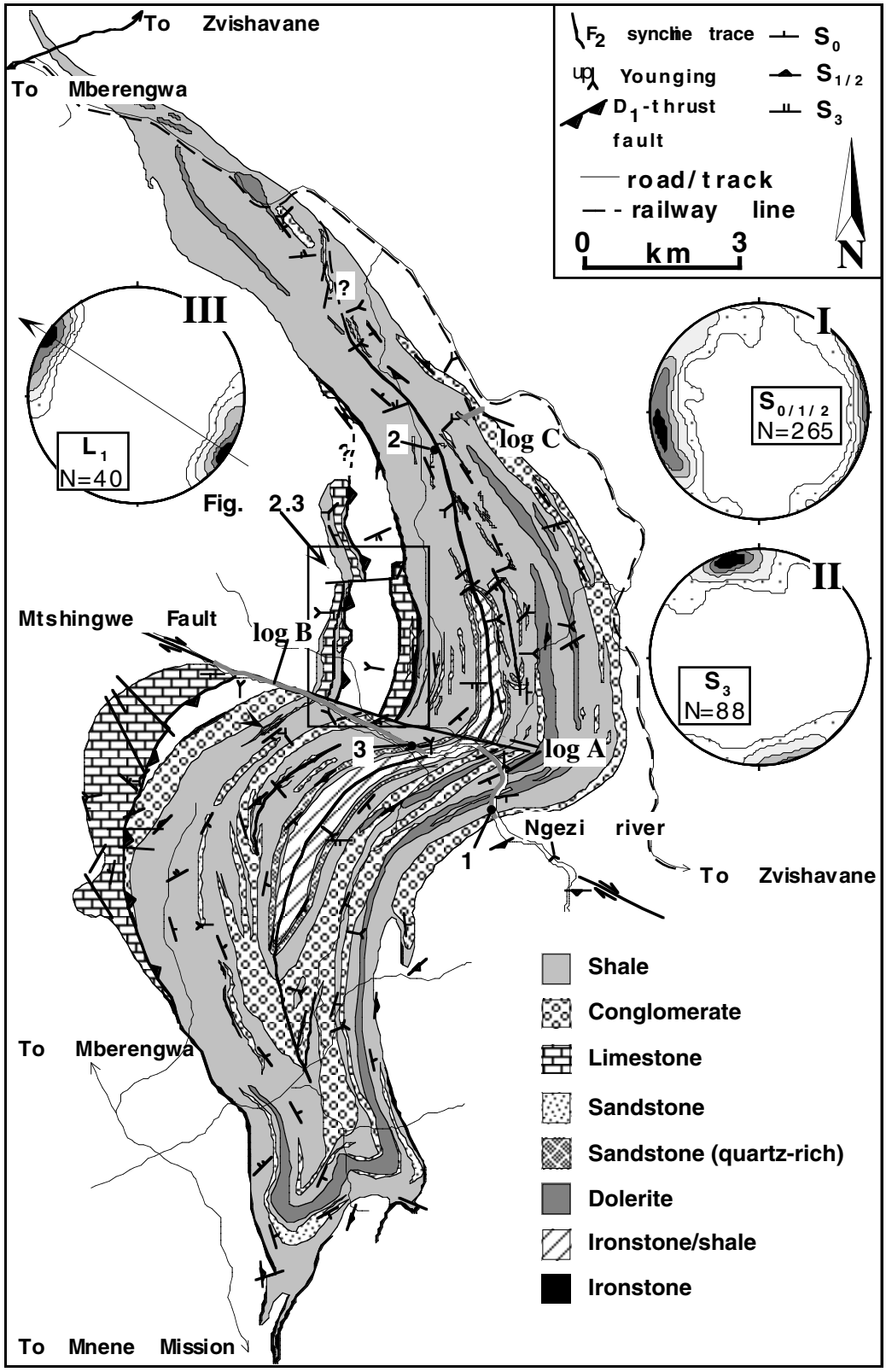

Fig. 2.2. Geological map of the Cheshire Formation (after Martin, 1978; Orpen et al., 1986; Nisbet et al., 1993 and own mapping). 1-3 are localities discussed in the text. A-C are areas of graphic logging (Fig. 2.4). I-III are lower hemisphere stereographic projections of contoured bedding, foliation and lineation data. Foliations S_1 and S_2 are mostly parallel to bedding S_0 and are shown together. L_1 data is shown as a pre-D_2 restoration and comprises mineral lineations in ironstones (n=17) and the elongation of inclusions in the mélange zone (n=26). Tectonic transport direction (arrow) is to the northwest (see text).

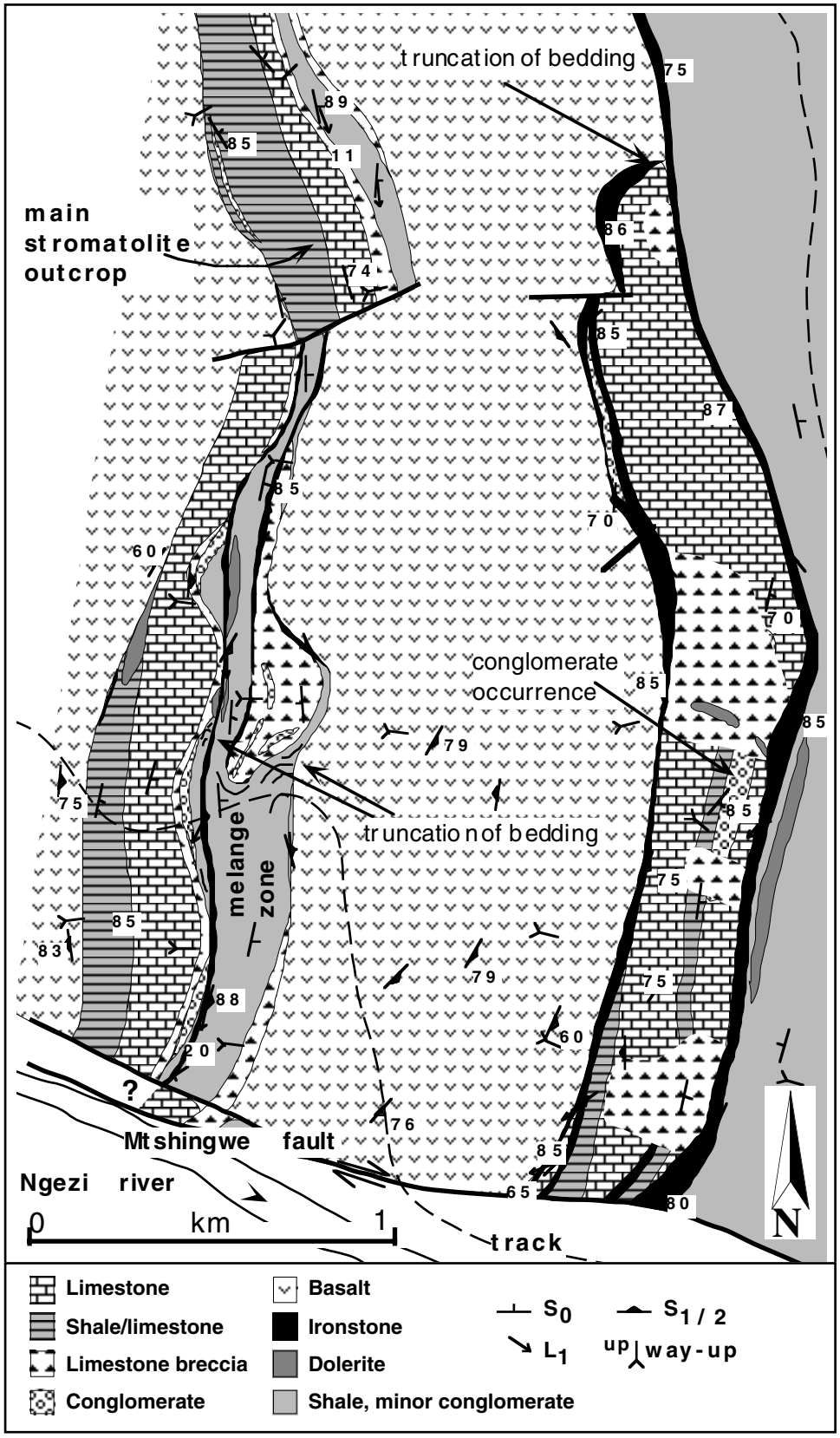

Fig. 2.3. Detailed map of the Zeederbergs/Cheshire Formation contact from the western limb of the syncline (refer to Fig. 2.2 for location). Note the transection of bedding along structural contacts, which are commonly occupied by ironstones, and the occurrence of basalt pebble conglomerate intercalated with limestone. The area south of the Mtshingwe fault consists of intercalated conglomerate and shale.

Previous studies of the Cheshire carbonates concentrated on a particular outcrop belt around the "main stromatolite outcrop" (Fig. 2.3), a well exposed limestone horizon near the top of the succession. Martin et al. (1980) noted a cyclical arrangement of stromatolitic facies and interpreted the cyclicity to reflect repetitive sea level changes in a restricted, shallow-water lagoon, giving rise to shallow subtidal to intertidal deposits. Sumner and Grotzinger (2000) reinvestigated the succession around the main stromatolite outcrop. They described a lower siliciclastic-dominated part of shale interstratified with silt- and sandstone storm deposits, and oolitic limestone and domal stromatolite. A shallow subtidal environment with water depths of 5-50 m in a wave- or storm-dominated open marine shelf setting was envisaged. The upper carbonate-dominated part comprises asymmetric cycles with subtidal shale, ooid-intraclast grainstone/packstone lags or rare flat pebble conglomerate at the base, beds of shallow subtidal aragonite pseudomorph fans alternating with small domal to columnar stromatolites in the centre and peritidal crinkly laminite facies at the top of cycles. Sumner and Grotzinger (2000) compared the cycles with those common in the record of Proterozoic shallow marine carbonate platforms.

The siliciclastic member forms the bulk of the Cheshire Formation. In the central part of the outcrop (Fig. 2.2) it consists of a lower conglomerate unit up to 220 m thick. The conglomerate is overlain by interstratified shale and conglomerate which form homogeneous horizons typically several 10´s of metres up to 150 m thick. Sandstone occurs in minor proportions except for a conspicuous unit of quartzose sandstone (20-50 m thick) near the top of the preserved section. Intercalated ironstone (typically 10 m thick) and hematitic shale overlie the quartzose sandstone. Both quartzose sandstone and ironstone form a prominent ridge with a folded outcrop pattern in the centre of the Cheshire outcrop, indicating strata continuity for at least 10 km (Fig. 2.2).

Structure

The Cheshire Formation has been affected by four deformational events (D_1-D_4), the characteristics of which are summarized below. A detailed account on the structural history of the Cheshire Formation will appear elsewhere.

D_1 is defined by shear zones that occur at the sharp contact between the Zeederbergs volcanics and Cheshire sediments, and within the Cheshire Formation, where they parallel the contact. Stratification in both the volcanics and the sediments is mostly parallel to the contact, but sedimentary bedding is locally transected along the contact (Fig. 2.3). Shearing is further evident in the occurrence of mylonitic fabrics in rocks adjacent to the contact and by the presence of blackish, graphitic, iron oxide and sulphide-impregnated rocks similar to banded ironstones of which their deformation-related origin will be discussed below. Sedimentary horizons modified by D_1-shearing resemble tectonic mélanges. Block-in-matrix structures as defined by inclusions of various lithologies wrapped around by a plastically deformed argillaceous matrix indicate that deformation affected unconsolidated to semiconsolidated sediment. The most prominent mélange (see below) occurs at the top of the carbonate unit where

it is overlain by an inlier of volcanic rocks (Figs. 2.2 and 2.3). This repetition of Zeederbergs rocks has formerly been interpreted by an anticline-syncline pair subsidiary to the main synclinal structure, with the inlier of volcanics in between the carbonate outcrops occupying the anticline (Martin, 1978; Bickle et al., 1993). This interpretation is not supported by stratigraphic younging indicators (Fig. 2.3). Instead, the stratigraphy of the western part of the Cheshire Formation and D_1 fabrics indicate that the inlier of Zeederbergs volcanics represents a tectonic thrust slice.

A foliation (S_1) is defined by the compositional layering in ironstone and by the lithological layering and the alignment of inclusion trains in mélange zones. A shallowly plunging lineation (L_1) is locally preserved as striations, mineral fibres and a mineral stretching lineation in tectonic ironstone, and by the elongation of inclusions in mélanges. Pre-D_2 restoration of the structural data combined with tectonic transport directions derived by kinematic indicators in the mélange zone such as the asymmetry of inclusions indicate a northwest-directed nappe transport (Fig. 2.2; chapter 3).

D_2 resulted in tight to isoclinal folding of the greenstone belt. A south-southeast oriented syncline developed with the Cheshire Formation forming the core (Fig. 2.2). The synclinal axis of the main Cheshire outcrop plunges to the north in the southern part of the Cheshire Formation and towards the south in the northern part (Fig. 2.2). The fold axis in the central part is probably subhorizontal as indicated by the occurrence of parasitic F_2 folds with subhorizontal fold axes (Bickle et al., 1993). An axial planar foliation (S_2) is oriented subparallel to bedding (Fig. 2.2).

A third, spaced foliation (S_3) occurs throughout the exposed area of the Cheshire Formation and is generally oriented at a high angle to bedding. The foliation is subvertical and strikes east-northeast (Fig. 2.2). It is thought to have formed as an axial planar foliation during gentle cross-folding of the BGB during D_3.

Dextral strike-slip faulting (D_4) is recorded along the Mtshingwe Fault (Fig. 2.2). Drag folding is absent, since rotation of S_3 has not been observed near the fault zone.

Metamorphism

Pelitic sediments of the Cheshire Formation contain very fine-grained chlorite-sericite-quartz assemblages with epidote typically lacking, which is indicative of sub-greenschist facies conditions (Martin, 1978; Bickle et al., 1993). The sedimentary rocks show evidence of recrystallization, but primary textures are commonly well preserved. Abell et al. (1985) attempted to constrain the thermal history of the Cheshire carbonates through a combined petrological and stable isotope study. They concluded that the Cheshire limestones experienced a maximum temperature of 200°C.

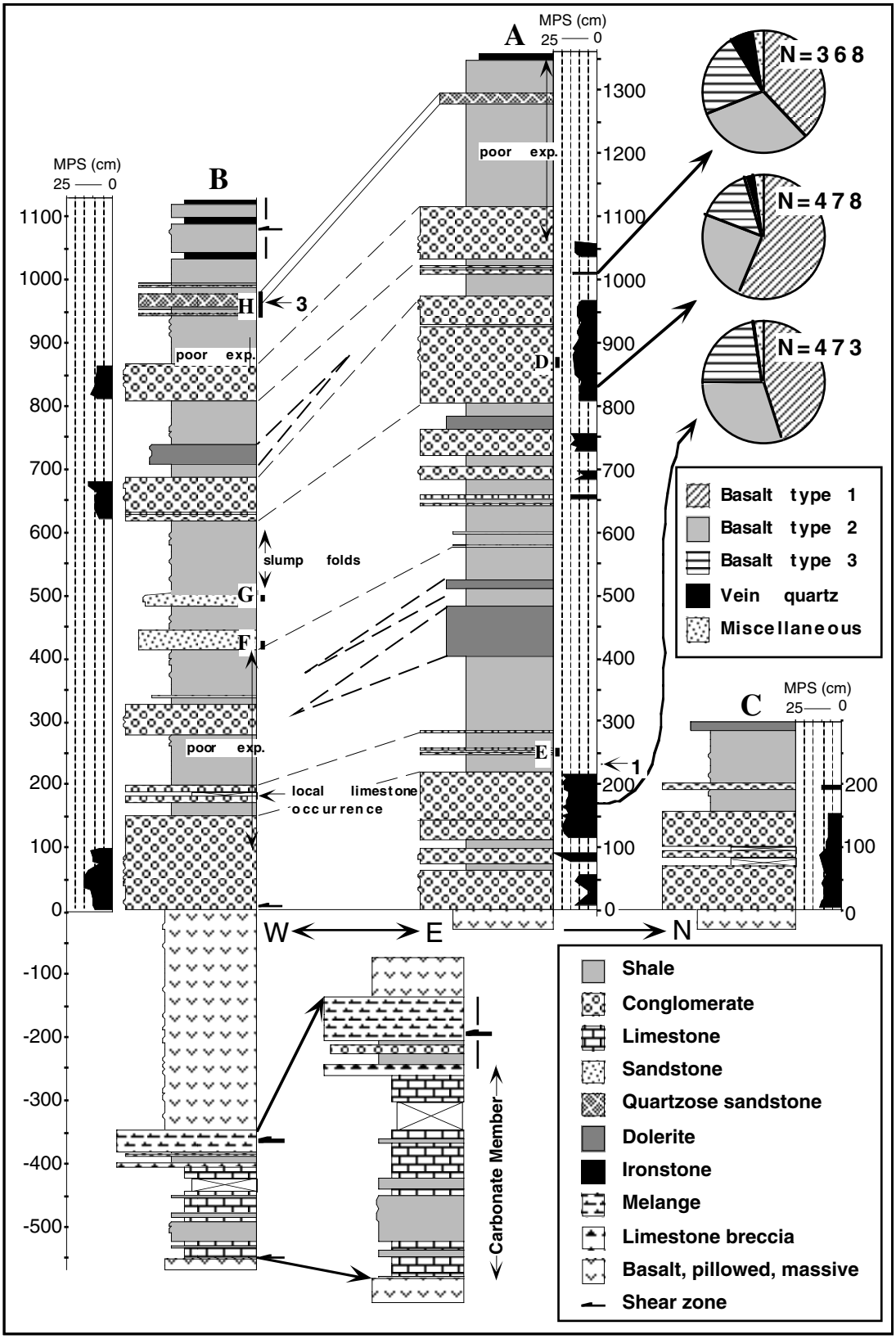

Fig. 2.4. Graphic logs measured on both sides of the syncline along the Ngezi river (A, B) and in the northern part of the outcrop (C) (Fig. 2.2). The carbonate member (base of log B) has been expanded for clarity. Maximum particle size (MPS) of conglomerates was determined where possible. Clast counts have been conducted at three localities of the eastern section (refer to text for description of different basalt clast types).

SEDIMENTOLOGY OF THE CHESHIRE FORMATION

The carbonate member

The carbonate member is well exposed in the Ngezi River where it has been logged in detail (Fig. 2.4B). The section consists of a cyclic succession of carbonates and shale, and is capped by a conspicuous limestone breccia. A detailed description of lithofacies and the controls of cyclicity is beyond the scope of this paper and will only shortly be summarized here.

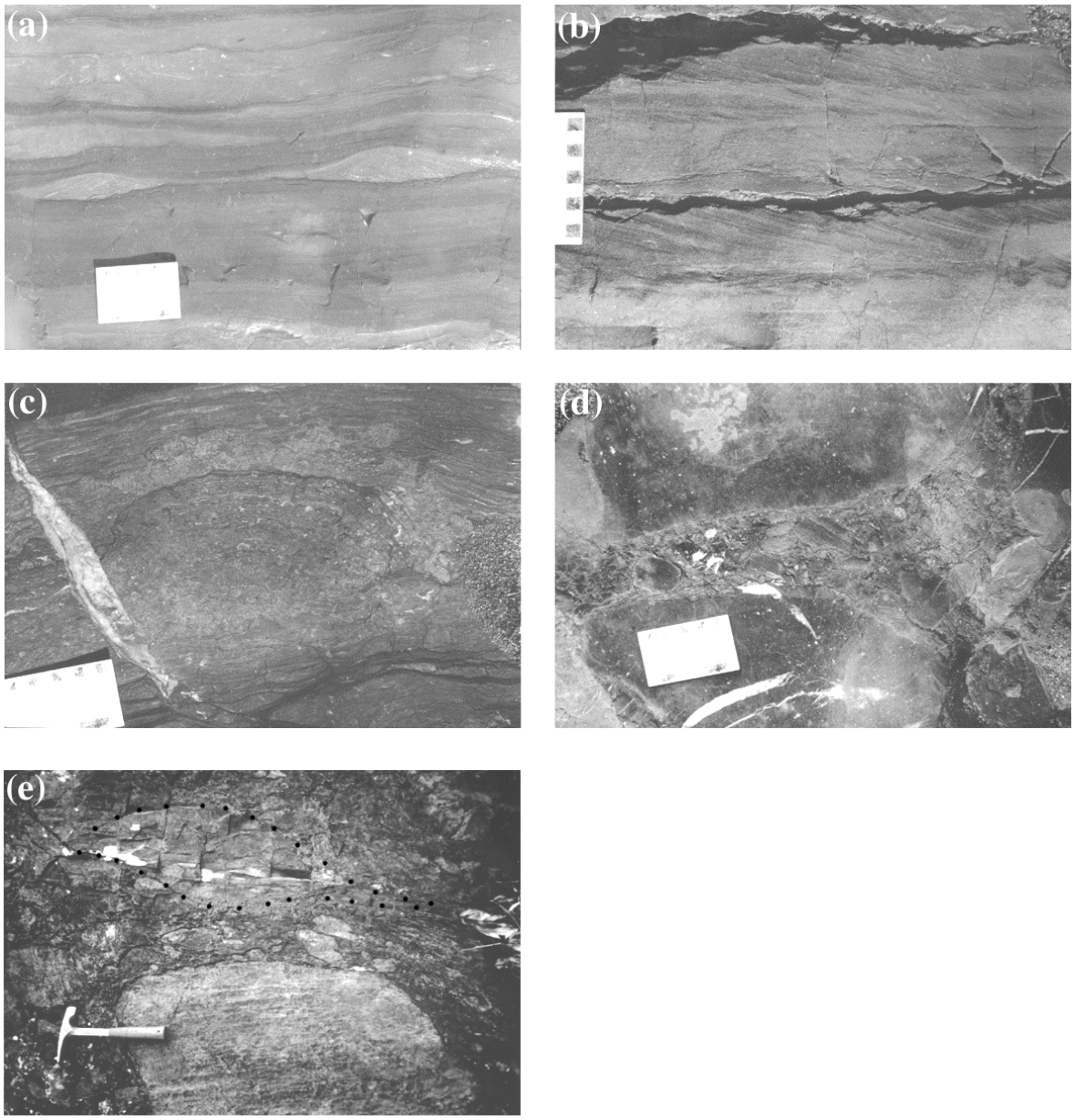

Fig. 2.5. Features of the carbonate member. (a) Shale (bottom) grading into wave-ripple laminated grainstone (top). Note bimodal cross-lamination in isolated ripple bedforms (centre). (b) Bedset of cross-bedded ooid grainstone. (c) Cauliflower-like, nodular stromatolites within flat- to undulatory laminated limestone are sharply overlain by shale along a cycle boundary (top). (d) Massive microbial boundstone transected by hourglass-shaped solution fissure filled with limestone breccia. (e) Blocks of limestone and shale in limestone breccia. Note the lenticular shape of the shale fragment (margin of fragment is marked for clarity).

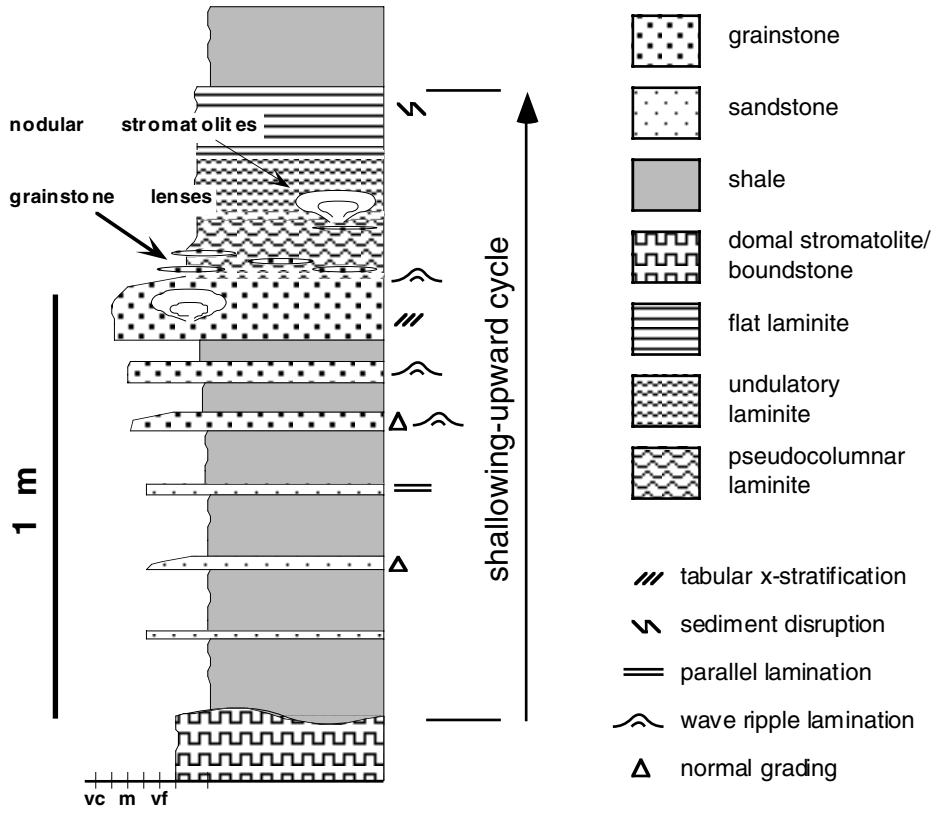

Fig. 2.6. Generalized sedimentary cycle of the measured section of the carbonate member.

Cyclic carbonates

Description. The lower 110 m of the section comprises 74 sedimentary cycles which are between 30 to 730 cm thick and have an average thickness of 150 cm. Two basic cycle types, shale-based cycles and carbonate cycles, can be distinguished. Shale-based cycles have a prominent bed of shale at the base which is intercalated with thin beds of wave-rippled and commonly normally graded sand-/grainstone that become more common and thicken upward (Fig. 2.5a). Shale is overlain by various ooid/intraclast grainstone subfacies including cross-bedded (Fig. 2.5b) and wave-rippled varieties which are, in turn, overlain by cryptmicrobial laminites. Cryptmicrobial laminites form the upper part of most cycles and typically comprise a lower pseudocolumnar subfacies which grades upsection into an undulatory and then into a flat laminite subfacies. Both grainstone and laminite facies commonly contain scattered nodular/domal stromatolites (Fig. 2.5c).

Carbonate cycles are different from shale-based cycles in the absence of the basal shale bed. They consist of ripple-laminated and massive grainstone subfacies at the base overlain by cryptmicrobial laminite. In general, the lower part of shale-based cycles shows a coarsening-upward from fine siliciclastic sediment to medium to coarse sand grainstones associated with a thickening-upward of event beds in shale, whereas the upper, carbonate-dominated part of shale-based cycles and carbonate cycles are characterized by a fining-upward from grainstone to

carbonate mud associated with a decrease in synoptic relief of microbial carbonates. Upper and lower contacts of cycles are sharp whereas internal boundaries between lithofacies are gradational (Fig. 2.6).

A cyclic arrangement of facies is poorly developed to absent in the uppermost 10 m of the section below the limestone breccia. In this part a bed of matrix-supported, resedimented limestone breccia has been observed. The bed contacts are sharp with clasts protruding into the overlying facies. The clasts consist of flat-laminated micrite and stromatolitic limestone, up to 25 cm in diameter, in a massive matrix of calcilutite.

Interpretation. The cyclic motif is a result of rapid submergence, followed by gradual shallowing of the sea level in the course of cycle formation. Shale formed in an open marine, shallow subtidal environment below fair-weather wave base. Intercalated sand-/grainstone beds represent storm-generated event deposits, and their upward increase and thickening are indices of higher energy as a result of progressive shoaling, a common feature of shale-bearing cycles of Phanerozoic carbonate platforms (Aigner, 1985; Calvet and Tucker, 1988; Osleger and Read, 1991). Ooid/intraclast grainstones formed at or above fair-weather wave base in an agitated shallow subtidal setting. They represent shoreface sand-sheets or low relief sand-shoals that prograded across open-marine shale in response to storm-, wind-, and/or tide-generated currents. Further shallowing resulted in the establishment of tidal flats where benthonic microbial communities aided in the formation of carbonate laminites. The decrease in synoptic relief of the laminites is an additional indicator for shallowing (Grotzinger, 1986a; Southgate, 1989). Cryptmicrobial laminites probably formed in the lower intertidal to lower supratidal zone and are similar to other peritidal laminites that commonly form the upper parts of shallowing-upward carbonate cycles (Hardie and Shinn, 1986; Koerschner and Read, 1989; James, 1994). Initial transgression during the formation of carbonate cycles lacking shale beds led to relative deepening of the depositional environment to fair-weather wave base only giving rise to basal grainstones which were overlain by microbial limestones during gradual shallowing.

The origin of shallowing-upward carbonate cycles has been discussed and reviewed in numerous studies (e.g., Grotzinger, 1986b; Osleger and Read, 1991; Demicco and Hardie, 1994). In most studies on cyclic carbonates the cyclicity has been attributed to external rhythmic or cyclic (allocyclic) forces, in particular small-scale (c. 10 m) but high-frequency eustatic sea-level changes (Fischer, 1964; Goodwin and Anderson, 1985; Grotzinger, 1986b; Koerschner and Read, 1989; Osleger and Read, 1991; Goldhammer et al., 1987, 1991) brought upon by the waxing and waning of alpine? glaciers/ice sheets.

Since the Cheshire Formation is interpreted to have formed in a tectonically active basin with the carbonate member overidden by a thrust sheet soon after its deposition (see below), episodic tectonic pulses during repeated thrust advance could have resulted in rhythmic tectonic loading of the lithosphere to abruptly generate the accommodation space needed for asymmetric cycle development. The local occurrence of basalt pebble conglomerates within the cyclic sequence (Fig. 2.3) may be a record of such tectonic events. The restricted spatial preservation of the carbonate member makes it impossible to explore the original lateral extent of the carbonate

cycles in order to provide evidence for or against cyclic subsidence. However, mainly three observations do not support a tectonic origin for the cyclicity. (1) Shale beds formed in a subtidal setting well below fair-weather wave base. The lower part of some shale beds is rich in clay and contains only rare storm deposits, indicating that water depth may have been >20 m at times. The shale-bearing cycles are commonly capped by tidal flat facies and, even when compaction is taken into account, are not thick enough to have reached a static sea level by simple aggradation. This discrepancy can only be explained if periodic subsidence was coupled with uplift or if the sea level fluctuated. (2) The thickness range of the sedimentary cycles is fairly narrow; cycles are typically 40 to 160 cm thick (Fig. 2.7a). Tectonically controlled subsidence events are non-periodic, which makes it difficult to explain the narrow thickness range of the Cheshire cycles. (3) A plot of cumulative cycle thickness (Fig. 2.7b) shows three groupings of cycles with a rather linear accumulation trend. The cumulative thickness distribution may give a hint on subsidence rate, because most cycles show a distinct facies stacking pattern, do not show evidence for prolonged time intervals of non-deposition/erosion, and are mostly capped by intertidal facies. Assuming that the cycle period was constant (Milankovitch-type orbital control), it can be supposed that subsidence rate during deposition of the first group of cycles was uniformly low. Starting with cycle 32, average subsidence rate suddenly increased. Since cycle 32 is unusually thick (Fig. 2.7a), it may record a tectonic event (advance of a thrust sheet?) which gave rise to an increase in subsidence rate. After a certain time period of high subsidence, the average subsidence rate decreased again starting with cycle 56. From the above discussion it appears likely that the cyclicity reflects eustatic, high-frequency oscillations in sea level.

The lack of cyclicity in the uppermost portion of the section may indicate changes in the depositional setting such as steepening of the palaeoslope as indicated by the occurrence of the resedimented limestone breccia. This facies is interpreted as a subaqueous, cohesive debris flow on account of upward protruding clasts which indicate deposition by sediment "freezing" due to a high matrix strength.

Limestone breccia

Description. Limestone brecciation is a common feature of the carbonate member. Brecciation is variable and ranges from breccia-filled fissures in an undisrupted, coherent limestone sequence to matrix- and clast-supported chaotic breccias (Figs. 2.5d and 2.5e).

The main limestone horizon in the western carbonate unit is continuously overlain by a 10-20 m thick breccia horizon which has an irregular relief (Fig. 2.3). Depressions are occupied by conglomerate and shale. In the Ngezi river section (Fig. 2.4B), this breccia horizon is dominated by stromatolitic limestone beds intercalated with bedding-parallel layers of commonly sheared brecciated rock. Irregular-shaped fissures, up to 30 cm in width and several decimetres in length, and perpendicular to bedding, transect the limestone beds and separate them into slab-like blocks 1-2 metres in length (Fig. 2.5d). The fissures are filled with granule- to pebble-sized, angular fragments of limestone (rare shale, mudstone and sandstone) in a matrix of muddy

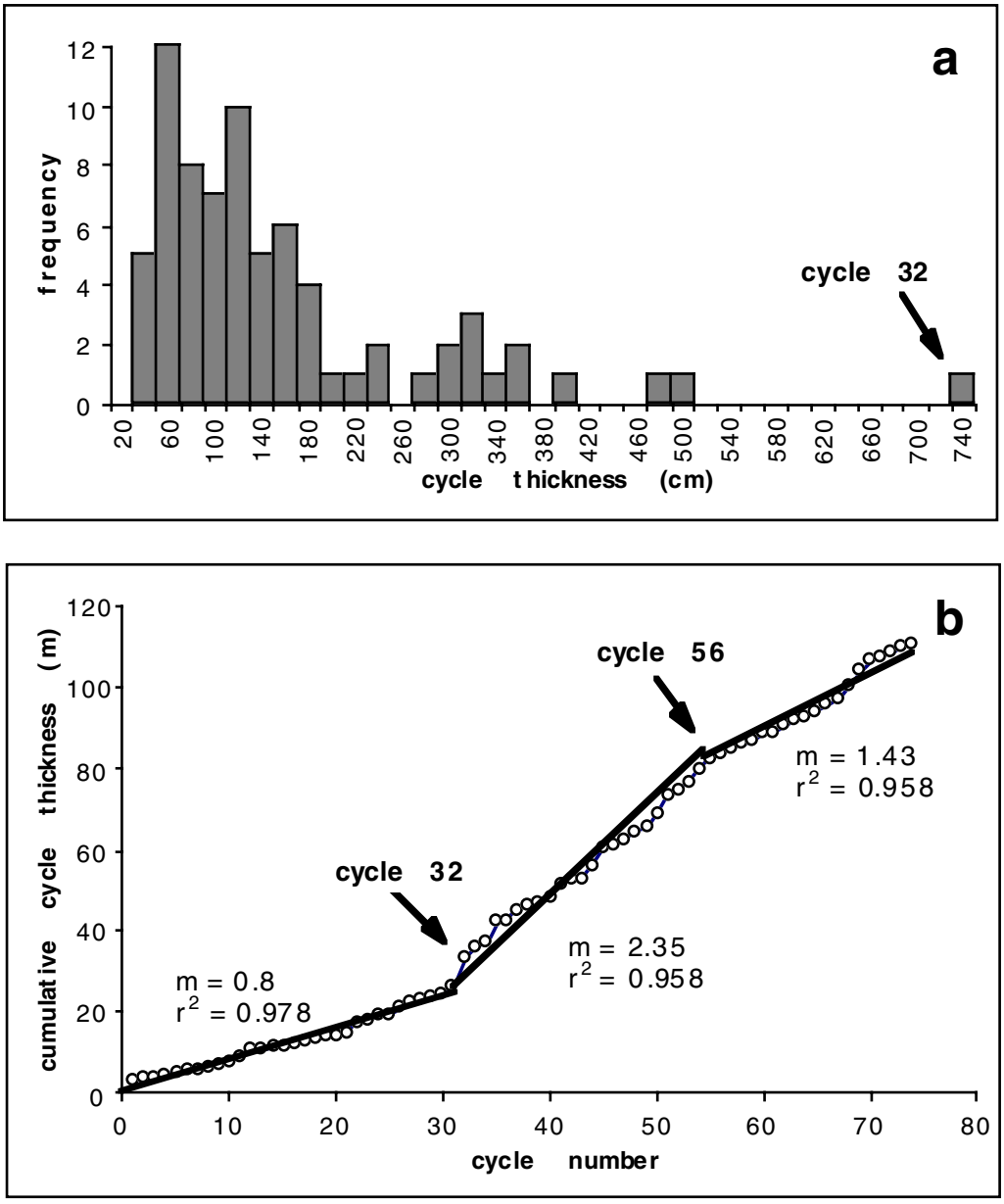

Fig. 2.7. (a) Frequency distribution of the thickness of measured cycles (thickness classes are 0-20 cm, 20-40 cm, etc.). The unusual thickness of cycle 32 probably reflects a tectonically induced subsidence event. (b) Cumulative cycle thickness graph showing three intervals with a different accumulation history. For each interval a regression line is shown (m: slope, r^2: regression coefficient).

sandstone or massive carbonate. Bedding is oriented parallel to the general structural trend, but the stratigraphy is locally inverted. In between less brecciated limestone horizons and along the contact with overlying shale occur bedding-parallel layers of sheared rock. These consist of various rock fragments wrapped around by a muddy arenaceous to argillaceous matrix in an anastomosing pattern. Mud-rich areas or mudstone inclusions in the sheared rock have sigmoidal to irregular, partly amoeboidal outlines, indicating that the rock was unconsolidated when deformation took place. At other localities, the same breccia horizon consists of poorly sorted, massive breccias with clast sizes between 0.5 and 200 cm (Fig. 2.5e).

In the eastern limestone unit of Figure 2.3, brecciated limestone occurs at high angles to bedding and grades laterally into an unbrecciated sedimentary sequence. Two stromatolitic

limestone horizons, each several metres thick, occur at one locality within the siliciclastic member in the west-central part of the Cheshire Formation (Figs. 2.2 and 2.4). They are intercalated with shale, massive pebble conglomerate and lenticular horizons of ironstone. The limestones are brecciated throughout; cross-cutting hematite-impregnated veins and dykes containing angular limestone and rare shale fragments are common.

Interpretation. Limestone brecciation could have been caused by: (1) disruption of the sequence during tectonic movements (tectonic breccia); (2) mass-flow action; (3) (subaerial) karstification; (4) in situ brecciation due to limestone dissolution by acidic fluids. Local inversion of the stratigraphy and bedding-parallel shear zones indicate that deformation affected the breccias. This must have taken place early in the depositional history, since shale fragments in the breccia have been plastically deformed and, hence, were not fully consolidated. However, an interpretation as a tectonic breccia does not account for the restricted occurrence of breccia in areas cross-cutting unbrecciated carbonate strata (Fig. 2.3). The same reasoning rules out the possibility of the breccias being mass-flow deposits such as olistrostromes.

Karst formation would have involved a major relative fall in sea level brought upon by tectonic uplift or an eustatic sea level fall and exposing the top of the carbonate sequence to subaerial weathering. After a later relative rise in sea level deeper water siliciclastic facies would then have covered the karst surface. The brecciation was mostly caused by limestone dissolution because of the occurrence of solution fissures. Similar fissures are a common feature of palaeokarsts and generally form due to the solution-widening of joints (grikes, e.g., James and Choquette, 1984). However, the fissures described here are filled with material derived from brecciation of adjacent material and not with material from the overlying deep water siliciclastics as would be expected for typical grikes.

Depressions that formed by the relief of the brecciated limestone horizon (Fig. 2.3) resemble karst sinkholes or karst valleys such as those described from Proterozoic palaeokarsts of Canada (Pelechaty et al., 1991; their Fig. 5). In their study, coarse limestone collapse breccias occupy the centre and margins of depressions and thin or pinch out rapidly towards intervening palaeotopographic highs which are covered by a thin veneer (< 1.5 m) of in situ brecciated limestone. The limestone breccia horizon described here is continuous and does not show marked thickness changes laterally, which is inconsistent with its interpretation as a solution collapse breccia. Its origin as a regolith is possible, but no evidence for subaerial weathering such as tepee structures or vadose pisoliths has been observed, and the underlying contact seems to be sharp. In addition, the local occurrence of stromatolitic limestone within the siliciclastic member (Fig. 2.4), which shows an identical style of brecciation, makes karstification as the sole mechanism for brecciation unlikely.

A model for the brecciation must also account for the observations of in situ limestone dissolution and early deformation of semi-consolidated sediments. Brecciation is interpreted to be partly related to deformation during D_1. Brecciation commonly affected carbonates situated near shear zones i.e. along ironstones and below the mélange zone. Limestone dissolution is therefore partly attributed to acidic fluids which were generated during shearing and which were

channelled through mostly bedding-parallel fault planes and possibly along cross-cutting fracture zones. However, karstification as a mechanism to form the continuous breccia horizon at the top of the main stromatolite outcrop and correlative strata seems most plausible, but it is likely that both karstification and limestone dissolution during shearing took place to form lithologically identical limestone breccias.

The siliciclastic member

No sedimentological work has previously been undertaken on the siliciclastic member which forms the overwhelming part of the Cheshire Formation and consists of a monotonous succession of mostly deep-water sediments. Several lithofacies are recognized, based on differences in texture and sedimentary structure. The observed facies are readily compared with well-established facies schemes (e.g., Bouma, 1962; Mutti and Ricci Lucchi, 1972; Lowe, 1982; Pickering et al., 1986). A description and interpretation of each lithofacies is given in Table 2.1. The reader is referred to the above authors for more detailed accounts on depositional processes and mechanisms.

Lithofacies occur in four facies associations which are defined on grounds of the spatial distribution of particular facies in the sedimentary succession. These are the conglomerate, sandstone, shale and quartzose sandstone facies association. Lateral facies relationships could not be investigated in any detail because of discontinuous exposure away from river beds.

Conglomerate facies association

Description. Conglomerates are clast-supported and consist of pebbles to pebbly cobbles with a poor to moderate sorting (Figs. 2.8a and 2.8b). The clasts locally include boulders up to 50 cm across, but the bulk is less than 10 cm in diameter. Granules are angular to subrounded, pebbles are subrounded to rounded and cobbles are very well rounded. The clasts are almost totally basaltic in composition. The matrix consists of poorly sorted sand ranging in size from angular fine sand to angular to rounded granules. Sand-sized basaltic rock fragments dominate at the base of the succession, whereas quartz sand becomes more common upsection. A matrix of clay and silt-sized material is rare.

The base of the central Cheshire Formation consists of massive conglomerate with rare thin sandstone beds and forms a homogeneous unit up to 220 m thick (Figs. 2.2 and 2.4). Intercalations of tabular (on outcrop-scale) shale horizons 0.5-15 m thick occur, suggesting a tabular geometry of adjacent conglomerate horizons. Bedding planes are commonly obscured due to the amalgamation of individual depositional units and later deformation. Imbrication is poorly developed to absent, possibly due to clast reorientation during deformation and a high degree of sphericity of the clasts. The basal conglomerate east of the outcrop axis is possibly sheared out in the south, whereas it grades into, and laterally interfingers with, shale towards the north (Fig. 2.2). The conglomerate unit is thickest in the east and thins both to the west and north. The coarsest clasts occur in the eastern section as indicated by the distribution of maximum clast sizes (Fig. 2.4).

Table 2.1. Description of lithofacies, classification after Pickering et al. (1986) and Lowe (1982), and environmental interpretation. Tabular bedding characteristics refer to outcrop-scale (typically 10 metres). HDTC: high-density turbidity current, LDTC: low-density turbidity current.

Facies	Texture	Sedimentary Structures	Bedding Characteristics	Pickering et al. (1986)	Lowe (1982)	Interpretation
Conglomerate facies association						
Massive conglomerate	Granules-boulders; poor sorting; c.-supported	Massive	10-?500 cm; tabular; planar to slightly erosive base with scours < 30 cm deep	A1.1		Rapid sedimentation of HDTC or debris flows
Inversely graded conglomerate	Granules-cobbles; poor-moderate sorting; c.-supported	Inverse grading; massive	5-50 cm; tabular	A2.2	R2	Frictional freezing of a traction carpet beneath a HDTC
Normally graded conglomerate	Granules-cobbles; poor-moderate sorting; c.-supported	Normal grading; massive	5-70 cm; tabular	A2.3	R3	Rapid suspension sedimentation from a HDTC
Horizontally stratified conglomerate	Granules-cobbles; c.-supported; pebbly, m-vc sand	Crude horizontal stratification; massive to horizontal lamination in sandstone; no grading	20-100 cm; very thin to thin discont. sandstone beds	A2.1		Deposition from traction bed-load beneath a HDTC
Thin bedded sandstone in conglomerate	Pebbly m-vc sand; silt-/sandstone intraclasts; m.-supported pebbles	Massive; normal and coarse-tail grading; horizontal lamination common in uppermost bed portions; rare low-angle cross-bedding	5-20 cm; discont.; sharp; irregular to concave-up lower and planar upper contacts; pinch out laterally within 1-15 m by thinning from base upwards	B1.2?		Traction sedimentation; winnowing by strong bottom currents
Pebbly sandstone	Pebbles to cobbles (< 20 cm) scattered in vc sand or forming conglomeratic layers	Crude horizontal stratification; discont. congl. (massive; rare inverse/normal grading) and sandstone beds (massive; horiz. lamination; rare low-angle cross-bedding)	20-100 cm; gravel-rich layers are typically 5-15 cm thick and are more common at base	A2.5	S1	Deposition from traction bed-load beneath a sandy HDTC
Sandstone/quartzose sandstone facies association						
Normally graded fine pebbly sandstone	f pebble conglomerate to f sand; mudstone intraclasts in lower portions	Normal size and coarse-tail grading; structureless; indistinct parallel lamination in upper bed portions; rare load casts	5-270 cm; tabular; small-scale scours	A2.7	S3	Rapid deposition from suspension from a sandy HDTC

Table 2.1. Continued.

Facies	Texture	Sedimentary Structures	Bedding Characteristics	Pickering et al. (1986)	Lowe (1982)	Interpretation
Massive sandstone	f sand to pebbly vc sand; poor sorting	Massive; no grading to coarse-tail grading; rare dish structures	5-200 cm; sharp; tabular; small-scale scours; discont. pebble bands	B1.1	S3	Rapid suspension sedimentation from a HDTC
Cross-stratified sandstone	c-vc sand	Trough cross-stratification; foresets 0.5-2 cm thick (typically 1 cm); angle of inclination 20°-31°	15-75 cm; planar, slightly erosive lower contacts; tabular; partly tabular bedsets	B2.2		Reworking of sands by tractional processes or strong bottom currents
Horizontally stratified sandstone	f-vc sand; granule-bearing; rare pebbles	discont. planar parallel lamination; locally convoluted at bed tops; dish structures common	5-85 cm; tabular; laminae 0.5-2 cm thick; rare concave-up scours <10 cm deep	B2.1		Freezing of successive traction carpets at the base of a HDTC
Shale facies association						
Medium- to thick-bedded sandstone/ mudstone	Ta: c-f sand, Tbcd: f sand-silt, Te: mud; scattered mudstone intraclasts (< 8 cm)	Sandstone: normal grading; partial or complete Tabcde sequences; Te-fallout: massive, Te-background: parallel lamination	Sandstone: 5-80 cm; tabular; sharp planar lower contacts; Mudstone: 5-100 cm	C2.1 to C2.2		Deposition from HDTC to LDTC
Thin-bedded sandstone/ mudstone	Silty vf-f sand (rare m-c sand); mudstone intraclasts in basal portions; silty clay to silt	Sandstone type 1: massive, current ripple lamination; type 2: normal grading; laminae with Tde; beds with Tabe, Tace, Tbce, Tbe; load casts in both types; mudstone: massive, horiz. lamination	Sandstone: 0.3-8 cm; continuous beds or lenticular laminae; lower contacts sharp, planar, slightly erosive; upper contacts sharp to gradational, planar or wavy; mudstone: 0.3-3 cm; cont.	C2.3 to D2.1		Deposition from LDTC
Interlaminated sandstone/ mudstone	Clayey silt/ silty f sand	Siltstone: lenticular lamination; load casts; fading ripples and load-casted ripples; current ripple trains; mudstone: planar horiz. lamination	Siltstone: 1-10 mm; lenticular, pinching-and-swelling; mudstone: 0.1-10 mm; both continuous and discont.	D2.2 to D2.3		Deposition from LDTC; suspension sedimentation
Ripple-laminated sandstone	Strongly carbonate-cemented f sand	Horizontal, current ripple and wave ripple lamination; mud drapes	3-10 cm; lenticular to tabular	————		Winnowing of sea floor sediments during storm events

The base of the central Cheshire Formation consists of massive conglomerate with rare thin sandstone beds and forms a homogeneous unit up to 220 m thick (Figs. 2.2 and 2.4). Intercalations of tabular (on outcrop-scale) shale horizons 0.5-15 m thick occur, suggesting a tabular geometry of adjacent conglomerate horizons. Bedding planes are commonly obscured due to the amalgamation of individual depositional units and later deformation. Imbrication is poorly developed to absent, possibly due to clast reorientation during deformation and a high degree of sphericity of the clasts. The basal conglomerate east of the outcrop axis is possibly

sheared out in the south, whereas it grades into, and laterally interfingers with, shale towards the north (Fig. 2.2). The conglomerate unit is thickest in the east and thins both to the west and north. The coarsest clasts occur in the eastern section as indicated by the distribution of maximum clast sizes (Fig. 2.4).

Upsection from the basal conglomerate occur homogeneous conglomerate horizons, typically several tens of metres thick, which are intercalated with shale horizons of similar thickness (Fig. 2.4). On average, maximum clast sizes are less than those of the basal conglomerate. Away from river-washed outcrops, individual horizons are difficult to trace but are continuous for a few kilometres. The conglomerates typically comprise thin to thick beds of massive conglomerate, horizontally stratified conglomerate and graded conglomerate (Fig. 2.9). Inversely graded conglomerate commonly grades into normally graded conglomerate (Fig. 2.8a). Imbrication locally occurs in thin conglomerate beds (Fig. 2.8b). Maximum particle size (MPS) correlates well with bed thickness (BTh), regardless of conglomerate facies type (Fig. 2.9). Conglomerates are commonly intercalated with thin sandstone beds or form amalgamated bedsets.

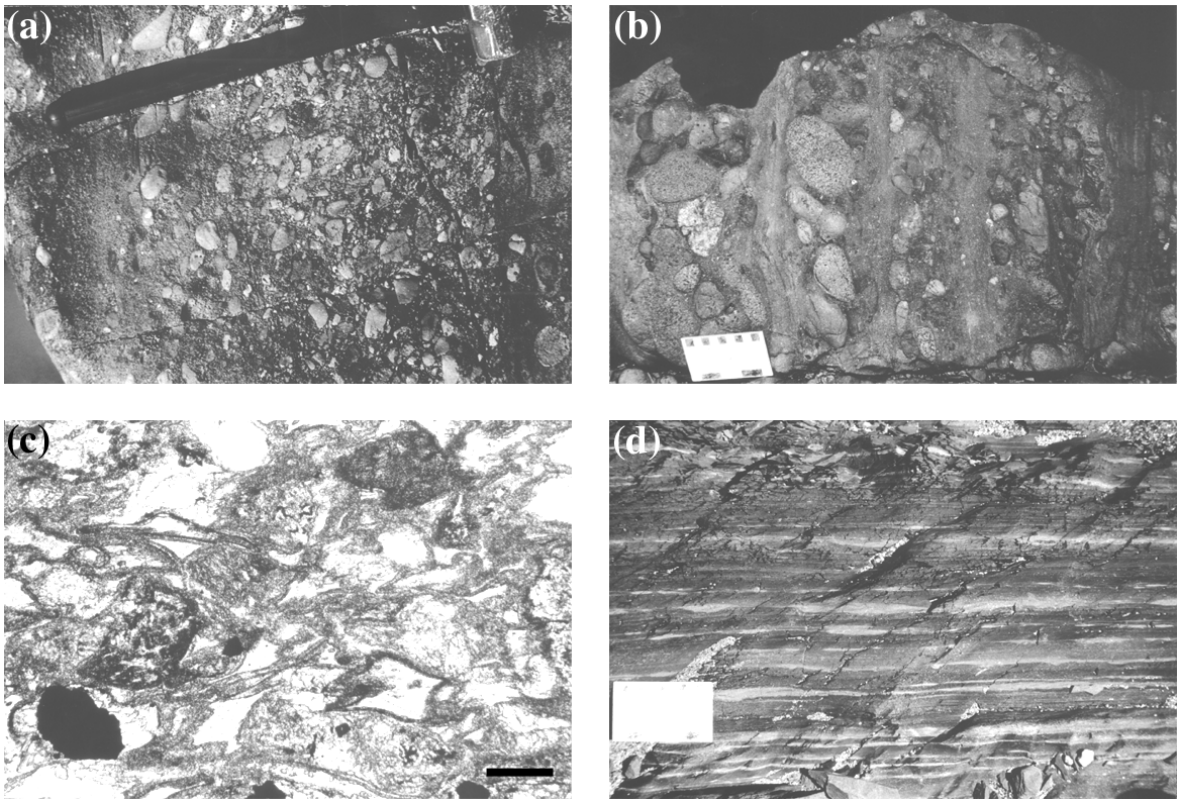

Fig. 2.8. Features of the siliciclastic member. (a) Inversely to normally graded conglomerate grading into pebbly sandstone facies. Lower bedding plane at hammerhead. (b) Thinly interbedded sandstone and conglomerate showing imbrication. (c) Photomicrograph (plane-polarized light) of medium-grained sandstone of sandstone facies association. Clasts predominantly consist of devitrified volcanic glass fragments with minor quartz and detrital pyrite. Scale bar is 200 µm. (d) Interlaminated sandstone/mudstone of shale facies association. Note spaced foliation (S_3) angular to bedding.

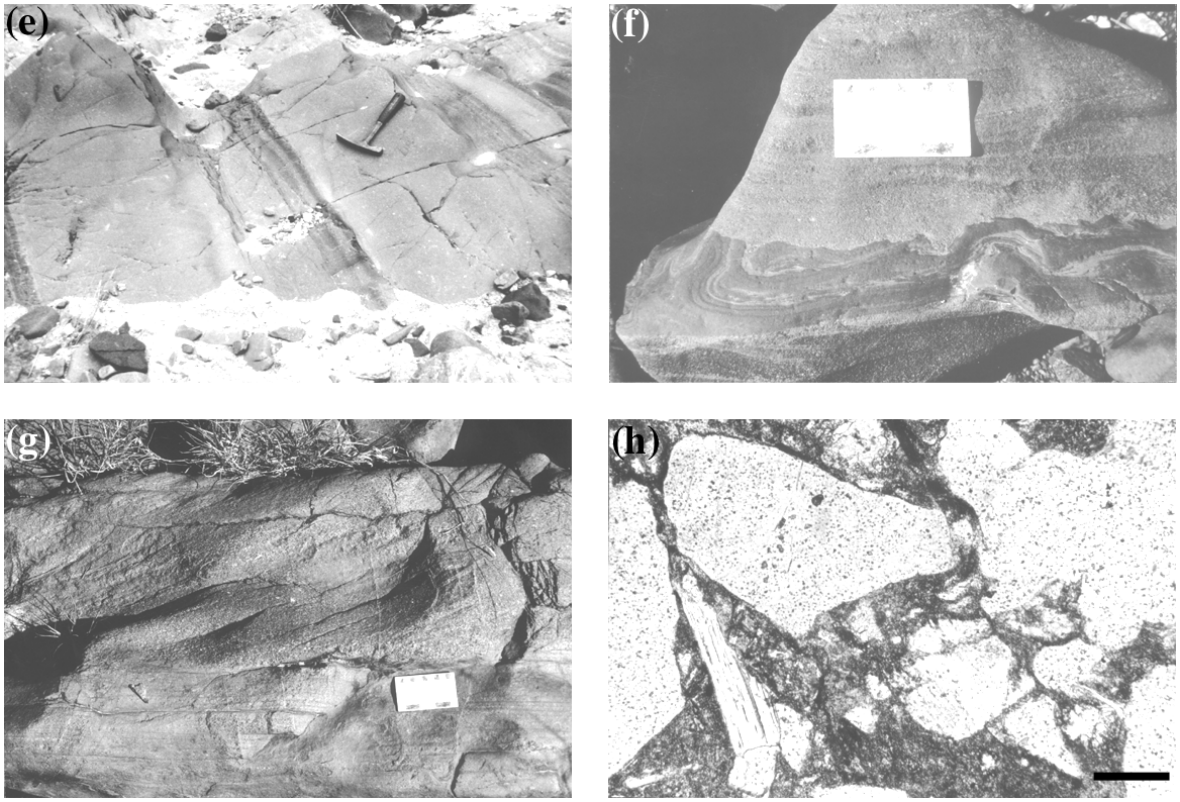

Fig. 2.8 (continued). (e) Normally graded sandstone beds of the medium- to thick-bedded sandstone/mudstone facies. (f) Slump fold in shale bed erosively overlain by massive to horizontally laminated sandstone (photo has been taken from a boulder in the Ngezi river). (g) Tabular bed of cross-stratified sandstone overlying horizontally stratified sandstone of the quartzose sandstone facies association. (h) Photomicrograph (plane-polarized light) of quartzose sandstone. Scale bar is 200 µm. Note the occurrence of muscovite (left centre).

The interbedding of sandstone and conglomerate varies from isolated sandstone beds bounding thick conglomerate beds to very complex, thin interbedding (Fig. 2.8b). Very thin beds are commonly diffuse and difficult to trace for more than one metre. The lenticular shape of sandstone beds is due to the concave-upward lower contacts and not due to the erosional activity of overlying conglomerate beds. Most sandstone beds sharply overlie conglomerate. Some sandstone beds have gradational lower contacts and form a graded bed together with the underlying conglomerate layer.

Pebbly sandstone occurs locally intercalated with, and gradationally resting on, conglomerate (Figs. 2.8a and 2.10). Pebbly sandstone is commonly overlain by horizontally laminated sandstone. Shale adjacent to conglomeratic units rarely contain erosive, isolated channels 1-30 m in width and 0.2-4 m thick. The channels are filled with massive conglomerate beds that are locally intercalated with pebbly sandstone and sandstone.

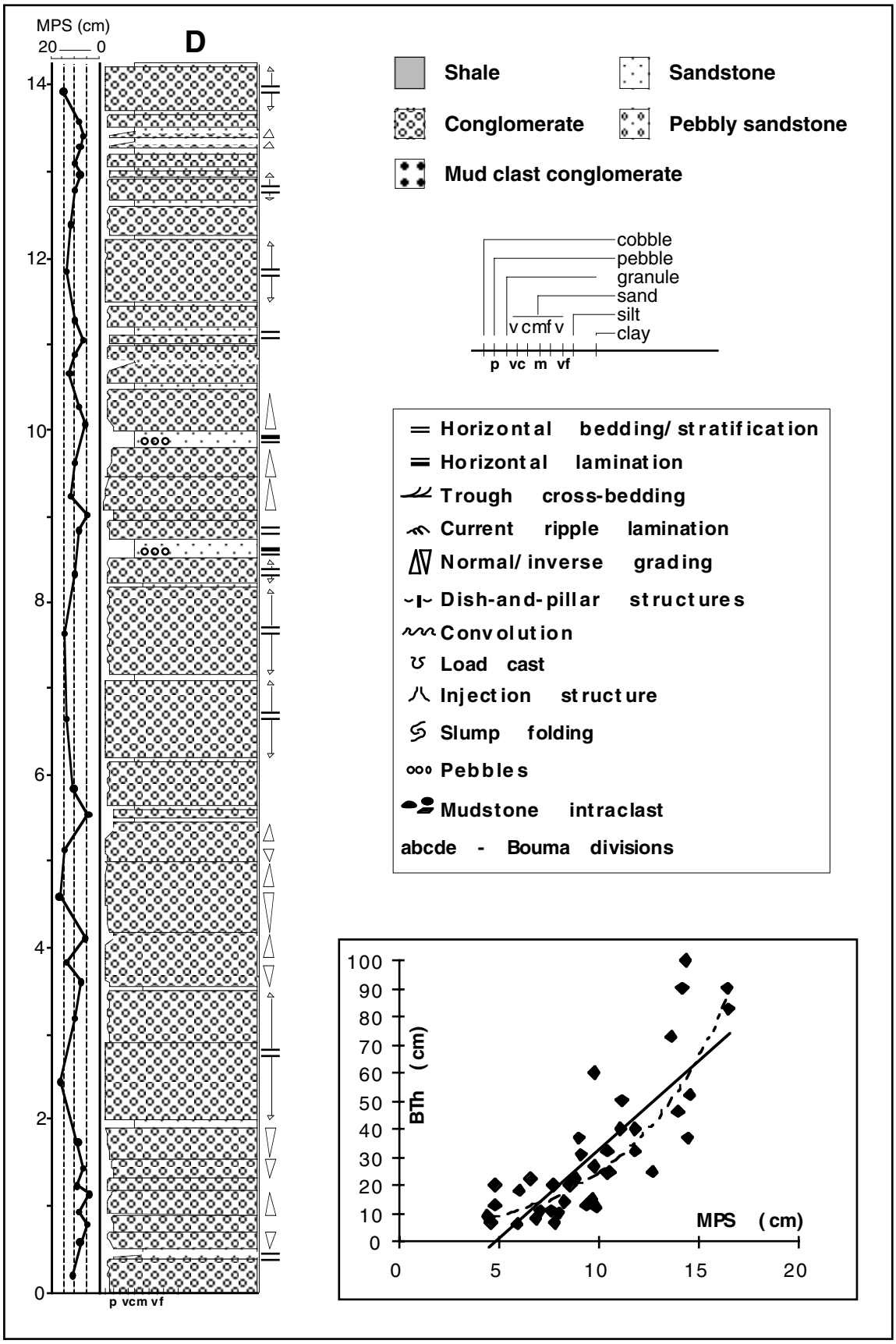

Fig. 2.9. Graphic log D measured at 860-874 m of log A (Fig. 2.4). Graph shows the positive correlation between maximum particle size (MPS) and bed thickness (BTh).

Interpretation. The conglomerate facies association consists of cohesionless debris flow and high-density turbidity current deposits (Table 2.1). Individual facies are generally sharply bounded and represent single depositional events, except for the inversely graded conglomerate facies which typically grades into the normally graded conglomerate facies (Fig. 2.9) and the pebbly sandstone facies which typically overlies the normally graded conglomerate facies (Figs. 2.8d and 2.10). This facies sequence is typical for the deposition of a single high-density turbidity current (R_2-R_3-S_1 divisions of Lowe, 1982).

The positive correlation between maximum particle size and bed thickness reflects an increase in competence with increasing capacity of depositing flows and is common for mass flows of both subaerial and subaqueous environments (e.g., Bluck, 1967; Steel, 1974; Porebski, 1984). The data distribution can either be described by a linear or an exponential function (Fig. 2.9), but this cannot be resolved due to the limited data set.

Conglomerates intercalated with the thin discontinuous sandstone beds strongly resembles the composite conglomerates reported by Hendry (1973) from Ordovician deep water deposits of Quebec and by Surlyk (1984) from the Jurassic/Cretaceous submarine fan deposits of East Greenland. Hendry (1973) suggested that deposition of individual compound conglomerate-sandstone beds took place as a series of pulses or events at very short time intervals. The composite beds have thus been interpreted by Hendry (1973) to be the products of successive pulses of coarse-grained mass flows resulting from progressive headward failure on a slope. Surlyk (1984) suggested that the composite nature may be a result of the segregation of grain size populations during flows. Alternatively, strong bottom currents may have reworked the bed tops of mass flow deposits, leaving behind discontinuous, channelized sandstone bodies.

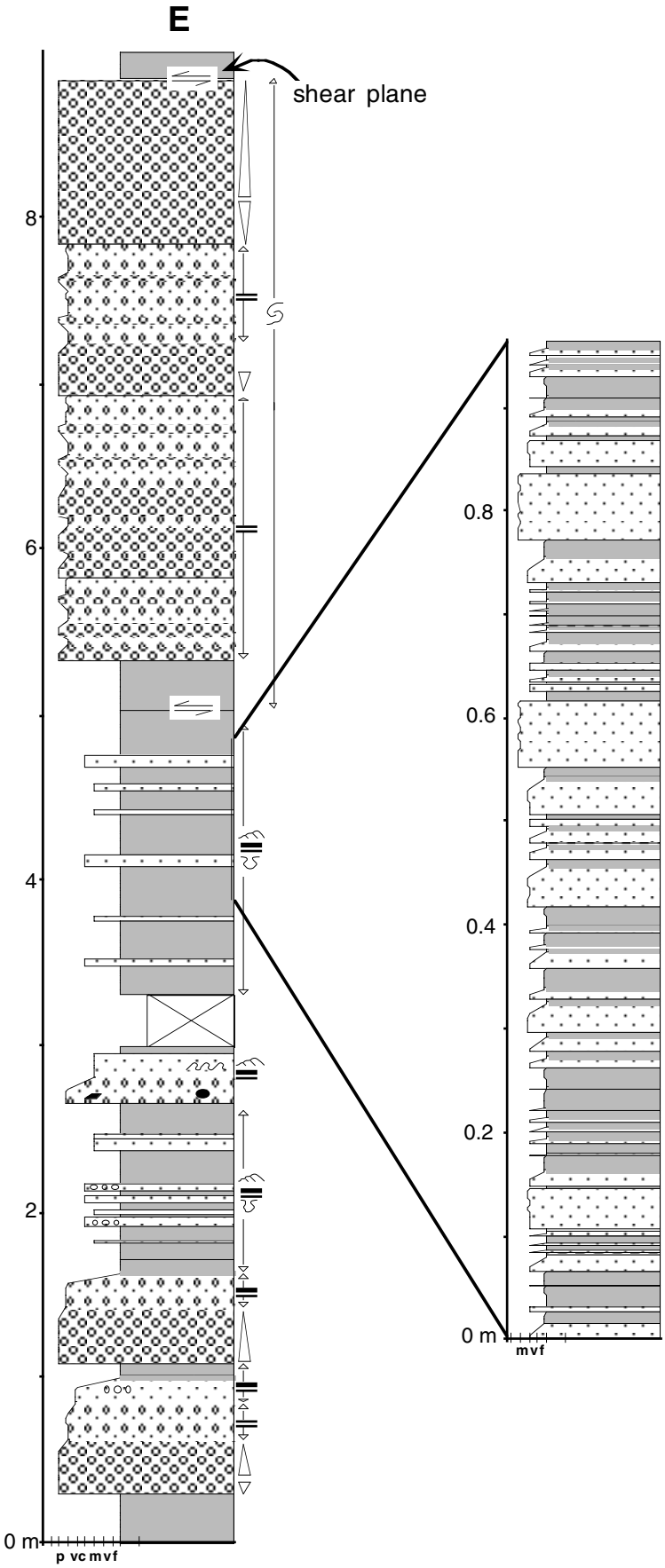

Fig. 2.10. Graphic log E measured at 246-254 m of log A (Fig. 2.4). See Figure 2.9 for legend.

Sandstone facies association

Description. Sandstone occurs in subordinate amounts in the Cheshire Formation as compared to conglomerate and shale. Sandstone is dark grey when fresh and consists predominantly of mafic rock fragments with variable amounts of quartz and feldspar, minor pyroxene and detrital pyrite (Fig. 2.8c). In weathered outcrop sandstone superficially resembles mudstone due to the high percentage of unstable constituents.

Major sandstone occurrences are restricted to the interval 420-500 m of the western section (Figs. 2.4B and 2.11F). Depositional units are 10-250 cm thick and comprise basal conglomerates of two types: (1) a clast-supported fine basalt pebble conglomerate; the clasts are 4-10 mm across and are moderately to well sorted; (2) a poorly sorted, monomict, clast-supported intraclast conglomerate; the clasts consist of massive mudstone and shale in a matrix of fine pebble conglomerate, are up to 40 cm across and are angular to rounded. Both types of conglomerate are mostly normally graded (R_3, Lowe, 1982), inverse-to-normally graded (R_2-R_3) or, rarely, massive or horizontally stratified.

Conglomerates are intercalated with, or gradationally overlain by, thin beds of pebbly sandstone (S_1) with scattered mudstone pebbles. This is gradationally overlain by massive, coarse-grained sandstone (S_3). Continuous to discontinuous bands of pebbly sandstone or isolated pebbles occur parallel to bedding. Scattered pebbles and granules commonly diminish in frequency and size upwards. Sandstone rarely grades into more fine-grained, horizontally laminated sandstone with convolutions and dish-and-pillar structures (S_3).

Interpretation. The sandstone facies association consists of stacked facies typical for sandy high-density turbidity current deposits (R_2-R_3-S_1-S_3; Lowe, 1982). The absence of the S_2 division may lie in the mean size of the suspended load that was unsuitable for traction carpet sedimentation (Lowe, 1982). The sandstone facies association cannot be correlated laterally with the conglomerate facies association, but may find its lateral expression in massive sandstone beds in the eastern section (Fig. 2.4). The rarity of sandstones as compared to conglomerate and shale is attributed to the predominantly mafic composition of the source terrain (see below).

Shale facies association

Description. The shale facies association forms homogeneous successions, typically several tens of metres to 150 m in thickness. It almost totally consists of a heterolithic facies of intercalated sandstone and mudstone (Table 2.1). Intercalations of massive sandstone and ripple-laminated sandstone are rare.

On average, the mud-dominated interlaminated sandstone/mudstone facies (Fig. 2.8d) and, less so, the thinly interbedded sandstone/mudstone facies (Fig. 2.10) predominate, and both facies are closely associated in the succession. The frequency and thickness of sandstone beds varies in the succession. However, no systematic vertical trend of thickness and grain size of sandstone beds were observed even though this may be partly a result of poor exposure and the overall fine grain size. In addition, sandstone beds thicker than 10 cm rarely occur intercalated with shale.

The medium to thickly interbedded sandstone/mudstone facies (Fig. 2.8e) is mostly restricted to the interval 490-510 m of the western outcrop (Figs. 2.4B and 11G) where it overlies sandstone. Tabular beds of massive sandstone up to 2 m thick occur at a few localities (e.g., Fig. 2.4A, 580-600 m) isolated within thick, homogeneous shale units. Ripple-laminated sandstone (Table 2.1) is intercalated with shale and is very rare in the stratigraphic sequence. It is intercalated with thin beds of graded sandstone and parallel-laminated siltstone. Ripple-laminated sandstone is commonly strongly cemented/replaced by carbonate.

Soft sediment deformational structures include small-scale asymmetric folds and rare syndepositional normal faults, and are restricted to a few shale horizons (e.g., Fig. 2.4B, 500-600 m). The asymmetric folds have a consistent sense of overturning, with a wavelength of 8-30 cm and an amplitude of 5-15 cm. Rarely, upper parts of folded strata are eroded, giving rise to truncation of fold hinges (Fig. 2.8f). At one locality (Fig. 2.10) a several metres thick, slump-folded conglomeratic unit is intercalated with shale and bounded by discrete shear surfaces.

Interpretation. Shale formed in a low-energy, mostly sub-wave base setting characterized by deposition of low-density, silt-dominated turbidity currents and quiet water background suspension sedimentation. Sand-rich intercalations formed by episodic low-density turbidity currents as indicated by partial to complete Bouma sequences (Fig. 2.11G). Parts of the succession may have formed from the tail-end of high-density turbidity currents, from deep-water bottom currents and/or from settling of fine material suspended in surface currents (Pickering et al., 1986). Rapid suspension sedimentation from rare high-density turbidity currents gave rise to deposition of massive sandstones. The ripple-laminated sandstone facies shows features characteristic of modern storm deposits (Table 2.1; e.g., Aigner, 1985). Its occurrence indicates that the sea floor was at least temporarily above storm weather wave base, possibly during times of relative sea level lows. The average water depth possibly ranged between 100 and 300 m. Preferential calcite-cementation of the ripple-laminated sandstone facies may indicate higher permeabilities of the sediments due to better sorting during sediment winnowing. Syndepositional deformational structures are attributed to gravity-induced slumping processes.

Quartzose sandstone facies association

Description. Fine-grained (rare) to granule-bearing, very coarse-grained (common) quartzose sandstone forms a 20-50 m thick succession near the top of the preserved section of the Cheshire Formation. Fine pebble conglomerate occurs locally. Sandstone beds are thin to very thick and mostly tabular in shape (Fig. 2.8g). Sand-sized grains are angular to subrounded and predominantly consist of vein quartz; pebble-sized grains are predominantly vein quartz with subordinate granite, massive basalt and minor siltstone intraclasts. Large detrital muscovite flakes are common. Unstable clasts such as mafic rock fragments and detrital pyrite form a minor proportion (Fig. 2.8h). Pebble-size mudstone intraclasts occur in some beds. The quartzose sandstone association mainly consists of the normally graded, horizontally stratified and cross-stratified sandstone facies (Table 2.1). The different sandstone facies are generally sharply bounded and partly form bedsets. One bed of cross-stratified sandstone which is overlain by shale has preserved a small-scale dune bedform some 10 cm in relief. Massive conglomerate occurs as rare, medium to thick beds or forms the base of graded sandstone beds (Fig. 2.12). It is a clast-supported, oligomict chert pebble conglomerate consisting of angular to rounded, tabular to ellipsoidal fragments of chert and mudstone with the chert clasts possibly representing silicified siltstone.

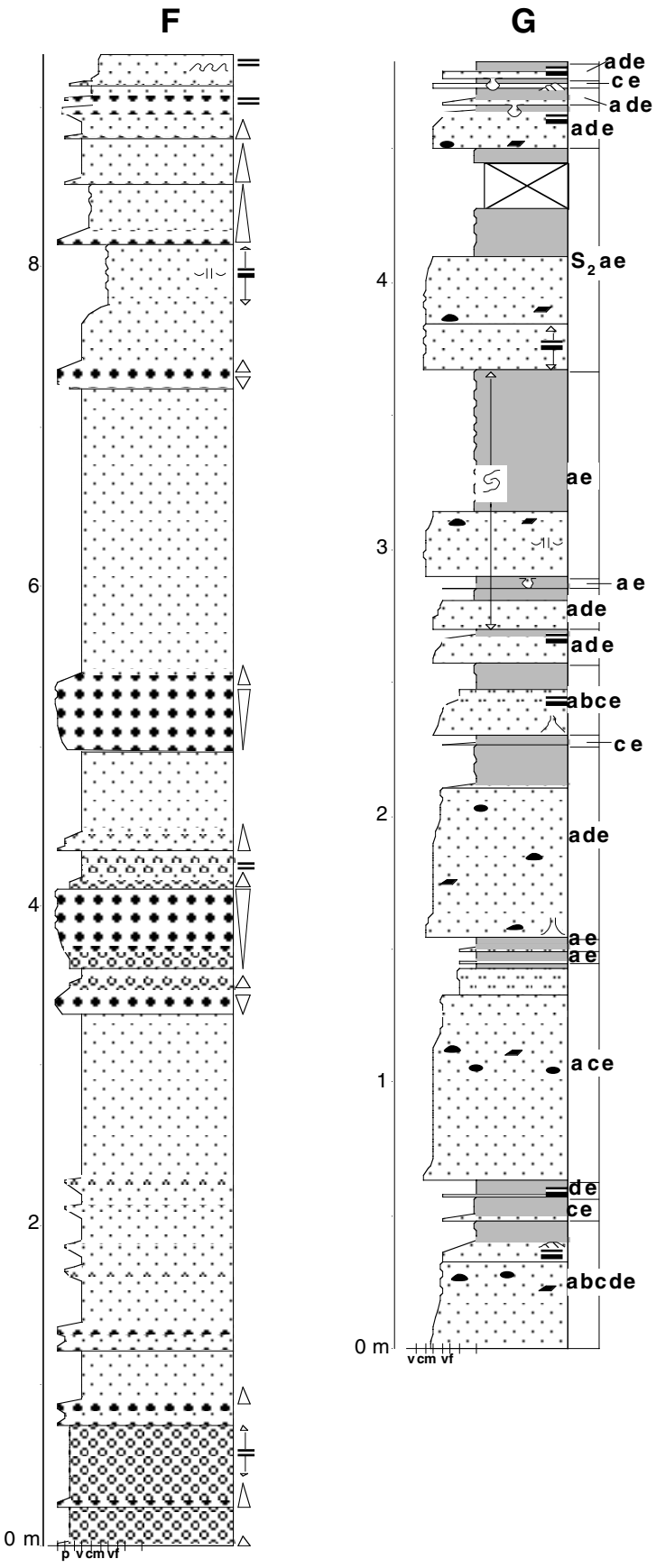

Fig. 2.11. Graphic logs F and G measured at 427-436 m and 490-495 m of log B (Fig. 2.4). See Figure 2.9 for legend.

Interpretation. Normally graded sandstones (S_3; Lowe, 1982) are most common and indicate rapid suspension sedimentation from sandy high-density turbidity currents. Horizontally stratified sandstones are probably analogous to S_2 of Lowe (1982) and formed by traction carpet sedimentation at the base of a sandy high-density turbidity current. The tabular geometry of cross-stratified sandstone beds (Fig. 2.8g), sharp bounding surfaces and their occurrence as sets indicate that they probably formed by strong bottom currents that reworked the sediments deposited by turbidity currents. Such currents commonly occur in confined channels and/or scours (Pickering et al., 1986). However, the lateral continuity of the quartzose sandstone association indicates that the sediments were deposited as sheets rather than as lenticular bodies in channels.

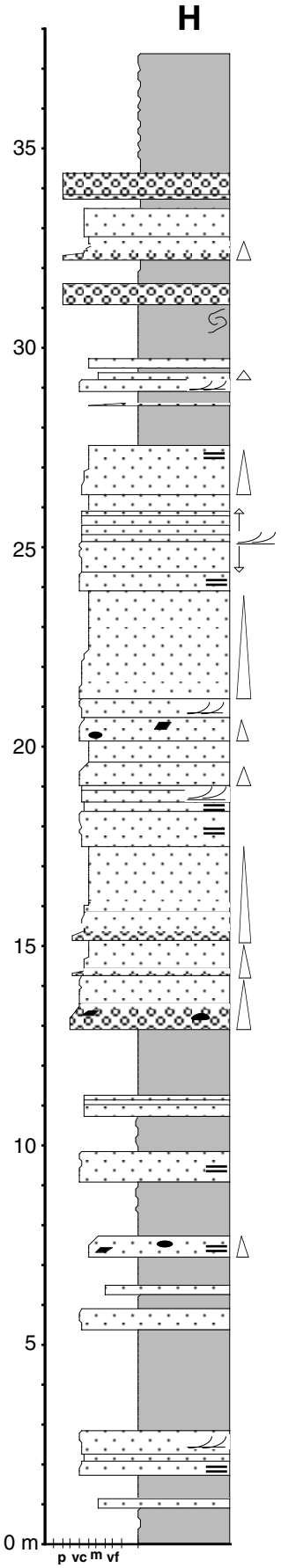

Fig. 2.12. Graphic log H measured at 941-978 m of log B (Fig. 2.4). See Figure 2.9 for legend.

Other lithological units

Basaltic rocks

Several dolerite sills, up to 80 m in width, occur within the sedimentary succession. Some sills can be traced for >10 km. Dolerite is medium-grained in sill centres and fine-grained along the margins. Decimetre-scale apophyses of dolerite are locally intrusive into the country rock. Contact metamorphism of shale adjacent to relatively thick dolerite sills is indicated by the occurrence of cherty, massive hornfels up to 4 m away from the contact.

Strongly altered igneous rocks occur in the northern part of the Cheshire Formation. They range from very fine- to medium-grained and are commonly strongly carbonatized with primary minerals mostly replaced by clayey material. The rocks have been interpreted by Martin (1978) to represent altered mafic lava flows. The geometry of the rock bodies and pseudomorphed plagioclase laths however indicate that they more likely represent strongly altered dolerite.

A few occurrences of tuff have been mapped in the southern part of the Cheshire Formation (Orpen et al., 1985), possibly on account of the dark brown colour of the rocks when weathered. However, the rocks consist of thin beds of commonly massive siltstone to medium-grained sandstone with relics of normal grading and current ripple lamination. Composition and structure is therefore not different from the shale facies described above. The supposed tuff typically occurs along fault zones. Rocks adjacent to faults are commonly silicified and hematite-impregnated.

Ironstone

Ironstone outcrops as discontinuous horizons up to 15 m thick and hundreds of metres to several kilometres in length. Ironstone is most common along the Zeederbergs-Cheshire contact and the contact between the carbonate and siliciclastic members. It further occurs in the upper part of the carbonate member close to the contact with the inlier of volcanic rocks and, more rarely, in the

lower to middle part of the siliciclastic member (Fig. 2.2). Continuous ironstone horizons are also common at the top of the sedimentary sequence where they are intercalated with hematitic shale and massive hematitic mud- to sandstone (Fig. 2.4).

Ironstone is a heterogeneous rock that consists predominantly of three varieties: (1) banded chert, (2) brecciated chert, and (3) chert horizons that are intercalated with hematite (sulphide)-impregnated sediments. Banded chert (1) consists of typically 1-3 cm thick (range 0.5-20 cm) and locally laminated chert bands that are intercalated with similarly thick bands of massive, hematite-rich rock. Hematitic layers are commonly continuous; chert layers are typically discontinuous, pinch-and-swell or are boudinaged. Hematitic layers commonly truncate chert bands and contain chert fragments. Layering is frequently deformed into small- to medium-scale, gentle to tight, commonly asymmetric and disharmonic folds. Isoclinal folds occur and represent strongly sheared asymmetric folds (Fig. 2.13a). Brecciated chert (2) was derived from the in situ disruption of banded chert with which it is intercalated. It comprises angular fragments of banded chert in a matrix of massive and vuggy, hematitic material (Fig. 2.13b). Type 3 ironstone comprises chert layers that are intercalated with hematite-impregnated sediments on a cm- to m-scale. The sediments include shale, brecciated shale and minor limestone and conglomerate.

Shale adjacent to ironstone horizons is iron-enriched, vuggy and sheared. Sandstone intercalations within shale are commonly dolomitized, typically disrupted and rotated, and partly sheared, resulting in lensoidal shapes. These inclusions are commonly intruded by massive, clayey material derived from adjacent shale, suggesting plastic behaviour of the fine-grained sediments during deformation. Limestone adjacent to ironstone shows various stages of replacement by chert and hematitic material parallel to bedding and along fractures.

The Cheshire ironstones have been interpreted as chemical precipitates that formed under sediment-starved, quiet-water conditions (Nisbet et al., 1993) , probably due to their similarity to banded iron formations. However, intercalated sediments are silicified, hematized and sulphurdized, are sheared in places, and show evidence that shearing took place prior to solidification. More strongly sheared rocks appear more strongly hematized, indicating that much of the silica and iron was introduced during deformation. Furthermore, ironstones in the lower part of the succession occur along lithological contacts where there is clear evidence of shearing. The ironstones therefore occur along D_1-shear zones as indicated by cross-cutting relationships with bedding of surrounding sediments (Fig. 2.3) and their formation can be attributed to silicification and hematization of predominantly fine-grained sediments (shale) by iron- and silica-rich fluids channelled trough mostly layer-parallel shear zones. Hematite-rich layers both represent in situ impregnated, fine-grained sediments and intrusive, commonly bedding-parallel veins. Intensive veining gave rise to brecciation of banded cherts.

Mélange zone

A distinct zone of deformed sediments occurs between the western carbonate unit and the inlier of Zeederbergs-type volcanics (Figs. 2.3 and 2.4). This zone, termed mélange zone,

comprises a deformed siliciclastic unit with minor carbonate horizons that preserves variable strain intensities. In less deformed areas intercalations of shale, conglomerate and brecciated limestone occur that are locally tightly folded (Fig. 2.3), whereas in more strongly deformed areas are various lithologies complexly intermingled and commonly forming inclusions in a strongly sheared matrix (Fig. 2.13c). Inclusions are up to a few metres in diameter and include limestone, basalt pebble conglomerate, sandstone, siltstone and shale. The inclusions are commonly elongated lenses in cross-section with "tails" that taper out in the plane of foliation. The matrix is a strongly sheared, argillaceous rock which is locally silicified, hematized and sulphide-bearing. Siltstone inclusions have very irregular, partly amoeboidal shapes and are commonly intruded by muddy matrix material (Fig. 2.13d), indicating that both the siltstone inclusions and the matrix were plastic (i.e. not consolidated) during deformation. The strong deformation of originally semi-consolidated sediment can best be explained by movement of the overlying volcanic unit relative to the carbonates shortly after their deposition.

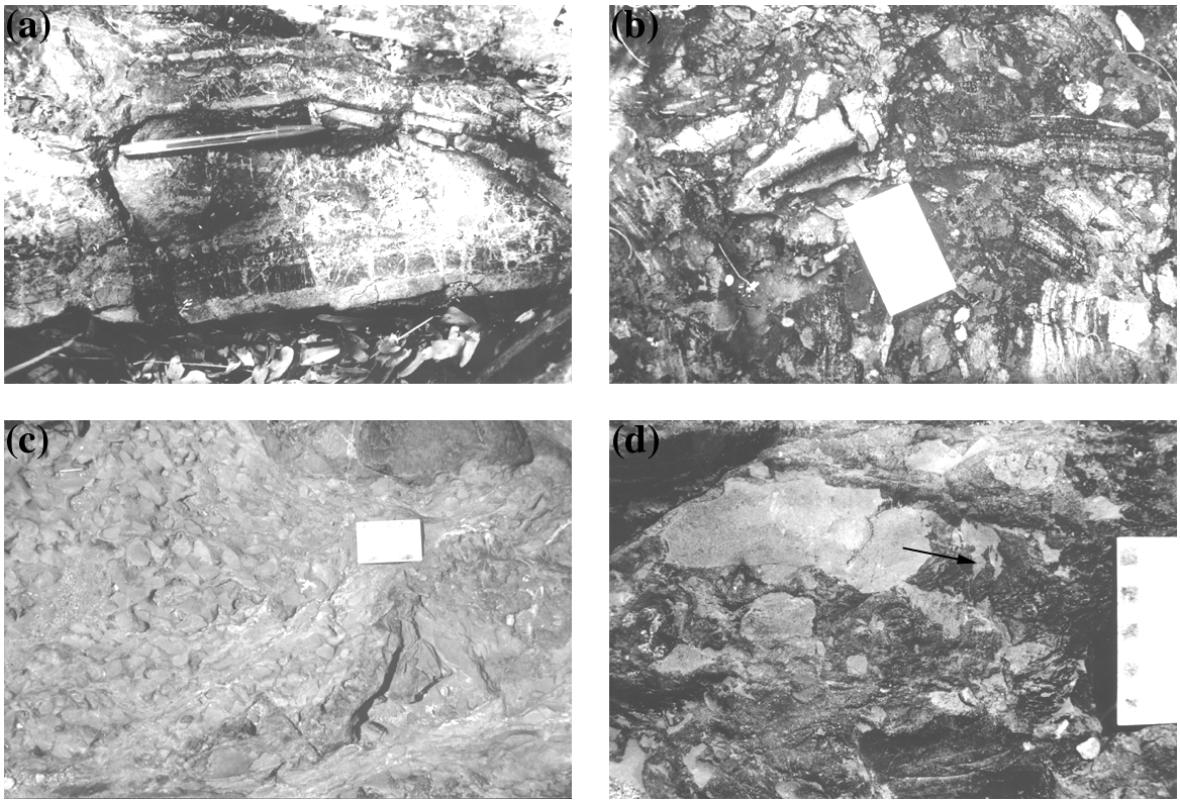

Fig. 2.13. Features of other lithological units. (a) Isoclinal fold in ironstone which shows incipient brecciation. (b) Brecciated ironstone consisting of angular fragments of banded chert in a massive hematitic matrix. (c) Inclusion of basalt pebble conglomerate (left) in the mélange zone. (d) Very irregular siltstone inclusions in the mélange zone which are partly intruded by muddy matrix material (arrow).

PROVENANCE

Basalt clasts form the bulk of the Cheshire conglomerates as indicated by pebble counting (Fig. 2.4). Several clast varieties have been distinguished (Fig. 2.14a). The most common clast type (1) is a massive, very fine-grained, light grey basalt containing a few, sub-mm calcite-filled vesicles. The second variety (2) is a dark grey, very fine-grained basalt with a cherty appearance.

This type commonly contains ocelli that are up to 2 cm in diameter (Fig. 2.14b). The third type (3) is a light grey, fine- to medium-grained basalt with macroscopic plagioclase laths. Much less common (< 2 %) is a medium- to coarse-grained dolerite (4) and a light grey, fine-grained rock with spinifex texture (5).

Non-basaltic clasts occur in subordinate amounts. Well rounded vein quartz clasts (<7 cm across) are most common (up to 6.3 %) and increase in frequency upsection (Fig. 2.4). Well rounded clasts, up to 10 cm in diameter, of medium- to coarse-grained granite and granitic gneiss occur throughout in minor proportions (less than 1 %). Clasts of detrital pyrite, up to 10 cm in diameter, and chert are locally common. Mud- to sandstone intraclasts are rare with the exception of the local occurrence of intraclast conglomerates.

Conglomerates with a contrasting composition locally occur in the upper part of the section in the vicinity of the quartzose sandstone unit. They contain abundant pebbles and cobbles of vein-quartz, granite and granitoid gneiss. The matrix is a very coarse, quartzose sand. No pebble count could be conducted because of poor exposure.

The basalt clasts are identical in composition and texture to the rocks of the Zeederbergs Formation. The first clast type is identical to basalt forming the core of pillows. The cherty appearance of type 2 clasts indicates that they may have been derived from the chilled margins of pillows. Ocelli are ubiquitous in Zeederbergs basalts (Fig. 2.14c) and are commonly concentrated along pillow margins. Clast type 3 is distinguished by its slightly coarser grain size as compared to type 1 and is possibly derived from the interior of thick, massive lava flows. Doleritic type 4 clasts are probably derived from the erosion of synvolcanic hypabyssal intrusions. Spinifex-textured clasts (type 5) indicate a provenance area with komatiites and/or komatiitic basalts. Such rocks are common in the Reliance Formation, but the Zeederbergs Formation also contains basaltic rocks with clinopyroxene spinifex textures (e.g., Martin, 1978).

The non-basaltic clasts could have been derived in part from the volcanic rocks. Coarse quartz mineralisation commonly occurs as fillings of voids between pillows as well as lava drainage tubes in pillow centres (e.g., Nisbet et al., 1993). The provenance of sand-sized quartz clasts could also be found in quartz-filled vesicles of basalt lava flows. Pyrite clasts were possibly derived from intercalations of massive sulphides within the Zeederbergs basalts which have since been eroded. Nevertheless, clasts of granite and granitoid gneiss clearly indicate a granitoid-gneiss source throughout the deposition of the siliciclastic member. The abundance of vein quartz together with granitoid rocks at the top of the sequence indicates that probably most of this vein quartz was derived from a granitoid-gneiss provenance. Such a source became more important during the depositional history of the Cheshire Formation as indicated by the systematic increase in vein quartz upsection. No trend in the frequency of granitoid clasts was observed, possibly because of their general scarcity in the lower to intermediate portion of the sedimentary succession.

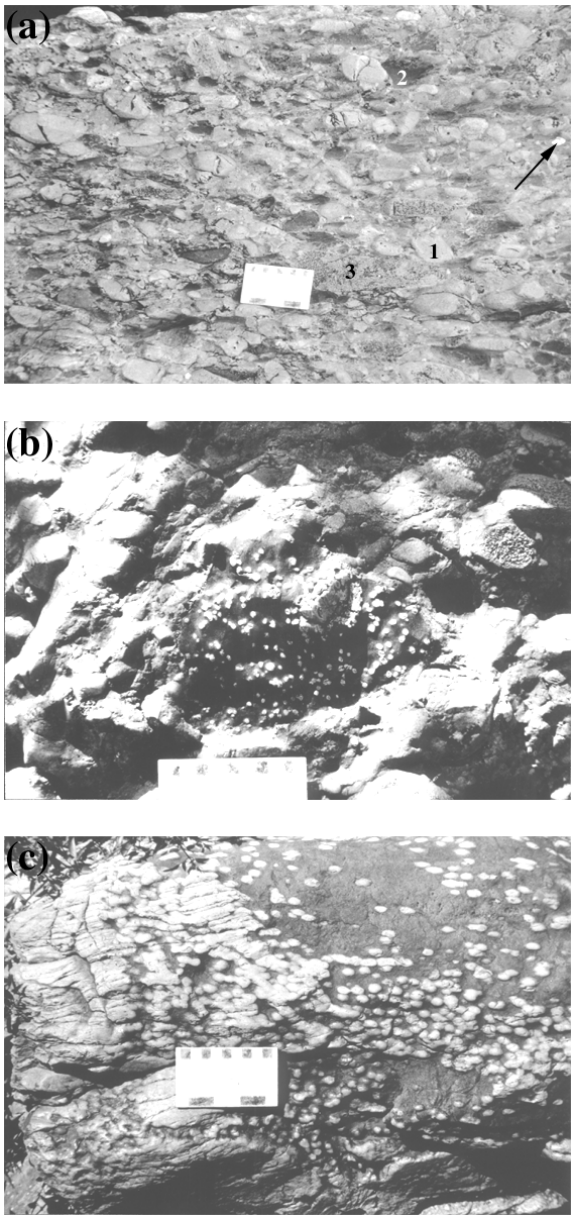

Fig. 2.14. (a) Massive conglomerate showing the main types of basalt clasts (1-3). Vein quartz clast is depicted by arrow. Photograph was taken near the lowermost locality of pebble counting. (b) Type 2 basalt clast with abundant ocelli. (c) Ocelli-rich pillow basalt in the upper part of the Zeederbergs Formation.

The marked grain size bimodality of the Cheshire sediments, i.e. abundant rudites and pelites but minor arenites, is striking. The major control on the size distribution of detritus derived by weathering is the size of the source grains formed from the parent rock (Pettijohn et al., 1987). The dearth of sand-rich sediments in the Cheshire Formation can be explained by a predominantly basaltic source terrain such as the Ngezi volcanics. They consist of fine-grained, mostly aphanitic ultramafic to mafic rocks with rare phenocrysts of olivine, clinopyroxene and fine-grained plagioclase (Scholey, 1992; Brake, 1996). The ferromagnesium minerals, which could form sand-size sediment upon decomposition of the host rocks, are unstable in a sedimentary environment; weathering and disintegration of the minerals preferably produced fine-grained material instead. Quartz, forming sand-sized grains upon decomposition, is not a common constituent of the Zeederbergs/Reliance Formations. On the other hand, weathering and erosion of the mafic rock sequence gave rise to a great quantity of basaltic rock fragments, typically in gravel size. However, the abrasion of pebbles gives rise to predominantly silt-sized material, not sand (e.g., Kuenen, 1959). Sandstones are mostly restricted to the top of the sequence. This is due to a marked increase of exposure of quartz-bearing granitoid rocks in the source area in the course of sediment deposition. Such rocks contain abundant quartz of sand-size, and their decomposition led to the formation of quartzose sandstones.

PALAEOFLOW, PALAEOSLOPE

Palaeocurrents were determined from both the carbonate and siliciclastic members (Fig. 2.15). Palaeocurrent analysis included data restoration to account for tectonic disturbance. Rotation to the pre-D_3 situation includes the assumption that the original strike of the D_2 fold axis is 160°. Pre-D_2 restoration, i.e. unfolding of the syncline, has been performed with the assumption of a horizontal fold axis in the central part of the Cheshire Formation. The D_2 fold axis at locality Z (Fig. 2.2) was determined to be 60° -> 156° (chapter 3).

Palaeocurrent data from the carbonate member have been obtained at the Ngezi river section (Fig. 2.4B) from cross-bedding and both wave and minor current ripple lamination. Cross-bedding has a trimodal distribution with a dominant flow to the south-southwest and a subordinate bipolar southeast-northwest flow. A similar picture emerges from ripple lamination, with the bipolar flow direction (east-west) more pronounced. The bipolar palaeoflow probably indicates the activity of wave-generated currents, whereas the south-southwest flow probably represents storm-generated currents.

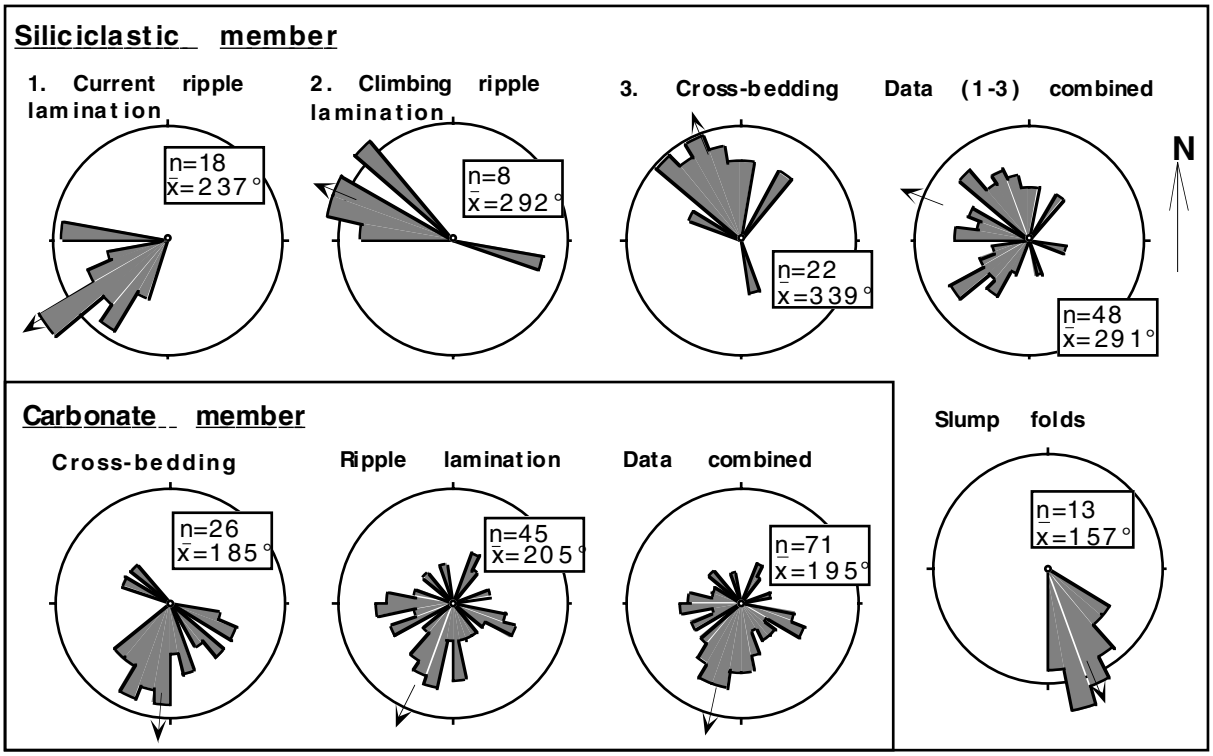

Fig. 2.15. Palaeocurrent/palaeoslope data (pre-D_2 restoration, see text) from the carbonate and siliciclastic members. The number of measurements and the vector mean is shown. Radius of the scale circle refers to 20% of the measurements.

Palaeocurrent data from the siliciclastic member have been obtained from ripple lamination at the base of the section (locality 1, Figs. 2.2 and 2.4A), from climbing ripple lamination in the centre (locality 2, Fig. 2.2), and from cross-bedding in the quartzose sandstone facies association at the top of the sequence (locality 3, Figs. 2.2 and 2.4B). All data show a unimodal distribution, with a southwesterly flow at the base, a west-northwesterly flow in the centre, and a north-northwesterly flow at the top. This indicates a gradual change of palaeoflow direction with time. All data combined suggest a west to northwesterly transport direction and indicate that the

provenance area of the siliciclastic member originally lay in the east. Small-scale asymmetric slump folds that are developed in one stratigraphic horizon in the centre of the succession (Fig. 2.4B) indicate a south-southeast-dipping palaeoslope.

DISCUSSION

The carbonate member is a shallow, wave- and storm-dominated, open marine sequence. The shallowing-upward cycles are very similar to sedimentary cycles reported from Proterozoic carbonate platforms (see also Grotzinger, 1986a; 1989; Sumner and Grotzinger, 2000). Deposition of the carbonate member probably took place on a carbonate ramp (e.g., Burchette and Wright, 1992) due to the stacking pattern of facies, the interpreted lateral facies distribution of the basal Cheshire sediments, palaeoflow/-slope data and shallow basinal water depths. Lower portions of shale-based cycles formed in an upper outer to mid ramp setting. Deposition was influenced by storms and resulted in the deposition of graded beds showing distal-proximal trends, a common feature of deep water ramp facies (Aigner, 1985; Calvet and Tucker, 1988). Upper parts of shale-based cycles and the carbonate cycles formed on the tidally influenced inner ramp which was characterized by sheet-like ooide shoreface deposits, sub- to intertidal stromatolite growth and the formation of tidal flat laminites. The rare occurrence of sediment gravity flows indicate a gently sloping depositional surface. Palaeocurrent data indicate a subordinate bipolar east-west flow, interpreted to reflect tide- or wave-generated currents which, in turn, are interpreted to be normal to the palaeoshoreline. The dominant palaeoflow to the south-southwest possibly indicates the effect of storm-generated geostrophic currents (e.g., Duke, 1990) subparallel to the shore.

The limestone sequence is capped by a continuous breccia horizon for which a karst origin is most likely, indicating subaerial emergence of the carbonate platform. The breccia is overlain by deep water siliciclastics (mélange zone), indicating net deepening and drowning of the carbonate platform either due to an eustatic sea level rise or due to tectonic subsidence. Relative sea level rise must have been slow to account for the local occurrence of carbonate horizons intercalated with conglomerate and shale. The restricted occurrence of sediment gravity flows at the top of the carbonate sequence indicates steepening of the otherwise gentle palaeoslope of the carbonate ramp near the termination of carbonate deposition. This relationship may indicate a tectonic origin for drowning. Brecciation of limestones in the mélange zone and higher up in the succession is attributed to in situ limestone dissolution by acidic fluids. These fluids are thought to have traveled along D_1 fault planes during overthrusting of the carbonate member.

The siliciclastic member consists of sub-wave base sediments which have been deposited by both high- and low-density turbidity currents. The succession lacks internal organization, as indicated by the lack of systematic vertical thickness trends of sandstone beds in shale, the lack of systematic grain size trends in conglomerate horizons, and by the rather random occurrence of conglomerate horizons in shale. In addition, channel/overbank and lobe facies (e.g., Mutti and Ricci Lucchi, 1972) that are common to canyon-fed submarine fans are indistinct to absent. Individual depositional units are laterally extensive instead. These features are characteristic for

submarine ramps where the sediment is derived from multiple feeder channels which act as a line source (Chan and Dott, 1983; Heller and Dickinson, 1985; Reading and Richards, 1994). The conglomerate and sandstone associations can be regarded as proximal ramp deposits, whereas the shale facies association represents distal ramp and basin plain deposits. The rare occurrence of wave-formed structures and stromatolitic limestones within the sequence, however, indicates shallow basinal water depth which was, at times, as shallow as 30-100 m.

The Cheshire Formation has preserved evidence for an early thrusting event. The inlier of mafic volcanics in between Cheshire sediments is interpreted as a tectonic nappe of Zeederbergs rocks which was thrust onto the carbonate sequence and overlying siliciclastic rocks from the southeast (Figs. 2.2 and 2.3). This interpretation is based on the identical appearance of the mafic volcanics to the rocks of the Zeederbergs Formation, the sheared lower contact and the intensely deformed underlying rocks (mélange zone), as well as kinematic indicators in the mélange zone and tectonic ironstone. Where the nappe pinches out in the south, the siliciclastic member is juxtaposed against the carbonate member along a sheared contact, indicating that during thrusting the nappe was already overlain by siliciclastic sediments. A similar relationship can be observed at the eastern carbonate outcrop (Fig. 2.3) where siliciclastic rocks rest on carbonates along an ironstone horizon that is interpreted as a shear zone. The two carbonate units separated by volcanics probably represent the same stratigraphic horizon which was tectonically duplicated during thrusting.

The carbonate unit is restricted to the western part of the Cheshire outcrop and is structurally overlain by the siliciclastic sediments which, together with the inlier of mafic volcanics, were probably thrust from the southeast as discussed above. The carbonates locally contain intercalations of basalt pebble conglomerate. At one locality in the western part of the siliciclastic member stromatolitic limestones occur near the top of the lower conglomerate horizon (Fig. 2.4), whereas limestones are absent in the eastern part. These relationships may indicate that the basal sedimentary units, i.e. conglomerate in the east and limestone in the west, formed synchronously and were juxtaposed during thrusting. If these assumptions are correct, the original facies distribution of the Cheshire Formation is asymmetric with shallow-water carbonates in the west and deeper water siliciclastic rocks in the east.

The palaeoslope was dipping to the southeast during deposition of the central siliciclastic member as indicated by the orientation of slump folds (Fig. 2.15). However, palaeoflow directions within the siliciclastic rocks are, on average, oriented towards the northwest (Fig. 2.15). Additionally, conglomerates are more abundant and coarse grained in the southeast than in the northwest (Figs. 2.2 and 2.4). These relationships indicate that detritus was shed from the southeast. Palaeoflow of the siliciclastic member is almost opposite to the inferred palaeoslope and indicate the ability of turbidity currents to move up-slope. However, the rarity of slump folds and the absence of chaotic slump and slide deposits suggest a rather gently sloping depositional surface. Taken all data into account, the sea floor was probably dipping towards the southeast in the western part of the sedimentary basin where carbonates formed and was northwestward-dipping in the eastern part (Fig. 2.16).

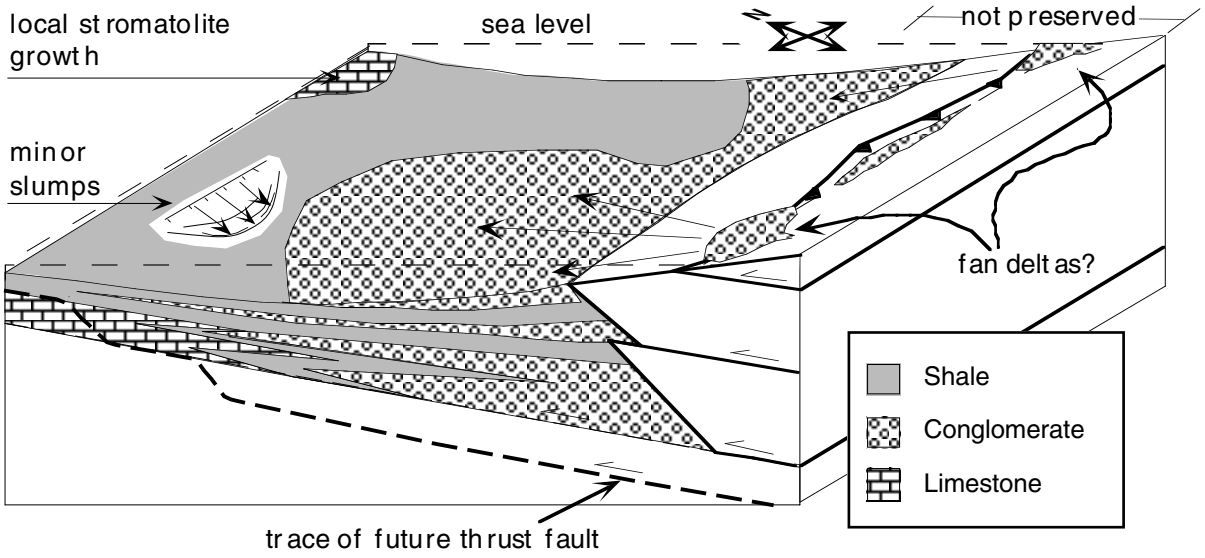

Fig. 2.16. Simplified facies model for the deposition of the Cheshire Formation in front of a northwestward advancing thrust stack (not preserved) of Zeederbergs-like rocks (no pattern).

The Cheshire Formation shares distinctive characteristics of the sedimentary fill of a foreland basin (papers in Allen and Homewood, 1986; Jordan, 1995; Miall, 1995). (a) It has an asymmetric facies and thickness distribution with deeper water sediments and thicker strata towards the thrust source in the southeast. (b) The basin fill has been incorporated into the thrust stack during or shortly after its formation as indicated by duplication of strata. (c) The clastic sediments have been derived from the erosion of Zeederbergs-like mafic volcanics which have been identified to form a thrust sheet in the sequence. (d) Sediment transport in the clastic sediments is in the same direction as the inferred tectonic transport, which is the most common setting for thrust-derived clastics (synthetic dispersal, Steidtmann and Schmitt, 1988). (e) The succession of a drowned carbonate platform sequence, overlain by deep water flysch-type deposits, is common to foreland basins. The subaerial exposure of the platform carbonates prior to drowning may be a consequence of flexural arching of the lithosphere some distance away from the tectonic load (stacked thrusts). (f) The inundation of the shallow water sedimentary environments (carbonate member) was not as rapid, and palaeoslope was not as steep as would be expected if the sediments formed, for example, in a rift basin; a gentle palaeoslope and gradually increasing subsidence rate might indicate lithospheric flexure.

Taken all data into account, it is likely that the Cheshire Formation formed in a foreland-type sedimentary basin that developed in front of a fold-and-thrust belt situated in the southeast. Accommodation space was probably provided by thrust loading and gave rise to an eastward deepening basin with the deposition of shallow-water sediments in the west and deep-water sediments in the east. Accelerated subsidence during thrust advance gave rise to drowning of the carbonate sequence which was then covered by more deep-water sediments (Fig. 2.16). The gradual change in the palaeoflow direction from southwest to northwest during deposition of the siliciclastic member could indicate a change from longitudinal sediment dispersal to a transverse dispersal pattern directed towards the foreland. Part of the sequence was then carried piggy-back on top of an active thrust, possibly during or shortly after deposition (see also Kusky and Kidd,

1992). The top of the sedimentary sequence is not preserved, but is occupied by tectonic ironstones which may represent the basal shear zone of another nappe, which has since been eroded.

Most gravel clasts were derived from a terrain remarkably similar, or laterally equivalent to the rocks preserved today as the Zeederbergs Formation. Clasts of granite, gneiss and vein quartz, however, indicate the presence of a granitoid-gneiss terrain in the source area. Such detritus becomes more abundant towards the top of the sedimentary sequence indicating increasing amounts of granitoid rocks as part of the source. Whether these rocks formed a (tectonic?) basement to the Ngezi volcanics and, during progressive unroofing, gave rise to an inverted stratigraphy in the composition of the detrital particles or whether they represent an active tectonic unit which was incorporated into the thrust stack cannot be resolved with the limited data set.

The contact between the Zeederbergs and Cheshire Formations is sharp. The volcanic sequence contains only minor sedimentary intercalations, mostly deep water shales and turbidites containing hyaloclastic material. The Cheshire Formation lacks volcanic rocks. This suggests that sedimentation took place some time after cessation of volcanism. Alternatively, it may indicate a long tectonic transport distance of Zeederbergs nappes between the site of active volcanism and the site of foreland sedimentation. However, where exposed, the Zeederbergs/Cheshire contact is sheared; the Cheshire Formation could therefore represent a thrust sheet in its own right, even though displacement was probably not large because most of the detritus forming the basal sediments was derived from erosion of Zeederbergs-like material.

Mafic magmatism in the Cheshire Formation is exemplified by the occurrence of dolerites which must have intruded prior to the syncline formation. Syndepositional mafic magmatism is a rare feature of recent foreland basins (Burke et al., 1986), but is rather common in Palaeoproterozoic foreland basins of Canada where it has been suggested to reflect a higher thermal regime of the Palaeoproterozoic lithosphere (Hoffman, 1987). Minor mafic lavas also occur in the late Archaean Witwatersrand basin of South Africa, which has been interpreted as a foreland basin (Burke et al., 1986; Winter, 1987).

CONCLUSIONS

Sedimentological-structural mapping enables us to develop a model for the depositional history of the Cheshire Formation and provides new constraints for the evolution of the Belingwe greenstone belt. The data is in accordance with a foreland-type setting for deposition of the Cheshire sediments northwest of an unidentified thrust belt.

The lower part of the Cheshire Formation was deposited in an eastward-deepening basin, characterized by shallow-water carbonate sedimentation in the west and deep-water siliciclastic sedimentation in the east. Basin formation is attributed to flexural loading of the crust by northwestward-moving thrust stacks. Uplift of the carbonate platform resulted in the formation of a karst surface and may have been caused by flexural bending of the crust. Accelerated subsidence, postulated to be due to thrust advance, gave rise to drowning of the carbonate

platform and deep-water sedimentation throughout. Detritus was shed from thrust sheets of Zeederbergs-like mafic volcanics and was deposited in a subaqueous ramp setting by high- and low-density turbidity currents flowing to the northwest. However, the basin remained relatively shallow, stromatolites formed locally and, at times, the sea floor was affected by winnowing during storm-induced currents. A felsic sediment source became more important in the course of sedimentation, possibly due to unroofing of granitoid crust. Shortly after deposition, the Cheshire Formation and underlying volcanics were incorporated into the thrust stack, and tectonic duplication took place. Shearing predominantly affected semi-consolidated shale horizons and was associated with the movement of silica- and iron-rich, acidic fluids along fault planes. This gave rise to local limestone brecciation and the formation of ironstone along shear zones. The timing of piggy-back thrusting of the Cheshire Formation with respect to its formation is unclear, but probably occurred shortly after deposition of the preserved part of the succession.

REFERENCES

Abell, P.I., McClory, J., Martin, A. and Nisbet, E.G., 1985. Archaean stromatolites from the Ngesi Group, Belingwe Greenstone Belt, Zimbabwe; preservation and stable isotopes-preliminary results. Precambrian Res., 27: 357-383.

Aigner, T., 1985. Storm depositional systems. Lecture Notes in Earth Sciences, Springer-Verlag, Berlin, 174 pp.

Allen, P.A. and Homewood, P. (Editors), 1986. Foreland Basins. Spec. Publ. Int. Ass. Sediment., 8, 453 p.

Bickle, M.J. and Nisbet, E.G. (Editors), 1993. The geology of the Belingwe Greenstone Belt, Zimbabwe. Spec. Publ. Geol. Soc. Zim., 2, 239 pp.

Bickle, M.J., Martin, A. and Nisbet, E.G., 1975. Basaltic and peridotitic komatiites, stromatolites and a basal unconformity in the Belingwe greenstone belt, Rhodesia. Earth Planet. Sci. Lett., 27: 155-162.

Bickle, M.J., Orpen, J.L., Nisbet, E.G. and Martin, A., 1993. Structure and metamorphism of the Belingwe Greenstone Belt and adjacent granite-gneiss terrain: The tectonic evolution of an Archaean craton. In: Bickle, M.J. and Nisbet, E.G. (Editors), The geology of the Belingwe Greenstone Belt, Zimbabwe. Spec. Publ. Geol. Soc. Zim., 2, pp. 39-68.

Bickle, M.J., Nisbet, E.G. and Martin, A., 1994. Archaean greenstone belts are not oceanic crust. J. Geol., 102: 121-138.

Blenkinsop, T.G., Fedo, C.M., Bickle, M.J., Eriksson, K.A., Martin, A., Nisbet, E.G. and Wilson, J.F., 1993. Ensialic origin for the Ngezi group, Belingwe greenstone belt, Zimbabwe. Geology, 21: 1135-1138.

Blenkinsop, T.G., Martin, A., Jelsma, H.A. and Vinyu, M.L., 1997. The Zimbabwe Craton. In: de Wit, M.J. and Ashwal, L.D. (Editors), Greenstone belts. Oxford University Press, pp. 567-580.

Bluck, B.J., 1962. Deposition of some Upper Red Sandstone conglomerates in the Clyde area; a stuy in the significance of bedding. Scott. J. Geol., 3: 139-167.

Bolhar, R., Hofmann, A., Woodhead, J.M., Hergt, J.M. and Dirks, P., 2000. Timing of deposition and provenance of stromatolitic carbonates from the 2.7 Ga Belingwe Greenstone Belt, Zimbabwe Craton: constraints from Pb/Pb and Sm-Nd systematics. Abstr. Geol. Soc. Aust., 62, pp.58.

Bouhallier, H., Choukroune, P. and Ballèvre, M., 1993. Diapirism, bulk homogeneous shortening and transcurrent shearing in the Archaean Dharwar craton, the Holenarsipur area, southern India. Precambrian Res., 63: 43-58.

Bouma, A.H., 1962. Sedimentology of some flysch deposits: a graphic approach to facies interpretation. Elsevier, Amsterdam, 168 pp.

Brake, C., 1996. Tholeiitic magmatism in the Belingwe greenstone belt, Zimbabwe. Ph.D. thesis, University of Edinburgh, 184 pp.

Burchette, T.P. and Wright, V.P., 1992. Carbonate ramp depositional systems. Sediment. Geol., 79: 3-57.

Burke, K., Kidd, W.S.F. and Kusky, T.M., 1986. Archean foreland basin tectonics in the Witwatersrand, South Africa. Tectonics, 5: 439-456.

Calvet, F. and Tucker, M.E., 1988. Outer ramp cycles in the Upper Muschelkalk of the Catalan Basin, northeast Spain. Sediment. Geol, 57: 185-198.

Campbell, S.D.G. and Pitfield, P.E.J., 1993. The use of structural techniques for gold exploration in Zimbabwe. Tech. Coop. Final Report, Zim. geol. Surv., 145 pp.

Card, K.D., 1990. A review of the Superior Province of the Canadian Schield, a product of Archaean accretion. Precambrian Res., 48: 99-156.

Chan, M.A. and Dott, R.H.Jr., 1983. Shelf and deep-sea sedimentation in Eocene forearc basin, western Oregon—fan or non-fan? Am. Assoc. Petrol. Geol. Bull., 67: 2100-2116.

Chauvel, C., Dupré, B. and Arndt, N.T., 1993. Pb and Nd istopic correlation in Belingwe komatiites and basalts. In: Bickle, M.J. and Nisbet, E.G. (Editors), The geology of the Belingwe Greenstone Belt, Zimbabwe. Spec. Publ. Geol. Soc. Zim., 2, pp. 167-174.

Demicco, R.V. and Hardie, L.A., 1994. Sedimentary structures and early diagenetic features of shallow marine carbonate deposits. Soc. Econ. Palaeont. Mineral. Atlas, 1, 255 pp.

de Wit, M.J., Roering, C., Hart, R.J., Armstrong, R.A., de Ronde, C.E.J., Green, R.W.E., Tredoux, M., Perbedy, E. and Hart, R.A., 1992. Formation of an Archaean continent. Nature, 357: 553-562.

Dirks, P.H.G.M. and Jelsma, H.A., 1998. Horizontal accretion and stabilization of the Archean Zimbabwe Craton. Geology, 26: 11-14.

Duke, W.L., 1990. Geostrophic circulation or shallow marine turbidity currents? The dilemma of palaeoflow patterns in storm-influenced prograding shoreline systems. J. Sediment. Petrol., 60: 870-883.

Fischer, A.G., 1964. The Lofer cyclothems of the Alpine Triassic. In: Merriam, D.F. (Editor), Symposium on cyclic sedimentation. Kans. geol. Surv. Bull., 169: 107-149.

Goodwin, P.W. and Anderson, E.J., 1985. Punctuated aggradational cycles: a general hypothesis of episodic stratigraphic accumulation. J. Geol., 93: 515-533.

Goldhammer, R.K., Dunn, P.A. and Hardie, L.A., 1987. High frequency glacio-eustatic sea-level oscillations with Milankovitch characteristics recorded in Middle Triassic platform carbonates in northern Italy. Am. J. Sci., 287: 853-892.

Goldhammer, R.K., Dunn, P.A. and Hardie, L.A., 1990. Depositional cycles, composite sea-level changes, cycle stacking patterns, and the hierarchy of stratigraphic forcing: Examples from Alpine Triassic platform carbonates. Geol. Soc. Am. Bull., 102: 535-562.

Grotzinger, J.P., 1986a. Cyclicity and palaeoenvironmental dynamics, Rocknest platform, northwest Canada. Geol. Soc. Am. Bull. 97: 1208-1231.

Grotzinger, J.P., 1986b. Upward shallowing platform cycles: a response to 2.2 billion years of low-amplitude, high-frequency (Milankovitch band) sea level oscillations. Paleoceanography, 1: 403-416.

Grotzinger, J.P., 1989. Facies and evolution of Precambrian carbonate depositional systems: emergence of the modern platform archetype. In: Crevello, P.D., Wilson, J.L., Sarg, J.F. and Read, J.F. (Editors), Controls on carbonate platform and basin evolution. Spec. Publ. Soc. Econ. Paleontol. Mineral., 44, pp. 79-106.

Grotzinger, J.P, Sumner, D.Y. and Beukes, N.J., 1993. Archaean carbonate sedimentation in an active extensional basin, Belingwe Greenstone Belt, Zimbabwe. GSA Annual Meeting, Abstracts, 25, p. A64.

Hardie, L.A. and Shinn, E.A., 1986. Carbonate depositional environments, modern and ancient. Part 3, tidal flats. Colorado School of Mines Quart., 81: 1-74.

Heller, P.L. and Dickinson, W.R., 1985. Submarine ramp facies model for delta-fed, sand-rich turbidite systems. Am. Assoc. Petrol. Geol. Bull., 69: 960-976.

Hendry, H.E., 1973. Sedimentation of deep water conglomerates in Lower Ordovician rocks of Québec—composite bedding produced by progressive liquefaction of sediment? J. Sediment. Petrol., 43: 125-136.

Hoffman, P.F., 1987. Early Proterozoic foredeeps, foredeep magmatism, and Superior-type iron-formations of the Canadian Shield. In: Kröner, A. (Editor), Proterozoic Lithospheric Evolution. American Geophysical Union Geodynamics Series, 17, pp. 85-98.

Horstwood, M.S.A., 1998. Stratigraphy, geochemistry and zircon geochronology of the Midlands greenstone belt, Zimbabwe. Ph.D. thesis (unpubl.), Univ. of Southampton, 215 pp.

Hunter, M.A., Bickle, M.J., Nisbet, E.G., Martin, A. and Chapman, H.J., 1998. Continental extensional setting for the Archean Belingwe Greenstone Belt, Zimbabwe. Geology, 26: 883-886.

James, N.P. and Choquette, P.W., 1984. Diagenesis 9. Limestones—the meteoric diagenetic environment. Geosci. Can., 11: 161-194.

James, N.P., 1994. Shallowing-upwards sequences in carbonates. In: Walker, R.G. (Editor), Facies Models (2nd edition). Geoscience Canada Reprint Series, 1: 213-228.

Jelsma, H.A. and Dirks, P.H.G.M., 2000. Tectonic evolution of a greenstone sequence in northern Zimbabwe: sequential early stacking and pluton diapirism. Tectonics, 19: 135-152.

Jordan, T.E., 1995. Retroarc foreland and related basins. In: Busby, C.J. and Ingersoll, R.V. (Editors), Tectonics of Sedimentary Basins. Blackwell, Cambridge, pp. 331-362.

Koerschner, W.F. and Read, J.F., 1989. Field and modelling studies of Cambrian carbonate cycles, Virginia Appalachians. J. Sediment. Petrol., 59: 654-687.

Kuenen, P.H., 1959. Sand—its origin, transportation, abrasion and accumulation. Annex. Geol. Soc. S. Afr., 62: 1-33.

Kusky, T.M., 1998. Tectonic setting and terrane accretion of the Archean Zimbabwe craton. Geology, 26: 163-166.

Kusky, T.M. and Kidd, W.S.F., 1992. Remnants of an Archaean oceanic plateau, Belingwe Greenstone Belt, Zimbabwe. Geology, 20: 43-46.

Kusky, T.M. and Winsky, P.A., 1995. Structural relationships along a greenstone/shallow water shelf contact, Belingwe greenstone belt, Zimbabwe. Tectonics, 14: 448-471.

Lowe, D. R., 1982. Sediment gravity flows: II. Depositional models with special reference to the deposits of high-density turbidity currents. J. Sediment. Petrol., 52: 279-297.

Martin, A., 1978. The geology of the Belingwe-Shabani shist belt. Rhod. geol. Surv. Bull. 83, 213 pp.

Martin, A., Nisbet, E.G. and Bickle, M.J., 1980. Archaean stromatolites of the Belingwe Greenstone Belt. Precambrian Res., 13: 337-362.

Martin, A., Nisbet, E.G., Bickle, M.J. and Orpen, J.L., 1993. Rock units and stratigraphy of the Belingwe Greenstone Belt: The complexity of the tectonic setting. In: Bickle, M.J. and Nisbet, E.G. (Editors), The geology of the Belingwe Greenstone Belt, Zimbabwe. Spec. Publ. Geol. Soc. Zim., 2, pp. 39-68.

McDonough, W. F. and Ireland, T. R., 1993. Intraplate origin of komatiites inferred from trace elements in glass inclusions. Nature, 365: 432-434.

Miall, A.D., 1995. Collision-related foreland basins. In: Busby, C.J. and Ingersoll, R.V. (Editors), Tectonics of Sedimentary Basins. Blackwell, Cambridge, pp. 393-424.

Mutti, E. and Ricci Lucchi, F., 1972. Le torbiditi dell'Appenino settentrionale all'analisi di facies. Mem. Soc. geol. Ital., 11: 161-199.

Myers, J.S., 1995. The generation and assembly of an Archaean super continent: evidence from the Yilgarn craton, western Australia. In: Coward, M.P. and Ries, A.C. (Editors), Early Precambrian processes. Geol. Soc. Spec. Publ., 95, pp. 143-154.

Nisbet, E.G., Martin, A., Bickle, M.J. and Orpen, J.L., 1993. The Ngezi Group: Komatiites, basalts and stromatolites on continental crust. In: Bickle, M.J. and Nisbet, E.G. (Editors), The geology of the Belingwe Greenstone Belt, Zimbabwe. Spec. Publ. Geol. Soc. Zim., 2, pp. 121-165.

Osleger, D.A. and Read, J.F., 1991. Relation of eustasy to stacking patterns of metre-scale carbonate cycles, late Cambrian, U.S.A.. J. Sediment. Petrol., 61: 1225-1252.

Orpen, J.L., Bickle, M.J., Nisbet, E.G. and Martin, A., 1986. Belingwe Peak, Zimbabwe. Zim. geol. Surv. Map, 1:100000.

Pelechaty, S.M., James, N.P., Kerans, C. and Grotzinger, J.P., 1991. A middle Proterozoic palaeokarst unconformity and associated sedimentary rocks, Elu Basin, northwest Canada. Sedimentology, 38: 775-797.

Pettijohn, F.J., Potter, P.E. and Siever, R., 1987. Sand and Sandstone, 2nd edition. Springer-Verlag, New York, 553 pp.

Pickering, K.T., Stow, D.A.V., Watson, M. and Hiscott, R.N., 1986. Deep-water facies, processes and models: a review and classification scheme for modern and ancient sediments. Earth Sci. Rev., 23: 74-174.

Porebski, S.J., 1984. Clast size and bed thickness trends in resedimented conglomerates: example from a Devonian fan-delta succession, southwest Poland. In: Koster, E.H. and Steel, R.J. (Editors), Sedimentology of gravels and conglomerates. Can. Soc. Petrol. Geol. Mem., 10, pp. 399-411.

Reading, H.G. and Richards, M., 1994. Turbidite systems in deep-water basin margins classified by grain size and feeder system. Am. Assoc. Petrol. Geol. Bull., 78: 792-822.

Scholey, S.P., 1992. The geology and geochemistry of the Ngezi Group volcanics, Belingwe Greenstone Belt, Zimbabwe. Ph.D. thesis, University of Southampton, 184 pp.

Southgate, P.N., 1989. Relationships between cyclicity and stromatolite form in the Late Proterozoic Bitter Springs Formation, Australia. Sedimentology, 36: 323-339.

Steel, R.J., 1974. New Red Sandstone floodplain and piedmont sedimentation in the Hebridean Province, Scotland. J. Sediment. Petrol., 44: 336-357.

Steidtmann, J.R. and Schmitt, J.G., 1988. Provenance and dispersal of tectogenic sediments in thin-skinned thrusted terrains. In: Kleinspeh, K. and Paola, C. (Editors), New perspectives in basin analysis. Springer-Verlag, New York, pp. 353-366.

Sumner, D.Y., and Grotzinger, J., 2000. Late Archaean aragonite precipitation: petrography, facies association and environmental significance. Spec. Publ. Soc. Econ. Paleontol. Mineral., in press.

Surlyk, F., 1984. Fan-delta to submarine fan conglomerates of the Volgian-Valanginian Wollaston Forland Group, East Greenland. In: Koster, E.H. and Steel, R.J. (Editors), Sedimentology of Gravels and Conglomerates. Can. Soc. Petrol. Geol. Mem., 10, pp. 359-382.

Wilson, J.F., Nesbitt, R.W. and Fanning, C.M., 1995. Zircon geochronology of Archaean felsic sequences in the Zimbabwe craton: a revision of greenstone stratigraphy and a model for crustal growth. In: Coward, M.P. and Ries, A.C. (Editors), Early Precambrian processes. Geol. Soc. Spec. Publ., 95, pp. 109-126.

Winter, H. de la R., 1987. A cratonic foreland model for Witwatersrand Basin development in a continental back-arc, plate-tectonic setting. S. Afr. J. Geol., 90: 409-427.

CHAPTER 3

Horizontal tectonic deformation geometries in a late Archaean sedimentary sequence, Belingwe greenstone belt, Zimbabwe

Axel Hofmann, Paul H.G.M. Dirks, and Hielke A. Jelsma

Tectonics, in press

Abstract—In the Belingwe greenstone belt of Zimbabwe, structural evidence from the c. 2.65 Ga old sedimentary Cheshire Formation which overlies and is imbricated with a mafic volcanic unit is consistent with thrusting of the greenstone sequence. The Cheshire Formation consists of a karstified carbonate ramp sequence, overlain by siliciclastic turbidite deposits that formed in a southeast-deepening basin. The earliest deformational structures formed during a syn- to postdepositional, thin-skinned thrusting event (D_1) that affected poorly consolidated sediments, and is recorded in bedding-parallel ductile shear zones, boudins, folds, and block-in-matrix structures. D_1 shear zones separate the volcanic sequence and the overlying sediments and occur between the carbonate and siliciclastic units. Syntectonic sulphide mineralization and silicification of mainly fine-grained sediments along the main thrust faults gave rise to the formation of rocks similar in appearance to banded iron formations. Stratigraphic units were locally duplicated along the D_1 thrust faults, including a tectonic slice of mafic volcanics that was emplaced onto carbonates along a chaotic unit similar to a tectonic mélange. The elongation of inclusions in the mélange zone and lineations in ironstones together with kinematic indicators suggest that stratigraphic duplication resulted from northwestward-directed tectonic transport. Deposition of the Cheshire Formation took place in an asymmetric, foreland-type basin contemporaneously with thrusting. Soon after deposition the formation was incorporated into the thrust stack. Subsequent deformation events include tight upright folding, gentle cross-folding, and dextral strike-slip faulting of the greenstone succession. Evidence for early thrusting suggests that horizontal tectonic processes played an important role in the evolution of the Belingwe greenstone belt.

INTRODUCTION

The significance of horizontal vs vertical tectonics in Archaean greenstone belts is far from being resolved. The granite-greenstone terrain of the Zimbabwe Craton is generally quoted as an example of vertically accreted Archaean crust in which the volcano-sedimentary sequences were laid down in rifts on older continental basement with magma under- and overplating above mantle plumes (Bickle et al., 1975; Blenkinsop et al., 1993; Bickle et al., 1994; Shackleton, 1995; Wilson et al., 1995; Ridley et al., 1997; Hunter et al., 1998). Subsequent compressional deformation is attributed to vertical tectonic processes, including liquid and solid state granite diapirism (Jelsma et al., 1993) and post tectonic strike-slip faulting (Campbell and Pitfield, 1994). This view is based on a range of arguments including: (1) the tri-cuspate outcrop pattern of greenstone belts enveloping subelliptical batholiths (Macgregor, 1951), (2) detailed descriptions of deformation patterns around the Chinamora Batholith in north Zimbabwe that illustrate the importance of ballooning diapirism in the deformation of greenstone sequences (Ramsay, 1989; Jelsma et al., 1993), (3) the recognition of unconformities at the base of major greenstone sequences overlying older continental crust with the type locality of such an unconformable contact in the Belingwe greenstone belt (Bickle et al., 1975; Hunter et al., 1998), and (4) the recognition of an apparently non-repetitive stratigraphy in the Belingwe belt that has been correlated across much of the Zimbabwe Craton (Wilson, 1979; Wilson et al., 1995). It has been suggested that prior to the diapiric rise of granite-gneiss domes, an extensive segment of continental crust existed (Horstwood et al., 1999) that was covered by one or a series of smaller greenstone basins.

In contrast, horizontal accretion models for the formation of Archaean crust suggest that greenstone belts represent remnant oceanic crust or island arc material that was amalgamated with continental fragments via a subduction-accretion related process (e.g., Swager and Griffin, 1990; Card, 1990; de Wit et al., 1992; Myers, 1995). Evidence for horizontal tectonics such as the occurrence of nappe-like structures has long been recognized in several Zimbabwean greenstone belts (Stowe, 1984), but it has generally been ascribed to gravity sliding induced by rising diapirs, i.e., as a secondary effect of vertical tectonic processes. More recently, data have been presented that suggest that thrust tectonics and associated horizontal tectonic stacking of stratigraphic units may have played an important role in the early evolution of the greenstone belts (Kusky and Kidd, 1992; Kusky and Winsky, 1995; Dirks and van der Merwe, 1997; Dirks and Jelsma, 1998a,b; Jelsma and Dirks, 2000). Kusky and Kidd (1992) and Kusky and Winsky (1995) argue that a major detachment zone exists in the Belingwe belt separating granitoid basement and overlying shallow-water clastics from obducted oceanic crust. The occurrence of possible decollement surfaces in the Archaean stratigraphy along which large coherent masses of rock emplaced as allochthonous thrust sheets has major implications. It means that the concept of craton wide stratigraphic correlation of greenstone sequences based on the stratigraphy of the Belingwe belt is incorrect, that oceanic crust may well exist in the greenstone belts and that the Zimbabwe Craton did not develop any differently

than the Yilgarn Craton in Australia or the Kaapvaal Craton in South Africa, where horizontal accretion is well established.

In the Belingwe belt no detailed structural-metamorphic and sedimentological studies have been performed that critically test the validity of the hypothesis put forward by Kusky and Kidd (1992) and Kusky and Winsky (1995) (horizontal tectonic stacking of stratigraphic units), and the contrary views of Blenkinsop et al. (1993) and Bickle et al. (1994) (no tectonic stacking; layer parallel shears are accommodation structures produced by folding). This paper summarizes the results of a detailed structural study of the c. 2.65 Ga old sedimentary Cheshire Formation, the youngest unit in the Belingwe belt. The geometries of deformational structures in combination with stratigraphic imbrications and the aspects of deformed lithologies suggest that horizontal thrust tectonics played an important role in the formation of the greenstone sequence.

GEOLOGICAL SETTING OF THE BELINGWE GREENSTONE BELT

The Belingwe greenstone belt (BGB) is situated in the south-central part of the Zimbabwe Craton (Fig. 3.1). It contains a well-preserved late Archaean sequence of predominantly mafic lavas and sedimentary rocks (Bickle and Nisbet, 1993). The supracrustal rocks overlie and are surrounded by a granitoid-gneiss terrain dominated by the 3.5 Ga Shabani gneiss complex to the east and the 2.9-2.8 Ga Chingezi gneiss complex to the west. The greenstone sequence is divided into two distinct units, the lower Mtshingwe and upper Ngezi Groups, respectively. The Mtshingwe Group is confined to the southern and western parts of the BGB. It comprises (1) ultramafic to mafic lavas and volcaniclastics, (2) minor felsic volcaniclastics, and (3) sediments including conglomerate, sandstone, shale, and ironstone (Martin et al., 1993). U-Pb zircon dates of Mtshingwe Group rocks range from 2.90 to 2.83 Ga (Wilson et al., 1995). The Ngezi Group forms the central part of the BGB (Fig. 3.1) and overlies the Shabani gneiss complex to the east and northeast and the Mtshingwe Group to the southeast and west. Chilimanzi Suite granites intrude the Ngezi Group in the northern and southern parts of the BGB.

Stratigraphy of the Ngezi Group

The Ngezi Group (Fig. 3.2) comprises a basal sedimentary succession (Manjeri Formation), overlain by ultramafic and mafic volcanics (Reliance and Zeederbergs Formations) and capped by another sedimentary unit (Cheshire Formation). The Reliance and Zeederbergs Formations are collectively termed Ngezi volcanics. The Manjeri Formation has been deposited unconformably on rocks of the Mtshingwe Group and granitoid basement (Bickle et al., 1975). Hunter et al. (1998) described the Manjeri Formation as a thin (0-120 m) clastic sedimentary unit with marked lateral thickness and facies variations. The lower part consists of fluvial to shallow-water sediments, including conglomerate, sandstone, shale, ironstone, and localized stromatolitic limestone. The upper part comprises immature, alluvial fan to fan delta clastics, mainly conglomerate and sandstone, and is

capped by ironstone (Hunter et al., 1998). Bolhar et al. (2000) determined a whole-rock Pb/Pb isochron date of 2698±48 Ma for stromatolitic limestones of the Manjeri Formation.

The overlying Reliance Formation is ~1 km thick and consists of komatiites, komatiitic basalts, and tholeiites. The volcanic rocks include layered, pillowed, and volcaniclastic flow units and high-level intrusives and pass without a distinctive geological break into the lavas of the Zeederbergs Formation (Scholey, 1992). The Zeederbergs Formation is a ~2.8 km thick pile of commonly pillowed, tholeiitic lava flows with minor intercalations of volcaniclastic sediment (Brake, 1996). Komatiitic basalts of the Reliance Formation have been dated by the whole-rock Pb/Pb isochron method at 2692±9 Ma (Chauvel et al., 1993). Ion microprobe trace element data of glass inclusions of Reliance Formation komatiites are similar to modern plume-related oceanic plateau and oceanic island basalts (McDonough and Ireland, 1993).

The ~1.3 km thick Cheshire Formation forms the uppermost stratigraphic unit of the BGB and is distributed along the synclinal axis of the belt. It consists of sedimentary rocks intruded by dolerite sills and can be subdivided into two lithostratigraphic units. The carbonate member consists of limestone/shale cycles and their brecciated equivalents, and the siliciclastic member consists predominantly of conglomerate and shale (chapter 2).

The carbonate member is restricted to two occurrences in the western part of the Cheshire Formation (Figs. 3.3 and 3.4). The westernmost unit rests on the Zeederbergs Formation and is overlain by Zeederbergs-type volcanics in the centre and siliciclastic rocks in the south. The second carbonate occurrence is situated at the western margin of the main Cheshire outcrop. The carbonate member consists of cyclically stacked, metre-scale sedimentary units interpreted to represent shallowing-upward sedimentary cycles. The cycles commonly consist of a basal unit of open marine, shallow subtidal shale. Shale grades into wave-rippled ooid/intraclast grainstone that formed close to fair-weather wave base. Cycles are capped by peritidal microbial laminites and boundstones (Grotzinger et al., 1993; Sumner and Grotzinger, 2000; chapter 2). The stromatolitic limestones yielded a whole-rock Pb/Pb date of 2600±48 Ma (Bolhar et al., 2000). The carbonate member has been interpreted as an eastward-deepening carbonate ramp sequence. Its top is formed by a karstic limestone breccia, indicating subaerial exposure and subsequent drowning of the ramp (chapter 2).

The siliciclastic member typically consists of a basal conglomerate which is overlain by a succession of intercalated conglomerates and shales. A laterally continuous quartzose sandstone horizon intercalated with, and overlain by, hematitic shales and ironstones occur at the top (Fig. 3.3). Massive, graded, and horizontally stratified conglomerates are common and are interpreted as high-density turbidity current deposits. Minor sandstones formed by sandy, high- to low-density turbidity currents. Shale is characterized by low-density turbidites and background suspension sediments. The rare occurrence of stromatolitic limestones intercalated with deeper water sediments indicate deposition, at least temporarily, within the photic zone. The siliciclastics are almost totally derived from erosion of Zeederbergs-like rocks situated in the east as indicated by the composition

of gravel in conglomerates and palaeoflow data (chapter 2). Rare granitic and gneissic pebbles, however, indicate the presence of felsic crust in the source terrain.

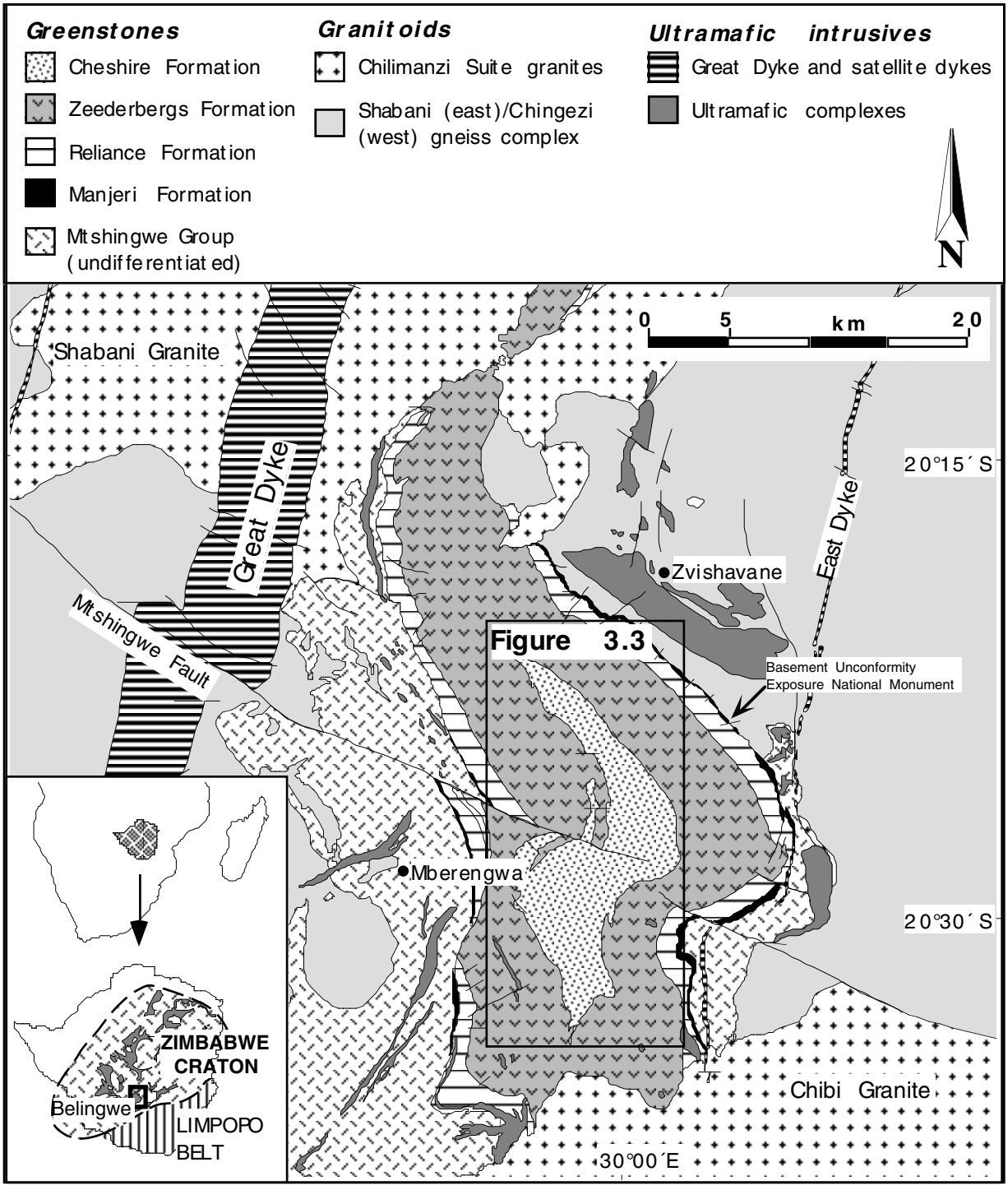

Fig. 3.1. Geological map of the Belingwe greenstone belt (after Martin et al., 1993, Fig. 2.1).

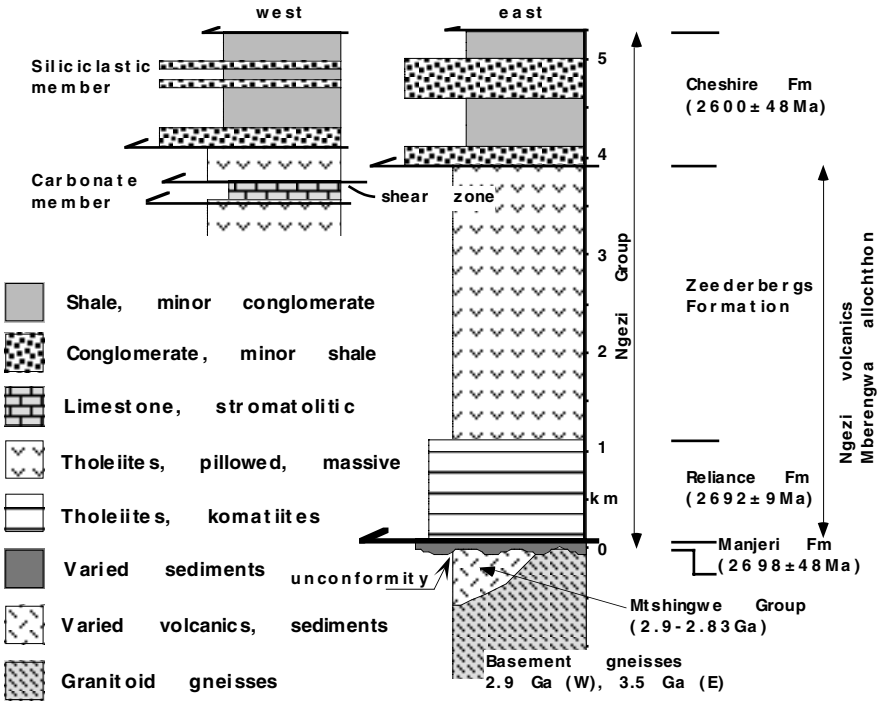

Fig. 3.2. Simplified stratigraphic column of the Ngezi Group (see text for references).

Structure

Controversy surrounds the tectonic setting in which the supracrustal rocks formed. The Ngezi Group has been interpreted by many authors (e.g., Bickle and Nisbet, 1993; Blenkinsop et al., 1993; Bickle et al., 1994; Hunter et al., 1998) as an autochthonous sequence deposited in an intracontinental rift basin. In contrast, Kusky and Kidd (1992) and Kusky and Winsky (1995) suggested the presence of a shear zone at the top of the Manjeri Formation. They argued that the Ngezi volcanics originated from an oceanic plateau and were emplaced as a large thrust sheet, the Mberengwa allochthon, onto the Manjeri Formation.

The structure of the BGB has generally been interpreted as a refolded syncline. According to Bickle et al. (1993), the first deformational event is recorded only in the Mtshingwe Group, which was folded about a NW-SE trending axis (D_g1, terminology of Bickle et al., 1993). The second event took place after the deposition of the Ngezi Group and is exemplified by the synclinal structure of the belt (D_g2). The rocks of the Ngezi Group are steeply dipping; stratigraphic younging is towards the core of the syncline. According to Blenkinsop et al. (1993), localized shear zones (most notably in the ironstones at the top of the Manjeri Formation) accommodated flexural slip associated with folding.

The intrusion of Chilimanzi Suite granites postdates D_g2 as indicated by truncation of the syncline of the Ngezi Group by the Chibi granite in the south (Fig. 3.1). A later greenschist facies cleavage-forming event is related to the folding of earlier structures about northeast striking axial planes in the south-central part of the belt (D_g3). According to Bickle et al. (1993), the Chibi granite

intruded prior to D_g3, because the granite has been recrystallized at greenschist facies conditions and locally shows a northeast-striking foliation. Following the intrusion of the Great Dyke at c. 2.58 Ga (Mukasa et al., 1998), dextral faulting along the Mtshingwe fault (D_g4) offset the stratigraphy of the greenstone belt.

Kusky and Winsky (1995) argued for a deformational event associated with obduction of the Ngezi volcanics between D_g1 and D_g2. They described high-strain zones in the lower 200 m of the Reliance Formation. At the Basement Unconformity Exposure National Monument (Fig. 3.1) the top of the Manjeri Formation is a strongly folded ironstone horizon which, according to Kusky and Winsky (1995), is overlain by a 1 m wide mylonitic ultramafic schist showing S-C fabrics; the overlying 15 m have been reported to consist of ultramafic schists, anastomosing mylonites, and phyllonites. Structural fabrics in mylonitic shear zones in the basal Reliance Formation indicate west- to southwestward movement and have been interpreted by Kusky and Winsky (1995) to reflect the transport direction of the Mberengwa allochthon after its detachment (their D_1). Relatively low-grade kinematic indicators such as fold asymmetries, fault ramps and fault bend folds in the ironstone indicate relative northward movement of the Ngezi volcanics (their D_2) and may have formed either during a change of transport direction during obduction or during a second extensional deformational event in response to collapse of the thickened crust (Kusky and Winsky, 1995). Table 3.1 summarizes the tectonic events proposed by the various authors.

Metamorphism

The metamorphic grade in the central part of the Ngezi Group reaches sub-greenschist to greenschist facies (Martin, 1978). Pelitic sediments of the Manjeri and Cheshire Formations contain fine-grained chlorite-sericite-quartz assemblages without epidote, which is indicative of sub-greenschist facies conditions (Martin, 1978; Bickle et al., 1993). The sedimentary rocks show evidence for recrystallization, but textures are commonly well preserved. Abell et al. (1985) attempted to constrain the thermal history of the Manjeri and Cheshire carbonates through a combined petrological and stable isotope study. They concluded that the limestones of the Manjeri Formation reequilibrated at ~200°C, whereas the Cheshire limestones experienced a maximum temperature of 200°C with a temperature of 80°C or less most likely. The Ngezi volcanics contain relic igneous assemblages variably replaced by greenschist facies mineral assemblages.

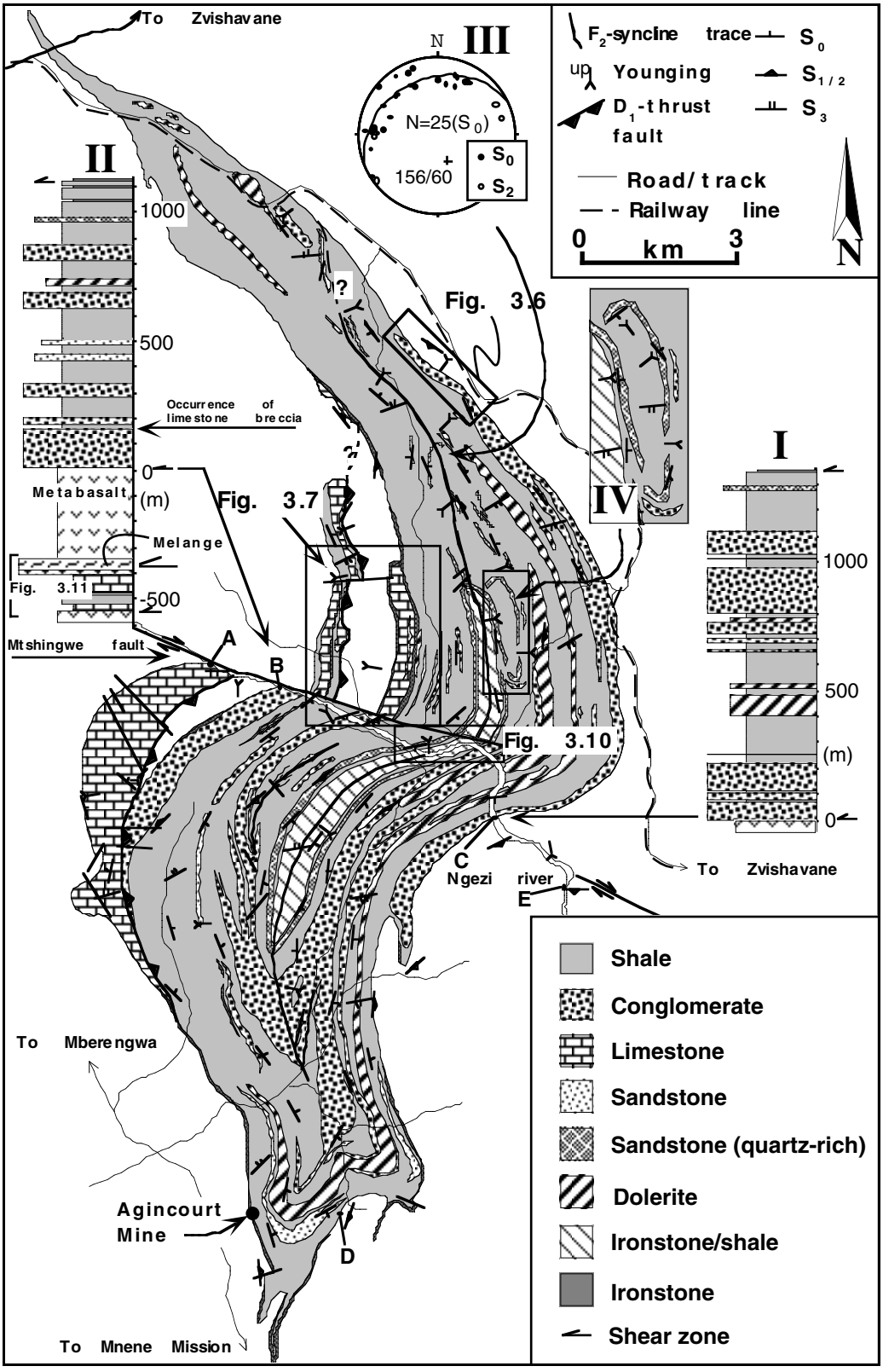

Fig. 3.3. Geological map of the Cheshire Formation (after Martin, 1978; Orpen et al., 1986; Nisbet et al., 1993, and own mapping). Graphic logs (I, II) have been measured in the bed of the Ngezi river. One area (IV) is enlarged for clarity. A-E are localities discussed in the text.

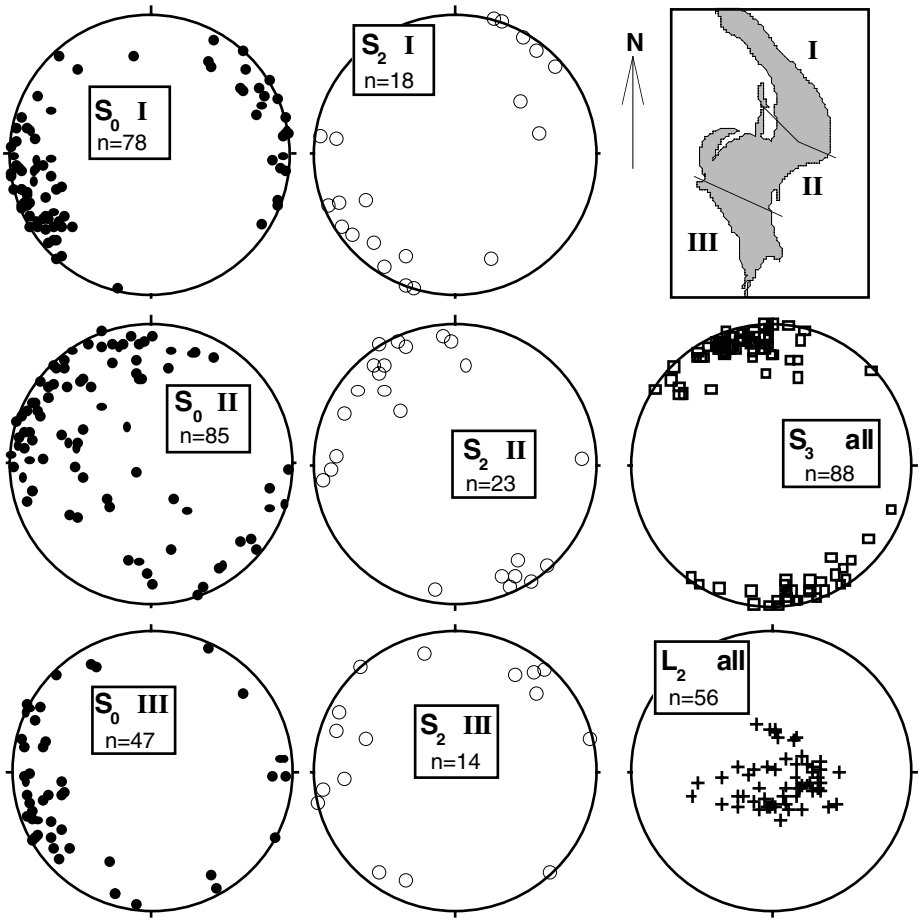

Fig. 3.4. Lower hemisphere stereographic projections of bedding, foliation, and lineation data from the Cheshire Formation. Cheshire outcrop has been divided into three structural domains I-III (see inset) to account for the reorientation of structural elements during D_3. Data from the mapped areas shown in Figures 3.6 and 3.7 are excluded.

Bickle et al. (1993) differentiated four distinct metamorphic events in the Ngezi Group: (1) syn-volcanic hydrothermal alteration on eruption of the Ngezi volcanics, (2) a greenschist facies event associated with D_g2, (3) amphibolite facies contact metamorphism associated with the intrusion of the Chilimanzi Suite granites, and (4) regional greenschist facies metamorphism associated with D_g3 (sub-greenschist facies in parts of the Cheshire Formation). Kusky and Winsky (1995) argued that the metamorphic grades are generally higher in the Ngezi volcanics than in the underlying Manjeri Formation, a relationship compatible with thrust displacement. However, the higher metamorphic grade may be related to initial sea-floor metamorphism of the Ngezi volcanics.

EARLY HORIZONTAL TECTONIC DEFORMATION OF THE CHESHIRE FORMATION

The sedimentary rocks of the Cheshire Formation have recorded an early horizontal tectonic event (D_1, this study) that is crucial for understanding the tectonic history of the BGB. D_1 was characterised by noncoaxial deformation at very low metamorphic grade, before full consolidation of the sediments had occurred, and resulted in tectonic duplication of sections of the stratigraphy. The D_1 event is manifested in (1) shear zones with associated silicification and sulphide mineralisation

of adjacent rocks to form tectonic ironstones, (2) a mélange-like shear zone along which tectonic duplication of strata took place, and (3) soft-sediment shear zones, folds, and brecciation of carbonates. This event has not been recognized in the Cheshire Formation before and possibly encompasses D_1 and D_2 of Kusky and Winsky (1995) (refer to Table 3.1).

Table 3.1. Summary of the tectonic events that affected the Belingwe greenstone belt (Bickle et al., 1993) and the deformational history of the Ngezi Group as proposed by Kusky and Winsky (1995) and this study.

Bickle et al. (1993)	Kusky and Winsky (1995)	This Study
D_g4, dextral faulting and folding	D_5, dextral faulting and folding (NW axis)	D_4, dextral faulting (Mtshingwe fault)
D_g3, folding and main cleavage formation	D_4, NNE sinistral faulting	D_3, cross-folding about ENE axis
D_g2, N-S synclinal folding of Ngezi Group	D_3, NNW-SSE synclinal folding	D_2, NNW-SSE synclinal folding
	D_2, northward obduction of Mberengwa allochthon or orogenic collapse	D_1, northwestward thrusting of Ngezi volcanics and foreland basin formation
	D_1, westward thrusting of Mberengwa allochthon	
D_g1, SW-NE folding of Mtshingwe Group		

Stratigraphic younging directions in the study area were established using the shape of pillows in basalt, erosional scours in conglomerate, stromatolites in limestone and load casts, flame structures, cross-lamination and, rarely, grading in shale. The analysis of structural data comprises the back rotation of structural measurements to identify the kinematics during D_1. Pre-D_3 restoration was done along a vertical axis and included the assumption that the original strike of the D_2 fold axis is 160°. Pre-D_2 restoration, i.e., unfolding of the syncline, has been done with the assumption of a horizontal fold axis in the central part of the Cheshire Formation (see below). The degree of unfolding was derived from the mean dip of S_0 in the area under consideration.

Tectonic ironstones

Tectonic ironstones bear similarities to banded iron formations. They form up to 10 m thick horizons, outcropping for hundreds of metres to several kilometres. Ironstones are most common along the Zeederbergs-Cheshire contact and along shear zones in the upper part of the carbonate member close to the contact with the inlier of Zeederbergs Formation. They more rarely occur in the lower to middle part of the siliciclastic member but are again common at the top of the preserved sedimentary sequence (Fig. 3.3).

Lithology and structural attributes

Ironstone is a heterogeneous rock that consists predominantly of three varieties: (1) banded ironstone, (2) brecciated banded ironstone, and (3) chert horizons that are intercalated with iron oxide-impregnated sediments. Banded ironstone (type 1) consists of thinly intercalated chert and hematite-rich layers. Chert bands are typically 1-3 cm in thickness (range 0.5-20 cm) and locally laminated. They are intercalated with equally thick bands of massive, hematitic fine-grained material and hematized, relictically laminated mudstone. Hematite-rich layers are commonly continuous; chert layers are typically discontinuous, pinch-and-swell or are boudinaged. The layering is commonly deformed into small- to medium-scale, gentle to tight, asymmetric and disharmonic folds. The disharmonic folding is partly produced by variably boudinaged chert layers, that is, chert layers commonly pinch out away from fold hinges (Fig. 3.5a). Lenticular quartz veins, both oblique and parallel to bedding, and axial planar to folds are common. Isoclinal folds occur and mostly represent strongly deformed, overturned asymmetric folds. Truncation surfaces occur where massive hematitic layers transect layered chert bands.

Brecciated banded ironstone (type 2 ironstone) is derived from the disruption of banded ironstone with which it is intercalated. It comprises lenticular to rectangular, angular fragments of banded ironstone in a matrix of massive and vuggy (moulds after former sulphides), fine-grained hematitic material identical to the material interlayered with chert.

Type 3 ironstone comprises chert that is interlayered (decimetre to m-thick layers) with sheared, hematite (sulphide)-impregnated sediments including: (1) hematitic shale, (2) brecciated shale with shale fragments in a massive hematitic matrix, (3) conglomerate with pebbles partly leached or replaced by iron oxides, and (4) quartzose sandstone at the top of the succession, where, in thin section, the quartz grains are partly replaced by chert or are fractured along hematite-filled veins (Fig. 3.5b). At one locality, silicified and hematized quartzose sandstone is intercalated with brecciated ironstone and massive hematite-rich rock containing chert lenses (Fig. 3.5c). The latter contains isolated quartz clasts that are identical to the constituents of the adjacent sandstone, indicating that the hematitic rock represents silicified and hematized primary sandstone. It is important to note that iron oxides in the ironstones and associated rocks are derived from the weathering of sulphides, mainly pyrite, which do occur in less weathered rocks or in the subsurface such as at Agincourt Mine.

Ironstones are locally cut by layer-parallel to irregular vein networks of quartz and hematitic material. Quartz veins are commonly intruded and brecciated by hematitic veins. Locally, intense brecciation gave rise to angular vein quartz fragments enveloped in a matrix of massive hematitic rock. Chert veins, similar to those forming layers in banded cherts, are locally preserved as intrusive layers in brecciated cherts.

Shale adjacent to ironstone horizons is ferruginized, strongly foliated to sheared, and complexly folded where it contains chert layers. Anastomosing shear zones are common. Sandstone beds within shale are locally disrupted into irregular geometries. These sandstone inclusions are

ellipsoidal to lenticular in shape and are commonly intruded by massive, clayey material, suggesting plastic behaviour of adjacent shales during disruption. Limestone intercalated with ironstone shows various stages of replacement by chert and hematitic material parallel to bedding and along fractures. Ironstone horizons adjacent to or intercalated with limestone breccia partly interfinger with the breccia. These ironstones are predominantly made up of brecciated cherts and locally contain limestone clasts.

The compositional layering of the banded cherts is defined as S_1, since it locally truncates S_0. High strain zones up to 2 m wide of strongly foliated graphitic shale occur within and along the margin of banded chert horizons and are subparallel to the layering in banded chert. A lineation (L_1) is locally preserved as striations, mineral fibres or as a mineral stretching lineation (e.g., quartz/calcite rods).

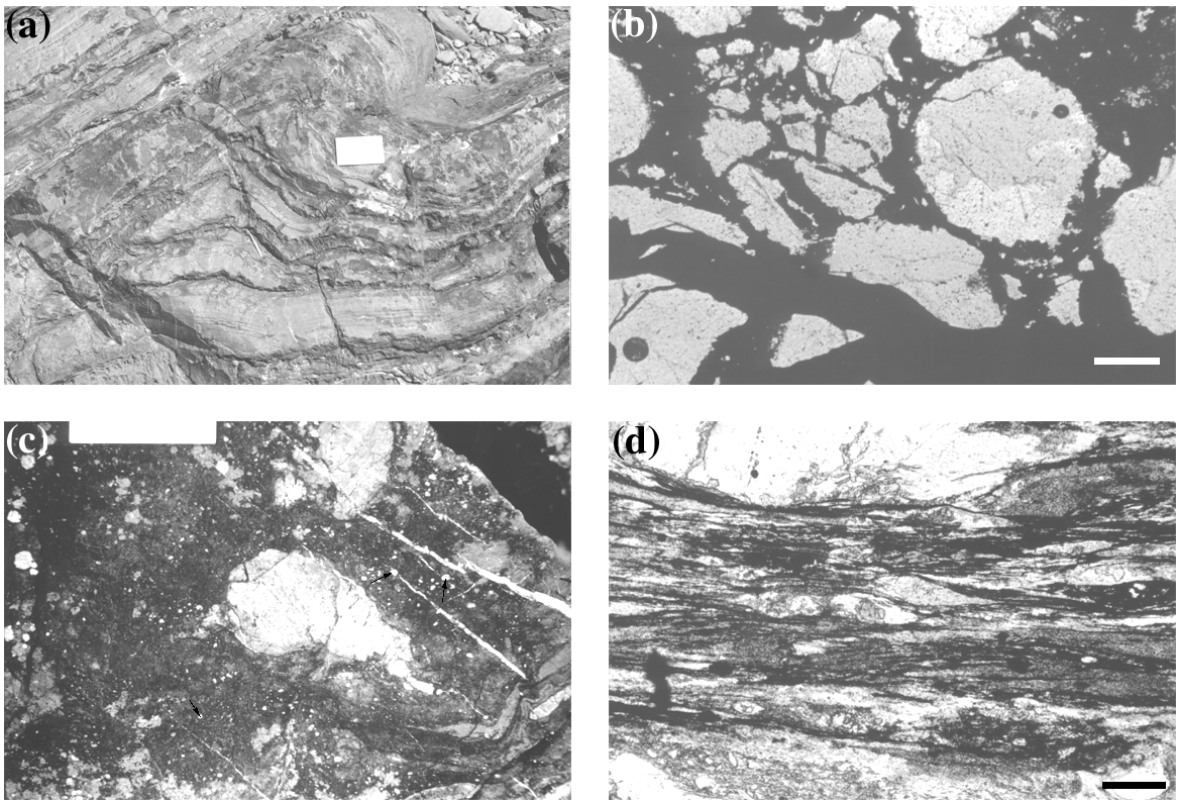

Fig. 3.5. Features of ironstone and sheared sediments. (a) Asymmetric fold in banded chert (type 1 ironstone) at the top of the Cheshire Formation. Note the lenticular chert layers in fold hinge (centre) which are sheared out away from the hinge zone (left). (b) Photomicrograph (plane-polarized light) of ferruginized quartzose sandstone. Brecciated quartz grains are intruded by opaque material, mostly hematite. Scale bar is 200 μm. (c) Ironstone consisting of disrupted banded cherts (lower right), an irregular-shaped disrupted chert lense (centre) and massive hematite-rich rock (left). White spots (arrows) are quartz granules, indicating that the protolith was a quartzose sandstone. (d) Photomicrograph (plane-polarized light) of mylonitic mudstone from Zeederbergs-Cheshire contact. Lens-shaped quartz aggregates are derived from the disruption of quartz veins. Scale bar is 200 μm.

Ironstones in relation to tectonic contacts and stratigraphic duplications, lower Cheshire Formation

The contact between the Zeederbergs volcanics and the Cheshire sediments is directly exposed at several localities where major ironstone horizons are absent (Table 3.2). The contact is variably sheared (Fig. 3.5d), silicified, and sulphide-mineralized with the sulphides mostly replaced by iron oxides. The strike of the contact is parallel to the stratification and parallel to S_2 in both basalts and sediments. Alteration effects due to sulphide mineralization and silicification decrease away from contacts, indicating that the alteration probably resulted from mineralized fluids infiltrating the contact zone during shearing. In the southwestern part of the Cheshire outcrop the contact was exploited for gold at Agincourt Mine (Fig. 3.3). This mine is situated in strongly foliated and graphitic shales intercalated with tectonic ironstone. The gold mineralization has been interpreted as shear zone-hosted (Worst, 1956).

Table 3.2. Description of contact relationships between the Zeederbergs and Cheshire Formation.

Location*	Lithology	Attributes
A	Hyaloclastite sharply overlain by 20 cm thick mylonitic mudstone	Hyaloclastite is Fe-impregnated; mudstone is silicified and characterized by a mylonitic foliation, lens-shaped quartz aggregates, and shear bands (Figure 5d)
B, C	Basalt sharply overlain by 50 cm thick ironstone overlain by conglomerate	Ironstone is a strongly foliated, graphitic, iron oxide and sulphide-impregnated rock
D	Vesicular basalt sharply borders on 1 m thick ironstone grading into shale	Basalt with 0.5-5 cm wide, anastomosing zones of cataclasite; ironstone is a hematite-impregnated sulphidic mudstone; degree of Fe-enrichment/sulphide mineralization in shale decreases away from the contact over a few meters
Others	Basalt-conglomerate (unexposed)	Conglomerate near contact is transected by an irregular network of hematite/ goethite-filled cracks; clasts are replaced by iron oxides (after former sulphides)
	Basalt-shale (unexposed)	Contact can be inferred from the presence of an Fe-enriched transition zone (5-10 m wide) in shale which is brecciated by hematite-filled vein networks

*see Figure 3.3 for localities

The tectonic significance of some of the ironstones can be clearly illustrated along the eastern Zeederbergs-Cheshire Formation contact (Fig. 3.6a) where pillow lavas sharply border on conglomerate. The conglomerate pinches out and grades into shale to the north. The contact between basalt and shale is occupied by an ironstone horizon which can be traced continuously in the mapped area. Lenticular bodies of ironstone further occur adjacent to the contact. Bedding is locally at an angle to and transected by ironstone, indicating that the ironstones are situated along shear zones (Fig. 3.6b).

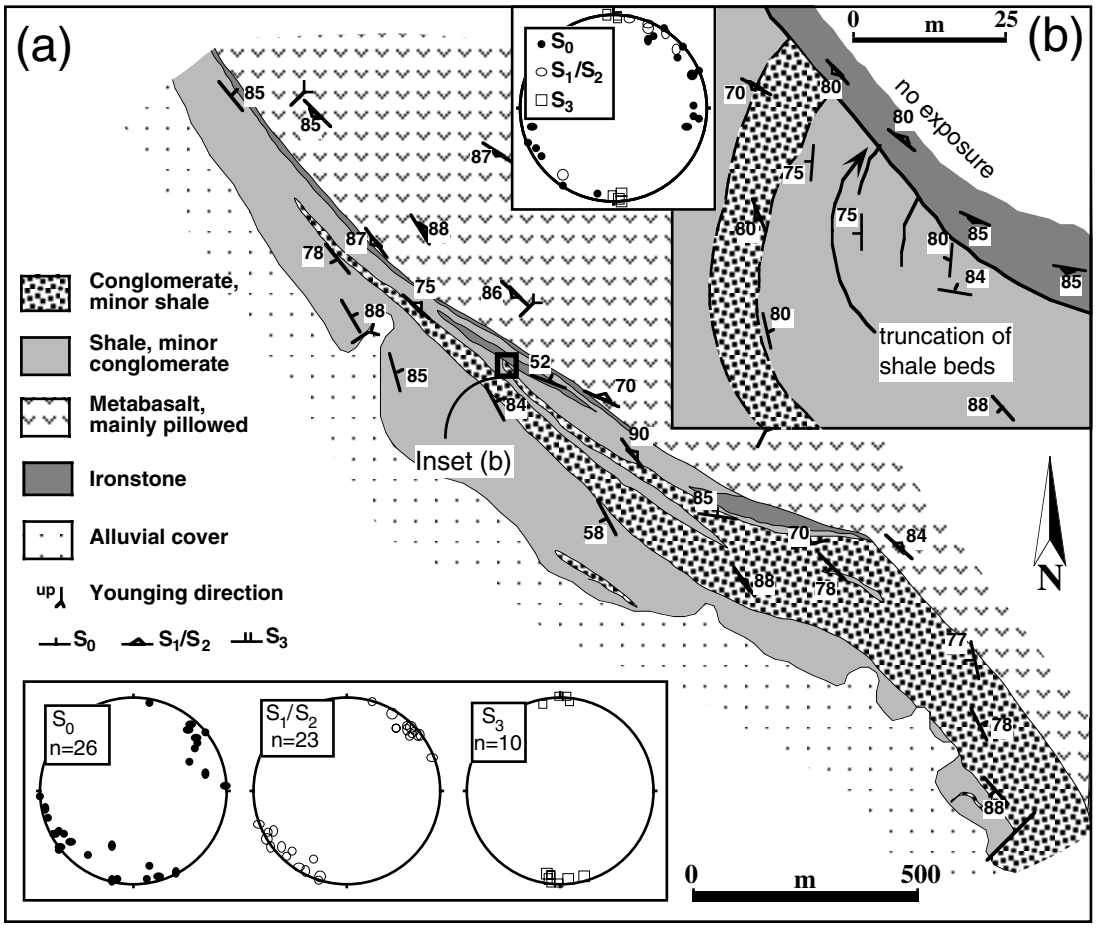

Fig. 3.6. (a) Detailed map of the eastern Zeederbergs-Cheshire contact (refer to Figure 3.3 for location). Lower hemisphere stereographic projections of bedding and foliation data are shown. Note the occurrence of lenticular ironstone horizons. (b) Bedding is locally transected by ironstones.

The relationship between ironstones and shear zones can also be demonstrated along the western contact, where pillow lavas are overlain by cyclical carbonates with limestone breccia at the top(Fig. 3.7). The breccia outlines an irregular karstic relief occupied by conglomerate and shale layers which are truncated by ironstone (Fig. 3.8a). The ironstone is overlain by a mélange zone (see below) in which S_0 is locally tight to isoclinally folded and transected by the overlying volcanic unit. Discontinuous ironstone horizons are developed along this contact and medium-scale, tight to isoclinal folds are common in shale adjacent to the contact. A second unit of locally brecciated carbonates overlies the volcanics and is completely bounded by ironstone. Structural fabrics such as S_0, S_2, L_2, and S_3 (Fig. 3.9, described below) have a similar orientation to similar fabrics within the rest of the Cheshire Formation (Fig. 3.4). Stratigraphic younging directions in the above sequence all point to the east except within folded horizons in the mélange zone. This contradicts previous studies, interpreting the volcanics-bounded carbonate unit as a synclinal structure and the intervening outcrop of Zeederbergs rock as an anticline (Martin, 1978; Bickle et al., 1993).

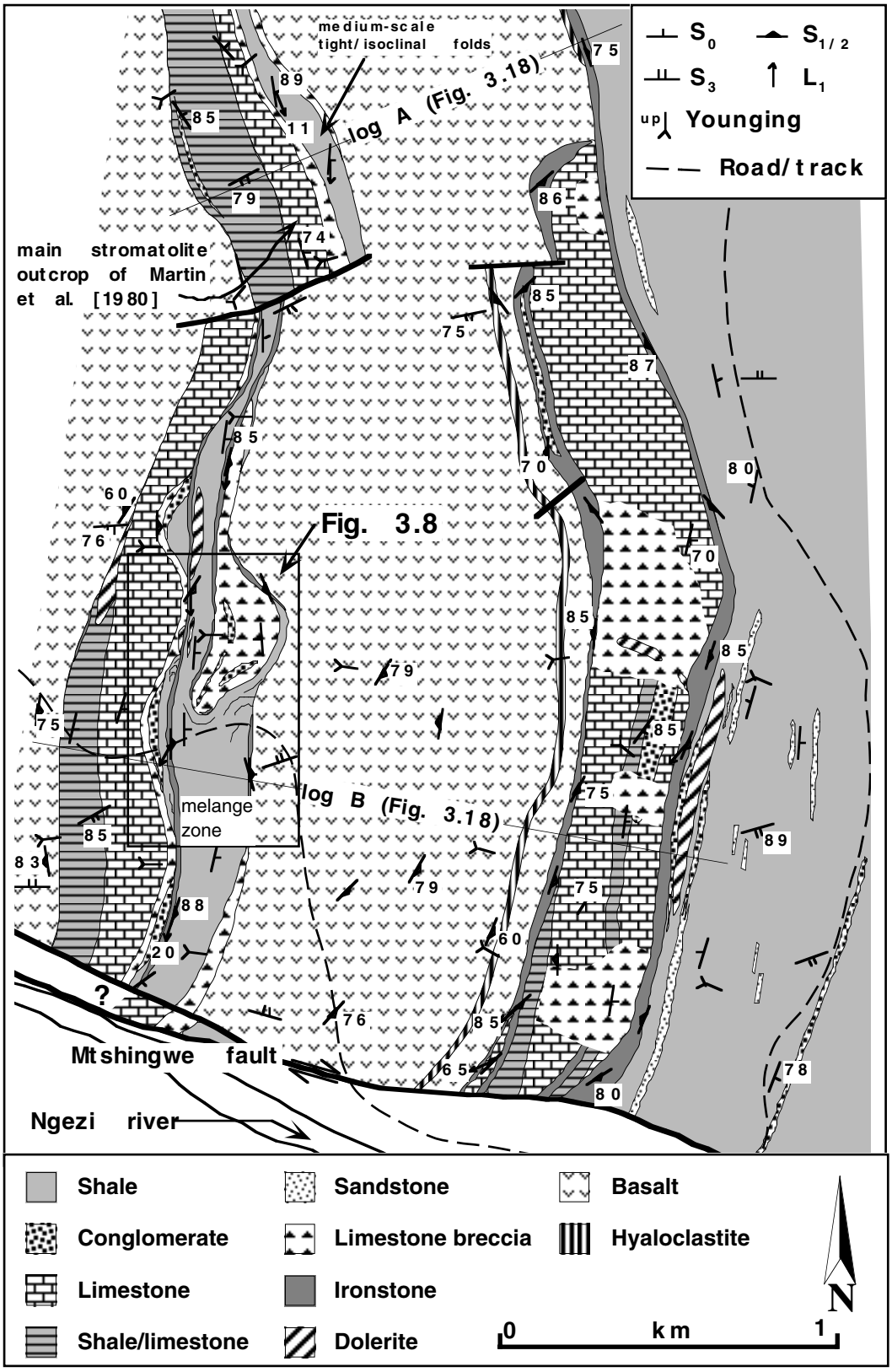

Fig. 3.7. Detailed map of the western Zeederbergs-Cheshire contact (refer to Figure 3.3 for location). Stereographic projections of structural data are shown in Figure 3.9. Note the ironstone which completely surrounds the carbonate unit in the eastern part of the map. The area south of the Mtshingwe fault comprises intercalated conglomerate and shale.

A mineral lineation (L_1) is locally preserved in the ironstones along the western contact. L_1 plunges at moderate to shallow angles to the south (Fig. 3.9). The lineation is parallel to the fold axes of small- to medium-scale folds in the mélange zone. The shallow plunge of the lineation and colinear fold axes in the deformed zone is inconsistent with D_2 as the cause of shearing. Furthermore, the lineation cannot be attributed to D_2, because it is restricted to certain lithotectonic units which show evidence for early, soft-sediment deformation (see below). Pre-D_2 data restoration of L_1 results in a southeasterly subhorizontal lineation (Fig. 3.9), which is interpreted to reflect the tectonic movement direction along the ironstone horizons during D_1.

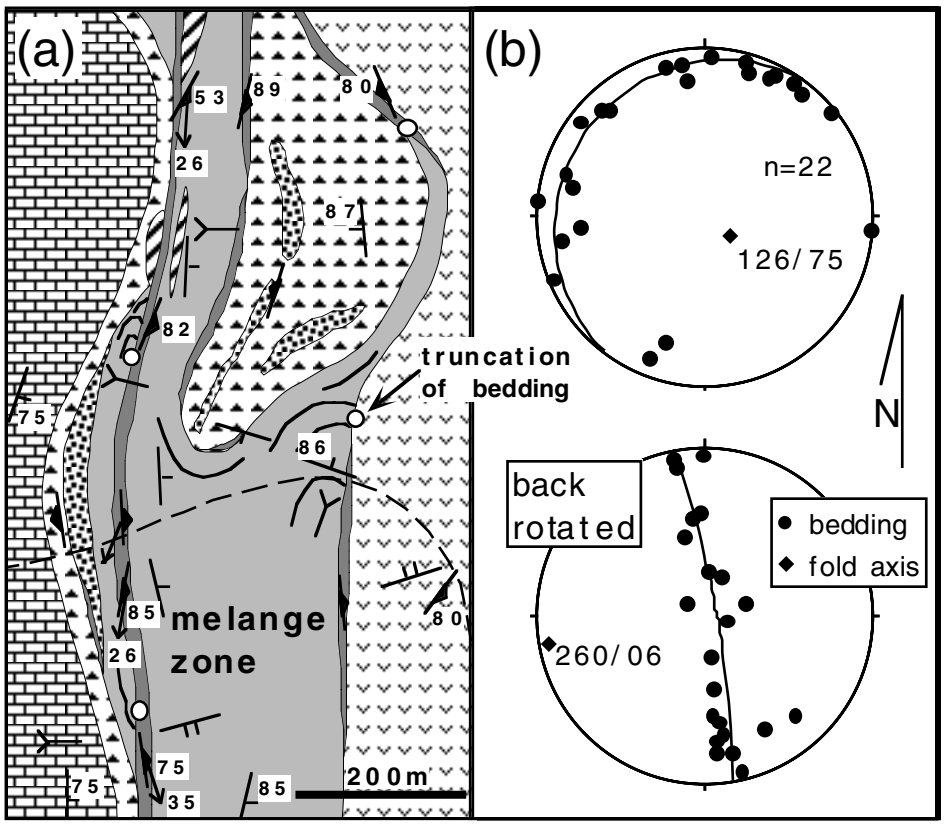

Fig. 3.8. (a) Enlargement of an area shown in Figure 3.7. Note the truncation of bedding along tectonic contacts. (b) Lower hemisphere stereographic projection of bedding measured along the hinge zone of the isoclinal fold and the same data back rotated to a pre-D_2 situation. Refer to Figure 3.7 for key of lithologies.

Tectonic ironstones, upper Cheshire Formation

Ironstone horizons are again common at the top of the sedimentary sequence (Fig. 3.3) above a unit of quartzose sandstone. The ironstones are similar in appearance (mostly types 1 and 3) to those developed along the lower contact with the Zeederbergs Formation and are complexly folded. They generally form 0.4-10 m thick horizons that are intercalated with hematitic shale and massive hematitic mud- to sandstone. Three major ironstone horizons are continuous throughout the central Cheshire Formation.

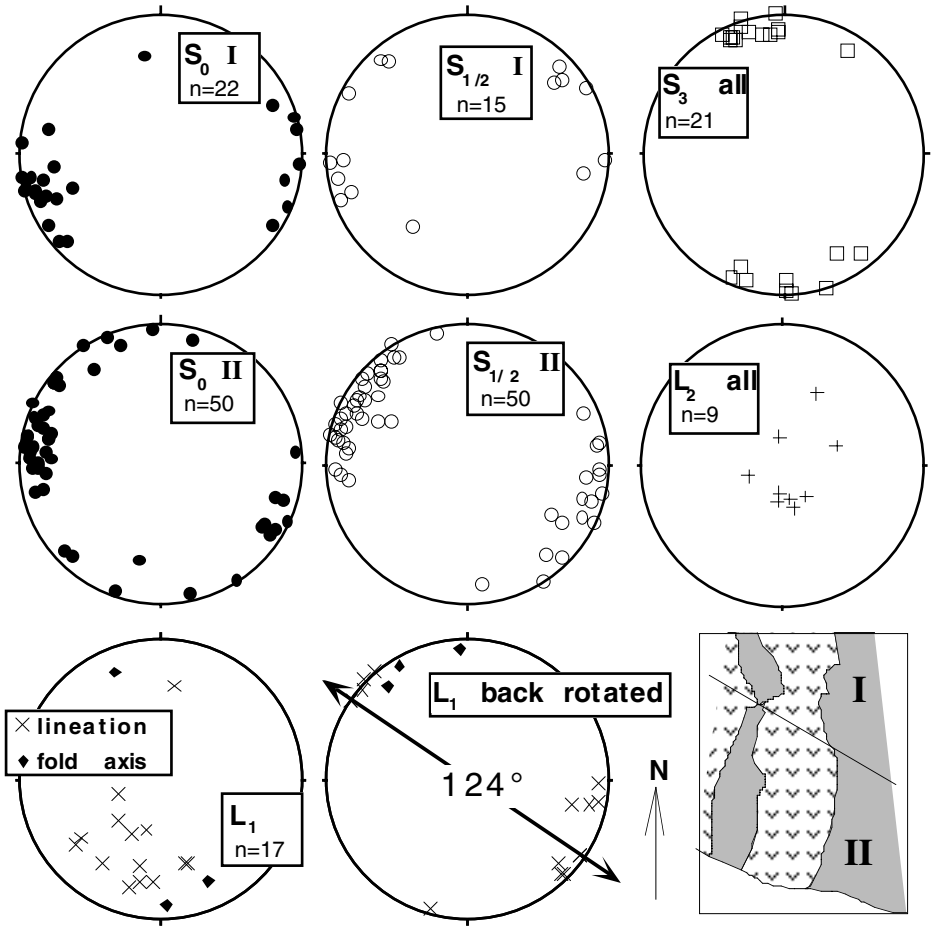

Fig. 3.9. Lower hemisphere stereographic projections of bedding, foliation, and lineation data from the area shown in Figure 3.7. Outcrop has been divided into two domains I and II to account for reorientation of structural elements during D_3. L_1 data include mineral lineations and fold axes of medium-scale folds (see Figure 3.7); pre-D_2 restoration gives rise to subhorizontal L_1 with a mean bearing of 124°.

The presence of ironstones in the central part of the syncline, i.e., at the top of the preserved sedimentary sequence, and their complex folding (Fig. 3.5a) need explanation. The presence of ironstone in the core of the D_2 syncline makes them prone to a structural overprint during D_2 such as parasitic folding. However, soft-sediment deformational structures in intercalated shales point to deformation during D_1. In order to constrain the nature and timing of deformation, fold axes and axial planes of small-scale folds within several horizons were measured (Fig. 3.10). The folds are commonly asymmetric with both Z- and S-geometries present in single horizons, but symmetric, partly vertical to reclined isoclinal folds also occur. The orientation of Z- and S-folds, symmetric folds, and associated fabrics is similar. Fold axes of the different horizons predominantly plunge towards the west, whereas axial planes have a variable strike and are steeply dipping.

Pre-D_3 restoration of fold data (Fig. 3.10) shows variably striking, steeply dipping axial planes, and moderately to steeply plunging fold axes both to the north and south. The fold axes orientations are inconsistent with parasitic folding related to D_2, since the plunge of the D_2 syncline axis in the central part of the Cheshire outcrop is expected to be subhorizontal (see below). Pre-D_2 restoration

results in subhorizontal fold axes with an east-southeast bearing. This orientation is identical to the restored orientation of L_1 in the basal ironstones (Fig. 3.9). Axial planes are variably dipping to the north and south and define a small circle distribution with the pole plunging shallowly to the east, much similar to the average orientation of the fold axes. These relationships together with the geometry of the folds suggest that the fold style is similar to sheath folds which formed during D_1, probably as a result of layer-parallel thrusting.

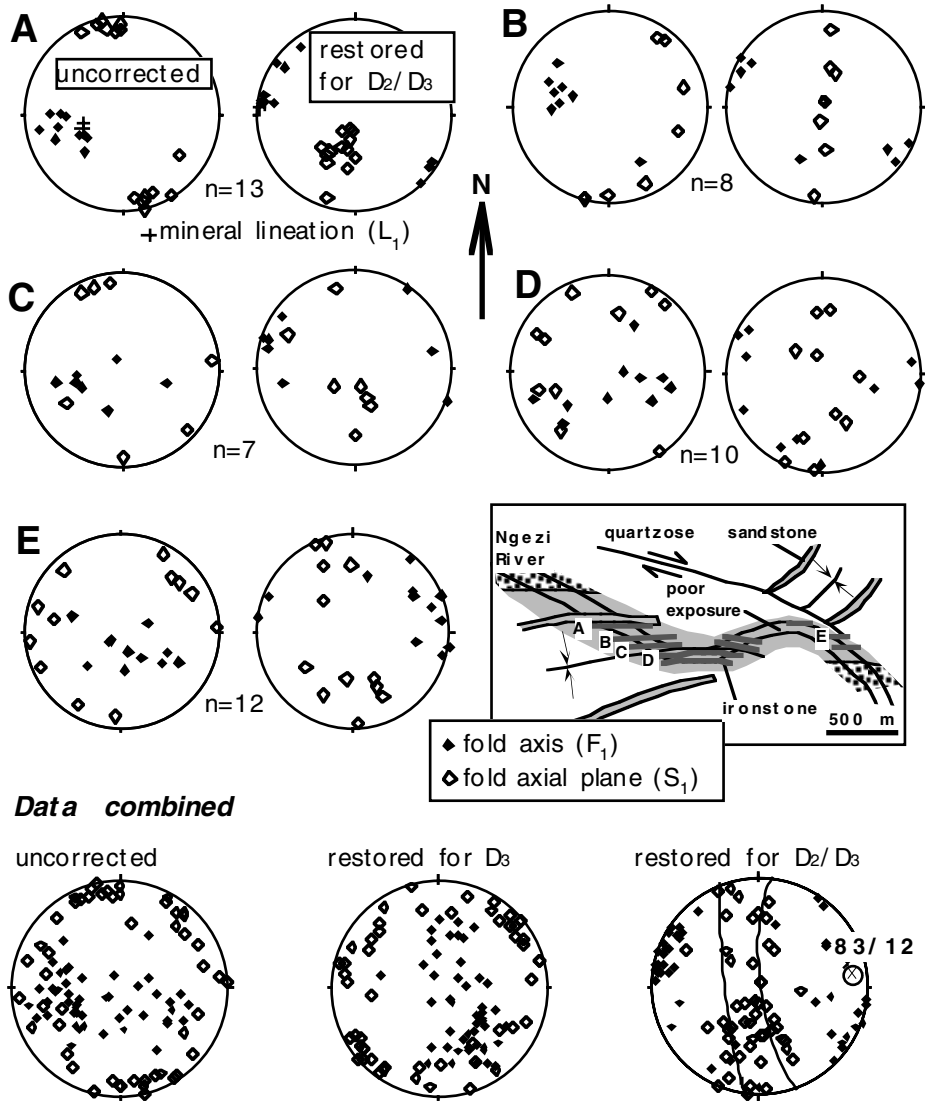

Fig. 3.10. Lower hemisphere stereographic projections of fold axes and axial planes (and mineral lineations in A) of five ironstone horizons (A-E) exposed in the central part of the Cheshire Formation in the Ngezi river (refer to Figure 3.3 for location). All the data combined have been corrected separately for D_3, and $D_{2/3}$.

Interpretation of ironstones as D_1-shear zones

The ironstones in the Cheshire Formation have previously been interpreted as deformed sedimentary banded iron formations (Martin, 1978). The ironstones commonly occupy lithological

contacts where there is clear evidence of shearing and stratigraphic duplication, and, locally, truncate bedding of surrounding sediments. Additionally, intercalated sediments are strongly sheared in places and show evidence that shearing took place prior to solidification. On the basis of these observations the ironstones are interpreted as rocks which gained their lithological characteristics during D_1.

The restricted occurrence of silicified and hematized sedimentary rocks in the vicinity of shear zones indicates that silica and iron were introduced after deposition during shearing. Also, more intensely sheared rocks appear more strongly hematized. Along the Zeederbergs-Cheshire contact ironstone is common at basalt-shale contacts, but it is rare at basalt-conglomerate contacts. The formation of ironstone can therefore be attributed to in situ silicification and iron(sulphide)-impregnation of predominantly fine-grained sediments (shale) by mineralized fluids adjacent to and within fault zones. Sandstone beds within shale may have been transformed into chert upon silicification, whereas clay-rich interbeds became preferentially ferruginized. However, ironstones probably formed from a variety of rock types as indicated by the replacement of limestone. In addition, a certain amount of chert and, in particular, hematitic rock represents newly formed, intrusive material as indicated by bedding-parallel and cross-cutting veins. Intrusion and hydraulic fracturing gave rise to brecciation of the banded rocks.

Most of the lithological aspects of ironstones and the deformation recorded in them such as tight to isoclinal folding is related to D_1, suggesting that ironstone formation took place syntectonically with D_1. The chert components were deformed in a brittle-ductile manner as indicated by brecciation on the one hand and boudinage, tight to isoclinal folding and sheath folding on the other, indicating that the chert precursor may have varied in the state of consolidation (cf. de Wit, 1982). Variable fluid pressure may have also played a role.

Mélange-like shear zone

The most prominent of the D_1 shear zones occurs at the stratigraphic top of the western outcrop of the carbonate member (Fig. 3.7) between a limestone breccia and structurally overlying basalts of the Zeederbergs Formation (Fig. 3.11). This shear zone is termed mélange zone (in the sense of Cowan, 1985; broken formation of Hsü, 1968, Raymond, 1984), since it is represented by a locally chaotic mixture of rock fragments enveloped by a sheared, fine-grained matrix.

At the Ngezi river section (Fig. 3.11) the mélange zone is ~50 m thick and comprises a deformed sedimentary sequence that preserves a spectrum of progressive stratal disruption. The stratigraphically lower 20 m of the mélange zone comprises a less disturbed succession of shale and conglomerate and overlies the limestone breccia along a sheared contact (Fig. 3.11). This grades into a more strongly deformed unit that consists of 0.5-10 m wide stratiform horizons of highly disrupted sediment that are intercalated with less deformed layers. Various lithologies are complexly intermingled and form lenticular inclusions (see Byrne, 1984) in a strongly sheared argillaceous matrix (Fig. 3.12a). The disrupted layers become more abundant upsection, but the uppermost few

metres of the mélange zone are slightly less deformed. The sediment-basalt contact is occupied by a 50 cm thick, massive, fine-grained cherty sediment containing disseminated sulphides. Basalt adjacent to the contact is strongly foliated and shows striations.

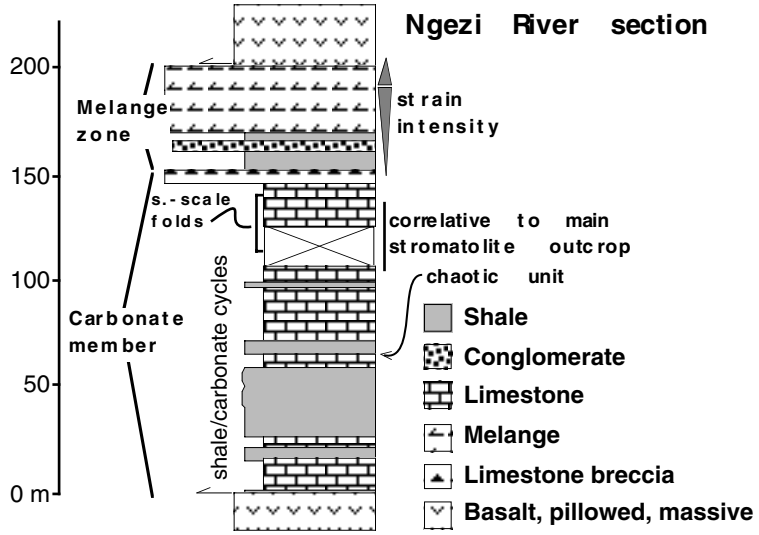

Fig. 3.11. Graphic log of the carbonate member and overlying mélange zone measured in the Ngezi river. The carbonate member consists of metre-scale shale/carbonate cycles. The uppermost limestone-dominated unit is correlative to the main stromatolite outcrop (Fig. 3.7) and is overlain by limestone breccia. The occurrence of small-scale folds and a chaotic unit as described in the text are indicated.

Inclusions in the mélange zone range from a few millimetres to a few metres in length. They include (1) limestone and dolostone, (2) clast-supported, basalt pebble conglomerate or individual pebbles, (3) massive sandstone, (4) chert probably representing silicified silt- to fine-grained sandstone, (5) massive mudstone/shale which commonly contains intermingled matrix material, (6) shale with boudinaged sandstone intercalations (Fig. 3.13a), (7) amoeboidal, massive siltstone clasts, some of which are broken and intruded by clayey matrix material (Fig. 3.13b), and (8) rare vein quartz fragments. Mud-rich inclusions have an irregular geometry, whereas others are mostly lenticular in cross-section. Along strike, less deformed sedimentary beds pinch-and-swell and, laterally, become boudinaged and cut by extensional shear zones thus forming isolated inclusions (Fig. 3.12a). Lensoid inclusions are commonly sigmoidal and have "tails" that taper out in the plane of foliation. Some of the inclusions show folding of primary bedding and represent rootless tight folds. In some horizons, inclusions are mostly angular fragments of dolomitic shale and irregular-shaped, massive mudstone forming up to 100 cm thick bedding-parallel breccia horizons. These are bounded by, and internally exhibit, anastomosing shear zones suggestive of a deformational origin for the breccias.

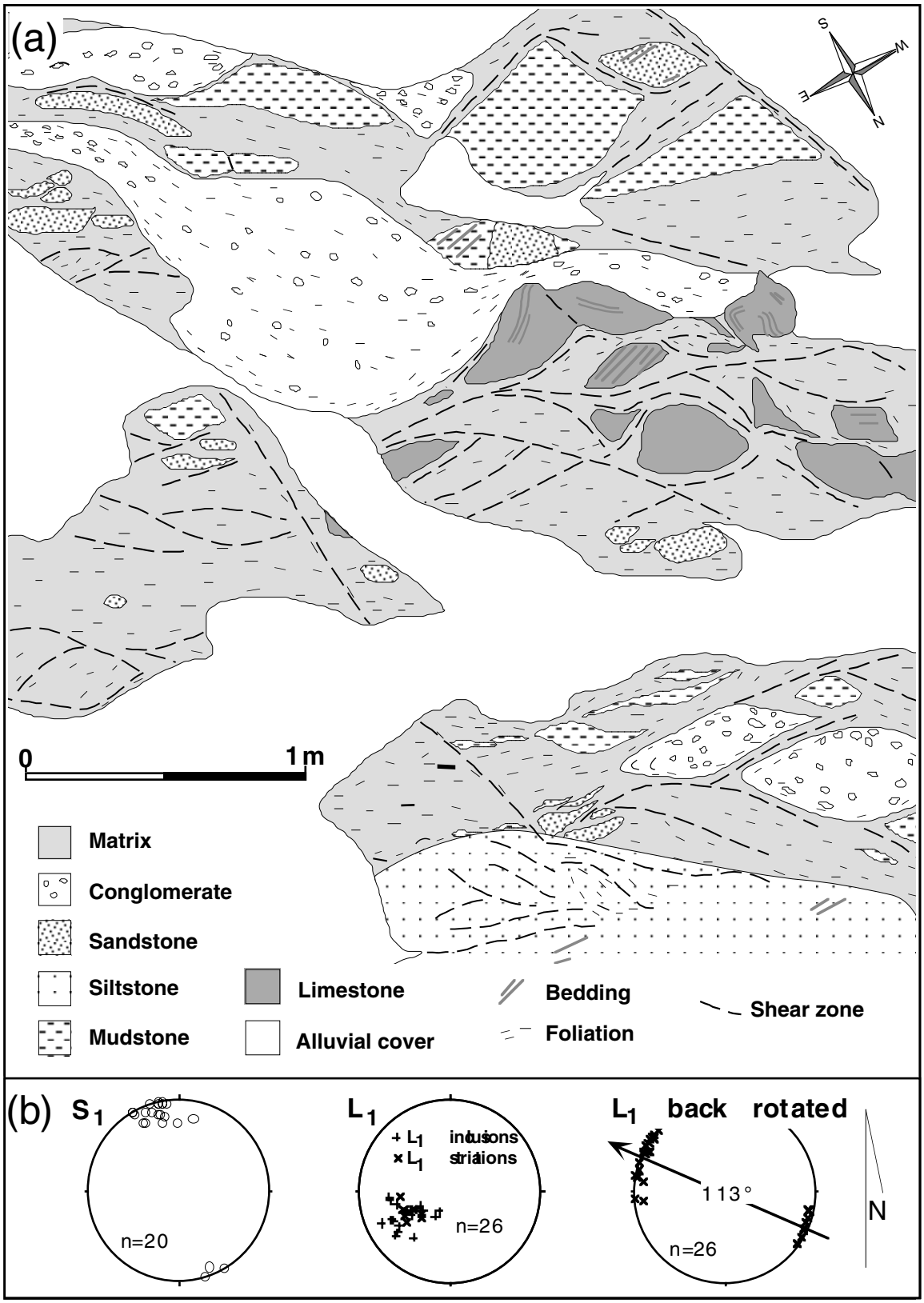

Fig. 3.12. (a) Detailed map of a selected area of the mélange zone. Lenticular inclusions of various rock types occur in a sheared argillaceous matrix. Note the boudinage of limestone inclusions along extensional shear zones. (b) Lower hemisphere stereographic projections of S_1 and L_1 data. L_1 is defined by the elongation of inclusions and by striations both in the mélange zone and overlying basalts. Restoration of L_1 gives a mean orientation of 113° for tectonic transport, which is towards the west-northwest, taking kinematic indicators into account.

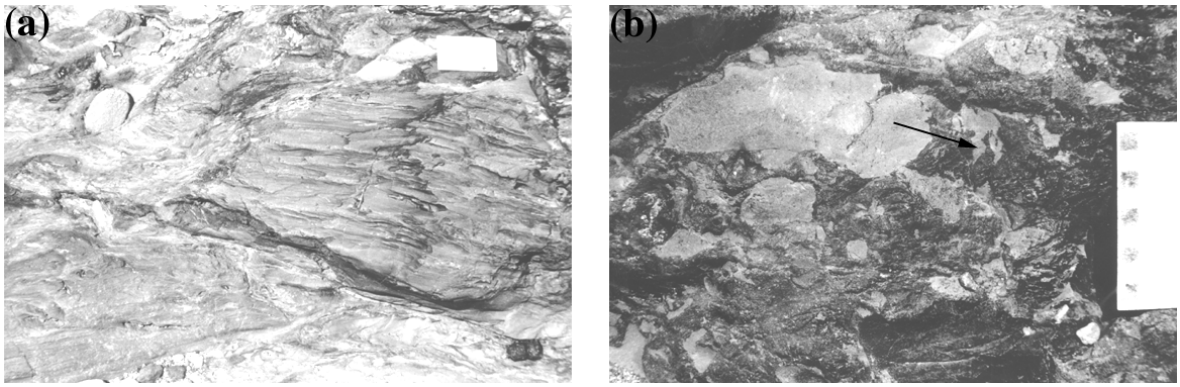

Fig. 3.13. Features of the mélange zone. (a) Shale inclusion (right) in the mélange zone. (b) Very irregular siltstone inclusions which are intruded by muddy matrix material (arrow).

The matrix is a sheared, argillaceous rock that is locally cherty and contains disseminated sulphides. Siltstone inclusions in the muddy matrix have very irregular, partly amoeboidal shapes, indicating that both siltstone and mudstone were not fully consolidated during deformation (Fig. 3.13b). Locally, silt- and mudstone are so intimately mixed that one forms irregular domains completely surrounded by the other, suggesting sediment mobility and fluidisation during deformation of only partly dewatered silts and muds. Basalt pebbles are scattered in the matrix and are derived from the disruption of conglomerate beds. The heterogeneous matrix material partly forms lenticular-shaped, shear zone-bounded objects which are surrounded by even more deformed matrix material, indicating that deformation was a progressive process.

A subvertical east-northeasterly striking planar fabric (S_1) is defined by the lithological layering and the alignment of inclusion trails forming a pseudostratigraphy. Primary bedding (S_0) can be identified where the mélange zone grades into less disrupted rocks and in less disrupted horizons within the zone. S_0 can also be recognized in several inclusions in which the internal layering has been rotated by 25° to 40° away from S_1 in either a clockwise or, less frequently, counter-clockwise direction (Fig. 3.12a). Shale horizons in between sheared units are locally tightly folded with S_1-parallel foliation domains cutting S_0 in fold hinges.

Both matrix material and mud-rich inclusions preserve a weak cleavage. This cleavage is attributed to D_1, but it was later overprinted by S_2. L_1 is defined by the elongation of inclusions as well as striations in the matrix and plunges at moderate angles towards the southwest (Fig. 3.12b). Anastomosing shear zones of various scales (from microscopic to outcrop-scale) occur in the matrix throughout the mélange zone. They are typically <1 cm wide, generally subparallel to S_1, and are most pronounced along inclusion margins (Fig. 3.12a). The shear zones partly truncate S_1 fabrics, indicating that they formed during a late stage of D_1. Kinematic indicators such as clast asymmetry, the common clockwise rotation of inclusions, and the bending of layering into shear zones are consistent with a sinistral movement direction with a reverse component (south-over-north) of the hanging-wall rocks along the mélange zone.

The structural features preserved in the mélange zone indicate noncoaxial deformation and stratal disruption of originally unconsolidated to semi-consolidated sediment. This shearing can be best explained by movement of the overlying Zeederbergs-type volcanics relative to the carbonates shortly after their deposition. Restoration of L_1 data gives an original WNW-ESE striking lineation (Fig. 3.12b). This data combined with the observed movement direction along the mélange zone suggest a west-northwest-directed transport direction of the mafic volcanics at the time of movement. The origin of the mélange as an olistostrome is not as likely because of the progressive noncoaxial deformation mechanism, the allochthony of the overlying unit, and the tectonic transport direction in relation to the inferred palaeoslope (see below). Furthermore, deformation can not be attributed to the D_2-event that formed the synclinal structure of the belt, e.g., by inner-arc thrusting of the western limb during folding, for several reasons: (1) the lineation should strike perpendicular to the fold axis of the syncline, i.e., ENE-WSW instead of WNW-ESE; (2) deformation would have affected already consolidated sediments due to the overlying sediment load and not unconsolidated to semi-consolidated sediments; (3) D_2 occurred at a higher metamorphic grade and was associated with the formation of a penetrative cleavage (see below).

The mélange zone continuously underlies the inlier of Zeederbergs volcanics and predominantly comprises variably deformed shales, but exposure is generally poor away from the Ngezi river section. In one area (Fig. 3.8a) the mélange zone mainly comprises shale and brecciated limestone, is variable in thickness, and shows tight to isoclinal folds. An isoclinal fold of brecciated limestone and intercalated conglomerate has a fold axis that is steeply plunging towards the southwest (Fig. 3.8b). Back rotation of S_0 data from the isoclinal fold gives a subhorizontal fold axis which shallowly plunges to the west-southwest (Fig. 3.8b). The orientation is much similar to the orientation of other F_1 folds developed locally in the carbonate member (discussed below). Folding is most probably related to the movement of the structurally overlying volcanics.

Soft-sediment shear zones, folds and carbonate breccias

The carbonate member shows D_1 structural features such as (1) sheared shale horizons and chaotic units, (2) disharmonic, open to closed folds, and (3) limestone brecciation. These have been investigated in detail at the Ngezi river section (Fig. 3.11).

Sheared shale and chaotic units

Shale horizons in the carbonate member are commonly deformed. A typical sedimentary cycle in the carbonate member consists of a lower part of shale intercalated with thin beds of sand/grainstone, and an upper part of limestone with rare shale beds. The clay-rich lower cycle portions are sometimes sheared; deformation becomes less pronounced in the upper cycle parts. Sheared shale horizons typically contain ellipsoidal sandstone inclusions, 3-40 cm in length and 0.5-5 cm thick, which are embedded in massive mudstone. Upper and lower inclusion margins are sharp, whereas the lateral margins are commonly diffuse and partly ragged. The inclusions have

both sigma and delta shapes (Fig. 3.14a); some inclusions bear geometries similar to mica fish structures; others represent tight rootless folds. In places, inclusions converge from bedding-parallel inclusion trails through pinching-and-swelling layers to tabular continuous beds, indicating that they originated from boudinaged sedimentary strata. Sandstone and, particularly, limestone beds exceeding ~5 cm in thickness, however, rarely show deformational features. On the other hand, thin shale beds bounded by thick sandstone or limestone beds are commonly strongly sheared (Fig. 3.14b). This is indicated by the occurrence of asymmetric, lenticular inclusions and transposed quartz and calcite veins. One sandstone bed intercalated with sheared shale has been observed to form a duplex structure (Fig. 3.15a). Other beds are transected by quartz/calcite-filled extension fractures (Fig. 3.15b). The fractures formed prior to compaction as indicated by differential compaction between non-fractured and fractured beds.

One stratigraphic interval of the cyclic succession is represented by a 2 m thick chaotic unit (Fig. 3.11). It comprises irregularly distributed lenticular rock fragments, up to 50 cm in length and 15 cm in width, in a muddy arenaceous matrix. The fragments include shale, dolomitized sandstone and limestone which are commonly complexly deformed and folded into isoclinal folds or folds with a closed outcrop pattern similar to sheath folds (Fig. 3.15c). Contacts of the chaotic unit to under- and overlying undeformed rocks are gradational.

The ductile deformation style of the sheared units together with the absence of an associated cleavage indicates that the sediments were not fully consolidated when shearing took place. Deformation preferentially affected more fine-grained, poorly dewatered cycle portions such as basal shale. The lack of deformation of relatively thick limestone beds can be attributed to early lithification of carbonates during or soon after burial. The asymmetry of inclusions and the occurrence of sheath folds indicate noncoaxial flow of the cyclical sedimentary stack prior to complete consolidation. The gradational nature of contacts between sheared horizons and chaotic units, and the undeformed rocks makes slumping as the cause of deformation unlikely. In addition, the general absence of a cleavage does not preclude deformation associated with tectonism, since tectonic deformation of unlithified sediments at low temperature (<200°-250°C) may result in uncleaved rocks with soft-sediment deformation-like features (Cloos, 1984).

Folds

At the main stromatolite outcrop (Fig. 3.7), gentle to closed folds deformed primarily horizontally stratified limestone and overprinted and accentuated domal stromatolites (Fig. 3.14c). Folding is indicated by a weak axial planar cleavage, cleavage fanning, and by the constant thickness of alternating stratiform stromatolite and siltstone beds in folded strata. The strike of the fold axial planes at the main stromatolite outcrop is east-northeast (Fig. 3.16a).

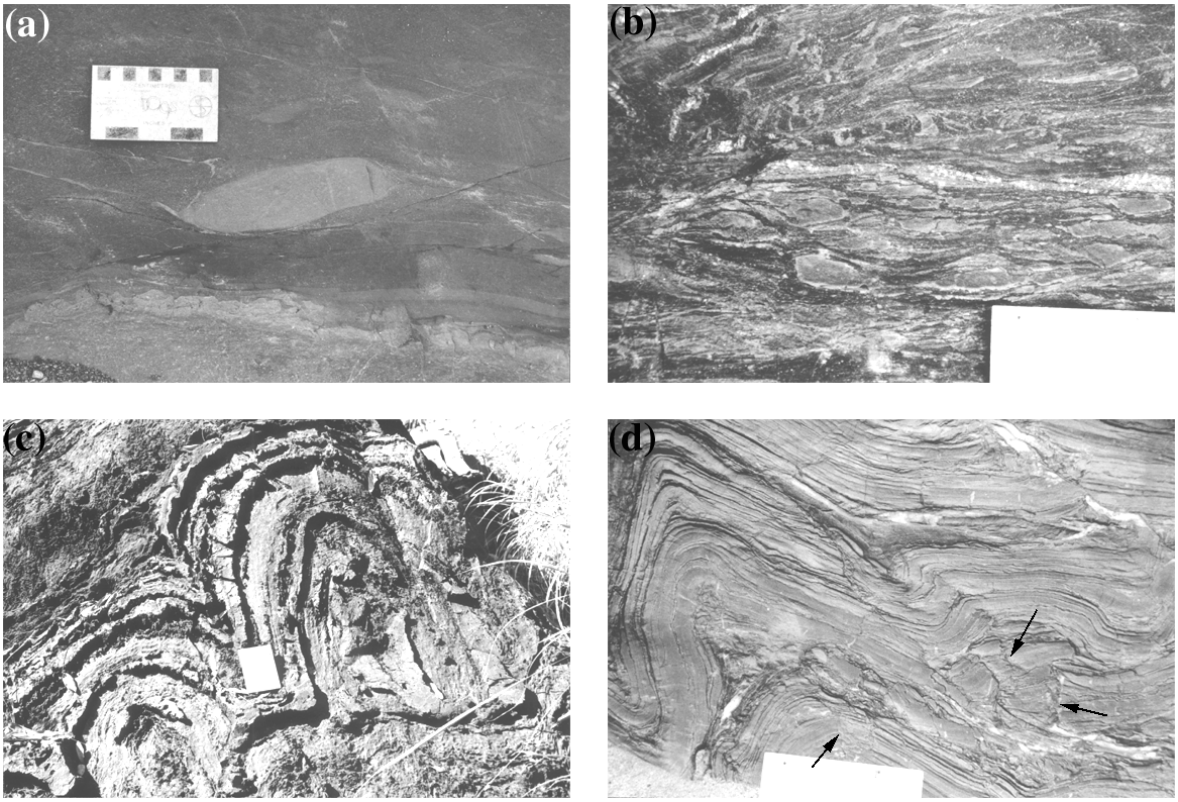

Fig. 3.14. Features of the carbonate member. (a) Asymmetric sandstone boudin in deformed shale. (b) Sheared shale with lenticular sandstone inclusions. (c) Stromatolitic limestone (mainly microbial laminites) overprinted by gentle to closed, upright folding (main stromatolite outcrop). (d) Small-scale asymmetric folds in flat-laminated limestone (Ngezi river section). Note mud-filled, axial planar and ptygmatically folded cracks (arrows).

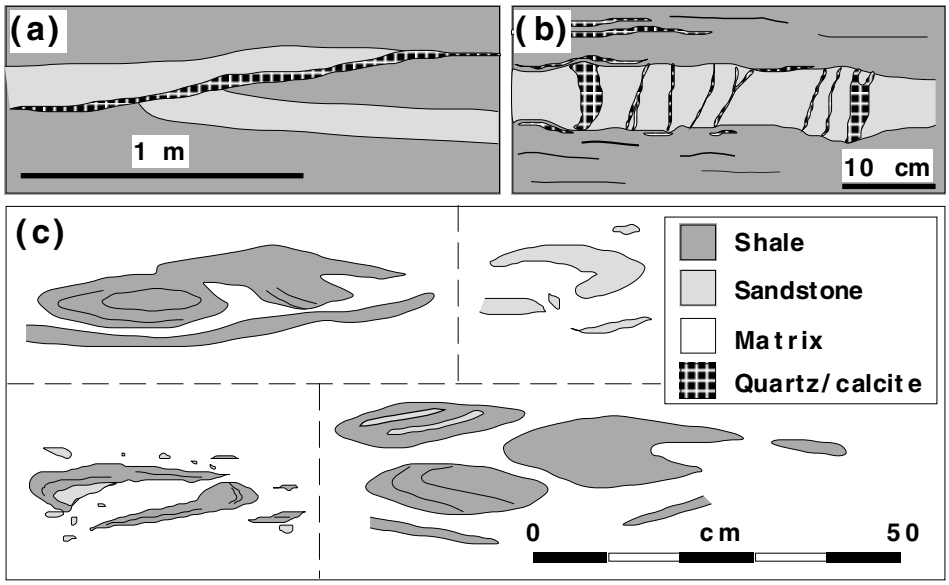

Fig. 3.15. Field sketches of structural features in the carbonate member. (a) Small-scale duplex structure. (b) Sandstone bed transected by pre-compaction quartz/calcite veins. (c) Examples of sandstone and shale inclusions in the chaotic unit.

At the Ngezi river section (Fig. 3.11), disharmonic, slightly asymmetric (z-shaped) open to closed folds are common in (and restricted to) the uppermost part of the cyclic limestone unit just below the limestone breccia. The strike of the axial planes is north-south (Fig. 3.16b). Folding affected beds of stromatolitic limestone, shale and silicified shale (now chert). An axial planar, spaced cleavage is present in the chert beds. Mud-filled, axial planar cracks cross-cutting the limestone beds are commonly associated with the folds. Cracks are sub-mm to 3 mm thick and are generally ptygmatically folded (Fig. 3.14d). Minor axial planar faulting is associated with folding. Fault planes are intruded by ptygmatically folded mud.

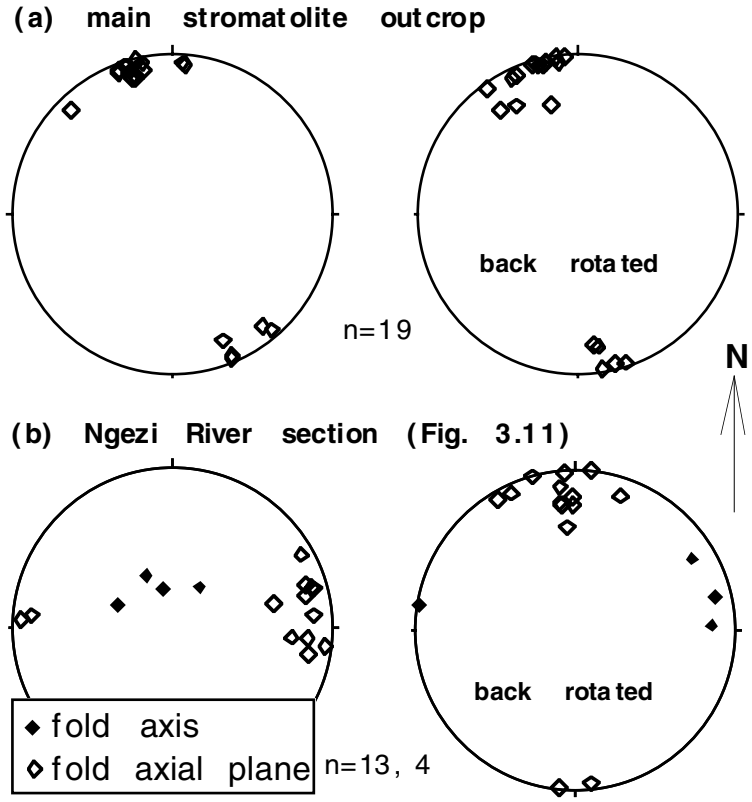

Fig. 3.16. Lower hemisphere stereographic projections of fold axial planes and fold axes of gentle to closed folds from (a) the main stromatolite outcrop (Fig. 3.7) and (b) the top of the carbonate section exposed in the Ngezi river (Fig. 3.11). Fold axes have only been measured at the Ngezi river section. Pre-D_2 restoration of the data yields east to east-northeast striking axial planes for both localities.

The strike of the axial planar cleavage of folds at the main stromatolite outcrop is identical to the strike of S_3 measured elsewhere (Fig. 3.4), and the folds could therefore be F_3 folds. However, the strike of the cleavage at the Ngezi river section is markedly different from S_3. The ptygmatic folding of mud-filled axial planar cracks indicates that folding must have occurred prior to compaction and, hence, lithification. Slump folding can be ruled out since the folding affects several beds, and the folds are disharmonic and not restricted to a deformed zone in between undisturbed beds. The folds occur in a relatively homogeneous unit of stromatolitic limestone at the top of the carbonate sequence just below the overlying limestone breccia and mélange zone. Underlying strata (sheared

shale horizons) and overlying strata (mélange zone) show evidence of noncoaxial shearing. Stress during movement on bounding shear zones may have resulted in folding of the limestone unit. After pre-D_2 data restoration, axial planes at both localities are steeply north-northwest verging (Fig. 3.16); this is a similar orientation to the fold structure in the mélange zone (Fig. 3.8a). Assuming that the folds developed in the limestones can be used as kinematic indicators for the overlying shear zone, and that the transport direction is towards the direction of fold vergence, the movement direction of the hanging-wall units is towards the north-northwest.

Limestone breccia

Brecciated limestone is a common component of the carbonate member. A laterally continuous but irregular, 10-20 m thick breccia horizon is situated at the top of the cyclic carbonate unit and below the mélange zone (Fig. 3.7, western unit; Fig. 3.11). In the eastern limestone unit of Figure 3.7, brecciated limestone occurs at high angles to bedding and grades laterally into an unbrecciated sedimentary sequence. Limestone breccias also form discontinuous and folded horizons in the mélange zone (Fig. 3.7). Two brecciated limestone horizons each several metres thick occur at one locality in the west-central part of the Cheshire Formation within the siliciclastic member (Fig. 3.3, II) where they are intercalated with shale, massive pebble conglomerate, and lenticular horizons of ironstone.

The intensity of brecciation is variable and ranges from matrix- and clast-supported chaotic breccias to breccia-filled fissures in an otherwise undisrupted, coherent limestone sequence. Chaotic breccias consist of poorly sorted fragments between 0.5 and ≥ 200 cm in diameter of limestone with minor sandstone, mudstone, and shale in a hematitic and/or dolomitic, commonly sheared muddy matrix. In less brecciated sequences, limestone beds are intercalated with bedding-parallel layers of commonly sheared brecciated rock. Irregular, partly hourglass-shaped and breccia-filled fissures, up to 30 cm in width and several decimetres in length, and perpendicular to bedding, transect the limestone beds and separate them into slab-like blocks which are locally upside-down.

Early tectonic fabrics are common in the breccias and include the alignment of tabular clasts, the wrapping of argillaceous to muddy arenaceous matrix material around the clasts, and the geometry of shale clasts. The clasts locally have lenticular, sigmoidal to irregular shapes, suggesting plastic behaviour of shales during deformation.

The origin of brecciated limestone has been discussed in detail in chapter 2. Brecciation has mainly been attributed to karstification of the carbonate sequence to account for the occurrence of breccias in areas cross-cutting unbrecciated strata and the sinkhole-like depressions in the continuous breccia horizon at the top of the sequence (Fig. 3.7). However, the local presence of stromatolitic limestones intercalated with deeper water sediments of the overlying mélange zone and siliciclastic member, and which show an identical style of brecciation, makes karstification as a sole mechanism unlikely (chapter 2). In addition, bedding-parallel shear zones indicate that deformation affected the breccias, and this must have taken place early in the depositional history, since shale

fragments in the breccia have been plastically deformed. It is suggested that brecciation of the carbonates intercalated with deeper water sediments is related to D_1. Brecciation is attributed to in situ limestone dissolution which preferentially affected carbonates situated near shear zones, i.e., along ironstones and within the mélange zone. Limestone dissolution is ascribed to the hydrothermal fluids which were generated during shearing and which were channeled through mostly bedding-parallel fault planes to form local ironstones.

Other D_1 features

In the siliciclastic member of the Cheshire Formation further up in the succession there are locally preserved D_1 fabrics. Some shale horizons comprise several metres wide soft-sediment shear zones parallel to the overall strike. Deformation is indicated by anastomosing shear zones and disruption, boudinage, and dolomitization of intercalated sandstone beds. Boudinaged sandstone beds form asymmetric inclusions in, and are enveloped by, a sheared muddy matrix. The orientation of S_0 is variable in these horizons. Veins filled with quartz, iron oxides, and sulphides are common.

In the north-central part of the Cheshire Formation, strata are complexly folded and faulted as indicated by the distribution of quartzose sandstone horizons and the variable orientation of younging directions (Fig. 3.3, IV). The abundance of quartzose sandstone is at least in part caused by repetition of strata. The intermingling of lithologies may be attributed to D_1, but large-scale slump folding could equally be possible.

D_1 structures are expected to occur in the Zeederbergs Formation, although shear zones may be obscured by the monotony of the volcanic sequence lacking marker horizons. Scholey (1992) described the Zeederbergs Formation as sheared throughout the exposed area, whereas Brake (1996) observed little or no evidence of deformation.

Pillows in the Zeederbergs Formation are commonly deformed in a plane parallel to stratification, giving rise to a weakly developed foliation. A lineation is defined by the stretching of pillows, spheroids, hyaloclastite fragments, and vesicles. These structural fabrics are attributed to D_2. Sheared tuff bands have been reported by Martin (1978), and this shearing may have taken place during D_1, but D_2 could equally be possible.

During the limited fieldwork a ~10 m wide bedding-parallel shear zone was observed which may have formed during D_1 (location E, Fig. 3.3). The shear zone consists of lenticular bodies and partly rotated, angular blocks of basalt and epiclastic sediment set in a sheared and brecciated matrix of fine-grained epiclastic material or tuff (Fig. 3.17). This horizon has been interpreted by Brake (1996, Figure 3.3) as a “large lava and debris flow”. Deformation of the basalt blocks has been attributed to their reincorporation in a flowing lava. It is of interest here that this shear zone separates an underlying, geochemically distinct (Brake, 1996) basalt unit containing abundant intercalations of shale and epiclastic sediment from a 1.5 km thick basaltic succession that completely lacks sedimentary horizons.

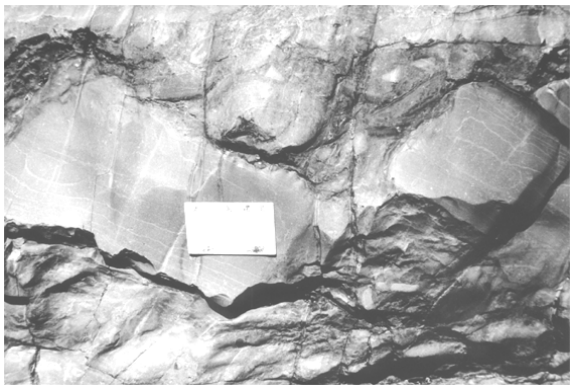

Fig. 3.17. Disrupted and rotated fragments of massive basalt in a sheared, fine-grained matrix, Zeederbergs Formation (location E, Fig. 3.3).

LATER DEFORMATION OF THE CHESHIRE FORMATION

Deformational events following D_1 are higher grade, post-lithification deformational episodes and include tight folding (Figs. 3.3 and 3.4) along a north-northwest-trending axis (D_2), gentle cross-folding with east-northeast-striking axial planes (D_3), and dextral strike-slip faulting along the Mtshingwe fault (D_4). Intrusion of dolerite sills took place between D_1 and D_2. D_2 correlates with D_g2 of Bickle et al. (1993), D_g3 with D_3 and so on (refer to Table 3.1).

D_2

D_2 resulted in tight, synclinal folding of the greenstone belt along a south-southeast striking axis with the Cheshire Formation forming the core of the syncline (Fig. 3.3). Rare parasitic medium to large-scale folds occur adjacent to the main syncline axis of the Cheshire outcrop, which plunges steeply to the north in the southern part of the Cheshire Formation and towards the south in the north-central part (Fig. 3.3, III). In the southern part the fold hinge is preserved, whereas to the north the axial trace of the syncline appears to be sheared out and possibly truncated along the northeastern contact between the Zeederbergs and Cheshire Formations (Fig. 3.3). Small- to medium-scale, open F_2 folds with subhorizontal fold axes rarely occur in the central part of the Cheshire outcrop, suggesting that the fold axis of the main syncline in this area is subhorizontal. S_0 in both limbs dips at steep angles mainly towards the east, indicating that the eastern limb of the syncline is overturned. A penetrative axial planar foliation (S_2) is striking subparallel to S_0 (Fig. 3.4). Towards the northern part of the Cheshire exposure the rocks are strongly foliated and mostly represented by slate. Liesegang rings are common and have been crenulated in the foliation plane, pointing to volume loss during D_2.

D_2 resulted in minor deformation and reorientation of clasts in conglomerate and brecciated limestone. With the exception of the northern section and the eastern margin of the Cheshire Formation, D_2 did not result in significant internal strain. Therefore sedimentary structures are generally well preserved in the central and western parts of the belt. In areas of higher strain, triaxially oblate clasts in conglomerates are generally oriented with their XY plane parallel to S_2. The long axis of the clasts defines a stretching lineation (L_2) which plunges at high angles, mostly towards the southeast (Fig. 3.4). This elongation direction is confirmed by the ellipsoidal shape of primary spherical ocelli in deformed basalt clasts in conglomerates. The lineation is locally subparallel to the intersection lineation between S_2 and S_3 and, hence, may have been reoriented during D_3. The age of D_2 is bracketed by the age of the greenstone sequence and the intrusion of

the Chilimanzi Suite Chibi granite. A granite of this suite has yielded an U-Pb zircon date of 2634±17 (Horstwood, 1998).

D_3

A spaced foliation (S_3) occurs throughout the study area and generally strikes at a high angle to S_0, S_1, and S_2, giving rise to pencil structures. S_3 is subvertical, strikes east-northeasterly (Fig. 3.4), and formed as an axial planar foliation during D_3 cross-folding of the BGB. This foliation is developed throughout the southern part of the BGB, including the Chilimanzi Suite Chibi granite (Bickle et al., 1993). Structural features of similar strike occur south of the BGB in the Buchwa-Mweza greenstone belt and the Northern Marginal Zone (NMZ) of the Limpopo Belt, where they have been related to northwestward thrusting of the NMZ onto the Zimbabwe Craton (Rollinson and Blenkinsop, 1995). The timing of D_3 is bracketed by the emplacement of the Chibi granite and the Great Dyke, dated at c. 2.58 Ga (Mukasa et al., 1998).

D_4

Dextral strike-slip faulting (D_4) is recorded along the Mtshingwe fault (Fig. 3.3). Drag folding is absent, since rotation of S_3 has not been observed near the fault zone. Additionally, the Great Dyke itself is not dragged (Fig. 3.1). The zetamoidal shape of the Cheshire outcrop is therefore solely a result of cross-folding during D_3. The fault zone is a few metres wide and has a strike separation of 3 km where it cuts the Great Dyke. Minor faults with separations of a few centimetres to several metres occur parallel to and in the immediate vicinity of the main fault. In the central part of the Cheshire exposure the fault zone forms a transpressional jog where strain was accommodated by small-scale faults and cataclasite zones.

DISCUSSION AND CONCLUSIONS

The Cheshire Formation contains strong evidence for a tectonic event (D_1) that affected the underlying volcanics and the sediments before they were fully consolidated. This event took place prior to the formation of the synclinal structure of the belt, suggesting a deformational history more complex than previously assumed. The stratigraphy of the western part of the Cheshire Formation, the distribution of D_1 shear zones, and the aspects of early formed structural fabrics indicate that D_1 was characterized by thin-skinned thrusting resulting in local stratigraphic repetitions. The inlier of Zeederbergs-type volcanics is interpreted as a thrust sheet which was emplaced onto the carbonate sequence and overlying siliciclastics. Thrusting was accompanied by noncoaxial, plastic deformation and stratal disruption of underlying, poorly consolidated and compacted sediments, and gave rise to the formation of a several tens of metres wide, mélange-like shear zone (Fig. 3.18). Where the Zeederbergs inlier pinches out in the south, the siliciclastic member is positioned on top of the carbonate member. This suggests that the basalts were already overlain by siliciclastic sediments during thrusting. A similar relationship can be observed at the eastern, fault(ironstone)-bounded

carbonate outcrop where siliciclastics tectonically rest on carbonates (Fig. 3.7). The two carbonate units separated by volcanics probably represent tectonic repetitions of the same stratigraphic horizon (Figs. 3.18 and 3.19) with the stratigraphically upper unit representing a horse structure. Linear features and kinematic indicators in different lithotectonic units indicate relative west-northwest to north-northwest directed tectonic movements of hanging-wall blocks which combine to a mean northwest-directed tectonic transport.

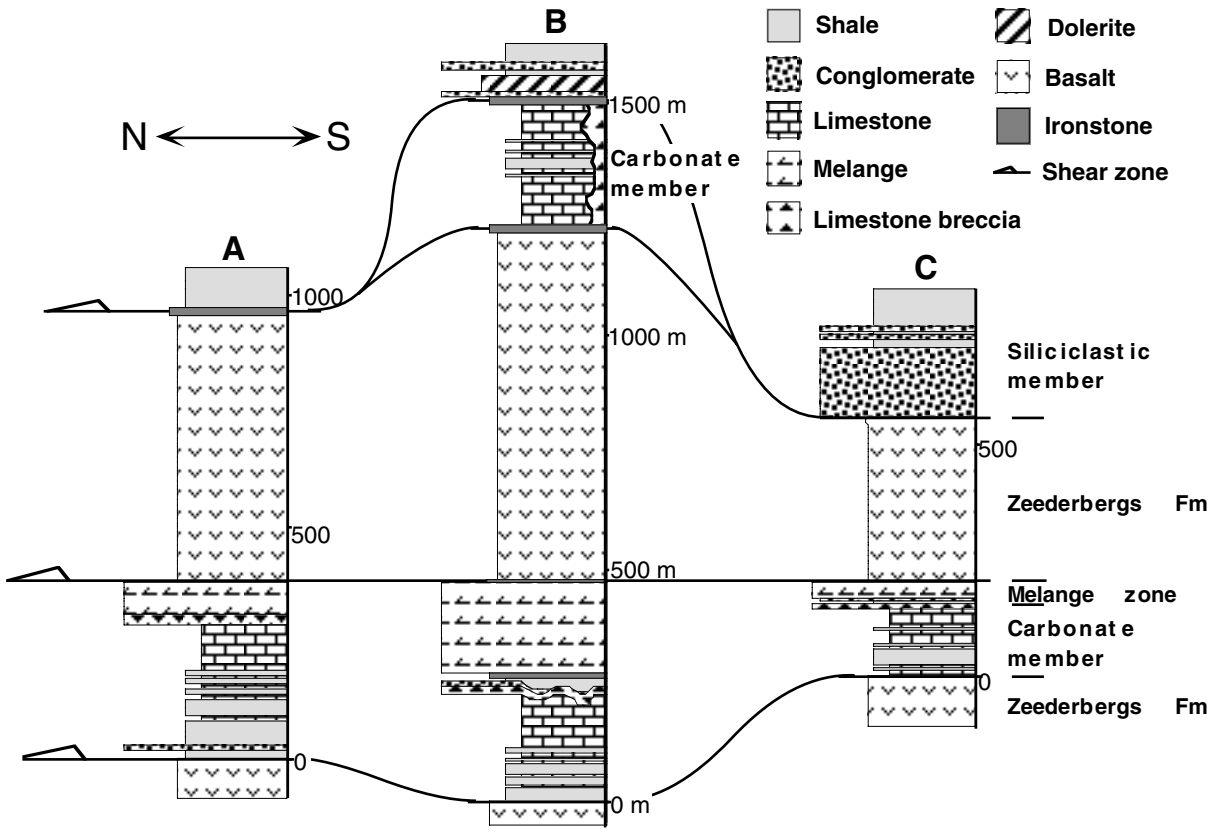

Fig. 3.18. Graphic logs showing the lateral distribution and vertical stacking of lithologic/lithotectonic units along the western Zeederbergs-Cheshire contact. Log C has been measured in the field (Ngezi river section), whereas logs A and B have been determined from the geological map (see Figure 3.7 for location) and are to some extent schematic. The mélange zone of logs A and B predominantly consists of variably deformed (including undeformed) shale.

Strain during horizontal tectonism was partitioned into shear zones mainly along lithological contacts. Deformation was associated with the generation and migration of mineralized fluids that traveled along the bedding-parallel fault zones. As a result, rocks adjacent to the fault zones, fine-grained sediments in particular, were silicified/sulphide-impregnated and, locally, tectonic ironstones formed. Some of the material forming the ironstones did not form via an alteration/replacement process of the host rocks but precipitated directly in the shear zones as indicated by intrusive veins of hematitic material and chert. Brecciation of previously formed banded rocks was part of this progressive alteration process. The relative amounts of replaced, primary sedimentary material and

newly formed and transposed intrusive veins which together resulted in the formation of ironstone remains unknown.

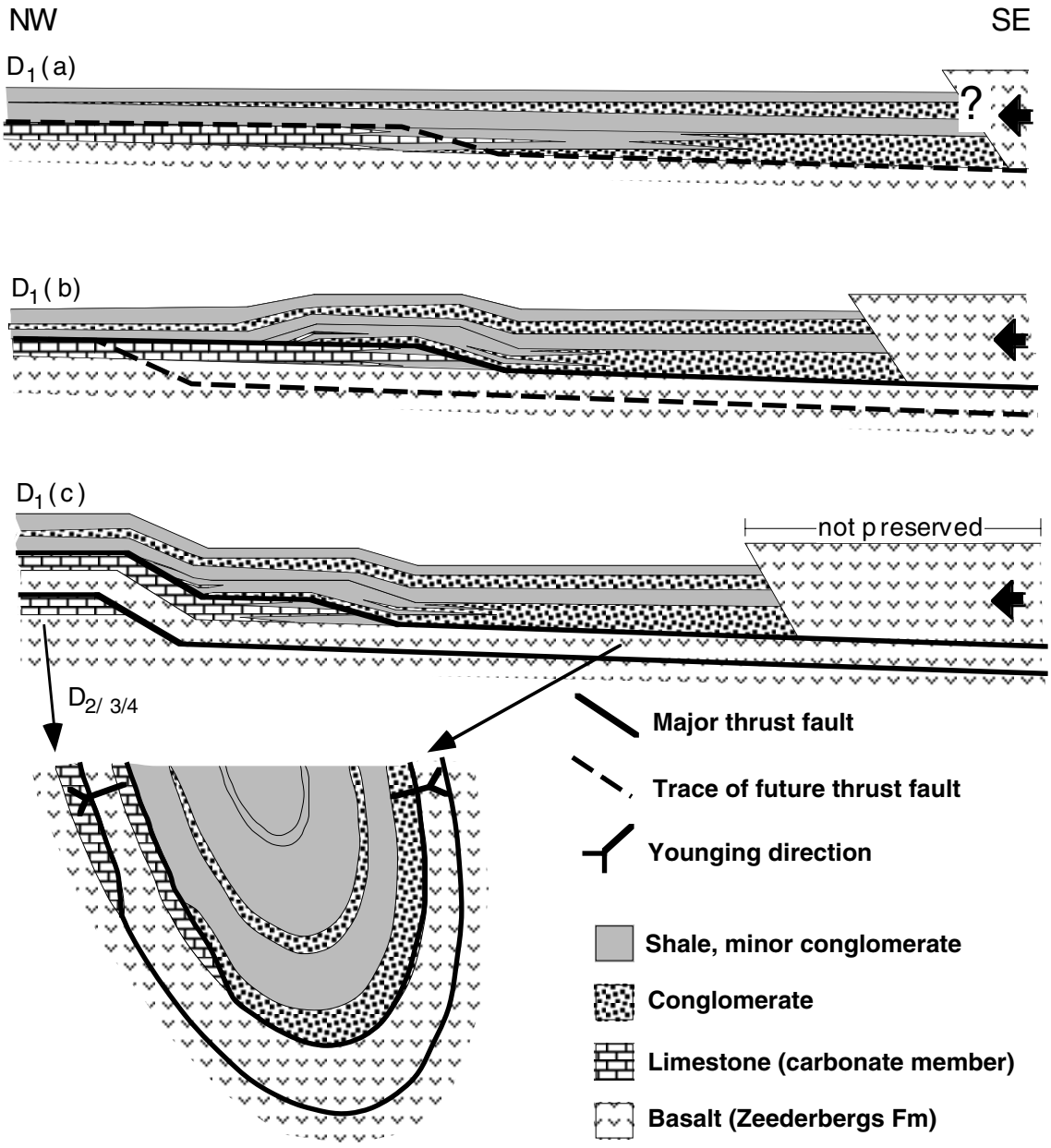

Fig. 3.19. Simplified tectonic model (not to scale) showing northwestward-directed thrusting and tectonic stacking during D_1 and subsequent deformation $D_{2/3/4}$ to give rise to the present synclinal structure of the belt (simplified cross-section, not to scale). The Cheshire Formation is interpreted as a foreland-type sedimentary basin fill (see also chapter 2, Figure 2.16). It remains unclear if thrusting occurred during or shortly after sedimentation of the preserved part of the Cheshire Formation. Model and cross-section are drawn for the outcrop configuration ~1.5 km north of the Ngezi river (compare log B of Figure 3.18). Dolerites and the upper part of the sedimentary sequence are not shown for clarity. Note that shearing was not only restricted to the lithological contacts shown as major thrust faults.

The carbonate member is restricted to the western part of the Cheshire outcrop and is sharply overlain by deeper water siliciclastics with rare limestone intercalations (mélange zone). The carbonates contain local intercalations of basalt pebble conglomerate similar to those in the

siliciclastic member. At one locality in the western section of the siliciclastic member (Fig. 3.3, II), stromatolitic limestones occur at the top of the basal conglomerate, whereas limestones are absent in the eastern section. These relationships suggest that the basal sedimentary units, i.e., conglomerate in the east and limestone in the west, formed synchronously in a basin with an asymmetric facies distribution and were juxtaposed during thrusting (Fig. 3.19). Siliciclastic detritus was shed from the southeast as indicated by palaeoflow data and lateral facies distribution and was most likely derived from the erosion of northwestward-advancing thrust sheets of Zeederbergs-like volcanics as implied by clast composition (chapter 2). Accommodation space was probably provided by thrust loading and gave rise to an eastward deepening foreland-type sedimentary basin with the deposition of shallow-water sediments in the west. Accelerated subsidence during thrust advance possibly gave rise to drowning of the carbonate sequence which was then covered by more deep-water sediments (chapter 2). Since the Zeederbergs inlier was already overlain by siliciclastic sediments during thrusting, at least part of the sedimentary sequence must have been carried piggy-back on top of active thrusts, possibly in a late stage of or shortly after deposition. The top of the sedimentary sequence is not preserved but is occupied by ironstones. It is likely that these ironstones represent the basal shear zone of another northwestward-moving thrust sheet which was emplaced on top of the Cheshire Formation and which has since been eroded.

The contact between the Zeederbergs and Cheshire Formations is sharp, planar, and sheared. No "intermingled suite of lavas and sediments" (Nisbet et al., 1993, p. 149) has been observed along the contact. The volcanic sequence contains minor intercalations of deep water shales and turbidites containing hyaloclastic material. The Cheshire Formation lacks volcanic rocks. This suggests that sedimentation took place some time after cessation of volcanism. However, where exposed, the Zeederbergs-Cheshire contact is sheared with an unknown magnitude of relative displacement along the shear zone. As a result, the Cheshire Formation may represent a thrust sheet in its own right. Nevertheless, most of the detritus forming the basal sediments was derived from erosion of Zeederbergs-like material (chapter 2), indicating that the succession was probably deposited on top of Zeederbergs volcanics and in front of Zeederbergs-type thrust sheets (Fig. 3.19).

Some may argue that the soft-sediment deformational fabrics such as contorted to chaotic strata and isoclinal folds as described from the Cheshire Formation are a characteristic feature of submarine slump deposits. Modern sediment slumps and slides are common along the submarine slopes of both active and passive continental margins and are triggered by slope failures due to gravitational instabilities (e.g., Jacobi, 1984). The emplacement of the inlier of volcanic rocks as a huge, internally undeformed slump block bounded below by a slump fault (mélange zone) can be discounted for various reasons. In the Cheshire Formation, unequivocal slump folds are of small scale and have only been observed at two localities in turbidite deposits, indicating a rather gentle palaeoslope during the depositional history. Sedimentological constraints suggest that the carbonate member represents a carbonate ramp sequence (chapter 2); such successions generally form along gently sloping (< 1°) depositional surfaces (Burchette and Wright, 1992). A gentle palaeoslope is

further indicated by the local occurrence of stromatolitic limestone interbedded with siliciclastics in the western part of the sequence. Additionally, the stratigraphy, facies distribution, and palaeoslope data of the Cheshire Formation (chapter 2; see above) indicate that the basin was deepening towards the southeast. This is opposite to the direction the volcanic unit moved and would imply that the slump block would have moved against the gravitational forces up the palaeoslope.

The D_2 and D_3 events are of higher metamorphic grade, gave rise to a penetrative cleavage, and formed after consolidation and lithification of the Cheshire sediments. D_2 may be an event related to D_1 insofar as continued shortening in a late stage of horizontal tectonic deformation combined with a possible switch to an east-west oriented stress field gave rise to the synclinal folding of the belt. D_3 is unrelated to the tectonic evolution of the BGB alone and indicates orogenic processes that affected a large section of the already consolidated Zimbabwe craton adjacent to the Limpopo belt. The same explanation possibly holds true for D_4.

Kusky and Kidd (1992), and Kusky and Winsky (1995) argued that the top of the Manjeri Formation, characterized by a complexly folded ironstone horizon and adjacent mylonite zones, represents a major tectonic discontinuity across which the overlying basalts were transported from their original position. In contrast, Blenkinsop et al. (1993) argued that the horizon in question is not a major shear zone and that any movement along it was minor and related to layer-parallel slip during synclinal folding of the greenstone sequence. No detailed work on the Manjeri Formation has been done within the framework of this project. However, the ironstone horizon at the Manjeri-Reliance contact is lithologically identical to the ironstones developed in the Cheshire Formation. The latter ironstones are interpreted as silicified and sulphide-impregnated D_1 shear zones. These shear zones seem to have acted as channels for mineralized, hydrothermal fluids. The common brecciation of the ironstones indicate that fluid pressures must have been high along these zones and high enough to overcome frictional and cohesion forces along the fault planes for thrusting to occur. Kusky and Winsky (1995) argued that the Ngezi volcanics were thrusted onto the Manjeri Formation in a west- to northward direction. This is in agreement with this study which indicates that the Cheshire Formation itself was affected by northwest-directed tectonic movements. Whether or not the ultramafic/mafic lava sequence of the Ngezi volcanics represents an obducted part of Archaean oceanic crust, this study indicates that horizontal tectonic processes played an important role in the evolution of the Belingwe greenstone belt.

REFERENCES

Abell, P. I., J. McClory, A. Martin, and E. G. Nisbet, Archaean stromatolites from the Ngesi Group, Belingwe Greenstone Belt, Zimbabwe: Preservation and stable isotopes-preliminary results, *Precambrian Res., 27*, 357-383, 1985.

Bickle, M. J., and E. G. Nisbet (Eds.), *The Geology of the Belingwe Greenstone Belt, Zimbabwe, Geol. Soc. Zimbabwe Spec. Publ., 2*, 239 pp., 1993.

Bickle, M. J., A. Martin, and E. G. Nisbet, Basaltic and peridotitic komatiites, stromatolites and a basal unconformity in the Belingwe greenstone belt, Rhodesia, *Earth Planet. Sci. Lett., 27*, 155-162, 1975.

Bickle, M. J., J. L. Orpen, E. G. Nisbet, and A. Martin, Structure and metamorphism of the Belingwe Greenstone Belt and adjacent granite-gneiss terrain: The tectonic evolution of an Archaean craton, in *The Geology of the Belingwe Greenstone Belt, Zimbabwe*, edited by M. J. Bickle, and E. G. Nisbet, *Geol. Soc. Zimbabwe Spec. Publ., 2*, 39-68, 1993.

Bickle, M. J., E. G. Nisbet, and A. Martin, Archaean greenstone belts are not oceanic crust, *J. Geol., 102,* 121-138, 1994.

Blenkinsop, T. G., C. M. Fedo, M. J. Bickle, K. A. Eriksson, A. Martin, E. G. Nisbet, and J. F. Wilson, Ensialic origin for the Ngezi group, Belingwe greenstone belt, Zimbabwe, *Geology, 21,* 1135-1138, 1993.

Bolhar, R., A. Hofmann, J. M. Woodhead, J. M. Hergt, and P. Dirks, Pb-Pb systematics of stromatolitic limestones from the 2.7 Ga Ngezi Group, Belingwe Greenstone Belt, Zimbabwe, in *Beyond 2000: New Frontiers in Isotope Geoscience*, edited by J.M. Woodhead, J.M. Hergt, and W.P. Noble, Abstracts and Proceedings, Lorne, Australia, 2000.

Brake, C., Tholeiitic magmatism in the Belingwe greenstone belt, Zimbabwe, Ph.D. thesis, 184 pp., Univ. of Edinburgh, Edinburgh, Scotland, U.K., 1996.

Burchette, T. P., and V. P. Wright, Carbonate ramp depositional systems, *Sediment. Geol., 79*, 3-57, 1992.

Byrne, T., Early deformation in mélange terranes of the Ghost Rocks Formation, Kodiak Islands, Alaska, in *Mélanges: Their Nature, Origin, and Significance*, edited by L. A. Raymond, *Geol. Soc. Am. Spec. Pap., 198*, 21-51, 1984.

Campbell, S. D. G., and P. E. J. Pitfield, Structural controls of gold mineralization in the Zimbabwe Craton: Exploration guidelines, *Geol. Surv. Zimbabwe Bull., 101*, 278 pp., 1994.

Card, K. D., A review of the Superior Province of the Canadian Shield: A product of Archaean accretion, *Precambrian Res., 48,* 99-156, 1990.

Chauvel, C., B. Dupré, and N. T. Arndt, Pb and Nd istopic correlation in Belingwe komatiites and basalts, in *The Geology of the Belingwe Greenstone Belt, Zimbabwe*, edited by M. J. Bickle and E. G. Nisbet, *Geol. Soc. Zimbabwe Spec. Publ., 2*, 167-174, 1993.

Cloos, M., Flow mélanges and the structural evolution of accretionary wedges, in *Mélanges: Their Nature, Origin, and Significance*, edited by L. A. Raymond, *Geol. Soc. Am. Spec. Pap., 198*, 71-79, 1984.

Cowan, D. S., Structural styles in Mesozoic and Cenozoic mélanges in the western Cordillera of North America, *Geol. Soc. Am. Bull., 96*, 451-462, 1985.

de Wit, M. J., Gliding and overthrust nappe tectonics in the Barberton Greenstone Belt, *J. Struct. Geol., 4,* 117-136, 1982.

de Wit, M. J., C. Roering, R. J. Hart, R. A. Armstrong, C. E. J. de Ronde, R. W. E. Green, M. Tredoux, E. Perbedy, and R. A. Hart, Formation of an Archaean continent, *Nature, 357*, 553-562, 1992.

Dirks, P. H. G. M., and H. A. Jelsma, Horizontal accretion and stabilization of the Archaean Zimbabwe Craton, *Geology, 26,* 11-14, 1998a.

Dirks, P. H. G. M., and H. A. Jelsma, Silicic layer-parallel shear zones in a Zimbabwean greenstone sequence: Horizontal accretion preceding doming, *Gondwana Res., 1,* 177-194, 1998b.

Dirks, P. H. G. M., and J. van der Merwe, Early duplexing in an Archaean greenstone sequence and its control on gold mineralization, *J. Afr. Earth Sci., 24,* 603-620, 1997.

Grotzinger, J. P, D. Y. Sumner, and N. J. Beukes, Archaean carbonate sedimentation in an active extensional basin, Belingwe Greenstone Belt, Zimbabwe, *Geol. Soc. Am. Abstr. Programs, 25*, 64, 1993.

Hofmann, A., P. H. G. M. Dirks, and H. A. Jelsma, Late Archaean foreland basin deposits, Belingwe greenstone belt, Zimbabwe, *Sediment. Geol., 141-142*, 131-168, 2001.

Horstwood, M. S. A., Stratigraphy, geochemistry and zircon geochronology of the Midlands greenstone belt, Zimbabwe, Ph.D. thesis, 215 pp., Univ. of Southampton, Southampton, England, U.K., 1998.

Horstwood, M. S. A., R. W. Nesbitt, S. R. Noble, and J. F. Wilson, U-Pb zircon evidence for an extensive early Archaean craton in Zimbabwe: A reassessment of the timing of craton formation, stabilization, and growth, *Geology, 27*, 707-710, 1999.

Hsü, K. J., Principles of mélanges and their bearing on the Franciscan-Knoxville paradox, *Geol. Soc. Am. Bull., 79*, 1063-1074, 1968.

Hunter, M. A., M. J. Bickle, E. G. Nisbet, A. Martin, and H. J. Chapman, Continental extensional setting for the Archean Belingwe Greenstone Belt, Zimbabwe, *Geology, 26*, 883-886, 1998.

Jacobi, R. D., Modern submarine sediment slides and their implications for mélange and the Dunnage Formation in north-central Newfoundland, in *Mélanges: Their Nature, Origin, and Significance*, edited by L. A. Raymond, *Geol. Soc. Am. Spec. Pap., 198*, 81-102, 1984.

Jelsma, H. A., and P. H. G. M. Dirks, Tectonic evolution of a greenstone sequence in northern Zimbabwe: Sequential early stacking and pluton diapirism, *Tectonics, 19*, 135-152, 2000.

Jelsma, H. A., P. A. van der Beek, and M. L. Vinyu, Tectonic evolution of the Bindura-Shamva greenstone belt (northern Zimbabwe): Progressive deformation around diapiric batholiths, *J. Struct. Geol., 15,* 163-176, 1993.

Kusky, T. M., and W. S. F. Kidd, Remnants of an Archaean oceanic plateau, Belingwe Greenstone Belt, Zimbabwe, *Geology, 20,* 43-46, 1992.

Kusky, T. M., and P. A. Winsky, Structural relationships along a greenstone/shallow water shelf contact, Belingwe greenstone belt, Zimbabwe, *Tectonics, 14,* 448-471, 1995.

Macgregor, A. M., Some milestones in the Precambrian of Southern Rhodesia, *Proc. Geol. Soc. S. Afr., 54,* 27-71, 1951.

Martin, A., The geology of the Belingwe-Shabani schist belt, *Bull. Rhod. Geol. Surv., 83*, 213 pp., 1978.

Martin, A., E. G. Nisbet, and M. J. Bickle, Archaean stromatolites of the Belingwe Greenstone Belt, *Precambrian Res., 13*, 337-362, 1980.

Martin, A., E. G. Nisbet, M. J. Bickle, and J. L. Orpen, Rock units and stratigraphy of the Belingwe Greenstone Belt: The complexity of the tectonic setting, in *The Geology of the Belingwe Greenstone Belt, Zimbabwe*, edited by M. J. Bickle and E. G. Nisbet, *Geol. Soc. Zimbabwe Spec. Publ., 2*, 13-37, 1993.

McDonough, W. F., and T. R. Ireland, Intraplate origin of komatiites inferred from trace elements in glass inclusions, *Nature, 365*, 432-434, 1993.

Mukasa, S. B., A. H. Wilson, and R. W. Carlson, A multielement geochronologic study of the Great Dyke, Zimbabwe: Significance of the robust and reset ages, *Earth Planet. Sci. Lett., 164*, 353-369, 1998.

Myers, J. S., The generation and assembly of an Archaean super continent: Evidence from the Yilgarn craton, western Australia, in *Early Precambrian Processes,* edited by M. P. Coward and A. C. Ries, *Geol. Soc. Spec. Publ., 95,* 143-154, 1995.

Nisbet, E. G., A. Martin, M. J. Bickle, and J. L. Orpen, The Ngezi Group: Komatiites, basalts and stromatolites on continental crust, in *The Geology of the Belingwe Greenstone Belt, Zimbabwe*, edited by M. J. Bickle and E. G. Nisbet, *Geol. Soc. Zimbabwe Spec. Publ., 2*, 121-165, 1993.

Orpen, J. L., M. J. Bickle, E. G. Nisbet, and A. Martin, Belingwe Peak, *Geol. Surv. Zimbabwe Map*, scale 1:100,000, Geol. Surv. of Zimbabwe, Harare, 1986.

Ramsay, J. G., Emplacement kinematics of a granite diapir: The Chinamora Batholith, Zimbabwe, *J. Struct. Geol., 11,* 191-209, 1989.

Raymond, L. A., Classification of mélanges, in *Mélanges: Their Nature, Origin, and Significance*, edited by L. A. Raymond, *Geol. Soc. Am. Spec. Pap., 198*, 7-20, 1984.

Ridley, J. R., J. R. Vearncombe, and H. A. Jelsma, Relations between greenstone belts and associated granitoids, in *Greenstone Belts,* edited by M. J. de Wit and L. D. Ashwal, pp. 376-397, Oxford Univ. Press, New York, 1997.

Rollinson, H. R., and T. Blenkinsop, The magmatic, metamorphic and tectonic evolution of the Northern Marginal Zone of the Limpopo Belt in Zimbabwe, *J. Geol. Soc. London, 152*, 65-75, 1995.

Scholey, S. P., The geology and geochemistry of the Ngezi Group volcanics, Belingwe greenstone belt, Zimbabwe, Ph.D. thesis, 184 pp., Univ. of Southampton, Southampton, England, U.K., 1992.

Shackleton, R. M., Tectonic evolution of greenstone belts, in *Early Precambrian Processes,* edited by M. P. Coward and A. C. Ries, *Geol. Soc. Spec. Publ., 95,* 53-65, 1995.

Stowe, C. W., The early Archaean Selukwe nappe, Zimbabwe, in *Precambrian Tectonics Illustrated,* edited by A. Kröner and R. Greiling, pp. 41-56, Nägele und Obermiller, Stuttgart, Germany, 1984.

Sumner, D. Y., and J. Grotzinger, Late Archaean aragonite precipitation: Petrography, facies association and environmental significance, in *Carbonate Sedimentation and Diagenesis in the Evolving Precambrian World*, edited by J. Grotzinger and N. P. James, *Soc. Econ. Palaeont. Mineral. Spec. Publ.*, 67, 114-131, 2000.

Swager, C., and T. J. Griffin, An early thrust duplex in the Kalgoorlie-Kambalda greenstone belt, Eastern Goldfields Province, Western Australia, *Precambrian Res., 48,* 63-73, 1990.

Wilson, J. F., A preliminary reappraisal of the Rhodesian basement complex, in *A Symposium on Mineral Deposits and Transportation and Deposition of Metals,* edited by C. Anhaeusser, R. P. Foster, and T. Stretton, *Spec. Publ. Geol. Soc. S. Afr., 5,* 1-23, 1979.

Wilson, J. F., R. W. Nesbitt, and C. M. Fanning, Zircon geochronology of Archaean felsic sequences in the Zimbabwe craton: A revision of greenstone stratigraphy and a model for crustal growth, in *Early Precambrian Processes,* edited by M. P. Coward and A. C. Ries, *Geol. Soc. Spec. Publ., 95,* 109-126, 1995.

Worst, B. G., The geology of the country between Belingwe and West Nicholson, *Bull. S. Rhod. Geol. Surv., 43*, 218 pp., 1956.

CHAPTER 4

Shallowing-upward carbonate cycles in the Belingwe greenstone belt, Zimbabwe: the possibility of orbital forcing in late Archaean times

Axel Hofmann, Paul H.G.M. Dirks, and Hielke A. Jelsma
submitted to Journal of Sedimentary Research

Abstract—In the Cheshire Formation of the Belingwe greenstone belt (Zimbabwe) c. 2650 Ma old shallowing-upward carbonate cycles have been observed that closely resemble their Proterozoic and Phanerozoic counterparts. The cycles build a karstified carbonate ramp sequence that is overlain by, and grades basinward into, siliciclastic turbidites. A single section of 74 cycles (1.5 m average thickness) has been studied in detail. The cycles have an asymmetric facies stacking pattern. Open marine subtidal shale formed below fair-weather wave base and constitutes the base of many cycles. Shale is intercalated with storm-generated sand/grainstone beds that become more common and thicken upward, indicating progressive shallowing. Wave-rippled ooid/intraclast grainstone beds/bedsets overlie shale and formed at or above wave base as shoreface sand-sheets in an agitated, shallow subtidal setting. Microbial laminites constitute cycle tops and are interpreted as a peritidal facies. Both grainstone and laminite facies contain scattered nodular/domal stromatolites. The laminite facies is sometimes capped by brecciated, stromatolitic limestone facies. Microbial boundstones with aragonite pseudomorphs are intercalated with, or overlie, laminites in the upper part of the studied section. The breccia and boundstone facies are interpreted as supratidal deposits. The vertical facies distribution within a cycle is the result of rapid submergence, followed by gradual shallowing of the sea-level. High-frequency eustatic sea-level changes are favoured over an allocyclic mechanism and tectonically induced autocyclicity as the controlling mechanism for the cyclicity. Hierarchies of stratigraphic cyclicity occur on different scales and may be the result of the combined effects of several orders of sea level oscillations. Cycle recurrence ratios correspond well to Milankovitch frequencies calculated for the late Archaean, suggesting that orbital climatic forcing may have been in operation in late Archaean times.

INTRODUCTION

Shallowing-upward sedimentary cycles are a common component of ancient carbonate platforms dating back to the Palaeoproterozoic (James 1984; Grotzinger 1986a, 1989; Pratt et al. 1992). Despite variations in the form of carbonate production through time associated with the evolutionary changes of carbonate-secreting organisms (Wilson 1975; Hoffman 1976; James 1984), the sedimentary history of Phanerozoic and Proterozoic carbonate platforms seems to be strikingly similar as indicated by the vertical and lateral arrangement of their basic building blocks, the shallowing-upward cycles (Beukes 1987; Grotzinger 1989). Accordingly, shallow marine carbonate depositional environments, the factors that govern carbonate sedimentation, and the mechanisms for cyclic deposition did not undergo significant changes through time, although the chemistry of ocean waters may have varied (cf. Sumner and Grotzinger 2000). Various auto- and allocyclic models have been proposed to explain the origin of cyclicity (e.g., Fischer 1964; Ginsburg 1971; Goodwin and Anderson 1985, Pratt and James 1986; Cisne 1986). In several studies evidence has been presented that the metre-scale cyclicity recorded in shallow-marine carbonates reflects repetitive eustatic changes in sea level (Goldhammer et al. 1987). High-frequency eustatic changes are possibly controlled by oscillatory climatic changes due to orbital forcing within the Milankovitch frequency band (Grotzinger 1986b; Goldhammer et al. 1987, 1990; Osleger and Read 1991). If we accept this as a likely mechanism, carbonate cycles potentially preserve important information on past climates, the nature and frequency of climatic changes, and information on the Earth orbital parameters for the past 2200 Ma or so, the maximum age for which possible eustasy-controlled cyclic carbonates have been reported (cf. Grotzinger 1986b).

Were there major differences in carbonate deposition in Archaean times? Limestones (and dolomites) have been documented from most Archaean cratons, e.g. in North America, southern Africa and Australia (e.g., Rothpletz 1916; Macgregor 1941; Winter 1963; Walter et al. 1980; Byerly et al. 1986). Most of these deposits are restricted to local, discontinuous occurrences within greenstone belts where they are tectonically interleaved with volcanic rock-dominated successions. The origin and tectonic setting of these ancient volcano-sedimentary sequences is still controversial (de Wit 1998; Hamilton 1998). It is common belief, however, that the supracrustal rocks formed in tectonically and volcanically active settings where stable, shallow-water environments were mostly absent and siliciclastic input was high. In addition, the rocks were typically affected by metamorphism and intense deformation, strongly modifying primary fabrics (e.g., Cameron and Baumann 1977). An exceptionally well preserved carbonate sequence was described by Martin et al. (1980) from one outcrop of the c. 2.65 Ga old Cheshire Formation of the Belingwe greenstone belt, Zimbabwe. A cyclic stacking of facies was observed in the stromatolitic limestones and attributed to cyclic changes in relative sea level. Sumner and Grotzinger (2000) revisited the outcrop and redefined the position of cycle boundaries, questioning the environmental interpretation of Martin et al. (1980). However, a detailed facies analysis has never been carried out. During sedimentological-structural mapping of the Cheshire Formation as part of this project a previously unrecognized outcrop was discovered where an

almost continuous section of carbonates of the Cheshire Formation is exposed. This section comprises distinct metre-scale, shallowing-upward cycles which are strikingly similar in lithofacies and facies stacking pattern to cyclic carbonates of much younger carbonate platforms. It is the scope of this paper to give a detailed account of the cyclic lithofacies and their vertical distribution, to give an interpretation of the depositional environment and to define the likely mechanisms that caused cyclic sedimentation 2650 million years ago.

GEOLOGICAL SETTING

The Belingwe greenstone belt (BGB), situated in the southern part of the Archaean Zimbabwe craton (Fig. 4.1), contains a well preserved volcano-sedimentary sequence. The supracrustal rocks overlie up to 3.5 Ga old granitoid gneisses and have been stratigraphically subdivided into the Mtshingwe Group and overlying Ngezi Group. The Mtshingwe Group is confined to the southeastern and western parts of the belt (Fig. 4.1). It mainly consists of mafic to intermediate lavas, volcaniclastics, and siliciclastic sediments (Martin et al. 1993) ranging in age from 2.90 to 2.83 Ga according to U/Pb zircon dates (Wilson et al. 1995).

Stratigraphy of the Ngezi Group

The Ngezi Group forms the central part of the BGB (Figs. 4.1 and 4.2). It overlies the ancient gneisses to the east and north-east and the Mtshingwe Group to the south-east and west. Granites of the c. 2.6 Ga old Chilimanzi Suite intrude the Ngezi Group in the northern and southern parts of the belt; these granites are cut by the 2.58 Ga old (Mukasa et al. 1998) Great Dyke. The Ngezi Group comprises a basal sedimentary succession (Manjeri Formation) overlain by ultramafic and mafic volcanic rocks (Reliance and Zeederbergs Formations, collectively termed Ngezi volcanics), and capped by a sedimentary unit (Cheshire Formation). The 0-120 m thick Manjeri Formation unconformably overlies the Mtshingwe Group and granitoid basement (Bickle et al. 1975). The lower part of the Manjeri Formation consists of shallow-water sediments, including conglomerate, sandstone, shale, ironstone and localized stromatolitic limestone (Martin et al. 1980). The upper part comprises alluvial fan to fan delta conglomerates and sandstones and is capped by ironstone (Hunter et al. 1998).

The 1 km thick Reliance Formation consists of komatiites, komatiitic basalts and tholeiites (Scholey 1992) and is gradationally overlain by the Zeederbergs Formation, a c. 3 km thick pile of commonly pillowed, tholeiitic lava flows with minor intercalations of volcaniclastic sediment (Brake 1996). Ion microprobe trace element data of glass inclusions of Reliance Formation komatiites are similar to modern plume-related oceanic plateau and oceanic island basalts (McDonough and Ireland 1993).

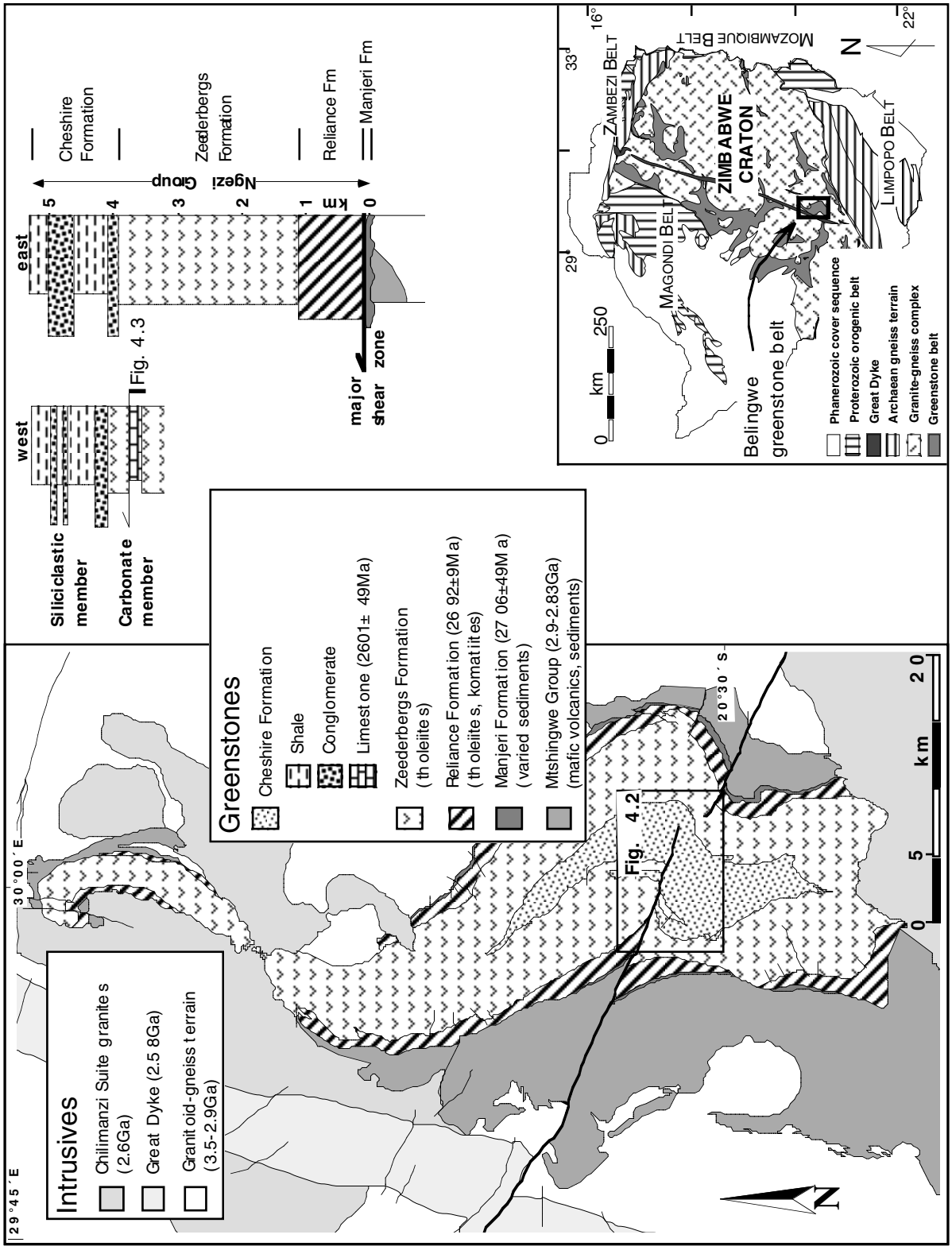

Fig. 4.1. Geological map of the Belingwe greenstone belt (after Fig. 2.1 of Martin et al. 1993), its location in the Zimbabwe craton, and simplified stratigraphic column of the volcano-sedimentary succession (see text for references).

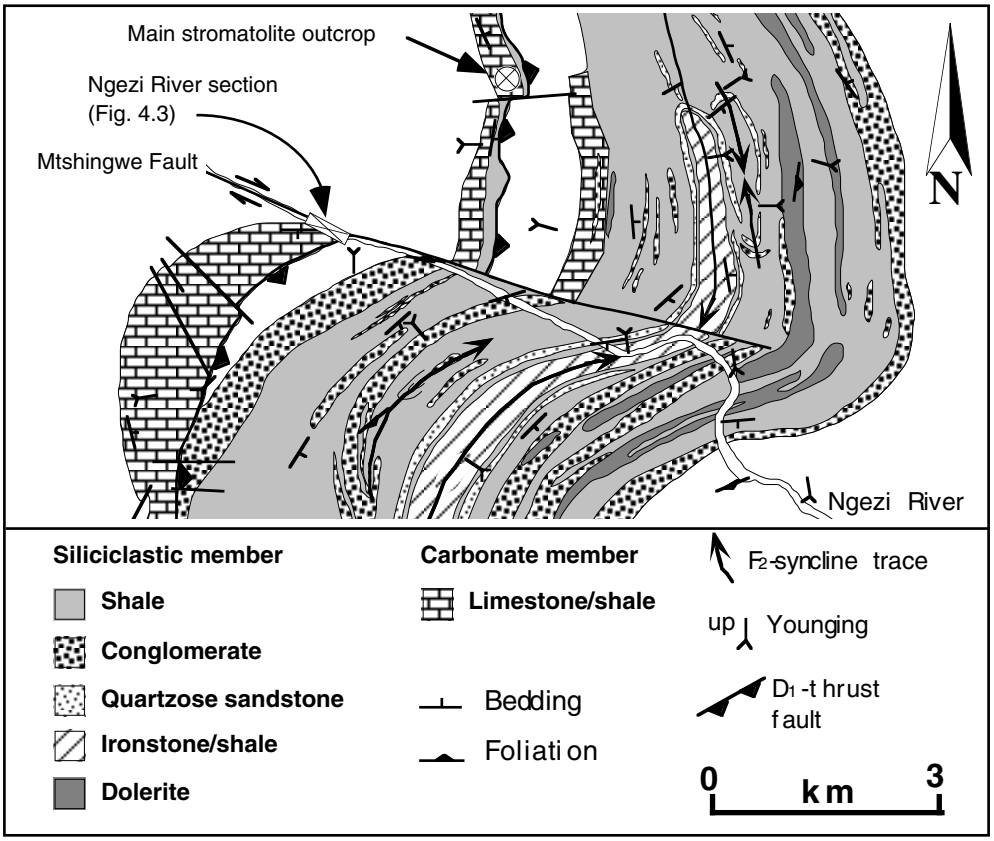

Fig. 4.2. Geological map of the central part of the Cheshire Formation. The Cheshire Formation is underlain by the Zeederbergs Formation (not shown).

The Cheshire Formation (c. 1.3 km thick) is the uppermost stratigraphic unit of the BGB and rests along a sharp and sheared contact on the Zeederbergs Formation. It has been subdivided into two informal stratigraphic units (chapter 2): (a) the carbonate member that consists predominantly of interbedded limestone and shale, and local limestone breccia, and (b) the siliciclastic member mainly comprising conglomerate and shale. The carbonate member is restricted to two occurrences in the western part of the Cheshire outcrop (Fig. 4.2). The westernmost occurrence rests on the Zeederbergs Formation and is structurally overlain by Zeederbergs-type volcanics. The second carbonate outcrop is shear zone-bounded and is situated at the western margin of the main Cheshire outcrop. At both localities, the carbonate member consists of metre-scale sedimentary cycles that are the focus of this paper.

The siliciclastic member in the central part of the Cheshire outcrop (Fig. 4.2) consists of a basal conglomerate unit which is overlain by a succession of intercalated conglomerate and shale with a conspicious sandstone horizon and ironstones at the top. Massive, graded and horizontally stratified conglomerates are common and are interpreted as high-density turbidity current deposits. Shale is characterized by low-density turbidites and background suspension sediments (chapter 2).

Age

Precise age data are scarce for the Ngezi Group. Komatiitic basalts of the Reliance Formation have been dated by the whole-rock Pb/Pb isochron method at 2692±9 Ma (Chauvel et al. 1993). Bolhar et al. (2001) determined whole-rock Pb/Pb dates of 2706±49 Ma and 2601±49 Ma for stromatolitic limestones of the Manjeri and Cheshire Formations, respectively. A minimum age for deposition of the Cheshire Formation is provided by the intrusion of the Chibi granite (Fig. 4.1) which is part of the Chilimanzi Suite granites. Rocks of this suite have yielded U-Pb zircon dates of 2601±14 Ma in the northern part of the craton (Jelsma 1993) and of 2634±17 in the central part (Horstwood 1998). Coarse clastic sediments of the Shamvaian Supergroup which occur in other greenstone belts in Zimbabwe and which may be time-correlative to the Cheshire Formation have been dated at around 2.65 Ga (Wilson et al. 1995; Jelsma et al. 1996). Taken all these data into account, the Cheshire Formation may have formed close to 2650 Ma.

Structure

Kusky and Kidd (1992) and Kusky and Winsky (1995) suggested that the Ngezi volcanics originated as part of an oceanic plateau and were emplaced as a large allochthonous sheet onto the Manjeri Formation during an early thrusting event (D_1). In the Cheshire Formation, early thrusting gave rise to tectonic duplication of parts of the stratigraphy during juxtaposition of a thrust slice of Zeederbergs basalts onto Cheshire sediments, forming the inlier of mafic volcanics in between the carbonate and siliciclastic members (Fig. 4.2; chapter 3). This deformation affected poorly consolidated sediments and is recorded in ductile fabrics such as shear zones, boudins, folds, and block-in-matrix structures. Shear zones are commonly occupied by tectonic ironstones which are similar in appearance to banded iron formations (chapter 3). Subsequent deformation of the BGB include tight folding (D_2) of the greenstone succession forming the southeast-striking synclinal structure, gentle cross-folding (D_3) along an east-west axis, and dextral strike-slip faulting (D_4) along the Mtshingwe fault (Figs. 4.1 and 4.2).

Cheshire sedimentary basin

Sedimentological and structural data indicate that deposition of the Cheshire Formation took place in an asymmetric, foreland-type basin contemporaneously with D_1-thrusting (chapter 2 and 3). The carbonate member is interpreted as a shallow, wave- and storm-dominated, open marine sequence that formed in an eastward-deepening carbonate ramp setting. This interpretation is based on the stacking pattern of facies, the interpreted lateral facies distribution of the basal Cheshire sediments, palaeoflow/-slope data and shallow basinal water depths (chapter 2). The limestone sequence is capped by a continuous karst breccia horizon which, in turn, is overlain by more deep water siliciclastic sediments, indicating subaerial emergence and subsequent drowning of the carbonate platform. The siliciclastic member consists of sub-wave base sediments, which have been deposited by both high- and low-density turbidity currents. Palaeoflow directions are, on average, towards the northwest. Conglomerates are thicker and

coarser grained in the southeast than in the northwest, suggesting that detritus was shed from the southeast, probably from the tips of northwestward-advancing thrust sheets of Zeederbergs volcanics. Facies relationships indicate that the basal sedimentary units, i.e. shallow-water carbonates in the west and deeper water siliciclastic sediments in the east, may have formed synchronously, giving rise to an asymmetric facies distribution, and were juxtaposed during thrusting (chapter 2 and 3).

Metamorphism

The metamorphic grade in the central outcrop of the Ngezi Group is low, reaching sub-greenschist to greenschist facies (Martin 1978). Cheshire Formation pelites contain very fine-grained chlorite-sericite-quartz assemblages and lack epidote, indicating sub-greenschist facies conditions (Martin 1978; Bickle et al. 1993). The sedimentary rocks show evidence for recrystallization, but sedimentary structures are commonly well preserved. Abell et al. (1985) attempted to constrain the thermal history of the Cheshire carbonates through a combined petrological and stable isotope study. They concluded that the limestones of the Cheshire Formation experienced a maximum temperature of 200°C with a temperature of 80°C or less most likely.

PREVIOUS STUDIES OF THE CHESHIRE CARBONATE CYCLES

Limestones are locally well exposed in the volcanic rocks-bounded lithotectonic unit along the western margin of the Cheshire Formation (Fig. 4.2). This unit consists of a lower interval of metre-scale limestone/shale cycles which are capped by a homogeneous limestone horizon, the main stromatolite outcrop (Fig. 4.2), described in detail by Martin et al. (1980). Limestones are overlain by a continuous, locally irregular layer of karstic limestone breccia. The upper interval consists of locally folded and sheared siliciclastic facies with discontinuous horizons of limestone breccia. The rocks show features similar to a tectonic mélange and are structurally overlain by a tectonic thrust slice of Zeederbergs-type volcanics (chapter 3).

Previous studies of the carbonate member concentrated on a well exposed limestone horizon at the main stromatolite outcrop (Fig. 4.2) which consists of stromatolitic limestones with rare shale intercalations. Martin et al. (1980) noted a cyclical arrangement of facies and measured 22 sedimentary cycles, ranging in thickness from 0.4 to 4.3 metres. Ideally, cycles in this outcrop consist of three “zones”, a lower, middle and upper zone. The lower zone forms the bulk of each cycle and consists of crinkly laminated limestone with minor chert and argillaceous laminae (description after Martin et al. 1980). Three lamination types were observed, a lowermost crinkle lamination, a smooth type which builds broad domical features and a clotty planar lamination defining small columns. The middle zone is a few to 20 cm thick, shows rare lamination and is lacking in several cycles. Pseudomorphs after radiating crystals, now calcite, are common in this zone; they start from a point source and form bundles up to 10 cm in width. Martin et al. (1980) interpreted the radiating crystals as pseudomorphs after aragonite or, less likely, gypsum. The upper zone is only a few centimetres thick. It consists of a dolomitic limestone with a well-

defined, smooth lamination. The laminae partly inherit the underlying morphologies or form small nodular and domical stromatolites. Sand-sized detrital calcareous clasts together with very fine-grained siliciclastic detritus are common.

Martin et al. (1980) interpreted the cyclicity to reflect repetitive environmental changes in a barred, shallow-water lagoon with restricted communication to sea. The lower zone of each cycle is interpreted to reflect carbonate deposition/accretion under relatively quiet water conditions and minimal terrigeneous sedimentation. The middle zone represents the closing of lagoon access to open water due to a fall in sea level. Aragonite or gypsum precipitated due to evaporative concentration of the lagoon waters. The upper zone is interpreted to reflect a sudden influx of fine-grained terrigeneous and calcareous detritus due to breaching of a barrier associated with a rise in water level.

Grotzinger et al. (1993) and Sumner and Grotzinger (2000) refined the sedimentological framework in which the carbonates were deposited. They reinvestigated the Cheshire carbonates around the main stromatolite outcrop, emphasizing the fanning pseudomorphs, interpreted as former aragonite crystals. Sumner and Grotzinger (2000) described a lower siliciclastic-dominated part comprising oolitic limestones, beds of fanning pseudomorphs and domal stromatolites interstratified with shale, siltstone and sandstone with symmetrical ripples, hummocky cross-stratification and slump structures. A wave- or storm-dominated open marine shelf settings with water depths of 5-50 m was envisaged. The upper carbonate-dominated part (the main stromatolite outcrop) was described by Sumner and Grotzinger (2000) to consist of asymmetric carbonate cycles bounded by erosional surfaces. The base of cycles comprises shale, transgressive lags of ooid-intraclast grainstone/packstone and rare flat pebble conglomerate. Overlying this are thin to thick beds of pseudomorph fans alternating with small domal to columnar stromatolites. These facies grade into a crinkly laminite facies forming the top of cycles.

Sumner and Grotzinger (2000) compared the cycles with those common in the record of shallow marine carbonate platforms rather than a restricted, evaporitic setting as suggested by Martin et al. (1980). Flooding of subaerial exposure surfaces was thought to have given rise to the formation of grainstone lags or shale drapes. Fanning pseudomorphs formed in a shallow subtidal setting. Gradual shallowing to the peritidal zone gave rise to the transition into crinkly laminites. This interpretation is different from that of Martin et al. (1980), who placed cycle boundaries between the pseudomorph/stromatolitic facies (middle/upper zone) and the laminite facies (lower zone).

SHALLOWING-UPWARD CYCLES, NGEZI RIVER SECTION

During sedimentological-structural mapping of the Cheshire Formation a well exposed section of the carbonate member was observed in the Ngezi River (Fig. 4.3). The section rests along a sheared, planar contact on hyaloclastites and basalts of the Zeederbergs Formation. The contact is occupied by a 20 cm thick mylonitic mudstone (chapter 3). The lower 111 metres of the section have been measured in detail (Figs. 4.3 and 4.4), which will herein be referred to as

the lower section. Logging was sometimes restricted to a narrow, 1 m wide outcrop revealed by trenching because the exposure is partly covered by alluvium. Above the lower section is a c. 35 m stretch of poor exposure where two additional sections have been measured (middle and upper section, Fig. 4.4). The carbonate sequence ends with a horizon of limestone breccia which, in turn, is overlain by a locally strongly sheared chaotic unit (mélange zone) and a thrust slice of pillowed mafic flows of the Zeederbergs Formation.

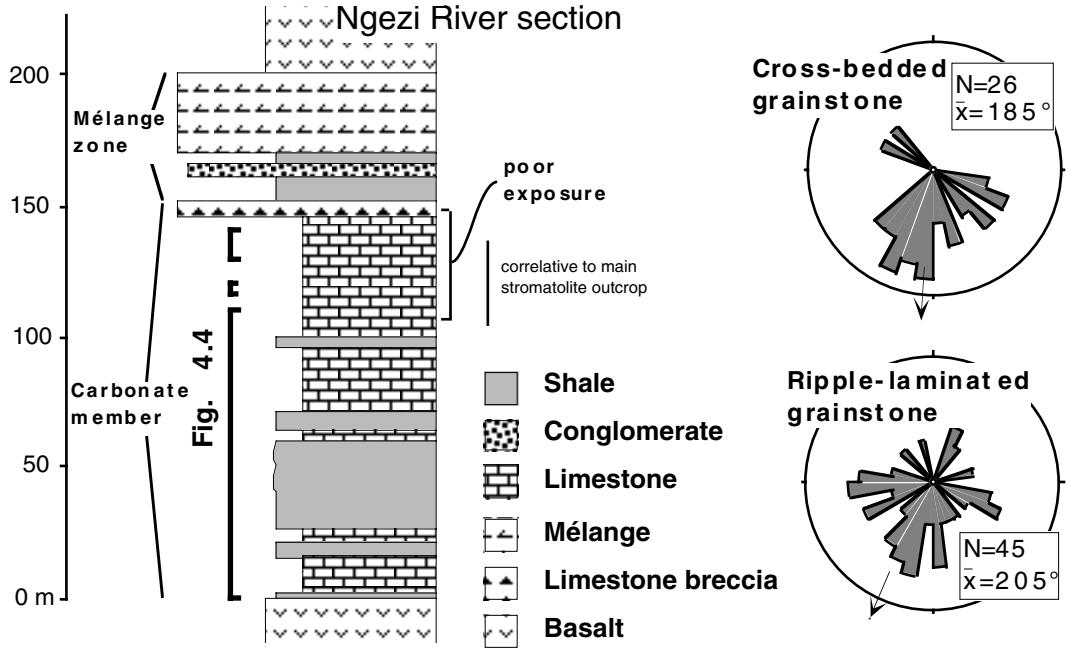

Fig. 4.3. Simplified graphic log of the carbonate member and overlying rocks measured in the Ngezi River. The uppermost limestone-dominated unit is correlative to the main stromatolite outcrop (Fig. 4.2) and is overlain by limestone breccia.

Non-coaxial strain affected the carbonate section during thrusting of the overlying volcanic unit. Thrusting occurred when the sediments were not fully consolidated and gave rise to the formation of sheared shale horizons, chaotic units and disharmonic open to closed folds in the Ngezi River section (chapter 3). Evidence for tectonic duplication or omission has not been observed in the measured section. It is thus assumed that the stratigraphy of the section reflects the stratigraphy as it was originally laid down and that shearing only slightly affected the true thickness of incompetent lithological units such as shale beds.

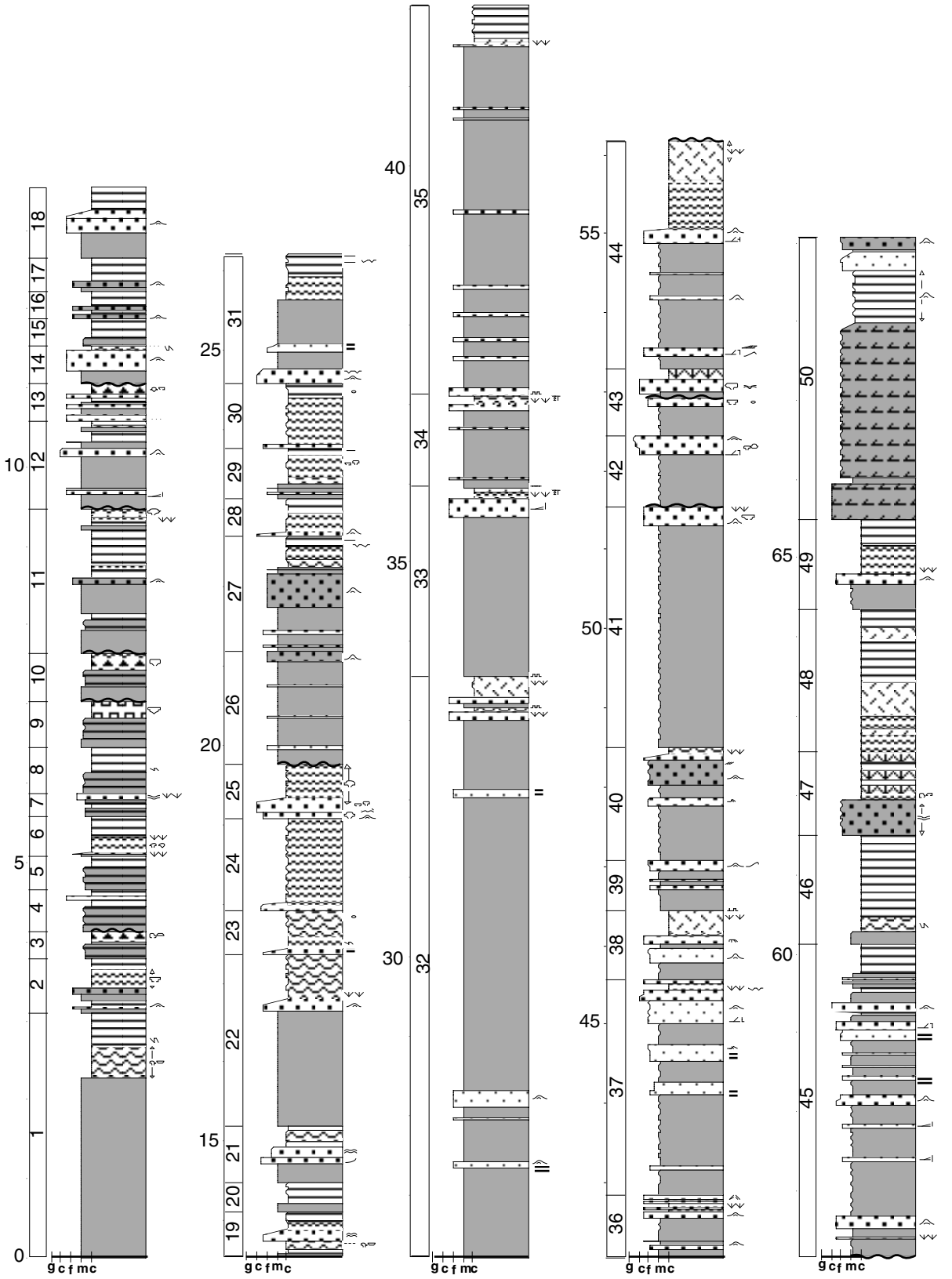

Fig. 4.4. Simplified graphic log of the Ngezi River section. Middle and upper sections are separated by poor exposure or shear zones. The top of the upper section occurs c. 6 m below the karstic limestone breccia (compare with Fig. 4.3).

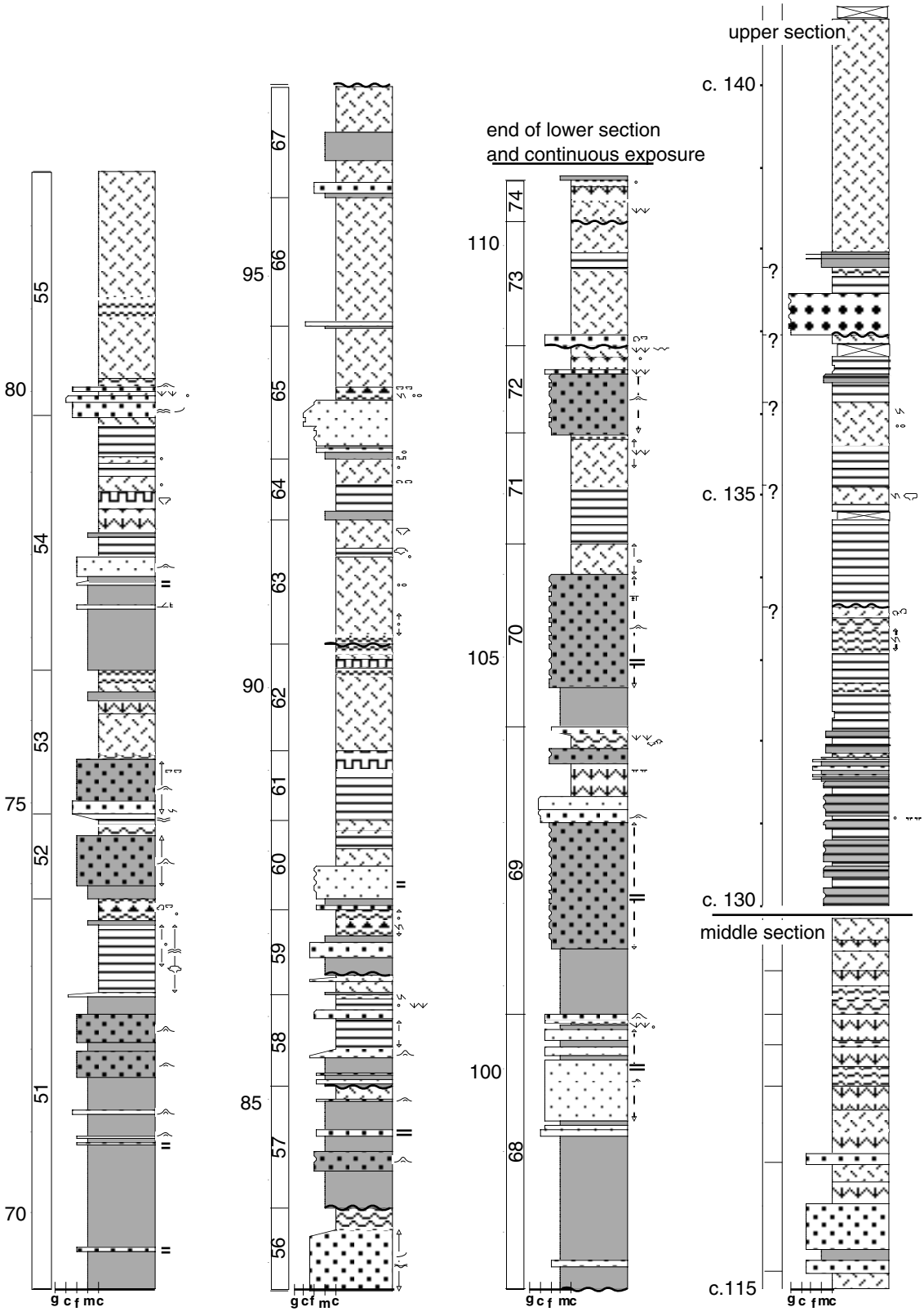

Fig. 4.4 (continued)

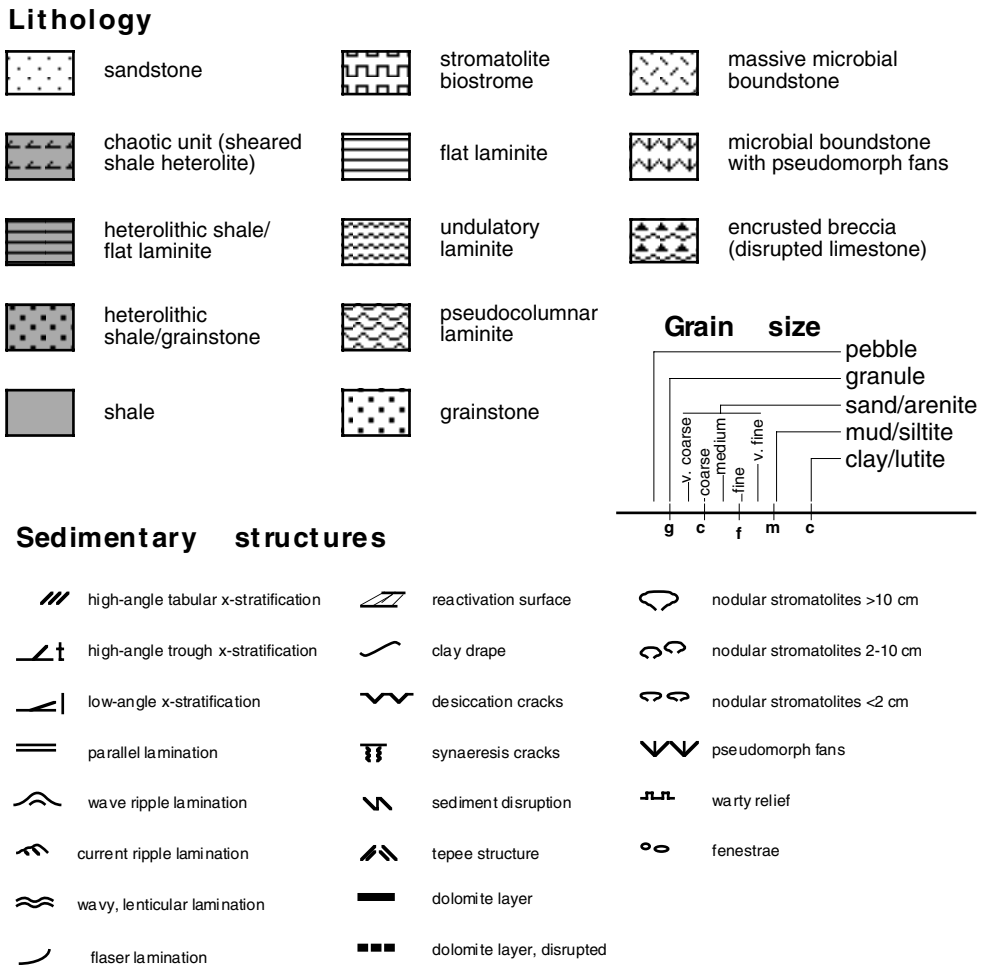

Fig. 4.4 (continued)

Repeated stacking patterns of facies in the measured sections were recognized to be cyclic and were classified as small-scale sedimentary cycles (microcycles). 74 cycles were observed in the lower section (Fig. 4.4). The cycles are between 29 to 734 cm thick (average 150 cm, Table 4.1). Lateral facies relationships could not be investigated due to the spatial restriction of the carbonates in the Cheshire Formation and generally poor, discontinuous outcrop away from the Ngezi River section. Within the river bed some cycles could be traced for up to 100 m along strike; lateral changes in facies/thickness were not observed.

The limestones have been recrystallized into a neomorphic spar (50-200 µm grain size) so that primary microstructures have been destroyed. Consequently, the former presence of microorganisms or biogenic filaments can no longer be ascertained. Larger scale elements such as sedimentary structures and stromatolitic lamination are generally well preserved. The nomenclature of Walter (1976) and Walter et al. (1992, p. 254) is used for the description of morphological aspects of stromatolites. The outline of domal microbial features in plan could not be investigated due to the lack of three-dimensional exposure.

Table 4.1. Number of cycles, their thickness range and average thickness of the basic cycle types of the Cheshire carbonates.

Cycle type	Number of cycles	Cycle thickness range (m)	Average cycle thickness (m)
Shale-based cycle	42	0.37-7.34	1.89
Carbonate cycle	32	0.29-2.97	0.98
Cycles combined	74	0.29-7.34	1.50
Carbonate cycle (m. stromat. outcrop)	22	0.3-4.3	0.99

Lower section in the Ngezi River

Within the measured section, several lithofacies have been defined, which are partly subdivided into subfacies. Lithofacies include (1) shale, (2) grainstone, (3) microbial laminite, (4) nodular/domal stromatolitic limestone and (5) microbial boundstone. In places, thin interbedding of facies and subfacies gives rise to heterolithic deposits.

A facies relationship diagram (Fig. 4.5) has been erected following a Markov chain analysis (Carr 1982; Powers and Easterling 1982) to define characteristic stacking patterns of facies and determine facies variations within cycles. The definition of common cyclic patterns was aided by visual examination of the graphic log. Two basic cycle types can be defined on the basis of the presence or absence of shale beds. Shale-based cycles have a prominent bed of shale at the base, which is rarely underlain by a thin bed of basal grainstone subfacies. Shale is typically overlain by various grainstone subfacies (cross-bedded, ripple-laminated, massive varieties) which are, in turn, overlain by microbial laminites (Fig. 4.6). Microbial laminites typically comprise a lower pseudocolumnar subfacies which grades upsection into an undulatory and then into a flat laminite subfacies. Both grainstone and laminite facies contain scattered nodular/domal stromatolites. The laminite facies can be capped by locally disrupted, stromatolitic limestone facies (Fig. 4.7).

Cycles lacking shale beds consist of ripple-laminated and massive grainstone subfacies at the base overlain by microbial laminite, and only differ from shale-based cycles in the absence of the basal shale bed. In the upper part of the measured section, the laminite facies of both cycle types is commonly intercalated with, or overlain by, microbial boundstones (Fig. 4.7).

Several cycles in the lower part of the section have a heterolithic laminite/shale facies at the base which grades into flat laminite upsection. Such cycles as well as those containing only a thin shale bed at their base (less than 25% of cycle thickness) have been grouped together with the carbonate cycles. A few shale-based cycles are capped by grainstone without grading into laminite, or heterolithic laminite/grainstone facies, which are sharply overlain by shale of the next cycle (Fig. 4.7). The basic cycle types and the variations thereof are genetically linked to one another since they share common lithofacies. The cyclic motif is asymmetric inasmuch as the transition from basal shale or grainstone to microbial carbonates is gradational, whereas shale or grainstone commonly sharply overlie microbial carbonates of the underlying cycle.

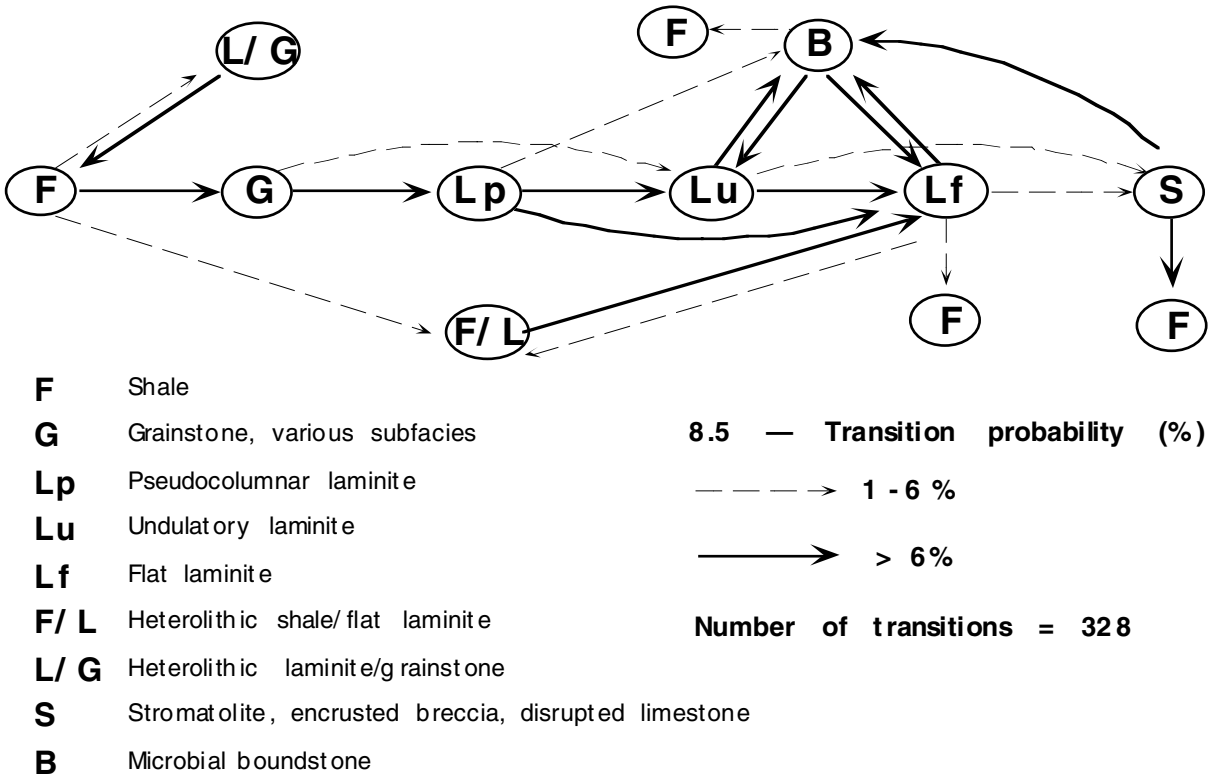

Fig. 4.5. Facies relationship diagram for the lower section. Grainstone includes massive, ripple-laminated, cross-bedded, flaser-bedded and the heterolithic shale/grainstone subfacies. Stromatolitic limestone includes stromatolite biostrome, encrusted breccia and disrupted facies. Boundstone encompasses the massive and pseudomorph-rich varieties. Note that facies L/G, F/L and S are rare with only 6, 11, and 12 upward transitions, respectively.

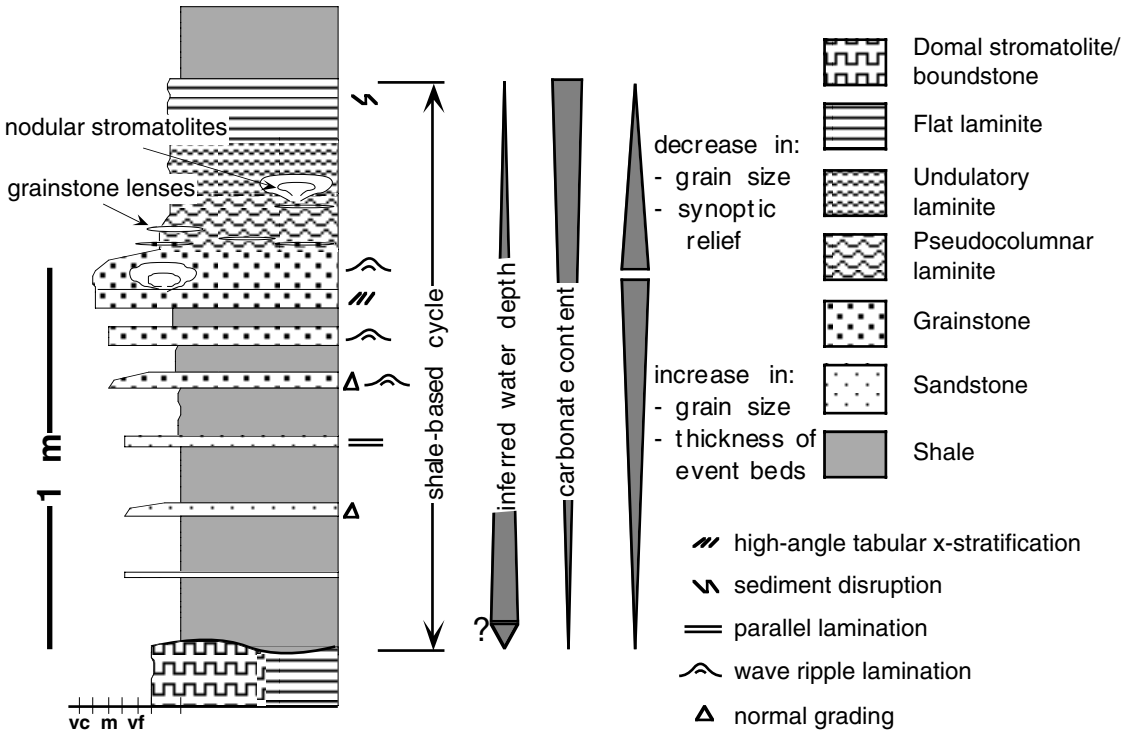

Fig. 4.6. Generalized shale-based sedimentary cycle of the lower section.

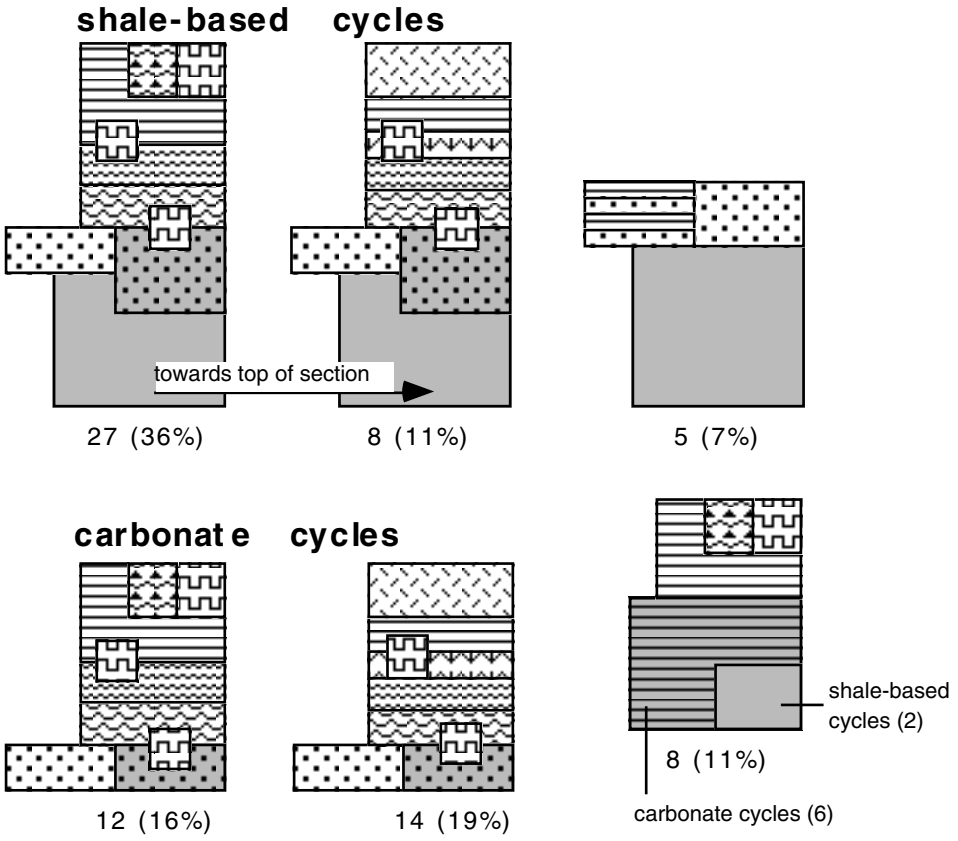

Fig. 4.7. Generalized types of sedimentary cycles observed in the lower section, their frequency and relative abundance (see Fig. 4.4 for key of lithologies).

1) Shale

Shale forms the lower part of shale-bearing cycles and comprises planar-laminated mud/siltstone intercalated with event beds of sand/grainstone (Table 4.2). These beds show normal grading, a waning flow sequences and wave ripple cross-lamination in upper bed portions. Shale sharply overlies and drapes the relief of underlying beds such as domed biostromes. Shale horizons are, on average, more clayey in their lower part. Clay-rich portions are commonly sheared, giving rise to massive mudstones with discontinuous layers or lenses of boudinaged, commonly dolomitized sandstone or grainstone beds. In several cases, sand/-grainstone intercalations become more numerous and partly amalgamate upsection (Fig. 4.8a).

Interpretation: Sedimentary structures of the event beds is characteristic for storm deposits (Aigner and Reineck 1982). Undulating cross-lamination may represent hummocky cross-stratification, which was reported by Grotzinger et al. (1993) and Sumner and Grotzinger (2000). The thickening upward trend of storm deposits, which is associated with an increase in average grain size upsection, and which partly culminates in the amalgamation of storm deposits, is indicative of progressive proximality due to water shallowing (Aigner and Reineck 1982). Silt-mud rhythmite can be interpreted as more distal storm layers or deposits of less severe storms that accumulated by storm-surge ebb currents below storm wave base, with each silty storm bed overlain by fair-weather, suspension fall-out mud. Soft sediment deformation such as convoluted bedding indicates dewatering and associated contortion after rapid sedimentation. Lower, more-fine-grained portions of shale horizons rarely contain thin event beds which

possibly formed near mean storm-weather wave base during exceptional storm events; upper parts of shale beds that comprise abundant event deposits formed between storm and fair-weather wave base.

Table 4.2. Description of shale and grainstone facies.

Facies	Shale (1-680 cm)	Grainstone	
Subfacies		Basal grainstone (5-15 cm)	Heterolithic shale/grainstone (5-160 cm)
Bedding characteristics	Heterolithic, thinly bedded/laminated rock (Fig. 4.8a). Tabular sand/grainstone beds with sharp lower contacts and gradational upper contacts (typically a few cm thick) are common.	Thin, tabular beds of dolomitic pack/grainstone.	Continuous to lenticular grainstone beds (1-4 cm) intercalated with continuous to discontinuous layers (0.3-1 cm, but up to 2 cm thick) of mudstone. Thin layers and patches of calcilutite/siltite are associated with grainstone.
Lithology	Dark grey clayey siltstone with minor very fine-grained sand is intercalated with laminae/thin beds (0.1-2 cm thick, typically 0.5 cm thick) of siltstone. Sandstone is very fine to fine-grained; grainstone is medium-grained. Both contain angular, tabular mud intraclasts (less than 1 cm across) in basal bed portions.	Fine- to coarse-grained (mainly medium-grained) rounded micrite clasts and coated grains, mainly ooides. The intergranular volume is occupied by sparite; a micrite matrix is less common. Tabular calcilutite/siltite intraclasts (typically 1 cm in length and 1 mm thick) occur. Angular to rounded shale intraclasts (up to 1 cm across) are locally common; similar sized fragments of chert, coarsely crystalline calcite, basaltic? rock fragments and quartz occur in subordinate amounts.	
Sedimentary structures	Siltstone laminae are normally graded and show rare ripple lamination; the lamination is rarely contorted. Sandstone beds show common normal grading; typically, the base is a massive, discontinuous horizontally or undulatory laminated fine sand, which grades into massive, horizontally or current to wave ripple-laminated silty fine sand to clayey silt at top. Mm-scale scours (up to 20 cm in length, 1 cm deep) are common. Grainstone beds are mostly ungraded and show low-angle to undulating cross lamination.	Horizontal and wave ripple lamination, but dolomitization obliterated most structures. Poor sorting; irregular, discontinuous, partly disrupted mudstone laminae and pseudomorph fans occur. Mud-filled cracks (1-2 mm in width, a few cm in length) are sub-vertical to bedding (desiccation cracks?).	Wave ripple and rare parallel-laminated grainstone, the latter partly containing rock fragments up to 2 cm across. Mudstone is horizontally laminated. Calcilutite/siltite layers are flat, wrinkly or undulatory laminated; the lamination is partly brecciated.

2) Grainstone

Grainstone and, less frequently, calcareous sandstone beds occur in between shale and overlying microbial carbonates of shale-bearing cycles. Sandstone is fine- to medium-grained, and contains varying proportions of carbonate material. It does not differ in sedimentary structures and stratigraphic position to grainstone and is thus included in the grainstone facies. Grainstone mainly consists of sand-sized, rounded micrite clasts and ooides, and larger tabular micrite intraclasts. Grainstone forms thin tabular beds that are interbedded with shale or arranged into tabular bedsets a few decimetres thick. Beds have sharp and planar erosive contacts. Several grainstone subfacies have been defined and are described below. Palaeocurrent data have been obtained from cross-bedding and ripple lamination (Fig. 4.3) and were corrected to account for tectonic disturbance (refer to chapter 2 a for details).

Table 4.2 (continued).

Facies	Grainstone			
Subfacies	Cross-stratified grainstone (5-25 cm)	Ripple-laminated grainstone (5-30 cm)	Massive pack/grainstone (5-30 cm)	Flaser-bedded grainstone (10-75 cm)
Bedding charateristics	Tabular, thin to medium cross-stratified beds and medium bedsets. Foresets are defined by differences in grain size/type e.g. siliciclastic fine sand vs medium sand-sized ooids.	Isolated ripples in shale (Fig. 4.8c), lenticular thin beds or tabular, thin to rare medium beds, several dm thick bedsets. Lower contacts are sharp and rarely erosive.	Tabular thin to medium beds; some horizons have a wavy relief of up to 10 cm (domed biostromes). Hemispherical to ellipsoidal, unlinked domes 5-10 cm in width are rare. Thin intercalations of flat laminite are minor.	Tabular thin to thick beds; pinching-and-swelling layers and lenses are commonly draped or separated by thin veneers of mudstone in an anastomosing pattern (Fig. 4.8d).
Lithology	Same as previous; local mudstone intraclasts.	Same as previous.	Same as previous; micrite matrix common. Domes consist of massive fine grainstone; the interstices are filled with very coarse to granule grainstone.	Calcisiltite to fine-grained calcarenite.
Sedimentary structures	Tabular and trough cross-bedding; partly herring-bone stratification (Fig. 4.8b). Foresets are rarely draped by c. 1 mm mud films; rare reactivation surfaces.	Wave ripple and minor current ripple lamination. Thin to medium mudstone laminae drape ripple bedforms. Isolated ripples comprise bidirectional and bidirectional bundled lenses (up to 4 cm in heigth, 25 cm in length). Mud-filled, downward-tapering cracks; some cracks start from the lower contact and taper upward.	Massive to ill-defined, even to irregular, discontinuous horizontal lamination to thin bedding (1-3 cm). Layers are partly draped by 1-2 mm thick mud laminae. Mud drapes can be irregular and disrupted. Wave ripple lamination is rare. Fenestrae are common to absent.	Non-parallel, very thin flaser to wavy-bedded rock. Grainstone layers/lenses are massive or wave ripple-laminated; some lenses are oversteepened beyond the angle of repose.

Basal grainstone

Thin, tabular beds of ripple-laminated and massive grainstone (Table 4.2) rarely occur at the base of shale-bearing cycles and sharply rest on laminite or stromatolite facies of the underlying cycle.

Interpretation: The basal grainstone subfacies may represent a transgressive lag deposit that formed during a rapid sea level rise (e.g., Hoffman 1975; James 1984; Grotzinger 1986a). In contrast, evidence for reworking of underlying sediments is absent. The subfacies more likely represents storm deposits that formed in the early phase of a relative sea level rise.

Heterolithic shale/grainstone

This subfacies commonly occurs between shale and microbial laminite or between shale and grainstone bedsets. In some cases it forms cycle tops. The facies is characterized by thinly interbedded grainstone and mudstone with minor, partly brecciated microbial laminite (Table 4.2).

Interpretation: Each grainstone layer represents a storm deposit that is interbedded with fair-weather suspension mud. Rare parallel-lamination in pebbly grainstone indicate deposition in a high-energy upper-flow regime. Microbial mats temporarily flourished in this shallow subtidal

environment, forming laminites which rarely became disrupted, possibly as a result of strong storm currents or subaerial exposure.

Cross-stratified grainstone

Tabular and trough cross-bedded grainstone (Table 4.2) occurs as single beds in the upper part of shale horizons (Fig. 4.8b) and in between shale and microbial limestones where it is interbedded with the ripple-laminated and massive grainstone subfacies. Cross-bedding has a trimodal distribution with a dominant flow to the south-southwest, and a subordinate bipolar southeast-northwest flow (Fig. 4.3).

Interpretation: This subfacies formed as straight-crested to crescentic dunes which probably covered the sea floor as thin, sheet-like units at or above fair-weather wave base. Rare herring-bone cross-beds, mud films and reactivation surfaces indicate unsteady flow conditions, probably due to a minor tidal influence characterised by tidal current and slack water phases. Tidal activity is further indicated by the bipolar southeast-northwest palaeoflow. The dominant south-southwest palaeoflow probably records storm-generated alongshore currents.

Ripple-laminated grainstone

Ripple-laminated grainstone (Table 4.2) is common in the upper part of shale horizons; beds commonly amalgamate upsection to form several decimetres thick bedsets (Fig. 4.8c). Ripple-laminated grainstone further occurs at the base of carbonate cycles. Palaeocurrent data (Fig. 4.3) has a trimodal distribution similar to the cross-bedded subfacies with a south-southwest flow, and a pronounced bipolar east-west flow.

Interpretation: This subfacies is dominated by wave ripple lamination (de Raaf et al. 1977) and formed as thin ooide sheets subjected to oscillatory currents close to fair-weather wave base. Ripple-laminated grainstone with relatively thick shale intercalations formed below mean wave base. Mudcracks are not related to desiccation as indicated by their upward tapering geometry. The activity of wave- and/or tide-generated currents is more strongly recorded in this facies as compared to the cross-bedded variety, suggesting that ripple-laminated grainstones are fair-weather deposits.

Massive pack/grainstone

Massive grainstone exhibits stromatolitic fabrics and relics of ripple lamination (Table 4.2). It occurs at the base of carbonate cycles and in between shale and microbial limestones where it is intercalated with ripple-laminated grainstone.

Interpretation: The occurrence of flat lamination and domal stromatolites indicates microbial activity. Microbial mats may have trapped and binded coarse-grained sediment to give rise to poorly stratified grainstone. Sediment disruption probably took place upon periodic subaerial exposure in a shallow sub- to intertidal environment.

Flaser-bedded grainstone

This subfacies is characterised by flaser to wavy-bedded fine-grained grainstone (Fig. 4.8d, Table 4.2). It is most common between ripple-laminated grainstone and overlying microbial limestone, and is rare at the base of carbonate cycles.

Interpretation: The stratification style indicates alternating phases of current/wave action and slack water, and resembles similar structures of shallow subtidal and intertidal deposits of siliciclastic tidal flat environments (Reineck and Wunderlich 1968). Oversteepened lamination is attributed to the presence and stabilizing effect of microbial mats.

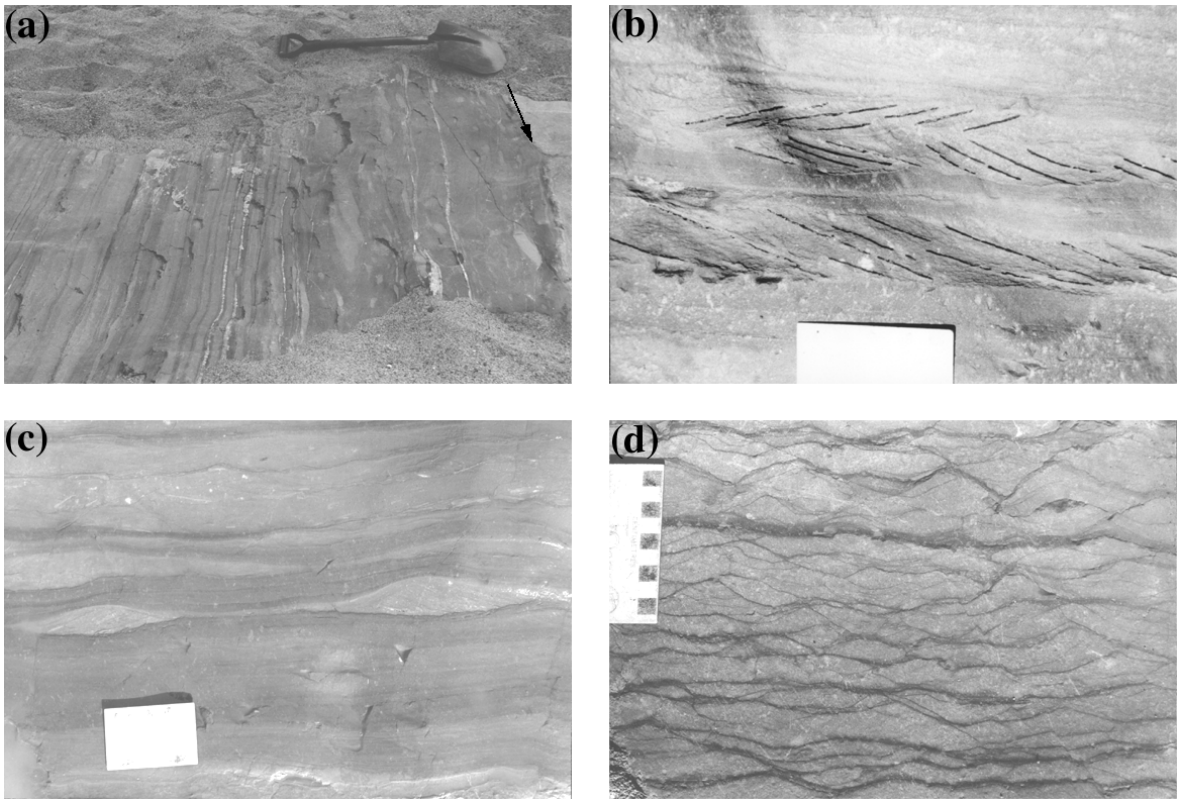

Fig. 4.8. Features of shale and grainstone facies from the lower section in the Ngezi River. a) Lower part of a sedimentary cycle comprising basal sheared shale that overlies a domed biostrome along a cycle boundary (arrow) and that grades into less deformed shale with thickening-upward sand/grainstone event beds. b) Thin beds of cross-bedded grainstone in shale; note herringbone pattern (lamination is enhanced with a marker pen). c) Shale (bottom) grading into wave-ripple laminated grainstone (top). Note bimodal cross-lamination in isolated ripple bedforms (centre). d) Flaser-bedded grainstone; note partly oversteepened lamination.

3) Microbial laminite

Microbial laminite (Fig. 4.9, Table 4.3) frequently forms cycle tops and includes a flat and undulatory laminite subfacies (corresponding to stratiform stromatolites with flat/undulatory lamination), and a pseudocolumnar laminite subfacies (or pseudocolumnar stromatolite, see Walter et al. 1992; Hofmann 2000). A heterolithic shale/flat laminite subfacies further occurs. The different laminite types are discussed together since they are closely associated within a cycle. Pseudocolumnar laminite commonly underlies, or is intercalated with, undulatory laminite, which, in turn, commonly underlies, or is intercalated with, flat laminite (Fig. 4.5). Microbial laminites thus show a decrease in synoptic relief upsection. Beds are tabular, thin to thick and

share gradational contacts. The lamination is defined by (1) colour contrasts (light and medium grey) between individual laminae, which may be related to contrasts in grain size and/or organic content, and, subordinately, by (2) the occurrence of thin to sub-mm mud-laminae, and (3) the occurrence of sand-sized carbonate grains in particular laminae in some beds. The lamination is enhanced by bedding-parallel stylolites. The laminites consist of calcilutite to calcisiltite. Sand-sized intraclasts, ooids and rare oncoids occur in lenses, irregular layers or scattered. Sand-sized grains are particularly common in the basal part of pseudocolumnar laminites, which comprise up to 50% of calcarenite decreasing in frequency upsection. Tabular micrite intraclasts with the same thickness as adjacent, undisturbed laminae, and nearly in-place occur frequently. Continuous thin layers of dolomite-cemented micrite locally occur, mostly near and along cycle tops. Pseudocolumnar and undulatory laminites, when overlain by shale, have an irregular relief up to 4 cm in hight, indicative of slightly domed biostromes, whereas flat laminites have a planar upper contact. In a few cycles, the uppermost 20 cm below heterolithic flat laminite/shale or shale of the next cycle show an upward increase in calcarenite material and synoptic relief or contain intercalations of shale laminae/thin beds, giving rise to a more conformable cycle boundary.

Interpretation: The microbial laminites appear to have formed by carbonate precipitation and trapping and binding of sediment by microbial mats. The former presence of microbes is indicated by (1) the geometry of laminae comprising detrital sediment which indicates microbial "stickiness" (e.g. convex-upward wrinkly features with lateral margins beyond the angle of repose), (2) features indicating an encrusting relationship, (3) jelly roll structures, (4) the association with domal stromatolites and small-scale stromatolitic bumps, (5) matrix-supported outsize grains (e.g. oncoides), indicating sediment trapping (cf. Aitken 1967; Hardie and Ginsburg 1977). Calcarenitic sediment probably represents storm-deposited as well as wave-reworked material either sticking to the mucilagineous sheaths, trapped by the filaments of microbial mats, or forming ripple-laminated, purely mechanically deposited sediment later stabilized by microbial mat overgrowths. Carbonate mud either settled from suspension, agglutinated by microbial activity or precipitated within the mats by biogenic and/or abiogenic processes. The mm-scale warty features common to the flat laminites indicate an originally pustular surface of the mats. Stratiform and pseudocolumnar stromatolites are the most common types in Archaean carbonates (Hofmann 2000). The ones described here are much similar in lamination style to, for example, the stromatolites described by Henderson (1975) from the Archaean Slave Province of Canada.

Table 4.3. Description of microbial laminite and associated heterolithic subfacies.

Facies	Microbial laminite		
Subfacies	Pseudocolumnar laminite (5-55 cm)	Undulatory laminite (5-105 cm)	Flat laminite (5-105 cm)
Bedding characteristics	Thin to thick beds gradational to undulatory laminite. Isolated, hemispherical to nodular forms (1-5 cm wide, up to 3 cm in hight, synoptic relief up to 2 cm) are common, and partly combine to form cauliflower-like structures (Fig. 4.9d). Rare other laminated limestones with columnar-layered, cumulate and chevron-type lamination.	Thin to thick beds gradational to other laminite facies (Fig. 4.9a). Hemispherical to cumulate, mostly isolated forms (up to 2 cm across) are locally common.	Thin to thick beds that commonly form cycle tops. Hemispherical forms (up to 2 cm across, synoptical relief less than 1 cm) and thin intercalations or patchy, ellipsoidal occurrences (up to 20 cm in width, 13 cm in hight) of massive limestone are rare. Thin mudstone laminae are common where flat laminite grades into the heterolithic shale/flat laminite subfacies.
Lithology	Calcilutite/siltite with common grainstone layers and lenses/patches in basal bed portions; anastomosing mud laminae and disrupted dolomite-cemented thin layers occur locally.	Calcilutite/siltite; rare grainstone lenses; anastomosing mudstone laminae are common.	Calcilutite/siltite with minor calcarenite lenses and mudstone laminae. Oncolites (0.5 - 2 mm across, micrite matrix-supported) are common in particular laminae. Tabular micrite clasts (up to 2 cm in length, a few mm thick) subparallel to bedding are common in certain layers in a sparry matrix. Some beds contain thin, continuous, dolomite-cemented layers.
Lamination style/ sedimentary structures	Lamination is wavy to wrinkled, gently to steeply convex, and rectangular to rhombic. Nodular forms have wavy rhombic to steeply convex lamination. The lamination is locally disrupted giving rise to a patchy, irregular fabric with intraclasts. Pseudomorph fans are common in a few beds and nucleate at the centre of growth forms. Fenestrae are common to absent. The synoptic relief of the lamination partly decreases upsection from 2 cm to less than 0.5 cm; this is sometimes associated with an increase of fenestrae upsection. Other non-columnar stromatolite types have smooth to wrinkly to wavy laminae and partly contain or grade into centrimetric nodular, rhombic forms or hemispherical to turbinate forms. Laterally linked, chevron-type stromatolites are mostly associated with massive limestone and have up to 13 cm of synoptic relief.	Smooth to wrinkly, undulatory laminated to thinly bedded. Layers or irregular domains with disrupted lamination occur locally. Stratiform spar-filled fenestrae are rare. Downward tapering and partly bifurcating, desiccation cracks up to 0.8 cm in width occur. The cracks are filled with coarse to very coarse-grained coated grains which are restricted to the cracks (unbridged cracks; Allen, 1984).	Continuous to discontinuous, horizontal, planar to wrinkly laminae (0.5-10 mm thick, mostly less than 5 mm). Thick laminae are continuous for up to a few metres, and are pinching and swelling with wavy upper and planar lower contacts; superposed lenticular features bearing an encrusting, gravity-defying relationship are common. Thin laminae are continuous for a few dm only; the discontinuity is partly related to irregular pressure solution seams. Calcisiltite lenses (1-2 dm long, up to 2 cm thick) are common (Fig. 4.9b). Rarely occur lenses to thin beds/laminae of calcarenite with faint wave ripple lamination and overlain by thin micrite laminae. Small-scale disconformities (up to 2 mm relief) occur. Warty to knotty, internally massive features (1 mm in diameter) are common. Mud drapes have cuspate lower contacts mimicking the warty surface of underlying limestone beds. Stratiform spar-filled fenestrae are rare. The lamination in some beds is uparched, disrupted and brecciated; jelly roll structures (Demicco and Hardie, 1994) are rare (Fig. 4.9c). Mudstone partly occurs as anastomosing layers sub-parallel to bedding and in sub-vertical cracks. The cracks are up to 0.5 cm wide, ptygmatically folded, and are downward but also upward tapering.

Table 4.3 (continued).

Facies	Microbial laminite	
Subfacies	Heterolithic shale/flat laminite (5-65 cm)	Heterolithic laminite/grainstone (5-40 cm)
Bedding characteristics	Typically 1 cm thick layers of planar tabular interstratified laminite and shale.	Flat- to undulatory laminite thinly intercalated with massive or discontinuous horizontal to ripple-laminated grainstone.
Lithology	Calcilutite/siltite and shale heterolite; rare grainstone lenses.	Calcilutite/siltite and grainstone heterolite; rare shale intercalations; uppermost few cm of sediment below cycle boundaries and thin layers within beds are cemented by dolomite.
Lamination style/ sedimentary structures	Limestone is flat to undulatory laminated or massive. Limestone-shale contacts are sharp and warty with a typical relief of 1 mm. Thin layers/lenses of massive or wave rippled grainstone (up to 1 cm thick) are less common. Centrimetric domical forms occur locally. Rare disruption is indicated by uparched laminae and micrite clasts. Subvertical and stratiform, mud-filled shrinkage cracks (partly filled from below) are common.	Grainstone is wave ripple and unidirectional cross laminated. Some beds have an irregular disrupted fabric and contain irregular fenestrae up to 3 cm across filled by sparite and dolomitic mud. Small-scale, laterally-linked growth forms occur locally forming wavy thin beds with a low synoptic relief. Ellipsoidal to spherical stromatolitic patches (up to 30 cm across) occur scattered or preferably at bed tops. These patches are composed of small-scale subspherical stromatolites. Pseudomorph fans are common in layers with a stromatolitic fabric, and less common in lenticular grainstone beds. Thin strongly dolomite-cemented layers (0.5-1 cm thick) form concave-upward, crescent-shaped layers similar to tepee structures. Dolomitic rock along cycle tops contains lenticular cracks up to 4 cm in length that partly cross-cut each other.

Periodic subaerial exposure of the undulatory and flat laminite subfacies is indicated by desiccation cracks, fenestrae as well as common in situ sediment disruption, suggesting that they formed in a peritidal environment. Most of the mud-filled cracks, however, have a non-desiccation origin and may have formed by syneresis or substratal compaction dewatering (cf. Demicco and Hardy 1994). The infrequent occurrence of unequivocal desiccation cracks may indicate that subaerial exposure of the sediments was not a frequent process or that the groundwater table rarely dropped below the sediment surface. However, the binding of surface sediment of intertidal to supratidal flats by microbial mats can also prevent mudcracks to form (Demicco and Hardy 1994, their Figure 70A, B). The dolomitic layers near cycle tops may represent early cemented surface crusts similar to the dolomitic crusts of the supratidal flats of the Bahamas (Shinn et al. 1969), indicating periods of non-deposition at the end of cycle formation. The pseudocolumnar subfacies possibly formed in a wave-swept, very shallow subtidal to lower intertidal environment which remained submerged for most of the time. The abundance of calcarenitic material in the pseudocolumnar subfacies and its near absence in the flat laminite subfacies may depend on variations in the ambient sediment supply. However, microbial mats with an irregular surface topography are more prone to trap coarse sediment than smooth mats (Riding 2000). The heterolithic shale/laminite facies probably formed in a relatively quite-water, shallow subtidal to intertidal environment, and part of the carbonate material was mechanically deposited, possibly during storms. The common change in stratification style from pseudocolumnar to flat lamination, the associated decrease in synoptic relief, and the gradual increase in the amount of fenestrae is typical for a gradual shallowing of the water (see below).

Heterolithic laminite/grainstone

Flat- to undulatory laminite is thinly intercalated with massive or rippled grainstone. This rare facies forms continuous medium beds that either occur between grainstone and laminite facies or form the top of a few cycles where it is strongly dolomitic. Tepee structures, irregular fenestrae, small-scale stromatolitic growth forms and pseudomorph fans are common (Table 4.3).

Interpretation: This facies is similar to the massive grainstone facies and represents an amalgam of mechanically deposited to microbially agglutinated coarse-grained sediment, and agglutinated and precipitated carbonate mud. Deposition possibly took place in an intertidal to supratidal setting. Dolomitic layers may represent dolomitic crusts that originated by lithification of the tidal flat sediments during subaerial exposure as indicated by tepee structures. Tepees are a common feature of supratidal crusts of the Bahamas (Hardie and Ginsburg 1977). The lenticular shape and the cross-cutting relationship of cracks in the dolomitic crust below cycle boundaries resembles moulds after former interpenetrating gypsum crystals (cf. Astin and Rogers 1991). If the cracks are truly moulds, gypsum may have grown in the final stages of cycle development due to the evaporative concentration of groundwaters in the supratidal environment.

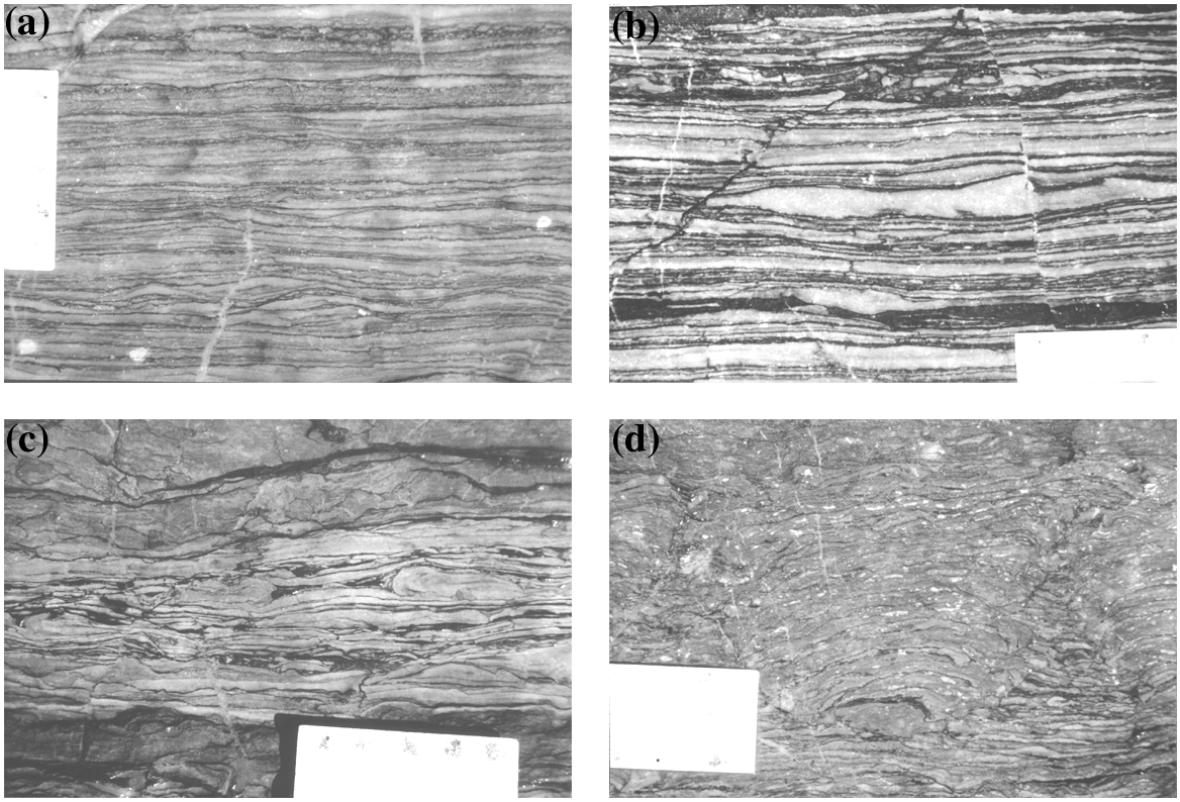

Fig. 4.9. Features of microbial laminite from the lower section in the Ngezi River. a) Undulatory to flat laminite. b) Flat laminite with shale laminae, discontinuos calcilutite/siltite lenses, local brecciation and mudcracks. c) Disrupted flat laminite with mud cracks and jelly roll structures; note the presence of stylolites. d) Pseudocolumnar laminite forming nodular to bulbous stromatolitic forms; note the presence of laminoid fenestrae.

4) Nodular/domal stromatolitic limestone

Three subfacies containing convex-upward stromatolitic growth forms are distinguished, namely the stromatolite, encrusted intraclast breccia and disrupted, fenestrae-rich limestone subfacies.

Stromatolite

The stromatolite subfacies includes non-branching columnar growth forms (Table 4.4). They occur mostly as isolated forms in the microbial laminite facies (Fig. 4.10a), and the ripple-laminated and massive grainstone subfacies. Stromatolites are rare in heterolitic laminite/grainstone, flaser-bedded grainstone and massive microbial boundstone subfacies. The stromatolites are partly laterally linked and, in several cases, coalesce upwards to form tabular to domed bioherms. Upward coalescence is generally associated with a decrease in synoptic relief. Domed bioherms forming the top of depositional cycles commonly have an undulating (convex-upward) relief of up to 20 cm. The uppermost few centimetres are commonly strongly dolomitized, giving rise to yellowish brown, weather-resistant crust-like rock.

Interpretation: The stromatolites formed by trapping and binding of detrital sediment in addition to possible carbonate precipitation by benthic microbial communities. Sediment trapping is indicated by the selection of the finer-size fractions of available detritus (e.g., Hardie and Ginsburg 1977). The stromatolites occur in various facies interpreted to have formed in subtidal to intertidal environments and, hence, are not precise indicators for a particular depositional environment. However, isolated, unlinked forms preferentially formed in shallow subtidal settings (grainstone facies), possibly due to greater wave agitation. Early sea-floor cementation during periods of non-deposition may have provided firm substrates for the stromatolites to form. Shallowing to the intertidal zone was accompanied by lateral linkage of the domes, probably due to a decrease in current velocity and intensity of erosion between domes (Grotzinger 1986a).

Encrusted intraclast breccia

The breccia subfacies comprises clasts of microbial laminites encrusted by stromatolites (Fig. 4.10b, Table 4.4). It forms individual beds at cycle tops or, less frequently, is gradationally intercalated with or forms discontinuous lenses and irregular-shaped patches within less disrupted flat- to undulatory stratified laminite.

Interpretation: The gradational contact of intraclast breccias to adjacent, undisrupted laminites and the absence of basal erosional scours indicate that the facies formed by in situ disruption of tidal flat laminites. Disruption may have taken place by erosional rip-up during storm wave processes or, more likely, by desiccation of the laminites during prolonged subaerial exposure under supratidal conditions. Encrustation of the intraclasts by micritic material may have been aided by microbial communities covering the breccias and forming stromatolitic fabrics, but direct, anaerobic precipitation of carbonate during periods of subaerial exposure and non-deposition is equally possible, giving rise to the formation of thin caliche crusts (Esteban

and Klappa 1983). Koerschner and Read (1989) and Osleger and Read (1991) observed similar breccias at the top of some Cambrian peritidal cycles and interpreted them as thin regoliths that resulted from prolonged subaerial emergence of the tidal flats during sea level lows.

Table 4.4. Description of stromatolite, microbial boundstone and matrix-supported breccia facies.

Facies	Nodular/domal stromatolitic limestone		
Subfacies	Stromatolite	Encrusted intraclast breccia (5-25 cm)	Disrupted, fenestrae-rich limestone (5-35 cm)
Bedding characteristics	Hemispherical to nodular to bulbous, non-branching columnar stromatolites scattered in various facies; individual forms sometimes coalesce and form beds (10-25 cm thick). The stromatolites have ellipsoidal to rhombic shapes and are 5-70 cm in width with a hight to width ratio between 0.35 and 0.7 (typically 0.4). Scattered stromatolites have sharp and rarely gradational to diffuse margins where the stromatolitic fabric interfingers with adjacent facies (Fig. 4.10a).	Clast-supported intraclast breccia; cauliflower-like, hemispherical to bulbous, partly rhombic domes are intercalated with the breccia and partly enclose and encrust it. The domes are either unlinked (hight to width ratio: 0.3-0.5), or become laterally linked upsection to form tabular biostromes. Synoptic relief decreases upsection from c. 5 cm to less than 1 cm.	Thin to medium tabular beds (partly domed biostromes) of disrupted flat- to undulatory laminated limestone.
Lithology	Calcilutite/siltite; irregular to anastomosing mudstone laminae are infrequent. Stromatolites associated with grainstone comprise up to one third of fine and minor medium sand-sized grains which are concentrated in certain laminae and, less frequently, are irregularly distributed. Coarse sand-sized grains common in adjacent grainstone is absent in the stromatolites.	Clasts are angular to subrounded, tabular to irregular, light grey calcilutite/siltite (1-8 cm in length, 0.1-1 cm thick); they are internally massive or laminated. The clasts are either embedded in a medium grey, massive micrite matrix or are encrusted by irregular layers (up to a few mm thick) of light grey calcilutite (Fig. 4.10b). Disrupted dolomitic layers occur locally.	Calcilutite/siltite; shale and micrite intraclasts are abundant; calcarenitic material is absent.
Lamination style/ sedimentary structures	Pseudocolumnar to undulatory and partly cumulate lamination; laminae are thin to thick (mostly less than 3 mm), smooth to wavy to wrinkled, moderately to steeply convex to rectangular. Commonly, stromatolites consist of subspherical, nodular forms (typically 1 cm across) with wrinkled steeply convex laminae which give the stromatolites a cauliflower-like appearance (Fig. 4.10a). Laminoid spar-filled fenestrae are common at the top of some domes whereas irregular fenestrae occur at stromatolite margins.	Clast long axes are subparallel to bedding and, less frequently, random or perpendicular (edgewise) to bedding. Encrusting stromatolites have wrinkly steeply convex laminae. Encrustation occurs on both sides of the clasts. Spar-filled laminoid fenestrae surround clasts and, in particular, occur below clasts as shelter voids. Irregular-shaped mud-filled cracks are rare along bed tops.	Wrinkly, flat- to undulatory lamination partly building domes up to 8 cm in height. Laminae are disrupted/brecciated and commonly deformed into tepee-like shapes (Fig. 4.10c, similar to polygonal stromatolite of Aitken 1967); the ridges have a subequal spacing of 3-4 cm and represent uparched, rarely disrupted laminae. Laminoid fenestrae (up to 3 cm long, 0.5 cm high) are common in brecciated intervals and below uparched laminae (shelter voids). Fenestrae are spar-filled; some contain minor amounts of calcilutite (geopetal structures).

Table 4.4 (continued).

Facies	Microbial boundstone		Matrix-supported breccia (50 cm)
Subfacies	Massive microbial boundstone (5-155 cm)	Mass. microb. boundst. with pseudomorph fans (10-40 cm)	
Bedding characteristics	Tabular to slightly domed lithostromes. Upper contacts are wavy (2-10 cm relief) with a superimposed warty relief due to knobby columnar features up to 1 cm in diameter. Intercalations of shale are typically lacking, but, when present, drape a wrinkled irregular surface relief of up to 2 cm.	Tabular to domed lithostromes with 20 cm of relief and sharp, planar contacts.	Tabular breccia bed with a sharp and non-erosive lower contact draping the relief of underlying bed; sharp upper contact with irregular relief.
Lithology	Medium to dark grey, homogeneous rock of calcilutite/siltite; sand-sized sediment is restricted to spherical to irregular patches (typically 1 cm across) and comprises fine sand-sized detrital carbonate and siliciclastic sediment.	Calcilutite/siltite with rare scattered sand-sized grains	Angular limestone clasts (sand to cobble size, up to 25 cm across) in a matrix of massive calcilutite.
Lamination style/ sedimentary structures	Massive to irregular patchy fabric with rare occurrences of flat, wrinkled or wavy lamination. The lamination appears disrupted. Lower bed portions (up to one-third) commonly comprise structured layers of undulatory to cumulate laminite intercalated with massive layers. Structured limestone grades upward into massive rock where lamination is rarely preserved (Fig. 4.10d). Structured bed portions are partly discontinuous layers or irregular domains surrounding patches (5-10 cm across) of massive rock. Ellipsoidal-shaped nodular stromatolites (0.45 hight to width ratio) with internal wrinkly lamination and concentrically surrounded by fenestrae are rare. A network of irregular tubular or elongate patchy features (0.5 cm across) occurs in several beds subvertical to bedding and radial to domical bed forms. The tubes consist of light grey calcilutite with some sparite, reddish, chert-bearing material and dolomitic mud. Pseudomorph fans occur and are common only in the uppermost parts of some beds. Irregular, hieroglyphics-like spar-filled fenestrae are locally common. Where fenestrae are variably filled with mudstone, the muddy material appears to have been infilled from above along now mud-filled, downward tapering cracks. Wavy, in situ disrupted dolomitic layers (partly fitted fabric) are rare.	Similar to massive boundstone, but pseudomorph fans are ubiquitious (Fig. 4.10e and 10F); the rock is massive with a locally developed, wrinkly lamination which is transected by fans. The lamination is best preserved at the base and vanishes upsection; fans are most common at bed tops. Fans are concentrated in certain layers where they have an even hight and a ±constant spacing. The fans are closely associated with dolomitic mud which preferentially occurs in domical layers and patches at the outer margin of the fans in a concentric arrangement; these layers get transsected by the pseudomorphs. Large irregular sparite-filled vugs (up to 2 cm across) occur.	Matrix-supported; tabular, massive to flat-laminated micrite clasts (typically 1-3 cm in length, 2-3 mm thick) most common. Cobble-sized clasts include massive to parallel-laminated chert and massive boundstone. Clasts protrude up to 10 cm into overlying flat-laminited limestone.

Disrupted, fenestrae-rich limestone

This rare subfacies is a laminated limestone with decimetre-scale domal growth forms, abundant fenestrae and evidence of in situ disruption (Fig. 4.10c, Table 4.4). It occurs at cycle tops or, less frequently, intercalated with microbial boundstone.

Interpretation: In situ disruption, tepees and the abundance of fenestrae indicate deposition/carbonate precipitation in the upper intertidal to supratidal zone which was affected by frequent subaerial exposure.

5) Microbial boundstone

Two subfacies can be differentiated, a fanned microbial boundstone and a massive microbial boundstone, depending on the presence of pseudomorph fans. Microbial boundstone occurs in the upper part of several sedimentary cycles and commonly forms tabular to slightly domed biostromes. It is commonly gradationally intercalated with or overlies undulatory and flat laminites.

Massive microbial boundstone

This is a homogeneous rock with an irregular, mottled or massive fabric, which contains discontinuous layers and patches with a stromatolitic fabric (Fig. 4.10d). Tubular features, pseudomorph fans and fenestrae are common (Table 4.4).

Interpretation: The occurrence of stromatolitic fabrics, the association with stromatolites, and the geometry of the biostromes suggest a microbial origin; the rocks are therefore denoted as microbial boundstones (Kennard and James 1986). The patchy fabric resembles the clotted fabric typical for thrombolites; intergradations between layers with a stromatolitic and a massive, patchy fabric are also common in thrombolites (Aitken 1967; Kennard and James 1986). However, the boundstones contain much less detrital material than Phanerozoic thrombolites and, hence, more closely resemble Palaeoproterozoic thrombolites of the Rocknest Formation (Kah and Grotzinger 1992).

Massive microbial boundstone is intercalated with or overlies intertidal laminite facies and frequently forms the top of depositional cycles (Fig. 4.5). Evidence for subaerial exposure is present in the form of mud-filled desiccation cracks and disrupted dolomitic layers. The mottled fabric may be partly related to disruption of an originally more regular, laminated fabric upon desiccation in a predominantly supratidal environment. Much similar to the boundstones described here are aragonite tufa mounds from the Great Salt Lake, Utah (Halley 1976); the internal structure of the mounds ranges from laminated stromatolitic to unlaminated clotted. Halley (1976) attributed their formation to microbially induced aragonite precipitation during an earlier fresher water stage of the lake.

Fanned microbial boundstone

This subfacies is much similar to the massive boundstone subfacies but contains ubiquitious pseudomorph fans (Fig. 4.10e, Table 4.4). It is intercalated with or occupies the same stratigraphic position as the more common massive boundstone.

Interpretation: The limestones made up of aragonite fans (discussed below) resemble modern tufas/travertines (Demicco and Hardie 1994), which in recent shallow-marine carbonate environments occur in seasonally flooded coastal freshwater marshes landward of the main tidal flats (Hardie and Shinn 1986). Tufas are a common facies of the inner shelf cycles of the Proterozoic Rocknest Formation, where they typically overlie stromatolitic limestones or microbial laminites and form the top of depositional cycles (Grotzinger 1986a).

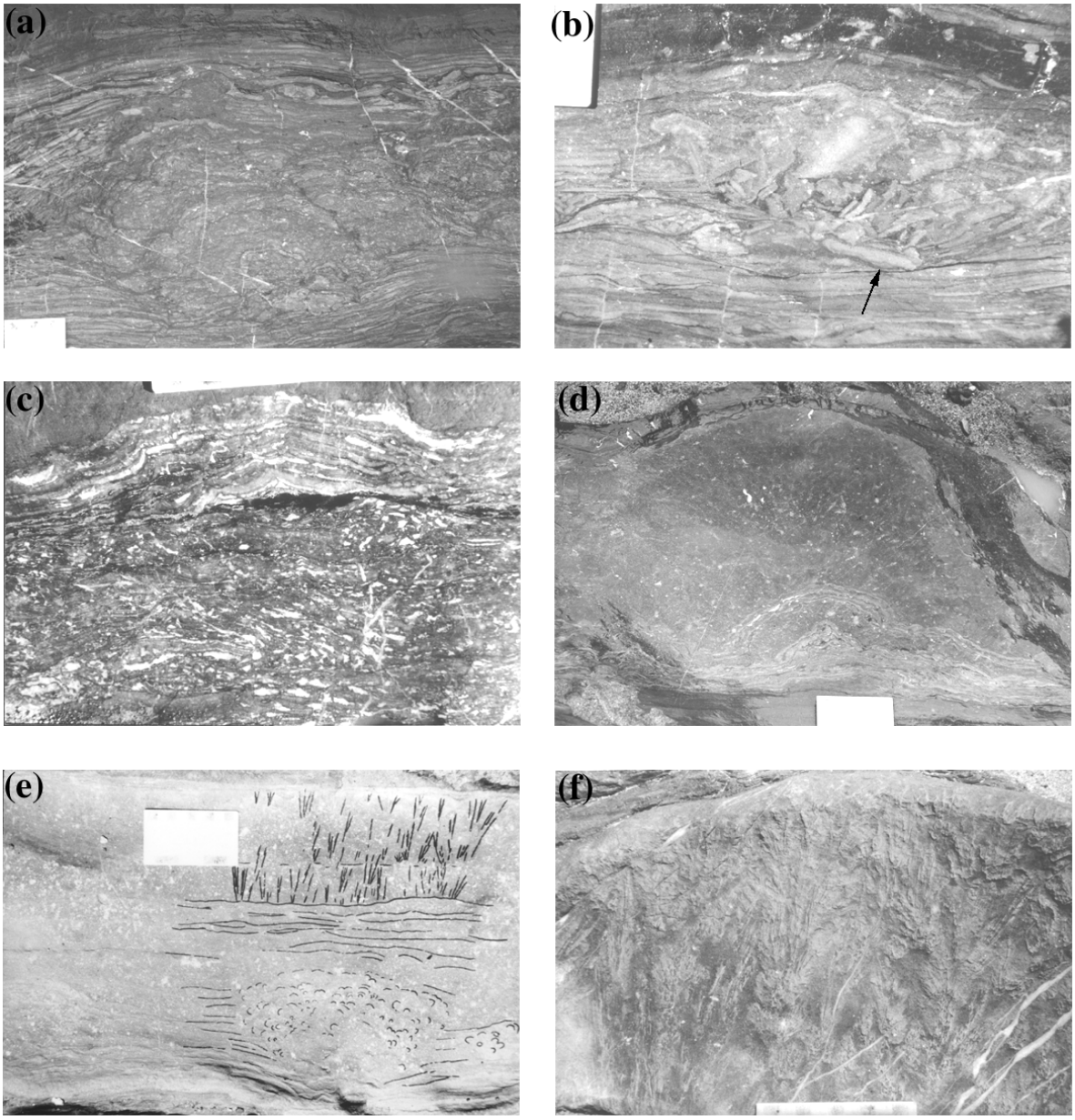

Fig. 4.10. Features of stromatolite facies, microbial boundstone facies and pseudomorph fans from the lower section in the Ngezi River. a) Hemispherical, cauliflower-like stromatolite within laminite facies. b) Pocket of encrusted intraclast breccia in laminite facies. Laminite is overlain by shale of the next cycle (top). Note clast encrustation by micrite (arrow). c) Disrupted, fenestrae-rich limestone facies; note disruption of lamination into small-scale tepees (top centre). d) Domed biostrome of microbial boundstone at the top of a cycle; note stromatolitic fabric in lower bed portion. e) Wave-rippled grainstone with cauliflower-like stromatolitic patches sharply overlain by tabular bed of fanned microbial boundstone (fabrics are enhanced with a marker pen). This is sharply overlain by shale of the next cycle. f) Fanned microbial boundstone at the top of a domed biostrome.

Pseudomorph fans

The pseudomorph fans are bundles of radiating, needle- to blade-shaped crystal pseudomorphs after aragonite. Crystal pseudomorphs are up to 20 cm in length, and blades are up to 2 mm in width. The fans have been studied in detail by Sumner and Grotzinger (2000) at the main stromatolite outcrop; localized buildups or laterally continuous beds of pseudomorph fans have been described. Commonly, the crystals nucleated on single surfaces such as erosional surfaces or lag deposits and grew into each other laterally forming continuous layers of fans. The fans are associated with stromatolitic laminae coating and mimicking the relief of underlying fans.

Troughs between fans are commonly filled with oolitic grainstone. Sumner and Grotzinger (2000) reported that the pseudomorph fans occur together with stromatolitic facies at the base of cycles and are gradationally overlain by crinkly laminites at cycle tops. Based on this, the pseudomorph fans have been interpreted as a shallow subtidal facies.

In contrast, this study of the Ngezi River section shows that pseudomorph fans are most common in the uppermost parts of sedimentary cycles (Fig. 4.10f) where they typically occur in microbial laminite or massive boundstone facies. Pseudomorph fans in laminites preferentially nucleate from the upper bedding plane of intercalated siliciclastic or grainstone layers. They also occur adjacent to the gradational contact between the grainstone and the laminite facies. Pseudomorph fans are rare in grainstone beds intercalated with shale in the lower part of depositional cycles. Grainstone beds with internal pseudomorph fans commonly have wavy upper contacts with the swell overlying a fan. Fans locally occur in the centre of stromatolitic growth forms.

Interpretation: Pseudomorph fans in the microbial boundstone facies have been interpreted as a supratidal precipitate similar to modern tufa/travertine (see above). The fans are morphologically similar to the "ray crystals" described by Chafetz and Folk (1984) from the Quaternary travertine deposits of Italy. The aragonite fans are interpreted as an inorganic precipitate that formed out of a supersaturated solution by nucleation and crystal growth on a stable substrate. The nucleation of fans at the centre of stromatolitic growth forms may indicate that microbial activity favoured fan growth and that the fans precipitated within and on microbial mats.

However, fans, although rare, are associated with subtidal facies, suggesting that the ancient sea water, in general, was supersaturated with respect to aragonite (Sumner and Grotzinger 2000). Nevertheless, the abundance of pseudomorph fans at the top of depositional cycles where they are associated with tidal flat facies suggest somewhat more restricted conditions associated with higher ion concentrations of sea/groundwater in the final phase of cycle formation. In addition, since the fans also occur in grainstone beds which formed under relatively high energy conditions and which lack clasts derived from the erosion of fans, these features are at least in part postdepositional forms, and possibly very early diagenetic due to the evaporative concentration of pore water at the end of cycle history.

Middle section in the Ngezi River and main stromatolite outcrop

The middle section is a 5 m thick, continuous section that was measured in detail (Fig. 4.11). It occurs a few metres above the lower section (Fig. 4.4) but is separated from it by faulted and sheared limestone, questioning its exact stratigraphic position. Some cycles contain shale at the base which is overlain by wave-rippled or massive grainstone, the latter containing irregular spar-filled fenestrae. Other cycles directly start with microbial laminites which contain laminoid fenestrae. The laminites are typically overlain by thin to medium beds of boundstone with fanned pseudomorphs; the fans commonly increase in size upwards (Fig. 4.12a). Pseudomorph fans are variably replaced by chert; clots of chert also occur. Digitate stromatolites are sometimes associated with the fans and increase in abundance upwards. Cycle tops are formed by limestone with an irregular, patchy fabric. Pseudomorph fans (more or less chertified) occur to-

gether with digitate stromatolites (up to 3 cm in height); the intercolumn space is filled by detrital carbonate mud. Some concentrically laminated features occur which may represent the cross-section of digitate stromatolites.

The middle section is similar and possibly correlative to rocks of the main stromatolite outcrop (Fig. 4.2). At this locality logging is hampered by D_1 folding (chapter 3) which makes the distinction between tectonic folds and domical microbial features difficult. In addition, certain horizons, especially those with pseudomorph fans, have been affected by chert replacement, whereas others have been altered by limestone dissolution and iron-impregnation. Chert further occurs as cross-cutting layers and as patches which are irregularly distributed in the limestones. Despite the alterations, a cyclic stacking of facies is evident (Martin et al. 1980; Sumner and Grotzinger 2000). The cycles can be traced across the outcrop (200-300 m) and do not show lateral changes in facies or thickness. Most cycles consist of a thin bed of wave-rippled or massive grainstone at the base which sharply, but not erosively rests on limestone of the underlying cycle. Grainstones are dolomitic and sometimes ferruginized. Grainstone commonly grades into a laminite facies, which partly builds domal stromatolites. The domes locally broaden upward resulting in a decrease in synoptic relief. Cycle tops are commonly formed by massive boundstone containing abundant pseudomorph fans (Fig. 4.12b). Digitate stromatolites rarely occur in between the laminite and boundstone facies. In several cycles either the grainstone facies or the boundstone facies is missing. Two distinct cycles consist of spaced pseudomorph fans enveloped by grainstone and overlain by digitate stromatolites (Fig. 4.12c).

Significance: Sedimentary facies and their vertical distribution are much similar to those of the lower section. Cycles, however, lack significant subtidal deposits and are dominated by intertidal laminites and supratidal boundstones. The increase in the amount of pseudomorph fans in parts of cycles possibly reflects a trend towards more restricted conditions on supratidal flats. The digitate columnar stromatolites common in the upper portions of cycles are similar to the microdigitate structures in tufa deposits at the top of the shallowing-upward cycles of the Rocknest Formation (Grotzinger 1986a). Digitate stromatolites are generally associated with supratidal settings in the fossil record (Grey and Thorne 1985).

Upper section in the Ngezi River

The measured 10 m thick upper section (Fig. 4.4) occurs c. 20 m above the lower section and rests on 1 m of sheared brecciated limestone. It predominantly consists of tidal flat facies such as microbial laminites and massive boundstones. The top of this section is separated from the overlying limestone breccia by 6 m of poor exposure of chertified laminite facies. The section shows a cyclic arrangement of facies, but cycle boundaries are poorly defined. Possible cycles may consist of a lower part of shale, heterolithic shale/laminite or flat laminite facies. One cycle contains a bed of matrix-supported breccia facies (Table 4.4) at the base. Cycle tops may consist of a massive boundstone facies with a locally disrupted, irregular lamination which may form nodular to bulbous growth forms. Pseudomorph fans have not been observed.

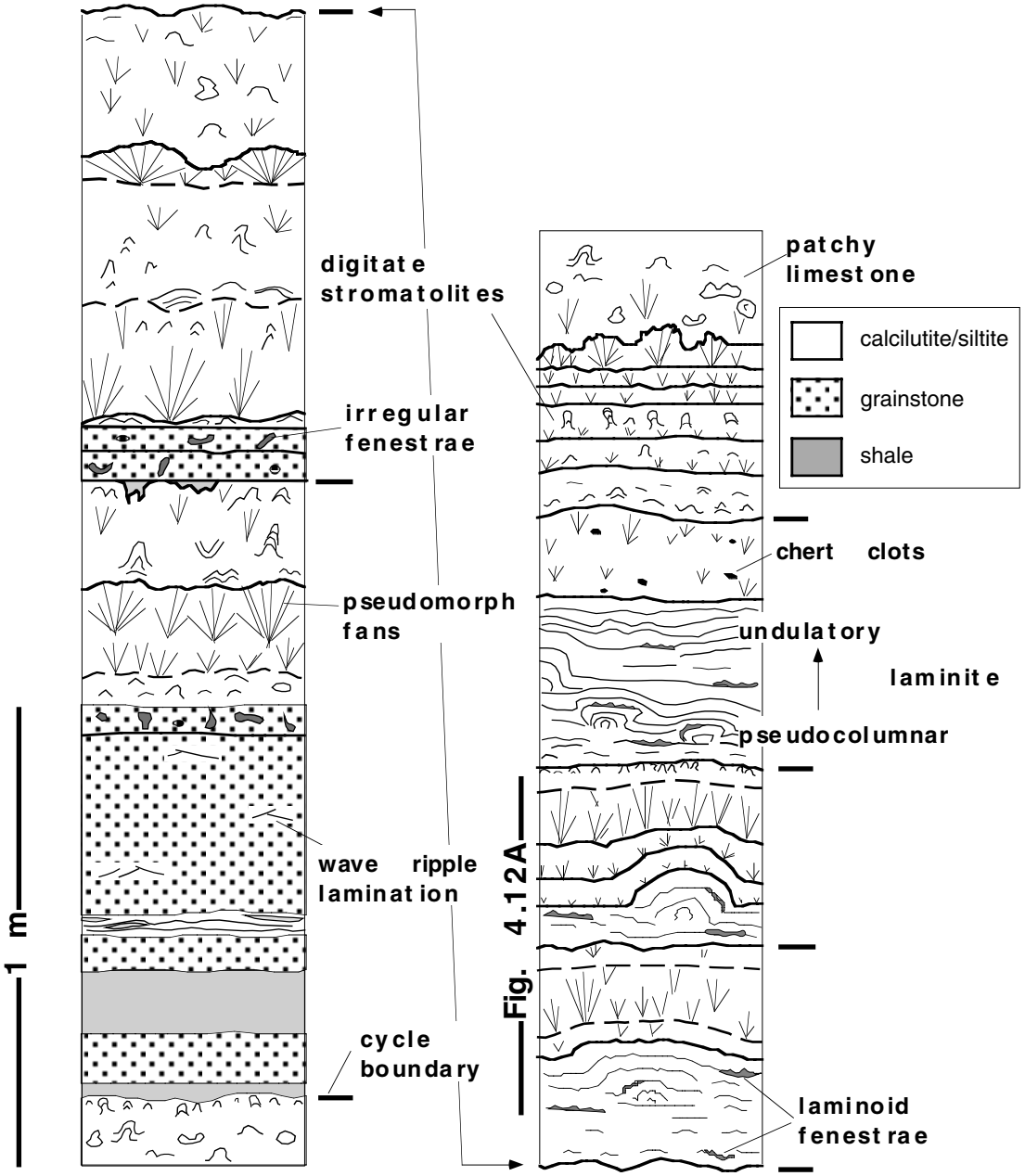

Fig. 4.11. Detailed log of cyclic carbonates of the middle section in the Ngezi River. Section is separated from the top of the lower section by 2-3 m of faulted and sheared limestone (see Figures 4.3 and 4.4).

Significance: The cause of the less well defined cyclicity of the section may indicate changes in the depositional setting. The matrix-support, sharp and non-erosive contacts, and the draping of relief indicates a subaqueous, cohesive debris flow origin for the breccia bed. The occurrence of clasts protruding into the overlying facies suggest deposition by sediment "freezing" due to a high matrix strength. The restricted occurrence of the resedimented limestone breccia at the top of the carbonate sequence may indicate tectonic movements resulting in changes in the basinal parameters such as steepening of the otherwise gentle palaeoslope. The overlying karst breccia is thougth to have formed upon subaerial exposure during uplift of the carbonate platform (chapter 2).

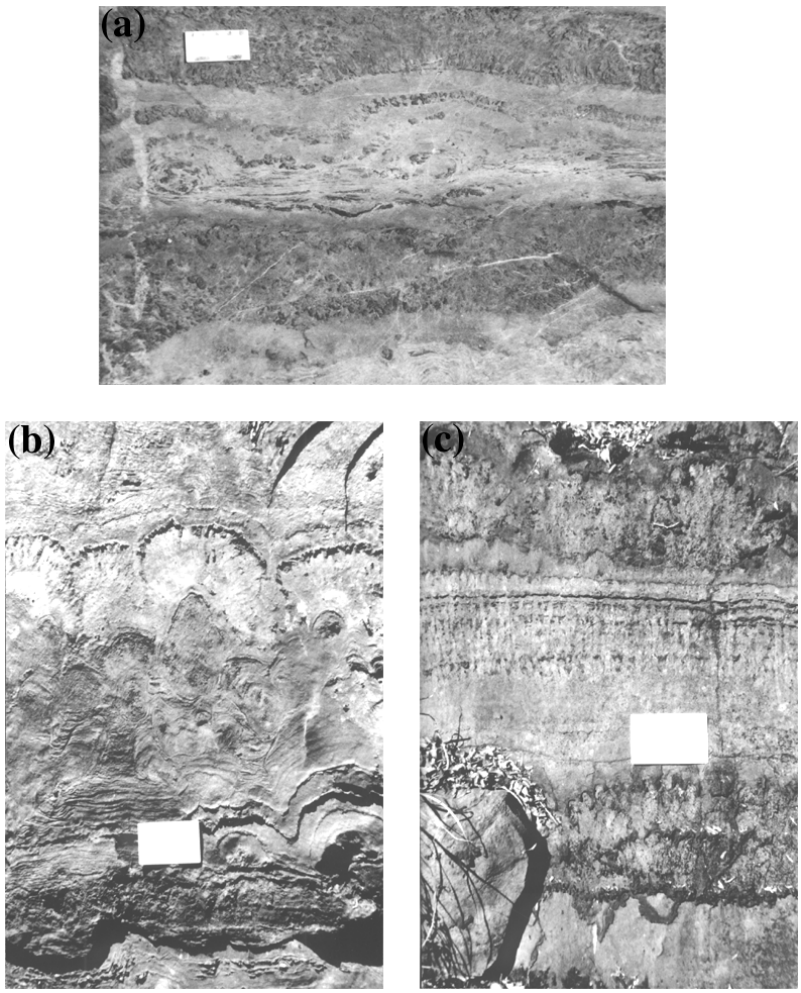

Fig. 4.12. Sedimentary features of other sections. a) Two sedimentary cycles of the middle section in the Ngezi River, consisting of laminite facies at the base and fanned boundstone at the top; pseudomorph fans are replaced by chert (see Fig. 4.11 for location of photograph). b) Cycle of ferruginized grainstone at the base overlain by hemispherical to bulbous stromatolites and capped by pseudomorph fans (photo taken at main stromatolite outcrop). c) Pseudomorph fans enveloped by grainstone and overlain by digitate stromatolites which are overlain by pseudomorph fans of the next cycle (photo taken at main stromatolite outcrop).

Facies stacking pattern

Cycles have an asymmetric facies stacking pattern. Cycle boundaries are sharp whereas internal contacts between lithofacies are gradational. In general, the lower part of shale-based cycles shows the following trends (Fig. 4.6): (1) thickening-upward of event beds in shale, (2) coarsening-upward from fine siliciclastic sediment to medium to coarse sand grainstone, (3) upward increase in carbonate content. The carbonate cycles and upper part of shale-based cycles are characterized by: (1) fining-upward from grainstone to carbonate mud, (2) decrease in synoptic relief of microbial carbonates.

The observed trends are the result of rapid submergence, followed by a gradual shallowing of the sea level during the course of cycle formation. The lower coarsening-upward part of shale-based cycles is represented by subtidal facies and resembles subtidal cycles of Phanerozoic carbonate platforms (Aigner 1985; Calvet and Tucker 1988; Osleger and Read 1991). The upper fining-upward part comprises peritidal facies and closely resembles typical peritidal cycles (James 1984; Hardie and Shinn 1986; Koerschner and Read 1989). Shale-based cycles were

initiated by abrupt flooding of tidal flats. Deposition of shale took place below fair-weather wave base and possibly even below storm wave base for the lower part of some shale horizons. The upward increase and thickening of storm deposits together with the increase in average grain size are indices of higher energy as a result of progressive shallowing when storm-generated currents were able to affect the sea bottom more frequently with time. Furthermore, the increase in clastic carbonate indicate progressive proximity to landward carbonate shoals and tidal flats.

Ooid/intraclast grainstone overlying shale formed at or above fair-weather wave base in an agitated shallow subtidal setting, possibly in water depths of less than 10 m. The grainstones represent shoreface sand-sheets or low relief sand-shoals that prograded across open-marine shale in response to storm-, wind-, and/or tide-generated currents. The association of ooid/intraclast grainstone and unlinked stromatolites resembles modern ooid sand dunes enveloping stromatolitic bioherms in current-swept, subtidal channels (7-8 m water depth) in the Bahamas (Dill et al. 1986).

Further shallowing resulted in the establishment of tidal flats where benthonic microbial communities were able to agglutinate detrital carbonate and possibly influenced carbonate precipitation. Microbial laminites are thought to have formed in the intertidal zone. The change in stratification style from pseudocolumnar through undulatory to flat lamination upsection is associated with a decrease in synoptic relief. In several studies a correlation has been described between inferred palaeowater depth and stromatolite form such that shallower water forms have a lower synoptic relief (Grotzinger 1986a; Southgate 1989; Walter et al. 1992). Facies overlying the laminite facies and commonly forming cycle tops such as encrusted breccia and microbial boundstone formed on supratidal flats. In this setting, periodic flooding and desiccation resulted in the disruption of the sediment, evaporative concentration of flood/groundwaters possibly aided in the chemical and/or biologically mediated precipitation of aragonite within microbial mats to form boundstones. A conformable, reversing sequence in the uppermost part of a few cycles (e.g., increase in calcarenite material and synoptic relief) indicates gradual submergence of the tidal flats to subtidal depths. Most commonly, however, are peritidal facies sharply overlain by subtidal facies along a paraconformable cycle boundary. Carbonate cycles lacking basal shale beds formed when initial transgression led to deepening of the depositional environment to around fair-weather wave base only. Basal grainstones formed and were overlain by microbial limestones during gradual shallowing.

Cycle boundaries

Cycle boundaries sharply separate facies of a contrasting texture and of a different palaeoenvironment (e.g., intertidal microbial laminite overlain by subtidal shale). Cycle boundaries and underlying sediments show evidence of dolomitization: (1) Flat laminites just below the top of some cycles contain massive, continuous, dolomite-cemented layers a few mm thick which commonly occur as multiple layers spaced a few mm to a few cm apart; these layers are locally disrupted. (2) In the heterolithic laminite/grainstone facies which forms the top of several cycles, 0.5-1 cm thick layers of dolomitic mud occur that form tepee structures. (3) Stromatolite bioherms/stromes and other carbonate facies of cycle tops preserve a few cm thick dolomitic crust.

The dolomitic layers are indicative of early cementation of the substrate during periods of non-deposition. Their association with sediment disruption such as tepee structures indicates that early cementation took place subaerially and gave rise to the formation of supratidal dolomitic crusts. Dolomitization in both ancient and modern carbonate environments is commonly an indicator for emergence in inter- to supratidal facies (e.g., Wilson 1975). Supratidal crusts and thin regoliths in the form of encrusted breccia facies are restricted to the top of several cycles, indicating subaerial exposure during periods of non-deposition and non-erosion (James and Choquette 1990). Dolomitization of carbonates below cycle boundaries is a typical phenomenon of shallowing-upward cycles (e.g., Southgate 1989).

In sediments underlying cycle boundaries, features characteristic for emergence such as desiccation cracks, fenestrae etc. are not as common as in modern supratidal deposits. In this respect, the Cheshire cycles are similar to the Cambrian peritidal cycles of the Appalachians (Hardie and Shinn 1986; Koerschner and Read 1989; Osleger and Read 1991). However, the occurrence of encrusted breccias and biostromes at the top of the Cheshire cycles indicates that desiccation/disruption and erosion was inhibited by microbial sediment binding, early cementation of the substrate and firm encrustation of surface sediments prior to transgression and deposition of the next cycle.

Facies distribution

The distribution of the main facies types within the measured section is not random (Fig. 4.13). Shales dominate the centre of the section, whereas laminites and boundstones dominate at the base and top, respectively. This relationship indicates that deposition in the central part took place under mostly subtidal conditions during a relative sea-level high, whereas inter/supratidal sedimentation dominated at the base and top suggestive of a low average sea-level. Excursions from this large-scale trend are represented by regularly recurring peaks (approximately every 10th cycle) in relative shale thickness and associated lows in relative laminite/boundstone thickness, indicating shorter term cyclic changes in relative sea-level. Grainstones occur throughout the section in similar proportions, indicating that a wave-swept shallow subtidal setting was present throughout. Boundstones are absent in the lower half of the section and then gradually increase in frequency towards the top. This may indicate a gradual trend towards more restricted conditions towards the top of the succession either due to a change in the palaeogeographic parameters of the platform (such as the formation of a reefal barrier) or a change in palaeoclimate. The absence of standard evaporite minerals like halite (gypsum may not have been a common evaporite mineral in Archaean times; Grotzinger and Kasting, 1993) and the lack of haloturbational features do not favour an arid climate during deposition of the Cheshire carbonates. However, evaporation on the supratidal flats must have been high enough to generate the aragonite fans of the tufa/travertine deposits. Using tufa deposits that form today in brackish coastal marshes in rainy climates (Hardie and Shinn 1986) as a modern analogue for the boundstones would indicate a humid tropical palaeoclimate during deposition of the Cheshire carbonates.

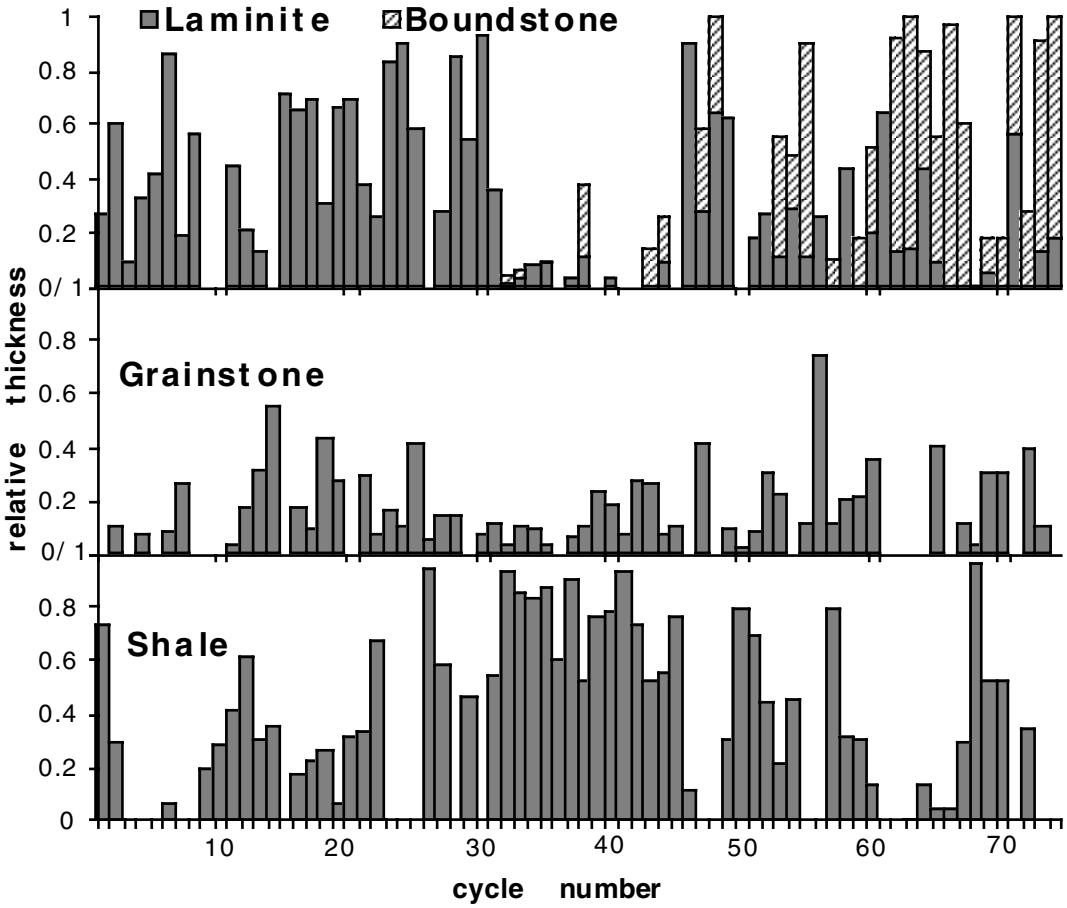

Fig. 4.13. Distribution of the main lithofacies within the lower section in the Ngezi River.

CONTROLS ON CYCLICITY

The mechanisms thought to result in the formation of shallowing-upward carbonate cycles have been discussed and reviewed in numerous studies (Hardie and Shinn 1986; Grotzinger 1986b; Strasser 1991; Demicco and Hardie 1994). There are two basic models to explain the origin of cyclicity, the autocyclic model relating cyclic processes to self-regulating mechanisms internal to the depositional system (Ginsburg 1971; Pratt and James 1986; Cowan and James 1996) and the allocyclic model in which cyclic sedimentation is controlled by external forces such as eustatic sea level variations and episodic subsidence (Fischer 1964; Goodwin and Anderson 1985; Cisne 1986).

Autocyclic models

In the autocyclic model of Ginsburg (1971) carbonates are produced in a subtidal area ("carbonate factory") under a static sea level and are transported landward (during storms, spring tides) onto adjacent tidal flats which as a result prograde seaward. Progradation leads to shrinkage of the subtidal source area which, at a certain point in time, is unable to provide sufficient sediment for progradation to continue. In addition, the prograding tidal flat wedge requires increasing sediment supply to maintain its rate of advance because of platform slope (Hardie and Shinn 1986). Carbonate production eventually comes to a halt, but basin subsidence continues, resulting in a relative sea level rise and the formation of a cycle boundary. Sea level

rises until the carbonate factory is again established and is able to act as a sediment source for the next cycle of tidal flat progradation. This model predicts that cycles always shoal to sea level, which is not the case for many cyclic carbonates of Proterozoic and Phanerozoic carbonate platforms. In addition, subsidence rates for common depositional settings of 5th order carbonate cycles are too low. Long lag times (Schlager 1981) of non-deposition are necessary for a relative sea level rise to occur in order to resume effective carbonate production (Grotzinger 1986b; Osleger and Read 1991; Read et al. 1991).

Vertical accretion of islands scattered in a shallow epeiric sea where tidal flats form and prograde laterally has been suggested by Pratt and James (1986) as a mechanism for cycle development. Cycle boundaries are thought to form when the tidal flats subside due to a shift in the focus of sedimentation. Cowan and James (1996) developed an autocyclic model for laterally discontinuous Cambrian shallowing-upward subtidal cycles. The cycles range from mud to ooid grainstone and are capped by hardgrounds. Cyclicity is attributed to in-place sediment production resulting in the growth and migration of ooid shoals and eventual sea-floor lithification due to internal or external factors. Other models have been proposed such as the migration of tidal channel on tidal flat complexes. Cycles formed by autocyclic processes as described above can be laterally persistent over the length of the system (Strasser 1991), but lateral correlation is commonly not possible even over short distances.

Allocyclic models

Allocyclic models attribute cyclicity to external rhythmic or cyclic forces such as repeated pulses of rapid (tectonically controlled) subsidence and high-frequency eustatic sea-level changes. Events of rapid subsidence on carbonate platforms (e.g., repeated stick-slip faulting, Cisne 1986) can give rise to a sudden relative rise in sea level and a cessation of carbonate sedimentation. After the passage of a certain lag time for carbonate production to reach its full potential, submergence is followed by gradual aggradation and progradation of carbonate facies during periods of normal subsidence rates to form a shallowing-upward cycle. Tectonically driven subsidence events are expected to occur in extensional basins (episodic normal faulting), and in compressional foreland basins (episodic thrust loading), but cannot explain the formation of most cyclic carbonates which typically occur in passive margin sequences and intracratonic basins (Grotzinger 1986b). A great lateral extent of sedimentary cycles is generally stated as evidence against tectonically induced subsidence events which would affect only a small area (e.g., Grotzinger 1986a; Hardie and Shinn 1986). Tectonically driven changes in relative sea level have also been attributed to variations in intraplate stress (Cloetingh 1986), but they are too slow and non-periodic to produce the well developed metre-scale cyclicity (4th to 5th order) common to ancient carbonate platforms (e.g., Osleger 1991; Goldhammer et al. 1993).

In many studies the cyclicity recorded in carbonate platform successions has been attributed to small-scale (≤ 10 m), but high-frequency eustatic sea-level changes (Fischer 1964; Goodwin and Anderson 1985; Grotzinger 1986b; Koerschner and Read 1989; Osleger and Read 1991; Goldhammer et al. 1987, 1990) brought upon by glacio-eustatic sea-level changes. The forcing

mechanism behind the fluctuations is attributed to cyclic climatic changes, possibly within the Milankovitch frequency band. During periods of continental glaciation major changes in water volume of the ocean basins can take place under oscillating climates due to the waxing and waning of polar ice sheets. During periods of no known major glaciations the origin of sea level changes may be attributed to the changes in the volume of alpine glaciers. This can result in high-frequency, low-amplitude changes in sea level. Low-amplitude changes are generally favoured to have produced metre-scale carbonate cycles in the geological record, since the major glacio-eustatic sea level changes in the Pleistocene (≤ 200 m) led to karstification of entire carbonate platforms during falling sea-level and their drowning during subsequent, rapid sea-level rise outpacing the growth potential of carbonate platform margins (Schlager 1981; Hardie and Shinn 1986). Other causes for climatically driven low-amplitude sea-level changes fast enough to overcome carbonate sedimentation rates are, for example, the desiccation/flooding of confined basins (Donovan and Jones 1979) or changes in the volume of groundwater held in continental aquifers (cf. Dewey and Pitman 1998).

Glacio-eustatic sea level changes best explain the formation of cyclic carbonates for several reasons (Grotzinger 1986b). (1) Sea level changes are asymmetric with a rapid rise and a slower fall, since the melting of glaciers is faster than their growth (references in Hays et al. 1976). This can explain the asymmetry of most carbonate cycles insofar as rapid transgression leads to submergence, the termination of carbonate production and the formation of a cycle boundary, whereas slow regression leads to the gradual stacking of facies, indicating progressive shallowing. (2) In certain cases, sea level fall may outpace subsidence rate, nearshore carbonates get subaerially exposed, and cycles may form that contain pedogenic features and vadose cements in their uppermost parts. This is well exemplified by the "diagenetic cycles" of the Triassic Latemar buildup where subtidal sediments are directly overlain by vadose diagenetic caps negating shoreline progradation as a cause of cycle formation (Hardie et al. 1986; Goldhammer et al. 1987, 1990). (3) Amplitudes and frequencies of sea level changes vary. Depending on the position within the basin, cycles can form that lack tidal flat facies and, hence, did not shallow to sea level. However, the absence of intertidal sediments can also be related to the intrinsic processes of storm and wave reworking (Osleger 1991). (4) Hierarchies of stratigraphic cyclicity occur on different scales with small-scale (4th and 5th order) sedimentary cycles commonly superposed on cycles of a lower order (3rd order). This hierarchy can be explained by the combined effects of different orders of relative sea level oscillations (composite eustasy, Goldhammer et al. 1990).

Early studies on cyclic carbonate sequences remarked that estimated average cycle periods (total length of time divided by cycle number) fall into the range of the frequencies of the Milankovitch orbital parameters (cf. Algeo and Wilkinson 1988). These frequencies today are 19 and 23 ka (precession), 41 and 54 ka (obliquity), 95 and 128 ka (short eccentricity, mean 112 ka) and 413 ka (long eccentricity) (Schwarzacher 1993; Berger and Loutre 1994). However, it has been noted that the similarities between the average cycle periods of metre-scale cycles and

the Milankovitch frequencies are to be expected and are insufficient evidence for an orbital control of cycle formation (Hardie and Shinn 1986; Algeo and Wilkinson 1988).

Van Houten (1964), Olsen (1986) and Anderson (1986) used varve-calibrated sedimentation rate estimates to determine cycle periods in Palaeozoic and Mesozoic cyclic strata of continental lacustrine settings. Their findings were in good agreement with the Milankovitch frequencies, suggesting an orbital control on cyclicity. Spectral analysis of cyclic stratigraphic sequences to determine cycle periods has been used successfully in several studies, e.g. Quaternary deep-sea sediments (Hays et al. 1976), Triassic carbonate platforms (Goldhammer et al. 1987) and Triassic lacustrine deposits (Olsen and Kent 1996), to establish a Milankovitch control on the cyclicity. However, this approach is difficult to apply to ancient shallow platform carbonates due to uncertainties in formation ages, differential sedimentation rates, periods of non-deposition and variations in the record of the cyclic signal (Osleger and Read 1991).

A common approach to indirectly show a Milankovitch control on cyclic stratigraphic sequences is to demonstrate a hierarchy in cycle stacking patterns where the recurrence ratio of two different orders of cyclicity corresponds to one of the ratios between periods of the orbital parameters. In addition, the calculated periods of the sedimentary cycles have to correspond to the frequency of the anticipated orbital parameters. A 5:1 recurrence ratio of metre-scale microcycles within mesocycles is the most commonly reported ratio in cyclic carbonate sequences (Strasser 1991) and is generally interpreted to reflect the precession cycle modulated by the short eccentricity signal (e.g., Schwarzacher and Fischer 1982; Goldhammer et al. 1987), since the frequency of orbital precession is five times that of short eccentricity. A 4:1 ratio of cycle bundles is also common and may be related to the superposition of short and long eccentricity cycles (e.g., Osleger and Read 1991). Obliquity signals are commonly not directly obvious in cyclic carbonate sequences without the aid of spectral analysis.

Mechanism of Cheshire cyclicity

As discussed above, a common step in analysing sedimentary cyclicity is to estimate a long-term sedimentation rate and related maximum duration of a cycle period which in case of the Cheshire cycles can not be obtained, because of the limited thickness of the carbonate sequence and the absence of rocks suitable for precise dating. The estimation of short-term sedimentation rates of cyclic facies in order to define a minimum cycle period can not be determined as well due to the lack of suitable lithologies such as varved shales (e.g., Olsen 1986) and the absence (or recrystallization) of periodical growth bands in stromatolites (e.g., Pannella 1975).

The vertical facies succession within a cycle indicates a change in relative sea level. The carbonate member has been interpreted as a carbonate ramp sequence that formed in a foreland-type basin (see above). Subsidence rate may well have been high enough to overcome the lag depth in a short period of time without the formation of erosional surfaces, extensive hardgrounds or transgressive lag deposits; this would have been followed by the progradation of tidal flats as stated in the autocyclic model. However, several cycles do not contain peritidal facies at the top which is a prerequisite for the Ginsburg (1971) autocyclic model. The

occurrence of cycles that lack tidal flat caps in cyclic carbonate sequences and that consist entirely of subtidal facies is commonly stated as evidence against the autocyclic model (Grotzinger 1986b; Osleger and Read 1991; Osleger 1991).

More importantly, Hardie (1986) in his discussion of the Palaeoproterozoic Rocknest cycles studied by Grotzinger (1986a) emphasized the point that offshore environments preserved in the lower portion of shale-based cycles and represented by siliciclastic muds may not have been the carbonate factory for the establishment and progradation of carbonate tidal flats as suggested by the Ginsburg model. The same holds true for the shale-based Cheshire cycles where offshore deposits lack the organically and inorganically produced carbonate muds typical for Phanerozoic marine-lagoonal environments. Carbonates intercalated with shale have been derived from nearshore areas during storms. The carbonate factory of the Cheshire carbonates was represented by the shallow subtidal ooid sand sheets/shoals, shallow subtidal stromatolites, and, most importantly, the tidal flats. In the latter environment, microbes aided in the precipitation of carbonate muds, and aragonite crystals formed from supersaturated waters on supratidal flats.

Tectonism during deposition of the Cheshire Formation was active. The carbonate member was overidden by a thrust sheet prior to complete consolidation and, hence, soon after deposition (chapter 3). Tectonic pulses during the repeated advance of thrust sheets may have resulted in rhythmic tectonic loading of the lithosphere, to abruptly generate the accomodation space necessary for asymmetric cycle development. The local occurrence of basalt pebble conglomerates within the cyclic sequence may record such sudden tectonic events. However, three observations do not support a tectonic origin for the cyclicity. (1) Shale formed in a subtidal setting well below fair-weather wave base. The lower parts of some shale horizons are rich in clay and contain only rare storm deposits, indicating that water depth may have been > 15 m at times. The shale-bearing cycles are commonly capped by tidal flat facies and, even when compaction is taken into account, are not thick enough to have reached a static sea level by simple aggradation. This discrepancy can only be explained if periodic subsidence was coupled with uplift ("yo-yo tectonics", no actualistic analog) or if the sea level fluctuated. (2) The thickness range of sedimentary cycles is fairly narrow; cycles are typically 40 to 180 cm thick (Fig. 4.14). Regular, cyclic tectonic subsidence events, giving rise to shallowing-upward cycles with the narrow thickness range of the Cheshire cycles are difficult to evoke. (3) A plot of cumulative cycle thickness (Fig. 4.15) shows three groupings of cycles with a rather linear accumulation trend. The cumulative thickness distribution may give a hint on subsidence rate, because most cycles show a distinct facies stacking pattern, do not show evidence for prolonged time intervals of non-deposition/erosion, and are mostly capped by intertidal facies. Assuming that the cycle period was constant (such as with a Milankovitch-type orbital control), it may be supposed that subsidence rate during deposition of the first group of cycles was uniformly low. Starting with cycle 32, the average subsidence rate suddenly increased. Since cycle 32 is unusually thick (Fig. 4.14), it may record a tectonic event (advance of thrust sheet?) which gave rise to an increase in average subsidence rate. After a certain time period of high subsidence, the

average subsidence rate lowered again. This relationship may indicate that tectonic events played a role in the evolution of the carbonate sequence, but were of a lower frequency than the mechanism that formed individual sedimentary cycles.

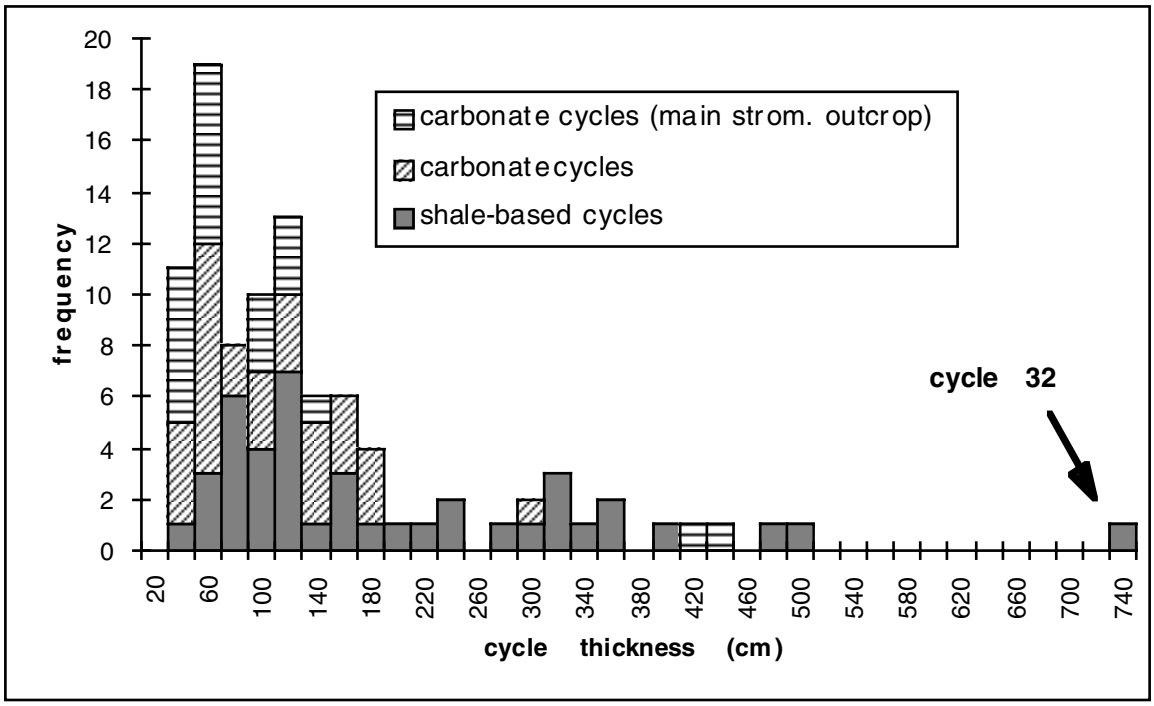

Fig. 4.14. Frequency distribution of the thickness of shale-based cycles and carbonate cycles of the lower section, including the carbonate cycles measured at the main stromatolite outcrop by Martin et al. (1980). Thickness classes are 0-20 cm, 20-40 cm, etc. Cycle 32 is unusually thick.

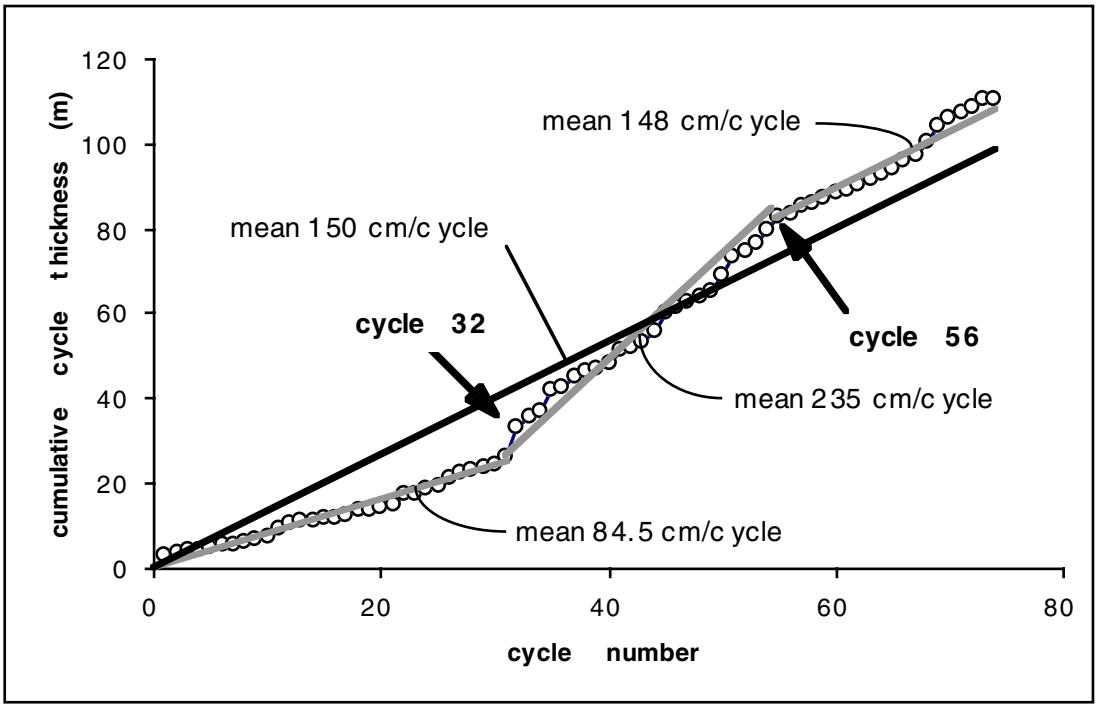

Fig. 4.15. Cumulative cycle thickness graph showing three intervals with a different accumulation history. For each interval a regression line is shown.

Cycle stacking patterns and Fischer plots

The mechanisms that controlled the Cheshire cyclicity can be investigated further by studying the vertical arrangement of cycles. The deposition of shale-based cycles in favour of carbonate cycles reflects differences in the depositional conditions on the platform. If the cyclicity is attributed to eustatic sea level oscillations, difference in cycle type can be asigned to differences in the amplitude of sea level variations. In the initial phase of deposition of a shale-based cycle the sedimentary surface was well below fair-weather wave base, indicating relatively high average sea-level. In contrast, carbonate cycles formed above fair-weather wave base and always shallowed to the inter/supratidal zone, suggesting lower amplitudes of sea level changes.

Systematic changes in the stacking pattern of cycles have been investigated with the aid of Fischer plots (Fig. 4.16a) assuming that each cycle formed during the same period of time. Fischer plots comprise a horizontal axis representing time (or number of time-equivalent successive cycles) and a vertical axis of cumulative cycle thickness of successive cycles minus the mean cycle thickness (which is an indication of average subsidence rate). Two curves have been drawn (Fig. 4.16a), one with a constant subsidence rate and one using different rates for the three parts of the section showing different accumulation histories (see Fig. 4.15). The plots illustrate relative changes in accomodation space through time with any slope between two cycles, indicating a change in relative sea level (Fischer 1964; Goldhammer et al. 1987, 1990; Read and Goldhammer 1988; Osleger and Read 1991). Bundles of thicker-than-average cycles plot with positive slopes and are interpreted to reflect an increase in accommodation space due to a larger scale relative sea-level rise; bundles of relatively thin cycles may reflect a decrease/fall in accomodation space/relative sea-level. The Fischer plot of the Cheshire cycles shows a systematic, asymmetric pattern of bundles of 9-11 cycles. These bundles (mesocycles) are 7.5 to 22 m thick and are characterized by a sharp increase, followed by a slow decrease of cumulative thickness/relative sea-level. A comparison of the Fischer plot with the stratigraphic section (Fig. 4.16a) shows that lower cycles of each bundle are represented by shale-based cycles, whereas carbonate cycles are restricted to the upper part. In addition, lower portions of cycle bundles comprise cycles dominated by subtidal facies; upper portions consist of cycles dominated by inter/supratidal facies (Fig. 4.16a). Cycles with only thin intertidal/supratidal facies or completely lacking such facies caps (Fig. 4.7) preferentially occur at the base of a mesocycle (Fig. 4.16a). The bundled nature of the cycles is visually accentuated by means of a mirror plot (Fig. 4.16b). The asymmetric pattern of the cycle bundles is due to higher thickness values of the first (and sometimes the second) cycle in a bundle (see Sadler et al. 1993 for other causative factors of Fischer plot asymmetry). The asymmetric pattern is similar to the stacking pattern of the Middle Triassic Latemar carbonate cycles where bundles consist of 5 cycles on average (Goldhammer et al. 1987, 1990).

The same mechanism responsible for the small-scale cyclicity can be evoked as the cause for the formation of mesocycles. Each mesocycle was initiated during a relative, lower order sea-level rise. Rising sea-level led to an increase in accommodation space during which shale-based cycles formed in a predominantly subtidal environment. The thickness of shale based-cycles is,

on average, twice as much as the thickness of carbonate cycles (Table 4.1), indicating that accomodation space provided was beyond that generated by subsidence alone. Sea-level rise was relatively rapid and was followed by a slower fall which was associated with a decrease in accommodation space. Relatively thin carbonate cycles constituting the upper part of a mesocycle then formed, mainly in inter/supratidal settings with minor subtidal shale deposition. Mesocycles may further be grouped into macrocycles, which on the Fischer plots are characterized by cycle bundles showing a net negative slope of the subsidence-corrected cumulative cycle thickness curve (Fig. 4.16a). In the stratigraphic section, macrocycles show a net increase in the amount of carbonate cycles as well as intertidal/supratidal facies upsection (Fig. 4.16a). The first macrocycle is represented by the first three cycle bundles (cycles 1-31), but it remains unclear if the bundles represent a complete macrocycle. The second macrocycle encompasses four cycle bundles (cycles 32-67). The first bundle comprises shale-based cycles only, whereas the overlying bundles contain successively more carbonate cycles. Cycle 32 has been interpreted, due to its excessive thickness, to possibly reflect one or the onset of a tectonic subsidence event (see above), whereas it is here interpreted to record a sea-level rise at the beginning of macrocycle formation. If both assumptions are valid, this apparent discrepany can be explained by supposing that water-loading during a sudden major sea-level rise led to increased subsidence which may have triggered tectonic thrust faulting in the foreland, resulting in further flexural loading.

The metre-scale Cheshire cycles show a systematic, hierarchically-arranged stacking pattern which is strikingly similar to cycle hierarchies in younger sedimentary sequences (e.g., Fischer 1964; Goldhammer et al. 1987, 1990; Osleger and Read 1991; Olsen and Kent 1996). Cycle hierarchies can best be explained by the combined effects of several orders of eustasy-driven, relative sea level oscillations (Goldhammer et al. 1990). Since most metre-scale carbonate cycles of Proterozoic and Phanerozoic carbonate platforms seem to record the precession cycle (Grotzinger, 1986b; Goldhammer, 1987), it can simply be assumed that the metre-scale Cheshire cycles relate to orbital precession and are bundled in cycle groups due to superposition of the eccentricity cycle. In using such arguments, it has to be remembered that the periodicities of the orbital parameters may have changed in geological time due to tidal friction. According to Berger and Loutre (1994) the two main periods of precession were around 11 ka and 12.2 ka (mean 11.6 ka) 2650 Ma ago (see Laskar 1989 for a contrasting view). Eccentricity is believed to have remained more or less constant (112 and 413 ka, see above). If these assumptions are correct, recurrence ratios of 9-10:1 (precession:short eccentricity), 35-36:1 (precession:long eccentricity) and 4:1 (short eccentricity: long eccentricity) can be expected to occur in the cyclic sequence. The recalculated precession:short eccentricity ratio of Berger and Loutre (1994) is similar to the ratio of microcycles in a mesocycle observed here. Seven mesocycle have been measured in the section (Fig. 4.16) comprising 7-11 microcycles each (9.6 cycles on average).

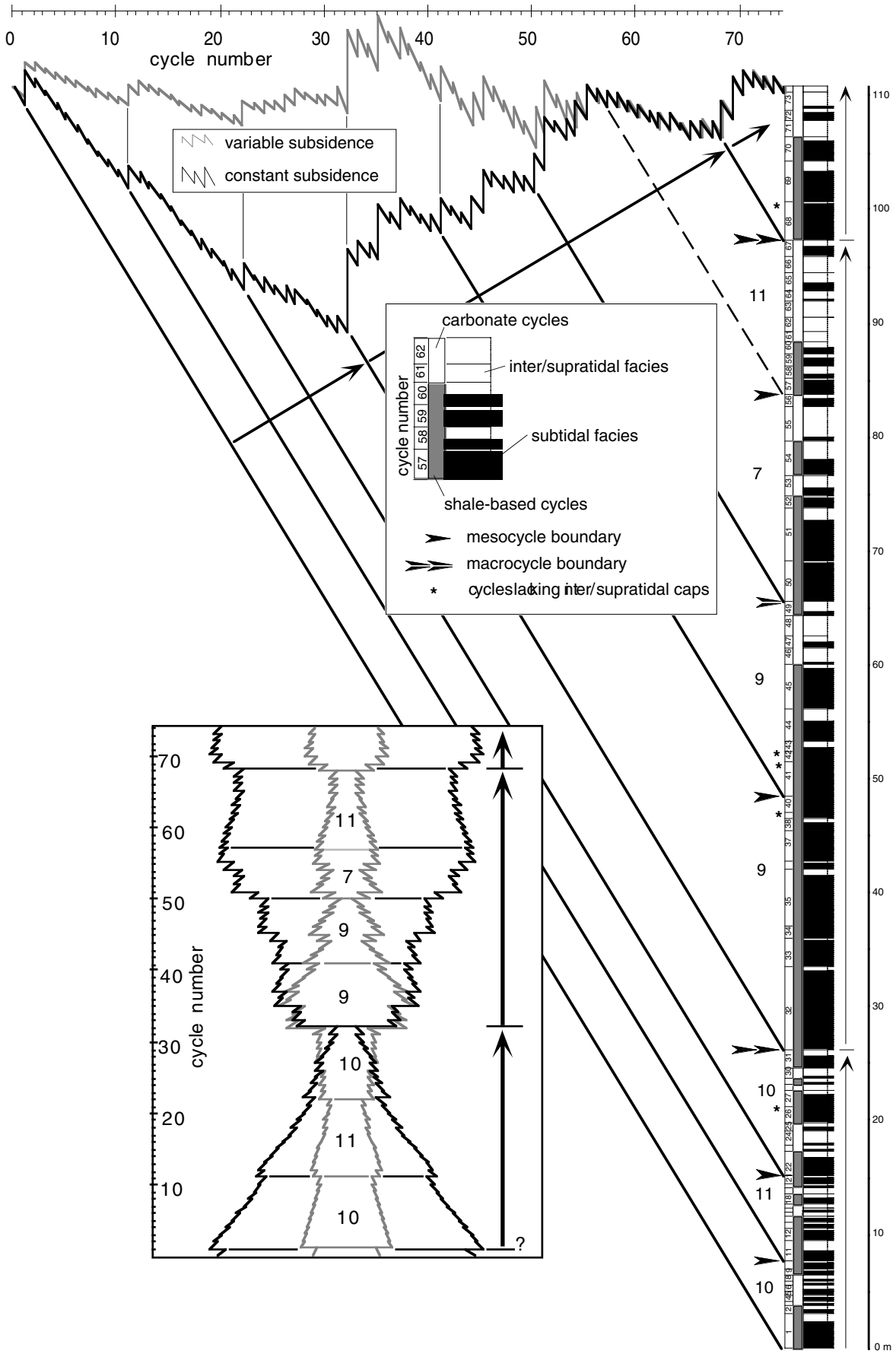
0
10
20
30
40
50
60
70
cycle number
variable subsidence
constant subsidence
carbonate cycles
inter/supratidal facies
subtidal facies
shale-based cycles
cycle number
mesocycle boundary
macrocycle boundary
* cycles lacking inter/supratidal caps
11
7
9
9
10
11
10
70
60
50
40
30
20
10
cycle number
11
7
9
9
10
11
10
?
110
100
90
80
70
60
50
40
30
20
10
0 m

Fig. 4.16 (previous page). a) Simplified log of the lower section in comparison with Fischer plots. One curve is corrected for uniform subsidence (i.e. mean cycle thickness of 150 cm), the other curve is corrected for three different mean cycle thickness values as shown in Figure 4.15. Subtidal facies include shale and grainstone facies, whereas inter/supratidal facies encompass the others. Diagonal lines reflect the mean subsidence vector (Fischer 1964) assuming that each cycle formed during a time-equivalent period. The lines separate individual cycle bundles (mesocycles), and the numbers refer to the number of cycles in each bundle. The mesocycles have been grouped into macrocycles (arrows). Cycles lacking an inter/supratidal cap are marked by asterisks. b) Diagram of vertically oriented Fischer plots and their mirror image. Boundaries of cycle bundles (mesocycles) are characterised by thick basal cycles overlying thinner ones of the bundle below.

Mesocycles are possibly grouped into macrocycles. Due to the limited thickness and incomplete exposure of the Cheshire carbonates, only one complete macrocycle has been observed comprising 35 cycles. This is identical to the recalculated precession:long eccentricity ratio. Furthermore, the macrocycle comprises four mesocycles, identical to the short eccentricity: long eccentricity ratio (see also Drummond and Wilkinson 1993 for a cautionary view on the relationship between cycle stacking patterns and orbital forcing frequencies).

CONCLUSIONS

1. The carbonate member of the Cheshire Formation comprises subtidal shales, shallow subtidal grainstones, intertidal microbial laminites, and supratidal breccias and tufa-like microbial boundstones. These facies are arranged into asymmetric, metre-scale cycles of which each has recorded a gradual fall in relative sea level. The metre-sale cycles are bundled into groups of cycles which seem to reflect a lower order of relative sea level variations.
2. Lithofacies of the Cheshire carbonates and their stacking into shallowing-upward cycles are similar to those of the Proterozoic and Phanerozoic rock record. This observation suggests that the mechanisms controlling shallow marine carbonate deposition have not significantly changed in the last 2650 million years.
3. A facies common to Palaeoproterozoic and Archaean carbonate platform successions, but rare in younger rocks, are carbonates consisting of radiating fans of aragonite crystals. In the Cheshire Formation this type of rock preferentially occurs at the top of depositional cycles and is interpreted to have formed in a supratidal setting, possibly due to the evaporation and concentration of sea/groundwater on the tidal flats.
4. The cyclicity recorded in the Cheshire carbonates is interpreted to reflect high-frequency eustatic sea-level changes based on evidence including (a) the absence of an offshore carbonate factory negating a Ginsburg-type model of tidal flat progradation, (b) the accumulation history of the cyclic sequence and the relationship between cycle thickness and inferred palaeowater depth not favouring tectonic subsidence cycles, and (c) the hierarchical arrangement of various orders of cycles.
5. The data presented here fit well with a Milankovitch-type model of orbital cyclic forcing. The deposition of metre-scale cycles is attributed to small-scale eustatic changes in tune with orbital precession with a frequency of c. 12 ka. The bundling into groups of 9-10 cycles suggests modulation by the ~100 ka short eccentricity cycle. Long eccentricity signals seem to be recorded in the succession too, as indicated by Fischer plots.

6. The mechanisms behind the origin of cyclic sedimentation on carbonate platforms has been discussed intensely in the past and probably will be discussed for some years to come. In this study a Milankovitch-type model of oscillating sea level changes is proposed for the Cheshire carbonate cycles but, like so many others, unequivocal evidence for this type of model cannot be presented. Other interpretations are possible, but are less likely.
7. The deposition of shallowing-upward carbonate cycles is as old as the Archaean, irrespective of changes in ocean water chemistry, composition of the atmosphere, climate, faunal elements, and possible changes in tectonic processes. The basic principle has remained the same.

REFERENCES

ABELL, P.I., MCCLORY, J., MARTIN, A. AND NISBET, E.G., 1985, Archaean stromatolites from the Ngesi Group, Belingwe Greenstone Belt, Zimbabwe; preservation and stable isotopes-preliminary results: Precambrian Research, v. 27, p. 357-383.

AIGNER, T., 1985, Storm depositional systems: dynamic stratigraphy in modern and ancient shallow-marine sequences: Lecture Notes in Earth Sciences, Berlin, Springer-Verlag, 174 p.

AIGNER, T., AND REINECK, H.E., 1982, Proximality trends in modern storm sands from the Helgoland Bight (North Sea) and their implications for basin analysis: Senckenbergiana maritima,v. 14, p. 183-215.

AITKEN, J.D., 1967, Classification and environmental significance of cryptalgal limestones and dolomites with illustrations from the Cambrian and Ordovician of southwestern Alberta: Journal of Sedimentary Petrology, v. 37, p. 1163-1178.

ALLEN, J.R.L., 1984, Sedimentary structures: their character and physical basis: Developments in Sedimentology 30, New York, Elsevier, 1256p.

ANDERSON, R.Y., 1986, The varve microcosm: propagator of cyclic bedding: Paleoceanography, v. 1, p. 373-382.

ASTIN, T.R., AND ROGERS, D.A., 1991, "Subaqueous shrinkage" or "syneresis" cracks in the Devonian of Scotland reinterpreted.: Journal of Sedimentary Petrology, v. 61.

BERGER, A., LOUTRE, M.F., AND LASKAR, J., 1992, Stability of the astronomical frequencies over Earth's history for paleoclimatic studies: Science, v. 255, p. 560-566.

BERGER, A., AND LOUTRE, M.F., 1994, Astronomical forcing through geological time: International Association of Sedimentologists Special Publication 19, p. 15-24.

BERGER, A., 1978, Long-term variations of caloric insolation resulting from the Earth`s orbital elements: Quaternary Research, v. 9, p. 139-167.

BEUKES, N.J., 1987, Facies relations, depositional environments and diagenesis in a major early Proterozoic stromatolitic carbonate platform to basinal sequence, Campbellrand Subgroup, Transvaal Supergroup, southern Africa: Sedimentary Geology, v. 54, p. 1-46.

BICKLE, M.J., MARTIN, A., AND NISBET, E.G., 1975, Basaltic and peridotitic komatiites, stromatolites and a basal unconformity in the Belingwe greenstone belt, Rhodesia: Earth and Planetary Science Letters, v. 27, p. 155-162.

BICKLE, M.J., ORPEN, J.L., NISBET, E.G., AND MARTIN, A., 1993, Structure and metamorphism of the Belingwe Greenstone Belt and adjacent granite-gneiss terrain: The tectonic evolution of an Archaean craton.

in Bickle, M.J., and Nisbet, E.G., eds., The geology of the Belingwe Greenstone Belt, Zimbabwe: Geological Society of Zimbabwe Special Publications 2, p. 39-68.

BOLHAR, R., HOFMANN, A., WOODHEAD, J.M., HERGT, J.M., AND DIRKS, P., 2001, Pb- and Nd-isotope systematics of stromatolitic limestones from the 2.7 Ga Ngezi Group of the Belingwe Greenstone Belt: constraints on provenance, deposition and deformation: Precambrian Research, in press.

BRAKE, C., 1996, Tholeiitic magmatism in the Belingwe greenstone belt, Zimbabwe [unpublished Ph.D. dissertation]: University of Edinburgh, 184p.

BYERLY, G.R., LOWE, D.R., AND WALSH, M.M., 1986, Stromatolites from the 3,300-3,500-Myr Swaziland Supergroup, Barberton Mountain Land, South Africa: Nature, v. 319, p. 489-491.

CALVET, F., AND TUCKER, M.E., 1988, Outer ramp cycles in the Upper Muschelkalk of the Catalan Basin, northeast Spain: Sedimentary Geology, v. 57, p. 185-198.

CAMERON, E.M., AND BAUMANN, A., 1972, Carbonate sedimentation during the Archean: Chemical Geology, v. 10, p. 17-30.

CARR, T.R., 1982, Log-linear models, Markov chains and cyclic sedimentation: Journal of Sedimentary Petrology, v. 52, p. 905-912.

CHAFETZ, H.S., AND FOLK, R.L., 1984, Travertines: depositional morphology and the bacterially constructed constituents: Journal of Sedimentary Petrology, v. 54, p. 289-316.

CHAUVEL, C., DUPRÉ, B., AND ARNDT, N.T., 1993, Pb and Nd istopic correlation in Belingwe komatiites and basalts. *in* Bickle, M.J., and Nisbet, E.G., eds., The geology of the Belingwe Greenstone Belt, Zimbabwe: Geological Society of Zimbabwe Special Publications 2, p. 167-174.

CISNE, J.L., 1986, Earthquakes recorded stratigraphically on carbonate platforms: Nature, v. 323, p. 320-322.

CLOETINGH, S., 1986, Intraplate stresses: A new tectonic mechanism for relative fluctuations of sea level: Geology, v. 14, p. 617-620.

COWAN, C.A., AND JAMES, N.P., 1996, Autogenic dynamics in carbonate sedimentation: meter-scale, shallowing-upward cycles, Upper Cambrian, western Newfoundland, Canada: American Journal of Science, v. 296, p. 1175-1207.

CRAFT, J.H., AND BRIDGE, J.S., 1987, Shallow-marine sedimentary processes in the Late Devonian Catskill Sea, New York State: Geological Society of America Bulletin, v. 98, p. 338-355.

DEMICCO, R.V., AND HARDIE, L.A., 1994, Sedimentary structures and early diagenetic features of shallow marine carbonate deposits: SEPM Atlas 1, Tulsa, Oklahoma, 255p.

DEWEY, J.F., AND PITMAN, W.C., 1998, Sea-level changes: mechanisms, magnitudes and rates: SEPM Special Publication 58, p. 1-16.

DE WIT, M.J., 1998, On Archaean granites, greenstones, cratons and tectonics: does the evidence demand a verdict? Precambrian Research, v. 91, p. 181-226.

DILL, R.F., SHINN, E.A., JONES, A.T., KELLY, K., AND STEINEN, R.P., 1986, Giant subtidal stromatolites forming in normal salinity waters: Nature, v. 324, p. 55-58.

DONOVAN, D.T., AND JONES, E.J.W., 1979, Causes of worldwide changes in sea level. Journal of the Geological Society of London, v. 136, p. 187-192.

DRUMMOND, C.N., AND WILKINSON, B.H., 1993, Carbonate cycle stacking patterns and hierarchies of orbitally forced eustatic sealevel change: Journal of Sedimentary Petrology, v. 63, p. 369-377.

ESTEBAN, M., AND KLAPPA, C.F., 1983, Subaerial exposure, *In* Scholle, P.A., Bebout, D.G., and Moore, C.H., eds., Carbonate Depositional environments: American Association of Petroleum Geologists Memoir 33, p. 1-54.

FISCHER, A.G., 1964, The Lofer cyclothems of the Alpine Triassic, *in* Merriam, D.F., ed., Symposium on cyclic sedimentation: Kansas State Geological Survey Bulletin, v. 169, p. 107-149.

GINSBURG, R.N., 1971, Landward movement of carbonate mud: New model for regressive cycles in carbonates (abstract): American Association of Petroleum Geologists Bulletin, v. 55, p. 340.

GOODWIN, P.W., AND ANDERSON, E.J., 1985, Punctuated aggradational cycles: a general hypothesis of episodic stratigraphic accumulation: Journal of Geology, v. 93, p. 515-533.

GOLDHAMMER, R.K., DUNN, P.A., AND HARDIE, L.A., 1987, High frequency glacio-eustatic sea-level oscillations with Milankovitch characteristics recorded in Middle Triassic platform carbonates in northern Italy: American Journal of Science, v. 287, p. 853-892.

GOLDHAMMER, R.K., DUNN, P.A., AND HARDIE, L.A., 1990, Depositional cycles, composite sea-level changes, cycle stacking patterns, and the hierarchy of stratigraphic forcing: Examples from Alpine Triassic platform carbonates: Geological Society of America Bulletin, v. 102, p. 535-562.

GOLDHAMMER, R.K., LEHMANN, P.J., AND DUNN, P.A., 1993, The origin of high-frequency platform carbonate cycles and third-order sequences (Lower Ordovician El Paso Gp, west Texas) constraints from outcrop data and stratigraphic modeling: Journal of Sedimentary Petrology, v. 63, p. p. 318-359.

GREY, K. AND THORNE, A.M., 1985, Biostratigraphic significance of stromatolites in upward shallowing sequences of the Early Proterozoic Duck Creek dolomite, Western Australia: Precambrian Research, v. 29, p. 183-206.

GROTZINGER, J.P., 1986a, Cyclicity and palaeoenvironmental dynamics, Rocknest platform, northwest Canada: Geological Society of America Bulletin, v. 97, p. 1208-1231.

GROTZINGER, J.P., 1986b, Upward shallowing platform cycles: a response to 2.2 billion years of low-amplitude, high-frequency (Milankovitch band) sea level oscillations: Paleoceanography, v. 1, p. 403-416.

GROTZINGER, J.P., 1989, Facies and evolution of Precambrian carbonate depositional systems: emergence of the modern platform archetype, *in* Crevello, P.D., Wilson, J.L., Sarg, J.F., and Read, J.F., eds., Controls on carbonate platform and basin evolution: SEPM Special Publication 44, p. 79-106.

GROTZINGER, J.P., AND KASTING, J.F., 1993, New constraints on Precambrian ocean composition: Journal of Geology, v. 101, p. 235-243.

GROTZINGER, J.P, SUMNER, D.Y., AND BEUKES, N.J., 1993, Archaean carbonate sedimentation in an active extensional basin, Belingwe Greenstone Belt, Zimbabwe (abstract): Geological Society of America Annual Meeting, v. 25, p. A64.

HALLEY, R.B., 1976, Textural variation within Great Salt Lake algal mounds, *in* Walter, M.R., eds., Stromatolites: Amsterdam, Elsevier, p. 435-445.

HAMILTON, W.B., 1998, Archean magmatism and deformation were not products of plate tectonics: Precambrian Research, v. 91, p. 143-179.

HARDIE, L.A., AND GINSBURG, R.N., 1977, Layering: the origin and environmental significance of lamination and thin bedding, *in* Hardie, L.A., ed., Sedimentation on the modern carbonate tidal flats of northwest Andros Island, Bahamas: Baltimore, Studies in Geology 22, The John Hopkins University Press, p. 50-123.

HARDIE, L.A., AND SHINN, E.A., 1986, Carbonate depositional environments, modern and ancient, Part 3, tidal flats: Colorado School of Mines Quarterly, v. 81, p. 1-74.

HARDIE, L.A., BOSELLINI, A., AND GOLDHAMMER, R.K., 1986, Repeated subaerial exposure of subtidal carbonate platforms: evidence for high-frequency sea level oscillations on a 10^4 year scale: Paleoceanography, v. 1, p. 447-457.

HAYS, J.D., IMBRIE, J., AND SHACKLETON, J.J., 1976, Variations in the Earth`s orbit: Pacemaker of the Ice Ages: Science, v. 194, p. 1121-1132.

HENDERSON, J.B., 1975, Archaean stromatolites in the northern Slave Province, Northwest Territories, Canada: Canadian Journal of Earth Sciences, v. 12, p. 1619-1630.

HOFFMAN, P.F., 1975, Shoaling-upward shale-to-dolomite cycles in the Rocknest Formation (lower Proterozoic), N.W. Territories, Canada, *in* Ginsburg, R.N., ed., Tidal deposits: New York, Springer-Verlag, p. 257-265.

HOFFMAN, P.F., 1976, Environmental diversity of Middle Precambrian stromatolites, *in* Walter, M.R., eds., Stromatolites: Amsterdam, Elsevier, p. 599-612.

HOFMANN, H.J., 2000, Archean stromatolites as microbial archives, *in* Riding, R.E. and Awramik, S.M., eds., Microbial Sediments: Berlin, Springer-Verlag, p. 315-327.

HORSTWOOD, M.S.A., 1998, Stratigraphy, geochemistry and zircon geochronology of the Midlands greenstone belt, Zimbabwe [unpublished Ph.D. dissertation]: University of Southampton, 215 p.

HUNTER, M.A., BICKLE, M.J., NISBET, E.G., MARTIN, A., AND CHAPMAN, H.J., 1998, Continental extensional setting for the Archean Belingwe Greenstone Belt, Zimbabwe: Geology, v. 26, p. 883-886.

JAMES, N.P., 1984, Shallowing-upwards sequences in carbonates, *in* Walker, R.G.,ed., Facies Models (2nd ed.): St. Johns, Newfoundland, Geoscience Canada Reprint Series 1, p. 213-228.

JAMES, N.P., AND CHOQUETTE, P.W., 1990, Limestones- The sea floor diagenetic environment: St. Johns, Newfoundland, Geoscience Canada Reprint Series 4, Geological Association of Canada, p. 13-34.

JELSMA, H.A., 1993, Granites and greenstones in Northern Zimbabwe: tectono-thermal evolution and source regions [unpublished Ph.D. dissertation]: Free University, Amsterdam, 268 p.

JELSMA, H.A., VINYU, M.L., VALBRACHT, P.J., DAVIES, G.R., WIJBRANS, J.R., AND VERDURMEN, E.A.T., 1996, Constraints on Archaean crustal evolution of the Zimbabwe craton: a U-Pb zircon, Sm-Nd and Pb-Pb whole-rock isotope study: Contributions to Mineralogy and Petrology, v. 124, p. 55-70.

KAH, L.C., AND GROTZINGER, J.P., 1992, Early Proterozoic (1.9 Ga) thrombolites of the Rocknest Formation, Northwest Territories, Canada: Palaios, v. 7, p. 305-315.

KENNARD, J.M., AND JAMES, N.P., 1986, Thrombolites and stromatolites: two distinct types of microbial structures: Palaios, v. 1, p. 492-503.

KOERSCHNER, W.F., AND READ, J.F., 1989, Field and modelling studies of Cambrian carbonate cycles, Virginia Appalachians: Journal of Sedimentary Petrology, v. 59, p. 654-687.

KUSKY, T.M., AND KIDD, W.S.F., 1992, Remnants of an Archaean oceanic plateau, Belingwe Greenstone Belt, Zimbabwe: Geology, v. 20, p. 43-46.

KUSKY, T.M., AND WINSKY, P.A., 1995, Structural relationships along a greenstone/shallow water shelf contact, Belingwe greenstone belt, Zimbabwe: Tectonics, v. 14, p. 448-471.

LASKAR, J., 1989, A numerical experiment on the chaotic behaviour of the Solar System: Nature, v. 338, p. 237-238.

MACGREGOR, A.M., 1941, A pre-Cambrian limestone in Southern Rhodesia: Geological Society of South Africa Transactions, v. 43, p. 9-15.

MARTIN, A., 1978, The geology of the Belingwe-Shabani shist belt: Rhodesia Geological Survey Bulletin 83, 213p.

MARTIN, A., NISBET, E.G., AND BICKLE, M.J., 1980, Archaean stromatolites of the Belingwe Greenstone Belt: Precambrian Research, v. 13, p. 337-362.

MARTIN, A., NISBET, E.G., BICKLE, M.J., AND ORPEN, J.L., 1993, Rock units and stratigraphy of the Belingwe Greenstone Belt: The complexity of the tectonic setting: *in* Bickle, M.J. and Nisbet, E.G., eds., The geology of the Belingwe Greenstone Belt, Zimbabwe, Geological Society of Zimbabwe Special Publications 2, p. 39-68.

MCDONOUGH, W. F., AND IRELAND, T. R., 1993, Intraplate origin of komatiites inferred from trace elements in glass inclusions: Nature, v. 365, p. 432-434.

MUKASA, S.B., WILSON, A.H., AND CARLSON, R.W., 1998, A multielement geochronologic study of the Great Dyke, Zimbabwe: significance of the robust and reset ages: Earth and Planetary Science Letters, v. 164, p. 353-369.

OLSEN, P.E., 1986, A 40-million-year lake record of early Mesozoic climatic forcing: Science, v. 234, p. 842-848.

OLSEN, P.E., AND KENT, D.V., 1996, Milankovitch climate forcing in the tropics of Pangaea during the Late Triassic: Palaeogeography, Palaeoclimatology, Palaeoecology, v. 122, p. 1-26.

OSLEGER, D.A., 1991, Subtidal carbonate cycles: implications for allocyclic versus autocyclic controls: Geology, v. 19, p. 917-920.

OSLEGER, D.A., AND READ, J.F., 1991, Relation of eustasy to stacking patterns of metre-scale carbonate cycles, late Cambrian, U.S.A.: Journal of Sedimentary Petrology, v. 61, p. 1225-1252.

PANNELLA, G., 1975, Biological time, paleontological clocks and the history of the Earth-Moon system. Geophys. Rev., p. 253-284.

POWERS, D.W., AND EASTERLING, R.G., 1982, Improved methodology for using embedded Markov chains to describe cyclical sediments: Journal of Sedimentary Petrology, v. 52, p. 913-923.

PRATT, B.R., AND JAMES, N.P., 1986, The St George Group (Lower Ordovician) of western Newfoundland: tidal flat island model for carbonate sedimentation in shallow epeiric seas: Sedimentology, v. 33, p. 313-343.

PRATT, B.R., JAMES, N.P., AND COWAN, C.A., 1992, Peritidal carbonates, *in* Walker, R.G., and James, N.P., eds., Facies, models and response to sea-level changes: St John´s, Newfoundland, Geological Association of Canada, p. 303-322.

DE RAAF, J.F.M., BOERSMA, J.R., AND VAN GELDER, A., 1977, Wave generated structures and sequences from a shallow marine succession, Lower Carboniferous, County Cork, Ireland: Sedimentology, v. 4, p. 1-52.

READ, J.F., AND GOLDHAMMER, R.K., 1988, Use of Fischer plots to define 3rd order sea level curves in peritidal cyclic carbonates, Early Ordovician, Appalachians: Geology, v. 16, p. 895-899.

REINECK, H.E., AND WUNDERLICH, F., 1968, Classification and origin of flaser and lenticular bedding: Sedimentology, v. 11, p. 99-104.

RIDING, R., 2000, Microbial carbonates: the geological record of calcified bacterial-algal mats and biofilms: Sedimentology, v. 47 (Supplement 1), p. 179-214.

ROTHPLETZ, A., 1916, Über die systematische Deutung und die stratigraphische Stellung der ältesten Versteinerungen Europas und Nordamerikas mit besonderer Berücksichtigung der Cryptozoen und Oolithe. Über Cryptozoon, Eozoon, und Atikokania. Bayrische Akademie der Wissenschaften, Abhandlungen Mathematik-Physik, v. 28, p. 92.

SADLER, P.M., OSLEGER, D.A., AND MONTAÑEZ, I.P., 1993, On the labeling, length, and objective basis of Fischer plots: Journal of Sedimentary Petrology, v. 63, p. 360-368.

SCHLAGER, W., 1981, The paradox of drowned reefs and carbonate platforms: Geological Society of America Bulletin, v. 92, p. 197-211.

SCHOLEY, S.P., 1992, The geology and geochemistry of the Ngezi Group volcanics, Belingwe Greenstone Belt, Zimbabwe [unpublished Ph.D. dissertation]: University of Southampton, 184p.

SCHWARZACHER, W., 1993, Cyclostratigraphy and the Milankovitch Theory: Developments in Sedimentology 52, Amsterdam, Elsevier, 225 p.

SHINN, E.A., 1968, Practical significance of birdseye structures in carbonate rocks: Journal of Sedimentary Petrology, v. 38, p. 215-223.

SHINN, E.A., LLOYD, R.M., AND GINSBURG, R.N., 1969, Anatomy of a modern carbonate tidal flat, Andros Island, Bahamas: Journal of Sedimentary Petrology, v. 39, p. 1202-1228.

SOUTHGATE, P.N., 1989, Relationships between cyclicity and stromatolite form in the Late Proterozoic Bitter Springs Formation, Australia: Sedimentology, v. 36, p. 323-339.

STRASSER, A., 1991, Lagoonal-peritidal sequences in carbonate environments: autocyclic and allocyclic processes, *in* Einsele, G., Ricken, W., and Seilacher, A., eds., Cycles and events in stratigraphy: Heidelberg, Springer, p. 709-721.

SUMNER, D.Y., AND GROTZINGER, J., 2000, Late Archaean aragonite precipitation: petrography, facies association and environmental significance, *in* Grotzinger, J., and James, N.P., eds., Carbonate sedimentation and diagenesis in the evolving Precambrian world: SEPM Special Publication 65, in press.

VAN HOUTEN, F.B., 1964, Cyclic lacustrine sedimentation, Upper Triassic Lockatong Formation, New Jersey and adjacent Pennsylvania: Kansas Geological Survey Bulletin, v. 169, p. 497-531.

WALTER, M.R., 1976, Glossary of selected terms, *in* Walter, M.R., ed., Stromatolites: Amsterdam, Elsevier, p. 687-692.

WALTER, M.R., GROTZINGER, J.P., AND SCHOPF, J.W., 1992, Proterozoic stromatolites, *in* Schopf, J.W., and Klein, C., eds., The Proterozoic biosphere; a multidisciplinary study: Cambridge, Cambridge University Press, p. 253-260.

WALTER, M.R., BUICK, R., AND DUNLOP, J.S.R., 1980, Stromatolites 3,400-3,500 Myr old from the North Pole area, Western Australia: Nature, v. 284, p. 443-445.

WILSON, J.F., NESBITT, R.W., AND FANNING, C.M., 1995, Zircon geochronology of Archaean felsic sequences in the Zimbabwe craton: a revision of greenstone stratigraphy and a model for crustal growth, *in* Coward, M.P., and Ries, A.C., eds., Early Precambrian processes: Geological Society Special Publication 95, p. 109-126.

WILSON, J.L., 1975, Carbonate facies in geologic history: New York, Springer-Verlag, 470p.

WINTER, H. DE LA R., 1963, Algal stromatolites in the sediments of the Ventersdorp System: Geological Society of South Africa Transactions, v. 65, p. 115-121.

CHAPTER 5

The geochemistry of Archaean shales derived from a mafic volcanic sequence, Belingwe greenstone belt, Zimbabwe: provenance, source area unroofing and submarine vs subaerial weathering

Axel Hofmann, Robert Bolhar, Paul H.G.M. Dirks, and Hielke A. Jelsma
submitted to Geochimica et Cosmochimica Acta

Abstract—Shales of the ~2.7 Ga Zeederbergs Formation, Belingwe greenstone belt, Zimbabwe, form thin (0.2-2 m) horizons intercalated with submarine lava plain basalts. Shales of the overlying Cheshire Formation, a foreland basin sedimentary sequence, form 1-100 m thick units intercalated with shallow-water carbonates and deep-water, resedimented basalt pebble conglomerates. Zeederbergs shale is characterized by high contents of MgO and transition metals and low concentrations of K_2O and LILE as compared to average Phanerozoic shale, indicative of an (ultra)mafic source terrain. Cheshire shales have similar major and trace element contents as compared to Zeederbergs shales, but MgO and transition metals are less enriched, and the LILE are less depleted. Zeederbergs shales have smoothly fractionated REE patterns (La_N/Yb_N=2.84-4.45) and no significant Eu anomaly (Eu/Eu*=0.93-0.96). REE patterns are identical to those of the surrounding basaltic rocks, indicating local derivation from submarine reworking. Cheshire shales have rather flat REE patterns (La_N/Yb_N=0.69-2.19) and a small but distinct negative Eu anomaly (average Eu/Eu*=0.85), indicative of a mafic provenance with minor contributions of felsic detritus. A systematic change in REE patterns and concentrations of transition metals and HFSE upwards in the sedimentary succession indicates erosion of progressively more ultramafic volcanic rocks and unroofing of granitoid crust. Weathering indices confirm the submarine nature of Zeederbergs shale, whereas Cheshire shale was derived from a source terrain subjected to intense chemical weathering.

INTRODUCTION

The geochemistry of shale has been a useful tool in the study of provenance, tectonic setting and palaeoclimatic conditions of Archaean sedimentary sequences (Wronkiewicz and Condie, 1987; Feng and Kerrich, 1990; McLennan and Taylor, 1991) and has provided important constraints on the evolution of continental crust through time (Taylor and McLennan, 1985). In the case of strongly deformed and metamorphosed rock sequences, deeply eroded terrains, and volcano-sedimentary rocks of greenstone belts, sediment geochemistry may be one of the few tools to obtain information on the depositional setting and sediment provenance (e.g., Taylor et al., 1986; Maas and McCulloch, 1991). Geochemical studies of fine-grained siliciclastic rocks of the greenstone belts of the Zimbabwe craton are rare, despite bearing the potential of providing important constraints on the evolution of this terrain. The only relevant study has been conducted on c. 3.0 Ga old shales of the Buhwa greenstone belt in southern Zimbabwe in which Fedo et al. (1996) were able to provide constraints on provenance and source-area weathering.

Situated north of Buhwa, the Belingwe greenstone belt (BGB) has been the focus of considerable geological research for more than two decades (Bickle et al., 1975; Bickle and Nisbet, 1993). The BGB comprises two stratigraphically distinct volcano-sedimentary sequences, the Mtshingwe and Ngezi Groups, that overlie up to 3.5 Ga old granitoid gneisses (Fig. 5.1). The Mtshingwe Group consists of mafic to intermediate lavas, volcaniclastics, and siliciclastic sediments (Martin et al., 1993) ranging in age from 2.90 to 2.83 Ga (Wilson et al., 1995, U/Pb zircon). The Ngezi Group comprises a sedimentary succession (Manjeri Formation), overlain by ultramafic and mafic volcanics (Reliance and Zeederbergs Formations, collectively termed Ngezi volcanics), and capped by a sedimentary unit (Cheshire Formation). Granites of the ~2.6 Ga old Chilimanzi suite are intrusive into the Ngezi Group in the northern and southern parts of the belt (Fig. 5.1).

Most studies of the BGB have concentrated on the Ngezi Group, given the good preservation and low metamorphic grade of this stratigraphic unit. Several, mostly unpublished geochemical studies have been conducted on the mafic volcanic rocks of the Reliance Formation, including extremely fresh komatiites (Nisbet et al., 1987; Scholey, 1992; McDonough and Ireland, 1993; Silva, 1997; Bolhar, 2001), and the overlying tholeiites of the Zeederbergs Formation (Brake, 1996; Bolhar, 2001). Most workers have suggested a mantle plume origin for the volcanic sequence, but the tectonic setting is controversial. Some have argued that the volcanics extruded onto stretched continental crust, a setting similar to continental flood basalt provinces (e.g., Bickle et al., 1994). In this type of model, the Cheshire Formation was regarded as a late syn- to post-volcanic sedimentary sequence with subsidence possibly related to continued extension (Nisbet et al., 1993). Others have suggested that the volcanic succession represents the uppermost part of an oceanic plateau that has been obducted as a large allochthonous sheet onto the Manjeri Formation and underlying basement (Kusky and Kidd, 1992; Kusky and Winsky, 1995). Recent sedimentological and structural work (chapters 2, 3) has indicated that the Cheshire Formation shares features characteristic of a foreland

basin sequence and formed during thrusting of the underlying Zeederbergs lavas, thus providing support for an allochthonous origin of the Ngezi volcanics.

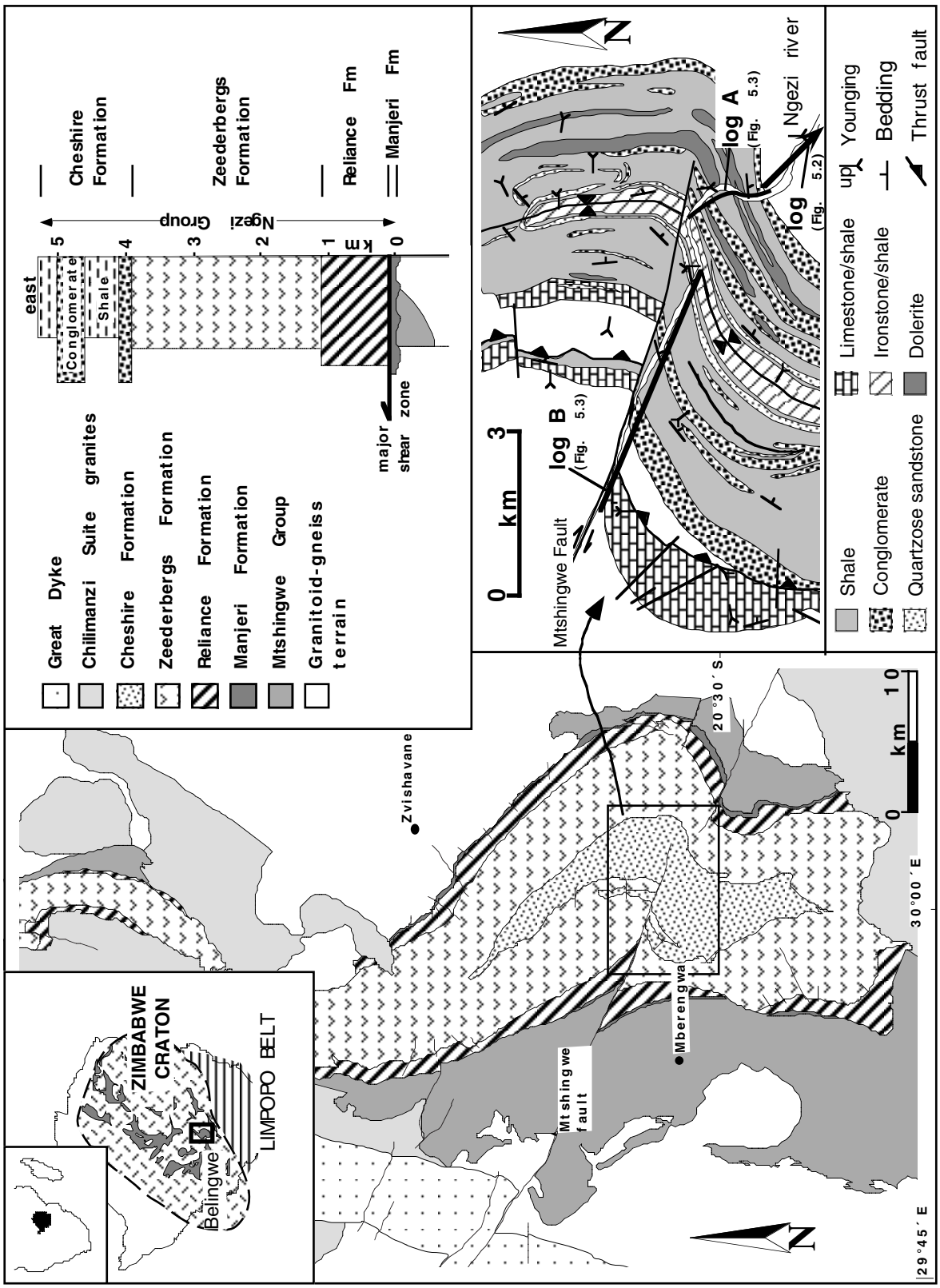

Fig. 5.1. Geological map of the Belingwe greenstone belt, simplified stratigraphic column of the Ngezi Group and geological map of the central part of the Cheshire Formation.

This paper reports analytical data of shales from the Zeederbergs and Cheshire Formations and attempts to refine the existing models for provenance and tectonic setting. The shales are somewhat unusual in chemical composition, since they have been derived almost entirely from erosion of a mafic volcanic provenance.

GEOLOGICAL SETTING OF THE NGEZI GROUP

Stratigraphy

The Manjeri Formation unconformably overlies the Mtshingwe Group and granitoid basement (Bickle et al., 1975) and has a maximum thickness of ~250 m. Hunter et al. (1998) described the Manjeri Formation to comprise three stratigraphic units, a lower unit of fluvial to shallow-water sediments, a middle unit of alluvial fan to fan delta clastics, and an upper unit represented by a 5-10 m thick horizon of sulphide-facies banded ironstone.

The Reliance Formation is ~1 km thick and can be divided into three stratigraphic units. The lower unit (500-600 m) consists of partly pillowed tholeiitic and komatiitic basalt. The central unit (300 m) comprises a komatiite suite of pillow lavas and lava flows with a few cross-cutting dykes. The upper unit (200 m) includes poorly exposed komatiitic basalt, tholeiitic basalt and tuff and passes upwards, without a distinctive geological break, into the lavas of the Zeederbergs Formation (Nisbet et al., 1977; Scholey, 1992). Komatiitic basalt of the Reliance Formation has been dated by the whole-rock Pb/Pb isochron method at 2692±9 Ma (Chauvel et al., 1993). Ion microprobe trace element data of glass inclusions in komatiites are similar to modern plume-related oceanic plateau and oceanic island basalts (McDonough and Ireland, 1993).

The Zeederbergs Formation (~2.8 km thick, Brake, 1996) consists of pillowed and massive basalt, and minor basaltic andesite and andesite at two stratigraphic levels in the centre and near the top of the sequence. Massive and pillowed rocks form randomly intercalated units several metres up to 200 m in thickness (Fig. 5.2). Pillows are typically 0.5-1 m in diameter and exhibit chilled margins and calcite- and quartz-filled vesicles. Pillow breccia commonly fills the space between pillows or forms rare discrete horizons. Massive basalt locally grades into pillow basalt, indicating that the massive variety represents, at least in part, extrusive lava flows. Intrusive rocks are rare in the Zeederbergs Formation and include narrow (<2 m), cross-cutting basaltic dykes and up to several metres thick ultramafic sills (Brake, 1996). Hyaloclastite forms a minor proportion of the sequence and consists of spherical, ellipsoidal or irregular, shard-like basalt clasts, ranging from sand size to 2 cm in diameter. It forms crudely parallel-stratified, continuous horizons, several decimetres up to 10 metres thick, intercalated with basalt flows. Rare epiclastic sedimentary rocks include continuous, several decimetres thick beds of shale. Graded beds 0.1-1 m thick are commonly intercalated with shale. The base of such beds consists of normally graded, fine basalt pebble conglomerate with varying amounts of angular, medium to coarse basalt pebbles. Conglomerate grades into parallel- and ripple-laminated sandstone and siltstone. Load and water escape structures are common. The graded beds show partial and complete Bouma (1962) sequences indicative of turbidites.

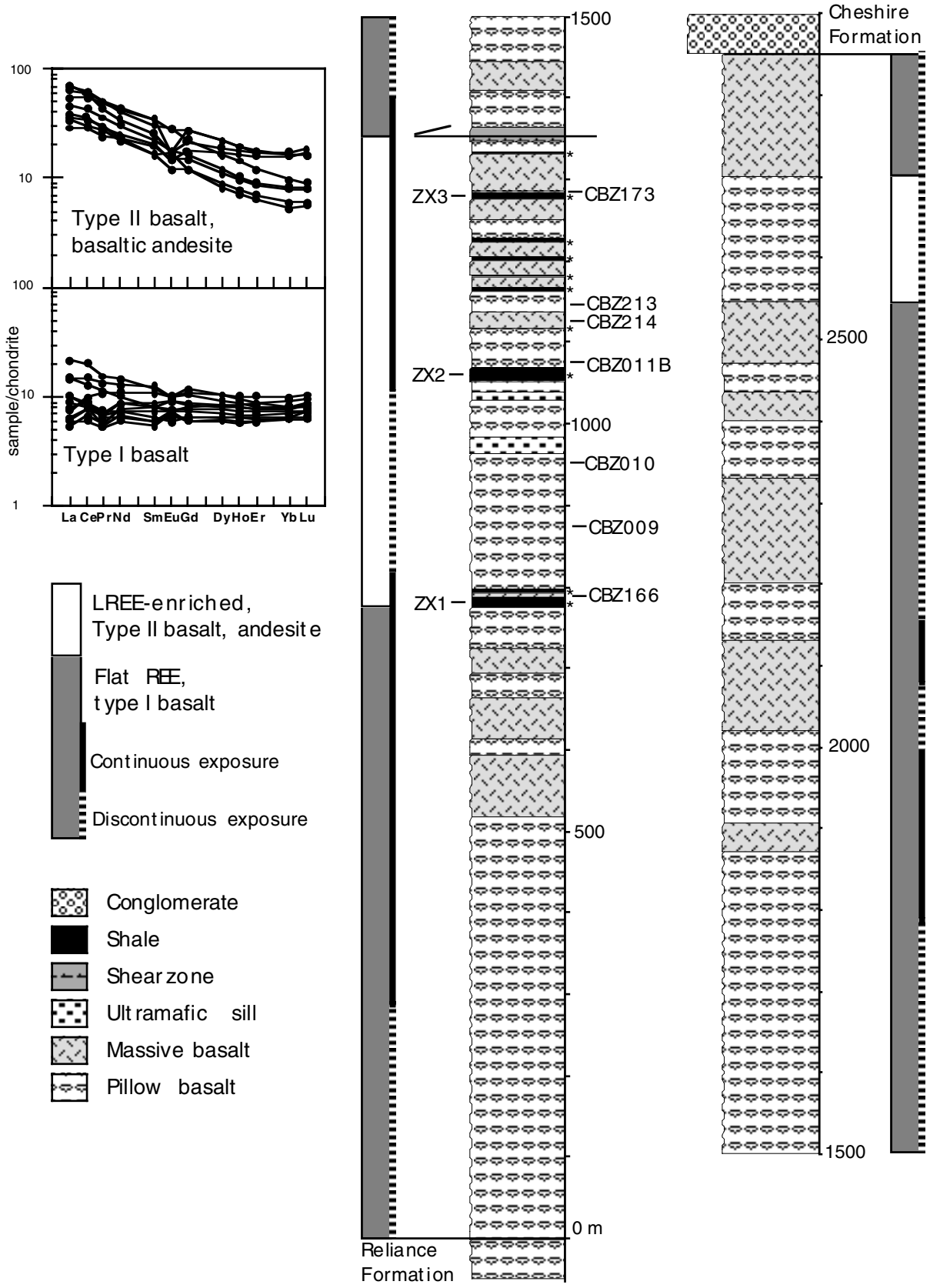

Fig. 5.2. Simplified stratigraphic log of the Zeederbergs Formation measured along the Ngezi River at the eastern margin of the belt (Fig. 5.1), and geochemical characteristics of the sequence (modified after Brake, 1996). Sample localities of Brake (1996, samples CBZ) are shown. Shale samples analysed by Brake (1996) from certain horizons (marked with asterisks) have been included in the discussion of Zeederbergs shale geochemistry.

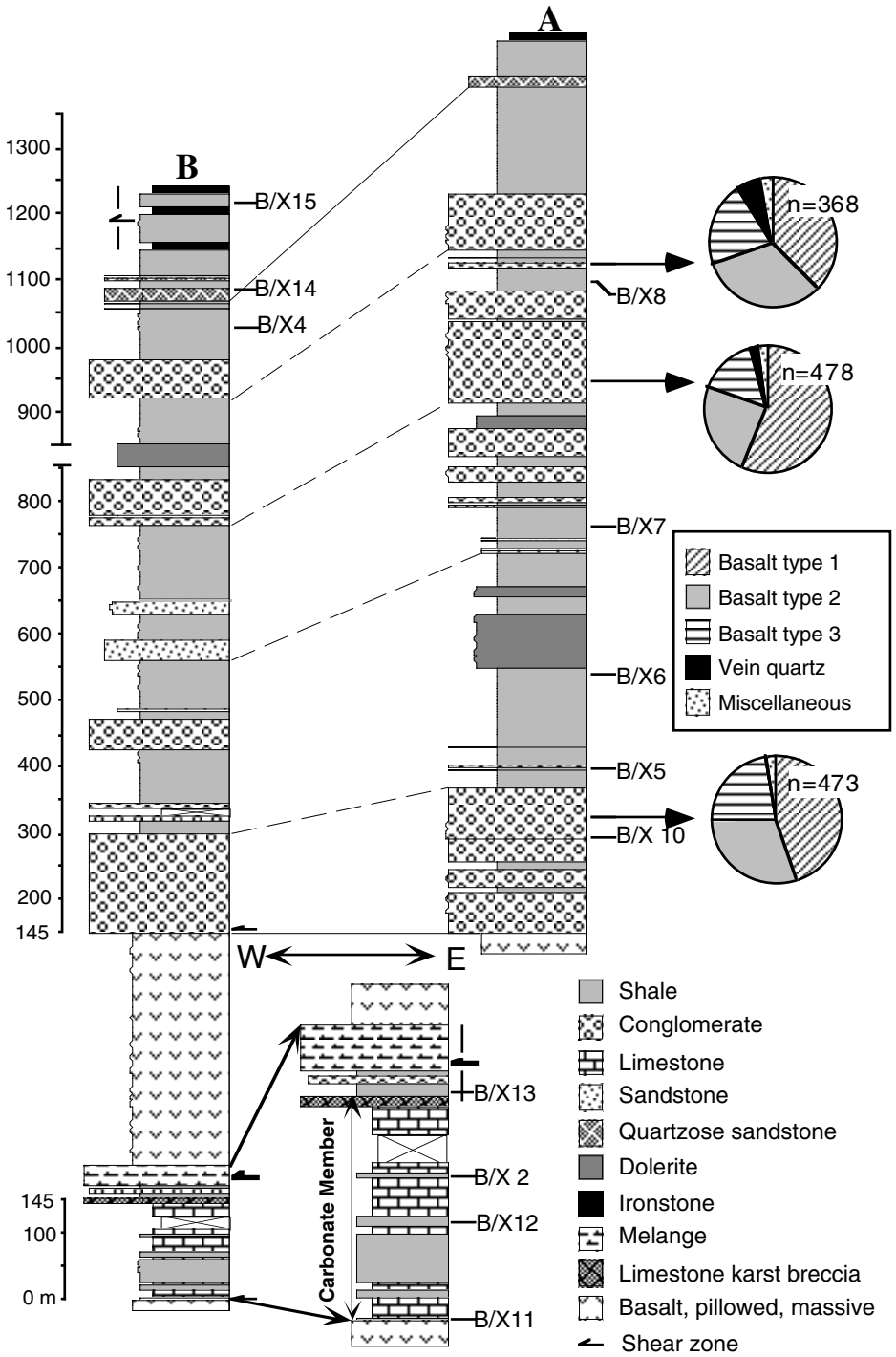

Fig. 5.3. Graphic logs measured on both sides of the syncline along the Ngezi River (A, B; Fig. 5.1) and sample localities. The carbonate member (base of log B) has been expanded for clarity. Pebble counts from three localities are shown (refer to text for clast description).

The Cheshire Formation (~1.3 km thick) is the uppermost stratigraphic unit of the BGB and rests along a sharp and sheared contact on the Zeederbergs Formation. It has been subdivided into two informal stratigraphic units, the carbonate and siliciclastic members (chapter 2). The carbonate member consists of interbedded limestone and shale and local limestone karst breccia and is

overlain by the siliciclastic member and a thrust slice of Zeederbergs volcanics. The siliciclastic member (Fig. 5.1) consists of a basal conglomerate unit which is overlain by a succession of intercalated conglomerate and shale with a conspicious quartzose sandstone horizon and ironstone at the top (Fig. 5.3). Massive, graded and horizontally stratified conglomerates are common and are interpreted as high-density turbidity current deposits. Shale is characteristic of low-density turbidite and background suspension deposition (chapter 2).

An early thrusting event gave rise to tectonic duplication of part of the Cheshire Formation stratigraphy and juxtaposition of a thrust slice of Zeederbergs basalt onto the carbonate member (Figs. 1 and 3; chapter 3). Subsequent deformation of the BGB included tight folding of the greenstone succession, forming the distinctive southeast-striking synclinal structure, gentle cross-folding along an east-west axis, and dextral strike-slip faulting along the Mtshingwe fault (Fig. 5.1).

Depositional and tectonic setting

The Manjeri Formation has been interpreted by many workers as the fill of an extensional rift basin. Crustal stretching has been attributed to the ascent of a mantle plume that gave rise to the extrusion of continental flood basalts of the Ngezi volcanics (Hunter et al., 1998). In contrast, Kusky and Kidd (1992) and Kusky and Winsky (1995) interpreted the Manjeri Formation as a foreland sequence that formed in front of the allochthonous thrust sheet of the Ngezi volcanics.

A shallow subaqueous to subaerial origin has been inferred for the Ngezi volcanics (e.g., Blenkinsop et al., 1993) mainly based on the occurrence of (1) vesicles in pillow lavas, indicating eruption in moderate to shallow water depths, (2) accretionary lapilli in tuffs, suggesting subaerial phreatoplinian eruption, and (3) locally developed cross-bedding in intercalated sediments. However, none of these features give an unambigious indication for shallow-water conditions. First, the vesicularity of pillow basalts is not only related to the confining pressure of the environment (consider volatile content) and is thus not a reliable indicator of water depth (Fisher and Schmincke, 1984). Second, beds of accretionary lapilli show sedimentary features reminiscent of turbidites (A. Hofmann, unpubl. data). Much similar lapilli have been observed by Stanistreet et al. (1981) in the Fig Tree Group, Barberton greenstone belt, where they occur in graded beds interpreted as deep-water turbidite deposits (but see Lowe, 1999 for a shallow-water interpretation). Third, in this study cross-bedding has only been observed as cross-lamination of the Bouma Tc division of turbidites. Nevertheless, cross-bedding, albeit rare, occurs in submarine turbidity current deposits (Pickering et al., 1986). The Ngezi volcanics are thus interpreted as a lava-plain sequence (cf. Dimroth et al., 1982) that extruded in a subaqueous setting well below wave base, as indicated by pillow basalts and intercalated turbidite deposits. A near-continental evolutionary setting has been suggested on the basis of the observation of local quartz sand in a drill core from the Reliance Formation (e.g., Blenkinsop et al., 1993). However, the core has since been lost (A. Martin, pers. comm. 1999), and no evidence for quartzose sediment has been found in outcrop. The Ngezi volcanics have been

interpreted either as an obducted oceanic plateau (Kusky and Kidd, 1992) or as continental flood basalts (Bickle et al., 1994).

The Cheshire Formation has been interpreted as the fill of an asymmetric foreland basin that formed contemporaneously with thrusting of the Ngezi volcanics (chapters 2, 3). The carbonate member is interpreted as a shallow, open marine sequence that formed in an eastward-deepening carbonate ramp setting (chapter 2). The limestone sequence is capped by a karst breccia horizon, which is overlain by deeper water siliciclastic sediments, indicating subaerial emergence and subsequent drowning of the carbonate platform. The siliciclastic member consists of sub-wave base turbidity current deposits that were shed from the southeast, possibly from the tips of northwestward-advancing thrust sheets of Zeederbergs volcanics. Facies relationships indicate that the basal sedimentary units (shallow-water carbonate in the west, deeper water siliciclastic sediment in the east) may have formed synchronously and were juxtaposed during thrusting (chapters 2, 3).

ANALYTICAL TECHNIQUES

A total of fifteen shale samples were analysed for major and trace elements by X-ray fluorescence spectrometry (XRF). Three samples are from the Zeederbergs Formation, three samples are from the carbonate member and nine samples are from the siliciclastic member of the Cheshire Formation. In the discussion on major and trace element geochemistry of Zeederbergs shale, the XRF results of twelve shale samples (star symbols in Fig. 5.2) analysed by Brake (1996) are included to supplement the data set. Fresh rock samples were typically 500 g and were reduced by jaw crusher and roller mill to a grain size of <500 μm. A representative fraction of this material was pulverized to <60 μm using an agate swing mill. From this, glass fusion disks (lithium metaborate flux) and powder pellets were prepared for major and trace element analysis by XRF, using a Philips PW 1404 spectrometer at the University of Mainz. Loss on ignition was determined after heating powdered samples at a temperature of 1000 °C for two hours.

Rare earth elements (REE's) were analysed from seven samples (two samples of Zeederbergs shale and five samples of Cheshire shale) at the Centre for Ore Deposit Research, University of Tasmania. Solutions were prepared using a sodium peroxide sinter to ensure decomposition of all resistant phases and analysed with a Finnigan MAT Element ICP-mass spectrometer using international and in-house rock standards for calibration. Analytical procedures, instrumental settings and estimates of precision/accuracy are reported in Yu et al. (2001). Results of major and trace element analysis are presented in Table 5.1, REE concentrations are shown in Table 5.2.

GEOCHEMISTRY

Previous geochemical studies of the BGB have focused on the Ngezi volcanics. The Reliance Formation is characterized by LREE-depleted to LREE-enriched komatiitic basalt and tholeiite with minor LREE-depleted komatiite and peridotitic cumulate with chondritic trace element ratios (Scholey, 1992; Bolhar, 2001). According to Brake (1996) and Bolhar (2001), the lavas of the

Zeederbergs Formation can be subdivided, on the basis of their trace and rare earth element patterns, into a slightly depleted to unfractionated group (type I) and an enriched group (type II). Type I basalt, the most common rock type, has relatively flat REE patterns (Fig. 5.2). Type II basalt, which includes basaltic andesite and andesite, is restricted to two stratigraphic units and differs from the previous type by strong LREE enrichment (Fig. 5.2) and distinct enrichment in LILE and depletion in HFSE (Bolhar, 2001). The different basalt types are not related to each other by crystal fractionation processes and may have been derived from different sources or from melting at different depths in the mantle (Brake, 1996; Silva, 1997). However, Nb-Th-LREE relationships indicate assimilation of material with the signature of continental crust, giving rise to the enriched type II volcanics (Bolhar, 2001). Shale horizons in the Zeederbergs Formation seem to be more commonly associated with type II basalts (Fig. 5.2), including the unit at the stratigraphic top which is, however, less well exposed than the central unit.

Table 5.1. Mayor element (in wt% oxide) and trace element (in ppm) concentrations for Zeederbergs Formation shales (ZX) and Cheshire Formation shales (BX). Data is ordered from left to right with increasing stratigraphic height.

Sample	ZX1	ZX2	ZX3	BX11	BX12	BX2	BX13	BX10
SiO_2	48.66	50.66	48.75	62.95	60.59	55.08	57.37	53.37
TiO_2	0.99	1.00	0.82	1.54	0.80	0.99	1.21	1.10
Al_2O_3	6.77	5.83	11.81	21.06	16.01	18.34	17.97	21.07
Fe_2O_3	16.21	15.34	13.74	8.06	13.71	15.20	13.29	10.41
MnO	0.23	0.21	0.22	0.07	0.03	0.26	0.22	0.19
MgO	16.48	13.24	17.55	0.90	3.77	2.76	2.35	2.98
CaO	10.36	12.28	6.93	0.35	1.12	3.83	3.53	3.75
Na_2O	0.04	1.24	0.05	1.58	2.84	0.87	0.83	7.05
K_2O	0.18	0.11	0.06	3.45	1.06	2.60	3.15	0.03
P_2O_5	0.08	0.08	0.08	0.04	0.07	0.07	0.09	0.04
LOI	3.53	1.73	7.45	3.69	4.53	8.42	7.18	2.41
Total	100.32	100.18	100.73	100.00	100.32	100.07	100.06	99.50
Sc	26	23	34	48	32	41	43	45
V	168	157	272	398	231	295	362	308
Cr	1306	1013	2298	197	230	225	267	489
Co	71	66	77	27	41	56	50	55
Ni	488	460	578	60	99	134	107	160
Cu	152	195	86	96	89	102	106	31
Zn	108	110	99	52	114	186	132	120
Ga	10	10	14	24	18	21	22	20
Rb	5	6	5	107	30	74	86	3
Sr	17	73	10	78	24	48	36	205
Pb	3.0	n.d.	2.5	4.8	4.2	7.6	4.4	2.4
Th	n.d.	0.5	n.d.	6.4	2.4	3.8	4.7	2.2
Y	18	13	17	36	17	24	24	19
Zr	78	66	62	188	105	121	135	104
Nb	7	5	4	9	5	7	8	5
Ba	48	n.d.	6	533	297	557	419	148
CIA	26.5	19.4	52.6	76.9	73.4	81.2	79.0	53.6
CIW	26.7	19.5	52.8	89.0	77.4	92.7	92.9	53.6

Note: all elements are recalculated to 100% volatile free; totals represent the sum of oxides and LOI in the original analysis; CIA=$[Al_2O_3/(Al_2O_3+CaO^*+Na_2O+K_2O)]100$; CIW=$[Al_2O_3/(Al_2O_3+CaO^*+Na_2O)]100$

Table 5.1 (continued).

Sample	BX5	BX6	BX7	BX8	BX4	BX14	BX15
SiO_2	59.89	54.64	54.62	52.15	54.87	67.85	54.14
TiO_2	0.86	0.86	1.06	1.04	1.04	0.84	0.83
Al_2O_3	19.97	20.47	21.41	22.84	23.99	17.83	16.25
Fe_2O_3	11.84	17.30	14.85	13.92	13.18	8.29	23.75
MnO	0.08	0.20	0.25	0.16	0.06	0.02	0.09
MgO	4.04	4.71	4.45	6.01	3.66	1.64	4.50
CaO	0.32	0.11	0.94	0.71	0.50	0.15	0.03
Na_2O	0.58	1.11	1.41	0.94	1.30	0.73	0.07
K_2O	2.37	0.57	0.94	2.20	1.34	2.63	0.27
P_2O_5	0.04	0.03	0.05	0.03	0.05	0.02	0.05
LOI	4.67	5.05	5.56	5.52	6.72	5.17	5.64
Total	99.82	100.22	100.03	100.18	100.65	100.07	100.47
Sc	49	54	50	60	60	34	34
V	302	341	333	381	365	235	247
Cr	500	438	464	858	492	375	422
Co	45	72	47	60	68	11	26
Ni	159	243	251	224	215	92	134
Cu	82	47	130	63	97	31	52
Zn	108	351	176	116	128	93	205
Ga	19	24	24	21	23	22	18
Rb	73	20	30	57	39	109	18
Sr	31	27	60	55	49	62	21
Pb	2.9	7.9	5.3	4.0	3.9	9.2	5.1
Th	1.4	2.2	1.4	2.0	2.3	2.5	3.3
Y	16	18	23	19	18	16	15
Zr	85	92	126	71	97	87	80
Nb	4	5	6	3	4	5	5
Ba	292	92	195	329	217	614	54
CIA	84.1	89.3	83.8	85.3	87.0	81.5	97.5
CIW	94.3	91.8	87.3	93.6	91.8	93.7	99.3

During this study, samples were taken from pelitic laminae/beds of shale horizons. Pelite of the Zeederbergs Formation typically contains albite-quartz-chlorite-amphibole-clinozoisite assemblages, suggestive of lower greenschist facies conditions (Brake, 1996). Coarser grained detritus consists entirely of (commonly hyaline) basalt fragments and rare clinopyroxene clasts. Cheshire Formation pelite contains very fine-grained chlorite-sericite-quartz assemblages and lacks epidote, indicating sub-greenschist facies grade (Martin, 1978; Bickle et al., 1993). Siltstone and sandstone intercalations consist of basalt fragments, some pyroxene clasts and varying proportions of detrital quartz and pyrite (chapter 2). The sedimentary rocks show evidence for recrystallization, but macroscopic primary textures are commonly well preserved. In following discussions on stratigraphic thickness of the Cheshire sedimentary sequence, the base of the carbonate member has been defined as 0 m and the top of the carbonate member (145 m) as the base of the siliciclastic member (Fig. 5.3). Furthermore, stratigraphic thickness has been corrected by substracting the thickness of dolerite sills in the sequence. Shale samples of the carbonate member do not differ geochemically from those of the siliciclastic member and are discussed together.

Major elements

Zeederbergs Formation: Zeederbergs shale has a low and narrow range of SiO_2 contents of 47.6 to 53.0% (average 50.8%), and systematic variations with other elements were not observed except for a positive correlation with Na_2O, possibly due to the presence of plagioclase. MgO contents are high and range from 7.84 to 17.76% (average 13.40%), indicating (ultra)mafic rocks as part of the source. Al_2O_3 shows negative correlations with Fe_2O_3, MgO and CaO, suggesting that these elements do not reside in clay minerals. TiO_2 contents correlate positively with Fe_2O_3, CaO, Na_2O and P_2O_5. CaO further shows a positive correlation with Fe_2O_3 and MnO. Compared to NASC (North American Shale Composite; Gromet et al., 1984), Zeederbergs shale is depleted in K_2O and enriched in ferromagnesian elements (Fig. 5.4). Relatively low Al_2O_3 values indicate that the source was not subjected to intense weathering.

Cheshire Formation: SiO_2 content in Cheshire shale ranges from 53.4 to 67.9% (average 57.3%), and the MgO content is much lower as compared to Zeederbergs shale (0.9-6.01%, average 3.48%). The Cheshire samples show variable degrees of negative correlation of SiO_2 versus Al_2O_3, Fe_2O_3 and MgO. There is a weak positive correlation between Al_2O_3 and TiO_2, indicating chemical weathering in the source area and giving rise to a relative concentration of these residual elements. K_2O and CaO are depleted, whereas Fe_2O_3 is enriched as compared to NASC (Fig. 5.4).

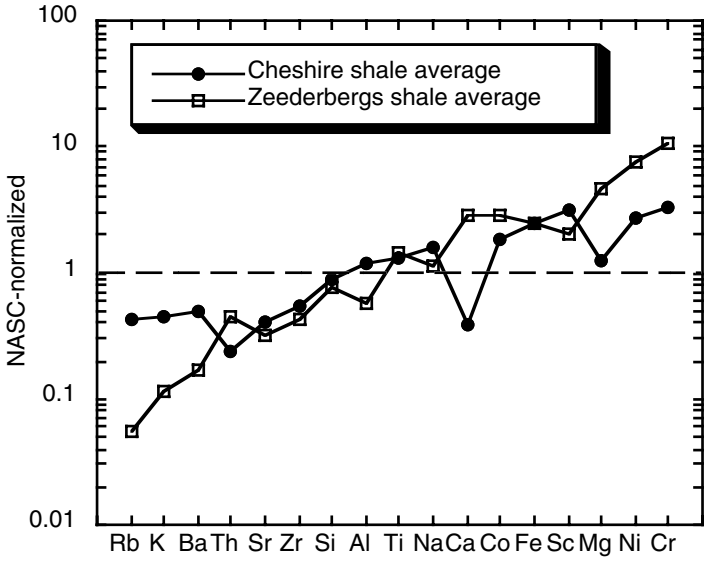

Fig. 5.4. Normalized distribution of selected major and trace elements of average Zeederbergs and Cheshire shales. Elements are ordered from left to right in terms of increasing enrichment in average shale compared to NASC of Gromet et al. (1984).

Large ion lithophile elements (LILE; Rb, Sr, Ba)

Zeederbergs Formation: Concentrations of the LILE are variable (Rb: 0.2-35, Sr: 3.5-122, Ba: 2.5-568 ppm), probably due to their mobility during alteration processes. Sr shows a negative correlation with MgO (and Cr, Ni) and a positive correlation with TiO_2 and Na_2O. Rb and Ba positively vary with K_2O, suggesting a control of these elements by K-bearing minerals. The LILE are strongly depleted as compared to NASC (Fig. 5.4).

Cheshire Formation: Concentrations of Rb, Sr and Ba are variable and higher as compared to Zeederbergs shale (3-103, 20-199, 51-583 ppm). The LILE generally show marked negative correlations with MgO contents. No correlation exists between the LILE and K_2O, possibly due to

disturbance of primary element distribution due to K-metasomatism (see below). Sr and, less so, the other LILE are depleted as compared to NASC.

Table 5.2. Rare earth element concentrations (in ppm) for Zeederbergs Formation shales (ZX) and Cheshire Formation shales (BX). Data is ordered from left to right with increasing stratigraphic height.

Sample	ZX1	ZX2	BX12	BX10	BX6	BX7	BX8
La	9.41	6.72	7.82	6.70	4.45	5.03	2.16
Ce	21.42	17.00	15.78	15.67	9.21	10.82	5.55
Pr	3.04	2.63	1.97	1.89	1.24	1.50	0.84
Nd	13.53	12.24	8.15	8.26	5.47	6.73	4.13
Sm	3.38	3.22	1.98	2.21	2.05	1.94	1.54
Eu	1.05	0.97	0.55	0.75	0.80	0.44	0.47
Gd	3.32	3.18	2.28	2.61	2.52	2.53	2.17
Tb	0.54	0.49	0.39	0.51	0.46	0.49	0.44
Dy	3.10	2.65	2.63	3.25	2.94	3.28	2.98
Ho	0.62	0.51	0.59	0.71	0.64	0.77	0.68
Er	1.65	1.32	1.77	2.08	1.86	2.46	2.00
Yb	1.43	1.06	1.86	2.06	1.79	2.60	2.12
Lu	0.21	0.15	0.28	0.30	0.26	0.41	0.32
∑REE	62.69	52.15	46.04	46.99	33.69	38.99	25.40
$(La/Sm)_N$	1.75	1.31	2.49	1.90	1.37	1.63	0.88
$(Gd/Yb)_N$	1.88	2.43	0.99	1.02	1.14	0.79	0.83
$(La/Yb)_N$	4.45	4.29	2.84	2.19	1.68	1.31	0.69
Eu/Eu*	0.96	0.93	0.80	0.96	1.08	0.61	0.79

note: $Eu/Eu^* = Eu_N/\sqrt{[(Sm_N)(Gd_N)]}$

Transition trace metals (Sc, V, Cr, Co, Ni)

Zeederbergs Formation: MgO contents co-vary with Cr, Ni and Co which have high concentrations (average 1302, 436 and 72 ppm respectively) as compared to NASC. Cr, Ni and Co are negatively correlated with SiO_2, Na_2O and P_2O_5. Sc is positively correlated with Al_2O_3 and negatively correlated with Fe_2O_3 and CaO. The Cr/Th ratio, a good indicator for provenance (Condie and Wronkiewicz, 1990), has an average value of 231. Such relatively high concentrations of Cr (and Ni/Co) are a common feature of Archaean shales due to higher proportions of (ultra)mafic rocks in the source as compared to Phanerozoic shales (Taylor and McLennan, 1985; Wronkiewicz and Condie, 1987).

Cheshire Formation: MgO contents co-vary with Cr (478 ppm average), Ni (157 ppm average) and Co (46 ppm average). All transition metals have concentrations higher than NASC (Fig. 5.4). They show a marked positive correlation with Al_2O_3, indicating that they are associated with clay minerals and have been enriched during weathering. The Cr/Th ratio averages 143, less as compared to the Zeederbergs shales, indicating a more felsic source.

High field strength elements (HFSE; Y, Zr, Nb, Th)

Zeederbergs Formation: The HFSE show positive correlations with TiO_2, Na_2O, P_2O_5, Cu and Zn and negative correlations with MgO (and Cr, Ni), an expected trend due to their incompatible

behaviour. Zr and Nb further show a positive correlation with Fe_2O_3 and MnO. The Th/Sc ratio, a good indicator for bulk composition of the provenance (McLennan and Taylor, 1991), has an average value of 0.18.

Cheshire Formation: There are no systematic trends between the incompatible elements and the other elements analysed except for a marked positive correlation between Zr and TiO_2 and a negative correlation between Th and MgO (and Cr, Ni). The Th/Sc ratio averages 0.06. HFSE concentrations of both shale types are depleted as compared to NASC, indicating a mafic provenance.

Rare earth elements (REE's)

The Zeederbergs and Cheshire shales have distinct REE patterns (Fig. 5.5). Zeederbergs shales have smoothly fractionated patterns with moderate LREE enrichment (La_N/Sm_N=1.31-1.75) and HREE depletion (Gd_N/Yb_N=1.88-2.43) with no significant Eu anomaly (Eu/Eu*=0.93-0.96). Cheshire shales have flat to variably enriched LREE patterns (La_N/Sm_N=0.88-2.49) and flat HREE patterns (Gd_N/Yb_N=0.79-1.14). Several samples show a distinct negative Eu anomaly (average Eu/Eu*=0.85). Total REE contents are higher in the Zeederbergs shales (average ∑REE=57.42 ppm) as compared to the Cheshire shales (average ∑REE=38.22 ppm).

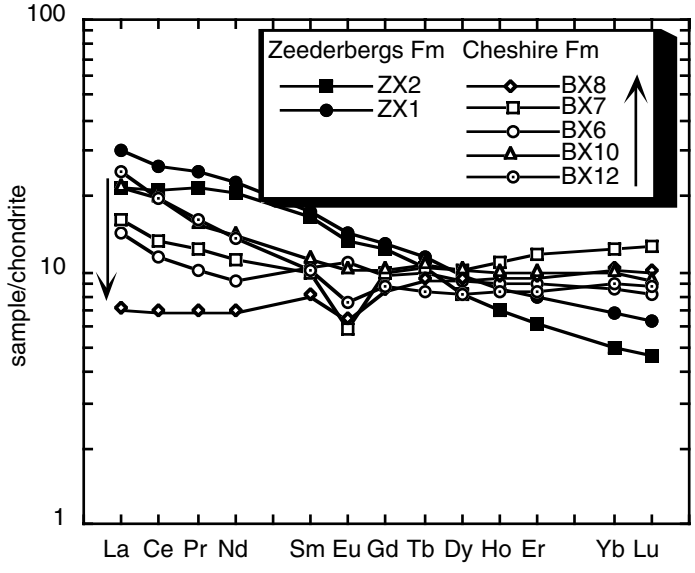

Fig. 5.5. Chondrite-normalized (Boynton, 1984) rare earth element plot of Zeederbergs and Cheshire shales. Arrow indicates increase in stratigraphic height of Cheshire Formation samples.

DISCUSSION

Of the several factors that contribute to the distribution of elements in siliciclastic sediments the more important ones are (1) mobilization/redistribution of elements during diagenesis and metamorphism, (2) bulk composition and tectonic setting of the source area, and (3) degree of chemical weathering of the source rocks (McLennan and Taylor, 1985; Taylor et al., 1986; Wronkiewicz and Condie, 1987; Johnsson, 1993). Grain-size effects due to hydraulic sorting during transport/deposition is probably not important, because (a) sampling focused on pelitic laminae of shale horizons thought to be geochemically homogeneous, (b) detrital phyllosilicates, which could become sorted during transport, are absent in the inferred, primary source rocks (cf. Argast and Donnelly, 1987) and (c) low Zr and normal P_2O_5 contents of the shales sampled relative to average shale do not indicate enrichments of heavy minerals, such as zircon or monazite (cf. Taylor et al., 1986). Adsorption of

ions by clay minerals seem to have affected the distribution of some transition metals in the shales studied (see below), a feature also observed in Archaean shales of the Witwatersrand (Wronkiewicz and Condie, 1987).

Metamorphism

Numerous studies have focused on the effects of diagenesis and metamorphism on the mobility of elements (e.g., Shaw, 1954; Ferry, 1983; Fleet, 1984). Except for certain alkali and alkaline earth elements and the LILE, large-scale element redistribution is not expected during burial and low-grade metamorphism. This may be true for the fine-grained, poorly permeable sediments investigated in this study. Furthermore, the metamorphic grade in the central outcrop of the Ngezi Group is low, reaching sub-greenschist to greenschist facies grade (Martin, 1978), suggesting that metamorphism did not greatly affect shale composition. Abell et al. (1985) concluded, on the basis of petrological and stable isotope data, that limestone of the Cheshire Formation experienced a maximum temperature of 200°C. The freshness of the rocks in the central part of the Belingwe belt is further exemplified by the unique preservation of olivine phenocrysts in komatiite of the Reliance Formation (Nisbet et al., 1987). The effects of alteration and element mobility on the chemistry of the Ngezi volcanics has been extensively discussed (Scholey, 1992, Brake, 1996, Silva, 1997, Bolhar, 2001). There is general agreement that Al_2O_3, TiO_2, P_2O_5, Cr, Ni, HFSE and the REE have not been significantly mobilized during water-rock interaction. The problem of alteration effects will be discussed further after potential source rocks of the studied shales have been identified.

Provenance of Zeederbergs shale

Useful elements for defining the composition of a sediment source area are those which are least mobile during weathering, transport and diagenetic and metamorphic processes, such as the REE, Th, Sc and the HFSE (Taylor and McLennan, 1985; McLennan and Taylor, 1991). Zeederbergs shales form thin intercalations within submarine lava flows and may have been deposited (1) by low-density, silt-dominated turbidity currents, (2) out of suspension following density currents and (3) from background suspension sedimentation. Some coarser grained turbidite beds intercalated with shale contain basalt clasts at the base, suggesting that the detritus represents reworked material directly derived from surrounding or laterally equivalent rocks. Turbidity currents may have been triggered by violent submarine eruptions (as indicated by abundant hyaloclastites in the sequence) or from failure of gravitationally unstable piles of volcanic rock. Shale horizons sampled during this study occur in a certain stratigraphic unit of the volcanic sequence that consists of type II basalts (Fig. 5.2). The REE patterns of the shale samples are identical to those of the basalts (Fig. 5.6), which are thus easily identified as the sediment source. The average Th/Sc ratio of the Zeederbergs shales (0.18) falls into the range of the ratios (0.14-0.29) for selected samples of the enclosing basalts (Fig. 5.6), confirming the usefulness of this ratio for provenance studies (Taylor and McLennan, 1985).

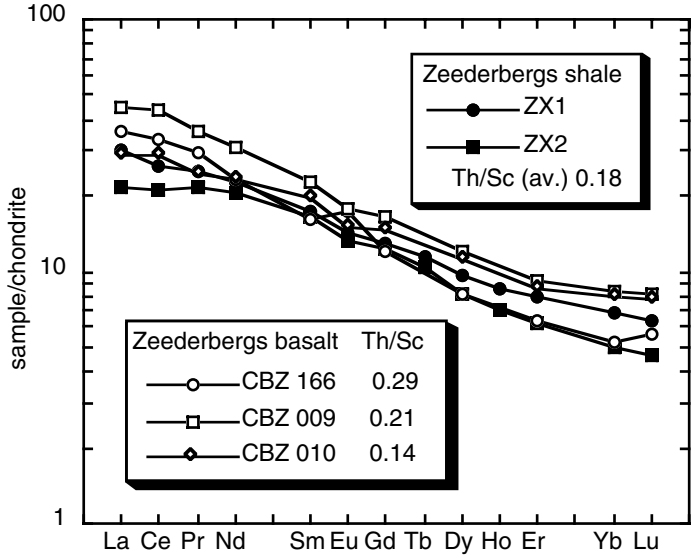

Fig. 5.6. Chondrite-normalized rare earth element plot of Zeederbergs shale and selected samples of type II basalt (Brake, 1996). Basalt samples selected are those with lowest ∑REE contents (cf. Fig. 5.2). Th/Sc ratios for basalt samples and average Zeederbergs shale are shown. See Figure 5.2 for sample locations.

Submarine alteration

Comparing the major and trace element geochemistry of shale with basalt flows directly under- or overlying the sampled shale horizons may be a useful means of further defining possible element redistribution during hydraulic sorting, submarine weathering, diagenesis and/or adsorption of ions by clay minerals. This includes the assumptions that shale was more subjected to alteration than the basalts (due to higher permeability and higher reactivity of fine-grained detritus) and that the basalts were not subjected to subaerial weathering (as confirmed by weathering indices, see below). The depletion-enrichment diagram for major and trace elements (Fig. 5.7) shows strong depletion of Na_2O, K_2O, Sr and Ba. FeO, MnO, MgO, and, in particular, Cr and Ni are enriched relative to basalt. The other elements do not show major variations, particularly TiO_2, CaO, Sc and V. All three sample pairs show the same depletion-enrichment patterns, suggesting basic mechanisms for the loss or gain of individual elements.

The fine-grained, detrital material of shale beds is interpreted to have been derived from submarine reworking of adjacent basalts, suspension settling and possibly directly from fragmented lava during submarine volcanic eruptions. Since the adjacent lavas are generally aphyric and the clastic material is composed of rock fragments, hydraulic sorting changing the bulk composition of the sediment as compared to the host rock can be discounted.

Since the discovery of seafloor hydrothermal activity, abundant data have been collected on the submarine alteration of basaltic rocks. Two types of alteration are generally distinguished, low temperature basalt-seawater interaction, i.e. submarine weathering, and high temperature, hydrothermal alteration related to hydrothermal systems near areas of magmatic activity, such as along mid-ocean ridges (Alt, 1995; Von Damm, 1995; Elderfield and Schultz, 1996; Staudigel et al., 1996). During hydrothermal alteration most metals are leached from basalts during interaction with up to ~400° C hot fluids, whereas Mg and sometimes Na are added. In contrast, low temperature weathering commonly results in a gain of alkali metals and Ca and a loss of other metals. However, fluxes of many elements can be variable at different depths in crustal sections (Staudigel et al., 1996).

In the shales studied, the depletion of all alkali metals points to a relatively high temperature alteration process that possibly operated some time after sedimentation and burial. The gain of Mg,

resulting in the formation of smectite or chlorite, may be related to water-rock interaction, but such a process should be balanced by the release of Ca (Seyfried, 1987), a feature not observed here. The observation that Ca behaved immobile may thus be related to the absence of such cation exchange processes, including albitization (Na is depleted rather than enriched), and/or the composition of the hydrothermal fluid (Von Damm, 1996). Furthermore, the decoupling of the chemical behavior of Ca (conservative) and Sr (depleted) is striking. Sr contents positively vary with Na in the analysed samples (see above). Loss of both Sr and Na may be related to alteration of detrital volcanic glass in the Zeederbergs shale (Staudigel and Hart, 1983).

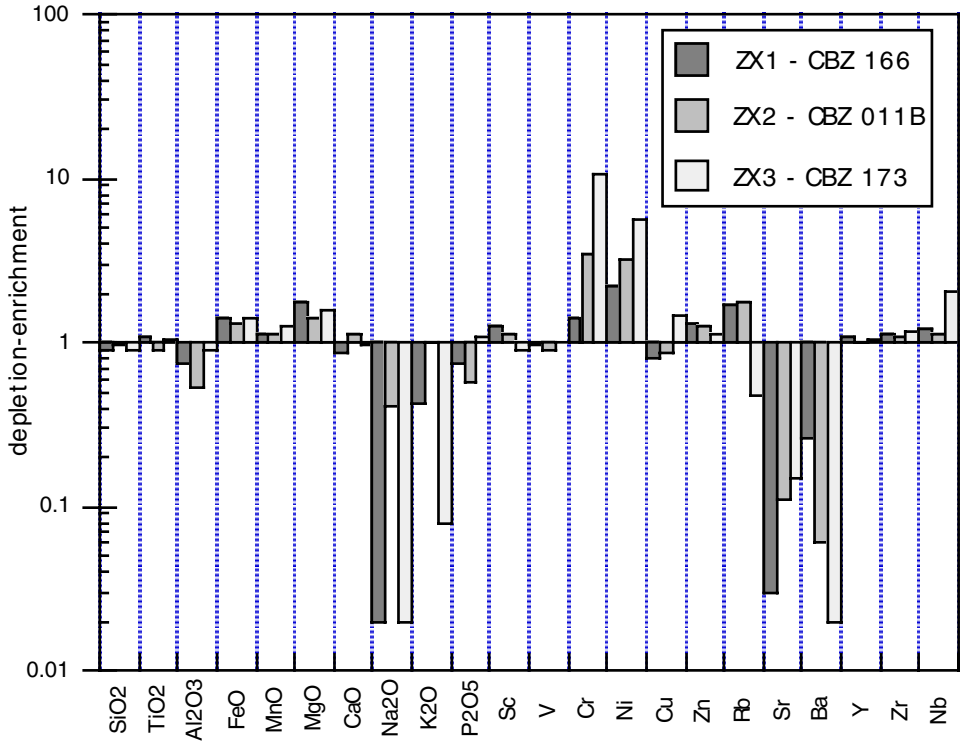

Fig. 5.7. Depletion-enrichment diagram of Zeederbergs shale as compared to basalt sampled by Brake (1996) directly below or above the shale horizon. See Figure 5.2 for sample location.

In contrast, the enrichment of Fe, Mn, Cr and Ni cannot be explained by hydrothermal alteration. This gain may have taken place early in the depositional history, such as from the settling of metal-rich sulfide, sulfate and oxide particles out of hydrothermal plumes emanating from nearby submarine hot spring systems. Massive sulfides as a record of such hydrothermal systems may have been originally present in the Zeederbergs Formation, as indicated by the abundance of detrital pyrite in the Cheshire Formation (chapter 2). However, simple particle fallout from hydrothermal plumes alone cannot contribute to the enrichment of Cr and Ni up to a factor ten. Archaean shales are commonly enriched in these elements which is generally attributed to a more mafic provenance as compared to Phanerozoic shales (e.g., Danchin, 1967; Taylor and McLennan, 1985). The enrichment of Cr (and Ni) in shales, as compared to their concentrations in inferred source rocks,

has been reported, for example, from Archaean shales of the Witwatersrand basin (Wronkiewicz and Condie, 1987; Condie and Wronkiewicz, 1990). Enrichment may be related to adsorption of these metals onto sediment particles during transport and deposition in seawater (Balistrieri and Murray, 1984). Scavenging of the trace metals by metal oxides precipitating in the hydrothermal plumes is an alternative interpretation.

Alkali metals such as K become released from basalts at temperatures of 150° C and above (Seyfried, 1987), whereas the solubility of most metals increases significantly at temperatures above 350° C (Seewald and Seyfried, 1990). The depletion of alkalis and the metal enrichment of Zeederbergs shale thus suggests temperatures of the hydrothermal fluids in between 150° and 350° C. Evidence of focused hydrothermal upflow zones have not been observed in the Zeederbergs Formation, suggesting diffuse upflow of the hydrothermal fluids through the basalts and sediments.

When comparing the REE patterns of Zeederbergs shale and type II basalt, REE contents in shale are somewhat lower (Fig. 5.6). Normalizing Zeederbergs shale using the average of the three type II basalt analyses shown in Figure 5.6 and using the average of all seven type II basalt samples analysed by Brake (1996) from the type II basalt unit in the central part of the Cheshire Formation illustrates depletion of all REE (Fig. 5.8), but, in particular, the LREE (La, Ce, Pr) and HREE (Yb, Lu). One sample shows a distinct negative Ce anomaly. REE depletion of basaltic rocks during submarine weathering is a commonly observed feature, especially the HREE (Frey et al., 1974; Nesbitt, 1979). A negative Ce anomaly is a characteristic feature of sea water. Ce depletion relative to the other REE is attributed to the oxidation of Ce^{3+} to more insoluble Ce^{4+} (Elderfield and Greaves, 1982). A negative Ce anomaly has also been reported from Archaean BIF and used as evidence for oxygenated bottom seawater in the Archaean (Ohmoto et al., 2001).

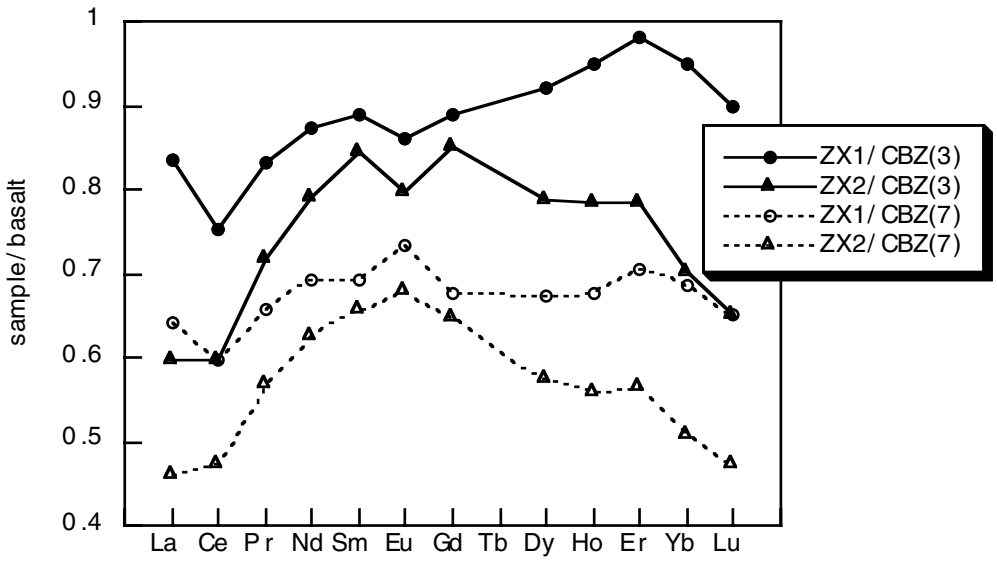

Fig. 5.8. REE concentrations of Zeederbergs shale (ZX1, ZX2) normalized to the average of three selected type II basalt samples with low ∑REE contents as shown in Fig. 5.6 (black symbols) and to the average of all seven type II basalt samples (white symbols) analysed by Brake (1996) from the central stratigraphic unit of type II basalt.

Provenance of Cheshire shale

A petrographic study of Cheshire Formation conglomerate has shown that the clastic detritus was predominantly derived from erosion of a terrain similar, or laterally equivalent, to the rocks preserved as the Zeederbergs Formation (chapter 2). Three common basalt clast types (Fig. 5.3), inferred to have been derived from pillow centres (type 1), quenched pillow margins (type 2) and from massive lava flows (type 3) of Zeederbergs volcanics, have been described. Rare spinifex-textured clasts indicate derivation from Reliance Formation komatiites. A mafic provenance is indicated geochemically by low concentrations of total REE and HFSE, low Th/Sc, high concentrations of ferromagnesian elements and high Cr/Th. Incompatible element distributions are much similar to Zeederbergs shale and Zeederbergs basalt (Fig. 5.9).

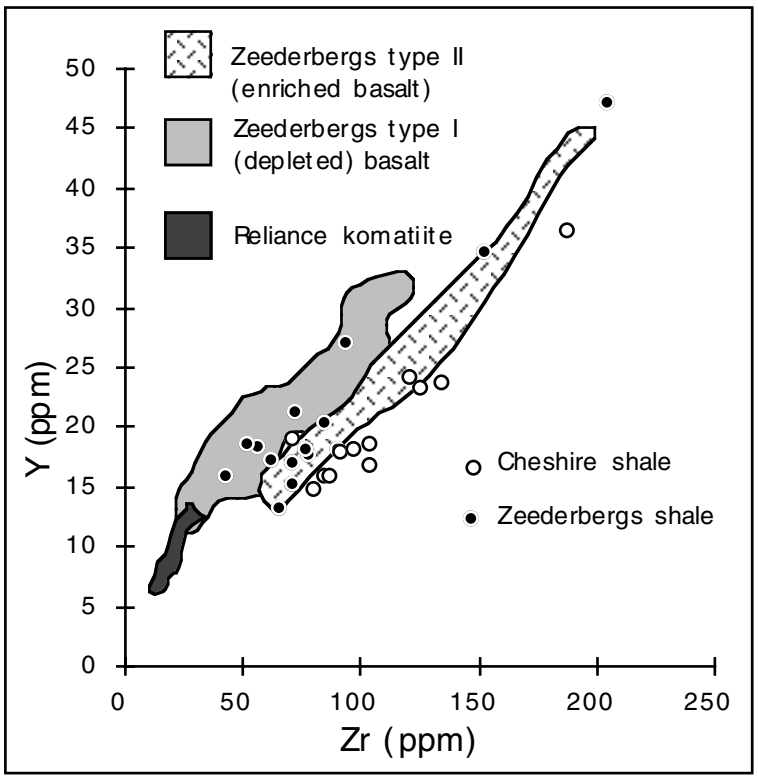

Fig. 5.9. Zr/Y diagram showing the compositional similarity between Zeederbergs basalt (compositional fields modified after Silva, 1997), Zeederbergs shale and Cheshire shale.

Minor vein quartz clasts (rarely exceeding 5% in abundance) occur together with mafic detritus in conglomerate (Fig. 5.3). Vein quartz increases in abundance upwards in the sedimentary sequence and even forms beds of quartzose sandstone that are restricted to the top of the sequence (Fig. 5.3). At one locality near the stratigraphic top such clasts are associated with fragments of granite and granitoid gneiss and are, thus, interpreted to have been derived from a granitoid-gneiss terrain (chapter 2). This upward increase in felsic detritus has been interpreted to reflect unroofing of granitoid crust, either representing a (tectonic?) basement to the Ngezi volcanics or an active thrust unit (chapter 2). A change in provenance upsection is well defined in the REE patterns and ferromagnesian trace element contents. A plot of REE ratios vs stratigraphic height (Fig. 5.10a) indicates a linear decrease in $(La/Sm)_N$ and $(La/Yb)_N$ ratios as well as ΣREE upsection, suggesting a change in provenance from LREE-enriched to LREE-depleted rocks. No trend can be observed in the distribution of $(Gd/Yb)_N$ and Eu/Eu*. In addition, the abundance of Cr and Ni, and the Cr/Th ratio shows a linear increase to about 1000 m stratigraphic height (Fig. 5.10b) above which there is a sharp decrease in the content of the ferromagnesian trace elements. Sc, Co and Co/Th (not shown) have a similar trend. The Th/Sc ratio distribution is a mirror image of the

previous trends and shows decreasing values up to 1000 m stratigraphic height, after which the values increase sharply further upwards in the succession (Fig. 5.10c). Quartzose sandstone only occurs above this stratigraphic level. Unfortunately, no REE data is available for this part of the sequence.

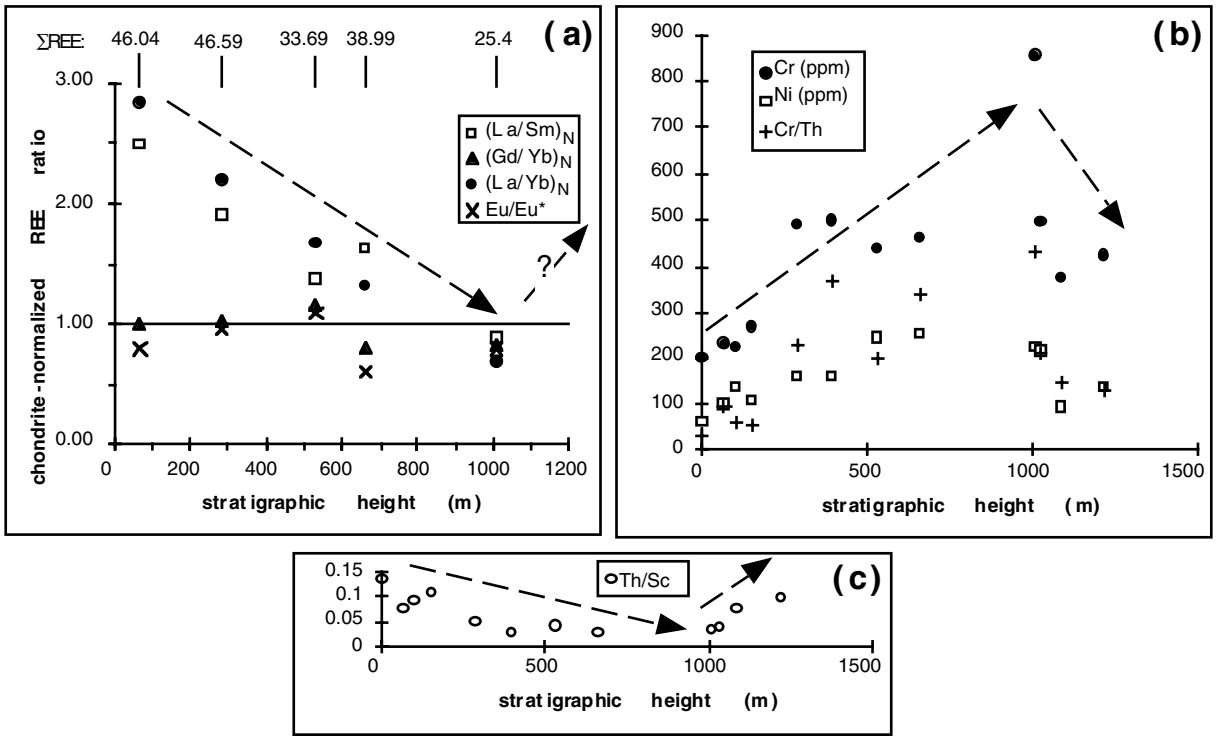

Fig. 5.10. (a) Chondrite-normalized REE ratios, Eu/Eu*, and ∑REE vs stratigraphic height. (b) Transition element contents and Cr/Th ratio vs stratigraphic height. (c) Th/Sc ratio vs stratigraphic height.

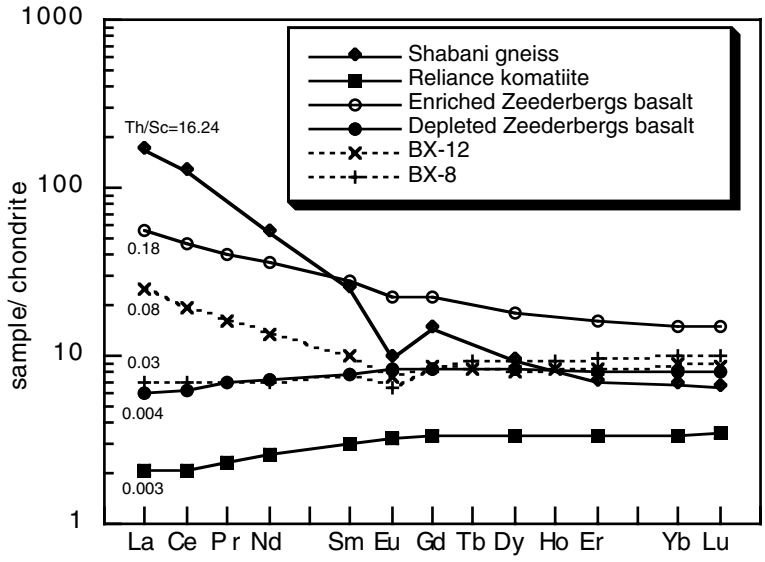

Fig. 5.11. Chondrite-normalised REE diagram showing the lowermost (BX12) and uppermost (BX8) Cheshire shale samples, together with a sample of Shabani gneiss (Hunter, 1997), Reliance komatiite and average compositions of incompatible element enriched (type II, based on three samples) and depleted basalt samples (type I, based on three samples) from the Zeederbergs Formation (Bolhar, 2001). Numbers indicate Th/Sc ratios.

Constraining source rock composition: mixing calculations

A comparison between the REE patterns of samples from the base (BX12) and top (BX8) of the Cheshire Formation with selected rock analyses of the Shabani Gneiss (sample MHZ327 of Hunter, 1997), Reliance Formation komatiite and average enriched and depleted Zeederbergs basalt (Bolhar, 2001) suggests that the composition of the Cheshire shales can

be modelled by mixing of various types of the Ngezi volcanics (Fig. 5.11). Simple mixing relationships are further indicated in Fig. 5.12, where the shales are compared with the likely mixing endmembers in terms of $(La/Sm)_N$ vs Th/Sc and Th/Sc vs Cr. It is obvious in the former diagram that the geochemical variation of the shales may be sufficiently explained by intermixing of variable proportions of the enriched and depleted Zeederbergs basalts. However, Th/Sc vs Cr relationships suggest that at least one sample incorporated a komatiitic component, as indicated by the shift towards higher Cr abundances, whereas a number of other samples most likely inherited combined low Cr abundances and elevated Th/Sc ratios from a more differentiated source, such as the Shabani Gneiss. Variable relative depletions of Eu relative to the neighbouring REE (Fig. 5.5) may also point to a differentiated source component (average granite: Eu/Eu* ~0.3, average tonalite: Eu/Eu* ~0.8, Condie and Wronkiewicz, 1990; Shabani Gneiss: Eu/Eu* ~0.7), although simple mixing cannot alone account for negative Eu anomalies, as indicated by the lack of correlation between Eu/Eu* and $(La/Sm)_N$, $(La/Gd)_N$. Alternatively, disturbed Eu/Eu* vs LREE/REE relationships may not reflect source characteristics, but instead may be accounted for by depositional processes, such as plagioclase accumulation or preferential decomposition of this mineral phase during weathering. Reduction of Eu^{3+} and subsequent leaching of Eu^{2+} during chemical weathering of the source or during diagenesis may result in a negative Eu anomaly in sedimentary rocks (Cullers et al., 1975; Nesbitt, 1979).

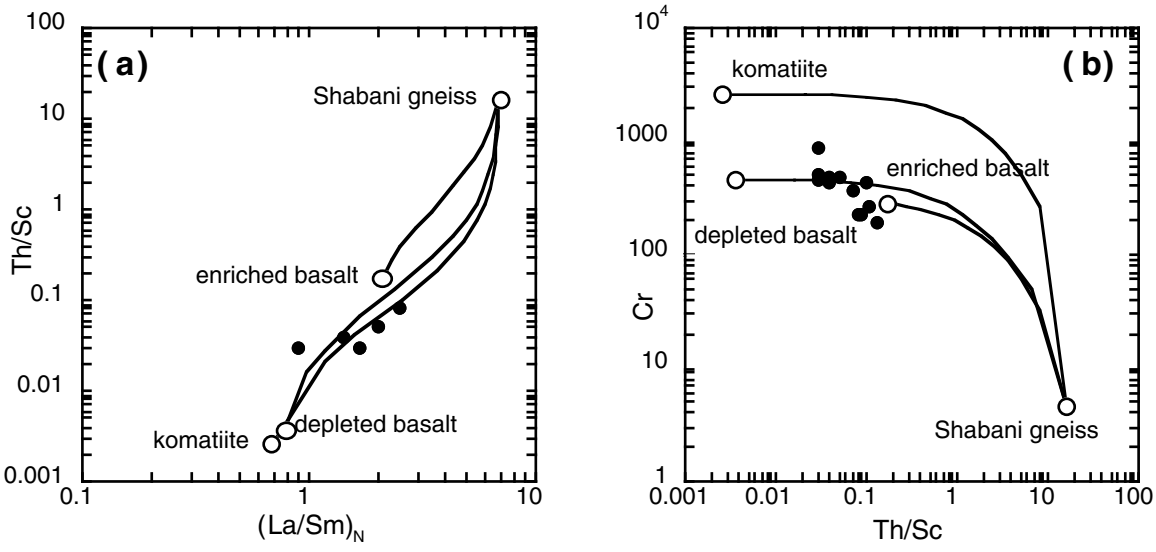

Fig. 5.12. Trace element ratio diagrams of (a) $(La/Sm)_N$ vs Th/Sc and (b) Th/Sc vs Cr, showing the shale samples (black dots), Reliance komatiite, Shabani gneiss, average Zeederbergs compositions and mixing trajectories. Note that shales plot broadly between these compositions, in support of simple mixing relationships between endmember compositions.

In order to quantitatively constrain the relative contribution of various endmembers to the compositonal features seen in the Cheshire shales, simple mixing calculations have been performed and are graphically illustrated in Fig. 5.13. The approach was to search for best-fit solutions which

would most closely reproduce the observed REE patterns and would also yield Th/Sc and $(La/Sm)_N$ ratios in agreement with the shale data (Table 5.3). The majority of the shale samples seems to require small quantities of highly evolved crustal material (i.e., Shabani Gneiss), while an ultramafic component may have been accommodated in the stratigraphically uppermost sample with an elevated Cr abundance (BX8). The contribution from material similar in composition to the average enriched Zeederbergs basalt is variable and broadly decreases upsection, with an estimated relative contribution of 20% in lowermost samples and 0% in the uppermost sample. Such a trend towards a LREE-depleted provenance up the Cheshire section may indicate erosion of successively lower levels of the Ngezi volcanics where LREE-depleted (and slightly more mafic, as indicated by increasing Cr contents) rocks are more common (Fig. 5.2). This is in accordance with ferromagnesian trace element variations to about 1000 m (Fig. 5.10b), indicating an increase in ultramafic rocks as part of the provenance. Komatiites as a likely ultramafic source are restricted to the Reliance Formation. Although the Cr/Th ratio (and Cr, Ni contents) does not directly reflect the corresponding value of the source due to enrichment processes as discussed above for the Zeederbergs shales, it does appear to monitor relative changes in source composition (Condie and Wronkiewicz, 1990). The Th/Sc ratio (and Cr content, Table 5.3) of proposed source basalts decreases with increasing LREE-depletion (Fig. 5.11), further explaining the change of Th/Sc ratio (and Cr content) with stratigraphic height (Fig. 5.10b). The addition of Shabani Gneiss appears to be necessary to reproduce the enrichment in the most incompatible REE in some of the samples, while a best-fit pattern for the slightly LREE-depleted sample BX8 also can be best modelled with 1% Shabani Gneiss. Eu anomalies are consistently too large in the shale samples when compared with the modelled patterns, and higher quantities of crust, as indicated by the distinct relative depletions in Eu, would invariably result in stronly enriched LREE not seen in the shale samples. Interestingly, the relative amount of incorporated crust seems to decrease upsection, based on REE patterns of the five shales. The calculated Th/Sc ratios for the various mixtures agrees well with those of the shales. However, it must be remarked that the calculated mixtures do not provide perfect matches. This is particularly the case for sample BX7 which displays a rather unusual REE pattern: LREE and HREE are enriched relative to the MREE, associated with a large negative Eu anomaly. Such a REE distribution cannot be perfectly reproduced by mixing of the endmembers used in the model calculations, and may point to an additional component with a rather unusual composition..

The sudden change in the proportions of different source rocks at c. 1000 m stratigraphic height is indicated by a sudden occurrence of quartzose sandstone as well as a decrease of ferromagnesian trace element contents, suggesting a major increase in the significance of a granitoid-gneiss source. No shear zone has been noted in the field, but exposure is poor at this stratigraphic level.

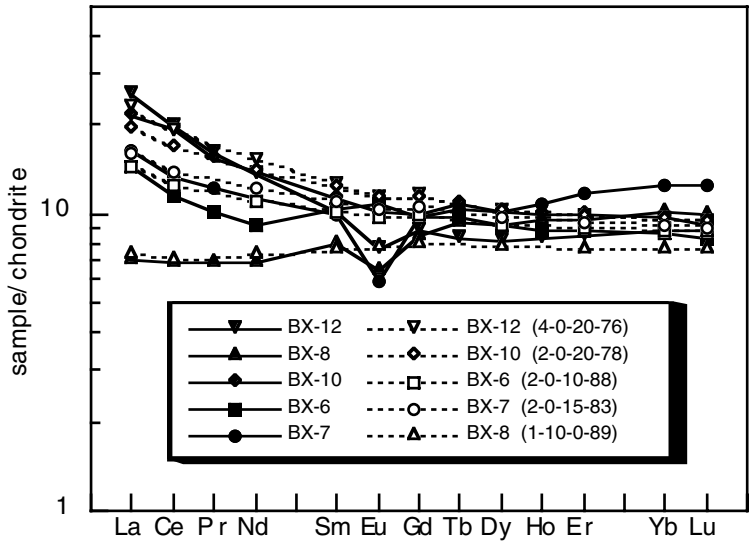

Fig. 5.13. Chondrite-normalised REE diagram showing best-fit results of mixing calculations (refer to Table 5.3). The observed REE patterns of the shales can be broadly reproduced by mixing relationships, while Th/Sc ratios thus obtained are similar to those in the shale samples. Numbers in parentheses give the relative contributions of the used mixing endmembers in the order of (Shabani gneiss, Reliance komatiite, enriched Zeederbergs basalt, depleted Zeederbergs basalt).

Table 5.3. Results (in ppm) of mixing calculations. ZB, Zeederbergs basalt

	Mixing end-members				Best-fit mixing results for				
	Shabani gneiss	Reliance komat.	enriched ZB	depleted ZB	BX-12 4:0:20:76	BX-10 2:0:20:78	BX-6 2:0:10:88	BX-7 2:0:15:83	BX-8 1:10:0:89
La	52.11	0.64	17.56	1.87	7.02	6.01	4.44	4.98	2.25
Ce	99.75	1.66	37.50	5.01	15.30	13.40	10.15	11.30	5.62
Nd	32.82	1.56	21.60	4.40	8.98	8.41	6.69	7.41	4.40
Sm	4.88	0.59	5.38	1.53	2.43	2.37	1.98	2.16	1.47
Eu	0.71	0.24	1.66	0.61	0.82	0.82	0.72	0.77	0.57
Gd	3.72	0.86	5.88	2.15	2.96	2.93	2.55	2.73	2.04
Dy	3.01	1.09	5.80	2.64	3.29	3.28	2.96	3.12	2.49
Er	1.45	0.70	3.42	1.71	2.04	2.05	1.88	1.96	1.61
Yb	1.38	0.70	3.17	1.71	1.99	2.00	1.85	1.92	1.61
Lu	0.21	0.11	0.48	0.26	0.30	0.30	0.28	0.29	0.24
Th	47.10	0.07	4.60	0.15	2.92	1.98	1.53	1.52	0.61
Sc	2.90	25.20	26.00	39.60	35.41	36.15	37.51	37.01	37.79
Th/Sc	16.24	0.00	0.18	0.004	0.08	0.05	0.04	0.04	0.02
La/Sm_N	6.72	0.68	2.05	0.77	1.81	1.60	1.41	1.45	0.96

Subaerial weathering

The effect of variable degrees of weathering in source areas can be important in influencing alkali and alkaline earth element abundances in siliciclastic sediments. Cations such as Rb and Ba are often fixed in weathering profiles, whereas cations with smaller ionic radii, such as Na, Ca and Sr, are more rapidly removed as dissolved species from weathering profiles (Nesbitt et al., 1980). A common approach to quantify the degree of source area weathering is to use the chemical index of alteration (CIA; Nesbitt and Young, 1982). CIA values (see Fedo et al., 1995, for corrections) for Zeederbergs shales range from 19 to 53 (Table 5.1) with an average of 33, a value typical of unweathered mafic rocks. The Cheshire shales have CIA values of 75-90 with an average of 84 (excluding one outlier, sample BX10), indicating a high degree of chemical weathering in the source area.

On the Al_2O_3-(CaO^*+Na_2O)-K_2O (A-CN-K) diagram (Fig. 5.14) of Nesbitt and Young (1984, 1989) Zeederbergs shale, as expected, plot along the A-CN joint. Two shale samples plot closer to the CN corner as selected samples of komatiite and basalt of the Ngezi volcanics, possibly indicating errors in the carbonate correction. The unweathered state of the Zeederbergs shale indicates that the source rocks were not exposed to subaerial weathering agents, but remained submerged, providing additional evidence for their local derivation.

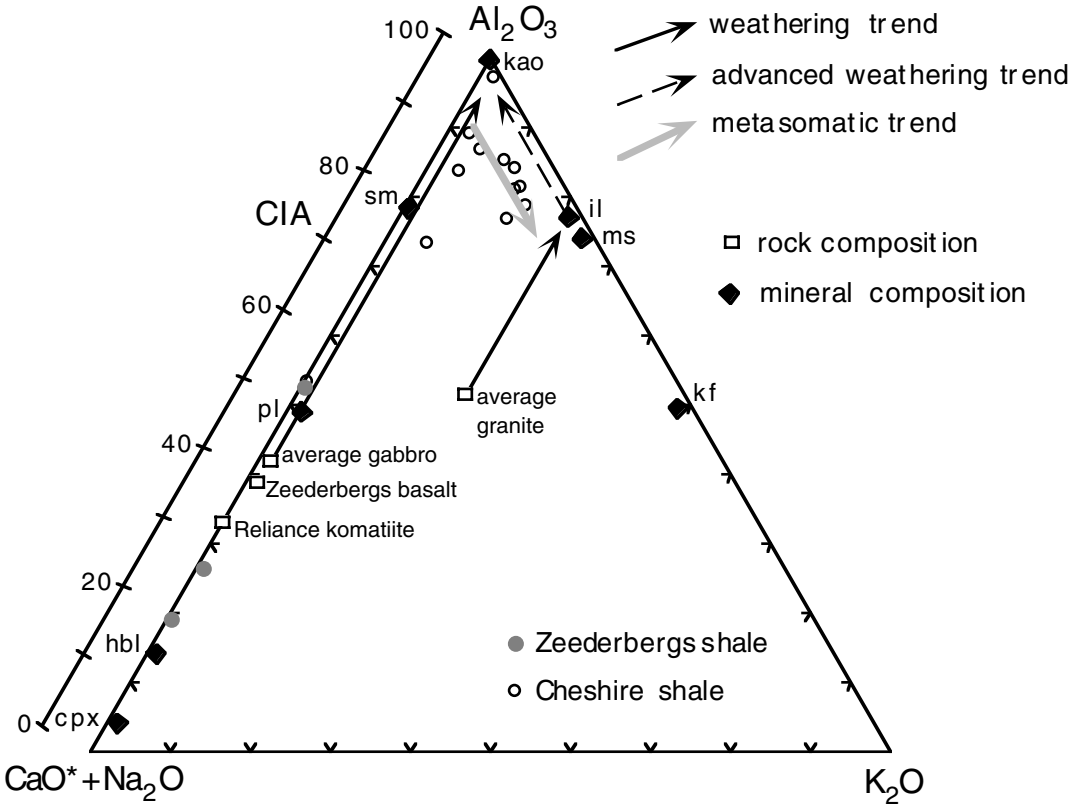

Fig. 5.14. Al_2O_3-(Na_2O+CaO^*)-K_2O diagram of Zeederbergs and Cheshire shales (compositions as molar proportions, CaO^* represents CaO of the silicate fraction only). Selected rock and mineral compositions and weathering trends (cf. Nesbitt and Young, 1984) are shown. kao: kaolinite, il: illite, ms: muscovite, kf: alkali-feldspar, sm: smectite, pl: plagioclase, hbl: hornblende, cpx: clinopyroxene; average granite and gabbro from Nesbitt and Young (1984), Reliance komatiite and Zeederbergs basalt from Bolhar (2001).

The Cheshire shales, which have been derived from the weathering and erosion of the Ngezi volcanics, plot away from the expected weathering trend of mafic rocks along the A-CN joint. Similar trends have been observed in ancient weathering profiles (Nesbitt and Young, 1989) and in shale of the Buhwa greenstone belt (Fedo et al., 1995, 1996) and interpreted as a result of K-metasomatism, possibly some time after normal weathering and removal of Na and Ca. The data points of the Cheshire samples define a linear array parallel to the A-K joint. This line intersects the A-CN joint at c. 93 which can be interpreted as the premetasomatized CIA value, indicating that kaolinite or other clay minerals produced during weathering were converted to illite with the introduction of K. The premetasomatized CIA value is similar to the chemical index of weathering

(CIW; Harnois, 1988), which does not utilize K_2O for determination of the degree of weathering. CIW values (Table 5.1) are typically in the order of 85 to 95 and have an average of 91 (excluding sample BX10). The high values of the weathering indices, which are similar to modern residual clays or muds from rivers draining highly weathered tropical areas (Nesbitt and Young, 1982; Kronberg et al., 1986), indicate intense chemical weathering of the source area. The degree of chemical weathering is mainly a function of climate and erosion rate, the latter of which is controlled by relief and vegetation cover of the source area. Assuming high erosion rates (as indicated by the abundance of coarse clastics in the Cheshire sequence) due to the tectonically active setting of the basin and the lack of vegetation in the Archaean, the degree of weathering suggests a strong influence of climate on chemical weathering. Severe weathering may have been related to a CO_2-rich atmosphere, elevated surface temperatures and a humid climate postulated for the Archaean (e.g., Young, 1991; Kasting, 1993; des Marais, 1994). Intense chemical weathering may also explain the abundance of vein quartz clasts as compared to granitoid rock fragments in, for example, the quartzose sandstone at the top of the sequence, the former being mechanically and chemically more stable, but less abundant in granitoid gneisses.

Implications for the tectonic setting

Geochemical data presented here do not, in themselves, provide evidence for the tectonic setting of the volcanic and overlying sedimentary sequence. Zeederbergs shale does not contain extrabasinal detritus, suggesting an environment removed from the influence of continental crust. This observation, however, does not rule out the possibility that the volcanic sequence extruded on top of continental crust, thus sealing its potential influence, despite the fact that the base of the volcanic sequence is a major shear zone (Kusky and Winsky, 1995; A. Hofmann, unpubl. data). The geochemistry of Cheshire Formation shale indicates a rather simple unroofing sequence. LREE-depleted basalts, the most common rock type of the Zeederbergs Formation, were eroded throughout deposition of the Cheshire Formation. Erosion of LREE-enriched Zeederbergs basalts took place in the early stage of basin filling, whereas Reliance Formation komatiites were eroded in a late stage. Small amounts of granitoid detritus seem to have been delivered to the basin throughout its history, except for the latest stage when the sudden appearance of abundant granitoid detritus indicates unroofing of a large tract of a granitoid-gneiss terrain, possibly the Shabani gneiss complex. This relationship indicates that the volcanic sequence already covered granitoid crust at least in the later stages of basin formation. Unroofing could be related to rifting, granite doming/diapirism or foreland thrusting. However, sedimentological and structural data are consistent with a foreland model of the Cheshire Formation (chapters 2, 3). Similar trends of granitoid basement unroofing, commonly coupled with an increase in the proportion of an ultramafic component, have been reported from several Archaean sedimentary sequences such as the Fig Tree-Moodies Group, Barberton greenstone belt, and the Witwatersrand sequence of South

Africa (Condie et al., 1970; Wronkiewicz and Condie, 1987), both of which have been interpreted as foreland basin strata (Jackson et al., 1987; Burke et al., 1986; Winter, 1987).

Clear evidence for stratigraphic duplication related to thin-skinned thrusting has been observed in the Cheshire Formation (chapter 3). In the Zeederbergs Formation, any evidence for tectonic stacking is difficult to obtain due to the homogeneity of the lava succession and the absence of marker horizons. However, one ~10 m wide shear zone has been observed (chapter 3) which coincides with the top of the first type II basalt horizon (Fig. 5.2). This observation, combined with the geochemical evidence of a simple unroofing trend as discussed above, strongly suggests that the Zeederbergs Formation is tectonically duplicated in a way that the upper half of the formation (depleted basalt overlain by enriched basalt) is basically the same stratigraphic unit as the lower half. A tectonic model incorporating the geochemical evidence is shown in Fig. 5.15.

One further observation is worth mentioning. Shale horizons (and other clastic sediments) in the Zeederbergs Formation are more commonly associated with type II basalt (Fig. 5.2). This observation may be explained by either less frequent submarine eruptions, providing more time for the deposition of sedimentary rocks in between extrusion events, or more violent submarine eruptions, providing more clastic material and triggering density currents. The latter may be related to a higher volatile content of the magma, or eruption in shallower waters.

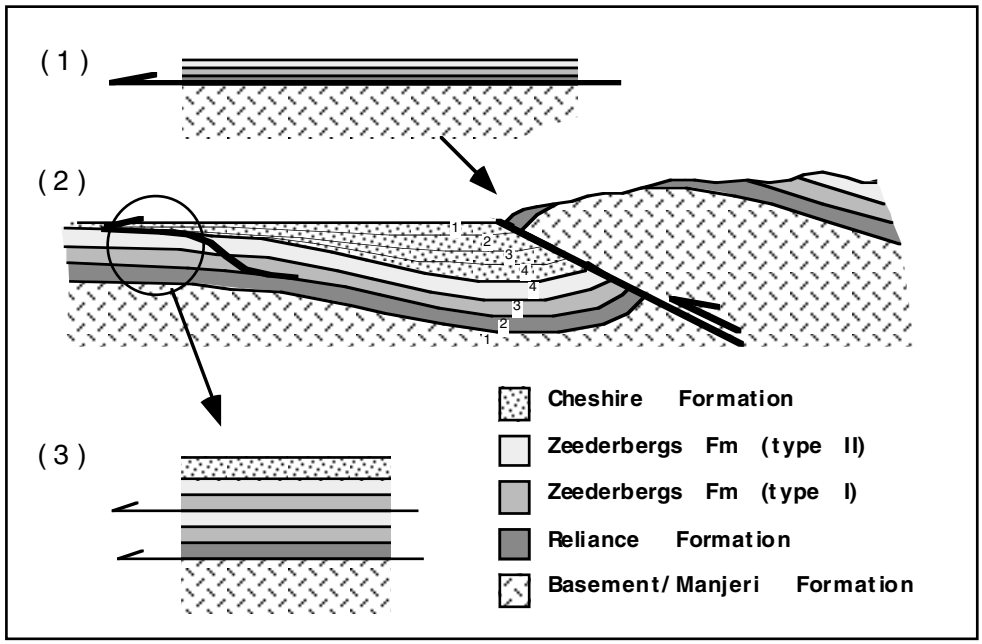

Fig. 5.15. Schematic model showing (1) obduction of the Ngezi volcanics, followed by (2) fold and thrust belt-style deformation with the development of the Cheshire foreland basin, followed by (3) tectonic stacking of the Zeederbergs Formation. Note inverse relationship between rock formation sequence (1-4) and sequence of erosion (4-1).

CONCLUSIONS

1. Shale of the Zeederbergs Formation formed in a submarine lava plain setting and represents suspension sediments and distal deposits of density flows that were possibly triggered by submarine eruptions. The depositional setting of Cheshire Formation shale ranges from wave-reworked shallow-marine (carbonate member) to turbiditic deep-marine (siliciclastic member).

2. REE geochemistry indicates that the sediment source of Zeederbergs shales can be directly related to the basalts with which they are intercalated. Comparison of the chemical composition of basalt and shale indicates that shale lost alkali metals and gained ferromagnesian metals. The compositional changes may be related to a combination of hydrothermal processes and adsorption of elements by clay minerals during deposition.

3. Shale in the lower part of the Cheshire sedimentary sequence was derived from the erosion of LREE-enriched, mafic volcanic rocks geochemically similar to enriched basalts of the Zeederbergs Formation. Towards the upper part of the Cheshire Formation, progressively more (ultra)mafic and LREE-depleted volcanics, geochemically similar to Reliance Formation komatiite and depleted basalt of the Zeederbergs Formation, were eroded in the source area. Unroofing of a large tract of granitoid rock took place after deposition of c. 1000 m of Cheshire sediment, as indicated by sedimentological data and variations in the transition metal contents.

4. The simple unroofing sequence recorded in the Cheshire Formation may indicate tectonic duplication of the Zeederbergs Formation.

5. Chemical indices for subaerial weathering indicate that the source of Zeederbergs shale was not affected by weathering in accordance with their submarine origin. Cheshire shales have values suggestive of intense chemical weathering of the source terrain. An event of K-metasomatism affected the Cheshire shales possibly during diagenesis below the sea floor.

REFERENCES

Abell P. I., McClory J., Martin A., and Nisbet E. G. (1985) Archaean stromatolites from the Ngesi Group, Belingwe Greenstone Belt, Zimbabwe; preservation and stable isotopes-preliminary results. *Precambrian Res.* 27, 357-383.

Alt J. C. (1995) Subseafloor processes in mid-ocean ridge hydrothermal systems. In *Seafloor Hydrothermal Systems: Physical, Chemical, Biological, and Geological Interactions* (ed. S. E. Humphris, R. A. Zierenberg, L. S. Mullineaux, and R. E. Thompson). Geophys. Monogr. 91, pp. 85-114.

Argast S. and Donnelly T. W. (1987) The chemical discrimination of clastic sedimentary components. *J. Sediment. Petrol.* 57, 813-823.

Balistrieri L. S. and Murray J. M. (1984) Marine scavenging: Trace metal adsorption by interfacial sediment from MANOP Site H. *Geochim. Cosmochim. Acta* 48, 921-929.

Bickle M. J. and Nisbet E. G. (Editors) (1993) *The geology of the Belingwe Greenstone Belt, Zimbabwe.* Spec. Publ. Geol. Soc. Zim. 2, 239 pp.

Bickle M. J., Martin A., and Nisbet E. G. (1975) Basaltic and peridotitic komatiites, stromatolites and a basal unconformity in the Belingwe greenstone belt, Rhodesia. *Earth Planet. Sci. Lett.* 27, 155-162.

Bickle M. J., Nisbet E. G., and Martin A. (1994) Archaean greenstone belts are not oceanic crust. *J. Geol.* 102, 121-138.

Bickle M. J., Orpen J. L., Nisbet E. G., and Martin A. (1993) Structure and metamorphism of the Belingwe Greenstone Belt and adjacent granite-gneiss terrain: The tectonic evolution of an Archaean craton. In *The geology of the Belingwe Greenstone Belt, Zimbabwe* (ed. M. J. Bickle and E. G. Nisbet). Spec. Publ. Geol. Soc. Zim. 2, pp. 39-68.

Blenkinsop T. G., Fedo C. M., Bickle M. J., Eriksson K. A., Martin A., Nisbet E. G., and Wilson J. F. (1993) Ensialic origin for the Ngezi group, Belingwe greenstone belt, Zimbabwe. *Geology* 21, 1135-1138.

Bolhar R. (2001) *Archaean mafic magmatism and crust formation in the eastern Pilbara craton (Western Australia) and Belingwe greenstone belt (Zimbabwe).* Ph.D. thesis, University of Melbourne, 183 pp.

Bouma A. H. (1962) *Sedimentology of some flysch deposits: a graphic approach to facies interpretation.* Elsevier, Amsterdam, 168 pp.

Boynton W. V. (1984) Geochemistry of the rare earth elements: meteorite studies. In *Rare earth element geochemistry* (ed. P. Henderson). Elsevier, Amsterdam, pp. 63-114.

Brake C. (1996) *Tholeiitic magmatism in the Belingwe greenstone belt, Zimbabwe.* Ph.D. thesis, University of Edinburgh, 184 pp.

Burke K., Kidd W. S. F., and Kusky T. M. (1986) Archean foreland basin tectonics in the Witwatersrand, South Africa. *Tectonics* 5, 439-456.

Chauvel, C., Dupré, B., and Arndt, N. T. (1993) Pb and Nd istopic correlation in Belingwe komatiites and basalts. In *The geology of the Belingwe Greenstone Belt, Zimbabwe* (ed. M. J. Bickle and E. G. Nisbet). Spec. Publ. Geol. Soc. Zim. 2, pp. 167-174.

Condie, K. C. and Wronkiewicz, D. J. (1990) The Cr/Th ratio in Precambrian pelites from the Kaapvaal Craton as an index of craton evolution. *Earth Planet. Sci. Lett.* 97, 256-267.

Condie, K. C., Macke, J. E., and Reimer, T. O. (1970) Petrology and geochemistry of early Precambrian greywackes from the Fig Tree Group, South Africa. *Geol. Soc. Am. Bull.* 81, 2759-2776.

Condie, K. C., Wilks, M., Rosen, D. M., and Zlobin, V. L. (1991) Geochemistry of metasediments from the Precambrian Hapschan Series, eastern Anabar Shield, Siberia. *Precambrian Res.* 50, 37-47.

Cullers, R. L., Chaudhuri, S., Arnold, B., Moon, L., and Wolf, C. W. (1975). Rare earth distributions in clay minerals and in the clay-sized fraction of the Lower Permian Havensville and Eskridge shales of Kansas and Oklahoma. *Geochim. Cosmochim. Acta* 39, 1691-1703.

des Marais, D. J. (1994) The Archaean atmosphere: ist composition and fate. In *Archaean Crustal Evolution* (ed. K.C. Condie). Developments in Precambrian Geology 11, Elsevier, Amsterdam, 528 pp.

Danchin, R.V. (1967) Chromium and nickel in the Fig Tree Shale from South Africa. *Science* 158, 261-262.

Elderfield, H. and Greaves, M. J. (1982). The rare earth elements in seawater. *Nature* 296, 214-219.

Elderfield, H. and Schultz, A. (1996) Mid-ocean ridge hydrothermal fluxes and the chemical composition of the ocean. *Annu. Rev. Earth Planet. Sci.* 24, 191-224.

Fedo, C. M., Nesbitt, H. W., and Young, G. M. (1995) Unraveling the effects of potassium metasomatism in sedimentary rocks and paleosols, with implications for paleoweathering conditions and provenance. *Geology* 23, 921-924.

Fedo, C. M., Eriksson, K. A., and Krogstad, E. J. (1996) Geochemistry of shales from the Archaean (~3.0 Ga) Buhwa Greenstone Belt, Zimbabwe: Implications for provenance and source-area weathering. *Geochim. Cosmochim. Acta* 60, 1751-1763.

Feng, R. and Kerrich, R. (1990) Geochemistry of fine-grained clastic sediments in the Archean Abitibi greenstone belt, Canada. Implications for provenance and tectonic setting. *Geochim. Cosmochim. Acta* 54, 1061-1081.

Ferry, J. M. (1983) Mineral reactions and element migration during metamorphism of calcareous sediments from the Vasselboro Formation, south-central Maine. *Amer. Mineral.* 68, 334-354.

Fisher, R. V. and Schmincke, H. U. (1984) *Pyroclastic Rocks.* Springer-Verlag, Berlin, 472 pp.

Fleet, A. J. (1984) Aqueous and sedimentary geochemistry of the rare earth elements. In *Rare earth element geochemistry* (ed. P. Henderson). Elsevier, Amsterdam, pp.343-373.

Frey, F. A., Bryan, W. B., and Thompson, G. (1974) Atlantic ocean floor: geochemistry and petrology of basalts from legs 2 and 3 of the Deep-Sea Drilling Project. *J. Geophys. Res.* 79, 5507.

Gromet, L. P., Dymek, R. F., Haskin, L. A., and Korotev, R. L. (1984) The "North American Shale Composite": its compilation, major and trace element characteristics. *Geochim. Cosmochim. Acta* 48, 2469-2482.

Harnois, L. (1988) The CIW index: A new chemical index of weathering. *Sediment. Geol.* 55, 319-322.

Hunter, M. (1997) *The tectonic setting of the Belingwe Greenstone Belt, Zimbabwe.* Unpublished PhD thesis, University of Cambridge, 223p.

Hunter, M. A., Bickle, M. J., Nisbet, E. G., Martin, A., and Chapman, H. J. (1998) Continental extensional setting for the Archean Belingwe Greenstone Belt, Zimbabwe. *Geology* 26, 883-886.

Jackson, M. P. A., Eriksson, K. A., and Harris, C. W. (1987) Early Archaean foredeep sedimentation related to crustal shortening: a reinterpretation of the Barberton Sequence, Southern Africa. *Tectonophysics* 136, 197-221.

Johnsson, M. J. (1993) The system controlling the composition of clastic sediments. In *Processes controlling the composition of clastic sediments* (ed. M. J. Johnsson and A. Basu). Geol. Soc. Am. Spec. Pap. 284, 1-19.

Kasting, J. F. (1993) Earth´s early atmosphere. *Science* 259, 920-926.

Kronberg, B. I., Nesbitt, H. W., and Lam, W. W. (1986) Upper Pleistocene Amazon deep-sea fan muds reflect intense chemical weathering of their mountainous source lands. *Chem. Geol.* 54, 283-294.

Kusky, T. M. and Kidd, W. S. F. (1992) Remnants of an Archaean oceanic plateau, Belingwe Greenstone Belt, Zimbabwe. *Geology* 20, 43-46.

Kusky, T. M. and Winsky, P. A. (1995) Structural relationships along a greenstone/shallow water shelf contact, Belingwe greenstone belt, Zimbabwe. *Tectonics* 14, 448-471.

Lowe, D. R. (1999) Shallow-water sedimentation of accretionary lapilli-bearing strata of the Msauli Chert: Evidence of explosive hydro-magmatic komatiitic volcanism. In *Geologic Evolution of the Barberton Greenstone Belt, South Africa* (ed. D. R. Lowe and G. R. Byerly). Geol. Soc. Am. Spec. Pap. 329, 213-232.

Maas, R. and McCulloch, M. T. (1991) The provenance of Archaean clastic metasediments in the Narryer Gneiss Complex, Western Australia: Trace element geochemistry, Nd isotopes, and U-Pb ages for detrital zircons. *Geochim. Cosmochim. Acta* 55, 1915-1932.

Martin, A. (1978) *The geology of the Belingwe-Shabani schist belt.* Rhod. Geol. Surv. Bull. 83, 213 pp.

Martin, A., Nisbet, E. G., Bickle, M. J., and Orpen, J. L. (1993) Rock units and stratigraphy of the Belingwe Greenstone Belt: The complexity of the tectonic setting. In *The geology of the Belingwe Greenstone Belt, Zimbabwe* (ed. M. J. Bickle and E. G. Nisbet). Spec. Publ. Geol. Soc. Zim. 2, pp. 39-68.

McDonough, W. F. and Ireland, T. R. (1993) Intraplate origin of komatiites inferred from trace elements in glass inclusions. *Nature* 365, 432-434.

Nesbitt, H. W. (1979) Mobility and fractionation of rare earth elements during weathering of a granodiorite. *Nature* 279, 206-210.

Nesbitt, H. W. and Young, G. M. (1982) Early Proterozoic climate and plate motions inferred from major element chemistry of lutites. *Nature* 299, 715-717.

Nesbitt, H. W. and Young, G. M. (1984) Prediction of some weathering trends of plutonic and volcanic rocks based on thermodynamic and kinetic considerations. *Geochim. Cosmochim. Acta* 48, 1523-1534.

Nesbitt, H. W. and Young, G. M. (1989) Formation and diagenesis of weathering profiles. *J. Geol.* 97, 129-147.

Nesbitt, H. W., Markovics, G., and Price, R. C. (1980) Chemical processes affecting alkalis and alkaline earths during continental weathering. *Geochim. Cosmochim. Acta* 44, 1659-1666.

Nisbet, E. G., Bickle, M. J., and Martin, A. (1977) The mafic and ultramafic lavas of the Belingwe greenstone belt, Rhodesia. *J. Petrol.* 18, 521-566.

Nisbet, E. G., Martin, A., Bickle, M. J., and Orpen, J. L. (1993) The Ngezi Group: Komatiites, basalts and stromatolites on continental crust. In *The geology of the Belingwe Greenstone Belt, Zimbabwe* (ed. M. J. Bickle and E. G. Nisbet). Spec. Publ. Geol. Soc. Zim. 2, pp. 121-165.

Nisbet, E. G., Arndt, N. T., Bickle, M. J., Cameron, W. E., Chauvel, C., Cheadle, M., Hegner, E., Martin, A., Renner, R., and Roedder, E. (1987). Uniquely fresh 2.7 Ga old komatiites from the Belingwe Greenstone Belt, Zimbabwe. *Geology* 15, 1147-1150.

Ohmoto, H., Watanabe, Y., Yamaguchi, K. E., Ono, S., Bau, M., Kakegawa, T., Naraoka, H., Nedachi, M., and Lasaga, A. C. (2001). The Archaean atmosphere, oceans, continents and life. In *4th International Archaean Symposium 2001, Extended Abstracts* (ed. K.F. Cassidy et al.). AGSO-Geoscience Australia, Record 2001/37, pp. 19-21.

Pickering, K. T., Stow, D. A. V., Watson, M., and Hiscott, R. N. (1986) Deep-water facies, processes and models: a review and classification scheme for modern and ancient sediments. *Earth Sci. Rev.* 23, 74-174.

Scholey, S. P. (1992) *The geology and geochemistry of the Ngezi Group volcanics, Belingwe Greenstone Belt, Zimbabwe.* Ph.D. thesis, University of Southampton, 184 pp.

Seewald, J. S. and Seyfried, W. E. (1990) The effect of temperature on metal mobility in subseafloor hydrothermal systems: constraints from basalt alteration experiments. *Earth Planet. Sci. Lett.* 101, 388-403.

Seyfried, W.E. (1987). Experimental and theoretical constraints on hydrothermal alteration processes at mid-ocean ridges. *Ann. Rev. Earth Planet. Sci.* 15, 317-335.

Shaw, D. M. (1954) Trace elements in pelitic rocks. Part I. *Geol. Soc. Amer. Bull.* 65, 1151-1166.

Silva, K. E. (1997) *Komatiites from the Belingwe greenstone belt, Zimbabwe: constraints on the development of Archaean greenstone belts.* Ph.D. thesis, University of London, UK.

Staudigel, H. and Hart, S. R. (1983). Alteration of basaltic glass: mechanisms and significance for the oceanic crust-seawater budget. *Geochim. Cosmochim. Acta* 47, 337-350.

Staudigel, H., Plank, T., White, W., and Schmincke, H.-U. (1996). Geochemical fluxes during seafloor alteration of the basaltic upper oceanic crust: DSDP sites 417 and 418. In *Subduction: Top to Bottom* (ed. G. Bebout, D. W. Scholl, S. H. Kirby, and J. P. Platt). Geophys. Monogr. 96, pp. 19-37.

Taylor, S. R. and McLennan, S. M. (1985) *The continental crust: its composition and evolution.* Blackwell, Oxford, 312pp.

Taylor, S. R., Rudnick, R. L., McLennan, S. M., and Eriksson, K. A. (1986) Rare earth element patterns in Archaean high-grade metasediments and their tectonic significance. *Geochim. Cosmochim. Acta* 50, 2267-2279.

Von Damm, K. L. (1995) Controls on the chemistry and temporal variability of seafloor hydrothermal systems. In *Seafloor Hydrothermal Systems: Physical, Chemical, Biological, and Geological Interactions* (ed. S. E. Humphris, R. A. Zierenberg, L. S. Mullineaux, and R. E. Thompson). Geophys. Monogr. 91, pp. 222-247.

Wilson, J. F., Nesbitt, R. W., and Fanning, C. M. (1995) Zircon geochronology of Archaean felsic sequences in the Zimbabwe craton: a revision of greenstone stratigraphy and a model for crustal growth. In *Early Precambrian processes* (ed. M. P. Coward and A. C. Ries). Geol. Soc. Spec. Publ. 95, pp. 109-126.

Winter, H. de la R. (1987) A cratonic foreland model for Witwatersrand Basin development in a continental back-arc, plate-tectonic setting. *S. Afr. J. Geol.* 90, 409-427.

Wronkiewicz, D.J. and Condie, K.C. (1987) Geochemistry of Archaean shales from the Witwatersrand Supergroup, South Africa: Source-area weathering and provenance. *Geochim. Cosmochim. Acta* 51, 2401-2416.

Young, G.M. (1991) The geologic record of glaciation: relevance to the climatic history of the Earth. *Geosci. Can.* 18, 100-108.

Yu, Z., Robinson, P., and McGoldrick, P. (2001) Chemical decomposition of geological materials for trace element determination using ICP-MS. *Geostandards Newsletter*, in press.

CHAPTER 6

Clastic sedimentation in a late Archaean accretionary terrain, Midlands greenstone belt, Zimbabwe

Axel Hofmann, Paul H.G.M. Dirks, and Hielke A. Jelsma
submitted to Precambrian Research

Abstract—Late Archaean (~2.65 Ga) clastic sediments of the Shamvaian Group occur as a shear zone-bounded lithotectonic unit in the Midlands greenstone belt of Zimbabwe. The sediments are tectonically intercalated with mid-Archaean granitoid gneisses and mafic and bimodal volcanics of oceanic and island arc affinity. The lower part of the sedimentary sequence consists of marine turbidite deposits successively overlain by high-energy shelf sandstone, fluvial braid-plain pebbly sandstone and alluvial fan conglomerate. The thick, monotonous sequence of shallow-marine and fluvial facies and the absence of quiet-water and eolian deposits suggests high sedimentation rates and perennial discharge, possibly in a humid climate. Deposition took place in a northward-deepening basin with local felsic volcanic input and with fluvial systems draining a source dominated by granitoid gneiss and banded chert. Basin formation was associated with a west-directed thrusting event, and the basin fill was incorporated into the thrust stack soon after deposition. The Shamvaian sediments show features similar to modern foreland and forearc successions and possibly accumulated during collision of a continental fragment with an oceanic plateau that developed into an island arc. The Midlands greenstone belt is thus regarded as an amalgamation of crustal fragments that accreted during horizontal tectonic processes.

INTRODUCTION

The Zimbabwe craton is an Archaean granitoid-greenstone terrain with a history ranging from 3.6 to 2.6 Ga ago. The majority of the rocks formed between 2.9 and 2.6 Ga and include volcano-sedimentary sequences of the Belingwean (2.9 Ga), Lower Bulawayan (2.8 Ga), Upper Bulawayan and Shamvaian (2.7-2.6 Ga) stratigraphic units, and intrusive granitoids of the Chingezi (2.9 Ga), Sesombi and Wedza (2.7-2.65 Ga), and Chilimanzi (2.6 Ga) suites (Wilson et al., 1995). The Shamvaian is a siliciclastic sedimentary succession and represents the uppermost and youngest unit of the greenstone belt stratigraphy. The time of deposition is unknown, but age determinations of adjacent rocks in various greenstone belts bracket sedimentation to between 2680 and 2640 Ma (Wilson et al., 1995; Jelsma et al., 1996). Two main models for the geological history of the Shamvaian have so far been presented, linked to the proposed tectonic evolution of the Zimbabwe craton. One group of tectonic models suggests cyclic deposition of greenstones and associated sediments in intracontinental rifts on preexisting continental basement forming autochthonous sequences of a distinct age (e.g., Bickle et al, 1994; Wilson et al., 1995). In this type of model the Shamvaian is regarded as the fill of extensional basins unconformably overlying greenstones and possibly onlapping on adjacent basement. An alternative model emphasizes the importance of layer-parallel shear zones along the margins and within greenstone belts and suggests that granite-greenstone terrains represent an amalgamation of oceanic crust, oceanic plateaus, island arcs, back-arc basins and continental crust that accreted due to plate tectonic processes (e.g., Kusky and Kidd, 1992; Kusky, 1998; Dirks and Jelsma, 1998). According to this view, the Shamvaian is regarded as the fill of compressional or transtensional basins that formed during horizontal accretion and/or formed in extensional basins upon collapse of the thickened crust.

In this paper, sedimentological data from the Shamvaian of the Midlands greenstone belt, the largest greenstone outcrop in the Zimbabwe craton, are presented. The data will be discussed in the light of new structural and geochemical results available from the greenstone belt in order to define the tectonic setting in which the Shamvaian sedimentary sequence and adjoining Bulawayan volcanics were formed.

GEOLOGICAL SETTING

The Midlands greenstone belt (MGB) occurs in the central part of the Zimbabwe craton and consists of a large marginal unit of Bulawayan volcanics and a central unit of Shamvaian sediments striking north-northeast (Fig. 6.1). The Rhodesdale granitoid-gneiss terrain forms the eastern flank of the belt. A simple layer-cake stratigraphic model has been developed for the MGB with the gneissic basement of the Rhodesdale terrain overlain by Bulawayan volcanics which are, in turn, overlain by Shamvaian sediments. The contacts between stratigraphic units have been regarded as unconformities (Macgregor, 1951; Harrison, 1970; Bliss, 1970; Robertson, 1976; Wilson, 1979; Wilson et al., 1995), even though many such contacts are strongly sheared (Campbell and Pitfield, 1994). Except for the amphibolite-grade Rhodesdale granitoid-gneiss terrain, metamorphism in the

MGB is generally characterised by greenschist facies mineral assemblages (Bliss, 1970; Robertson, 1976). The MGB has been an object of geological interest for many decades since it hosts major gold deposits (Macgregor, 1930, 1932; Harrisson, 1970; Robertson, 1976; Foster et al., 1986; Campbell and Pitfield, 1994). The Shamvaian sediments were assumed to have a low potential as a host for gold mineralization and, thus, remained relatively unexplored.

Lithologies and field relations

Lithologies in the MGB can be divided into several tectonostratigraphic units characterized by a unique structural-metamorphic history (Dirks et al., 2001). These units are the Rhodesdale granitoid-gneiss terrain, the Kwekwe Ultramafic Complex, the Bulawayan volcanics, and the Shamvaian sediments. Various workers have established a stratigraphy of the Bulawayan volcanic rocks (Bliss, 1970; Harrison, 1970; Robertson, 1976; Wilson, 1981; Foster, 1985). The most commonly used stratigraphic scheme subdivides the rocks into a Mafic Formation, Maliyami Formation and Felsic Formation. The Mafic Formation is wedged in between the Rhodesdale terrain/Kwekwe Ultramafic Complex and the Shamvaian sediments, whereas the Maliyami and Felsic Formations occur west of the Shamvaian outcrop. Contacts between the tectonostratigraphic units are occupied by major shear zones containing sheared, carbonated and silicified equivalents of adjacent lithologies. Lithological characteristics of each unit are summarized in Table 6.1.

Rhodesdale granitoid-gneiss terrain

The Rhodesdale granitoid-gneiss terrain forms the eastern margin of the greenstone belt and is separated from the supracrustal rocks by a strongly sheared contact of quartz-sericite schist (Sherwood shear zone). A sample of the Kwekwe gneiss, which occurs along the contact with the greenstone belt (Harrison, 1970), has yielded a U-Pb zircon age of 3456 ± 6 Ma (Horstwood, 1998).

Kwekwe Ultramafic Complex

Strongly deformed ultramafics, the Kwekwe Ultramafic Complex (KUC) of Harrison (1970), form a unit up to 5 km wide along the contact between Bulawayan greenstones to the west and the Rhodesdale granitoid-gneiss terrain to the east. Harrison (1970) postulated that it intruded into Bulawayan volcanics, contrary to earlier views (Macgregor, 1951) interpreting the KUC as a mid-Archaean greenstone sequence (Sebakwe Group). On the basis of field relationships, Dirks et al. (2001) suggested intrusion of the ultramafics during tectonic juxtaposition of the greenstones and granitoids.

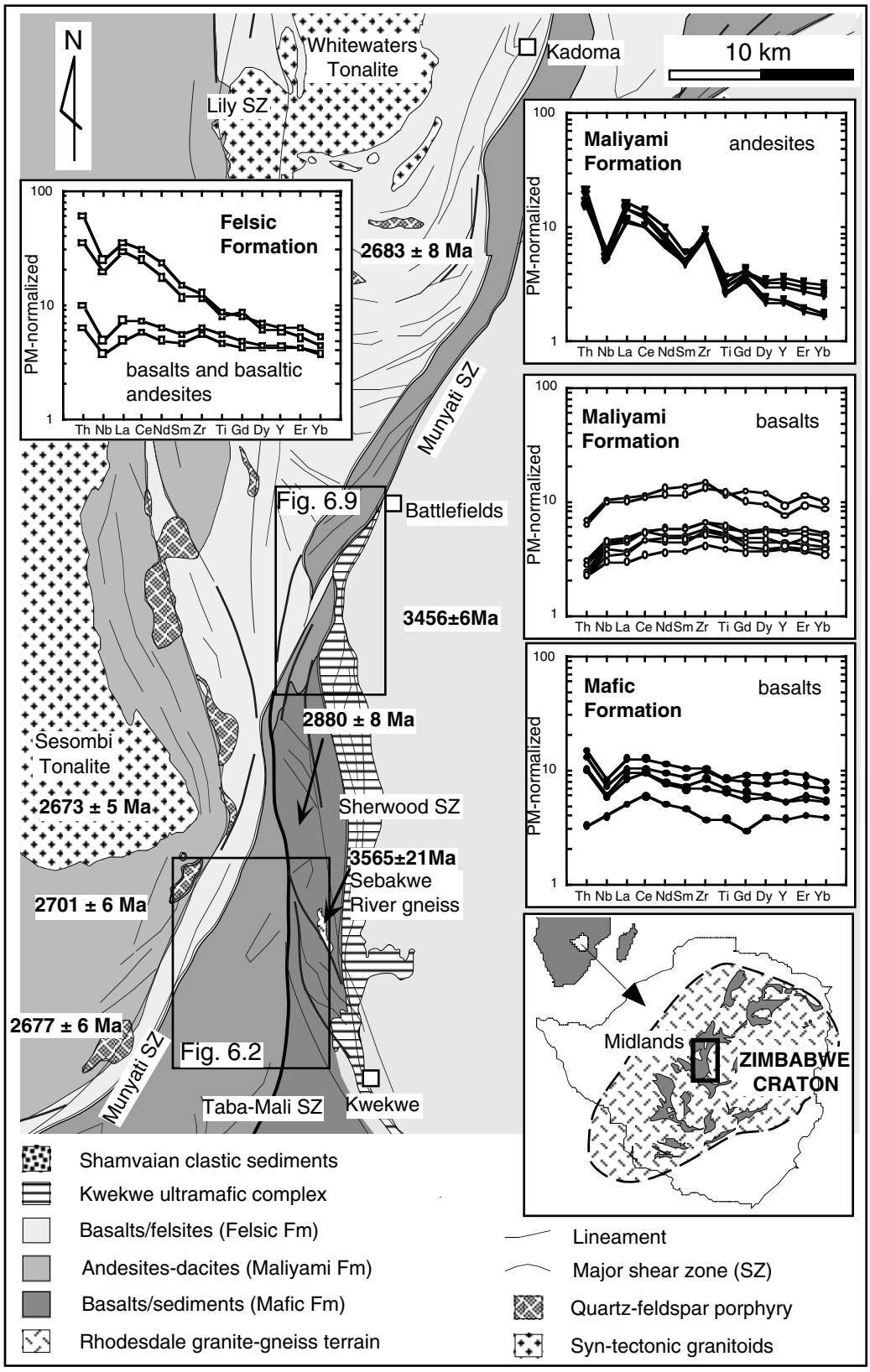

Fig. 6.1. Geological map of the east-central part of the MGB, its position in the Zimbabwe craton (inset), and location of study areas (adapted from Campbell and Pitfield, 1994). Geochronological data (Wilson et al., 1995; Horstwood, 1998) and primitive mantle-normalised trace element and REE diagrams (data from Horstwood, 1998) from Bulawayan formations are also shown.

Mafic Formation

The Mafic Formation is bounded by the Sherwood shear zone to the east and the Taba-Mali shear zone to the west. It is a heterogeneous unit of various lithologies that, in an area near the Sebakwe River, are arranged in ten asymmetric cyclic sequences each c. 500 m thick and interpreted as tectonic duplications of the same horizon (Dirks et al., 2001). A typical cycle consists of basalt, sandstone, turbiditic shale, and jaspilitic banded iron-formation (BIF). Cycle boundaries are marked by strongly foliated ironstone, interpreted as sulphide-mineralized shear zones (Dirks et al., 2001). Zircons from a dacitic tuff yielded a U-Pb age of 2880 ± 8 Ma interpreted as the time of formation of the Mafic Formation (Horstwood, 1998). An isolated occurrence of amphibolitic to dioritic gneiss within the Mafic Formation along the Sebakwe River (Sebakwe River gneiss, Fig. 6.1) has been dated at 3565 ± 21 Ma (Horstwood, 1998) and correlated with gneisses of the Rhodesdale terrain.

Table 6.1. Lithological description of the main stratigraphic units of the MGB.

Stratigraphic unit	Lithological description
Rhodesdale granitoid-gneiss terrain	Migmatitic, layered TTG-gneisses intruded by non-layered granodioritic to granitic gneisses and mafic dykes, now amphibolites. Enclaves of tightly folded greenstone (e.g., fuchsitic quartzite, calc-silicate, ultramafic rock) are attributed to the Sebakwian Group.
Kwekwe Ultramafic Complex	Variably carbonated and silicified serpentinite, talc schist and chlorite schist. Olivine pseudomorphs arranged in a cumulate texture (Harrison, 1970) suggest an intrusive nature of the complex.
Mafic Formation	Cyclic rock units; massive or pillowed tholeiitic basalt is commonly overlain by sandstone/grit. Sandstone is massive, very coarse-grained, and contains quartz and quartzite fragments in a cherty matrix. Sandstone locally grades upward into turbiditic shale indicating a deep-water origin. Cycle tops are formed by jaspilitic BIF which is overlain by sulphide-impregnated, gossaneous ironstone breccia and bound by sulphide-mineralized shear zones (Dirks et al., 2001). Other lithologies include dacitic agglomerate, tuff, and rare conglomerate containing cobbles of granite and granitoid gneiss (Harrison, 1970).
Maliyami Formation	Monotonous sequence of tholeiitic basalt, calc-alkaline andesite and minor (rhyo)dacite. Basalt and andesite are commonly porphyritic and vesicular and either pillowed or massive. A characteristic feature of the formation is the presence of bimodal tuff and agglomerate comprising felsic fragments in a basaltic matrix.
Felsic Formation	Pillowed and massive basalt and andesite dominate this unit and are intercalated and infolded with intermediate to felsic volcanics including agglomerate, volcanic breccia and tuff. Tuff locally shows graded bedding and ripple lamination indicative of subaqueous deposition and reworking. Horstwood (1998) reported the local occurrence of oolitic limestone, suggesting a shallow water environment.

Maliyami Formation

The Maliyami Formation is a thick, monotonous sequence of tholeiitic basalt and calc-alkaline andesite in the western part of the belt. Its continuation to the west is unknown due to later cover. Maliyami Formation andesites have been dated at 2702 ± 6 Ma (SHRIMP U-Pb zircon, Wilson et

al., 1995). The formation is intruded by tonalitic to granodioritic plutons such as the Sesombi tonalite (Fig. 6.1) dated at c. 2670 Ma (Dougherty-Page, 1994; Horstwood, 1998).

Felsic Formation

The Felsic Formation is situated in between the Maliyami Formation and Shamvaian sediments. It differs from the Maliyami Formation by the absence of bimodal agglomerate and the more common occurrence of felsic volcanics (Horstwood, 1998). A felsic clast in a reworked volcanic breccia of the Felsic Formation has been dated at 2683 ± 8 Ma (SHRIMP U-Pb zircon, Wilson et al., 1995). Harrison (1970) and Horstwood (1998) regarded the Felsic Formation to conformably overlie the Maliyami Formation, whereas Campbell and Pitfield (1994) described the contact as a major shear zone (Lily shear zone). The boundary of both units is accentuated by elongated bodies of quartz-feldspar porphyry, one of which (Giraffe porphyry) yielded a U-Pb zircon age of 2677 ± 6 Ma (Horstwood, 1998). The contact between the Felsic Formation and the Shamvaian sediments is sharp and sheared and dips steeply.

Structure

The MGB is characterized by mesoscale, upright fold zones of distinct rock associations with well preserved igneous and sedimentary textures. These zones of low strain are wrapped around by anastomosing high strain zones such as the Munyati, Sherwood, Lily and Taba-Mali shear zones (Fig. 6.1). A regionally developed penetrative fabric occurs in the belt, axial planar to the major fold zones. The structure of the MGB was previously explained by a two-stage tectonic model, an early event of upright folding linked to vertical tectonic processes (granite diapirism) and a later event of multistage strike-slip faulting forming the complex network of shear zones during the final stages and post-dating stabilisation of the Zimbabwe craton (Wilson, 1990; Campbell and Pitfield, 1994; Herrington, 1995). Complex isoclinal folding leading to younging reversals marks an earlier event, and this deformation has generally been attributed to syn-sedimentary slumping.

Campbell and Pitfield (1994) and earlier workers (e.g., Stowe, 1980) proposed a spatial and genetic relationship between structures and Shamvaian sediments in the MGB. They argued that the Shamvaian sediments had been deposited in narrow, fault-bounded, transtensional pull-apart basins or transpressional basins synchronous with deformation. The sheared contacts of the Shamvaian outcrops have been regarded as transcurrent fault systems bounding the sedimentary basins.

On the basis of a detailed structural analysis, Dirks et al. (2001) presented a different view of the tectonic evolution of the greenstone belt. They suggested an early episode of west-directed thrusting of different lithotectonic domains that underwent distinctly different sedimentary and structural-metamorphic histories prior to their juxtaposition. Concomitant with thrusting along domain boundaries, upright folding and minor shear accommodated strain internal to the domains. This event has been interpreted as terrane accretion, possibly associated with a subduction system. Strike-slip faulting reactivating the earlier thrust faults was assumed to have occurred late in the tectonic

history due to a shift of the compressional field stress from E-W to N-S. This shift is attributed to extensional collapse after a long period of E-W shortening at the end of an Archaean compressional cycle leading to crustal thickening and cratonisation of the Zimbabwe craton. Basin formation and deposition of the Shamvaian clastics has been related to thrusting. Soon after deposition the sedimentary sequence was caught up in the accretionary process (Dirks et al., 2001).

Geochemistry

A geochemical study of the Bulawayan volcanics has been conducted by Condie and Harrison (1976) and Horstwood (1998). Primitive mantle-normalized (Sun and McDonough, 1989) trace and REE data of volcanic rocks reported in Horstwood (1998) are shown in Figure 1. REE patterns are nearly flat to slightly LREE-enriched for Mafic Formation basalts (see Table 6.2 for REE ratios) and flat but slightly LREE-depleted for Maliyami Formation basalts. Felsic Formation basalts and basaltic andesites show nearly flat to positively fractionated REE patterns. Andesites of the Maliyami Formation are distinct if compared to the basalts, since they are enriched in LREE and depleted in HREE. Except for Maliyami Formation basalts, all rock units show a distinct negative Nb anomaly. Maliyami andesites are further characterized by a pronounced positive Zr anomaly. Andesites and rhyodacites of the Maliyami and Felsic Formation record a 2.8 to 2.9 Ga T_{DM} model age (Table 6.2), whilst basalts from all formations record a 3.3 to 3.5 Ga T_{DM} model age (Horstwood, 1998).

Condie and Harrison (1976) and Horstwood (1998) suggested a different origin for basalts and andesites-rhyodacites, the former directly derived from partial melting of lherzolitic mantle which experienced a depletion event in the early to mid-Archaean (Nägler et al., 1997), the latter derived by melting of a previously existing basaltic source, possibly rocks equivalent to those of the Mafic Formation as indicated by T_{DM} model ages. This source has been attributed to a 2.9 Ga mafic underplate in the mantle rather than a subducted slab of Mafic Formation. Crustal contamination of the lavas in the MGB has been regarded as minor to absent due to positive and only slightly varying $\varepsilon_{Nd(t)}$ values of between +1.53 and +3.49 (Table 6.2, Horstwood, 1998).

Condie and Harrison (1976) proposed a plate tectonic model for the Bulawayan greenstones. The Mafic Formation has been interpreted as either an oceanic back-arc basin that formed east of a volcanic arc represented by the Maliyami and Felsic Formations or a closing large ocean basin between the volcanic arc and continental crust to the east. The former model is, however, not supported by recent geochronological data (Horstwood, 1998) suggesting that the Felsic and Mafic Formation differ by 200 Ma in age, although the geochemical signatures of the Mafic and Felsic Formation are remarkably similar (Fig. 6.1).

Table 6.2. Lithologies, normalized REE ratios, Nd isotope data and inferred tectonic setting of the Bulawayan volcanics (analytical data reported in Horstwood, 1998).

Formation	Lithology	$(La/Sm)_{PM}$	$(Gd/Yb)_{PM}$	T_{DM}	$\varepsilon_{Nd(t)}$	Tectonic setting
Felsic Formation	tholeiitic basalt, basaltic andesite (4)	1.05-2.5	1.14-1.97	3.6 Ga (2.8-2.9 in intermediate volcanic)	1.7 (1.8-2.6)	arc, continental flood basalt (incipient rift)
Maliyami Formation	calk-alkaline andesite (3)	2.25-3.09	1.3-2.06	2.8-2.9 Ga	2.0-2.9	crustally contaminated greenstones, arc
	tholeiitic basalt (2)	0.74-0.88	1.05-1.25	3.0-3.5 Ga	2.6-3.5	oceanic plateau
Mafic Formation	tholeiitic basalt (1)*	1.09-1.31	0.77-1.18	3.4-4.3 Ga	1.5-2.0	arc, continental flood basalt (incipient rift)

*Samples (Horstwood, 1998): (1) Zim 23, 135, 136, 137, 151, (2) Zim 61, 62, 64, 72, 177, 184, 186, 188), (3) Zim 46, 194, 195, 198, 213, (4) Zim 28, 34, 173, 208

SEDIMENTOLOGY OF THE SHAMVAIAN SEDIMENTS

The Shamvaian in the MGB forms a narrow belt of siliciclastic sediment including conglomerate, sandstone and shale. The sediments are in tectonic contact with Bulawayan greenstones of the Felsic Formation to the west; to the east they border on greenstones of the Mafic Formation, serpentinites of the KUC and gneisses of the Rhodesdale terrain (Fig. 6.1). Two areas in the MGB have been chosen for detailed sedimentological studies. One area is located northwest of Kwekwe and is termed the Sebakwe area after the Sebakwe River. The second study area occurs south-southwest of Kadoma and is termed Munyati area after the Munyati River.

Sebakwe area

The Shamvaian Group in the Sebakwe area (Fig. 6.2) has been subdivided by Macgregor (1932) into a Lower and Upper Sedimentary Series and by Harrison (1970) into four formations the characteristics of which are summarized in Table 6.3. The Shamvaian in the Sebakwe area (Fig. 6.2) forms a broad synformal structure. Poles to bedding define a great circle with the fold axis plunging at shallow angles to the north-northwest. The contacts to adjacent greenstone units are sheared. Palaeocurrent measurements have been conducted at several locations within the UGF. Data were corrected to account for tectonic disturbance. To overcome variations in bedding orientation at different localities, bedding has been rotated to an average strike of 20° prior to unfolding. Unfolding has been done using an average fold axis of 022/22 (see Fig. 6.2).

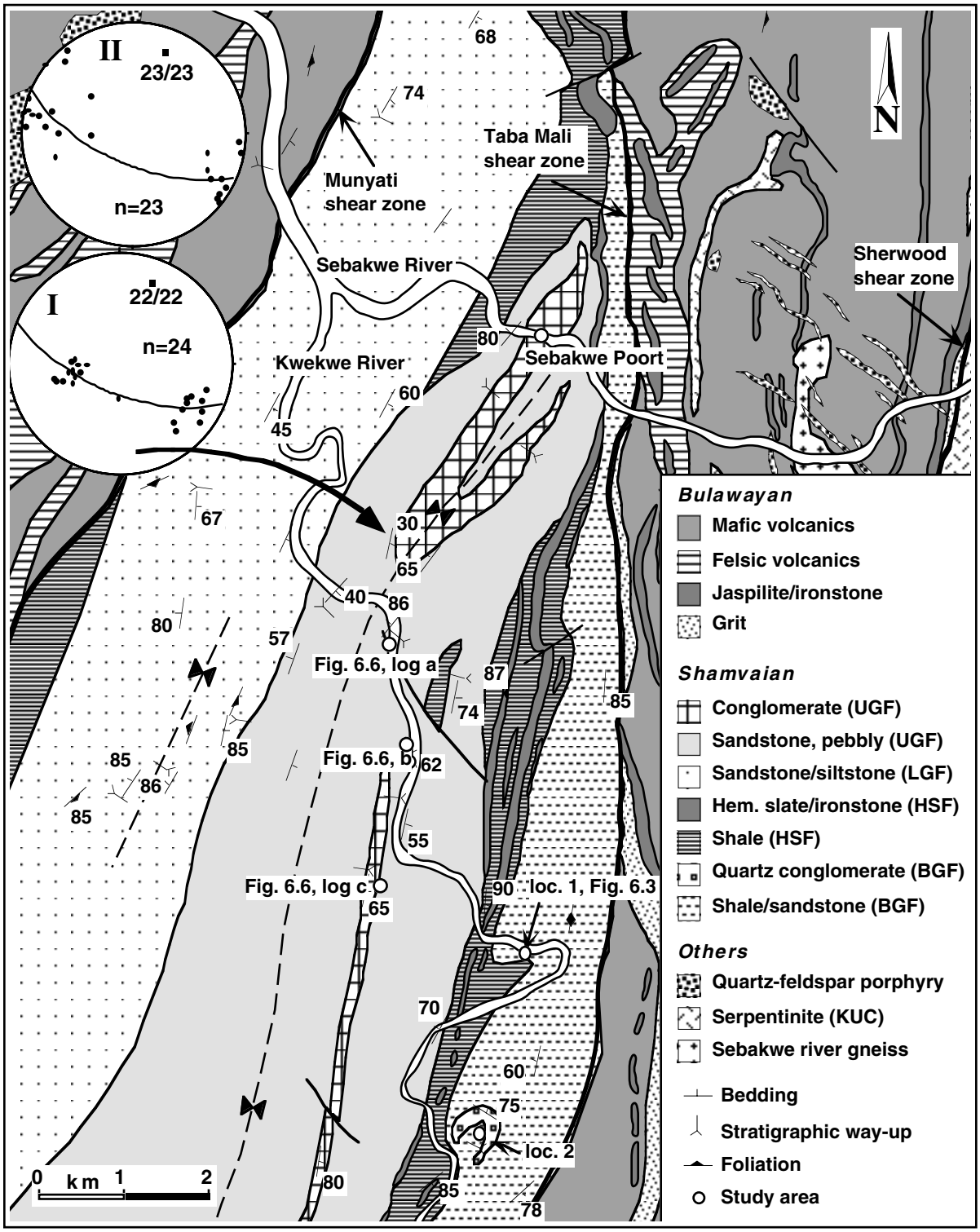

Fig. 6.2. Geological map of the Sebakwe area (modified after Macgregor, 1932; Harrison, 1970). Lower hemisphere stereographic projections of poles to bedding from a fold closure south of Sebakwe Poort (I) and from other localities (II) are shown.

Table 6.3. Lithological description of the stratigraphic units of the Shamvaian Group.

Lithostratigraphy Macgregor (1932)	Lithostratigraphy Harrison (1970), Robertson (1976)	Lithological description
		Sebakwe area
Upper Shamvaian Series	Upper Greywacke Formation (UGF)	Thin to thick beds of trough and hummocky cross-stratified coarse-grained sandstone locally intercalated with massive or normally graded conglomerate.
	Lower Greywacke Formation (LGF)	Thin to thick beds of fine- to coarse-grained, ripple-laminated and cross-bedded sandstone intercalated with thin shale beds; conglomerate is absent.
Lower Shamvaian Series	Hematite Slate Formation (HSF)	Thinly laminated to very thinly bedded shale intercalated with ironstone; well-developed cleavage planes parallel to the lamination give rise to a slaty rock. Banded ironstone consists of 1-5 cm thick, continuous to lenticular layers of chert and massive hematitic layers; brecciated ironstone is a poorly layered, gossaneous rock with fragments of chert and silicified sediment in a massive hematitic matrix.
	Basal Grit Formation (BGF)	Medium to very thick beds of massive quartzose sandstone/grit and local conglomerate intercalated with shale. Several metres to several 10´s of metres thick sandstone bedsets are common. Tight folding is common.
		Munyati area
	Volcaniclastic Formation (Munyati north)	Tightly folded units of conglomerate, sandstone/grit and minor shale. Conglomerate and coarse-grained sandstone/grit is characterized by massive or normally graded, medium to very thick beds. Intercalations of coarse sandstone and shale are locally common. Shale (slate) consists of parallel-laminated silt- to mudstone with thin, normally graded beds of fine-grained sandstone.
	Basal Grit Formation (Munyati south)	Medium to very thick beds of massive, quartzose coarse sandstone/grit forming metres to 10`s of metres thick horizons within homogeneous shale. Shale is characterized by parallel lamination, a slaty cleavage, and contains minor thin silt/sandstone beds. Small-scale kink folds, asymmetric folds and crenulations are common.

Basal Grit Formation (BGF)

Description. The BGF occurs on the eastern side of the belt and on the western side farther to the south of the study area (Harrison, 1970). Exposure is poor except for a small river section where intercalated sandstone and shale are exposed (Fig. 6.2, location 1; Fig. 6.3a). Sandstone beds are tabular and planar (on outcrop-scale), thin to thick, and range from fine to very coarse-grained (Figs. 6.3b and 6.4a). Sandstone is mostly massive and normally graded with rare parallel lamination at bed tops. Shale is a homogeneous rock with laminae/thin beds of graded siltstone interbedded with mudstone. Diagenetic pyrite nodules up to 1 cm across occur locally. Open to tight folds with an axial planar cleavage and a northeastward plunging fold axis are common (Figs. 6.3c and 6.3d). Sandstone beds are locally discontinuous due to disruption and boudinage of the sequence (Fig. 6.3e). The lateral bed geometry and vertical facies distribution could not be investigated due to lack of exposure and intense deformation.

At location 2 (Fig. 6.2) there occurs a tightly folded, ~30 m thick horizon of pebble conglomerate intercalated with grit. Conglomerate beds are thick to very thick and tabular. The

conglomerate is clast-supported and consists of massive and normally graded (partly coarse-tail graded) facies; horizontal stratification is associated with more fine-grained (gritty) sediment. A pebble count (Fig. 6.5a) indicates the dominance of well rounded vein quartz followed by well rounded granite clasts. Less common are clasts of massive dark grey chert, granitoid gneiss and banded jaspilitic chert. Clasts of hematitic shale, grit/shale intraclasts and fuchsitic quartzite are rare.

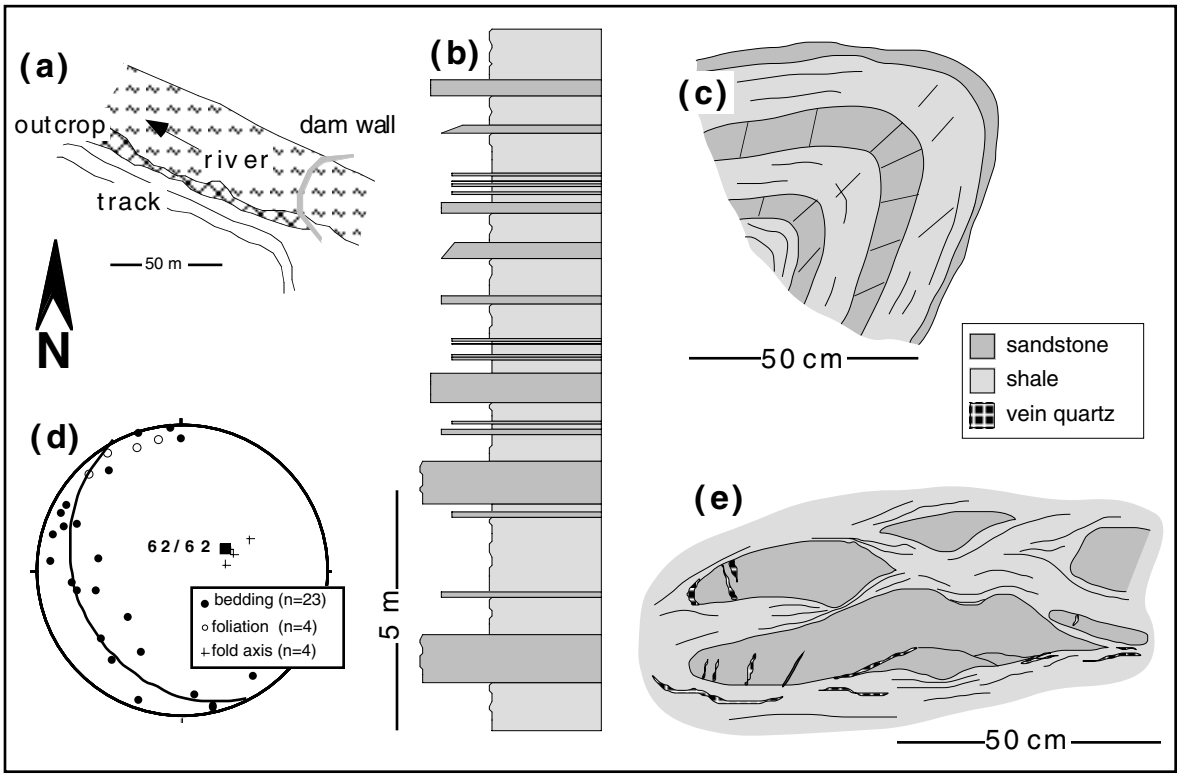

Fig. 6.3. Location map (a), graphic log (b), sketch of a fold (c), lower hemisphere stereographic projections of structural data (d), and sketch of deformation geometries (e) of intercalated sandstone and shale of the BGF exposed in a section of the Kwekwe River (see Fig. 6.2 for locality).

Interpretation. Bedding characteristics, sedimentary structures and facies association indicate sub-wave base deposition by turbidity currents. Normally graded conglomerate (R_3 division of Lowe, 1982; A2.3 facies of Pickering et al., 1986) and massive sandstone with poorly developed grading (S_3 division; B1.1 facies) are common facies in coarse-grained deep-sea clastics and formed by rapid suspension sedimentation and rapid deposition by suspension freezing from high-density turbidity currents. Shale formed in a low-energy setting characterized by the deposition of low-density, silt-dominated turbidity currents and quiet-water background suspension sedimentation. The occurrence of both granite and vein quartz clasts suggests a granitoid source area compositionally similar to the Rhodesdale granite-gneiss terrain. Granitic detritus was blended with chert clasts, the source of which may be found in banded cherts of the Mafic Formation. Harrison (1970) postulated that the Lower Shamvaian has been folded and eroded prior to deposition of the Upper Shamvaian. However, the orientation of fold axes of folds developed in the Lower and Upper

Formations are similar (Figs. 6.2 and 6.3d), suggesting that folding affected both formations after deposition.

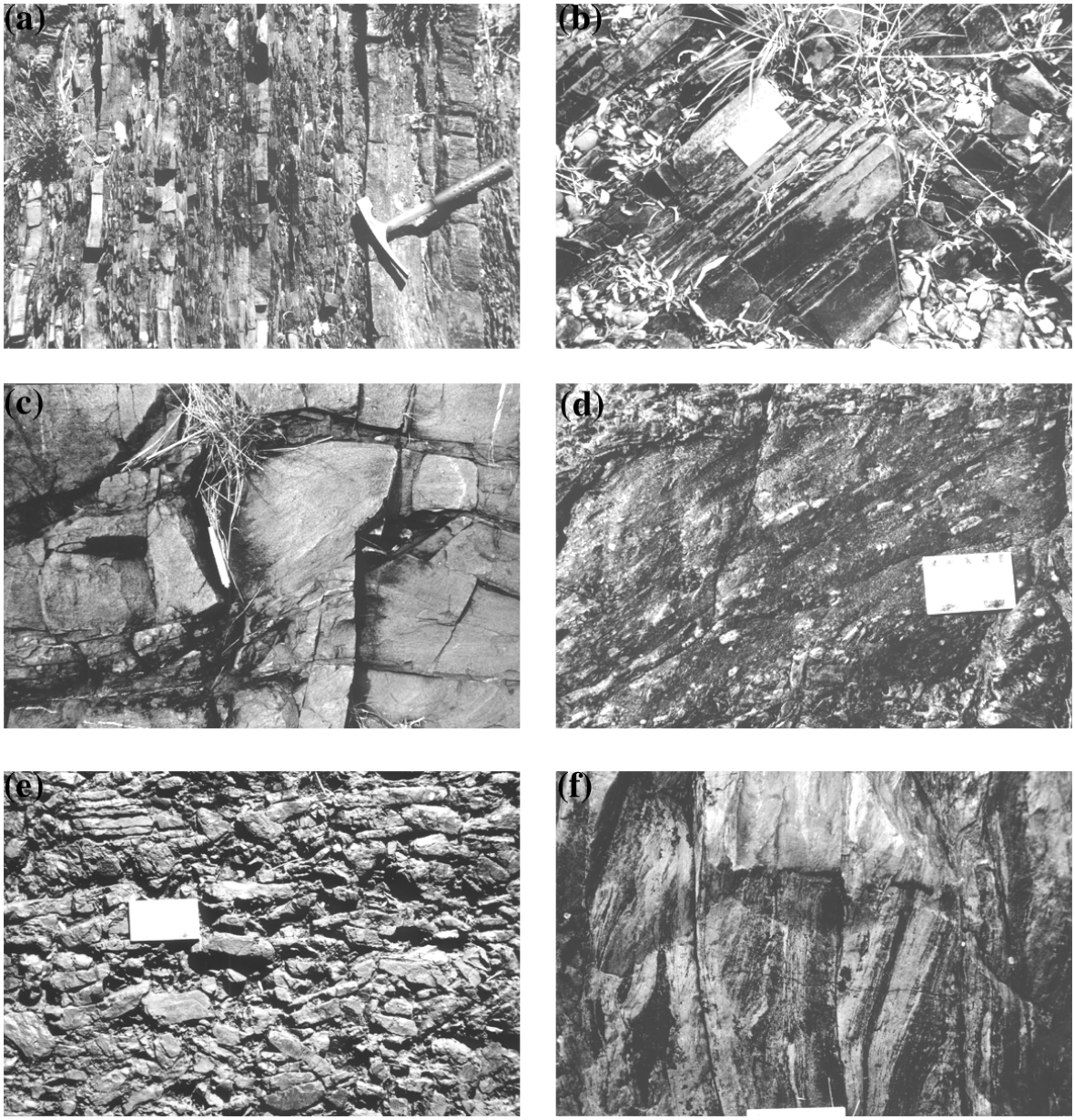

Fig. 6.4. Features of Shamvaian sediments in the Sebakwe area. (a) Thin to medium sandstone beds intercalated with shale of the BGF. (b) Thin to medium beds of ripple-laminated sandstone of the LGF. (c) Hummocky cross-stratified sandstone of the UGF (marker pen for scale). (d) Cross-bedded pebbly sandstone with chert pebbles, UGF, Sebakwe Poort. (e) Massive chert cobble conglomerate, UGF, Sebakwe Poort. (f) Backrotated foliation boudins and truncation surfaces in a bedding-parallel shear zone, UGF, Sebakwe Poort.

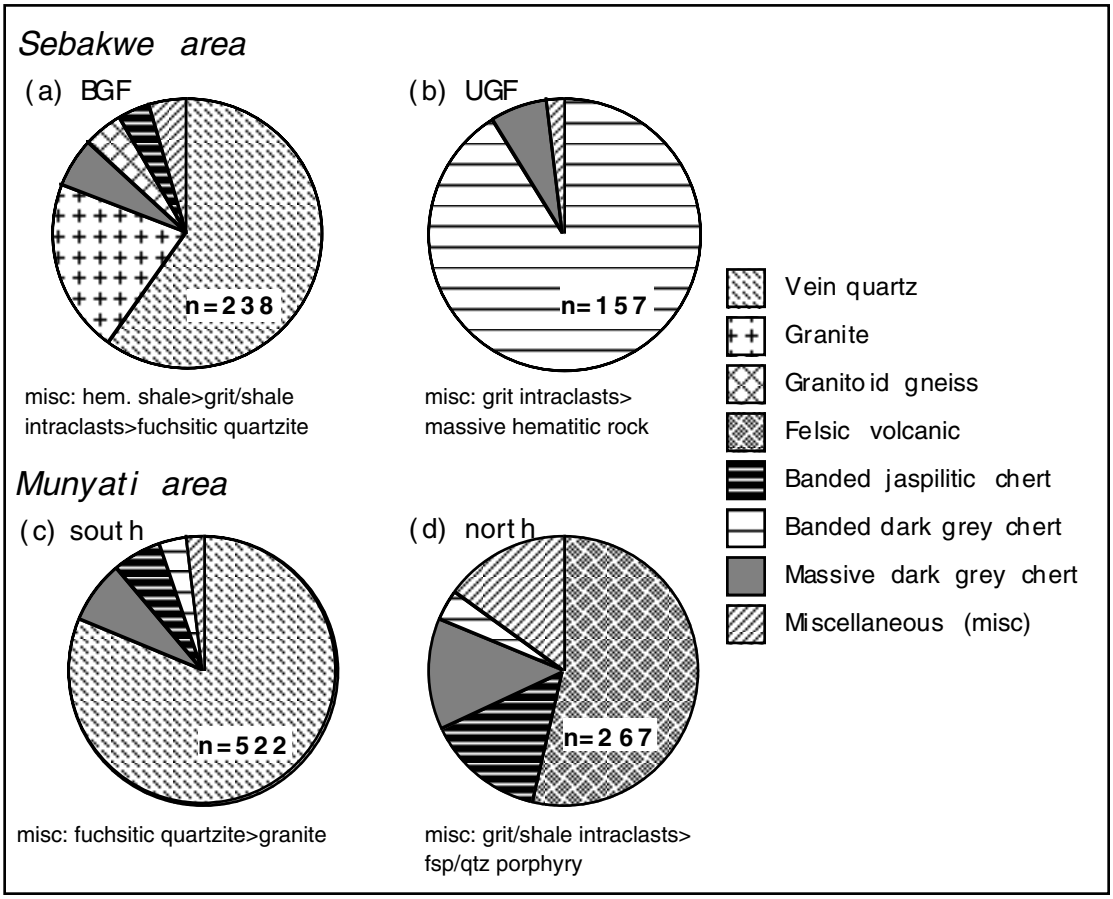

Fig. 6.5. Results from pebble counts. All clasts exceeding 10 mm were counted on a certain outcrop surface. (a) Conglomerate in BGF, Sebakwe area (Fig. 6.2). (b) Conglomerate in UGF, Sebakwe area (Fig. 6.2). (c) Munyati south; synthesis of three different sites of pebbly sandstone (Fig. 6.9). D. Munyati north; river section (Fig. 6.10).

Hematite Slate Formation (HSF)

Description. The HSF is a homogeneous unit of schistose shale intercalated with decimetre to metre thick, continuous layers of ironstone. Locally, what superficially looks like undeformed shale shows large-scale boudinage as indicated by up to 2 m wide and several metres long boudins of shale within shale. Ironstone consists of mainly two types, a banded and brecciated variety, both of which show complex folding and are commonly intercalated and grade into each other laterally. Ironstone is associated with quartz veins that are locally strongly disrupted and brecciated to give rise to vein quartz breccias. Isoclinal folds and truncation planes bounding lenticular objects are common. Shale adjacent to ironstone is Fe-enriched (haematitic slate) and locally contains fine-grained, disseminated sulphides. In some shale horizons layers of laminated chert occur along anastomosing foliation planes.

The contact between the BGF and HSF seems to be gradational and is marked by a decrease to total absence of sandstone intercalations in shale. However, a tectonic contact cannot be ruled out due to the generally poor exposure of the BGF. Towards the contact to the overlying LGF, shale comprises alternating thin continuous beds (1-5 cm thick) of normally graded siltstone/fine sandstone intercalated with mudstone. Parallel lamination, ripple cross lamination and wavy

lamination are common. Soft sediment deformation includes slump folds and load casts. Contorted bedding is sometimes truncated by the overlying bed.

Interpretation. The lack of decimetre-thick sandstone beds suggests a sub-wave base depositional environment similar to the BGF but without the periodic influx of coarse clastics by high-density turbidity currents. The lack of coarse detritus may be related to a retreat of the sediment source due to a relative sea level rise or to a lowering of the topographic relief in the hinterland such as during times of tectonic quiscence. Shales probably formed from low-density turbidity currents, deep-water bottom currents and settling of background suspension material. A submarine environment with low clastic influx is generally conducive for the chemical precipitation of banded iron-formations in the Archaean (Barret and Fralik, 1989). However, the ironstones in the HSF are similar to rocks observed in other Zimbabwean greenstone belts where they represent silicified and ferruginized shales adjacent to shear zones (chapter 3). The more strongly deformed nature of ironstone and adjacent sediment and the local presence of ironstone restricted to anastomosing cleavage domains in shale strongly suggest a temporal relation between deformation and ironstone formation. The absence of genuine sedimentary banded iron-formation may suggest that the supply of fine-grained clastic material was continuous and high, such as in the proximity of a delta or a siliciclastic shoreline. The interbedded shale and graded siltstone beds in the upper part of the HSF are similar to inferred outer shelf deposits of the Precambrian rock record (Harris and Eriksson, 1990; Eriksson et al., 1998). Sedimentary structures resemble those of Bouma-type beds that reflect deposition from waning suspension currents, possibly related to storm events.

Lower Greywacke Formation (LGF)

Description. The LGF is confined to the western part of the belt where exposure is very poor and tight folding is common. It is characterized by thin to medium beds of parallel-, current and minor wave ripple-laminated as well as flaser-bedded silt to fine-grained sandstone (Fig. 6.4b). Bimodal current ripple cross-lamination is common. Some beds are normally graded. Medium to thick beds of cross-bedded, medium- to coarse-grained sandstone further occur. Beds are draped by shale partings which can be mudcracked. Current ripple bedforms are commonly preserved on bedding planes. The contact to the underlying HSF is gradational as indicated by a gradual decrease in sandstone beds within shale. The contact to the overlying UGF is gradational as indicated by an increase in grain size, decrease in shale partings, and an increase in the abundance of cross-bedded sandstone.

Interpretation. The LGF formed in a tide-influenced shallow marine to litoral-fluvial environment which was subjected to periodic subaerial exposure. A tidal influence is indicated by bimodal sediment transport and flaser bedding (Reineck and Wunderlich, 1968). Cross-bedded sandstones draped by desiccation-cracked mud partings may have formed in shallow ephemeral channels providing sediment to the tidal flats or represent overbank deposits of fluvial channels. The lower gradational contact with the HSF indicates progressive shallowing of the depositional

environment from deeper marine, sub-wave base deposition to a very shallow water to subaerial setting.

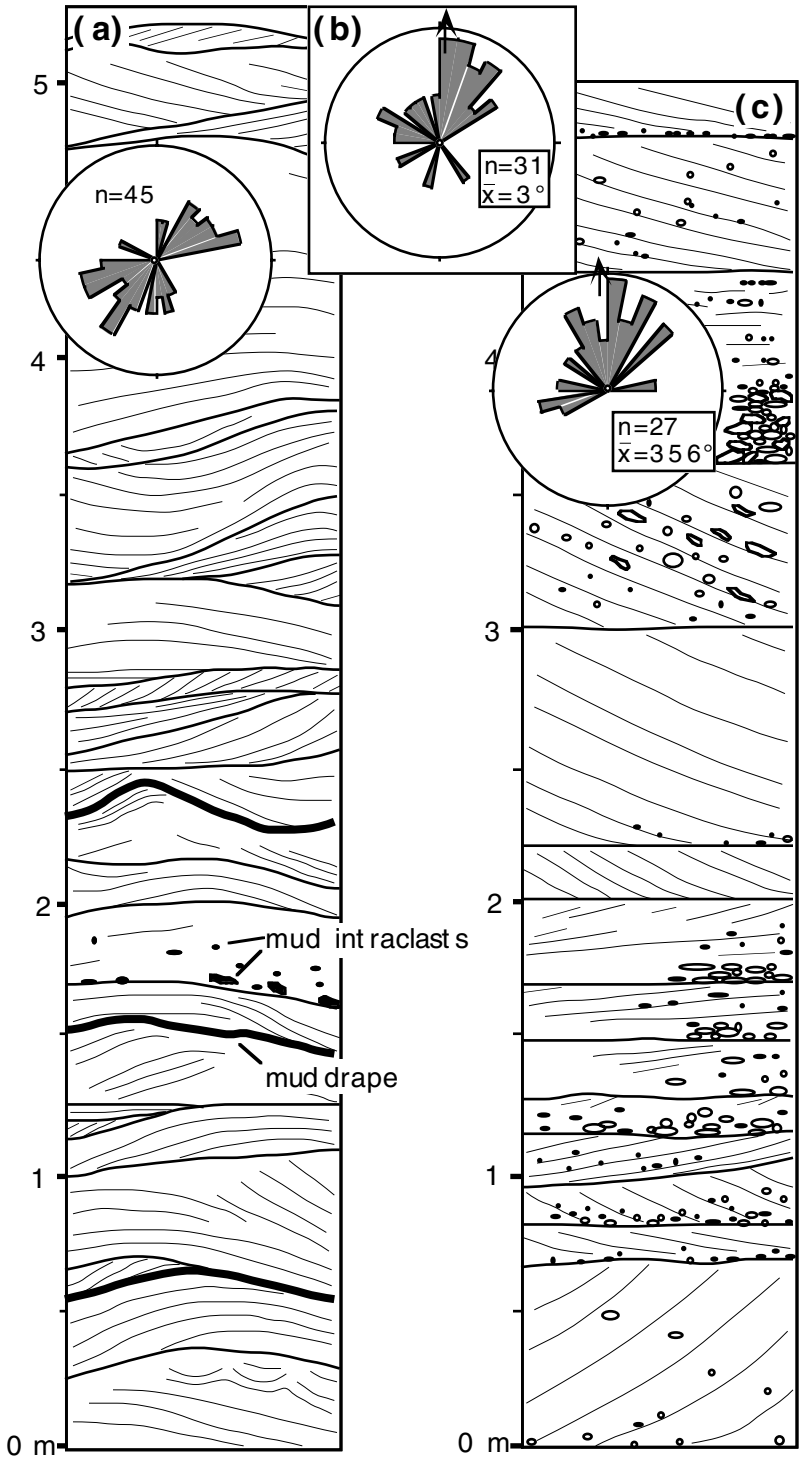

Fig. 6.6. Sedimentological data from the Upper Greywacke Formation (refer to Fig. 6.2 for locations a-c). (a) Graphic log of hummocky cross-bedded sandstone and palaeoflow data. (b) Palaeoflow data from hummocky cross-bedded sandstone. (c) Graphic log of cross-bedded pebbly sandstone and palaeoflow data. The radius of the scale circle refers to 10% of the palaeoflow measurements; the number of measurements and the vector mean are indicated.

Upper Greywacke Formation (UGF)

Description. The UGF forms the central part of the Shamvaian outcrop and is characterized by a monotonous sequence of medium- to coarse-grained sandstones that are locally well exposed. Beds are thin to thick and lenticular to wavy. Trough cross-bedding and hummocky cross-stratification are ubiquitious (Fig. 6.4c); parallel-lamination is less common. Upper bedding planes rarely show current ripple bedforms which, in that case, are draped by thin shale beds. Angular to rounded chert granules and pebbles up to 4 cm across are scattered throughout; shale intraclasts occur locally in basal bed portions. The geometry of some beds is wavy to fold-like with the bedding planes too steep to be of depositional origin. A representative log of this facies is shown in Figure 6a. Palaeoflow orientations have been determined at two localities and either show a bimodal northeast-southwest flow (Fig. 6.6a), or a somewhat variable unimodal flow to the north (Fig. 6.6a).

Pebbly sandstone and conglomerate occur in discrete horizons in the upper part of the UGF (Fig. 6.2). A ~60 m thick horizon of conglomerate is continuous for several km and consists of planar tabular, medium to thick beds of clast-supported pebble conglomerate. Beds are massive or normally graded. A pebble count (Fig. 6.5b) shows that all clasts consist of chert which is mostly banded. The conglomerate horizon occurs in between pebbly sandstone and sandstone with minor intercalations of conglomerate. One section below the conglomerate horizon was logged in detail (Fig. 6.6c). Beds are lenticular to tabular, thin to thick, and consist of cross-bedded pebbly sandstone and sandstone, partly with conglomerate or pebble lags at the base. Palaeocurrent data indicate a palaeoflow to the north (Fig. 6.6c).

A well exposed section of the UGF through the central and stratigraphically uppermost part of the Shamvaian outcrop is exposed at Sebakwe Poort, a gorge cut through a ridge of folded, coarse clastic sediments (Fig. 6.2). A lithostratigraphic log of the succession forming the western to central part of the fold structure has been compiled (Fig. 6.7). The measured section starts with a thick unit of shale, either part of the HSF or an intercalation of shale within the LGF. Shale is sharply overlain by a homogeneous sandstone unit lacking shale interbeds. The lower contact of the sandstone unit occurs in an unexposed zone of <1 m in width. This sharp lithological break points to a sheared contact. The sandstone unit consists of thin to medium, tabular, pinching-and-swelling or lenticular beds of massive, trough cross-stratified and undulating to hummocky cross-stratified, medium- to coarse-grained sandstone. Pebbles are lacking except for angular mudstone intraclasts up to 5 cm in length. Palaeocurrent data indicate a unimodal north-northwest flow (Fig. 6.7). Open to tight, asymmetric slump folds with an amplitude of up to 50 cm are common in one distinct sandstones horizon (Fig. 6.7). Extension fractures occur along fold hinges, suggesting that the sediments were already consolidated to some degree. The orientation of the slump folds indicates a north-northeast-dipping palaeoslope (Fig. 6.7).

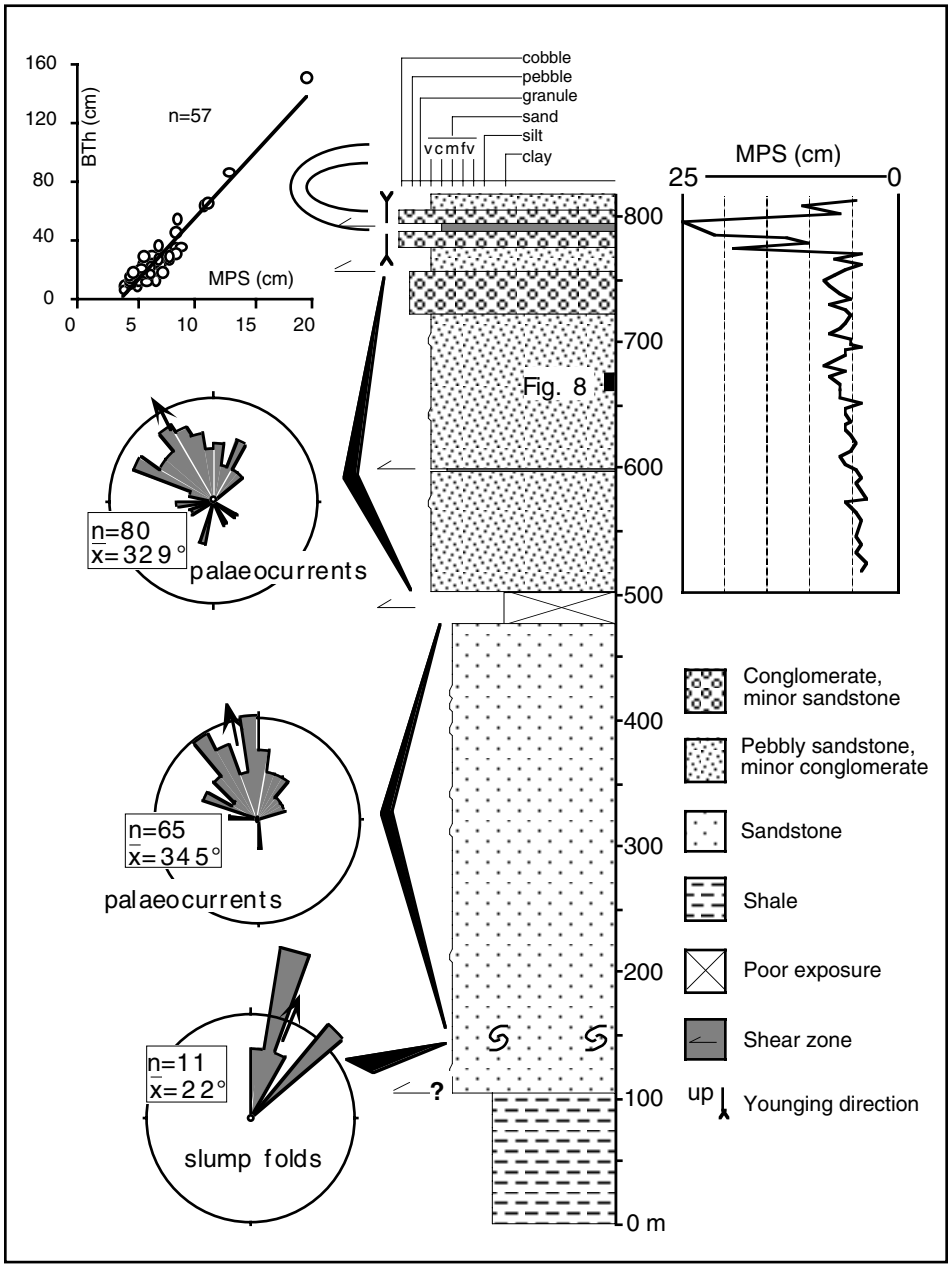

Fig. 6.7. Graphic log of the sedimentary succession forming the western to central part of the Sebakwe Poort fold structure (see Fig. 6.2 for location). Maximum particle size (MPS) has been determined for the upper conglomerate-bearing portion and has been plotted against bed thickness (BTh). Several bedding-parallel shear zones occur in the section. The uppermost shear zone is overlain by the same sedimentary sequence as below, but the stratigraphy is inverted. Palaeocurrent data are derived from cross-bedding. Slump folds in sandstone are well developed in one horizon and provide palaeoslope data.

The sandstone unit is sharply overlain by pebbly sandstone with minor conglomerate beds along a shear zone several decimetres in width (Fig. 6.8). Conglomerate is clast-supported, dominated by pebbles, and forms thin to rare thick beds, which are massive or normally graded. Some beds are inversely graded at the base. Clast imbrication is common. Maximum particle size, i.e. the average of the twelve largest clasts observed in a conglomerate bed after omitting the two largest, gradually increases upsection. The frequency and thickness of conglomerate beds also increases upsection, so

that there is a significant linear correlation between maximum particle size and bed thickness (Fig. 6.7). Conglomerate is intercalated with or grades into pebbly very coarse-grained sandstone. Beds are thin to thick and massive, normally graded, horizontally stratified or trough cross-stratified (Fig. 6.4d). Discontinuous thin beds of horizontally laminated, trough cross-stratified to massive, coarse- to very coarse-grained sandstone also occur. The orientation of cross-bedding indicates a northwest-directed palaeoflow (Fig. 6.7).

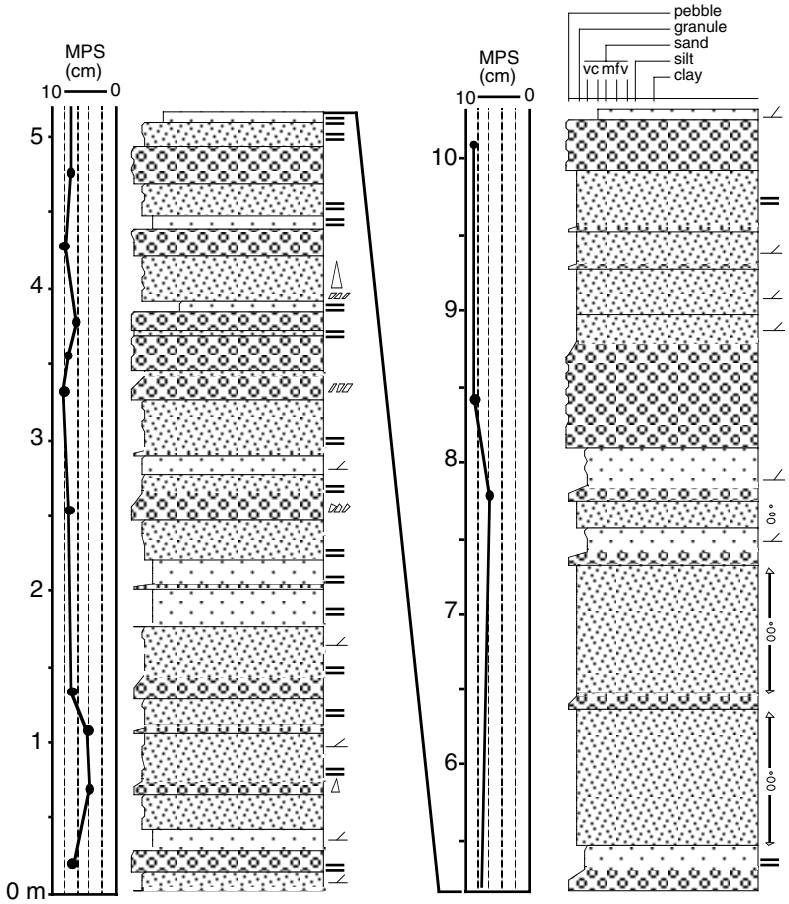

Fig. 6.8. Graphic log of intercalated conglomerate and pebbly sandstone at Sebakwe Poort (see Fig. 6.7 for location of measured section and Fig. 6.10 for key of symbols).

Medium to very thick, tabular and planar beds of pebble to cobble conglomerate form the uppermost portion of the section. The conglomerate is massive or normally graded (Fig. 6.4e). Lenticular thin beds of coarse-grained, partly pebbly sandstone are intercalated with or gradationally overlie graded conglomerate. Clast imbrication is well developed. Beds thicken and coarsen upward. A several metres wide shear zone marks the top of the succession and is overlain by parts of the same but inverted sequence.

Clasts in pebbly sandstone/conglomerate almost totally consist of banded chert. Banding is typically on a mm- to a few cm-scale and defined by colour variations from white to dark grey to red. Banding in some clasts is folded, whereas in others the banding is brecciated. Clast shape

ranges from angular to rounded with most clasts being subrounded. The angularity of some clasts can be attributed to the breaking up of large clasts during transport. Clasts of well rounded vein quartz are rare.

Several bedding-parallel shear zones ranging from a few mm to 2 m in width occur in the upper part of the measured section (Fig. 6.7). Shear zones are characterised by foliated, very fine-grained, silicified cherty material that represents anastomosing foliation domains. These domains surround mm- to decimetre-scale lenticular objects of the host sediment or boudinaged and rotated foliation domains (Fig. 6.4f). The shear zones are commonly enriched in iron oxides and sulphides. Truncation surfaces are common and probably formed during one progressive event. Kinematic indicators in the shear zones indicate an original (prior to folding) east-over-west tectonic transport (Dirks et al., 2001). A major shear zone occurs at the top of the sequence and bounds conglomerate horizons with opposite stratigraphic way-up. The shear zone consists of conglomerate with a strongly iron oxide- and sulphide-impregnated matrix.

Interpretation. The homogeneous succession of cross-bedded and hummocky cross-stratified sandstone which forms most of the lower and intermediate part of the UGF was deposited in a storm-dominated, high-energy shoreface environment. Storm-generated currents giving rise to hummocky cross-stratified and parallel-laminated sands (Dott and Bourgeois, 1982; Nottvedt and Kreisa, 1987) and strong, fair-weather longshore, onshore, or offshore currents forming cross-bedded sands of subaqueous dunes led to continuous sediment reworking, sand bed amalgamation and bypassing of fine siliciclastic sediment. The rare occurrence of shale draping hummocky crossbeds indicates the rarity of relatively quiet-water conditions. The common undulatory geometry of beds is partly a primary characteristic of sediment deposition (HCS), and partly attributed to soft-sediment deformation. Some folding may be related to fluid escape due to very rapid deposition, whilst the asymmetric folds observed at Sebakwe Poort are a result of graviational movements, indicating an original depositional slope. The lack of sedimentary structures of massive sandstone may be a result of rapid sediment deposition and/or fluid escape. Homogeneous successions of storm-dominated shoreface shelf sandstone hundreds of metres thick are common in the Precambrian rock record, possibly due to a fine balance between subsidence rate and sediment influx and a more evenly sediment redistribution due to strong semipermanent wind-driven and tidally driven current systems (Cant and Hein, 1986; Soegaard and Eriksson, 1989; Eriksson et al., 1998).

Above the shoreface sandstones, individual beds of pebbly sandstone with trough cross-bedding and horizontal stratification suggest deposition in braided, shallow bedload channels as part of migrating longitudinal and transverse bars. The stacked sheets of composite beds of conglomerate and pebbly sandstone show features indicative of both mass and stream/sheet flow deposits. Characteristic features for a mass flow origin include the absence of stratification in conglomerate, and a linear correlation between maximum particle size and bed thickness (e.g., Bluck, 1967; Steel, 1974). The tabular bed geometry and a waning flow sequence (conglomerate gradationally overlain

by sandstone showing traction structures) are consistent with a sheet flow origin. Similar composite units have been described from several ancient alluvial fan sequences (Allen, 1981; Ballance, 1984). Todd (1989) interpreted such conglomerates as *en masse* deposits from high-density dispersions in channels during high magnitude floods, whereas caps of pebbly sandstone and sandstone resulted from the dissipation of floods. Sand deposition took place either directly from suspension, forming massive or graded sandstone, or experienced traction under upper flow regime, producing parallel lamination, or lower flow regime conditions, producing cross-stratification.

The facies association is suggestive of a braid-plain to stream-dominated alluvial fan environment with an increase in proximality towards the top of the preserved sequence and with a consequent shift from sheetflood to debris flow processes. Deposition occurred in pulses or was episodic, but the time interval between individual flood events cannot be determined without the presence of, for example, mudstone intercalations which could preserve the effects of subaerial exposure.

Palaeoflow is, on average, directed towards the north, suggesting northward propagation of the clastic wedge. This is in accordance with a northward-dipping palaeoslope. The bimodal sediment transport path in the hummocky cross-bedded shoreface sandstones indicates the importance of oscillatory currents in the formation of this facies type. The rare presence of vein quartz clasts may indicate the presence of granitoid crust in the source (see above), but this influence is masked by the abundance of chert clasts which may have been derived from banded iron-formation. Folding and brecciation of chert clasts indicate their deformation prior to erosion and incorporation into the sediment.

Munyati area

In the Munyati area the Shamvaian sediments occur in two geographically distinct areas roughly situated north and south of the Munyati River (Fig. 6.9). These are separated by a prominent shear zone and tectonically intercalated felsic volcanic rocks attributed to the Felsic Formation (Robertson, 1976). In this study the northern area is designated Munyati north and the southern area Munyati south.

Robertson (1976) subdivided the Shamvaian Group of the Munyati area into three formations (Table 6.3). The Basal Grit Formation represents the Munyati south area and consists of coarse-grained, partly pebbly sandstone and shale. The Volcaniclastic Formation represents the Munyati north area and mainly consists of conglomerate and pebbly sandstone containing felsic volcanic rock fragments. Shales of the Hematite Slate Formation are poorly exposed both to the north and south of the two areas and are not discussed further. The rocks wedged in between the northern and southern Shamvaian outcrops consist of poorly exposed massive felsic rocks, possibly former lava flows, and a well exposed rhyolite pebble conglomerate and associated sediment representing epiclastic material derived from an entirely volcanic source.

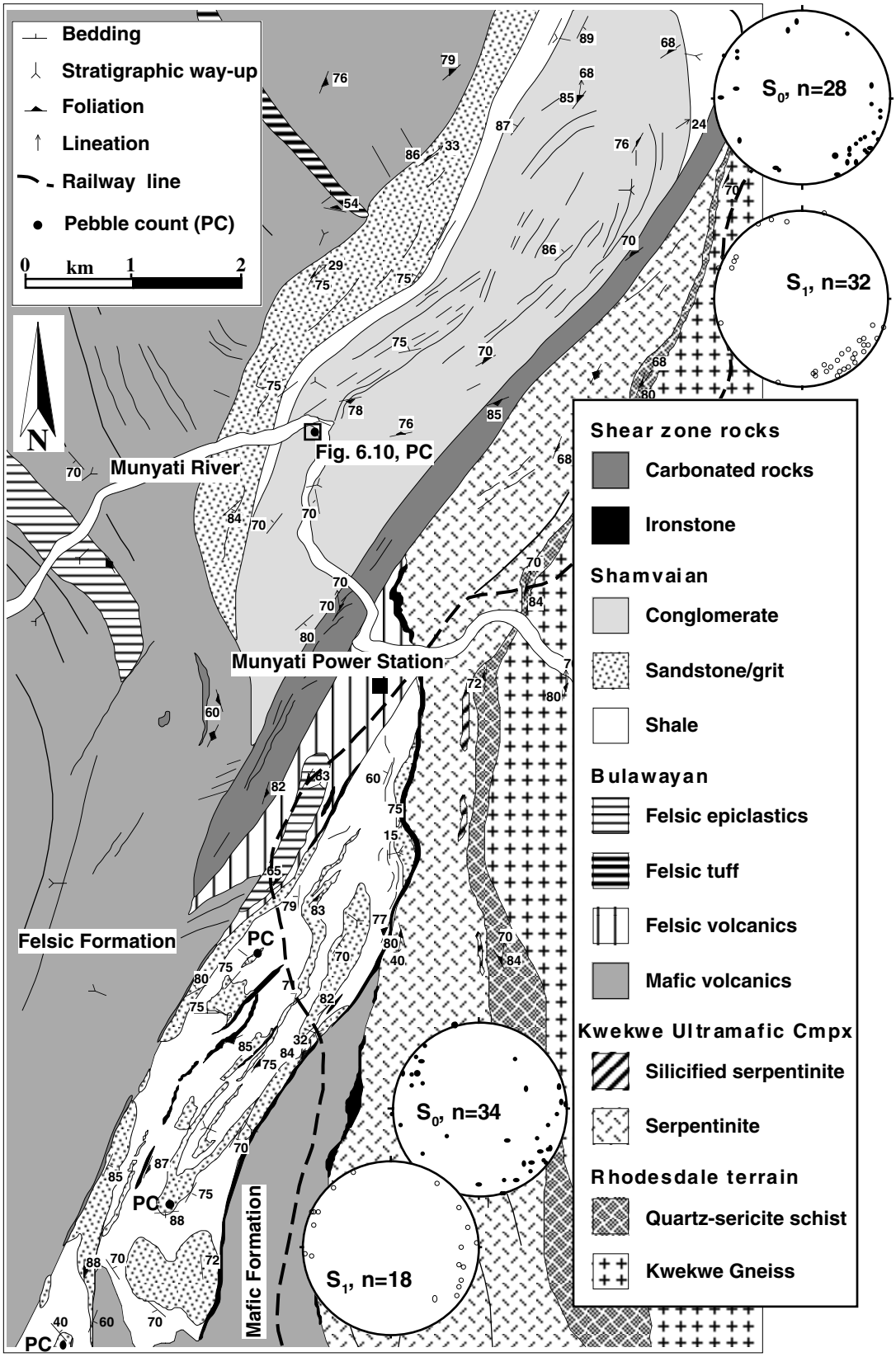

Fig. 6.9. Geological map of the Munyati area. Lower hemisphere stereographic projections of poles to bedding (S_0) and foliation (S_1) of the northern and southern Shamvaian outcrop are shown.

Basal Grit Formation (Munyati south)

Description. The area is characterized by several metres to several 10`s of metres thick horizons of sandstone/grit intercalated with shale. The sediments are tightly folded, and the fold limbs are commonly sheared (Fig. 6.9). Sandstone forms ridges, whereas shale is poorly exposed in the intervening topographic lows. Sandstone is composed of coarse sand to grit (2 mm average clast size) and locally contains scattered, well rounded pebbles rarely exceeding 3 cm in diameter. Clast-supported pebble conglomerate is rare. The abundance of vein quartz (both in sand and pebble size) gives the rock a quartzitic appearance. Beds are tabular, planar, 0.2 to >2 m thick and massive. Normal grading and parallel-laminated bed tops are rarely preserved. Graded beds are locally capped by thin shale beds. Shale forms homogeneous horizons with minor thin silt/sandstone beds.

Ironstone horizons up to 20 m thick locally occur within the succession and are common along the eastern margin of the Shamvaian outcrop. Ironstone consists of alternating layers of chert and hematite (former sulphide)-rich material; the layering is frequently brecciated. Contacts with intercalated shale and sandstone are gradational. In general, ironstone grades vertically and laterally into sediment that is more strongly foliated, Fe-impregnated and transected by quartz veins. Various stages of iron-impregnation can be observed.

Graphic logging was not possible because of discontinuous exposure and the uniformity of sandstone/grit. Pebble counting in pebbly sandstone was done at three sites. The clast composition at the different sites is similar, and the data are treated together (Fig. 6.5c). Well rounded milky white vein quartz clasts are the dominant pebble type, followed by subangular clasts of chert which comprise a banded jaspilitic, banded grey and a massive grey variety. The least common pebbles are fuchsitic quartzite clasts with a gneissic fabric and granite clasts. Fuchsitic quartzite and muscovite are relatively common as sand-sized grains.

Interpretation. The rocks in the Munyati south area are similar in terms of facies and composition to the BGF of the Sebakwe area (cf. Robertson, 1976). The tabular geometry of sandstone beds, sedimentary structures, and the interbedding with thick shale horizons indicate sub-wave base deposition by turbidity currents. Massive sandstone (S_3, Lowe, 1982) and normally graded sandstone with a variable Bouma (1962) sequence are most common and indicate rapid suspension sedimentation from sandy high-density turbidity currents.

The gradational contact of ironstone horizons to adjacent, Fe-impregnated rocks, the more strongly strained nature of intercalated and adjacent sediments, the truncation of bedding planes by ironstone horizons and the presence along the sheared eastern contact of the Shamvaian outcrop all indicate that the ironstones represent silicified and sulphide-mineralized shear zones. These ironstones are lithologically identical to those described from other greenstone belts where they occupy structural contacts between distinct lithotectonic units (Kusky and Winsky, 1995; Dirks and Jelsma, 1998; chapter 3). The occurrence of granite clasts together with vein quartz and the lack of greenstone fragments suggest a granitic source for the Munyati south area. The Rhodesdale granite-gneiss terrain is a likely source area, since it contains abundant enclaves of fuchsitic quartzite.

Volcaniclastic Formation (Munyati north)

Description. The main lithologies are conglomerate, sandstone/grit and minor shale, which are tightly folded. The eastern contact of the sedimentary sequence is formed by sheared carbonated ultramafics of the KUC. Shale adjacent to the contact is strongly foliated, sheared and Fe-enriched, whilst conglomerate is strongly foliated so that clasts form augen wrapped by a foliated matrix. Towards the western contact both Shamvaian and Bulawayan rocks are progressively more foliated, sheared and carbonated. This contact is locally occupied by a massive, iron-enriched, very fine-grained rock with abundant cross-cutting quartz veins. Lithological trends in both units are cut obliquely along the contact (Robertson, 1976).

Conglomerate occupies the eastern side of the Munyati north outcrop (Fig. 6.9) and is characterized by massive or normally graded, medium-bedded pebble conglomerate. Intercalations of coarse sandstone/grit and shale are locally common. Massive coarse sandstone to fine pebble conglomerate occurs along the western side. Clasts consist of quartz, silicified felsic rock fragments and chert. Beds are 0.5 to >5 m thick and massive or normally graded. Some graded beds are capped by parallel-stratified fine to coarse sand- or siltstone. A continuous horizon of shale (slate) separates the sandstone from conglomerate facies (Fig. 6.9). At one locality a several metres thick horizon of agglomerate was observed within this unit. The rock consists of subrounded to rounded felsic volcanic clasts embedded in a felsic tuffaceous matrix.

Sedimentary rocks of the northern area are well exposed along the Munyati River (Fig. 6.10), even though the sequence is transected by numerous shear zones disrupting the primary stratigraphy. The sediments consist of pebble conglomerate and pebbly sandstone with minor sandstone and rare shale. Conglomerate is clast-supported, and sorting is poor to moderate. The matrix consists of poorly sorted coarse-grained sand mainly comprising quartz and various rock fragments. Beds are thin to very thick and tabular with rare concave-upward scours. Beds with erosive scours have a relief of up to 1 m and contain intraclasts up to 50 cm across. Massive and normally graded conglomerate are common (Fig. 6.11a), whereas inversely graded conglomerate is rare. A crude horizontal stratification occurs in thicker beds defined by discontinuous layers of more fine or more coarse than average pebbles. Clast imbrication and discontinuous lenses of pebbly sandstone are locally common.

Pebbly sandstone consists of sandstone/grit with matrix-supported pebbles. Beds are tabular and planar and show normal grading; thin lenticular beds are rare. Common horizontal stratification is defined by an indistinct parallel lamination and discontinuous horizontal layers of fine pebble to granule conglomerate and sandstone.

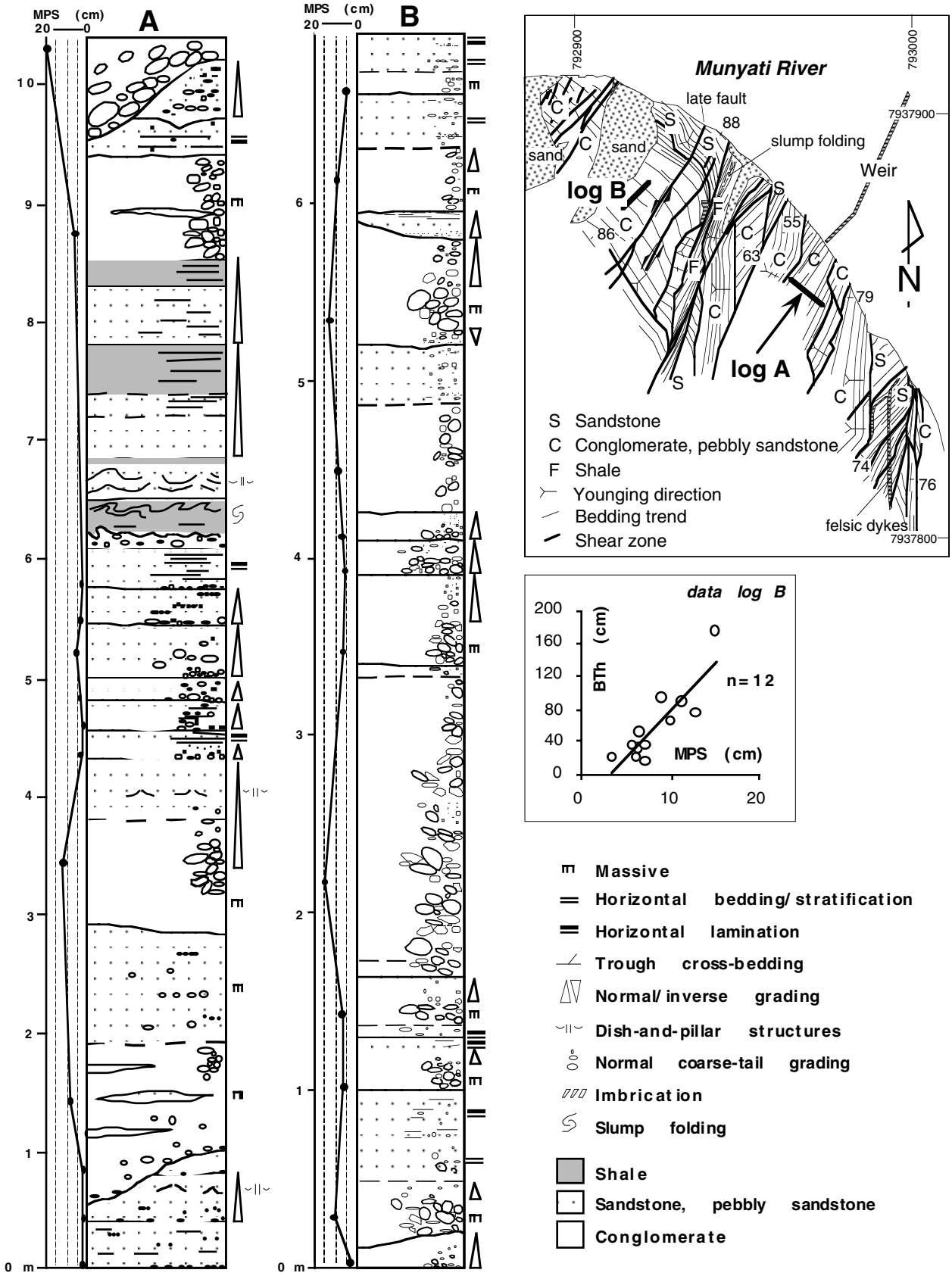

Fig. 6.10. Graphic logs of two sections of the Munyati north area and geological map (inset, modified after Dirks et al., 2001) of a rock pavement at the south bank of the Munyati River. Note the disruption of the stratigraphy. Maximum particle size (MPS) has been determined and plotted against bed thickness (BTh) for log B.

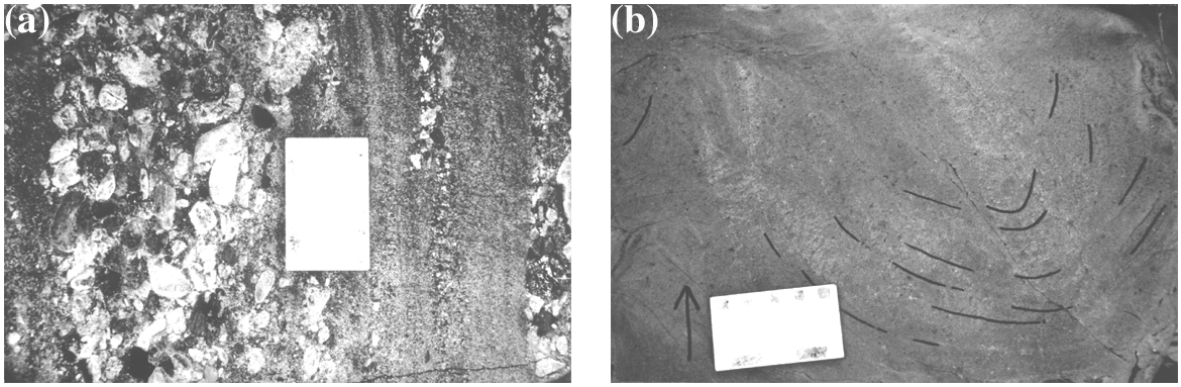

Fig. 6.11. Features of Shamvaian sediments in the Munyati north area. (a) Tabular bed of massive conglomerate is overlain by normally graded conglomerate that grades into pebbly sandstone (younging to the right). Pebbles include felsic volcanic (light grey) and jaspilitic chert (blackish) clasts. (b) Large-scale dish structure in sandstone (lamination enhanced with marker pen).

Sandstone is fine (rare) to coarse-grained with or without scattered pebbles. Pebble lags are common at the base of beds. The common horizontal lamination is locally distorted into dish structures (Fig. 6.11b). Discontinuous thin layers with pebbles/granules as well as granule lenses 5-10 cm in length and up to 1 cm thick are common. Siltstone/shale is parallel-laminated and forms rare thin to medium beds. Slump folding is common.

The different facies are arranged into upward-fining beds (Fig. 6.10). Conglomerate in the basal bed portion consists of rare inversely graded conglomerate overlain by massive and then normally graded conglomerate. The conglomerate beds show a positive correlation between maximum particle size and bed thickness (Fig. 6.10). Conglomerate grades upsection into pebbly sandstone associated with a decrease in clast size and, less frequently, associated with an increase in sand matrix. Sandstone typically overlies pebbly sandstone, and shale commonly rests gradationally on sandstone and forms the top of depositional units.

A pebble count at one locality of the river section shows fine-grained and commonly cherty, silicified felsic volcanics as the most common clast type (Figs. 6.5d and 6.11a). Chert clasts are also common and include a banded jaspilitic, a banded grey and a massive grey variety. Some chert clasts show internal folding and brecciation. Other clast types occur in subordinate amounts and include sandstone and shale intraclasts and rare quartz/feldspar porphyry clasts. The pebbles are mostly subrounded to rounded except for chert clasts which range from angular to subrounded.

Interpretation. Each individual bed represents a single depositional unit that formed during a high to low energy sedimentary event as indicated by a waning flow sequence. The absence of subaerial exposure marks and structures such as oscillatory ripples suggests deposition of the graded beds below wave base. The vertical facies distribution within a single bed is characteristic of turbidity current deposits. Massive conglomerate formed upon rapid deposition from cohesionless debris flow or high-density turbidity currents. The positive correlation between maximum particle size and bed thickness is typical for mass flow deposits (Nemec and Steel, 1984). The facies

sequence of massive conglomerate overlain by normally graded conglomerate and pebbly sandstone facies is typical for suspension sedimentation out of a high-density turbidity current when suspension fall-out rates are high, inhibiting the formation of traction structures (Lowe, 1982). Thin sandstone beds and sandstone-shale couplets, albeit rare, comprise incomplete Bouma sequences characteristic of sandy turbidites. The rarity of shale beds may indicate that the recurrence interval between successive density currents was short.

The abundance of felsic volcanic clasts and the occurrence of felsic agglomerate suggests an active volcanic terrain such as the Felsic Formation as part of the source. Banded cherts are a major component of the sedimentary rocks of both the northern and southern area, suggesting a common source. However, outcrops of such rocks are rare in the surrounding greenstones. Macgregor (1930) acknowledged this as a "remarkable feature" when the rarity of the jaspillites in the greenstones was taken into account. Folded and brecciated chert clasts indicate their deformation prior to erosion.

DISCUSSION

The Shamvaian, a strike-slip basin?

The age of the Shamvaian sediments relative to the adjacent Bulawayan rocks has been estimated on the basis of the nature of stratigraphic contacts and the composition of clasts in conglomerates. An angular discordance exists between structural trends of the Bulawayan greenstones and the contact to Shamvaian rocks (Fig. 6.1). Previous workers (Macgregor, 1932; Harrison, 1970; Robertson, 1976) have interpreted this relationship as an unconformity, thus considering the Shamvaian sediments to be the youngest rocks in the area. The greenstone-sediment contact is, however, always marked by major shear zones such as the Taba-Mali and Munyati shear zones making the construction of the age relationship on the basis of the contacts impossible (Dirks et al., 2001).

The Shamvaian sedimentary sequence forms elongate, shear zone-bounded rock units. Based entirely on this overall geometry, the Shamvaian has been interpreted as the fill of pull-apart basins which formed as a result of strike-slip along the bounding shear zones (Stowe, 1980; Campbell and Pitfield, 1994). This inference contradicts the following observations: (a) the bounding shears cut bedding in the sediments (Figs. 6.2 and 6.9); (b) mafic or intermediate volcanic clasts are absent in the sediments, in spite of the fact that such rocks surround the Shamvaian outcrops (Fig. 6.5; Macgregor, 1930; Harrison, 1970; Robertson, 1976); (c) the strike-slip shear zones represent reactivated reverse faults, and thrusting postdates deposition of the sedimentary sequences since layer-parallel early shear zones occur in the Shamvaian sequence (Fig. 6.7; Dirks et al., 2001). This suggests that the Shamvaian sedimentary basin and the source areas for the clastic sediments were removed from the greenstone domains that currently flank the Shamvaian outcrop, refuting a simple, pull-apart basin interpretation. Since contacts between the Shamvaian and adjacent rock units are in all cases sheared, the rocks originally forming the basin floor during deposition are unknown. In

fact, all distinct lithotectonic units in the MGB are shear zone-bounded and have unique lithological and structural-metamorphic characteristics. They thus represent terranes or thrust nappes. The shear zones have recorded an early west-directed thrusting event prior to strike-slip faulting, and juxtaposition of the lithotectonic units occured during thrusting (Dirks et al, 2001).

Vertical and lateral facies distribution

The Shamvaian succession in the Sebakwe area contains narrow, bedding-parallel shear zones which only in the exceptional case of good exposure such as at Sebakwe Poort can be noted in the field. Some shear zones are better discernible where they are occupied by tectonic ironstones. Tectonic displacement on these shear zones is difficult to determine, but for some shear zones it must have exceeded several kilometres (Dirks et al., 2001). Despite shearing the overall vertical facies distribution probably closely reflects the original sedimentary superposition since no structural overturning has been observed (except for the very top of the sequence at Sebakwe Poort), and the contacts between the individual formations seem to be, at least locally, gradational. If this is the case, the Shamvaian succession in the Sebakwe area consists of deep-water turbiditic facies in the lower part, shallow-water sandstone and shale in the middle, and coarse clastic alluvial sediments at the top. The middle to upper part of this large-scale shallowing-upward sequence is preserved in the coarsening-upward Sebakwe Poort section (Fig. 6.7). This trend indicates the gradual progradation of a clastic wedge into a standing water body, and the succession can be described as a large-scale deltaic sequence. This interpretation is consistent with the abundance of soft-sediment deformational features in the shoreface sandstones due to a relatively high slope of the depositional surface and high sedimentation rates. Thick, homogeneous deltaic sequences seem to be an Archaean phenomenon and have been related, among others, to a high generation rate of accomodation space, close proximity to source areas and a high sediment supply (Eriksson et al., 1998). The lack of stacked delta lobes may suggest a linear shoreline with coalescing braid-deltas related to an extensive braidplain as a sediment source. No indications for sea-level variations are observed in the sequence. However, the effect, for example, of a sea-level rise can be masked by a high sediment input, giving rise to continued progradation (Cant and Hein, 1986).

The absence of mudstone in the fluvio-deltaic sequence, both as individual beds and as intraclasts, is puzzling and can be attributed to the lack of availability of muddy material, thorough reworking of the deposits, or complete bypass of the sediment. The first interpretation is inconsistent with the occurrence of thick horizons of shale in inferred prodelta deposits, whereas the absence of shale intraclasts is inconsistent with reworking of previously deposited fines. A complete bypass of fine-grained sediment would suggest a rather perennial fluvial system with a pulsating discharge as indicated by sedimentary facies. A pulsating flow may be related to a permanent switching of the braided, low-relief channels. In addition, current systems acting on the shoreface must have been strong and permanently active. Dalrymple et al. (1985), in a model for the distribution of Cambrian shales in North America, suggested that fine-grained material bypassed an

alluvial system due to winnowing by the wind and direct transport to the ocean. Such a model is inconsistent with the complete absence of aeolian deposits within the Shamvaian fluvial facies. The rather tabular bed geometries and absence of channeling is a common feature of pre-Silurian fluvial deposits, probably due to the absence of land vegetation which, for example, affects fluvial bank stability (Schumm, 1968; Cotter, 1978; Long, 1978) resulting in the high vulnerability of overbank fines to erosion.

Interbedded sandstone and shale of the BGF are interpreted as deposits of a submarine ramp or slope apron, deep-sea depositional systems fed by a delta or a linear source (Chan and Dott, 1983; Heller and Dickinson, 1985; Reading and Richards, 1994). Shale of the HSF possibly represents a sub-wave base, prodelta deposit. Sedimentation may have been controlled by mud-dominated low-density turbidity currents that were triggered by high discharge events from the adjacent fluvial system. The muddy prodelta deposits are overlain by a thick sequence of shallow-water sandstone. The sandstones are interpreted to have formed in a high-energy shelf environment with abundant sediment influx and with a gradient to allow slumping. Shelf sandstones are overlain by fluvial braid-plain and alluvial fan conglomerates and pebbly sandstones, classifying the sequence as a braid-delta or fan-delta sequence (Nemec and Steel, 1988). The different fan-delta subenvironments exposed in the Sebakwe Poort section (pro-delta, delta front/shelf, alluvial fan) are partly separated by shear zones. A sudden increase in grain size in rocks overlying the shear zones indicates that more proximal facies were thrust onto more distal facies. A possible transitional facies (foreshore-beach/delta plain) between the shelf and fluvial sandstones is not preserved in the Sebakwe Poort section, possibly due to shearing. However, foreshore and beach deposits are rarely preserved in Archaean and Proterozoic clastic shelf sequences (Eriksson, 1998). This may indicate a dominance of the fluvial system tending to cannibalize beach deposits adjacent to the braided channels (cf. McCormick and Grotzinger, 1993). A possible transitional facies could be represented by the LGF, of which the exact position in the stratigraphic sequence is not established. The LGF seems to be restricted to the western part of the Shamvaian outcrop (Fig. 6.4) and may grade laterally to the east across the syncline axis trace either into deeper-water (HSF) shales or into shoreface sandstones of the UGF.

The association of lower deep-water (flysch) facies overlain by shallow-water and non-marine fluvial (molasse) facies is characteristic of foreland and forearc basins (e.g., Miall, 1995; Dickinson, 1995). Bedding-parallel thrust faults in the sedimentary sequence indicate that the sediments were incorporated into the thrust stack after deposition, a common feature of such basins. This relationship is particularly evident at the top of the sequence at Sebakwe Poort where a thrust nappe is preserved. Sandstone intraclasts are minor by volume but are a common component of the sediments (Fig. 6.5). Their presence may indicate erosion and cannibalization of previously deposited sediment at the basin margin during deformation. Thrusting was directed towards the west (Dirks et al., 2001), suggesting the presence of a thrust belt to the east, and gave rise to an elongate, north-south oriented basin. Palaeoflow directions in the molasse facies is generally to the north,

suggesting axial drainage, which is a common orientation in fluvial facies of foreland basins (e.g., van Houten, 1981).

The BGF and HSF can be traced northward from the Sebakwe River to the Munyati south area without major changes in composition and facies. The sediments become more strongly deformed, however, probably due to their attenuation between two major shear zones. The sediments of Munyati north are rather different in composition, but a sub-wave base depositional setting similar to those of Munyati south is inferred. The abundance of chert clasts may indicate that the sediments are laterally correlative with the Upper Shamvaian (LGF and UGF) in the Sebakwe area. This would imply that the Upper Shamvaian sediments formed in a basin that deepened to the north, an assumption that is corraborated by observed palaeocurrent and palaeoslope data.

Provenance

Clast composition of coarse clastics of the BGF favours the Rhodesdale granitoid-gneiss terrain or a compositionally similar terrain as the main sediment source. No palaeocurrent data are available to define the sediment transport path, but using the present-day geographical position of the Rhodesdale terrain suggests a westerly transport direction. For conglomerates in the upper Shamvaian, in which pebbles consist almost totally of banded chert, no direct source terrain can be identifed. The same source terrain must have been in existence during sedimentation of the lower Shamvaian formations where cherts are a common but volumetrically minor component. The absence of banded jaspilitic chert horizon in the Shamvaian suggests an extrabasinal origin. Banded jaspilitic cherts identical to the clasts in the Shamvaian sediments occur in the Mafic Formation at the top of a tectonically duplicated horizon of lower basalt, intermediate shale and grit, and upper BIF (see above; Dirks et al., 2001). If the clasts are indeed derived from the same BIF, this must have occurred prior to tectonic duplication, given the absence of basalt fragments in the sequence. Alternatively, intense chemical weathering under the influence of a CO_2-rich atmosphere, elevated surface temperatures and a humid climate postulated for the Archaean (e.g., Young, 1991; Kasting, 1993; des Marais, 1994) may have been responsible for the preferential removal of unstable mafic volcanic detritus. Such a mechanism may explain the abundance of vein quartz clasts over granitoid rock fragments in the BGF, the former being mechanically and chemically more stable but less abundant in granitoid gneisses. However, in other greenstone belts in Zimbabwe, well rounded mafic clasts are a common component of fluvial Shamvaian-type sediments (chapter 7). In addition, the transport distance of the chert clasts was probably short because of their thinly bedded nature and thus mechanical instability. Another possibility is that the same cherts overlying basalts of the Mafic Formation once covered the Rhodesdale terrain as well, thus making the Rhodesdale terrain the sole contributor for the Shamvaian detritus except for the felsic volcanic clasts in the Munyati north area. The increase in the amount of chert clasts upsection could then be explained by an increase in the proximity of the source area to the sedimentary basin. Simple unroofing should, however, yield more quartz clasts upsection in the sedimentary sequence rather than the other way round.

The Volcaniclastic Formation of Munyati north probably represents the lateral equivalent of the UGF due to the abundance of chert clasts (see above). In addition, common felsic volcanic clasts and the occurrence of felsic agglomerate in this unit suggests an active volcanic terrain as the part of the source with syndepositional volcanism. Felsic volcanic rocks of the Felsic Formation may well have been the source area. However, no traces of mafic clasts occur in the sedimentary sequence. This may imply that, during erosion, the felsites were geographically separated from the mafic greenstones with which they are now interlayered. Another possibility is that the now eroded part of the Felsic Formation had a much higher felsic to mafic rock ratio or that the detritus was shed solely from felsic volcanic centres.

Tectonic setting of the Bulawayan volcanics

In order to more fully understand the evolution of the Shamvaian sedimentary basin, the possible geodynamic setting of the adjacent volcanic rocks needs to be evaluated. Trace and REE patterns for Maliyami Formation basalts (Fig. 6.1) are similar to inferred Archaean oceanic plateau basalts (not shown) from the Abtibi belt in the Superior Province (e.g., Kerrich et al., 1999) and the Kostomuksha belt of the Baltic Shield (Puchtel et al., 1997). An oceanic origin may further be indicated by relatively high Nb (Nb_{PM}/La_{PM}=0.95-1.01) contents.

All other rock units show a conspicious negative Nb anomaly which is characteristic for rocks formed above subduction zones as well as crustally contaminated lavas (Taylor and McLennan, 1985). Similarly, correlations between $\varepsilon_{Nd(t)}$ and incompatible element ratios (e.g., $(Nb/Th)_{PM}$, $(La/Sm)_{PM}$, $(Nb/La)_{PM}$, not shown) exist, and $\varepsilon_{Nd(t)}$ values of +1.5 to +3.5 are conspicuously lower than values for depleted mantle at 2.7-2.9 Ga. The positive fractionation of the Felsic Formation volcanics and Maliyami Formation andesites is similar to modern island arc tholeiites and inferred crustally contaminated Archaean lavas of the Kambalda and Vetreny greenstone belts (Sun et al., 1988; Puchtel et al., 1997). In diagrams of Ce/Nb vs Th/Nb and $(Nb/La)_{PM}$ vs $(Nb/Th)_{PM}$ (Figs. 6.12a and 6.12b), basalt samples from the Maliyami Formation plot in the compositional field for oceanic plateaus, whereas Maliyami andesites are similar to modern oceanic arcs and crustally contaminated greenstones from Kambalda (Sun et al., 1988). Basalts from the Mafic and Felsic Formation are superimposed onto compositional fields for modern oceanic plateaus, continental flood basalts, and straddle the boundary to modern oceanic arc rocks. The positive Zr anomaly of the Maliyami andesites may point to a supra-subduction zone environment, since Zr enrichment is a characteristic feature of boninites (Crawford et al., 1989).

In summary, only the Maliyami Formation basalts can be unambigiously assigned to a geodynamic setting (oceanic plateau). For the rest, trace element criteria employed here cannot differentiate between an arc or continental (rift) setting (Table 6.2). However, on the basis of geochronologial and regional geological data discussed below, an arc origin is inferred except for the Mafic Formation basalts which may have formed upon continental break-up and rifting.

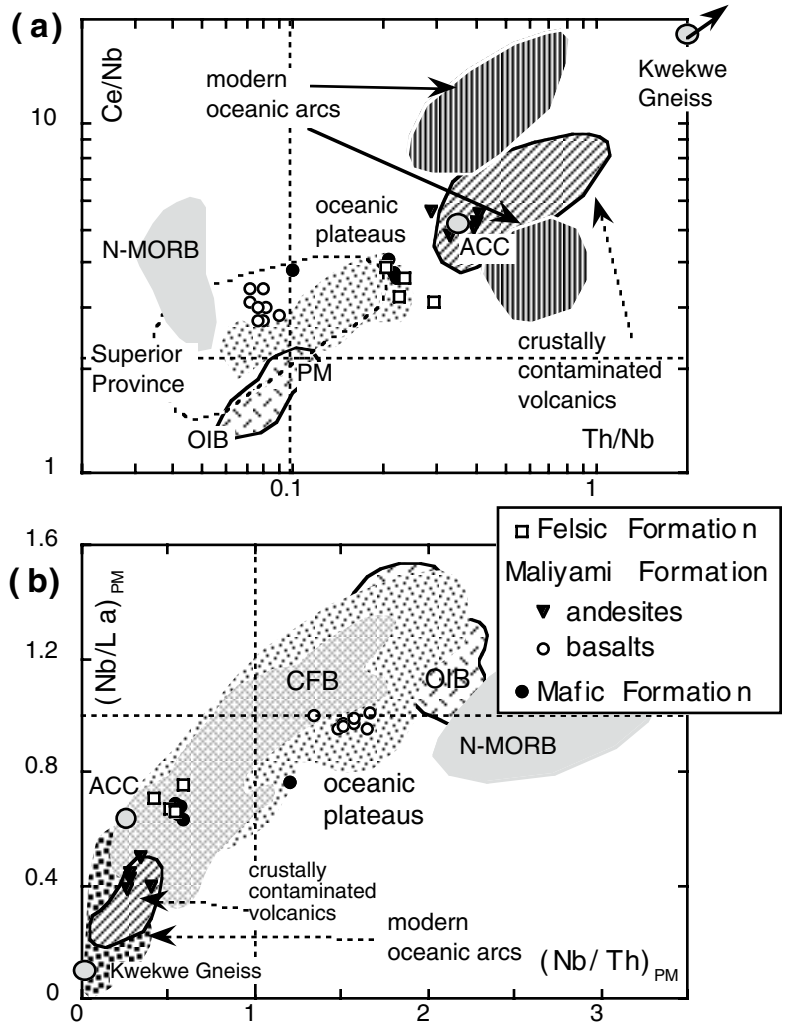

Fig. 6.12. Ce/Nb vs Th/Nb (a) and $(Nb/La)_{PM}$ vs $(Th/Nb)_{PM}$ (b) diagrams modified from Puchtel et al. (1998), Kerrich et al. (1999) and Bolhar (2001). Arc rock analyses cover a compositional spectrum between end-members with strong sediment and slab-derived fluid signatures (refer to Bolhar, 2001). ACC, Archaean continental crust; CFB, continental flood basalt; OIB, oceanic island basalt.

Towards a model for the Shamvaian in the Midlands greenstone belt

Any interpretation of the tectonic setting of the Shamvaian sequence relies heavily on geological information from the adjacent lithotectonic units. Deposition of the Shamvaian in an extensional rift and on top of an extrusive, rift-related volcanic sequence is inconsistent with the contrasting geology and age of the greenstones east and west of the Shamvaian outcrop. The Shamvaian may represent a lithologically exotic terrane that formed independently from the adjacent lithotectonic units before thrusting and lateral accretion. However, the facies sequence (flysch to molasse) and structural information (incorporation of the basin fill into the thrust stack) suggests that the Shamvaian formed in a compressional basin syntectonically with the deformation that resulted in terrane docking. A foreland or forearc setting is consistent with the deposition of the thick, monotonous sequence of shallow-marine and fluvial sandstones, given the presence of a high-relief drainage area and rapid and prolonged basin subsidence in such settings (McCormick and Grotzinger, 1993).

The following working model for the evolution of the MGB (Fig. 6.13) is suggested. The model relies heavily on recent geochronological data (Horstwood, 1998), the validity of which has not yet been rigorously tested. At c. 2.8 Ga two terrains were in existence: (1) mafic volcanics overlain by quartzose turbidites and BIF of the 2.88 Ga Mafic Formation, and (2) granitoid gneisses of the >3.4 Ga Rhodesdale terrain. The Mafic Formation may represent a rift sequence that formed during break-up of the Rhodesdale terrain and an unrecognized crustal block. A near-continental, proto-oceanic setting rather than an arc environment is indicated by the quartzose turbidite deposits di-

rectly overlying the pillow basalts as well as the lack of andesites and related rocks in the volcanic sequence. The turbidites may have formed in an early rift stage when abundant quartz sand was derived from the uplifted graben shoulders of the Rhodesdale terrain. The inclusion of Sebakwe River gneiss in the Mafic Formation may represent a remnant of the Rhodesdale terrain that was downfaulted during rifting. In the course of continued spreading leading to a narrow ocean setting, the graben shoulders possibly subsided below sea-level shutting the basin from further clastic input so that the quartzose sediments of the Mafic Formation (and maybe the Rhodesdale gneisses as well) were overlain by BIF. The preserved part of Mafic Formation may thus be classified as the upper layer of incipient oceanic or transitional crust with true oceanic crust farther to the west (present-day coordinates). Upon the onset of the relative westward movement of the Rhodesdale terrain due to a switch to convergent plate motion, most of the oceanic crust was underthrust or subducted back into the mantle, except for the possibly more buoyant transitional crust of the Mafic Formation.

At c. 2.7 Ga ago an oceanic plateau derived from a mantle plume and representing parts of the Maliyami Formation approached the continental nucleus, and parts of the Mafic Formation were underplated or subducted below the plateau. Continued plume activity resulted in the concomitant generation of basalts (from the mantle plume) and andesites (from partial melting of the slab of Mafic Formation), giving rise to the characteristic bimodality of the Maliyami rocks and explaining the difference in T_{DM} model ages. The trend towards a more felsic composition of volcanic rocks from the Maliyami to the Felsic Formation indicates eventual cessation of plume activity and an increase in more typical arc volcanism and arc differentiation. At the same time, the uppermost layer of the remaining Mafic Formation was tectonically imbricated during continued convergence. Between the suture of Mafic Formation/Rhodesdale terrain and Maliyami/Felsic Formation terrain a sedimentary basin developed that was filled, in the early stage, by deep-water clastics (Lower Shamvaian). In this stage of evolution the duplicated sliver of Mafic Formation remained mostly submerged so that the Rhodesdale terrain was the main source for the sedimentary basin fill. During continued compression the obducted mafic material was tectonically duplicated whereas probably most of the overlying banded cherts were detached from the lower unit, subaerially emerged, and eroded to give rise to abundant chert clasts in the upper part of the Shamvaian basin fill.

Throughout the basin evolution the oceanic plateau/volcanic arc to the west remained submerged except for the latest stage when felsic volcanic rocks became subjected to erosion to form detritus in the Shamvaian of Munyati north. These felsic rocks probably formed from concomitant volcanic eruptions as indicated by the presence of felsic agglomerate in the Shamvaian sequence. Continued east-west shortening resulted in the accretion, internal thrusting and, locally, upright folding of the individual lithotectonic units. Contemporaneous with tectonic stacking was the emplacement of the Kwekwe Ultramafic Complex as a large intrusive sheet along a major thrust zone between the greenstones and the granitoid-gneiss terrain. Horizontal accretion was followed by strike-slip faulting along the former thrust faults. Strike-slip motion represents a late phase of prolonged E-W shortening (Dirks et al., 2001) and possibly indicates that compression resulted from oblique

convergence and terrane accretion, a similar tectonic scenario to the Cordilleran orogen of western North America (e.g., Jones, 1990).

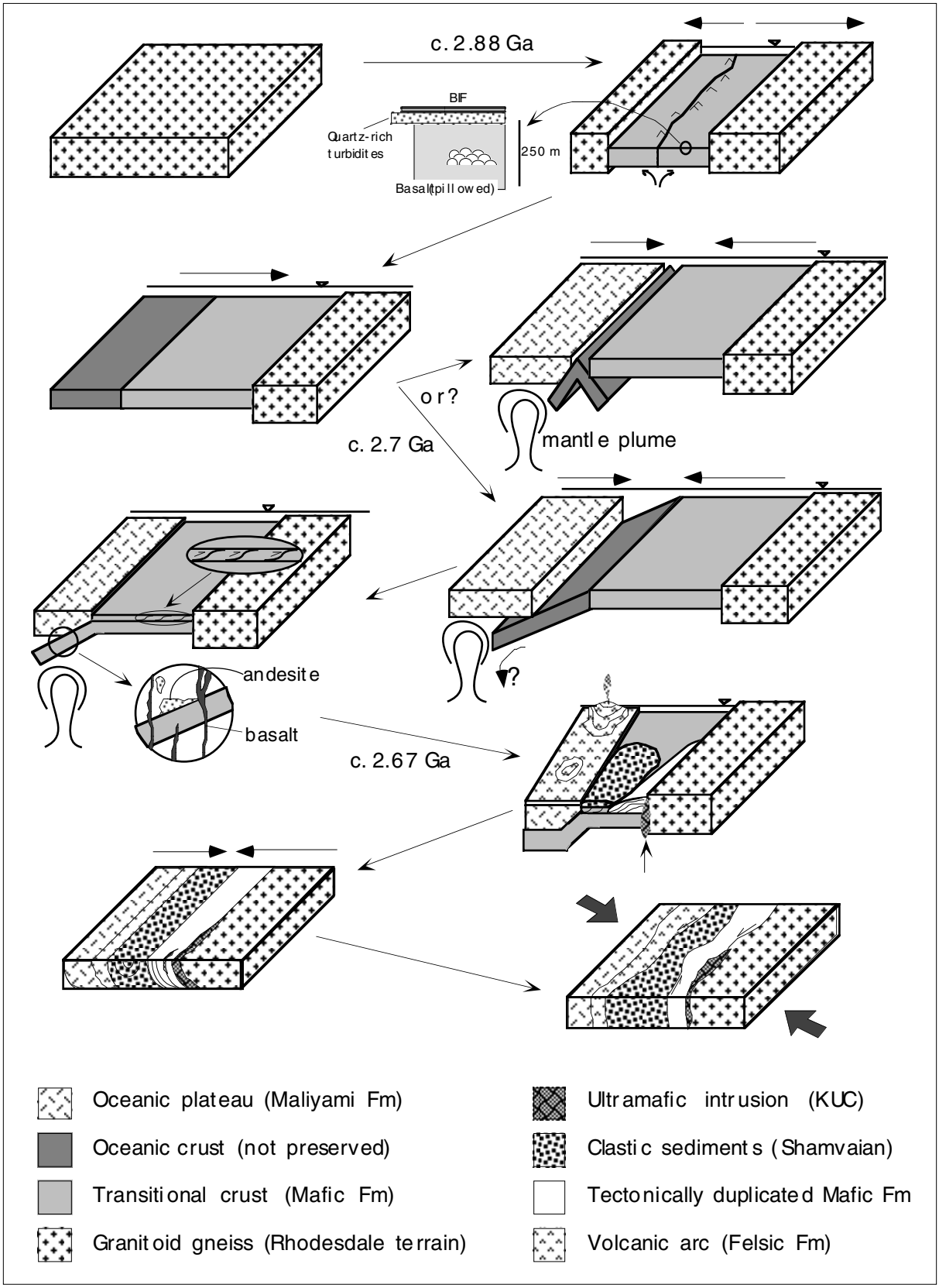

Fig. 6.13. Simplified (plate) tectonic model (not to scale) for the evolution of the MGB.

REFERENCES

Allen, P.A., 1981. Sediments and processes on a small alluvial stream-flow dominated Devonian alluvial fan, Shetland Islands. Sediment. Geol. 29, 31-66.

Ballance, P.F., 1984. Sheet-flow-dominated gravel fans of the non-marine Middle Cenozoic Simmler Formation, central California. Sediment. Geol. 38, 337-359.

Barrett, T.J., Fralick, P.W., 1989. Turbidites and iron-formations, Beardmore-Geraldton, Ontario: application of a combined ramp/fan model to Archaean clastic and chemical sedimentation. Sedimentology 36, 221-234.

Bickle, M.J., Nisbet, E.G., Martin, A., 1994. Archaean greenstone belts are not oceanic crust. J. Geol. 102, 121-138.

Bliss, N.W., 1970. The geology of the country around Gatooma. Rhod. Geol. Surv. Bull. 64, 240 pp.

Bluck, B.J., 1962. Deposition of some Upper Red Sandstone conglomerates in the Clyde area; a study in the significance of bedding. Scott. J. Geol. 3, 139-167.

Bolhar R., 2001. Archaean mafic magmatism and crust formation in the eastern Pilbara craton (Western Australia) and Belingwe greenstone belt (Zimbabwe). Ph.D. thesis, University of Melbourne, 183 pp.

Bouma, A.H., 1962. Sedimentology of some flysch deposits: a graphic approach to facies interpretation. Elsevier, Amsterdam, 168 pp.

Campbell, S.D.G., Pitfield, P.E.J., 1994. Structural controls of gold mineralization in the Zimbabwe Craton - Exploration guidelines. Zim. Geol. Surv. Bull. 101, 270 pp.

Cant, D.J., Hein, F.J., 1986. Depositional sequences in ancient shelf sediments: some contrasts in style. In: Knight, R.J., McLean, J.R. (Eds.), Shelf sands and sandstones. Can. Soc. Pet. Geol. Mem. 11, 303-312.

Chan, M.A., Dott, R.H.Jr., 1983. Shelf and deep-sea sedimentation in Eocene forearc basin, western Oregon—fan or non-fan? Am. Assoc. Petrol. Geol. Bull. 67, 2100-2116.

Condie, K.C., Harrison, N.M., 1976. Geochemistry of the Archaean Bulawayan Group, Midlands greenstone belt, Rhodesia. Precambrian Res. 3, 253-271.

Cotter, E., 1978. The evolution of fluvial style, with special reference to the central Appalachian Paleozoic. In: Miall, A.D. (Ed.), Fluvial sedimentology. Can. Soc. Pet. Geol. Mem. 5, 361-383.

Crawford, A.J., Falloon, T.J., Green, D.H., 1989. Classification, petrogenesis, and tectonic setting of boninites. In: Crawford, A.J. (Ed.), Boninites and related rocks. London, Unwin-Hyman, pp. 1-49.

Dalrymple, R.W., Narbonne, G.M., Smith, L., 1985. Eolian action and the distribution of Cambrian shales in North America. Geology 13, 607-610.

des Marais, D.J., 1994. The Archaean atmosphere: its composition and fate. In: Condie, K.C. (Ed.), Archaean Crustal Evolution. Developments in Precambrian Geology 11, Elsevier, Amsterdam, 528 pp.

Dickinson, W.R., 1995. Forearc basins. In: Busby, C.J., Ingersoll, R.V. (Eds.), Tectonics of Sedimentary Basins. Blackwell, Cambridge, pp. 221-261 .

Dirks, P.H.G.M., Jelsma, H.A., 1998. Horizontal accretion and stabilization of the Archean Zimbabwe Craton. Geology 26, 11-14.

Dirks, P.H.G.M., Jelsma, H.A., Hofmann, A., 2001. Thrust-related accretion of an Archaean greenstone belt in the Midlands of Zimbabwe. J. Struct. Geol., in press.

Dott, R.H., Bourgeois, J., 1982. Hummocky stratification: significance of its variable bedding sequences. Geol. Soc. Am. Bull. 93, 663-680.

Dougherty-Page, J.S., 1994. The evolution of the Archean continental crust of northern Zimbabwe. Ph.D. thesis (unpubl.), The Open University, Milton Keynes.

Eriksson, P.G., Condie, K.C., Tirsgaard, H., Mueller, W.U., Altermann, W., Miall, A.D., Aspler, L.B., Catuneanu, O., Chiarenzelli, J.R., 1998. Precambrian clastic sedimentation systems. Sediment. Geol. 120, 5-53.

Foster, R.P., Mann, A.G., Stowe, C.W., Wilson, J.F., 1986. Archean gold mineralization in Zimbabwe. In: Anhaeusser, C.R., Maske, S. (Eds.), Mineral deposits in Southern Africa. Geol. Soc. S. Afr., pp. 43-112.

Harris, C.W., Eriksson, K.A., 1990. Allogenic controls on the evolution of storm to tidal shelf sequences in the Early Proterozoic Uncompahgre Group, southwest Colorado, USA. Sedimentology 37, 189-213.

Harrison, N.M., 1970. The geology of the country around Que Que. Rhod. Geol. Surv. Bull. 67, 1-125.

Heller, P.L., Dickinson, W.R., 1985. Submarine ramp facies model for delta-fed, sand-rich turbidite systems. Am. Assoc. Petrol. Geol. Bull. 69, 960-976.

Herrington, R.J., 1995. Late Archean structure and gold mineralization in the Kadoma region of the Midlands greenstone belt, Zimbabwe. In: Coward, M.P., Ries, A.C. (Eds.), Early Precambrian Processes. Geol. Soc. Lond. Spec. Publ. 95, pp. 173-191.

Horstwood, M.S.A., 1998. Stratigraphy, geochemistry and zircon geochronology of the Midlands greenstone belt, Zimbabwe. Ph.D. thesis (unpubl.), Univ. of Southampton, 215 pp.

Horstwood, M.S.A., Nesbitt, R.W., Noble, S.R., Wilson, J.F., 1999. U-Pb zircon evidence for an extensive early Archean craton in Zimbabwe: a reassessment of the timing of craton formation, stabilization, and growth. Geology 27, 707-710.

Jelsma, H.A., Vinyu, M.L., Valbracht, P.J., Davies, G.R., Wijbrans, J.R., Verdurmen, E.A.T., 1996. Constraints on Archean crustal evolution of the Zimbabwe craton: a U-Pb zircon, Sm-Nd and Pb-Pb whole-rock isotope study. Contrib. Mineral. Petrol. 124, 55-70.

Jones, D.L., 1990. Synopsis of late Palaeozoic and Mesozoic terrane accretion within the Cordillera of western North America. Phil. Trans. R. Soc. Lond. A331, 479-486.

Kasting, J.F., 1993. Earth´s early atmosphere. Science 259, 920-926.

Kerrich, R., Polat, A., Wyman, D., Hollings, P., 1999. Trace element systematics of Mg-, to Fe tholeiitic basalt suites of the Superior Province: implications for Archaean mantle reservoirs and greenstone belt genesis. Lithos 46, 163-187.

Kusky, T.M., 1998. Tectonic setting and terrane accretion of the Archean Zimbabwe craton. Geology 26, 163-166.

Kusky, T.M., Kidd, W.S.F., 1992. Remnants of an Archaean oceanic plateau, Belingwe Greenstone Belt, Zimbabwe. Geology 20, 43-46.

Kusky, T.M., Winsky, P.A., 1995. Structural relationships along a greenstone/shallow water shelf contact, Belingwe greenstone belt, Zimbabwe. Tectonics 14, 448-471.

Long, D.G.F., 1978. Proterozoic stream deposits: some problems of recognition and interpretation of ancient sandy fluvial systems. In: Miall, A.D. (Ed.), Fluvial sedimentology. Can. Soc. Pet. Geol. Mem. 5, 313-341.

Lowe, D. R., 1982. Sediment gravity flows: II. Depositional models with special reference to the deposits of high-density turbidity currents. J. Sediment. Petrol. 52, 279-297.

Macgregor, A.M., 1930. The geology of the country between Gatooma and Battlefields. S. Rhod. Geol. Surv. Bull. 17, 144pp.

Macgregor, A.M., 1932. The geology of the country around Que Que, Gwelo district. S. Rhod. Geol. Surv. Bull. 20, 113pp.

Macgregor, A.M., 1951. Some milestones in the Precambrian of Southern Rhodesia. Proc. Geol. Soc. S. Afr. 54, 27-71.

McCormick, D.S., Grotzinger, J.P., 1993. Distinction of marine from alluvial facies in the Palaeoproterozoic (1.9 Ga) Burnside Formation, Kilohigok basin, N.W.T., Canada. J. Sediment. Petrol. 63, 398-419.

Miall, A.D., 1995. Collision-related foreland basins. In: Busby, C.J., Ingersoll, R.V. (Editors), Tectonics of Sedimentary Basins. Blackwell, Cambridge, pp. 393-424.

Nägler, T.F., Kramers, J.D., Kamber, B.S., Frei, R., Prendergast, M.D.A., 1997. Growth of subcontinental lithospheric mantle beneath Zimbabwe started at or before 3.8 Ga: Re-Os study on chromites. Geology 25, 983-986.

Nemec, W., Steel, R.J., 1984. Alluvial and coastal conglomerates: their significant features and some comments on gravelly mass-flow deposits. In: Koster, E.H., Steel, R.J. (Eds.), Sedimentology of gravels and conglomerates. Can. Soc. Petrol. Geol. Mem. 10, pp. 1-31.

Nemec, W., Steel, R.J., 1988. What is a fan delta and how do we recognize it? In: Nemec, W., Steel, R.J. (Eds.), Fan Deltas. Blackie, 3-13.

Nottvedt, A., Kreisa, R.D., 1987. Model for the combined-flow origin of hummocky cross-stratification. Geology 15, 357-361.

Pickering, K.T., Stow, D.A.V., Watson, M., Hiscott, R.N., 1986. Deep-water facies, processes and models: a review and classification scheme for modern and ancient sediments. Earth Sci. Rev. 23, 74-174.

Puchtel, I.S., Hofmann, A.W., Jochum, K.P., Mezger, K., Shchipansky, A.A., Samsonov, A.V., 1997. The Kostomiksha greenstone belt, NW Baltic Shield: remnant of a late Archaean oceanic plateau? Terra Nova 9, 87-90.

Puchtel, I.S., Arndt, N.T., Hofmann, A.W., Haase, K.M., Kröner, A., Kulikov, V.S., Kulikova, V.V., Garbe-Schönberg, C.D., Nemchin, A.A., 1998. Petrology of mafic lavas within the Onega plateau, central Karelia: evidence for 2.0 Ga plume-related continental crustal growth in the Baltic Shield. Contrib. Mineral. Petrol. 130, 134-153.

Reading, H.G., Richards, M., 1994. Turbidite systems in deep-water basin margins classified by grain size and feeder system. Am. Assoc. Petrol. Geol. Bull., 78, 792-822.

Reineck, H.E., Wunderlich, F., 1968. Classification and origin of flaser and lenticular bedding. Sedimentology 11, 99-104.

Robertson, I.D.M., 1976. The geology of the country around Battlefields, Gatooma District. Rhod. Geol. Surv. Bull. 76, 258p.

Schumm, S.A., 1968. Speculations concerning paleohydrologic controls of terrestrial sedimentation. Geol. Soc. Am. Bull. 79, 1573-1588.

Soegaard, K., Eriksson, K.A., 1989. Origin of thick, first cycle quartz arenite successions: evidence from the 1.7 Ga Ortega Group, Northern New Mexico. Precambrian Res. 43, 129-141.

Steel, R.J., 1974. New Red Sandstone floodplain and piedmont sedimentation in the Hebridean Province, Scotland. J. Sediment. Petrol., 44, 336-357.

Stowe, C.W., 1980. Wrench tectonics in the Archaean Rhodesian craton. Trans. Geol. Soc. S. Afr. 83, 193-205.

Sun, S.S., McDonough, W.F., 1989. Chemical and isotopic systematics of oceanic basalts, implications for mantle compositions and processes. Geol. Soc. Lond. Spec. Publ. 42, p. 313-345.

Sun, S.S., Nesbitt, R.W., McCulloch, M.T., 1988. Geochemistry and petrogenesis of Archaean and early Proterozoic siliceous high-Mg basalts. In: Crawford, A.J. (Ed.), Bonitites. London, Unwin Hyman, p. 148-173.

Taylor, S.R., McLennan, S.M., 1985. The continental crust: its composition and its evolution. Oxford, Blackwell, 312 p.

Todd, S.P., 1989. Stream-driven, high-density gravelly traction carpets: possible deposits in the Trabeg Conglomerate Formation, SW Ireland and some theoretical considerations of their origin. Sedimentology 36, 513-530.

van Houten, F.B., 1981. The odyssey of molasse. Geol. Assoc. Can. Spec. Pap. 23, 35-48.

Wilson, J.F., 1979. A preliminary reappraisal of the Rhodesian basement complex. In: Anhaeusser, C.R., Foster, R.P., Stretton, T. (Eds.), A symposium on mineral deposits and transportation and deposition of metals. Geol. Soc. S. Afr. Spec. Publ. 5, pp. 1-23.

Wilson, J.F., 1981. The granite-gneiss-greenstone shield, Zimbabwe. In: Hunter, D.R. (Ed.), Precambrian of the southern hemisphere. Elsevier, Amsterdam, pp. 454-488.

Wilson, J.F., 1990. A craton and its cracks: some of the behaviour of the Zimbabwe block fom the late Archean to the Mesozoic in response to horizontal movements, and the significance of some of its mafic dyke fracture patterns. J. Afr. Earth Sci. 10, 483-501.

Wilson, J.F., Nesbitt, R.W., Fanning, C.M., 1995. Zircon geochronology of Archaean felsic sequences in the Zimbabwe craton: a revision of greenstone stratigraphy and a model for crustal growth. In: Coward, M.P., Ries, A.C. (Eds.), Early Precambrian processes. Geol. Soc. Lond. Spec. Publ., 95, pp. 109-126.

Young, G.M., 1991. The geologic record of glaciation: relevance to the climatic history of the Earth. Geosci. Can. 18, 100-108.

CHAPTER 7

Late Archaean clastic sediments (Shamvaian Group) of the Zimbabwe craton: first observations from the Bindura-Shamva greenstone belt

Axel Hofmann, Paul H.G.M. Dirks, and Hielke A. Jelsma
submitted to Canadian Journal of Earth Sciences

Abstract—The ~2.65 Ga old Shamvaian Group sediments occur as a folded succession in the central part of the Bindura-Shamva greenstone belt of Zimbabwe. The sediments comprise distinct, shear zone-bounded tectonstratigraphic units which may be stratigraphically arranged as follows. The lower part of the sedimentary succession represents a transgressive, fining-upward sequence of alluvial fan conglomerate, overlain by fluvial braid-plain pebbly sandstone and marine shoreface sandstone. Detritus was derived from a mid-Archaean granitoid-gneiss terrain situated to the east. Sediment supply and subsidence rate must have been high. Shallow shelf sedimentation was followed by deep-water (sub-wave base) deposition by turbidity currents, giving rise to a thick succession of fine to coarse clastic material. The turbidite deposits were locally overlain by shallow-marine sandstone and fluvial to alluvial fan conglomerate. The upward increase in the abundance of intermediate and felsic volcanic clasts suggest an increase in the proximity of a volcanic terrain such as a volcanic arc. Deposition was followed by layer-parallel shearing during thrust belt-style tectonic deformation. Major shear zones developed preferentially along the contact between shallow and deep-marine facies associations. Basin initiation may have been related to extensional tectonics, possibly on stretched continental crust, whereas later stages of basin history may have been similar to compressional foreland or forearc settings. Sedimentary facies, stratigraphy and facies distribution are remarkably similar to some late Archeaen sedimentary sequences of the Superior Province in Canada.

INTRODUCTION

Much of the current understanding of the geology of Archaean greenstone belts, including many controversial views, originated from studies of the granitoid-greenstone terrain of the Zimbabwe craton (Macgregor 1951; Bickle et al. 1975; Stowe 1984; Ramsay 1989; Bickle et al. 1994; Shackleton 1995; Wilson et al. 1995; Blenkinsop et al. 1997; Ridley et al. 1997; Dirks and Jelsma 1998*a*). The volcano-sedimentary rocks of the Zimbabwean greenstone belts have been interpreted either as rift sequences that formed on pre-existing continental basement and were deformed during the diapiric rise of granite domes (Wilson et al. 1995) or as geologically distinct terranes that were amalgamated during horizontal tectonic processes (Dirks and Jelsma 1998*a*). The main episode of formation of supracrustal rocks in the Zimbabwe craton occurred in the late Archaean with the deposition of Upper Bulawayan Group greenstones (~2.7 Ga). This group is dominated by thick successions of tholeiitic basalts with komatiite intercalations and contains minor units of intermediate to felsic volcanic rocks and volcaniclastic sediments. Basaltic volcanism was followed by the deposition of Shamvaian Group siliciclastic sediments (~2.65 Ga), and at ~2.6 Ga stabilization of the craton occurred with the intrusion of large volumes of potassic granites of the Chilimanzi suite.

Sedimentary rocks that are remarkably similar in age, composition and stratigraphic position to the Shamvaian are common in greenstone belts of the Superior Province of Canada where they have been extensively studied for several decades (Pettijohn 1943; Turner and Walker 1973; Ojakangas 1985; Mueller and Corcoran 1998). In Zimbabwe, the Shamvaian sedimentary rocks have only been studied on a regional scale during mapping projects of the Geological Survey. As a result, the knowledge of the Shamvaian Group is limited, despite being the host of some major gold deposits, and sedimentological studies are lacking. This paper is aimed at providing basic sedimentological data of the Shamvaian sediments, understanding the stratigraphic framework on the scale of a single greenstone belt, deducing the depositional environments in which the sedimentary rocks formed, and defining the likely tectonic setting of sedimentary basin formation. For this purpose the Shamvaian was studied at its type locality in the Bindura-Shamva greenstone belt.

GEOLOGICAL SETTING

The Bindura-Shamva greenstone belt occurs in the northern part of the Zimbabwe craton (Fig. 7.1a) and comprises Upper Bulawayan volcanic lithologies and Shamvaian clastic sediments. The greenstone belt is bound by the Chinamora, Murehwa and Madziwa granite-gneiss terrains to the southwest, southeast and north, respectively. Upper Bulawayan rocks occupy the flanks, and Shamvaian sediments occur as a folded succession within the core of the greenstone belt. The basal succession of the Bulawayan greenstone sequence structurally overlies the Chinamora batholith (Fig. 7.1a) and is represented by felsic volcanics of the Iron Mask Formation (Table 1.1), followed by mafic volcanics of the Arcturus Formation. The base of the Arcturus Formation is interpreted as a shear zone (Baldock 1991; Ridley et al. 1997; Jelsma and Dirks 2000). The Arcturus Formation is overlain in the west by felsic volcanics of the Passaford Formation, whereas elsewhere it is overlain

by Shamvaian sediments. The Iron Mask and Passaford Formations have yielded identical U-Pb zircon dates (Table 1.1) and may represent the same but tectonically stacked and repeated lithotectonic unit (Jelsma and Dirks 2000). However, variable ages for the Iron Mask Formation have been reported as well (Table 1.1), indicating the complexity of this unit. Along the northern margin of the greenstone belt, the Upper Bulawayan comprises the Mungari Formation, similar in composition to the Arcturus Formation, but with intercalations of felsic volcanics of the Maparu Formation. The Shamvaian sediments overlie the Bulawayan greenstones, and the contact is mostly sheared but locally conformable. Available geological evidence summarized by Jelsma and Dirks (2000) indicate deposition of the Shamvaian sediments at ~2645 Ma ago. A U-Pb zircon date of 2672±12 Ma (Jelsma et al. 1996) for a feldspar porphyry intrusive into Shamvaian sediments has been interpreted as a mixed age and too old (Jelsma and Dirks 2000).

Table 1.1. Stratigraphic subdivision, lithologies and age of the Bindura-Shamva greenstone belt.

Stratigraphic unit	Lithology	Age
Shamvaian Group	conglomerate, sandstone, shale	2.7-3.2 Ga (provenance)[3]
Bulawayan Group north		
Maparu Formation	rhyolitic felsic volcanics, volcaniclastic sediments	2697±9 Ma[1]
Mungari Formation	pillowed and massive tholeiitic basalts	
Bulawayan Group south		
Passaford Formation	felsic volcanics and volcaniclastic sediments	2643±8 Ma[1]
Arcturus Formation	pillowed and massive tholeiitic basalt; minor komatiitic basalt, serpentinite, ultramafic schist; rare ironstone, chert, limestone, shale	
Iron Mask Formation	calc-alkaline rhyodacitic volcanic and volcaniclastic rocks; minor ironstone, limestone and chert	2645±4 Ma[1], 2715±15 Ma[2]

[1]Wilson et al. (1995, SHRIMP U-Pb zircon); [2]Jelsma et al. (1996, TIMS U-Pb zircon); [3]Dougherty-Page (1994, Kober Pb-Pb zircon evaporation)

Wilson et al. (1995) and Jelsma et al. (1996) interpreted the stratigraphic succession of the Bindura-Shamva greenstone belt as an upright synclinorium which pinches out eastward and is commonly sheared between closely spaced batholiths, but is open and little strained in cleavage triple points. Deformation was explained by ballooning plutonism or pluton diapirism (Ramsay 1989; Jelsma et al. 1993). Related deformation geometries include shear zones along the greenstone-granite contacts recording "off-the-dome" movements, radial lineation patterns around gneiss domes and finite strain distribution patterns in the greenstones. Movement along layer-parallel shear zones in the greenstone stratigraphy was related to pluton emplacement (Ramsay 1989; Jelsma et al. 1993).

In addition, Dirks and Jelsma (1998*a, b*) and Jelsma and Dirks (2000) reported the presence of two separate amphibolite facies metamorphic assemblages and two mineral lineations in shear zones,

suggestive of two distinct structural-metamorphic events in the Bindura-Shamva greenstone belt. An early set of amphibolite-grade D_1 structures and synkinematic M_1 metamorphic assemblages were attributed to an episode of layer-parallel shearing. This resulted in sequential west-directed imbricate stacking and recumbent folding of distinct tectonostratigraphic greenstone sequences. Deposition of the Shamvaian is envisaged as syntectonic with D_1. D_2/M_2 fabrics, strain patterns and contact aureoles overprint D_1 geometries and are related to the diapiric emplacement of granite domes such as the Chinamora batholith (Fig. 7.1a). The Bindura-Shamva greenstone belt is not a simple syncline, since (a) the stratigraphy of the Bulawayan greenstones along the northern limb of the belt is different from the stratigraphy along the southern limb (Stidolph 1977; Jelsma et al. 1996) and (b) younging indicators and stratigraphic asymmetries indicate that no large-scale syncline exists within the Shamvaian sediments in the core of the belt (Jelsma and Dirks 2000). Layer-parallel D_1 mylonite and schist zones have been reported to separate Shamvaian sediments from the greenstones to the north along which younging reversals and truncation of primary bedding occur. Locally, foliation trajectories and younging indicators within the Shamvaian sediments show complex folds and shear zones.

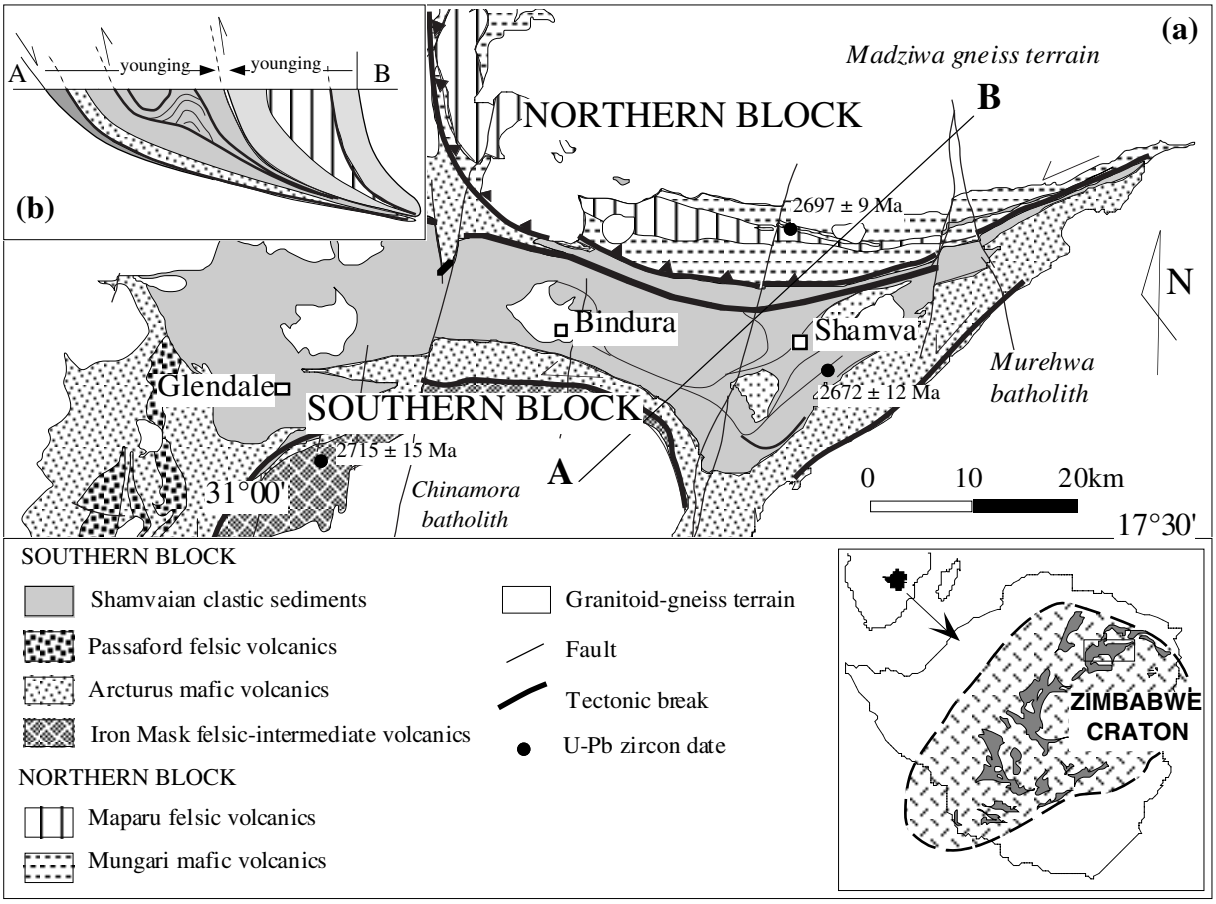

Fig. 7.1. (a) Geological map of the Bindura-Shamva greenstone belt and surrounding granitoid-gneiss terrains. Shown are prominent shear zones and selected age data (see text for references). (b) Schematic cross-section of the greenstone belt along section line A-B (modified after Dirks and Jelsma 1998a).

Jelsma and Dirks (2000) proposed a subdivision of the greenstone belt into two separate lithotectonic blocks, a southern (footwall) block and a northern (hangingwall) block that include internally stacked mafic-felsic greenstone stratigraphies (Figs. 7.1a, 7.1b). The volcanics of the southern block are capped by Shamvaian sediments that are tectonically overlain by the inverted northern block, interpreted as the downward facing limb of a large nappe that moved westward, overriding the greenstones of the southern block. The nappe is thought to be represented by gneisses of the Madziwa terrain enveloped by greenstones of the Maparu and Mungari Formations. In this model, the Shamvaian clastic sediments were interpreted as a syndeformational succession that formed in a foreland basin (Jelsma and Dirks 2000).

THE SHAMVAIAN SEDIMENTS

Stidolph (1977) subdivided the Shamvaian Group into two lithostratigraphic units, (1) the Lower Shamvaian consisting of volcaniclastic sediments and pyroclasts, and (2) the Upper Shamvaian consisting of a coarse-grained siliciclastic association characterized by the presence of granitic detritus.

In the course of this study three tectonostratigraphic units, termed the Tsambe, Pote, and Mazowe Formations that are separated from each other by shear zones (Fig. 7.2) were differentiated. The units differ in lithofacies and/or composition from each other. The Tsambe Formation is equivalent to the Lower Shamvaian of Stidolph (1977) and is restricted to the southern part of the Shamvaian outcrop. The Pote and Mazowe Formations represent the Upper Shamvaian of Stidolph (1977). The Pote Formation forms most of the central part of the Shamvaian outcrop, whereas the Mazowe Formation is restricted to a 1-3 km wide unit in the northern part of the outcrop. The southern contact of the Mazowe Formation is termed the Wolley shear zone. Along the northern contact with Bulawayan volcanics occurs a several tens of metres wide schistose zone termed the Wapley shear zone (Jelsma and Dirks 2000; Fig. 7.2).

The area around Shamva town comprises all three formations which are slightly better exposed than farther to the west where the sediments mostly occupy cultivated plains. Five localities have been investigated in detail and will be discussed below (Fig. 7.2). These have been chosen (a) to cover the different stratigraphic units of the Shamvaian, (b) to give an indication of the style of deformation of the sedimentary strata, and, importantly, (c) because of reasonably good exposure. The sedimentological analysis included graphic logging, palaeoflow determination and pebble counting. Logging was restricted to small, discontinuous outcrops. Palaeoflow directions were determined from cross-bedding orientation. The analysis included data restoration to account for E-W folding and subsequent N-S cross-folding of the sedimentary sequence. The orientation of fold axes was established at most localities. To account for variations in the orientation of bedding at the different localities due to cross-folding, an original east-west strike of the fold axes has been assumed. Despite being metamorphosed to greenschist and amphibolite facies grade, the rocks will be classified according to their unmetamorphosed state. Lithofacies and inferred depositional environment will be discussed first. The results of pebble counting at the different localities will be treated separately.

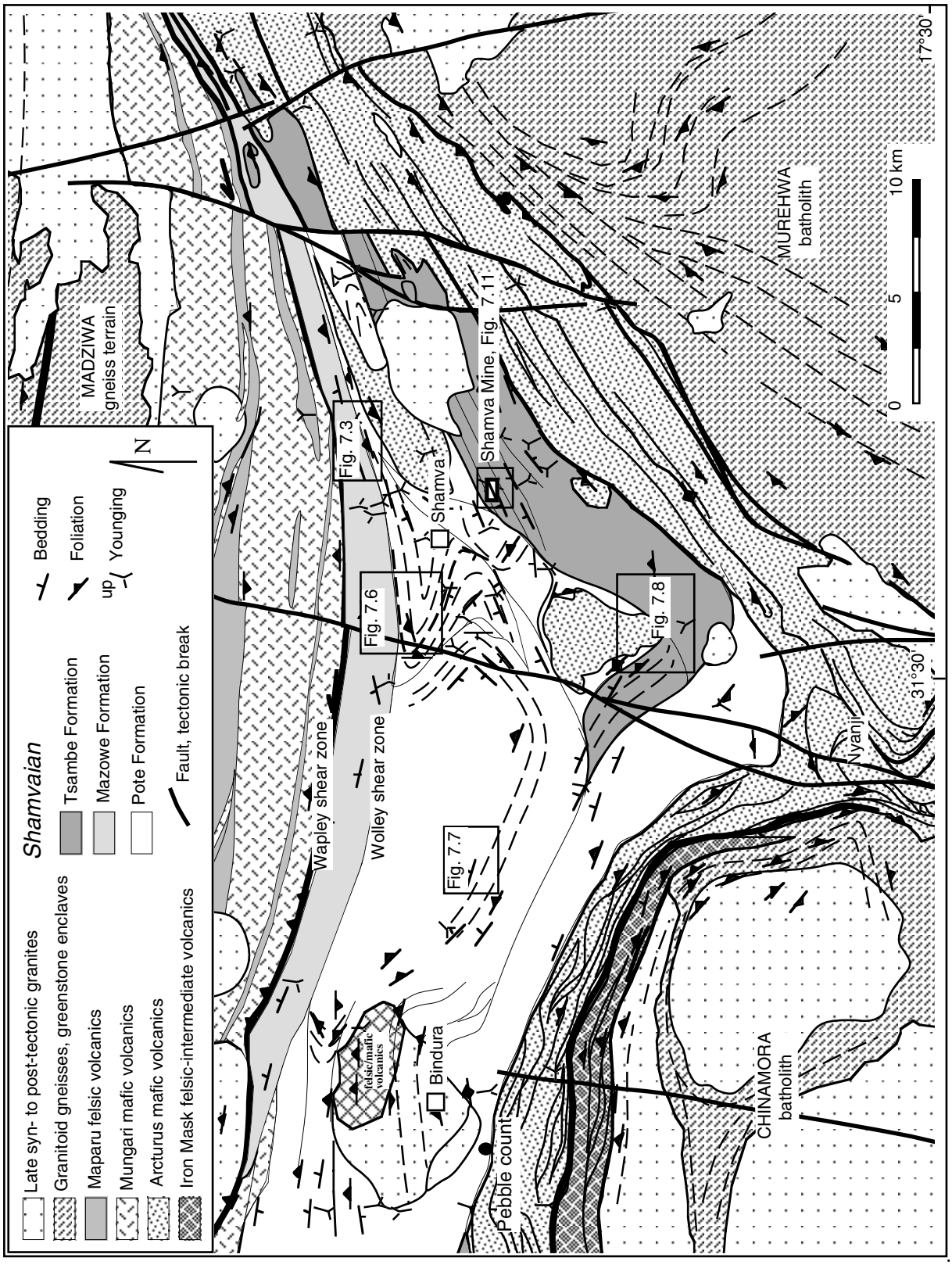

Fig. 7.2. Detailed geological map of the eastern part of the Bindura-Shamva greenstone belt (modified after Jelsma and Dirks 2000), showing the stratigraphic subdivision of the Shamvaian Group. Shear zone networks, foliation trajectories and younging indicators are shown.

Mazowe River section (Pote and Mazowe Formations)

Shamvaian sediments are well exposed in the bed of the Mazowe River northeast of Shamva (Fig. 7.3). The section can be subdivided into different lithological units (facies associations) which are conglomerate, pebbly sandstone, and sandstone facies associations of the Pote Formation and interbedded sandstone/shale of the Mazowe Formation. The two stratigraphic units are separated by the Wolley shear zone, and their primary stratigraphic relationship is uncertain. Sills and dykes of feldspar porphyry occur as small, irregular bodies in the river section. Basal conglomerate rests on fine-grained, structureless basaltic rock. The contact is sharp and remarkably planar for at least 50 m. Within a few decimetres of the contact, basalt is more strongly foliated and contains minor anastomosing shear zones. The amount of displacement along the contact (if any) is difficult to assess. The absence of mylonites is suggestive of a slightly deformed conformable contact.

The Wolley shear zone is a ~40 m thick unit of sheared sediment (Fig. 7.3). It is characterized by foliated mudstone/shale thinly intercalated with beds of siltstone and sandstone. Strong deformation resulted in disruption and boudinage of the sandstone beds. Narrow quartz veins are deformed together with the surrounding sediment. The lower contact of this unit is not exposed. The upper contact seems to be gradational as indicated by the occurrence of less disrupted tabular sandstone beds intercalated with mudstone.

Conglomerate

Conglomerate is clast-supported, polymodal, poorly sorted, and either massive or horizontally stratified. Beds are thin to very thick and commonly tabular on outcrop scale (Fig. 7.4a). Some beds exceed 4 m in thickness, possibly due to amalgamation. Thin beds locally wedge out within several metres. Lower bedding planes are sharp and planar with a maximum erosional relief of 10 cm. Each conglomerate bed is invariably overlain by sandstone along a sharp and, rarely, gradational contact, and gravel clasts commonly protrude into sandstone. Gravel clasts are rounded to well rounded and range from spherical to ellipsoidal to oblate in shape. The matrix consists of granule-bearing coarse- to very coarse-grained sand.

Massive conglomerate beds lack any form of grading (Fig. 7.5a), and the largest clasts are scattered. Imbrication is rarely developed; the clasts rather form trains with the ab-plane oriented parallel to bedding. Horizontally stratified conglomerate is characterized by a crude horizontal stratification that is defined by variations in clast size and intercalations of thin, discontinuous sandstone beds. Intervals with the coarsest clasts occur in various positions within a bed.

The conglomerate sequence is characterized by a coarsening-upward trend followed by fining-upward (Fig. 7.3), as indicated by variations in the maximum particle size (MPS, mean of twelve largest clasts per bed after omitting the two largest). Coarsening and fining is associated with thikkening and thinning of individual beds. Bed thickness (BTh) and maximum particle size thus show a positive linear correlation (Fig. 7.3). Palaeoflow directions, as determined from cross-bedded pebbly sandstones intercalated with conglomerate, are, on average, towards the southwest (Fig. 7.3). A

~30 m thick conglomerate horizon in the middle part of the section (Fig. 7.3) is distinct to the lower conglomerate in bed geometry, since individual beds are lenticular channel-fill deposits.

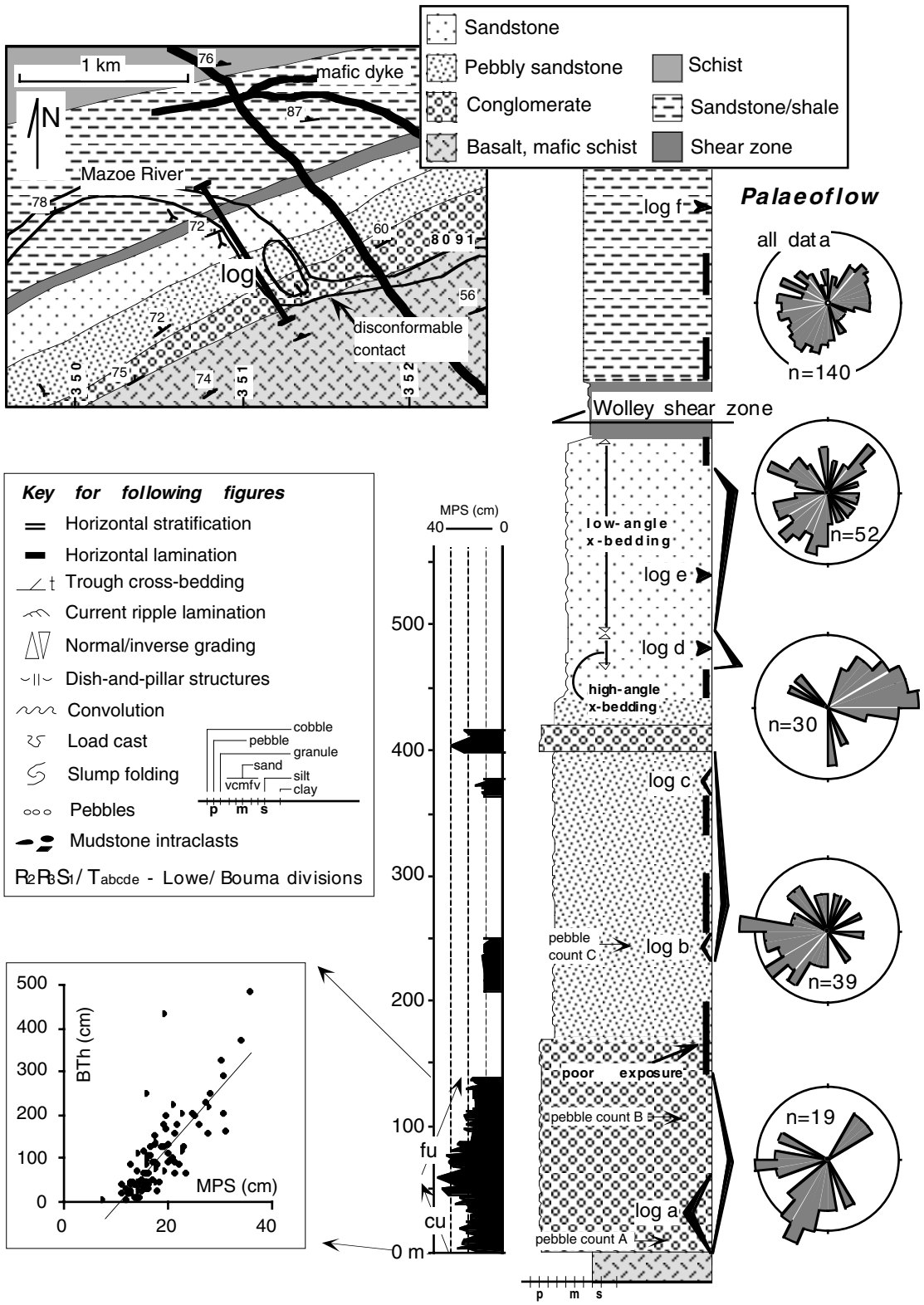

Fig. 7.3. Simplified geological map and graphic log of the Mazowe River section (see Fig. 7.2 for location). Palaeoflow diagrams (radius of the scale circle refers to 10% of the measurements, the same applies to following figures) and a plot of maximum particle size (MPS) vs bed thickness (BTh) are shown.

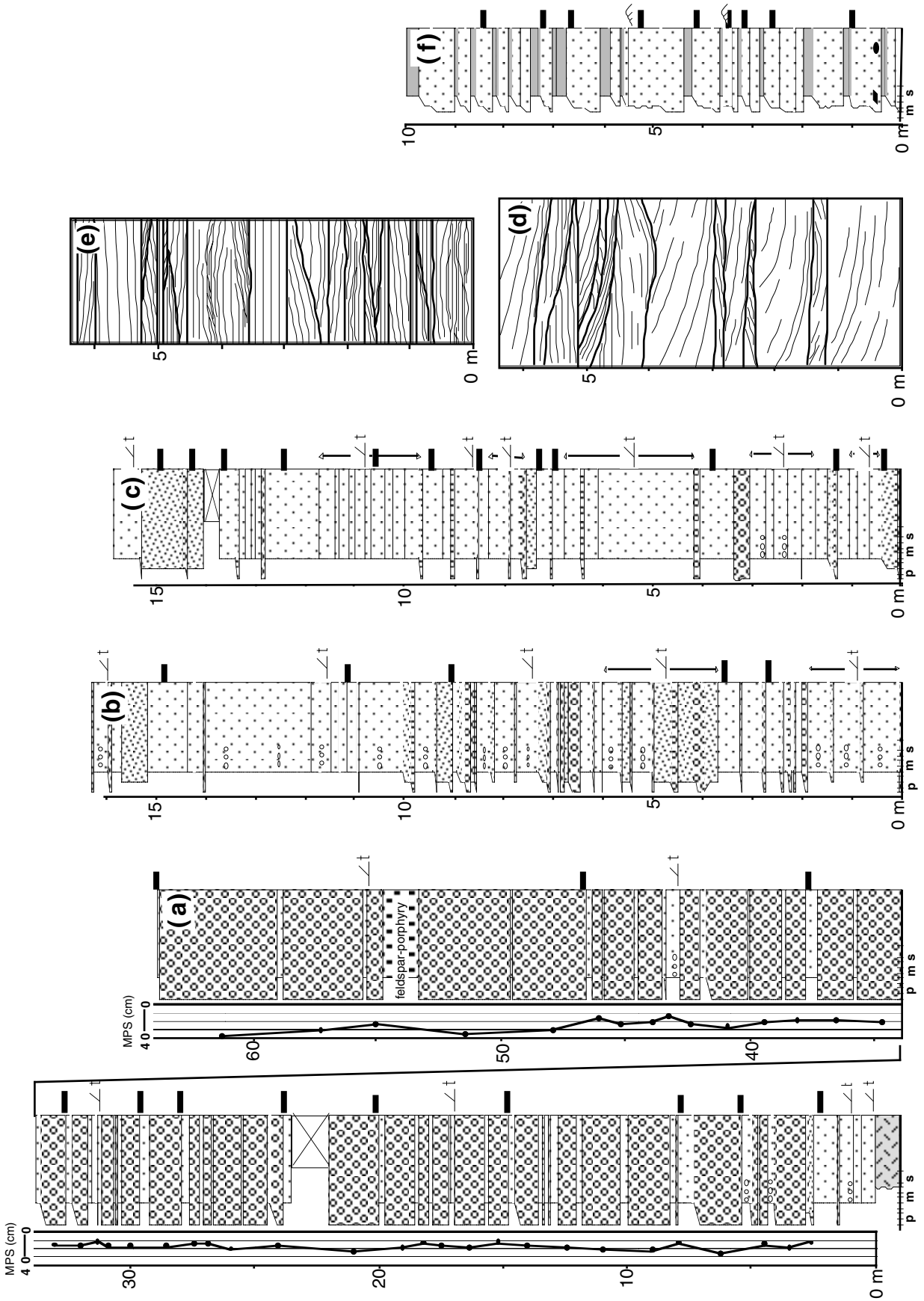

Fig. 7.4. Representative graphic logs of different lithological units of the Mazowe River section (see Fig. 7.3 for location and key of symbols).

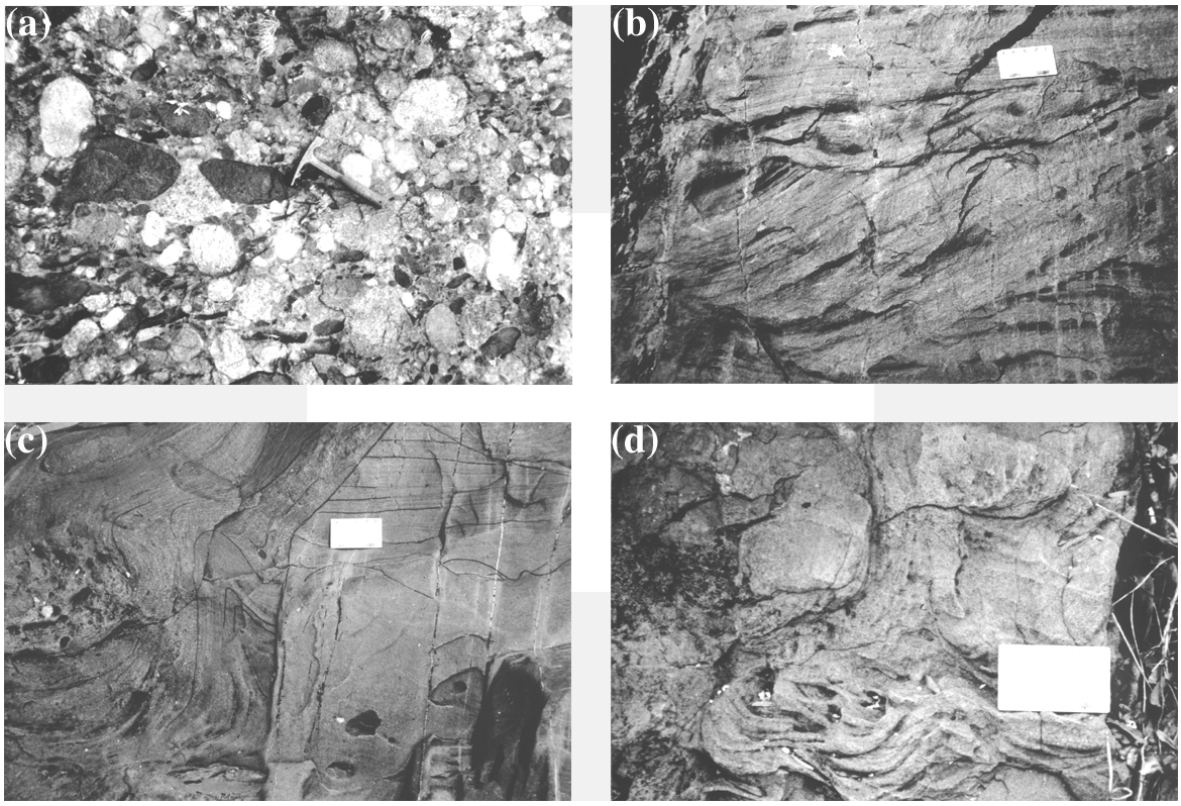

Fig. 7.5. Features of the Pote Formation. (a) Massive granite pebble conglomerate with large clasts of metagabbro (at hammerhead). (b) Medium-scale trough cross-bedding in coarse-grained sandstone. (c) Soft-sediment convolution and disruption of horizontally and cross-stratified sandstone. (d) Dewatering pipe in cross-bedded sandstone.

Pebbly sandstone

Pebbly sandstone forms the lower to intermediate part of the Mazowe River section (Figs. 3, 4b, 4c) and also occurs interbedded with conglomerate (Fig. 7.4a). Pebbly sandstone consists of thin to medium beds of granule-bearing, coarse sand with varying proportions of pebbles and cobbles up to 14 cm in diameter. Pebbles are either scattered in the sand matrix or form gravel-rich bands. The clasts gradually decrease in frequency and diameter up the Mazowe River section. Pebbly sandstone is either horizontally laminated or cross-stratified. Beds are broadly lenticular and partly pinch out laterally. Lower bed contacts are sharp (sometimes slightly erosive), gradational when overlying gravel and irregular when clasts protrude from underlying conglomerate beds.

Horizontally laminated pebbly sandstone consists of variably thick, planar parallel laminae. Bedding-parallel discontinuous bands, mostly one pebble thick, of pebbly sandstone or pebble/cobble conglomerate occur locally. If present, gravel occurs mostly at the base of beds and diminishes in frequency and size upwards; upper bed portions are mostly devoid of pebbles. Lower bedding planes are sharp; erosive lower contacts and associated pebble lags are rare.

Trough cross-bedded pebbly sandstone forms lenticular beds that wedge out within several metres to several tens of metres. Pebbles form discontinuous lags; scattered pebbles also occur and are aligned parallel to foresets. The cross-bedded facies commonly grades into horizontally

stratified facies and vice versa. Palaeoflow determinations indicate sediment transport to the southwest (Fig. 7.3).

Sandstone

A homogeneous succession of cross-bedded sandstone overlies the pebbly sandstone facies association (Figs. 3, 4d, 4e). Intercalations of both conglomerate and shale are absent, and scattered pebbles are rare. A ~30 m thick unit of medium- to large-scale, trough cross-stratified sandstone occurs in the lower part of the succession (Figs. 3, 4d). It consists of very coarse-grained sand rarely containing pebbles up to 8 cm across. Beds are medium to very thick with erosional, commonly concave-upward lower contacts (Figs. 4d, 5b). Foreset laminae (1-5 mm thick) are trough-shaped with steepening-upward angle of inclination. Rare pebbles either occur at the base of sets or are aligned in particular foresets. Thick beds are continuous on outcrop-scale. Palaeocurrent directions are uniformly to the east-northeast (Fig. 7.3).

Low-angle cross-stratified sandstone gradationally overlies the high-angle cross-bedded facies (Fig. 7.3). It consists of very coarse-grained sand rarely containing pebbles a few centimetres across. Bedding contacts are erosive, and beds are mostly discontinuous. Lamination (1-5 mm thick) is either planar, inclined at a low-angle or is undulating, partly forming convex-upward hummocks (Fig. 7.4e). Convolution and contortion of foreset laminae into fold-like structures is locally common. Palaeocurrent data have a somewhat variable distribution with a dominant flow to the southwest and two subordinate flows to the northwest and northeast (Fig. 7.3).

Interbedded sandstone/shale

Thin to thick beds of normally graded sandstone intercalated with shale form the >>200 m thick upper part of the section and are attributed to the Mazowe Formation (Figs. 3, 4f). Beds are tabular with a sharp to slightly erosive base (≤4 cm erosional relief) and commonly show Bouma (1962) T_{abde} and T_{bde} sequences. Massive to horizontally laminated, medium-grained sandstone, partly containing mudstone intraclasts up to 1 cm across, occurs at the base. This grades upwards into massive, horizontally laminated and/or current ripple-laminated, fine-grained sandstone which, in turn, is overlain by massive to laminated mudstone. Palaeocurrent data could not be collected due to the lack of three-dimensional exposure.

Depositional environment

Basal conglomerate shows features diagnostic of subaerial debris flows such as a sheetlike bed geometry with insignificant basal erosion, lack of grading, upward protruding clasts and a positive correlation between bed thickness and maximum clast size. Horizontally stratified conglomerate indicates deposition by surging mass flows (Nemec and Steel 1984). Sandstone layers capping conglomerate beds represent stream flow deposits that followed the debris flows. Subaerial environments dominated by mass flow processes are generally associated with alluvial fans. The

dominance of sediment deposited as sheets rather than forming channelled deposits on the Shamvaian alluvial fans may lie in the absence of vegetation in the Archaean, favouring unconfined sediment transport (Schumm 1968; Cotter 1978).

Cross-bedded pebbly sandstone may have formed by the migration of megaripples or low-relief sand lobes in broad unconfined channels. Horizontal lamination together with pebble layers and normal grading suggest deposition of the horizontally stratified pebbly sandstones facies under upper flow regime plane bed conditions. This facies is thus similar to laminated sand sheets that Miall (1985) interpreted as the product of flash floods. The broadly lenticular geometry of individual sedimentary units suggests deposition in virtually unconfined bedload streams on braid-plains, giving rise to a homogeneous sequence of stacked sheets and lenses of pebbly sandstone. A nearshore environment (cf. Bourgeois and Leithold 1984) for the pebbly sandstone facies is less likely, since sediment transport was directed towards the southeast, parallel to the flow direction of the alluvial fan conglomerates.

The deposition of the large-scale cross-bedded sandstone facies is inconsistent with a fluvial setting due to the reversed palaeoflow to the northeast. The sandstone may have formed as tidal sandbars or flood-tidal deltas at the mouth of an estuary where marine processes (waves and/or tidal currents) dominated, resulting in net bedload transport landward (Dalrymple et al. 1992). Low-angle and undulatory laminated sandstone strongly resembles amalgamated, hummocky cross-stratified sandstone which is thought to form at or above storm-wave base under combined flow conditions on the inner shelf (Dott and Bourgeois 1982). Convolution of bedding may indicate rapid sediment accumulation, followed by dewatering and associated contortion. As expected for this facies, palaeocurrent patterns are somewhat variable but indicate a subordinate northeast-directed (landward) flow and a dominant southwest-directed (offshore, shorenormal) flow. The northwest-directed palaeoflow may reflect a shore-parallel transport path, a common feature of storm-dominated shelf seas (cf. Duke 1990).

Graded sandstone beds of the interbedded sandstone/shale facies association of the Mazowe Formation show features typical of classical turbidites. The sheared shale unit occupying the Wolley shear zone possibly represents a primarily thin-bedded turbidite association that became tectonically disrupted.

The Range Farm area (Pote and Mazowe Formations)

Description

The Shamvaian of the Range Farm area occupies the northern and southern limb of a tight fold (Fig. 7.6). A hinge zone was not observed and may have been sheared out. In addition, the northern fold limb was affected by faulting along the Wolley shear zone. The northern area is laterally equivalent to the Mazowe River section. It comprises conglomerate overlain by homogeneous sandstone of the Pote Formation and an upper unit of the Mazowe Formation rocks consisting of planar and tabular beds of normally graded coarse-grained sandstone intercalated with shale and

representing turbidites. The Wolley shear zone separating the sandstone and the sandstone/shale succession is occupied by an intrusive ultramafic sill of now tremolite-actinolite-rich, schistose rock. The northern unit is poorly exposed.

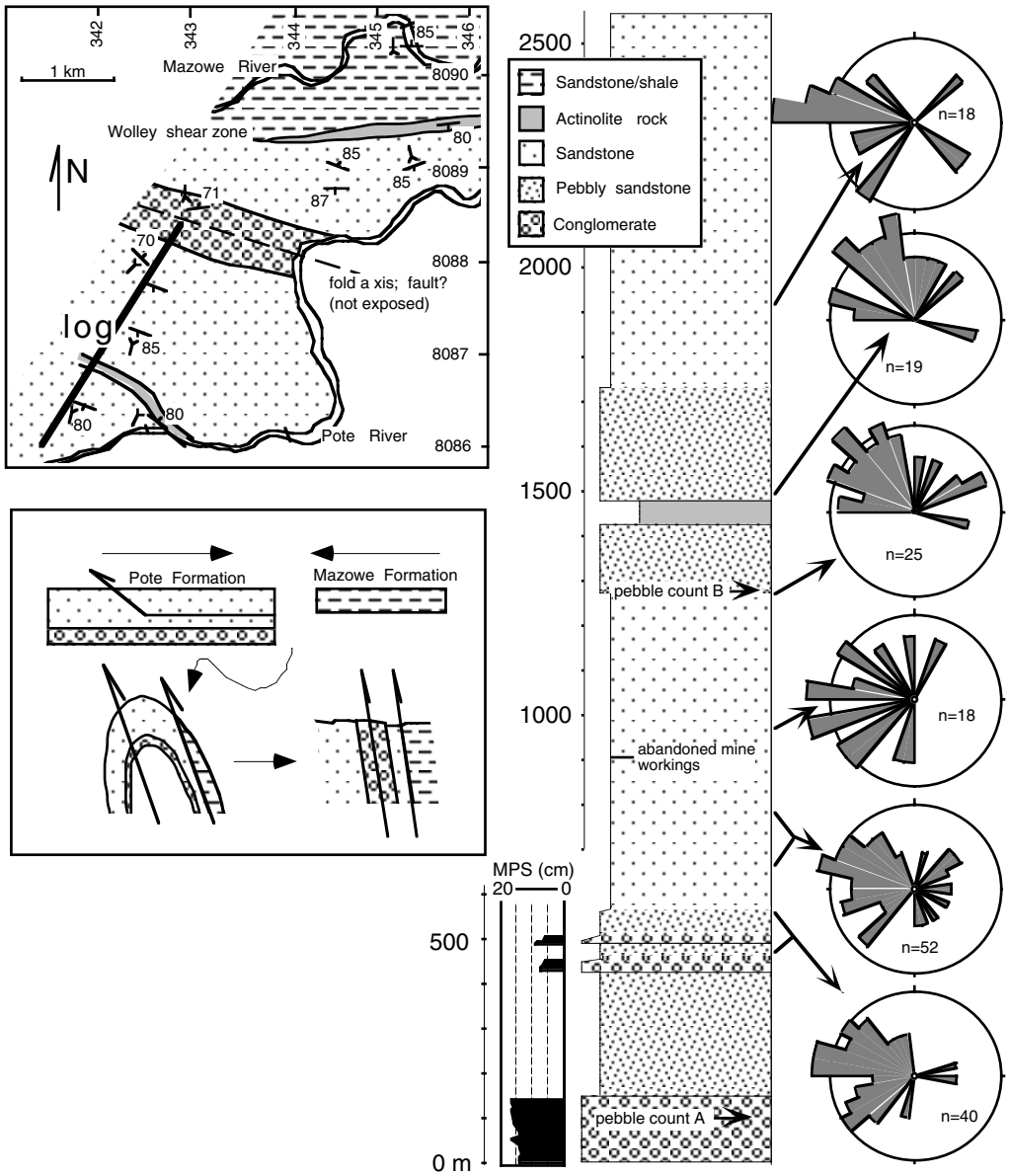

Fig. 7.6. Simplified geological map of the Range Farm area (see Fig. 7.2 for location), schematic tectonic model, graphic log of the southern part of the sedimentary succession and palaeoflow diagrams from certain stratigraphic horizons (arrows).

The southern unit consists of a ~150 m thick lower succession of tabular beds of massive pebble conglomerate. This is overlain by a monotonous sequence, >2500 m thick, of sandstone and pebbly sandstone with rare intercalations of conglomerate. Sandstone is medium- to thick-bedded, coarse-grained and contains fine pebbles in discrete laminae. Pebble layers and lags are common in sandstone at certain stratigraphic levels (logged as pebbly sandstone, Fig. 7.6). Intercalations of

mudstone are absent. Sandstone shows medium-scale trough cross-bedding, but planar parallel lamination, undulatory lamination and low-angle cross bedding also occur. Cross-bedding is locally convoluted; local overturning of foresets at bed tops, dish-and-pillar structures, dewatering pipes and small-scale internal unconformities suggest syndepositional deformation (Figs. 5c, 5d). Palaeoflow directions are unimodal and to the west in the lower part of the sequence, switching to a northwest-directed flow in the upper part (Fig. 7.6). Bedding-parallel shear zones were not observed in the southern area, but small-scale gold mining activity along a certain bedding-parallel horizon (Fig. 7.6) may indicate local shearing. In addition, a sill of ultramafic rock occurs in the sequence and, in comparison with the northern unit, may occupy a fault zone, although no evidence for shearing has been observed at this stratigraphic level.

Interpretation

The southern unit of the Range Farm area is distinct from the northern unit and the laterally equivalent Mazowe River section in its excessive thickness and lacks the turbidites of the Mazowe Formation. The different stratigraphy of the northern and southern units suggests that the Wolley shear zone in both the Mazowe River section and the northern area of the Range Farm is a major tectonic break along which distinct sedimentary rock units (fluvial to shallow-water sandstone of the Pote Formation, deeper-water turbidites of the Mazowe Formation) were juxtaposed during an event of tight folding and thrusting (Fig. 7.6). The shear zone was locally intruded by a sill of ultramafic rocks, probably during deformation due to the schistosity of the rock.

The lower stratigraphic unit of the southern fold limb consists of alluvial fan conglomerate that grades upsection into fluvial braid-plain pebbly sandstone and, probably, shallow-marine shoreface sandstone similar to the Mazowe River section. The depositional environment (fluvial, foreshore, shoreface) for individual portions of the middle to upper part of the sequence cannot be readily distinguished in the field because of limited exposure and homogeneity of the sequence. The unimodal palaeoflow direction and the abundance of scattered pebbles throughout may suggest a predominance of fluvial facies. Soft-sediment deformation further suggests high rates of sedimentation, possibly on a relatively high-relief depositional surface. Cross-bedding with overturned foresets is common in fluvial, unconsolidated sands due to sediment liquefaction (Allen and Banks 1982). The abundance of soft-sediment deformation features in the sequence suggests an external, allokinetic force of deformation. Earthquake shock in an active tectonic setting is the most commonly inferred trigger for extensive soft-sediment deformation and sediment liquefaction (Allen and Banks 1982; Owen 1987; Leeder 1987).

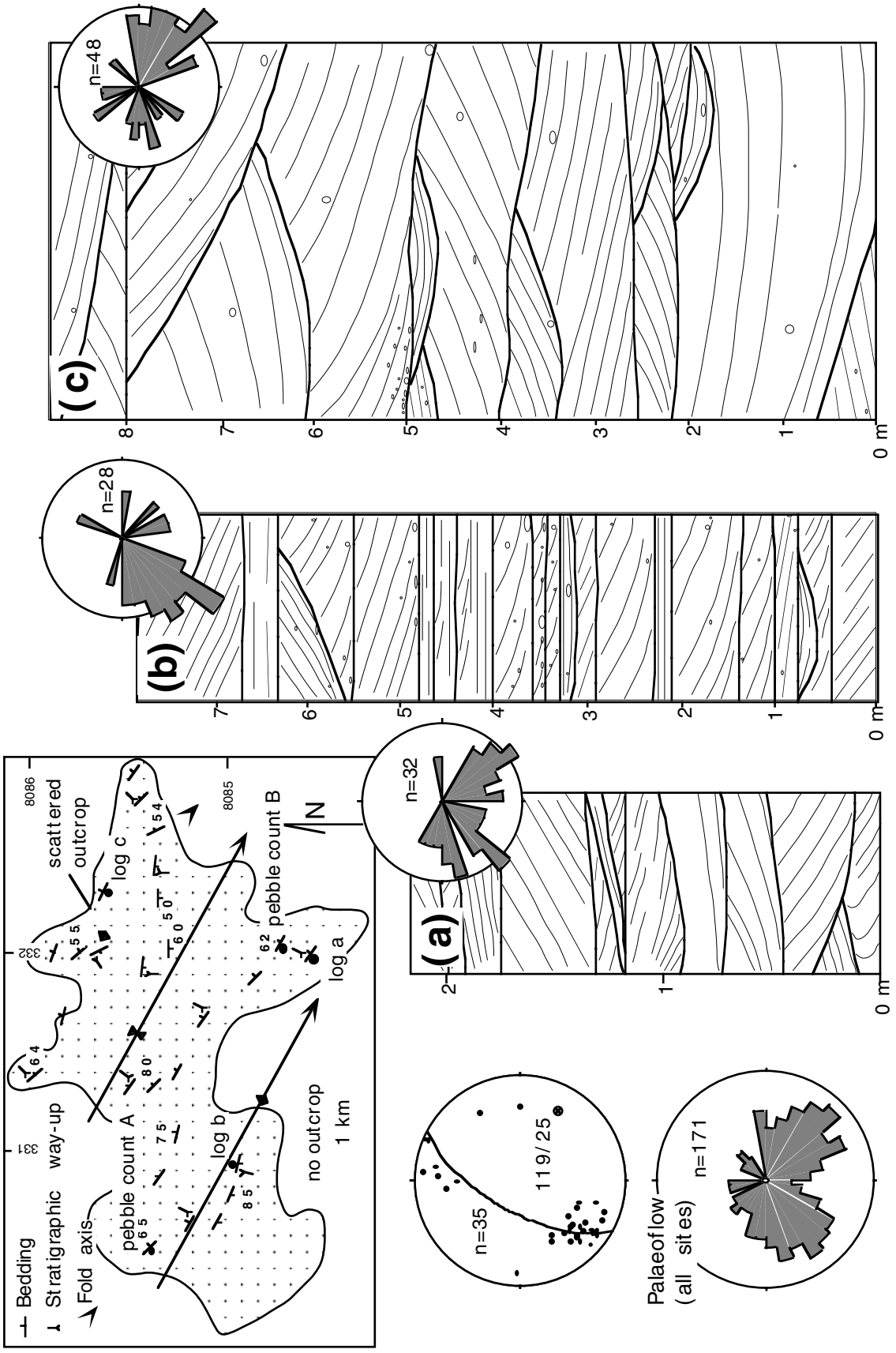

Fig. 7.7. Simplified geological map of the Arundel Farm area (see Fig. 7.2 for location), stereographic projection of poles to bedding and representative graphic logs of three sections together with palaeoflow data.

Arundel Farm area (Pote Formation)

Description

Shamvaian sediments at Arundel Farm consist entirely of sandstone of the Pote Formation which have been tightly folded about shallowly southeast-plunging fold axes. Folding led to repetition of strata which attain a minimum thickness of 600 metres. Rocks below and above the sandstones are not exposed at this locality. The sandstone facies do not differ from, and are probably laterally equivalent to, those described earlier. The sedimentary sequence consists of trough cross-bedded, very coarse-grained sandstone (Fig. 7.7). Well rounded pebbles of granite and mafic volcanics up to 6 cm across are scattered and, more rarely, concentrated in foresets and occur as lags or form conglomerate beds. Palaeoflow directions are, on average, bimodal with southwest and southeast-directed flow (Fig. 7.7).

Despite the homogeneity of the sequence, differences in bedding style can be observed. Medium-scale, trough cross-bedded sandstone is most common and typically shows a bimodal palaeoflow direction (Fig. 7.7a). Medium to thick and mostly tabular, pebble-rich sandstone beds occur at one locality (Fig. 7.7b). Trough cross-bedding is most common, but some beds show horizontal lamination which grades vertically into cross-bedding. Palaeoflow is uniform to the southwest. At another locality there occur large-scale trough cross-bedded sandstones with concave-upward contacts, recording a southeast-directed palaeoflow (Fig. 7.7c).

Interpretation

Medium to large-scale cross-bedded sandstones (Figs. 7a, 7c) may represent a variety of delta mouth, flood-tidal delta and/or shoreface sand bars that formed under the combined influence of fluvial, shoreface and wave/tidally influenced currents, possibly recording an offshore (southwestward) and longshore (southeastward) palaeoflow. Tabular bedded sandstone (Fig. 7.7b) represents fluvial deposits of unconfined bedload channels. Exceptional flood events deposited horizontally laminated sand grading into cross-bedded sand due to waning flow conditions. The uniform, southwest-directed palaeoflow of this facies is consistent with a fluvial interpretation.

Tafuna Hill area (Tsambe Formation)

Description

Tafuna Hill represents an inlier of Upper Bulawayan volcanics surrounded, and tectonically overlain, by Shamvaian sediment (Fig. 7.8). The volcanics include pillowed to massive basalt, dolerite, gabbro and minor mafic agglomerate. Stratigraphic younging is generally away from the centre of the greenstone inlier (Mukwakwami 1999). Tafuna Hill has been interpreted as an area of tectonic uplift due to diaprism of an underlying granite, or as the result of fold interference (Stidolph 1977). Shamvaian sediments north, east and west of Tafuna Hill are represented by the Pote Formation and are dominated by cross-bedded sandstone, pebbly sandstone and local boulder conglomerate with abundant granitic detritus (Fig. 7.2). Rocks south of Tafuna Hill are attributed to

the Tsambe Formation and conspiciously lack granitic clasts. Several lithofacies can be recognized and readily compared with well-established facies schemes (e.g., Bouma 1962; Lowe 1982).

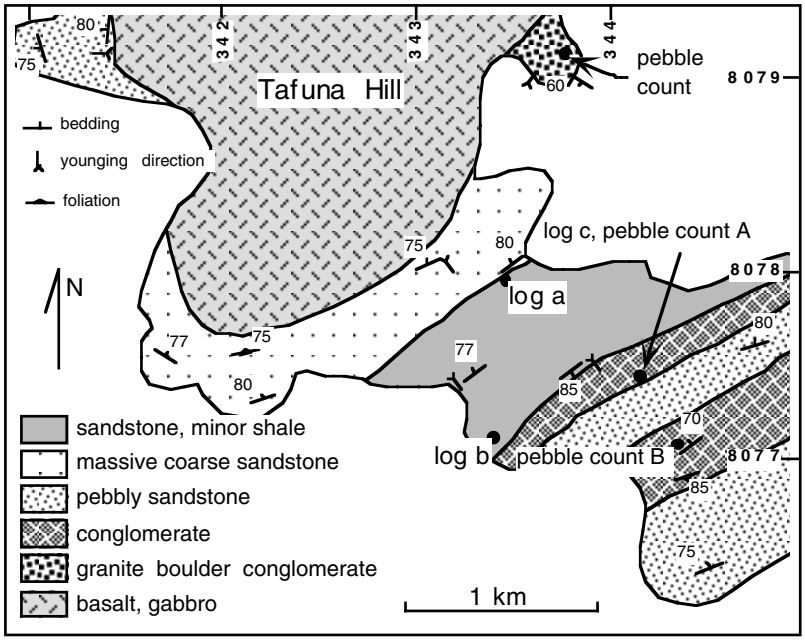

Fig. 7.8. Geological map of the area south of Tafuna Hill (see Fig. 7.2 for location).

The sediments south of Tafuna Hill form a continuous sequence of sandstone, conglomerate and minor shale that dip steeply to the northwest. Stratigraphic way-up is consistently towards the southeast (Fig. 7.8), suggesting a minimum original thickness of the sedimentary sequence of ~2000 m, although no younging indicators were observed in the far southeastern part of the outcrop. The sequence commences with massive very coarse-grained sandstone with rare intercalations of mudstone (associated with load casts of overlying sandstone), rare parallel and ripple lamination at bed tops and graded bedding. Bedding planes are poorly defined. The greenstone-sediment contact is not exposed, but adjacent rocks are strongly foliated, suggestive of a tectonic contact. Overlying the massive sandstone unit is a succession of sandstone and shale, varying from thinly bedded sand-mud couplets to very thick-bedded (>2 m) fine pebble conglomerate grading into shale. Two sections were measured in detail (Figs. 9a, 9b). Beds are thin to thick, tabular and planar (Fig. 7.10a) and show incomplete Bouma sequences (typically T_{ab}, T_{abe} and T_{ae}). Normally graded beds of conglomerate and pebbly sandstone are less common. Shale is commonly convoluted, partly due to load casts and ball-and-pillow structures derived from the overlying sandstone beds.

Above the shale-bearing unit are two conglomerate horizons intercalated with pebbly sandstone. Pebbly sandstone comprises massive, very coarse-grained sandstone with scattered pebbles up to 4 cm across. Conglomerate is clast-supported (Fig. 7.10b) and consists of subrounded to well rounded clasts (typically 2-4 cm, rarely 10 cm in diameter) in a matrix of silicified sand-sized

material, sometimes showing abundant neomorphic feldspar. One conglomerate section has been measured in detail (Fig. 7.9c). Individual beds are medium to very thick, tabular and planar and commonly consist of normally graded conglomerate (R_3, classification after Lowe 1982) grading into horizontally stratified pebbly sandstone (S_1) and massive (S_3, Bouma T_a) to horizontally laminated sandstone (T_b). Some conglomerate beds are inversely graded at the base (R_2).

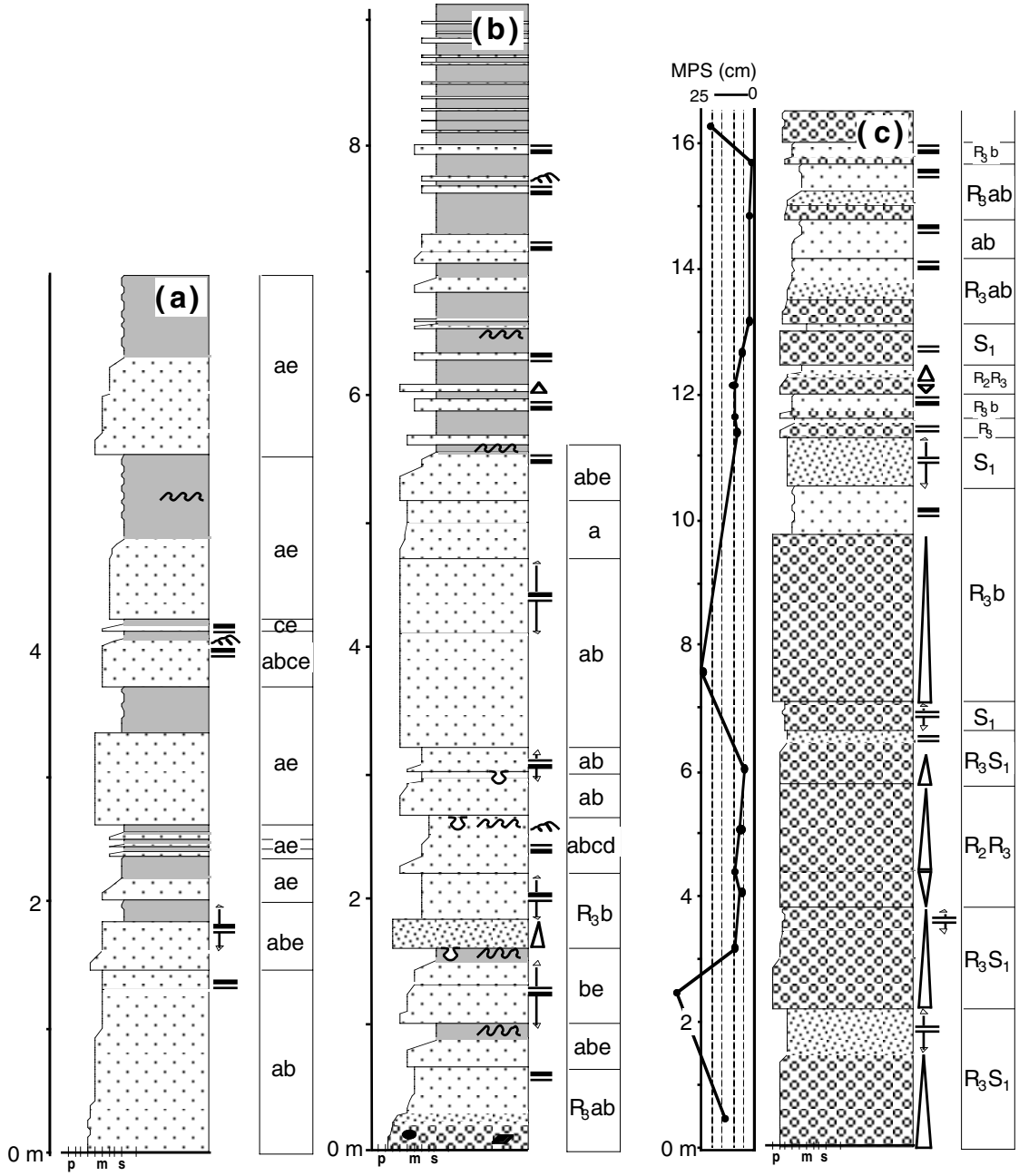

Fig. 7.9. Graphic logs of three sections measured in detail south of Tafuna Hill (see Fig. 7.3 for key of symbols).

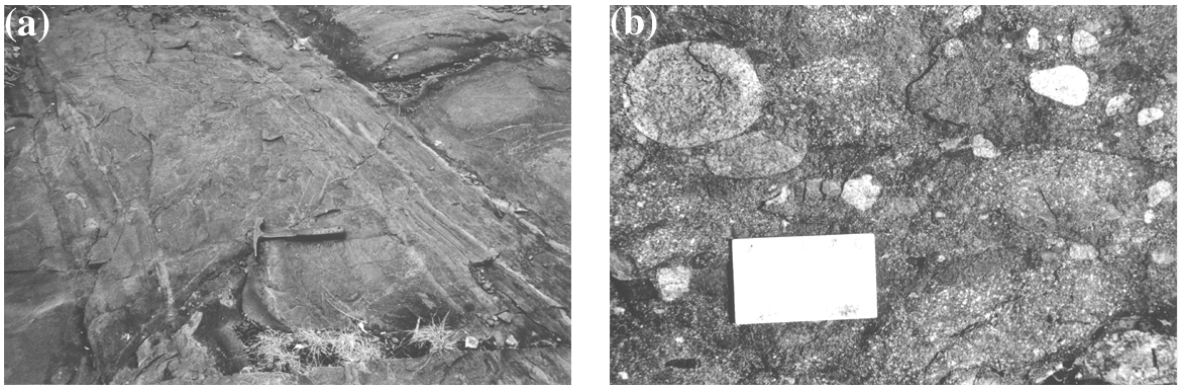

Fig. 7.10. Features of the Tsambe Formation. (a) Thick-bedded classical turbidites. (b) Massive porphyry pebble conglomerate with some felsic volcanic clasts (light grey); note the compositional similarity between clasts and matrix.

Interpretation

Intercalated sandstone/shale formed by episodic low-density turbidity currents, as indicated by partial to complete Bouma sequences. Rapid suspension sedimentation from sand-ladden, high-density turbidity currents gave rise to the deposition of the lower unit of massive sandstone. Conglomerate and pebbly sandstone consist of stacked facies typical for high-density turbidity current deposits (R_2-R_3-S_1; Lowe 1982). The absence of the S_2 division may lie in the mean size of the suspended load unsuitable for traction carpet sedimentation (Lowe 1982).

Shamva Mine (Tsambe Formation)

The sedimentary rocks at Shamva gold mine have been isoclinally folded and subsequently deformed along northeast-striking shear zones (Fig. 7.11); gold mineralization is associated with these shears (Foster et al. 1986). Rocks adjacent to the shear zones are strongly silicified, giving rise to weather-resistant rocks that form Shamva Hill. Southeast of Shamva Hill there occurs a heterolithic, thinly bedded facies of graded sandstone intercalated with shale. This facies shows partial to complete Bouma sequences indicative of turbidity current deposits. A few metres thick, continuous horizon of argillaceous rock with abundant cordierite crystals overlies the turbidites (Fig. 7.9). Argillite is followed by horizontally and ripple-laminated, fine- to medium-grained sandstone. Stratigraphic younging is to the north. In general, however, poor exposure hampered any detailed sedimentological work south of the hill.

The rocks forming Shamva Hill comprise three spatially closely related lithofacies associations. These include conglomerate, pebbly sandstone and sandstone facies associations. Primary sedimentary structures are locally obscured due to strong silicification. Three localities situated south, north and on top of Shamva Hill have been studied in detail (Fig. 7.11).

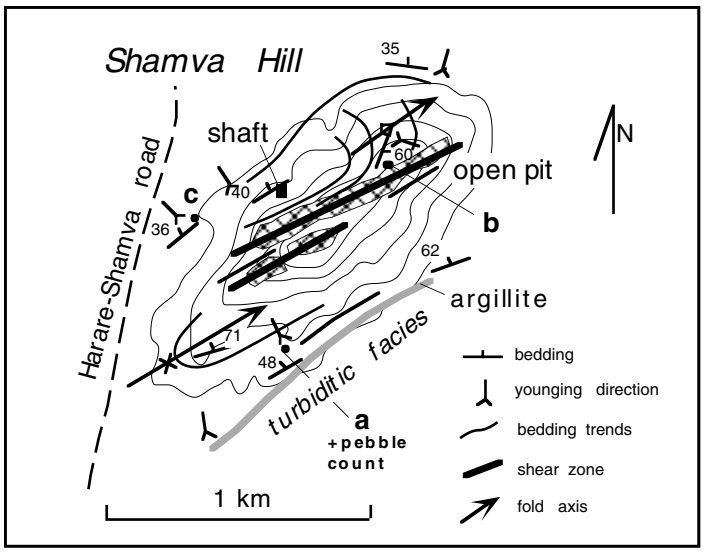

Fig. 7.11. Schematic map of Shamva Hill (see Fig. 7.2 for location).

Conglomerate

Conglomerate is restricted to the southern slope of Shamva Hill where a representative section has been measured (Fig. 7.12a). It includes massive, graded and horizontally stratified beds, ranging in thickness from 10 to 35 cm. Massive conglomerate is either matrix- or clast-supported, unstratified and displays no size grading. Graded conglomerate is clast-supported, shows normal coarse-tail grading and commonly grades into fine pebble conglomerate containing scattered larger clasts. Stratified conglomerate is matrix- to clast-supported, poorly sorted, lacks grading and shows crude horizontal stratification due to the alignment of tabular clasts of a particular size range parallel to bedding. Conglomerate is intercalated with trough cross-bedded and horizontally stratified pebbly sandstone. Bedding planes are planar without signs of significant erosion and bound sheet-like beds. The pebbles/cobbles are subrounded to well rounded and up to 15 cm in diameter. The matrix consists of granule-bearing very coarse sand. Palaeoflow directions are unimodal with a considerable range and a mean direction towards the northeast (Fig. 7.12a).

Pebbly sandstone

Coarse-grained pebbly sandstone is the most common rock type and includes trough cross-bedded, low-angle cross-bedded and horizontally laminated facies (Fig. 7.12b). Pebbles and rare cobbles up to 12 cm in diameter vary in abundance and are aligned parallel to the stratification within beds. Beds (5-30 cm thick) are tabular with mostly planar bedding planes. The trough cross-bedded facies partly forms lenticular beds with concave-upward erosive contacts that are commonly veneered by pebble lags. Most clasts are well rounded; subangular clasts are rare and may represent larger clasts broken up during sediment transport. Palaeocurrent data have a bimodal, bipolar distribution with the dominant flow towards the northeast (Fig. 7.12b).

Sandstone

Sandstone with only minor proportions of pebbles occur locally. A representative section could not be logged because of poor exposure. The rocks are characterized by very thin to thick bedded, medium to very coarse-grained sandstone. Pebble lags are rare. Facies include horizontally laminated, low-angle cross-bedded, trough cross-bedded and minor wavy to undulatory laminated sandstone, resembling hummocky cross-stratification. The palaeocurrent data distribution of the

sandstone facies association (Fig. 7.12c) is bimodal, bipolar with the dominant flow towards the east-northeast. A subordinate, bimodal, bipolar southeast-directed flow also occurs.

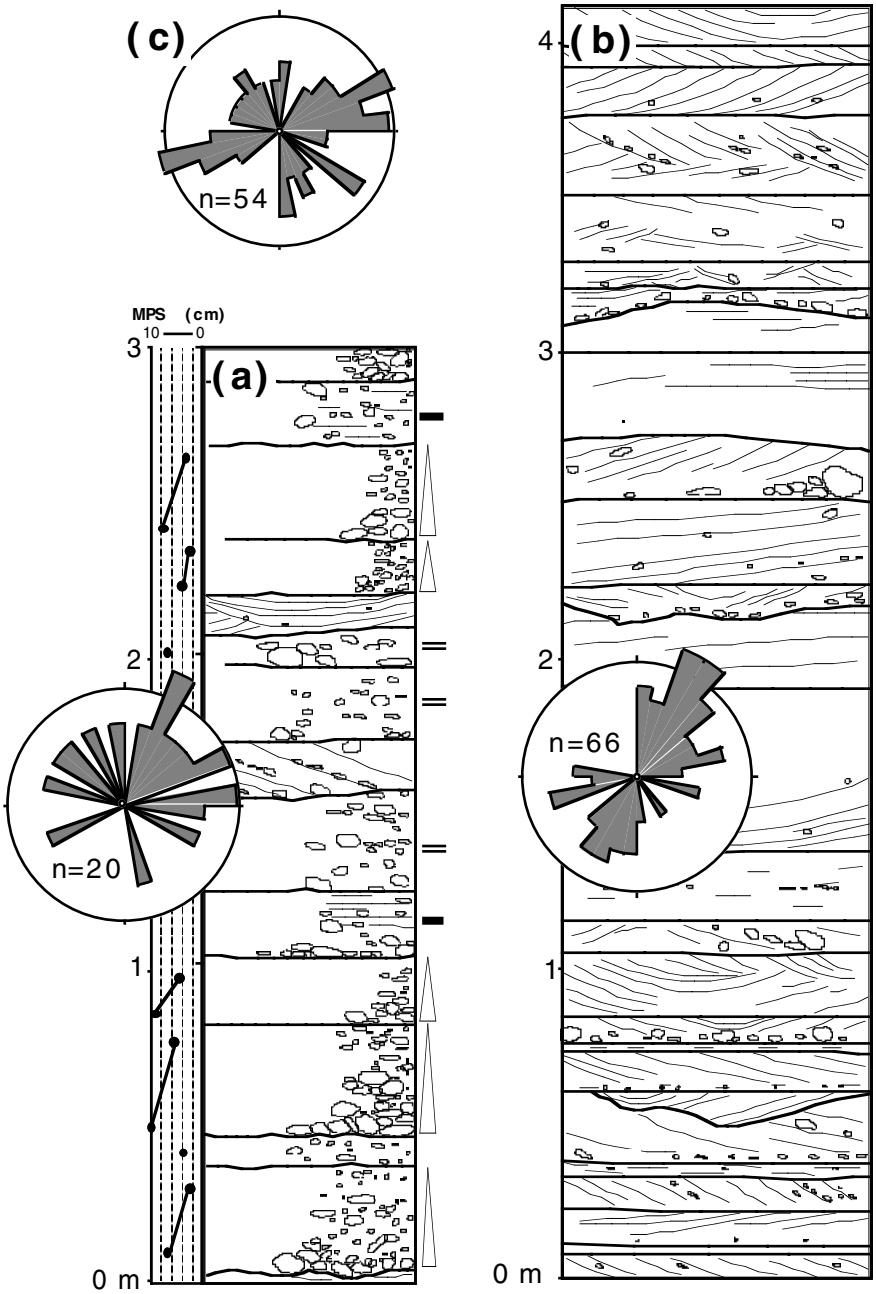

Fig. 7.12. Sedimentological data from three localities a-c at Shamva Hill (see Fig. 7.11).

Depositional environment

Massive and graded conglomerates are interpreted as mass flow deposits on account of lack of stratification and lack of obvious erosion surfaces between beds (Nemec et al. 1984). The horizontally stratified conglomerate and pebbly sandstone facies are interpreted as sheetflood (unchannelized flood-flow) deposits on the basis of sedimentary structures, tabular bed geometries

and only minor erosive contacts. Intercalations of cross-bedded pebbly sandstone possibly formed as transverse bars in shallow bed-load streams. The facies assemblage of mass-flow and sheet-flood deposits is consistent with an alluvial fan depositional setting. Palaeocurrent azimuths suggest outbuilding of fan lobes to the northeast.

The facies assemblage of pebbly sandstones, the mostly tabular geometry of depositional units, bipolar palaeoflow directions and the absence of mudstone intercalations are consistent with a high-energy shallow-marine environment. Cross-stratified pebbly sandstone is interpreted as the deposits of migrating lunate bars and megaripples, a common feature of upper shoreface environments (Bourgeois and Leithold 1984). Basal pebble lags may have formed during storm-wave reworking of underlying sediment. Horizontally to low-angle cross-stratified sandstone possibly represents foreshore deposits. The dominant northward-directed palaeocurrent indicate sediment transport offshore, whereas the southward, i.e. onshore-directed flow possibly suggests (storm) wave- or tide-induced currents.

Low-angle cross-stratification and hummocky cross-stratification of the sandstone facies association is typical for coarse-grained, lower shoreface environments, frequently affected by storms (Bourgeois and Leithold 1984). Palaeocurrent data indicate both offshore and onshore directed currents similar to the pebbly sandstone facies association. Storm-induced, longshore geostrophic currents (e.g., Duke 1990) may be indicated by southeast-oriented palaeoflow data (Fig. 7.12c).

Provenance

Pebble analysis of Pote and Tsambe Formation conglomerates (Figs. 5a, 10b) clearly indicates different source terrains. Tsambe Formation sediments are dominated by intermediate and felsic volcanic clasts, whereas Pote sediments are characterized by granite and greenstone clasts (Fig. 7.13). On the same basis, Stidolph (1977) subdivided the Shamvaian into the volcanics-derived Lower Shamvaian and the granite-derived Upper Shamvaian. Conglomerate in the Mazowe Formation is very rare. Reconnaissance sandstone petrography, however, indicates a predominantly granitic provenance similar to the Pote Formation.

Description

Pebble analyses of Pote Formation conglomerates at different localities are discussed together. Granitoid rock and mafic volcanic are the most common clast types followed by intermediate/felsic volcanic, feldspar- and quartz-porphyry, quartzite, chert and granitoid gneiss (Fig. 7.13). Granitoid clasts are mostly medium-grained granite; less common are fine-grained granodiorite and pegmatite pebbles. Mafic clasts consist of two varieties. The first variety is a fine-grained, massive mafic rock, probably basaltic in composition, and has a chert-like appearance due to silicification. The second variety is schistose and contains abundant biotite and hornblende. Both varieties have been counted together. Intermediate to felsic volcanic clasts are massive, commonly silicified, aphanitic rocks. Porphyry clasts are intermediate volcanic rocks that comprise euhedral feldspar and/or quartz

phenocrysts. Quartz crystals in some clasts have a distinct blue colour. Quartzite is an orange-weathering rock with a gneissic fabric. Chert clasts comprise a dark grey, massive variety and a banded variety which occur in subequal proportions. Gneissic clasts are restricted to leucocratic granitic gneiss. Rare miscellaneous components include strongly weathered calc-silicate and marble, foliated metagabbro (Fig. 7.5a), very coarse-grained pyroxenite clasts and vein quartz. The abundance of porphyry and intermediate/felsic clasts markedly increases upwards in the Range Farm section; a similar trend is less well developed in the Mazowe River section (Fig. 7.13). The conglomerate matrix consists of granule to coarse sand-sized clasts of quartz, feldspar and volcanic rock fragments.

The rocks south of Tafuna Hill and around Shamva Mine are part of the Tsambe Formation. At Tafuna Hill (Fig. 7.10b), conglomerate contains four compositionally similar clast types (Fig. 7.13) which are (in order of decreasing abundance): (1) feldspar-porphyry, (2) massive intermediate/mafic volcanic clasts with rare feldspar phenocrysts, (3) variably silicified intermediate/felsic volcanic clasts with spherical vugs (1-3 mm across), suggesting an extrusive origin and (4) clasts of mafic schist (typically less than 2 cm across). Sandstone and shale intraclasts are locally common. A granite pebble was observed at one locality. The conglomerate matrix is dominated by sand-sized volcanic rock fragments admixed with mud. Locally, subhedral feldspar crystals similar to those in porphyry pebbles occur in the matrix of the clastic sediments. They are particularly common along cracks and in halos around mudstone intraclasts. At Shamva Mine, four different clast types occur in conglomerates (Fig. 7.13) which are (in order of decreasing abundance): (1) feldspar-porphyry, (2) silicified, fine-grained intermediate volcanic, (3) silicified, fine-grained felsic volcanic and (4) calcareous, strongly weathered clasts. Quartzite pebbles are rare. Stidolph (1977) reported the occurrence of granite granules in the rocks at Shamva Mine.

Interpretation

Granite, granitoid gneiss and vein quartz suggest a granitoid-gneiss terrain such as the Madziwa and Murehwa terrains as part of the source of the Pote Formation. Granitic clasts within Shamvaian conglomerate from the Mazowe River section have yielded Pb-Pb zircon evaporation ages up to 3.2 Ga (Dougherty-Page 1994). Mafic clasts, including biotite-hornblende schist, metagabbro and pyroxenite, quartzite, chert and calc-silicate suggest a supracrustal source which experienced a metamorphic event prior to erosion. All such rocks occur as inclusions in migmatitic banded gneisses of both the Madziwa and Murehwa gneiss terrains and, as such, may be part of the mid-Archaean Sebakwe Group greenstones. Massive mafic volcanic clasts may well be derived from rocks similar to Arcturus Formation basalt. Porphyry and intermediate/felsic volcanic clasts, identical to those of the Tsambe Formation, suggest an additional source composed of volcanic rocks. The bluish colour of quartz grains in some porphyry clasts suggests the Maparu Formation as a possible source where quartz-porphyries with conspicious bluish quartz phenocrysts are common (Tyndale-Biscoe 1931). The occurrence of intermediate/felsic volcanic clasts in Pote

Formation granite conglomerate, the increase in the abundance of such clasts in the Pote Formation stratigraphy and the occurrence of granite pebbles in Tsambe Formation rocks indicate that both lithostratigraphic units contain clasts derived from similar source terrains, but the proportion of clasts derived from a particular source strongly varies in the succession.

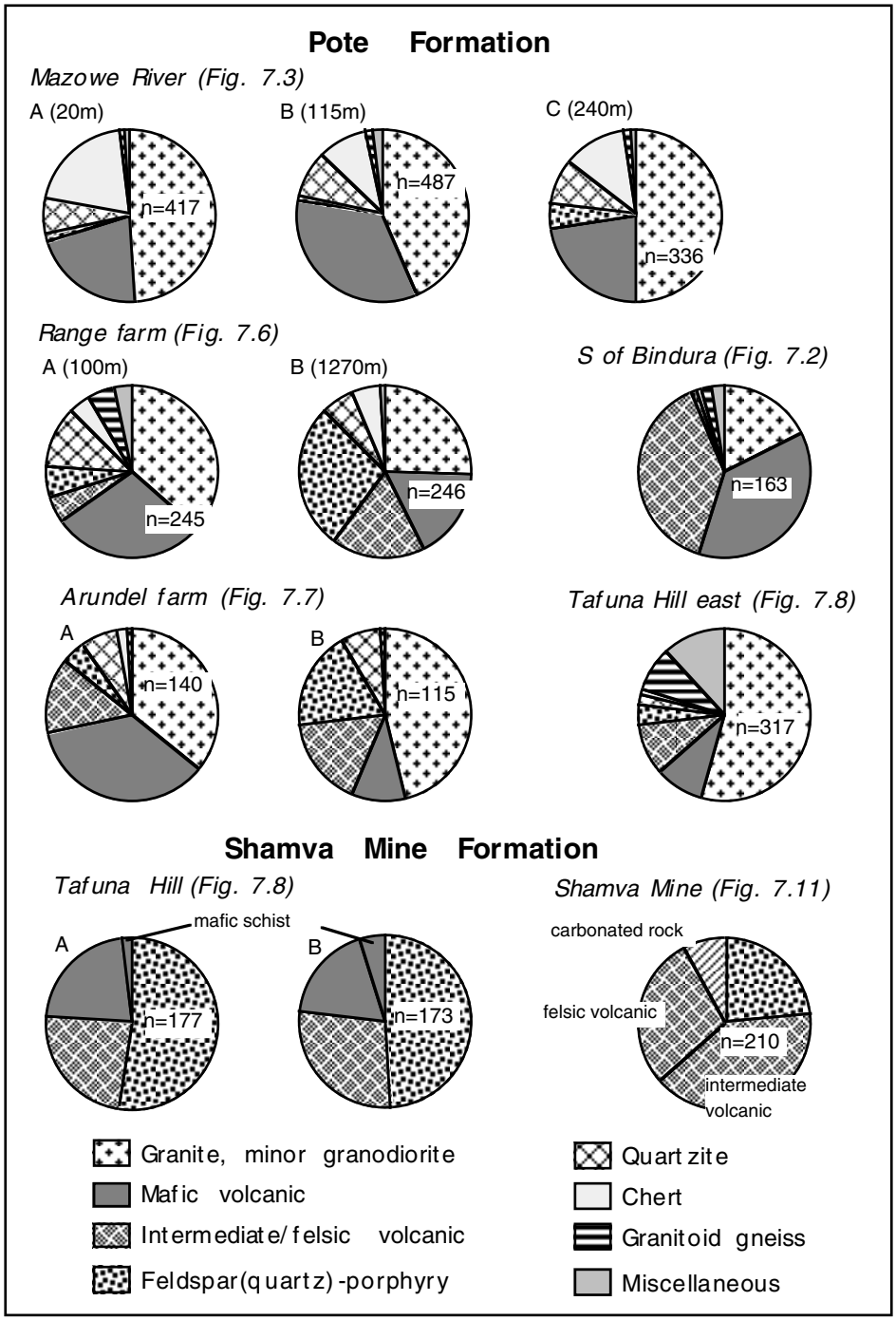

Fig. 7.13. Results of pebble counting from the study areas.

Part of the sequence south of Tafuna Hill has previously been mapped as dacitic tuff and dacitic agglomerate (Stidolph 1977). Besides the volcanic nature of the clasts, this reasoning may be based in the local occurrence of subhedral feldspar crystals in the sediment matrix. However, the feldspars more likely represent neomorphic crystals that formed during metamorphism of the sedimentary rocks, since feldspatization is more intense along cracks and in halos. Stidolph (1977) interpreted the rocks at Shamva Mine as reworked pyroclastic deposits derived from synsedimentary felsic volcanism. However, direct evidence for synsedimentary volcanism such as tuff beds or volcanic bombs has not been observed during this study. The occurrence of volcanic clasts in the sequence does not necessarily imply contemporaneous volcanism but provides evidence for a source terrain consisting predominantly of volcanic rocks. Nevertheless, active volcanism during the time of Shamvaian sedimentation is indicated by the U/Pb zircon ages of ~2645 Ma from felsic volcanic rocks of the Iron Mask and Passaford Formations of the BSGB (Wilson et al. 1995).

DISCUSSION

Stratigraphic relationships

In order to constrain the larger scale framework of the depositional setting of the Shamvaian Group it is of prime importance to reconstruct any original superposition or lateral correlation of the three tectonostratigraphic units defined in this study. No primary stratigraphic contacts between the units have been observed. Instead, all contacts are sheared. Stidolph's (1977) subdivision into Lower Shamvaian (herein termed Tsambe Formation) and Upper Shamvaian (Pote and Mazowe Formations) is justified by the compositional contrast of the sediments. However, Stidolph (1977) does not provide evidence for the Lower Shamvaian being stratigraphically below the upper unit. Indications for this reasoning may lie in Stidolph´s (1977) observation in the area around Shamva that the lower unit is predominantly situated in the southern part of the Shamvaian outcrop and stratigraphic younging is commonly towards the northwest. However, the structural framework of the sediments in this area is complex with common indications for younging reversals (Fig. 7.2). Additionally, the southern greenstone-sediment contact in the Shamva area is either not exposed or occupied by a feldspar porphyry sill and may be sheared.

The observation that the different tectonostratigraphic units are shear zone-bounded makes it difficult to assess the original stratigraphic relationship without detailed geochronological data. From the present picture, the different units are separate and tectonically juxtaposed sequences. Nevertheless, there are a number of field relationships which may indicate that the Pote Formation originally represented the lowermost stratigraphic unit of the Shamvaian Group. (1) The only relatively undeformed greenstone-sediment contact so far observed occurs at the Mazowe River section (Fig. 7.3) where basalts are overlain by Pote Formation conglomerate characterized by abundant granite clasts. Granitic detritus is the defining feature of Stidolph's (1977) Upper Shamvaian. A second possibly primary contact occurs south of Bindura where basaltic greenstone is directly overlain by Pote Formation granite pebble conglomerate (Figs. 7.2, 7.13). (2) The Tafuna

Hill greenstone inlier is surrounded by a veneer of Pote Formation granite clast-rich sediments (Fig. 7.2). The greenstone inlier probably represent a basement uplift so that the Pote Formation can be explained as a lower stratigraphic unit brought to the surface during uplift.

The compositional contrast between the Pote and Tsambe Formations does rule out the possibility that they represent laterally correlative units and, as such, may be different lithotectonic units altogether. However, clasts characterizing the Tsambe Formation (e.g., porphyry) become progressively more common towards the top of the Pote Formation, as observed in the Range Farm section (Fig. 7.13). This relationship may indicate that the Tsambe Formation originally overlay the Pote Formation. The Mazowe Formation may have been (1) a laterally correlative, deeper water facies association of the Pote Formation (due to similar compositional aspects) and was thrusted onto the shallow water equivalent, or (2) was deposited, prior to thrusting, in an intermediate position between the Pote and Tsambe Formations due to compositional affinities to the former and environmental affinities to the latter.

Depositional setting

If the above assumptions are correct the following picture emerges. The Shamvaian sediments overlie Bulawayan greenstones (Arcturus Formation) along a disconformable contact. Erosion of the underlying basaltic greenstones was minor. Instead, detritus was mostly derived from a mid-Archaean granitoid-gneiss terrain such as the Madziwa and/or Murehwa terrains containing previously metamorphosed portions of supracrustal rocks. Furthermore, sedimentation must have taken place some time after cessation of Bulawayan mafic volcanism due to the absence of such rocks in the sedimentary sequence. The lower part of the sedimentary succession (Pote Formation) represents a transgressive, fining-upward sequence. Alluvial fan conglomerate is overlain by fluvial braid-plain pebbly sandstone followed by braid-delta (?) to high-energy shoreface sandstone. The basin was of a marine nature due to the scale of wave/storm-induced features (e.g., HCS) and common bimodal palaeocurrents in shoreface sandstone. The complete absence of fine-grained sediment suggests a linear shoreline with coalescing braid-deltas related to an extensive braid-plain as a sediment source. Possible causes for transgression are eustatic sea level rise, decrease in sediment supply or rapid (tectonic) subsidence. Indications for sea-level variations such as shallowing-upward parasequences do not occur in the sequence. Foreshore and beach deposits between the shelf and fluvial sandstones have not been observed, possibly indicating a dominance of the fluvial system tending to cannibalize beach deposits adjacent to the braided channels (cf. McCormick and Grotzinger 1993). This observation, together with the excessive thickness of the fluvial to shallow marine sandstone sequence, suggest a high sediment supply in conjunction with a high subsidence rate. Such homogeneous sequences of both fluvial braid-plain and storm-dominated shoreface shelf sandstones hundreds of metres thick are common in the Precambrian rock record. This has been related to a fine balance between subsidence rate and sediment influx and a more evenly sediment redistribution due to strong semipermanent wind-driven and tidally driven

current systems on the shelf (Cant and Hein 1986; Soegaard and Eriksson 1989; Eriksson et al. 1998). The monotony of the shallow-marine and fluvial facies and the absence of quiet-water and aeolian deposits further suggest a perennial discharge, possibly in a humid climate.

Fluvial braid-plain to shallow shelf sedimentation may have been followed by deep-water, sub-wave base sedimentation by turbidity currents (Mazowe and Tsambe Formations), assuming an originally gradual sedimentary contact that later became sheared upon thrusting. The upward increase in the abundance of intermediate and felsic volcanic clasts suggests an increase in the proximity of a volcanic terrain, such as a volcanic arc. Deep-water sedimentation of fine to coarse clastic material of the Tsambe Formation, which was predominantly derived from a volcanic source terrain, gave rise to a thick turbidite succession, as preserved south of Tafuna Hill. The great thickness of the turbidite sequence again suggests a marine rather than a lacustrine basin. South of Shamva Hill, deep-marine turbidite deposits are overlain by shallow-marine sandstone and fluvial to alluvial fan conglomerate that form the host rocks of Shamva Mine. Such a coarsening-upward sequence is indicative of a braid- to fan-delta depositional setting (Nemec and Steel 1988) although, once again, the presence of a shear zone between the deep and shallow-water deposits cannot be ruled out. Coarse clastic sediments of the Shamva Mine strata were transported via mass flow and stream/sheet flow processes acting on an alluvial fan into a standing body of water where the sediments were reworked by wave and storm-induced currents.

Constraints for an understanding of the Shamvaian sequence

Besides the complexity of stratigraphic relationships, lateral thickness and facies distribution data for the individual tectonostratigraphic units were not obtained due to poor outcrop, making a basin analysis difficult. In addition, a feasible geodynamic scenario for sedimentary basin formation is difficult to evoke as long as the tectonic setting of the adjacent volcanic units of the Bulawayan Group and their stratigraphic relationship to each other has not been established. Any model for the evolution of the Bindura-Shamva greenstone belt, and the Shamvaian sequence in particular, has to take the following observations and inferences into account: (1) The contact between Bulawayan volcanics and underlying granitoids is sheared; this may suggest tectonic emplacement of the volcanic sequence. (2) The Arcturus Formation may have been tectonically emplaced onto the Iron Mask Formation due to the occurrence of a prominent silicified shear zone at its base (Dirks and Jelsma 1998*b*). (3) The abundance of pillow basalts and the lack of coarse siliciclastic intercalations may indicate an oceanic origin of the Arcturus Formation as a lava-plain sequence (cf. Dimroth et al. 1982). (4) The sharp contact between Arcturus Formation basalts and Shamvaian alluvial fan conglomerates is striking and suggests (a) that there was no major time lapse between basaltic volcanism and alluvial fan deposition due to the absence of intervening waterlain sediments and no indication for prolonged subaerial weathering of the basalts and (b) that the basin was initiated by a sudden tectonic event. (5) The Shamvaian sequence comprises a fluvio-deltaic fining-upward sequence with abundant granitic detritus and a coarsening and shallowing-upward sequence

dominated by intermediate/felsic volcanic detritus. (6) The provenance of the granitic detritus was a terrain compositionally similar to the Madziwa or Murehwa granitoid-gneiss terrains, whereas the provenance of the volcanic detritus was compositionally similar to the Iron Mask or Maparu Formations. (7) Palaeoflow orientations in the Shamvaian sequence are generally towards the west for the Pote Formation, indicating westward outbuilding of the clastic wedge. During deposition of the Tsambe Formation alluvial fans prograded into a postulated ocean to the north. (8) Deformation by westward thrusting (D_1) followed by vertical granite diapirism (D_2) affected all lithotectonic units of the Bindura-Shamva greenstone belt, including the Shamvaian sequence (Jelsma and Dirks 2000). However, an earlier, pre-D_1 (extensional?) deformation event cannot be ruled out.

Sedimentary basin model

A large-scale transgressive sequence from coarse, alluvial clastics to fine-grained, deep-water sediments, which, in turn, is overlain by shallowing-upward marine to fluvial facies is a typical motif of an extensional basin fill such as a short-lived continental rift or pull-apart basin (e.g., Schlische and Olsen 1990). Tectonism during sedimentation was probably active as recorded by common soft-sediment deformation features in the sedimentary sequence. A continental pull-apart basin interpretation is, however, inconsistent with the occurrence of thick, shallow-marine sandstones, recording evidence for high-energy current systems, thus necessitating a basin connected to the open ocean with a significant fetch. Furthermore, no basin-bounding strike-slip faults with fault displacement contemporaneous with sedimentation have been observed. In addition, it has to be noted that the basal coarse clastic sediments seem to be a basin-wide phenomenon and not a local occurrence along basin flanks and, as such, cannot be related to local formation of alluvial fans near basin-bounding faults. The upper part of the Shamvaian sequence, characterized by a regressive trend from turbiditic deposits at the base to alluvial fan deposits at the top, may indicate compressional tectonics in the later stage of the basin, culminating in thrust belt-style deformation of the basin fill together with the adjoining lithological units. Such an event of compressional deformation has been postulated for the BSGB. Jelsma and Dirks (2000) suggested westward emplacement of a tectonic nappe, comprising the Madziwa gneiss terrain enveloped by greenstones of the Maparu and Mungari Formation, onto the Shamvaian sediments (Fig. 7.1b). Due to incorporation of the sediments into the thrust stack, the Shamvaian Group has been interpreted as the fill of a foreland basin. However, the occurrence of coarse alluvial clastic sediments at the base of the succession is inconsistent with a foreland-type model; only the upper part may have formed in a foreland basin.

With respect to provenance, the question arises if there were compositionally distinct and geographically separated source terrains or only on terrain comprising both granitoid material and volcanic rocks. Unroofing of a single source terrain, consisting of granitoid basement and a cover of volcanic rocks, would yield an incease in granitoid detritus with time, a relationship not observed in the Shamvaian sequence. Two distinct source terrains may also explain the different palaeoflow directions recorded in the Pote and Tsambe Formations.

Tectonic scenarios

Several tectonic scenarios for the evolution of the Bindura-Shamva greenstone belt may be envisaged (Fig. 7.14) which can be modified or rejected when more geochemical and geochronological data become available. (1) Rifting of granitoid crust, possibly above a mantle plume, led to the formation of synrift felsic volcanics (Iron Mask Formation), followed by submarine basaltic volcanism (Arcturus Formation), followed by deposition of Shamvaian clastics possibly due to uplift of the graben shoulders. (2) E-W rifting of submerged continental crust resulted in the formation of oceanic crust (Arcturus Formation) in a narrow ocean setting. A passive margin sequence (Pote Formation) formed along the eastern rifted margin. Subsequent E-W shortening resulted in westward subduction of the oceanic crust under the western rifted margin and the formation of a volcanic arc (Iron Mask Formation) which became a source for Tsambe Formation clastics. During continent collision the upper part of oceanic crust and overlying sediments were obducted onto the arc sequence. (3) Rifting of a continental arc (granitoid gneisses overlain by Iron Mask Formation) gave rise to the formation of a back-arc basin on stretched continental crust. Stretching resulted in basaltic volcanism (Arcturus Formation) followed by deposition of the lower part (Pote Formation) of the Shamvaian sequence in an extensional regime. Closing of the back-arc basin during divergent plate motions and collision of the rifted arc with the rifted continental nucleus gave rise to deposition (and subsequent thrust deformation) of the upper part (Tsambe Formation) of the Shamvaian sequence in a compressional foreland or forearc regime.

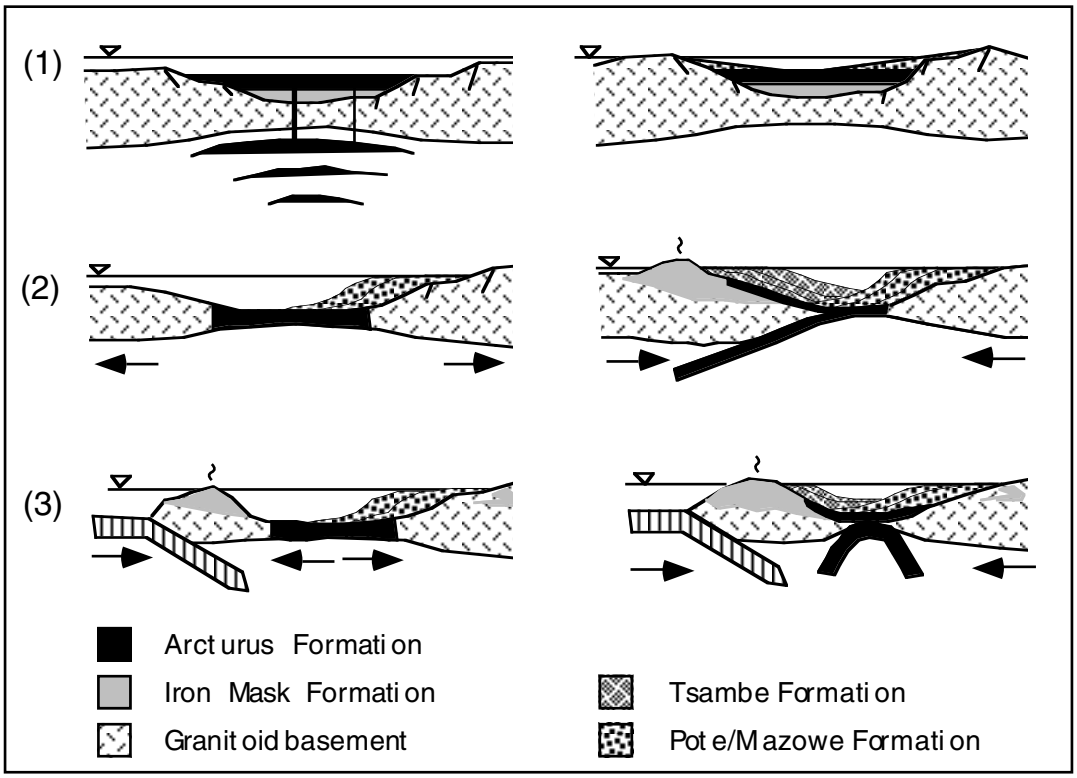

Fig. 7.14. Cartoons illustrating possible tectonic settings (1-3) for the deposition of the Shamvaian Group sediments. See text for discussion.

The Timiskaming connection

The current level of knowledge of the geology of the Bindura-Shamva greenstone belt does not allow us to pinpoint the geodynamic setting of the Shamvaian sedimentary sequence. It may be of interest, however, to compare the Shamvaian sediments with lithologically and temporally similar sediments which overlie volcanic rocks in greenstone belts of the Superior Province, Canada, commonly referred to as Timiskaming-type deposits (Thurston and Chivers 1990). Two main sedimentary facies associations have been described, a coarse-clastic alluvial-fluvial-shallow marine association and a deep-water turbidite association. The two associations occur in close proximity to each other and have been regarded as vertical as well as lateral facies variations (alluvial fan conglomerates grading rapidly both vertically and laterally into turbidites). In most cases, however, the actual contact does not crop out or is occupied by volcanic rocks or fault zones (Turner and Walker 1973; Hyde 1980; Dimroth et al. 1982; Ojakangas 1985). The sequence of submarine volcanic rocks overlain by non-marine sediments which are, in turn, overlain by deep-marine turbidites have puzzled many workers. Analogies to the Shamvaian sequence described herein are apparent. Recent studies have suggested two separate basin forming events, an early flysch-forming event dominated by turbidites and a late molasse-forming event characterized by alluvial conglomerates (Mueller et al. 1994; Mueller and Corcoran 1998). This interpretation is thus different from the earlier ones and regards the alluvial conglomerates to unconformably overlie the deep-water turbidites. Basin formation has been attributed to transtensional strike-slip faulting in terminal stages of arc-arc collision (late-orogenic strike-slip basins) on the basis of, for example, elongate basin geometry, bounding crustal-scale faults and basin margin unconformities (Mueller and Corcoran 1998). In Zimbabwe, strike-slip faults commonly bound outcrops of Shamvaian sediments as well, but faulting typically postdates sedimentation (e.g., Midlands greenstone belt, Dirks et al. 2001). However, we are just at the beginning of trying to understand the geology of the late Archaean sedimentary basins of the Zimbabwe craton. The many similarities to the Superior Province and other late Archaean granite-greenstone terrains (e.g., the Yilgarn craton) invites comparative studies.

REFERENCES

Allen, J.R.L., and Banks, N.L. 1972. An interpretation and analysis of recumbent-folded deformed cross-bedding. Sedimentology, 19: 257-283.

Baldock, J.W. 1991. The geology of the Harare greenstone belt and surrounding granitic terrain. Geological Survey of Zimbabwe Bulletin, 94, 213 pp.

Bickle, M.J., Martin, A., and Nisbet, E.G. 1975. Basaltic and peridotitic komatiites, stromatolites and a basal unconformity in the Belingwe greenstone belt, Rhodesia. Earth and Planetary Science Letters, 27: 155-162.

Bickle, M.J., Nisbet, E.G., and Martin, A. 1994. Archaean greenstone belts are not oceanic crust. Journal of Geology, 102: 121-138.

Blenkinsop, T.G., Martin, A., Jelsma, H.A., and Vinyu, M.L. 1997. The Zimbabwe Craton. *In* Greenstone Belts. *Edited by* M.J. de Wit and L.D. Ashwal. Oxford University Press, New York, pp. 567-580.

Bouma, A.H. 1962. Sedimentology of some flysch deposits: a graphic approach to facies interpretation. Elsevier, Amsterdam, 168 pp.

Bourgeois, J., and Leithold, E.L. 1984. Wave-worked conglomerates-depositional processes and criteria for recognition. *In* Sedimentology of gravels and conglomerates. *Edited by* E.H. Koster and R.J. Steel. Canadian Society of Petroleum Geologists. Memoir 10, pp. 331-343.

Cant, D.J., and Hein, F.J. 1986. Depositional sequences in ancient shelf sediments: some contrasts in style. *In* Shelf sands and sandstones. *Edited by* R.J. Knight and J.R. McLean. Canadian Society of Petroleum Geologists, Memoir 11, pp. 303-312.

Cotter, E. 1978. The evolution of fluvial style, with special reference to the central Appalachian Paleozoic. *In* Fluvial sedimentology. *Edited by* A.D. Miall. Canadian Society of Petroleum Geologists, Memoir 5, pp. 361-383.

Dalrymple, R.W., Zaitlin, B.A., and Boyd, R. 1992. Estuarine facies models: conceptual basis and stratigraphic implications. Journal of Sedimentary Petrology, 62: 1130-1146.

Dimroth, E.I., Laszlo, I., Rocheleau, M., and Goulet, N. 1982. Evolution of the south-central part of the Archaean Abitibi Belt, Quebec. Part I: Stratigraphy and paleogeographic model. Canadian Journal of Earth Sciences, 19: 1729-1758.

Dirks, P.H.G.M., and Jelsma, H.A. 1998*a*. Horizontal accretion leading to stabilization of the Archaean Zimbabwe Craton. Geology, 126: 11-14.

Dirks, P.H.G.M., and Jelsma, H.A. 1998*b*. Silicic layer-parallel shear zones in a Zimbabwean greenstone sequence; horizontal accretion preceding doming. Gondwana Research, 1: 177-194.

Dirks, P.H.G.M., Jelsma, H.A., and Hofmann, A. 2001. Thrust-related accretion of an Archaean greenstone belt in the Midlands of Zimbabwe. Journal of Structural Geology, in press.

Dott, R.H., and Bourgeois, J. 1982. Hummocky stratification: significance of its variable bedding sequences. Geological Society of America Bulletin, 93: 663-680.

Dougherty-Page, J.S. 1994. The evolution of the Archaean continental crust of northern Zimbabwe. Ph.D. thesis, Open University, Milton Keynes, England, 244 pp.

Duke, W.L. 1990. Geostrophic circulation or shallow marine turbidity currents? The dilemma of palaeoflow patterns in storm-influenced prograding shoreline systems. Journal of Sedimentary Petrology, 60: 870-993.

Eriksson, P.G., Condie, K.C., Tirsgaard, H., Mueller, W.U., Altermann, W., Miall, A.D., Aspler, L.B., Catuneanu, O., and Chiarenzelli, J.R. 1998. Precambrian clastic sedimentation systems. Sedimentary Geology, 120: 5-53.

Foster, R.P., Furber, F.M.W., Giligan, J.M., and Green, D. 1986. Shamva Gold Mine, Zimbabwe: A product of calc-alkaline-linked exhalative, volcaniclastic, and epiclastic sedimentation in the late Archaean. *In* Turbidite-hosted gold deposits. *Edited by* J.D. Keppie, R.W. Boyle, and S.J. Haynes. Geological Association of Canada, Special Paper 32, pp. 41-66.

Hyde, R.S. 1980. Sedimentary facies in the Archaean Timiskaming Group and their tectonic implications, Abitibi greenstone belt, northeastern Ontario, Canada. Precambrian Research, 12: 161-195.

Jelsma, H.A. 1993. Granites and greenstones in Northern Zimbabwe: tectono-thermal evolution and source regions. Ph.D. thesis, Free University of Amsterdam, Netherlands, 268 pp.

Jelsma, H.A., and Dirks, P.H.G.M. 2000. Tectonic evolution of a greenstone sequence in northern Zimbabwe: sequential early stacking and pluton diapirism. Tectonics, 19: 135-152.

Jelsma, H.A., van der Beek, P.A., and Vinyu, M.L. 1993. Tectonic evolution of the Bindura-Shamva greenstone belt (northern Zimbabwe): Progressive deformation around diapiric batholiths. Journal of Structural Geology, 15: 163-176.

Jelsma, H.A., Vinyu, M.L., Valbracht, P.J., Davies, G.R., Wijbrans, J.R., and Verdurmen, E.A.T. 1996. Constraints on Archaean crustal evolution of the Zimbabwe craton: A U-Pb zircon, Sm-Nd and Pb-Pb whole-rock isotope study. Contributions to Mineralogy and Petrology, 124: 55-70.

Leeder, M. 1987. Sediment deformation structures and the palaeotectonic analysis of sedimentary basins, with a case-study from the Carboniferous of northern England. *In* Deformation of sediments and sedimentary rocks. *Edited by* M.E. Jones and R.M.F. Preston. Geological Society, Special Publication 29, pp. 137-146.

Lowe, D. R. 1982. Sediment gravity flows: II. Depositional models with special reference to the deposits of high-density turbidity currents. Journal of Sedimentary Petrology, 52: 279-297.

Macgregor, A.M., 1951. Some milestones in the Precambrian of Southern Rhodesia. Proceedings of the Geological Society of South Africa, 54: 27-71

McCormick, D.S., and Grotzinger, J.P. 1993. Distinction of marine from alluvial facies in the Palaeoproterozoic (1.9 Ga) Burnside Formation, Kilohigok basin, N.W.T., Canada. Journal of Sedimentary Petrology, 63: 398-419.

Miall, A.D. 1985. Architectural-element analysis: a new method of facies analysis applied to fluvial deposits. Earth-Science Reviews, 22: 261-308.

Mukwakwami, J. 1999. The spatial and structural relationship between Tafuna Hill Formation and surrounding Shamvaian metasediments. BSc. Hons. thesis, University of Zimbabwe, 46p.

Mueller, W.U., Donaldson, J.A., and Doucet, P. 1994. Volcanic and tectono-plutonic influences on sedimentation in the Archaean Kirkland Basin, Abitibi greenstone belt, Canada. Precambrian Research, 68: 201-230.

Mueller, W.U., and Corcoran, P.L. 1998. Late-orogenic basins in the Archaean Superior Province, Canada: characteristics and inferences. Sedimentary Geology, 120: 177-203.

Nemec, W., Steel, R.J., Porebski, S.J., and Spinnangr, A. 1984. Domba conglomerate, Devonian, Norway: process and lateral variability in a mass flow-dominated, lacustrine fan-delta. *In* Sedimentology of gravels and conglomerates. *Edited by* E.H. Koster and R.J. Steel. Canadian Society of Petroleum Geologists, Memoir 10, pp. 295-320.

Nemec, W., and Steel, R.J. 1984. Alluvial and coastal conglomerates: their significant features and some comments on gravelly mass-flow deposits. *In* Sedimentology of gravels and conglomerates. *Edited by* E.H. Koster and R.J. Steel. Canadian Society of Petroleum Geologists, Memoir 10, pp. 1-31.

Nemec, W., and Steel, R.J. 1988. What is a fan delta and how do we recognize it? *In* Fan deltas: sedimentology and tectonic settings. *Edited by* W. Nemec and R.J. Steel. Blackie, pp. 3-13.

Ojakangas, R.W. 1985. Review of Archaean clastic sedimentation, Canadian Shield: major felsic volcanic contributions to turbidite and alluvial fan—fluvial facies associations. *In* Evolution of Archaean Supracrustal

Sequences. *Edited by* L.D. Ayres, P.C. Thurston, K.D. Card, and W. Weber. Geological Association of Canada, Special Paper 28, pp. 23-47.

Owen, G. 1987. Deformation processes in unconsolidated sands. *In* Deformation of sediments and sedimentary rocks. *Edited by* M.E. Jones and R.M.F. Preston. Geological Society, Special Publication 29, pp. 11-24.

Pettijohn, F.J. 1943. Archaean Sedimentation. Geological Society of America Bulletin, 54: 925-972.

Ramsay, J.G. 1989. Emplacement kinematics of a granite diapir: The Chinamora Batholith, Zimbabwe. Journal of Structural Geology, 11: 191-209.

Ridley, J.R., Vearncombe, J.R., and Jelsma, H.A. 1997. Relations between greenstone belts and associated granitoids. *In* Greenstone Belts. *Edited by* M. J. de Wit and L. D. Ashwal. Oxford University Press, New York, pp. 376-397.

Schlische, R.W., and Olsen, P.E. 1990. Quantitative filling model for continental extensional basins with application to early Mezosoic rifts of eastern North America. Journal of Geology, 98: 135-155.

Schumm, S.A. 1968. Speculations concerning paleohydrologic controls of terrestrial sedimentation. Geological Society of America Bulletin, 79: 1573-1588.

Shackleton, R.M. 1995. Tectonic evolution of greenstone belts. *In* Early Precambrian Processes. *Edited by* M. P. Coward and A. C. Ries. Geological Society, Special Publication 95, pp. 53-65.

Soegaard, K., and Eriksson, K.A. 1989. Origin of thick, first cycle quartz arenite successions: evidence from the 1.7 Ga Ortega Group, Northern New Mexico. Precambrian Research, 43: 129-141.

Stidolph, P.A. 1977. The geology of the country around Shamva. Geological Survey of Rhodesia Bulletin, 78, 249pp.

Stowe, C.W. 1984. The early Archaean Selukwe nappe, Zimbabwe. *In* Precambrian Tectonics Illustrated. *Edited by* A. Kröner and R. Greiling, Nägele und Obermiller, Stuttgart, Germany, pp. 41-56.

Thurston, P.C., and Chivers, K.M. 1990. Secular variation in greenstone sequence development emphasizing Superior Province, Canada. Precambrian Research, 46: 21-58.

Turner, C.C., and Walker, R.G. 1973. Sedimentology, stratigraphy and crustal evolution of the Archaean greenstone belt near Sioux lookout, Ontario. Canadian Journal of Earth Sciences, 10: 817-845.

Tyndale-Biscoe, R. 1931. The geology of the central part of the Mazowe Valley Gold Belt. Geological Survey of Southern Rhodesia Bulletin, 22.

Wilson, J.F., Nesbitt, R.W., and Fanning, C.M. 1995. Zircon geochronology of Archaean felsic sequences in the Zimbabwe craton: A revision of greenstone stratigraphy and a model for crustal growth. *In* Early Precambrian Processes. *Edited by* M. P. Coward and A. C. Ries. Geological Society, Special Publication 95, pp. 109-126.

CHAPTER 8

Field relationships of tectonic ironstone horizons in the Zimbabwe craton and their significance for greenstone belt geology

Axel Hofmann, Paul H.G.M. Dirks, Hielke A. Jelsma, and Nikadzino Matura
submitted to Journal of the Geological Society of London

Abstract—Metre-thick horizons of ironstone lithologically similar to "sulfide-facies" banded iron formation, but interpreted as silicified and sulfide-impregnated shear zones, are a common component of the greenstone stratigraphy of the Archaean Zimbabwe craton. Such tectonic ironstones separate different lithostratigraphic units commonly regarded as autochthonous rock sequences. On outcrop scale, shearing along ironstone horizons is indicated by anastomosing foliation domains, folding, boudinage, and mylonitic fabrics, and, on a regional scale, by truncation of bedding and/or foliation, an anastomosing geometry of the horizons, and duplication/ juxtaposition of lithostratigraphic units. Tectonic ironstone formation is attributed to in-situ silicification and iron (sulfide)-impregnation of rocks, commonly sediments, by mineralized fluids that penetrated the shear zones and their immediate wall rocks. The shear zones formed as a result of thin-skinned thrust tectonics that gave rise to horizontal accretion, imbrication and juxtaposition of volcanic and sedimentary rock units prior to deformation associated with granitoid diapirism. As a result, "layer-cake" stratigraphic models of greenstone sequences containing tectonic ironstone "layers" have to be treated with care, and the use of ironstone horizons as stratigraphic markers should be discouraged.

INTRODUCTION

The evolutionary history of Archaean greenstone belts is controversial and, to date, no tectonic model for their evolution has been agreed upon. Greenstone belts have been related to plate tectonic-style horizontal tectonic accretion of oceanic, island arc, and continental crustal fragments (Kusky, 1989; Card, 1990; Swager and Griffin, 1990; de Wit et al., 1992; Myers, 1995; Kusky and Vearncombe, 1997; Dirks and Jelsma, 1998a) or to superposition of rift-related sequences on already existing segments of differentiated crust (Campbell and Hill, 1988; Bouhallier et al., 1993; Bickle et al., 1994; Jelsma et al., 1996; Hamilton, 1998).

The evolution of the granitoid-greenstone terrain of the Zimbabwe craton involved a number of rock formation stages. Each of these is represented by the deposition of a volcano-sedimentary sequence and the emplacement of granitoids (Wilson et al., 1995). The oldest segment of granitoid crust is the 3.6-3.5 Ga old Tokwe Gneiss Complex (Fig. 8.1) which contains greenstone enclaves of the Sebakwean Group. Later stages of greenstone formation include the Belingwean (~2900 Ma), Lower Bulawayan (~2800 Ma), Upper Bulawayan (~2700 Ma), and Shamvaian (~2650 Ma) Groups. Stabilisation of the craton was achieved around 2600 Ma ago with the emplacement of large volumes of crustally derived Chilimanzi suite granites (Wilson et al., 1995; Jelsma et al., 1996; Horstwood, 1998), followed by intrusion of the Great Dyke.

Several workers have interpreted the Zimbabwe craton as vertically accreted crust. In this model, coherent units of volcano-sedimentary rocks were laid down in rifts (in fixed positions above mantle plumes) on top of older continental basement and underwent little deformation until the late-stage emplacement of granite-gneiss complexes (Bickle et al., 1975; Blenkinsop et al., 1993; Bickle et al., 1994; Shackleton, 1995; Wilson et al., 1995; Ridley et al., 1997; Horstwood et al., 1999). Vertical accretion of the Zimbabwe craton was first proposed by Macgregor (1951) to explain the geometry of arcuate greenstone belts surrounded by subelliptical granitoid batholiths. The model was supported by the recognition of an unconformity in the Belingwe greenstone belt where sedimentary rocks of the Bulawayan Group overlie granitoid gneisses and older greenstones (Bickle et al., 1975). The recognition of this unconformity had a chain effect, and, as a result, most angular stratigraphic relationships in Zimbabwean greenstone sequences were interpreted as unconformities. Many of the proposed unconformities are occupied by chert-rich, sulfide-mineralized and laterally persistent horizons (variably termed sulfide-facies banded iron formation, chert, ironstone, etc.) that have been interpreted to be of sedimentary origin. The presence of these ironstone horizons has placed important constraints on the proposed tectonic evolution of greenstone belts in Zimbabwe, because they have been regarded as stratigraphic marker horizons due to their exceptional lateral continuity. Both the unconformities and ironstone horizons have been correlated laterally and used to construct a craton-wide stratigraphy (Wilson, 1979; Wilson et al., 1995). The existence of such a layer-cake greenstone stratigraphy, underlain by a basement unconformity, led to the suggestion that continental crust was covered by one or several connected extensional greenstone basins, before they were disturbed by vertical diapiric processes. This interpretation ignored the occurrence of

shear zones parallel to the stratigraphy, many of which coincide with low-angle truncation planes. Layer-parallel shear zones have been recognised in the past, but they were generally interpreted as insignificant (Blenkinsop et al., 1993), or being the direct result of gravity sliding away from the centres of rising diapiric domes (Stowe, 1984; Jelsma et al., 1993). The commonly held belief was that these shears did not seriously affect the stratigraphy of the greenstone belts (e.g., Wilson et al., 1995). Recently, however, some workers have suggested otherwise (Kusky and Kidd, 1992; Dirks and van der Merwe, 1997; Dirks and Jelsma, 1998a,b; Jelsma and Dirks, 2000). Kusky and Kidd (1992), for example, interpreted a layer-parallel shear zone in the Belingwe greenstone belt as a major displacement zone across which oceanic crust was emplaced on top of granitoid basement and older greenstone sequences.

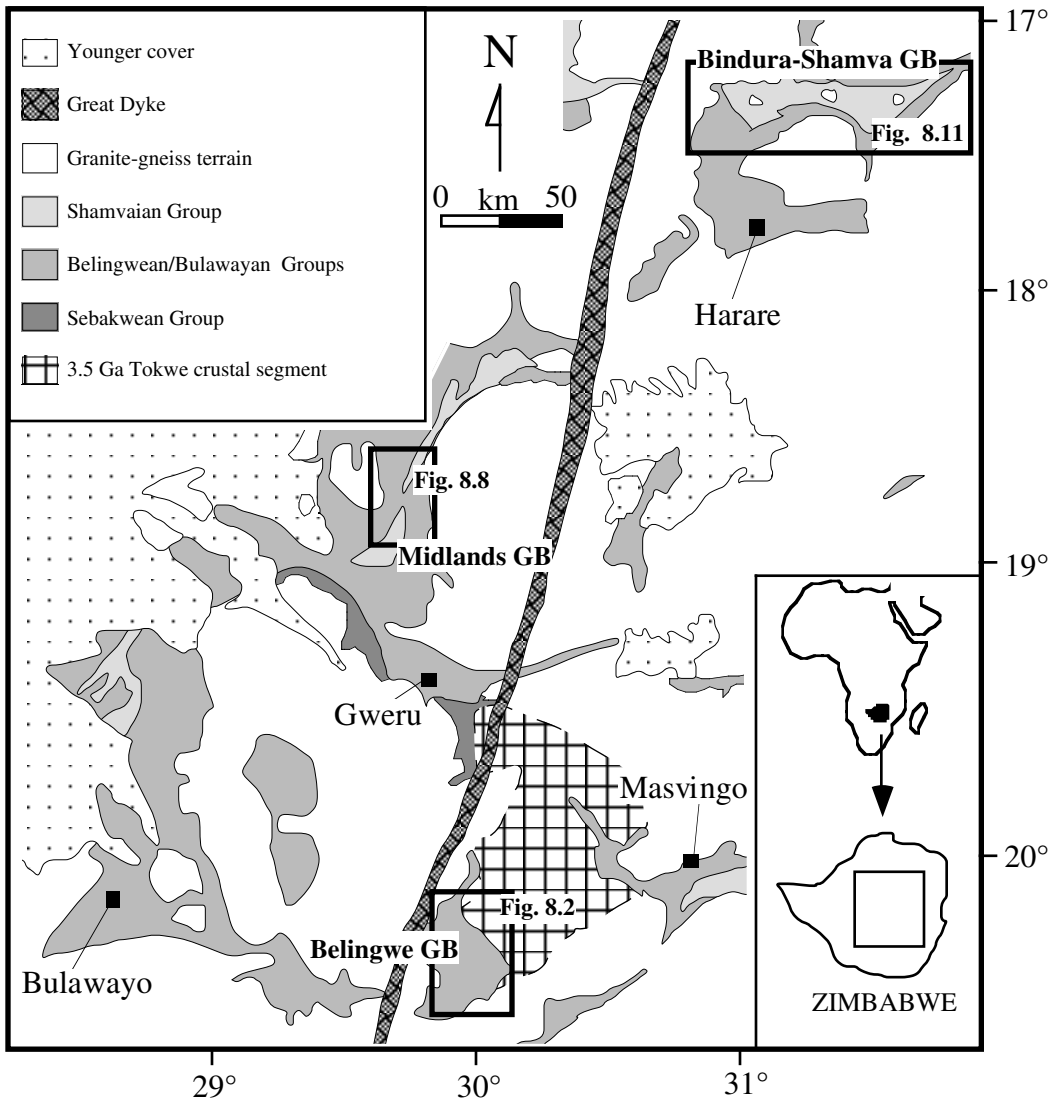

Fig. 8.1. Geological map of the central part of the Zimbabwe craton.

The tectonic interpretation of the Zimbabwe craton hinges on the correct recognition, interpretation and correlation of unconformities, stratigraphic marker horizons, and layer-parallel shear zones. Many of the silicified and sulfide-mineralized horizons, which are commonly

associated with proposed unconformities and are mostly regarded as banded iron formation, show features which are not conformable with a sedimentary origin. In this paper we present a detailed description of such horizons from three greenstone belts in Zimbabwe. Our aims are (1) to characterize the lithology, lithological variability, structure and relationships of tectonic ironstones to adjacent rocks, (2) to develop criteria for their recognition which sets them apart from chemical sedimentary rocks, (3) to provide a guidance for future field-related studies of greenstone sequences and (4) to redefine existing stratigraphic models in greenstone belts.

IRON FORMATIONS: SOME BACKGROUND

Much has been written on the classification of iron formations which are, according to Kimberley (1978), mappable rock units composed mostly of iron-rich chemical sedimentary rock (ironstone). The origin of iron formation, which is a common component of greenstone sequences worldwide, has been discussed for many decades and is still a controversial topic. Iron formation is generally regarded as sedimentary in origin, and has been classified mainly on the basis of mineralogical composition (James, 1954), proposed tectonic setting (Gross, 1965), and depositional environment (e.g., Kimberley, 1978; Simonson, 1985). The original facies concept of James (1954) for the description of iron formation, depending on the type of iron minerals present, included oxide, silicate and carbonate facies iron formation, thought to have been deposited in different water depths. An additional sulfide facies type was described as consisting of pyritic carbonaceous shale. Kimberley (1989) remarked that the sulfide facies type, by definition, is not iron formation, since the bulk of the rock does not represent chemical sediment. The description of pyritic mudrocks is markedly in contrast to proposed sulfide facies iron formations described by economic geologists to consist of interstratified chert and sulfide layers. These sulfidic rocks are commonly associated with other ironstone facies, commonly the oxide facies type, and host a number of important gold deposits in Archaean terrains (e.g., Fripp, 1976; Anhaeusser, 1976; cf. Chown et al., 2000). A syngenetic origin of sulfides and gold was suggested by early workers, mainly based on the stratiform and stratabound occurrence of the gold-bearing sulfides in ironstone (Fripp, 1976). More recent studies suggest an epigenetic origin (Phillips et al., 1984; Groves et al., 1987), indicating that sulfide-rich iron formation is a replacement type rather than a primary sedimentary facies. Sulfide and associated gold-mineralization is thought to have been preferentially deposited in iron-rich sedimentary rocks, such as oxide-facies iron formation, by sulfidation of iron oxide-rich layers from hydrothermal fluids. As a result, many sulfide facies iron formations described in the literature may not be iron formations and may not be of sedimentary origin.

For the purpose of this paper, we use the term ironstone for an iron-rich rock, not necessarily of sedimentary origin. Banded iron formation (BIF) refers to a mappable rock unit of iron-rich, chemical sedimentary rock, comprising cm-scale, alternating layers of chert and iron-rich material. BIF's described herein from greenstone belts in Zimbabwe can all be regarded as oxide-facies types (James, 1954) and are similar to BIF in other Archaean greenstone belts of the world (e.g.,

Goodwin, 1973; Beukes, 1973; Trendall, 1973). A certain rock type which is generally rich in iron and/or silica and which occurs along tectonic rather than primary lithological contacts is herein termed tectonic ironstone. Tectonic ironstone encompasses silicious and ferruginous rock types which are characterized by the presence of chert or cherty quartzite, iron oxides and/or sulfides. The mineralogy and chemistry of such ironstones have not yet been subjected to detailed study.

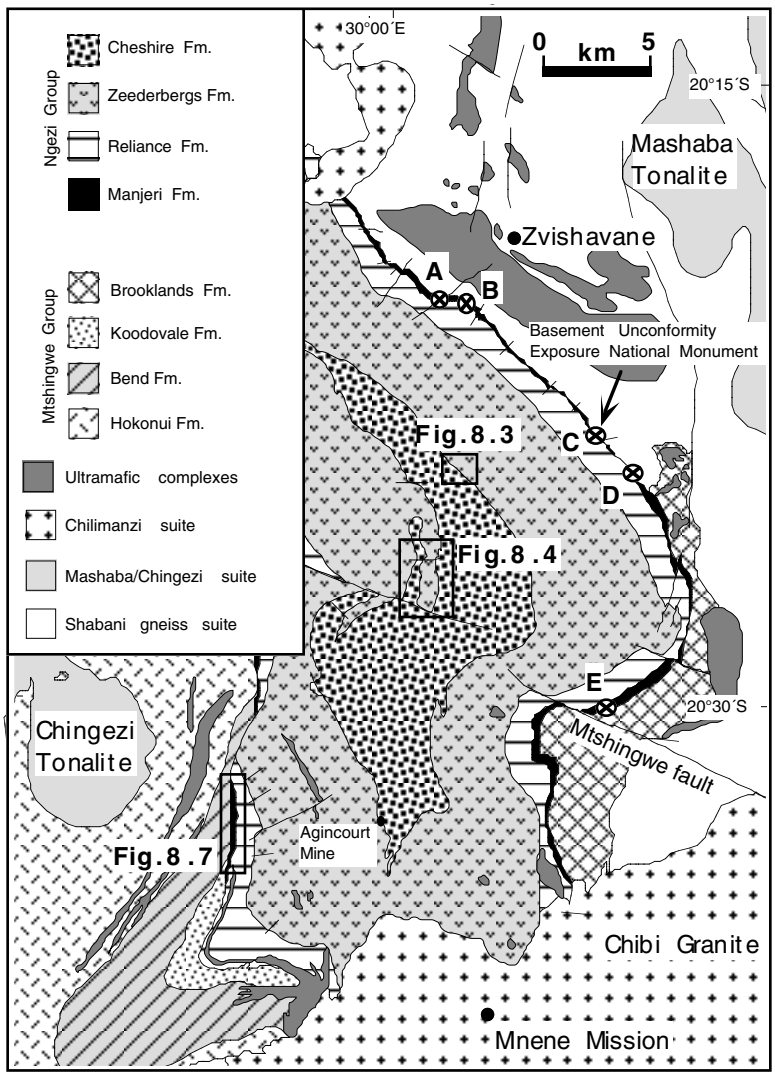

Fig. 8.2. Geological map of the Belingwe greenstone belt (after Martin et al., 1993).

TECTONIC IRONSTONES OF THE BELINGWE GREENSTONE BELT

The Belingwe greenstone belt (BGB) is situated in the southern part of Zimbabwe (Fig. 8.2) and contains a well preserved sequence of late Archaean supracrustal rocks that locally overlie a granitoid basement (Shabani gneiss complex) up to 3.5 Ga old. The stratigraphy of the BGB has been used by Wilson et al. (1995) as the basis for stratigraphic subdivision of the greenstones of the Zimbabwe craton. The Belingwe greenstones have been divided into the Mtshingwe Group at the base and the Ngezi Group at the top. The Mtshingwe Group comprises the Hokonui, Bend, Koodoovale and Brooklands Formations, all of uncertain tectonic environment. U/Pb zircon ages of these rocks range from 2.90 to 2.83 Ga (Wilson et al., 1995). The Ngezi Group comprises the Manjeri, Reliance, Zeederbergs and Cheshire Formations. The Manjeri Formation is a thin, clastic sedimentary unit which has been deposited unconformably on the Mtshingwe Group and granitoid basement (Bickle et al., 1975). The Manjeri Formation is overlain by 2692±9 Ma old (Chauvel et al., 1993) tholeiites, komatiitic basalts and komatiites of the Reliance Formation. The Zeederbergs Formation gradationally overlies the Reliance Formation (Scholey, 1992). It is a 3 km thick unit of commonly pillowed lava flows of tholeiite and minor andesite with rare intercalations of volcaniclastic sediment (Brake, 1996). The ca. 1.3 km thick

Cheshire Formation forms the uppermost stratigraphic unit of the BGB. It consists of sedimentary rocks intruded by dolerite sills and can be subdivided into two lithostratigraphic units (chapter 2), the carbonate member (shallow-water limestone and shale) and the overlying siliciclastic member (deep-water conglomerate and shale). Ironstones occur in the Manjeri Formation and in the Cheshire Formation, the latter of which will be described first.

Cheshire Formation

Tectonic ironstones are typically 5-10 m thick horizons that are continuous for hundreds of metres to several kilometres. They are common along the Zeederbergs-Cheshire Formation contact and along tectonic contacts in the carbonate member. The tectonic significance of ironstones can be observed along the eastern Zeederbergs-Cheshire Formation contact (Fig. 8.3a), where pillow lavas sharply border on conglomerate in the south and shale in the north. The basalt-shale contact is occupied by an ironstone horizon which can be traced continuously in the mapped area. Lenticular bodies of ironstone further occur adjacent to the contact. Bedding is locally at an angle to, and transected by, ironstone, indicating that the ironstone is situated along a shear zone (Fig. 8.3b).

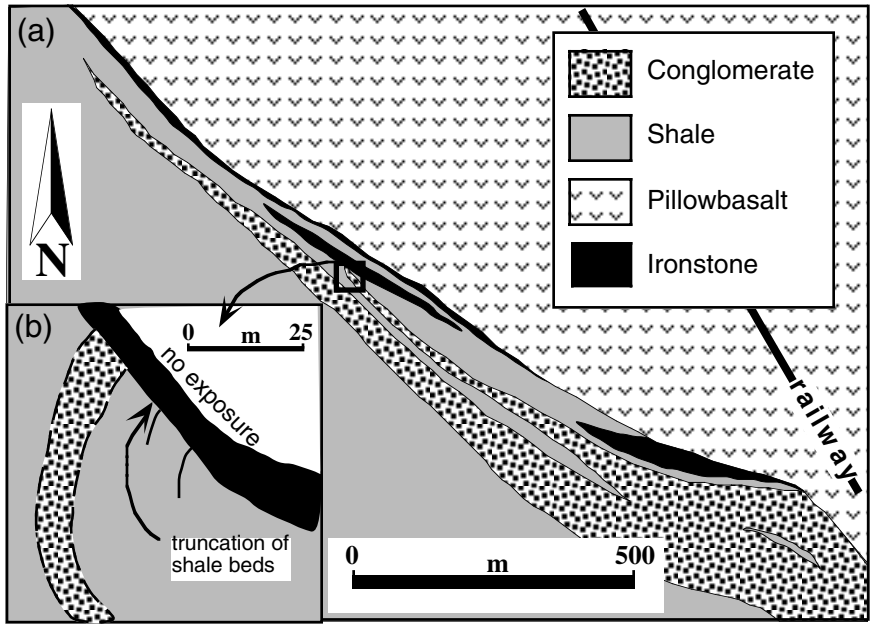

Fig. 8.3. (a) Detailed map of the eastern Zeederbergs-Cheshire Formation contact. (b) Bedding is locally transected by ironstone.

Along the western contact, pillow lavas of the Zeederbergs Formation are overlain by Cheshire carbonates (Fig. 8.4). The top of the carbonate sequence is formed by a karst breccia which outlines an irregular relief occupied by conglomerate and shale beds; bedding is truncated by a continuos ironstone horizon. The ironstone is overlain by a clastic unit in which bedding is locally tight to isoclinally folded. The clastic unit is transected by an overlying tectonic thrust slice of Zeederbergs Formation pillow lavas (chapter 3). Discontinuous ironstone horizons are developed along this

contact. A second, tectonically duplicated unit of Cheshire carbonates locally overlies the volcanics, is completely bound by ironstone (Fig. 8.4) and represents a tectonic horse structure.

Where the Zeederbergs-Cheshire contact lacks ironstone horizons, the contact is variably sheared, and adjacent rocks are silicified and characterized by mostly oxidized sulfide-impregnation. Alteration effects decrease away from the contact, indicating that the alteration resulted from mineralized fluids infiltrating the contact zone during shearing. In the southwestern part of the belt at Agincourt Mine, gold was extracted from the ironstone at the Zeederbergs-Cheshire contact (Fig. 8.2).

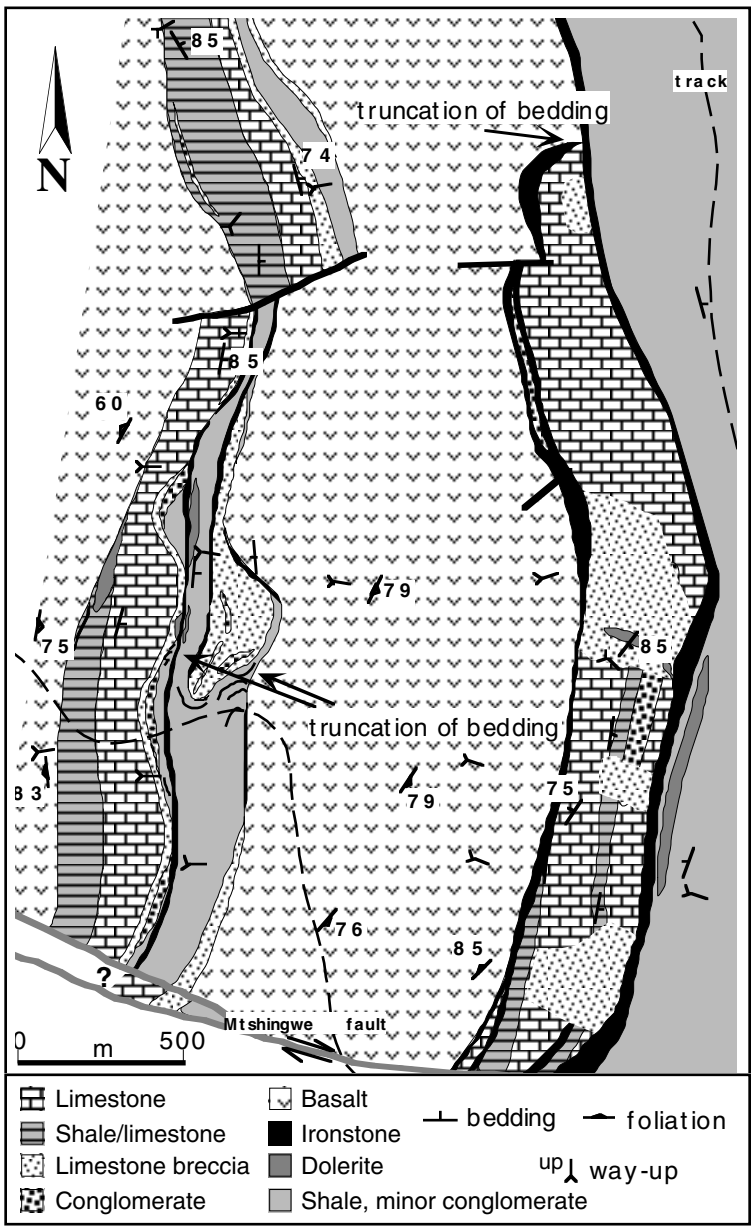

Fig. 8.4. Detailed map of the western Zeederbergs-Cheshire Formation contact. Note the ironstone which completely surrounds the carbonate unit in the eastern part of the map and local truncation of bedding.

Lithology and structure

Ironstone is a heterogeneous rock that consists predominantly of three varieties: (1) banded ironstone, (2) brecciated banded ironstone, and (3) mixed ironstone that consists of banded chert intercalated with various, iron oxide-impregnated sediments. Banded ironstone (type 1) consists of chert bands, typically 1-3 cm in thickness (range 0.5-20 cm), that are thinly intercalated with equally thick bands of massive, hematitic, fine-grained material, and, locally, hematized, relictically laminated mudstone. Chert layers are typically discontinuous, pinch-and-swell or are boudinaged, whereas hematite-rich layers are more continuous. The layering is commonly deformed into small- to medium-scale, gentle to tight, asymmetric and disharmonic folds (Fig. 8.5a). Lenticular quartz veins, both oblique and parallel to bedding, and axial planar to folds are common. Isoclinal folds occur and

mostly represent strongly deformed, overturned asymmetric folds. Truncation surfaces occur where massive hematitic layers cross-cut chert layers.

Brecciated ironstone (type 2 ironstone) is derived from the disruption of banded ironstone with which it is intercalated (Fig. 8.5b). It comprises lenticular to rectangular, angular fragments of banded ironstone in a matrix of massive and vuggy (moulds after former sulfides), fine-grained hematitic material identical to the material interlayered with chert.

Mixed (type 3) ironstone comprises chert layers that are intercalated (decimetre to metre-scale) with sheared, hematite (sulfide)-impregnated sediment including: (a) hematitic shale, (b) brecciated shale with shale fragments in a massive hematitic matrix (Fig. 8.5c), (c) conglomerate with pebbles partly leached or replaced by iron oxides, and (d) quartzose sandstone, where, in thin section, the quartz grains are partly replaced by chert (Fig. 8.5d) or fractured along hematite-filled veins. It is important to note that iron oxides in the ironstones and associated rocks are derived from the weathering of sulfides, mainly pyrite, which occur in less weathered rocks or in the subsurface.

Ironstones are locally cut by layer-parallel to irregular vein networks of quartz and hematitic material. Quartz veins are commonly intruded and brecciated by hematitic veins. Locally, intense brecciation gave rise to angular vein quartz fragments enveloped by a matrix of massive hematitic rock. Chert veins, similar to those forming layers in banded cherts, are locally preserved as both foliation-parallel and cross-cutting, intrusive veins in brecciated cherts (Fig. 8.5b).

Shale adjacent to ironstone horizons is ferruginized, strongly foliated, and complexly folded where it contains chert layers. Anastomosing shear zones are common. Limestone intercalated with ironstone shows various stages of replacement by chert and hematitic material parallel to bedding and along fractures.

Interpretation

The ironstones of the Cheshire Formation have previously been interpreted as deformed BIF (Martin, 1978). This assumption contradicts the observation that ironstones are restricted to lithological contacts where there is clear evidence of shearing, truncation of bedding and stratigraphic duplication. Additionally, sediments adjacent to, or intercalated with, ironstone are strongly sheared. Based on these observations, the ironstones are interpreted as rocks which gained their lithological characteristics during deformation.

The restricted occurrence of silicified and hematized sedimentary rocks in the vicinity of shear zones and ironstones indicates that silica and iron were introduced after deposition during shearing. In addition, more intensely sheared rocks are more strongly silicified/hematized due to the increase in alteration towards the shears. Along the Zeederbergs/Cheshire contact, ironstone is common where basalt borders on shale, but is rare at basalt-conglomerate contacts. This suggests that ironstone preferentially formed by in-situ silicification and iron (sulfide)-impregnation of fine-grained sediments (shale) by mineralized fluids adjacent to and within fault zones. However, ironstone formed by replacement from a variety of rock types such as sandstone and limestone. In

addition, a certain amount of chert and, in particular, former sulfides represent newly formed, intrusive material as indicated by bedding-parallel and cross-cutting veins. Progressive intrusion and hydraulic fracturing gave rise to brecciation of the banded rocks.

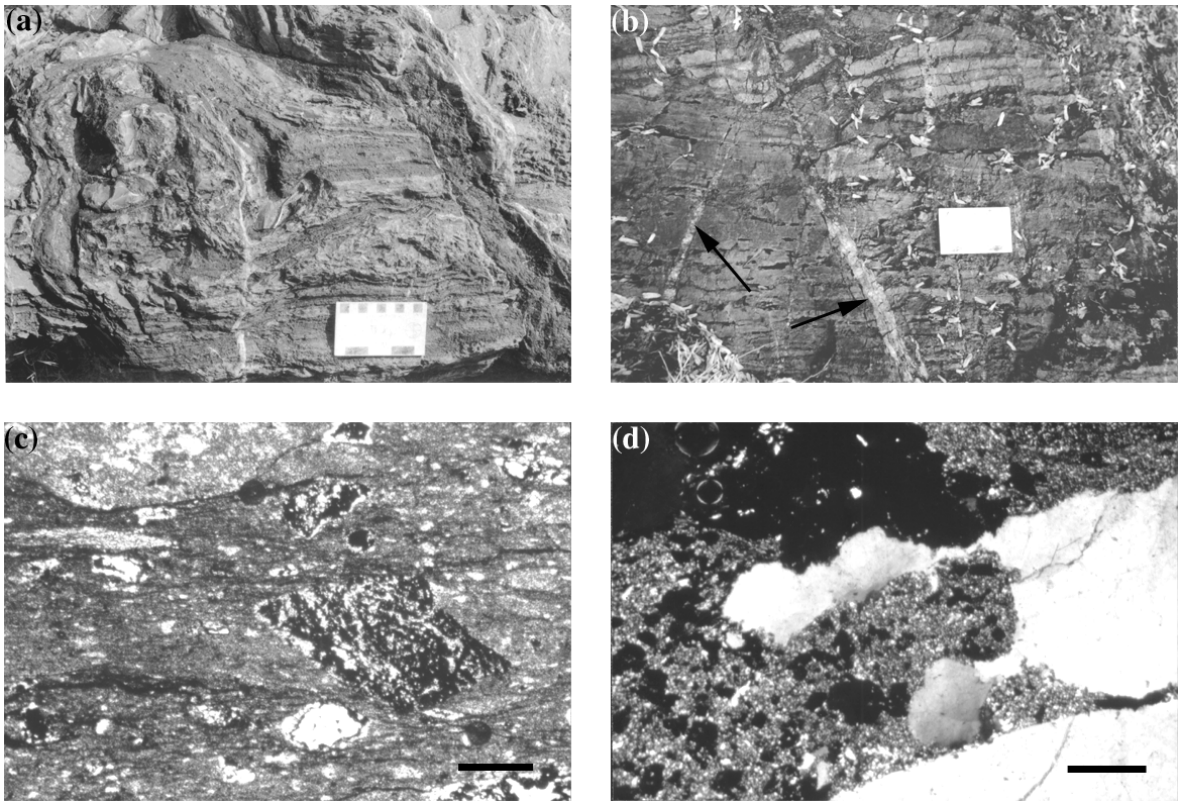

Fig. 8.5. (a) Complexly folded banded ironstone. (b) Vuggy banded ironstone intercalated with brecciated ironstone (top) and transected by chert veins (arrows). (c) Photomicrograph (plane-polarized light) of sheared hematitic shale intercalated with ironstone. Scale bar is 200 μm. (d) Photomicrograph (crossed-polarized light) of silicified quartzose sandstone. Note the replacement of quartz grains by iron oxide-rich chert. Scale bar is 200 μm.

Manjeri Formation

The Manjeri Formation lies unconformably on the Shabani Gneiss Complex in the east (Basement Unconformity Exposure National Monument, Fig. 8.2) and overlies the Mtshingwe Group in the south-east and west of the BGB. It has a maximum thickness of 250 m and is absent at several localities except for a continuous ironstone horizon. Hunter et al. (1998) described the Manjeri Formation to consist of three stratigraphic units. The lower Spring Valley Member consists of fluvial to shallow-water sediments including conglomerate, sandstone, shale, BIF and localized stromatolitic limestone. The middle Rubweruchena Member comprises immature alluvial fan to fan delta clastics, mainly conglomerate and sandstone, and is capped by a 5-10 m thick horizon (Jimmy Member) of sulfidic ironstone which will be the focus of this section. When comparing sections of the Manjeri Formation from the eastern side of the belt (Fig. 8.6), the lower Spring Valley Member appears laterally continuous and retains a similar thickness. The overlying Rubweruchena Member is discontinuous and shows marked facies changes over a short distance; the section resembles a

display of a horst-and-graben depositional setting. Rapid facies changes along strike have been stated as a characteristic feature of the Manjeri Formation (e.g., Orpen, 1978). In contrast, the overlying ironstone horizon is laterally continuous and equally thick. Similar relationships can be observed in other parts of the BGB where contacts between the Reliance Formation and underlying rocks (Mtshingwe Group greenstones, granitoids) are occupied by the Jimmy Member ironstone with or without variably thick Manjeri sediments below the ironstone.

Sulfidic ironstones identical to the Jimmy Member ironstone occur locally within or at the base of the Manjeri Formation. Along the western side of the BGB, Manjeri sediments sharply overlie mafic volcanics and intercalated continuous horizons of BIF of the Bend Formation, Mtshingwe Group (Fig. 8.7). The contact is mostly occupied by ironstone, and the stratification in the underlying rocks is at an angle to bedding in the Manjeri sediments. This angular relationship has been interpreted as evidence for an unconformable contact.

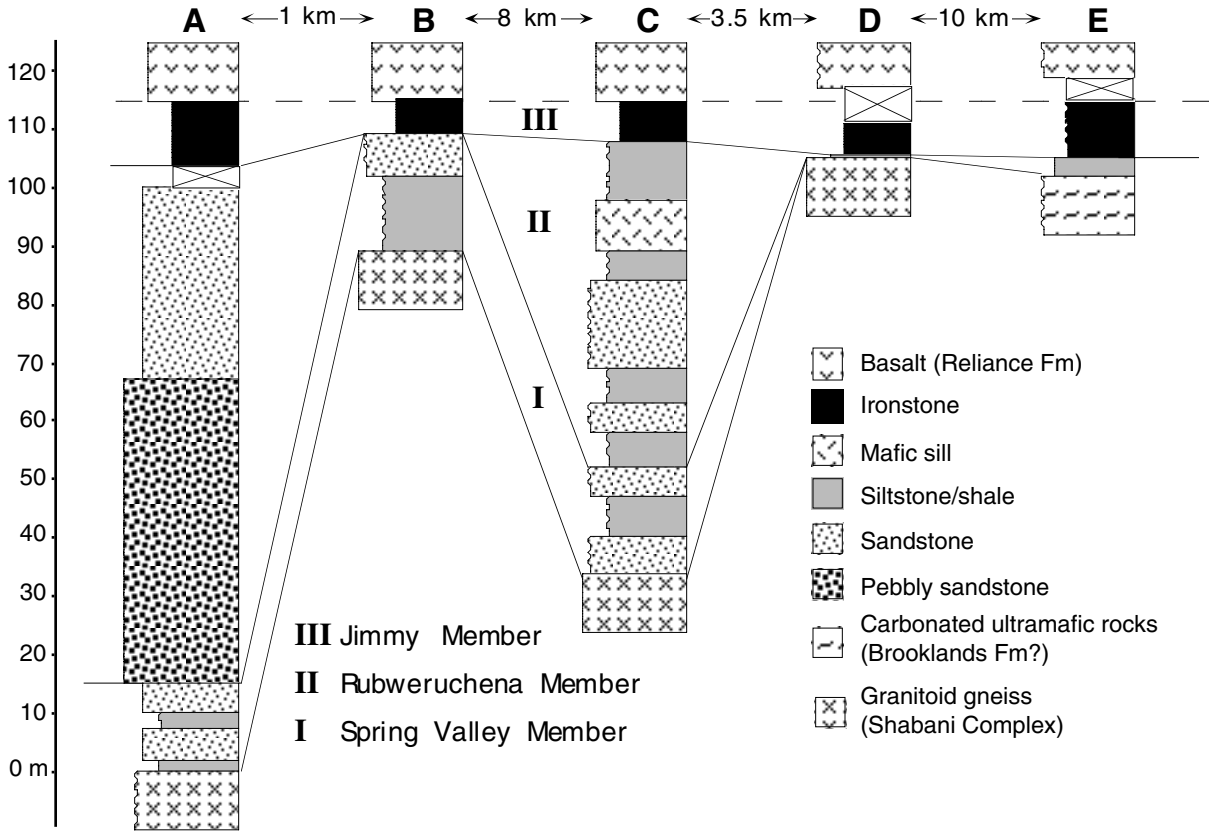

Fig. 8.6. Simplified graphic logs of the Manjeri Formation (see Fig. 8.2 for location of sections). Logs A-C are from Hunter (1997). Note the lateral discontinuity of the Spring Valley and Rubweruchena Members and the continuity of the Jimmy Member.

Lithology and structure

The ironstone horizon at the top of the Manjeri Formation is identical in composition and structural fabric to the Cheshire ironstones. It is dominated by banded ironstone and brecciated banded ironstone. Asymmetric folds and axial planar quartz veins, isoclinal folds and boudinage of

chert layers are common. Hunter (1997) described the rock as a highly-weathered, highly-deformed gossaneous ironstone in surface outcrop. In the subsurface, the ironstone is dominated by massive sulfide (pyrite, minor pyrrhotite) and chert, intercalated with chloritic shale, graphitic and carbonate mudstone and vein quartz. Zones of high strain as indicated by anastomosing cleavage domains, local mylonitic fabrics as well as intensely folded carbonaceous horizons showing an axial planar cleavage are common.

Ironstone at the Bend-Manjeri contact differs from sedimentary BIF of the Bend Formation by the discontinuity of banding, common brecciation and sulfide mineralization. Colour of the ironstone (whitish and dark grey chert layers, brownish-red hematitic bands) is in stark contrast to the bright red colours of the Bend jaspilitic BIF. The ironstone is locally represented by hematite matrix-supported vein quartz breccia. Shale intercalated with ironstone shows anastomosing cleavage domains and contains lens-shaped inclusions of ironstone. In places, intercalations of sandstone have mylonitic fabrics.

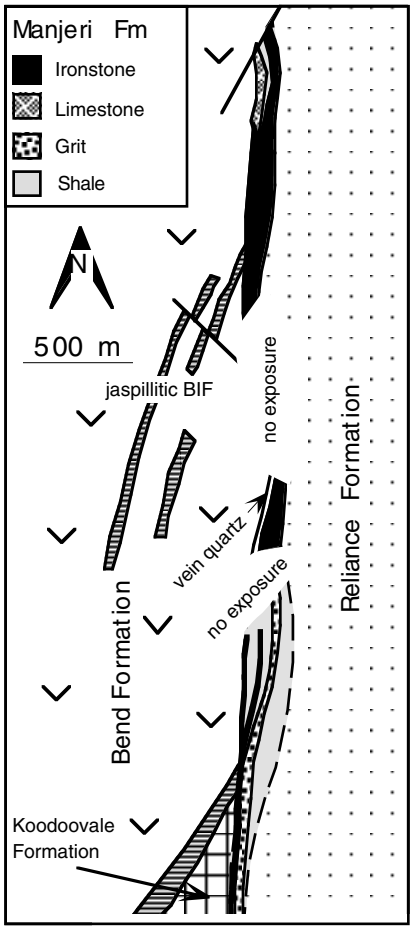

Fig. 8.7. Simplified geological map of the contact between the Mtshingwe Group and Manjeri Formation (modified after Orpen, 1978).

Interpretation

The Jimmy Member ironstone is generally regarded as a sulfide-facies BIF which was deposited in a low-energy, clastic-free environment (Hunter, 1977). Its state of deformation has been attributed to (a) soft sediment deformation, such as slumping prior to lithification (e.g., Nisbet et al., 1993), (b) accommodation of strain related to layer-parallel slip during synclinal folding of the greenstone sequence (Blenkinsop et al., 1993), and (c) thrusting of the Reliance Formation onto the Manjeri Formation (Kusky and Kidd, 1992). Soft-sediment deformation cannot explain the observed structural fabrics which need elevated temperatures to form. The second interpretation has been followed by many workers who regard the deformation recorded in the ironstones as minor. However, shear sense indicators do not support deformation during synclinal folding. Sense of shear from both the Manjeri ironstone east of the syncline fold axis trace and from shear zones at the Zeederbergs/Cheshire contact on the western side is towards the northwest (Kusky and Winsky, 1995; chapter 3). We thus favour the interpretation that the Jimmy Member ironstone represents a regional shear zone along which the overlying volcanic and sedimentary units were thrust towards the northwest. The local presence of similar tectonic iron-

stones within the Manjeri Formation suggests that the rapid lateral facies and thickness changes are not primary, sedimentary phenomena, but may be related to tectonic dismemberment of the Manjeri Formation during emplacement of the overlying rock units. A tectonic origin of the Jimmy Member is also consistent with vertical "facies variations" (Fig. 8.6), since the sudden superposition of alluvial/shallow-water clastics by a tabular BIF horizon in an active extensional basin consisting of numerous small-scale horst-and-grabens would be difficult to explain sedimentologically. The protolith of the Jimmy Member ironstone prior to sulfide-mineralization during shearing was possibly shale or true BIF, both of which are common in some parts of the Manjeri Formation.

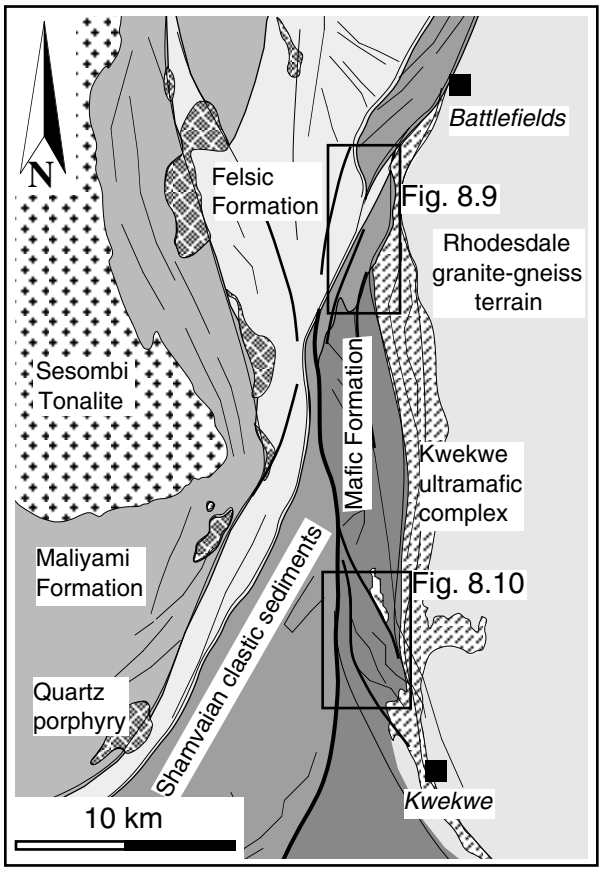

Fig. 8.8. Geological map of the east-central part of the Midlands greenstone belt (modified after Campbell and Pitfield, 1994).

TECTONIC IRONSTONES OF THE MIDLANDS GREENSTONE BELT

The Midlands greenstone belt (MGB) is located in the central part of the Zimbabwe craton and consists of a large marginal unit of Bulawayan volcanics and a central unit of Shamvaian sediments striking north-northeast (Fig. 8.8). The ca. 3.5 Ga old Rhodesdale granitoid-gneiss terrain forms the eastern flank of the belt which has been intruded by ultramafic rocks of the Kwekwe complex. Large-scale strike-slip shear zones run sub-parallel to the contacts between the greenstones, sediments and the gneisses. Dirks et al. (2001) suggested that the MGB north of Kwekwe consists of different lithotectonic domains (terranes) that were swept together during an early episode of west-directed thrusting and concomitant upright folding. Strike-slip faulting reactivated the earlier thrust faults and is assumed to have taken place late in the tectonic history. Many of the former thrusts are occupied by tectonic ironstones, and this can be well demonstrated at two localities.

Munyati area

In an area south of the Munyati River (Fig. 8.9), the contact between Shamvaian sediments to the west and Bulawayan mafic volcanics of the Mafic Formation and serpentinites of the Kwekwe ultramafic complex to the east is occupied by a continuous ironstone horizon. Towards the north,

this ironstone gives way to a strongly sheared and carbonated talc-tremolite schist. Similar ironstone horizons further occur intercalated with the Shamvaian sediments (Fig. 8.9).

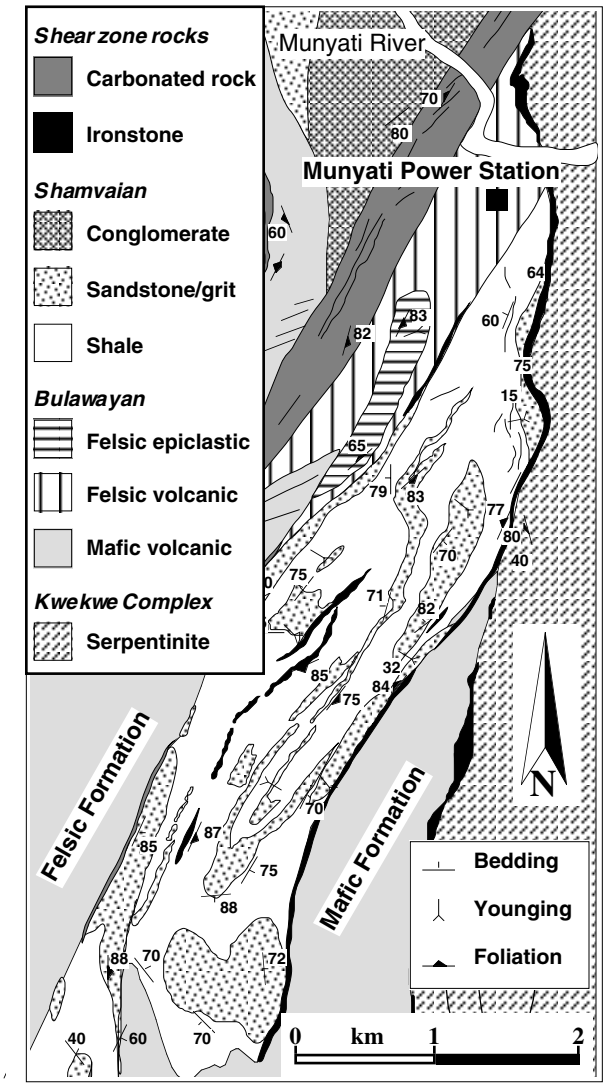

Fig. 8.9. Detailed geological map of an area south of the Munyati River (see Fig. 8.8 for location).

Lithology and structure

Ironstone forms up to 20 m thick, gossaneous horizons that consist of alternating layers of chert and hematite (former sulfide)-rich material. The layering is frequently brecciated so that chert fragments are enveloped by a matrix of gossaneous material. Quartz veins are common. Contacts to adjacent rocks are gradational, i.e. ironstone grades vertically into shale or sandstone that is more strongly foliated, Fe-impregnated and transected by quartz veins than rocks away from ironstone. Various stages of Fe-impregnation can be observed. For example, sandstone adjacent to ironstone may consist of sandstone lenses surrounded by anastomosing bands of Fe-impregnated rock. In the case of more intense Fe-impregnation, scattered quartz clasts supported by a ferruginous matrix may be the only remains of former sandstone. Ironstone adjacent to shale contains intercalations of strongly foliated and brecciated hematitic shale with an anastomosing, lenticular fabric. In some shale horizons, layers of laminated chert occur along anastomosing foliation planes which are subparallel to bedding. Chert-filled cracks may propagate from these planes and intrude into the host rock at high angles to bedding; chert fillings are laminated parallel to the crack walls.

Interpretation

The ironstones are not sedimentary BIF but formed as a consequence of silicification and sulfide-mineralization along shear zones. This is indicated by the restricted occurrence of ironstone along contacts between distinct lithostratigraphic units, the gradational contact of the ironstone horizons to adjacent, Fe-impregnated rocks, and the more strongly strained nature of intercalated

and adjacent sediments. Chert layers are, at least in part, intrusive, and their lamination can be related to crack-and-seal rather than to sedimentary processes.

Sebakwe area

In an area around the Sebakwe River (Fig. 8.10a), the contact that separates the Mafic Formation from Shamvaian sediments has been referred to as the Taba-Mali shear zone (Campbell and Pitfield, 1994). The Taba-Mali shear zone is a ca. 50-100 m wide, steeply westward-dipping schistose zone along which primary bedding and foliation trends in both adjoining domains are truncated. Ironstones are common in this zone.

East of the Taba-Mali shear zone, the Mafic Formation is a ca. 4500 m thick heterogeneous sequence of various lithologies that are arranged in ~10 asymmetric cyclic sequences (Fig. 8.10b). The base of each cycle consists of massive or pillowed basalt. Basalt is commonly overlain by a sandstone/grit unit that locally grades upward into shale. Cycle tops are formed by up to 20 m thick jaspilitic BIF which, in turn, is overlain by a chert breccia and strongly foliated and locally brecciated, sulfide-impregnated ironstone up to a few metres thick.

Lithology and structure

The Taba-Mali shear zone is characterized by intensely contorted and disrupted bedding planes within shale and silt horizons that are commonly carbonated and ferruginized. However, outcrops are mostly restricted to gossaneous ridges composed of highly brecciated, ferruginous horizons in which fragments of quartz-rich (either sandstone or vein quartz) material are embedded in a mesh of oxidized sulfide veinlets, commonly transected by quartz-carbonate veins. In places where brecciation is less intense, the rocks have the appearence of banded chert.

The chert breccia at the top of a cyclic unit of the Mafic Formation consists of angular blocks of jaspilitic BIF embedded in a network of gossaneous veins containing magnetite and pyrrhotite. At the lower contact of the breccia to undisrupted BIF, jaspilitic blocks commonly show a fitted fabric. This coherency is lost away from the contact as unoriented jaspilitic fragments are embedded in a more pervasive ironstone matrix. Ironstone overlying the breccia shows an intense foliation and mineral lineation as well as brecciation, sulfidisation and carbonatisation. An anastomosing foliation envelops quartz lenses that are locally isoclinally folded. Brecciated and sheared ironstones were exploited for gold at several localities in the Mafic Formation (Macgregor, 1932).

Interpretation

Alteration, ironstone formation and deformation can clearly be related along the Taba-Mali shear zone where there is abundant evidence of truncation of primary layering in adjacent sedimentary and volcanic rocks. The presence of tectonic ironstones in the Mafic Formation suggests that the ten repetitive sequences represent tectonic duplications of the same horizon, consisting of basalt overlain by siliciclastic sediment and BIF. Overpressured hydrothermal fluids were focused along bedding-

parallel shear zones along which stratigraphic duplication took place. The fluids resulted in sulfide-mineralization of the shear zones and brecciation of underlying BIF. The presence of tectonic ironstone adjacent to sedimentary BIF makes the distinction of the two difficult, especially in areas of poor exposure. The tectonic duplication of a basalt-BIF sequence several times is similar to what has been described by Ohta (1996) from the Pilbara craton.

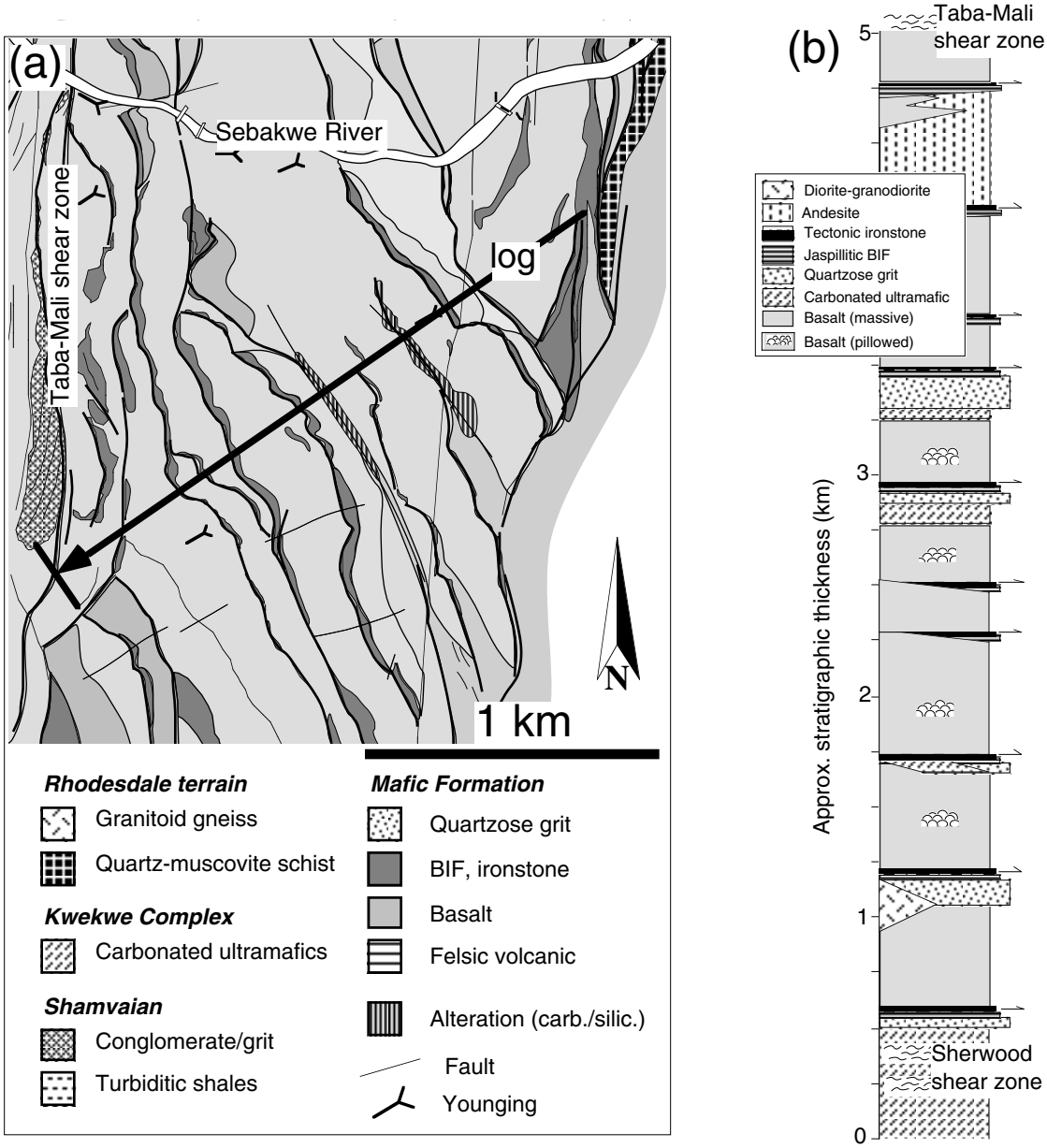

Fig. 8.10. (a) Detailed geological map of the Mafic Formation south of the Sebakwe River (see Fig. 8.8 for location). (b) Simplified graphic log of the Mafic Formation (arrow in Fig. 8.10a; modified after Dirks et al., 2001).

TECTONIC IRONSTONES OF THE BINDURA-SHAMVA GREENSTONE BELT

The Bindura-Shamva greenstone belt (BSGB) is situated in the northern part of the Zimbabwe craton (Fig. 8.1). It is a synformal greenstone belt wedged in between subelliptical granitoid-gneiss domes (Fig. 8.11; Jelsma et al., 1993, 1996). The stratigraphy of the BSGB is locally complex.

South of Bindura, the basal greenstone succession is represented by the Iron Mask Formation which comprises calc-alkaline rhyodacitic volcanic and volcaniclastic rocks variably dated at 2645±4Ma (Wilson et al., 1995) and 2715±15 Ma (Jelsma et al., 1996). The overlying Arcturus Formation is a volcanic pile of pillowed and massive tholeiitic basalt with intercalated komatiitic basalt, ultramafic schist and serpentinite and horizons of volcaniclastic sediment, ironstone, chert and marble. The basal contact of the Arcturus Formation is commonly represented by a thin quartzitic horizon which has been interpreted to unconformably overly the Iron Mask Formation (Wilson et al., 1995).

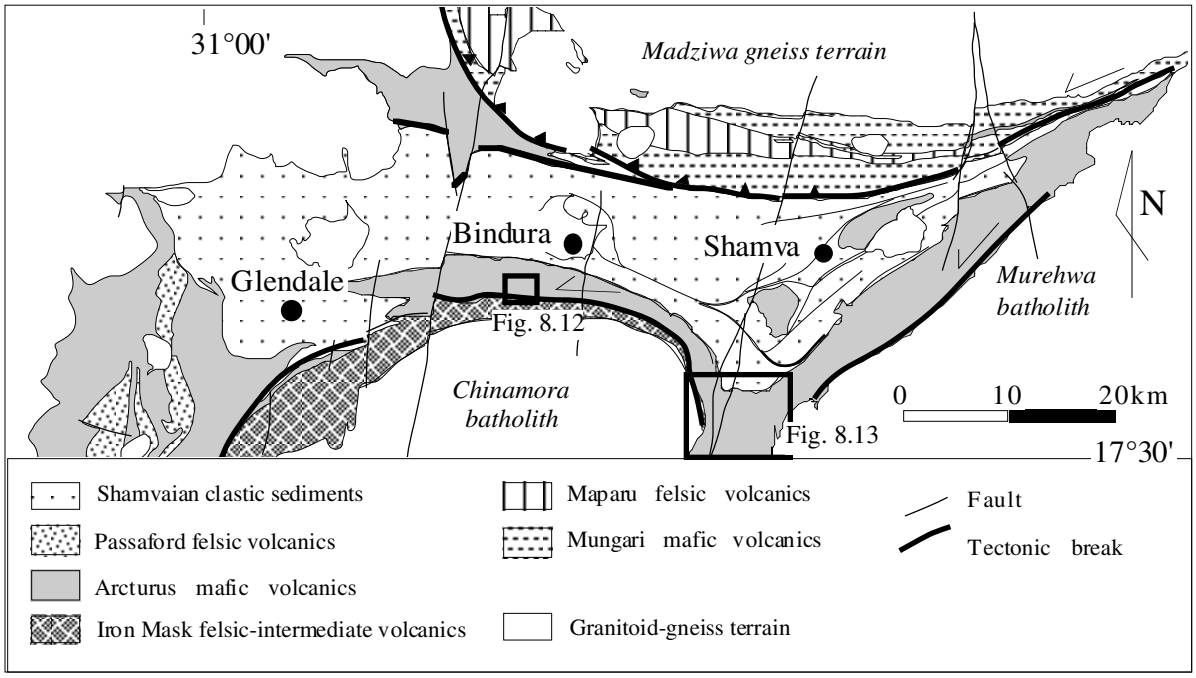

Fig. 8.11. Geological map of the Bindura-Shamva greenstone belt and surrounding granitoid-gneiss terrains (modified after Jelsma and Dirks, 2000).

Trojan nickel mine area

The geology of the Trojan nickel mine has been described in detail by Dirks and Jelsma (1998b). The mine is positioned in the centre of the Arcturus Formation within the southern flank of the BSGB (Fig. 8.12). Massive to pillowed tholeiitic basalt, komatiitic basalt and ultramafic rocks form a series of partly overlapping lensoidal bodies with typical sigmoidal outcrop patterns. The lenses are separated by locally discordant horizons of ferruginous, silicic or graphitic, strongly schistose sedimentary to volcanic rocks. Common lithologies include graphitic schist, chlorite-sericite schist, silicified carbonaceous schist and fine-grained quartzite. These layers are connected in an anastomosing pattern and are described in detail below. Where the schist zones are dominated by quartzitic horizons, such as in the vicinity of ultramafic horizons, they have been mapped as ironstone, sedimentary chert or BIF.

Lithology and structure

Silicified carbonaceous schist and graphitic quartzite are mostly confined to the immediate vicinity of ultramafic units. They occur as lenses or layers with extremely variable thickness. Fine-grained graphitic quartzite occurs in well-foliated to massive dark-grey layers; the fine grain size and layering give them the appearance of banded chert. Networks of layers and veins of Fe-sulfides (mostly pyrrhotite and pyrite) and Fe-oxides are locally common, giving rise to brecciation of the host rock. The quartzitic horizons change along strike into carbonaceous shale and sericite-chlorite schist. This change generally coincides with a change in wall rock lithologies. Quartzite is in contact with serpentinite lenses, whereas graphitic shale is in contact with mafic lithologies, suggesting that some of the quartzites resulted from silicification of sedimentary schist in the vicinity of serpentinized ultramafics. The quartzitic horizon at the contact between the Iron Mask and Arcturus Formation locally truncates primary layering in the footwall and hanging wall (Dirks and Jelsma, 1998b).

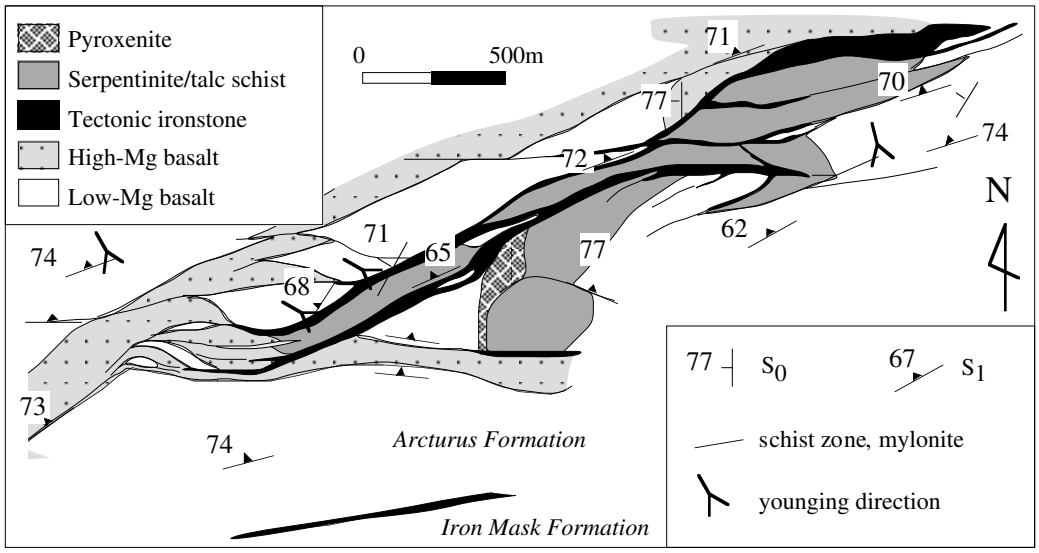

Fig. 8.12. Detailed geological map of the area around Trojan nickel mine (modified after Dirks and Jelsma, 1998a; see Fig. 8.11 for location).

In comparison to the centres of lenticular rock units, the anastomosing quartzite and schist zones preserve a more intensely developed foliation-lineation fabric and clear evidence of high, non-coaxial strain (Dirks and Jelsma, 1998b). Characteristics of the graphitic quartzites that differentiate them from primary sedimentary horizons include the anastomosing and discordant nature of the horizons, the occurrence of complex fold geometries unrelated to regional-scale folds, and the preferential occurrence of these horizons near serpentinized ultramafic units. Mesoscopic features characteristic of high strain include a penetrative foliation, anastomosing foliation domains (commonly Fe-oxide or Fe-sulfide seams), intrafolial folds, sheath folds and transposition fabrics, and brecciated "chert" inclusions infiltrated by Fe-oxide or Fe-sulfide seams. On a microscopic scale, the quartzites are commonly characterized by strong quartz c-axes fabrics, S-C fabrics, grain-

shape fabrics and asymmetric pressure fringes around chert fragments and pyrite cubes (Dirks and Jelsma, 1998b).

Interpretation

The schist zones are interpreted as shear zones, considering the intensity of deformation features and the high finite strains relative to the rocks they envelop. Most graphitic quartzite horizons in the Trojan area show at least some of the above mentioned deformation features suggesting (a) that they represent mylonites, (b) that the fine-grain size is a tectonic feature (and not chert), (c) that the origin of at least some of the quartz is secondary, and (d) that the horizons must be interpreted as silicified shear zones and not as stratigraphic units.

Nyanji Hill area

The area around Nyanji Hill has been described and mapped in detail by Matura (2000) and comprises complexly folded, commonly pillowed basalts and ultramafic schists of the Arcturus Formation (Fig. 8.13). 30 to 100 m thick BIF horizons and thin horizons of siltstone and shale are locally intercalated with basalt. Tectonic ironstone horizons occur and preserve features characteristic of shear zones which have undergone ferruginization and silicification.

Lithology and structure

Tectonic ironstone characteristically occurs as narrow horizons several metres to 10´s of metres thick. The horizons anastomose and bifurcate and truncate the general trend of other lithologies, especially serpentinite and basalt (Fig. 8.13). The ironstone is poorly layered, and the layers show anastomosing geometries. The layers mostly comprise oriented grunerite and haematite alternating with quartz-rich layers. Actinolite has been observed locally. Ironstone preserves penetrative mineral lineations and anastomosing foliation domains; intrafolial folds are common. Fe-oxides occur in narrow fracture zones, many of which are parallel to the grain fabric orientation. These fracture zones occur as parallel layers (~0.2 mm wide) alternating with cherty lithons, typically 5 mm wide, giving the rock a layered appearance. In thin section, quartz grains and mica inclusions define an S-C fabric. Rocks adjacent to ironstones are strongly sheared with the intensity of foliation and lineation decreasing away from ironstone horizon, signifying a pronounced strain gradient.

Interpretation

Tectonic ironstones typically truncate and anastomose around mafic and ultramafic lithologies and, as such, are interpreted as silicified and ferruginized shear zones. Deformation resulted in the fracturing of rocks adjacent to the shear zones, leading to the creation of pathways along which iron and silica-rich fluids were channeled. Fracturing took place parallel to the shear zone walls. The altered ironstone protoliths were probably variable in composition and may have included shale, BIF and mafic volcanic rocks, as evidenced by remnant mafic minerals (actinolite).

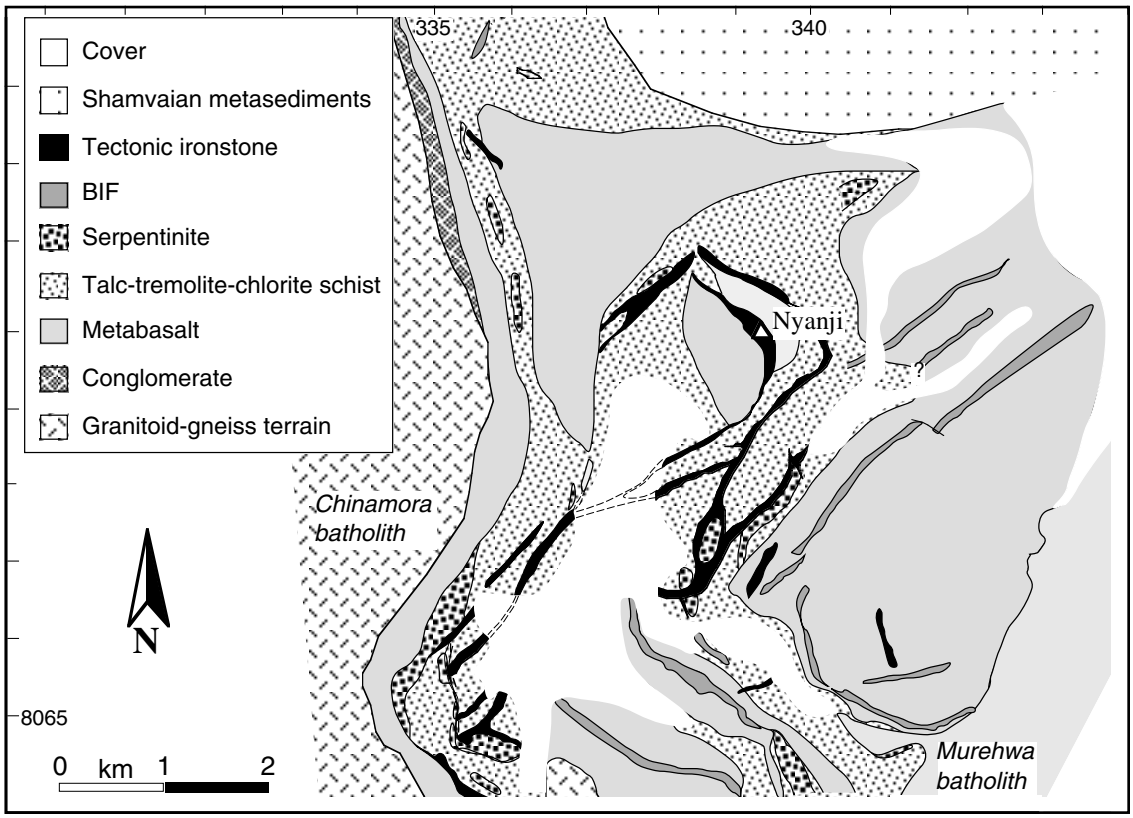

Fig. 8.13. Detailed geological map of the area around Nyanji Hill (modified after Matura, 2000; see Fig. 8.11 for location)

DISCUSSION

Regional synthesis

Ironstones, herein interpreted to have formed syntectonically along bedding-parallel shear zones, are a common phenomenon in Zimbabwean greenstone belts. The belts discussed above have preserved evidence for an early deformational event which was characterized by thin-skinned thrust tectonics prior to granite diapirism and upright folding (Kusky and Winsky, 1995; Dirks and Jelsma, 1998a,b; Jelsma and Dirks, 2000; Dirks et al., 2001; chapter 3). Thrust faults typically occur along lithological contacts and at the margins of distinct lithotectonic units. Tectonic ironstones are locally developed along these shear zones.

In the Cheshire Formation of the BGB, tectonic ironstones formed along shear zones that now separate tectonically duplicated strata (chapter 3). Shearing resulted from compressional deformation in a foreland thrust belt setting. The ironstone horizon at the Manjeri-Reliance contact is in many ways similar to the Cheshire ironstones and is interpreted to have formed during thrusting of the Ngezi volcanics onto the Manjeri Formation. The magnitude of displacement cannot be determined without the knowledge of the root zone of the thrust.

In the MGB, tectonic ironstones commonly occupy the contacts between distinct lithotectonic units (terranes) that show unique structural-metamorphic histories. These shear zones represent major tectonic breaks and were active during horizontal thrust tectonics and terrane accretion (Dirks

et al., 2001). One terrane (Mafic Formation) was internally duplicated and stacked along tectonic ironstone horizons that developed at the top of a sedimentary BIF horizon. The juxtaposition of lithological units with different ages and deformational histories indicate that displacement must have been large along the thrust faults.

In the BSGB, the anastomosing network of early shear zones formed during an episode of low-angle or layer-parallel shearing that resulted in imbricate stacking of the greenstone stratigraphy (Dirks and Jelsma, 1998a,b). Shearing was mostly partitioned into sedimentary horizons thinly intercalated with volcanic rock units. The sediments were transformed into tectonic ironstones upon shearing and associated silicification. Lateral displacement along the shear zones cannot be determined, since they separate rocks of similar composition and structural attributes.

Formation of ironstone

Ironstone formation is intricately associated with layer-parallel slip along fault/shear zones, which are zones of relatively high permeability and, thus, channelways for hydrothermal fluids (e.g., Franklin et al., 1981; Gibson et al., 1983). Deformation was associated with the migration of mineralized hydrothermal fluids along the fault planes. The mineralized fluids probably represented deep circulating waters enriched with silicon, sulphur and metals by the interaction with country rocks. These elements may have been released upon hydrothermal alteration (hydration, serpentinization, albitization, high-temperature metal leaching) of mafic and ultramafic volcanic rocks at deeper structural levels. Upward migration of heated hydrothermal fluids along fault planes may have been aided by seismic pumping. As a result, rocks adjacent to the fault zones, commonly siliciclastic sediments and BIF, were silicified and sulfide-mineralized and, locally, tectonic ironstones formed. The origin of ironstone can be thought of as a layer-by-layer replacement process of primarily stratified rocks that were subjected to shearing. However, some of the material constituting the ironstones did not form via an alteration/replacement process of primary host rocks, but precipitated directly in fractures within the shear zones, as indicated by intrusive chert and sulfide veins. The relative amounts of replaced, primary sedimentary material and newly formed, intrusive veins, which together resulted in the formation of ironstone, remains unknown. Layering is probably the result of the combined effects of replacement of originally stratified rocks (e.g., shale, BIF, limestone), chert intrusion and sulfide-mineralization parallel to shear zone walls and, less likely, transposition of intrusive veins during deformation. Brecciation was part of this progressive alteration process. The common feature of brecciation indicates that fluid pressures must have been high along the shear zones and high enough to overcome frictional and cohesion forces for thrusting to occur. Most of the lithological aspects of the ironstones and the deformation recorded in them, such as tight to isoclinal folding, is related to early thrusting, suggesting that the ironstones formed syntectonically. The chert components were deformed in a brittle-ductile manner, as indicated by brecciation on the one hand and boudinage, tight to isoclinal folding and sheath folding

on the other, indicating that the chert precursor may have varied in the state of consolidation (cf. de Wit, 1982). Variable fluid pressure may have also played a role.

Above we have proposed an intrusive or replacement origin for sulfides in tectonic ironstones, and, in addition, we think that banded cherts in tectonic ironstone not derived from the alteration of BIF have the same origin, i.e. by silicification and chert veining. Chert as an alteration or replacement product of sedimentary country rock is a feature commonly associated with hydrothermal massive sulfide deposits (e.g., Leistel et al., 1998). In the Barberton greenstone belt, South Africa, chert is a common replacement product of ultramafic to felsic lavas, pyroclastic deposits and sedimentary rocks (de Wit et al., 1982; Paris et al., 1983; Lowe, 1999). Chert veins and stockworks are also common and locally give rise to brecciation of the host rocks. Chert veins are both oblique and parallel to bedding and commonly display banding parallel to the walls of the fractures (Paris et al., 1983). In the Warawoona Group of the Pilbara craton, Western Australia, stratiform and discordant veins of black chert, commonly associated with barite, are a common phenomenon and have been related to hydrothermal fluids generated and emplaced during an event of extensional faulting (Nijman et al., 1998).

Tectonic ironstones in other greenstone belts

We suggest that tectonic ironstones similar to those described above are a common phenomenon in other Archaean greenstone terrains. In the Barberton greenstone belt, for example, stratiform silica (and carbonate) alteration zones, commonly separating different lithological units, have been described and interpreted as major decollement zones along which extensive horizontal translations took place (de Wit, 1982; de Wit et al., 1982). One such zone, a silicious, cherty horizon hosting the New Consort gold mine, occurs along the contact between the mafic volcanics of the Onverwacht Group and shales of the Fig Tree Group. Its origin has been related to the silicification and gold mineralization of the shear zone that occurs along the contact (references in Anhaeusser et al., 1976). This is a similar setting to the ironstone at the Zeederbergs-Cheshire Formation contact. Discontinuous bodies of "ironstone breccias, in appearance often reminiscent of slag", have been described from Barberton and interpreted as mineralized hydrothermal channels and chimneys (de Wit et al., 1982). These features are near the silica alteration zones interpreted as major shear zones (de Wit, 1982). Recently, a thick, laterally continuous breccia unit of banded chert in an iron oxide-rich matrix has been described from the Buck Ridge Chert at Barberton; brecciation has been attributed to hydrothermal activity (de Vries and Nijman, 2001).

In the Slave Province of Canada, mid-Archaean granitoid basement is overlain unconformably by a thin, discontinuous sedimentary cover sequence (Central Slave Cover Group, Bleeker et al., 1998), followed by a thick succession of tholeiitic basalts (Kam Group). The stratigraphy is thus remarkably similar to the stratigraphy of the Ngezi Group of the Belingwe belt. The top of the sedimentary sequence is represented by a laterally continuous unit of shale and silicate- and oxide-facies BIF. "A thin sulphidic chert horizon is locally present at the contact between BIF and the

overlying pillow basalts" (Bleeker et al., 1998), a rock apparently similar to what we have called tectonic ironstone at the top of the Manjeri Formation.

A possible hydrothermal-metasomatic origin of banded iron formation has also been discussed from greenstone belts in the Ukrainian and Baltic Shields (references in Alexandrov, 1973). This resulted from the observation of, for example, gradational contacts between pyroxenites-serpentinites and iron formation, the presence of relics of ultrabasic rocks in ironstone, and the asociation of mylonitic horizons with iron formation. Hydrothermal-metasomatic processes were thought to include silicification and iron metasomatism of various rock types by fluids derived from hydrothermal alteration of mostly ultramafic and mafic rocks. These findings are remarkably similar to our observations from, for example, the Trojan Mine area in the Bindura-Shamva greenstone belt.

Most of the tectonic ironstones in Zimbabwe have previously been interpreted as sedimentary rocks. The Manjeri Formation, meaning here the ironstone of the Jimmy Member, has been used as a marker horizon and has been correlated over long distances across many of Zimbabwe's greenstone belts, on the basis of the unusual lateral persistence of this rock type as compared to other greenstone lithologies (Wilson et al., 1995). This study considers such rocks as tectonic in origin. If major structural repetitions and tectonic intermingling occured along ironstone horizons, the preserved greenstone belt stratigraphy must be more complex.

CONCLUSIONS

1. The term "tectonic ironstone" summarizes a variety of rocks which are enriched in Fe and Si and which show evidence that their formation is related to shearing. Such rocks have been variably termed banded iron formation, gossaneous ironstone, chert, ferruginous chert, ferruginous quartzite, ferruginous schist, etc.
2. Tectonic ironstones are typically several metres to ~20 m in thickness and can be laterally continuous for tens of kilometres. They commonly occur along the contact between different lithological units that are frequently mapped as distinct stratigraphic units.
3. In outcrop, tectonic ironstone is a poorly layered rock of chert and iron-oxides, the latter representing replacements after sulfides, mostly pyrite. Surface weathering of the sulfides gives rise to a gossaneous appearance and obliterates primary structural features. Brecciation is very common so that fragments of chert and banded chert float in a matrix dominated by iron oxide.
4. Tectonic ironstone occurs along lithological contacts where there is clear evidence of shearing, such as bedding and/or foliation truncation. Sheared contacts between basalt and shale seem to be the most common site of ironstone occurrence, with shale being the host rock of the ironstone.
5. Ironstones formed syntectonically by silicification and sulfide-mineralization of rocks adjacent to shear zones. Thus, the degree of hydrothermal alteration decreases away from the shear zones.

6. Shear zones containing ironstones frequently represent detachment surfaces at the base of now juxtaposed lithotectonic units. Within lithotectonic domains, the shear zones are bedding-parallel and may give rise to stratigraphic duplication.
7. Displacement along the shear zones cannot be determined, but must have been large at many places (minimum of tens of kilometres) where terrane boundaries are concerned.
8. We finally want to encourage caution when using cherts or ironstones as stratigraphic marker horizons in greenstone terrains. Caution is particularly necessary when angular rock relationships are involved.

REFERENCES

ALEXANDROV, E.A. 1973. The Precambrian banded iron-formations of the Soviet Union. *Economic Geology,* 68, 1035-1062.

ANHAEUSSER, C.R. 1976. The nature and distribution of Archaean gold mineralization in southern Africa. *Minerals Science Engineering,* 8, 46-84.

BEUKES, N.J. 1973. Precambrian iron-formations of southern Africa. *Economic Geology,* 68, 960-1004.

BICKLE, M.J. & NISBET, E.G. (eds) 1993. *The geology of the Belingwe Greenstone Belt, Zimbabwe.* Geological Society of Zimbabwe Special Publications, 2, 239pp.

BICKLE, M.J., MARTIN, A. & NISBET, E.G. 1975. Basaltic and peridotitic komatiites, stromatolites and a basal unconformity in the Belingwe greenstone belt, Rhodesia. *Earth and Planetary Science Letters,* 27, 155-162.

BICKLE, M.J., NISBET, E.G. & MARTIN, A. 1994. Archaean greenstone belts are not oceanic crust. *Journal of Geology,* 102, 121-138.

BLEEKER, W., KETCHUM, J.W.F., JACKSON, V.A. & VILLENEUVE, M.E. 1998. The Central Slave Basement Complex, Part I: its structural topology and autochthonous cover. *Canadian Journal of Earth Sciences,* 36, 1083-1109.

BLENKINSOP, T.G., FEDO, C.M., BICKLE, M.J., ERIKSSON, K.A., MARTIN, A., NISBET, E.G. & WILSON, J.F. 1993. Ensialic origin for the Ngezi group, Belingwe greenstone belt, Zimbabwe. *Geology,* 21, 1135-1138.

BLISS, N.W. 1970. The geology of the country around Gatooma. *Rhodesia Geological Survey Bulletin,* 64, 240pp.

BOUHALLIER, H., CHOUKROUNE, P. & BALLÈVRE, M. 1993. Diapirism, bulk homogeneous shortening and transcurrent shearing in the Archaean Dharwar craton, the Holenarsipur area, southern India. *Precambrian Research,* 63, 43-58.

BRAKE, C. 1996. *Tholeiitic magmatism in the Belingwe greenstone belt, Zimbabwe.* Unpublished PhD thesis, University of Edinburgh, 184pp.

CAMPBELL, I.H. & HILL, R.I. 1988. A two-stage model for the formation of the granite-greenstone terrain of the Kalgoorlie-Norseman area, Western Australia. *Earth and Planetary Science Letters,* 90, 11-25.

CAMPBELL, S.D.G. & PITFIELD, P.E.J. 1994. Structural controls of gold mineralization in the Zimbabwe Craton—Exploration guidelines. *Geological Survey of Zimbabwe Bulletin,* 101, 270pp.

CARD, K.D. 1990. A review of the Superior Province of the Canadian Schield, a product of Archaean accretion. *Precambrian Research,* 48, 99-156.

CHAUVEL, C., DUPRÉ, B. & ARNDT, N.T. 1993. Pb and Nd istopic correlation in Belingwe komatiites and basalts. *In:* BICKLE, M.J. & NISBET, E.G. (eds) *The geology of the Belingwe Greenstone Belt, Zimbabwe.* Geological Society of Zimbabwe Special Publications, 2, 167-174.

CHOWN, E.H., N´DAH, E. & MUELLER, W.U. 2000. The relation between iron-formation and low temperature hydrothermal alteration in an Archaean volcanic environment. *Precambrian Research,* 101, 263-275.

DE VRIES, S.T. & NIJMAN, W. 2001. Environmental conditions and hydrothermal systems: Buck Ridge Chert complex, Barberton, SA. *In:* CASSIDY, K.F., DUNPHY, J.M. & VAN KRANENDONK, M.J. (eds) *4th International Archaean Symposium 2001, Extended Abstracts.* AGSO-Geoscience Australia, Record 2001/37, 224-226..

DE WIT, M.J., 1982. Gliding and overthrust nappe tectonics in the Barberton Greenstone Belt. *Journal of Structural Geology,* 4, 117-136.

DE WIT, M.J., HART, R.J., MARTIN, A. & ABBOTT, P. 1982. Archaean abiogenic and probable biogenic structures associated with mineralized hydrothermal vent systems and regional metasomatism, with implications for greenstone belt studies. *Economic Geology,* 77, 1783-1802.

DE WIT, M.J., ROERING, C., HART, R.J., ARMSTRONG, R.A., DE RONDE, C.E.J., GREEN, R.W.E., TREDOUX, M., PERBEDY, E. & HART, R.A. 1992. Formation of an Archaean continent. *Nature,* 357, 553-562.

DIRKS, P.H.G.M. & JELSMA, H.A. 1998a. Horizontal accretion and stabilization of the Archaean Zimbabwe Craton. *Geology,* 26, 11-14.

DIRKS, P.H.G.M. & JELSMA, H.A. 1998b. Silicic layer-parallel shear zones in a Zimbabwean Greenstone sequence; horizontal accretion preceding doming. *Gondwana Research,* 1, 177-194.

DIRKS, P.H.G.M. & VAN DER MERWE, J. 1997. Early duplexing in an Archaean greenstone sequence and its control on gold mineralisation. *Journal of African Earth Sciences,* 24, 603-620.

DIRKS, P.H.G.M., JELSMA, H.A. & HOFMANN, A. 2001. Accretion of an Archaean greenstone belt in the Midlands of Zimbabwe. *Journal of Structural Geology,* in press.

FRANKLIN, J.M., LYDON, J.W. & SANGSTER, D.M. 1981. Volcanic-associated massive sulfide deposits. *Economic Geology,* 75th Anniversary Volume, 485-627.

FRIPP, R.E.P. 1976. Stratabound gold deposits in Archaean banded iron-formation, Rhodesia. *Economic Geology,* 71, 58-75.

GIBSON, H.L., WATKINSON, D.H. & COMBA, C.D.A. 1983. Silicification: Hydrothermal alteration in an Archaean geothermal system within the Amulet Rhyolite Formation, Noranda, Quebec. *Economic Geology,* 78, 954-971.

GOODWIN, A.M. 1973. Archaean iron-formations and tectonic basins of the Canadian Shield. *Economic Geology,* 68, 915-933.

GROSS, G.A. 1965. Geology of iron deposits in Canada, V.1. General geology and evaluation of iron deposits. *Geological Survey of Canada Economic Geology Report,* 22, 181pp.

GROVES, D.I., PHILLIPS, N., HO, S.E., HOUSTOUN, S.M. & STANDING, C.A. 1987. Craton-scale distribution of Archaean greenstone gold deposits: predictive capacity of the metamorphic model. *Economic Geology,* 82, 2045-2058.

HAMILTON, W.B. 1998. Archean magmatism and deformation were not products of plate tectonics. *Precambrian Research,* 91, 143-179.

HARRISON, N.M. 1970. The geology of the country around Que Que. *Rhodesia Geological Survey Bulletin,* 67, 125pp.

HERRINGTON, R.J. 1995. Late Archean structure and gold mineralization in the Kadoma region of the Midlands greenstone belt, Zimbabwe. *In:* COWARD, M.P. & RIES, A.C. (eds) *Early Precambrian processes.* Geological Society Special Publication, 95, 173-191.

HORSTWOOD, M.S.A. 1998. *Stratigraphy, geochemistry and zircon geochronology of the Midlands greenstone belt, Zimbabwe.* Unpublished PhD thesis, University of Southampton, 215 pp.

HORSTWOOD, M.S.A., NESBITT, R.W., NOBLE, S.R. & WILSON, J.F. 1999. U-Pb zircon evidence for an extensive early Archaean craton in Zimbabwe: A reassessment of the timing of craton formation, stabilization, and growth. *Geology,* 27, 707-710.

HUNTER, M. 1997. The tectonic setting of the Belingwe Greenstone Belt, Zimbabwe. Unpublished PhD thesis, University of Cambridge, 223pp.

HUNTER, M.A., BICKLE, M.J., NISBET, E.G., MARTIN, A. & CHAPMAN, H.J. 1998. Continental extensional setting for the Archean Belingwe Greenstone Belt, Zimbabwe. *Geology,* 26, 883-886.

JAMES, H.L. 1954. Sedimentary facies of iron-formation. *Economic Geology,* 49, 235-293.

JELSMA, H.A., VAN DER BEEK, P.A. & VINYU, M.L. 1993. Tectonic evolution of the Bindura-Shamva greenstone belt (northern Zimbabwe): progressive deformation around diapiric batholiths. *Journal of Structural Geology,* 15, 163-176.

JELSMA, H.A., VINYU, M.L., VALBRACHT, P.J., DAVIES, G.R., WIJBRANS, J.R. & VERDURMEN, E.A.T. 1996. Constraints on Archaean crustal evolution of the Zimbabwe craton: a U-Pb zircon, Sm-Nd and Pb-Pb whole-rock isotope study. *Contributions to Mineralogy and Petrology,* 124, 55-70.

JELSMA, H.A. & DIRKS, P.H.G.M. 2000. Tectonic evolution of a greenstone sequence in northern Zimbabwe: sequential early stacking and pluton diapirism. *Tectonics,* 19, 135-152.

KIMBERLEY, M.M. 1978. Palaeoenvironmental classification of iron formations. *Economic Geology,* 73, 215-229.

KIMBERLEY, M.M. 1989. Exhalative origins of iron formations. *Ore Geology Reviews,* 5, 13-145.

KUSKY, T.M. 1989. Accretion of the Archean Slave Province. *Geology,* 17, 63-67.

KUSKY, T.M. & VEARNCOMBE, J.R. 1997. Structural aspects. *In:* DE WIT, M.J. & ASHWAL, L.D. (eds) *Greenstone belts.* Oxford University Press, 91-124.

KUSKY, T.M. & KIDD, W.S.F. 1992. Remnants of an Archaean oceanic plateau, Belingwe Greenstone Belt, Zimbabwe. *Geology,* 20, 43-46.

KUSKY, T.M. & WINSKY, P.A. 1995. Structural relationships along a greenstone/shallow water shelf contact, Belingwe greenstone belt, Zimbabwe. *Tectonics,* 14, 448-471.

LEISTEL, J.M., MARCOUX, E. & DESCHAMPS, Y. 1998. Chert in the Iberian pyrite belt. *Mineralium Deposita,* 33, 59-81.

LOWE, D.R. 1999. Petrology and sedimentology of cherts and related silicified sedimentary rocks in the Swaziland Supergroup. *In:* LOWE, D.R. & BYERLY, G.R. (eds) *Geologic Evolution of the Barberton Greenstone Belt, South Africa.* Geological Society of America Special Paper, 329, 83-114.

MACGREGOR, A.M. 1932. The geology of the country around Que Que, Gwelo district. *Southern Rhodesia Geological Survey Bulletin,* 20, 113pp.

MACGREGOR, A.M. 1951. Some milestones in the Precambrian of Southern Rhodesia. *Proceedings of the Geological Society of South Africa,* 54, 27-71.

MARTIN, A. 1978. The geology of the Belingwe-Shabani schist belt. *Rhodesia Geological Survey Bulletin,* 83, 213pp.

MARTIN, A., NISBET, E.G., BICKLE, M.J. & ORPEN, J.L. 1993. Rock units and stratigraphy of the Belingwe Greenstone Belt: The complexity of the tectonic setting. *In:* BICKLE, M.J. & NISBET, E.G. (eds) *The geology of the Belingwe Greenstone Belt, Zimbabwe.* Geological Society of Zimbabwe Special Publications, 2, 39-68.

MATURA, N.E. 2000. The tectonic history of the Bindura-Shamva Greenstone Belt, northern Zimbabwe, and the importance of ironstone as structural discontinuities. Unpublished M.Sc. thesis, University of Zimbabwe, 117pp.

MYERS, J.S. 1995. The generation and assembly of an Archaean super continent: evidence from the Yilgarn craton, western Australia. *In:* COWARD, M.P. & RIES, A.C. (eds) *Early Precambrian processes.* Geological Society Special Publication, 95, 143-154.

NIJMAN, W., DE BRUIJNE, K.H. & VALKERING, M.E. 1998. Growth fault control of Early Archaean cherts, barite mounds and chert-barite veins, North Pole Dome, Eastern Pilbara, Western Australia. *Precambrian Research,* 88, 25-52.

NISBET, E.G., MARTIN, A., BICKLE, M.J. & ORPEN, J.L. 1993. The Ngezi Group: Komatiites, basalts and stromatolites on continental crust. *In:* BICKLE, M.J. & NISBET, E.G. (eds) *The geology of the Belingwe Greenstone Belt, Zimbabwe.* Geological Society of Zimbabwe Special Publications, 2, 121-165.

OHTA, H., MARAYAMA, S., TAKAHASHI, E., WATANABE, Y. & KATO, Y. 1996. Field occurrence, geochemisty and petrogenesis of the Archaean Mid-Oceanic Ridge Basalts (AMORBs) of the Cleaverville area, Pilbara Craton, Western Australia. *Lithos,* 37, 199-221.

ORPEN, J.L. 1978. *The geology of the southwestern part of the Belingwe Greenstone Belt and adjacent country—The Belingwe Peak area.* Unpublished PhD thesis, University of Rhodesia.

ORPEN, J.L., BICKLE, M.J., NISBET, E.G. & MARTIN, A. 1986. Belingwe Peak, Zimbabwe Geological Survey Map, 1:100000.

PARIS, I., STANISTREET, I.G. & HUGHES, M.J. 1985. Cherts of the Barberton greenstone belt interpreted as products of submarine exhalative activity. *Journal of Geology,* 93, 111-129.

PHILLIPS, G.N., GROVES, D.I. & MARTYN, J.E. 1984. An epigenetic origin for Archaean banded iron-formation-hosted gold deposits. *Economic Geology,* 79, 162-171.

RIDLEY, J.R., VEARNCOMBE, J.R. & JELSMA, H.A. 1997. Relations between greenstone belts and associated granitoids. *In:* DE WIT, M.J. & ASHWAL, L.D. (eds) *Tectonic evolution of greenstone belts.* Oxford University Press, 376-397.

ROBERTSON, I.D.M. 1976. The geology of the country around Battlefields, Gatooma District. *Rhodesia Geological Survey Bulletin,* 76.

SCHOLEY, S.P. 1992. *The geology and geochemistry of the Ngezi Group volcanics, Belingwe Greenstone Belt, Zimbabwe.* Unpublished PhD thesis, University of Southampton, 184pp.

SHACKLETON, R.M. 1995. Tectonic evolution of greenstone belts. *In:* COWARD, M.P. & RIES, A.C. (eds) *Early Precambrian processes.* Geological Society Special Publication, 95, 53-65.

SIMONSON, B.M. 1985. Sedimentological constraints on the origins of Precambrian iron-formations. *Geological Society of America Bulletin,* 96, 244-252.

STOWE, C.W. 1984. The early Archaean Selukwe nappe, Zimbabwe. *In:* KRÖNER, A. & GREILING, R. (eds) *Precambrian tectonics illustrated.* Nägele und Obermiller, Stuttgart, 41-56.

SWAGER, C. & GRIFFIN, T.J. 1990. An early thrust duplex in the Kalgoorlie-Kambalda greenstone belt, Eastern Goldfields Province, Western Australia. *Precambrian Research,* 48, 63-73.

TRENDALL, A.F. 1973. Precambrian iron-formations of Australia. *Economic Geology,* 68, 1023-1034.

WILSON, J.F. 1979. A preliminary reappraisal of the Rhodesian basement complex. *In:* ANHAEUSSER, C.R., FOSTER, R.P. & STRETTON, T. (eds) *A symposium on mineral deposits and transportation and deposition of metals.* Geological Society of South Africa Special Publications, 5, 1-23.

WILSON, J.F. 1990. A craton and its cracks: some of the behaviour of the Zimbabwe block from the late Archaean to the Mesozoic in response to horizontal movements, and the significance of some of its mafic dyke fracture patterns. *Journal of African Earth Sciences,* 10, 483-501.

WILSON, J.F., NESBITT, R.W. & FANNING, C.M. 1995. Zircon geochronology of Archaean felsic sequences in the Zimbabwe craton: a revision of greenstone stratigraphy and a model for crustal growth. *In:* COWARD, M.P. & RIES, A.C. (eds) *Early Precambrian processes.* Geological Society Special Publication, 95, 109-126.

Lebenslauf

Persönliche Daten

Name	Axel Hofmann
Heimatanschrift	Maxdorf 1, 55571 Odernheim
Geburtsdatum/-ort	26.02.1971, Bad Kreuznach
Nationalität	Deutsch

Bildungsweg

1977-1981	Grundschule Odernheim
1981-1991	Gymnasium Sobernheim
05.91	Schulabschluß, Abitur
07.91-09.92	Zivildienst
10.92-08.97	Studium der Geologie an der Johannes Gutenberg-Universität Mainz
seit 08.97	Doktorand an der Universität Mainz
03.98	Beginn der vorliegenden Dissertation
seit 03.98	Research Associate an der Universität von Simbabwe in Harare

Förderungen

09/97-02/98	Förderungsstipendium der Universität Mainz
03/98-10/99	Doktorandenstipendium des DAAD im Rahmen des HSP III Programms
07/00-04/01	Stipendium nach dem Landesgraduiertenförderungsgesetzes

Mainz, 16.12.2001